UNIVERSIDAD COMPLUTENSE DE MADRID

FACULTAD DE CIENCIAS FÍSICAS
Departamento de Física de la Tierra, Astronomía y Astrofísica I

VARIABILIDAD DEL ATLÁNTICO TROPICAL: INTERACCIONES OCÉANO-ATMÓSFERA E IMPACTOS EN EL CLIMA = TROPICAL ATLANTIC VARIABILITY: OCEAN-ATMOSPHERE INTERACTIONS AND CLIMATE IMPACTS

MEMORIA PARA OPTAR AL GRADO DE DOCTOR

PRESENTADA POR

Irene Polo Sánchez

Bajo la dirección de los doctores
María Belén Rodríguez de Fonseca y Alban Lazar

Madrid, 2008

- **ISBN: 978-84-692-1094-9**

Departamento de Física de la Tierra, Astronomía y Astrofísica I
Universidad Complutense de Madrid

Variabilidad del Atlántico Tropical: Interacciones Océano-Atmósfera e Impactos en el Clima

Tropical Atlantic Variability: Ocean-Atmosphere Interactions and Climate Impacts

Memoria de Tesis presentada para optar al grado de Doctor

Dirigida por

Dra. María Belén Rodríguez de Fonseca
Dr. Alban Lazar

Irene Polo Sánchez

Madrid 2008

AGRADECIMIENTOS

Parece que fue ayer cuando asistí a la defensa de Tesis de Belén y las palabras variabilidad, Atlántico y temperatura del mar se colaron en mi existencia, hace ya siete años. Desde entonces y hasta hoy, Belén no ha dejado nunca de ofrecerme generosamente lo mejor de ella: su confianza, su apoyo, su diligencia, su entusiasmo, su empatía, su ímpetu, su constancia, tanto en lo profesional como en lo personal. En esto años no solamente he aprendido sino que he crecido con ella. Sencillamente, me temo que a día de hoy no podré escribir unos agradecimientos que le hagan justicia.

Agradezco también a Alban la confianza que puso en mí. La búsqueda del consenso en las largas discusiones ha logrado mejorar esta Memoria, a pesar de nuestras diferencias.

A modo testimonial, me gustaría agradecer a los que me han acompañado en estos años. Una lista sólo nombra, lo sé, pero en cada nombre hay una historia que requeriría otro libro.

Al departamento, especialmente a Elvira, Encarna y Carlos, por su apoyo en todo el proceso. A la parte administrativa y técnica por su eficacia y apoyo: Lucía, Salva y Pedro.

A los que empezaron conmigo aquellos cursos de doctorado: a Luis, Lucía, Isabel, Marta, Paco, y en sincronía a mis compañeras del centro de cálculo.

A los que fueron y van pasando por el laboratorio de Meteorología, haciendo de éste un espacio acogedor y estimulante donde es posible compartir algo más que trabajo y galletas: A Xavier, Alberto, Kike, Elena, Teresa, Javi, África, Samuel, Álvaro, Blanca, Tesa, Etor, David y Esteban.

A los compañeros geofísicos y no geofísicos por su compañía en las comidas y su apoyo siempre: a Ana, Víctor, Rafa, Carlos, Alicia, Simone, Javi Pavón, Elsa, Luis Dinis, Gianluca, Juan Luis y Juan.

A los que siempre han estado por aquí, animándome: A Óscar, Sonia, Óscar Vadillo, Nekane, Javi Galeano y Eduardo. A Roberto Mechoso por sus conversaciones en sus viajes a Madrid.

A Ensenada, al CICESE, especialmente a Julio Sheinbaum por su hospitalidad y su inspiración en el trabajo, a Dulce, Selene, Lucho, Píston, las perras de satán, el comando anfibio y el sauzal.

A París, al LOCEAN, especialmente a Sabine Arnault y a Serge Janicot por su cordialidad y su disponibilidad para ayudarme, a Gildas, Aziza, Thomas, Benjamin, Aurélie, Jhan Carlo, Flore, Alessandro y Gabi.

A los colegas de Vigo, Barna, Irun, Bangor y Torre, los de siempre. En especial a Marino y a Jaime por su amistad incondicional de años y que junto a Javi, Juan, Gorka y Marcos intuimos una vez que todo era posible, a Isa, Maca, Almu, Olivia, Jorge, Fernando, Tobias y Stefan.

A Samuel y a Roberto que me han sustentado y alimentado en los momentos más tensos de las últimas semanas. También en estas últimas semanas agradezco el apoyo y la ayuda de Nati, Henry y Adriana.

A mis padres y a mis tíos que siempre confían en mí, y muy especialmente a Nuria y a Sandra, mis hermanas, con las que crezco siempre.

Gracias

Mucho TROPA

Sat nam

Este trabajo ha sido financiado por el Ministerio de Educación y Ciencia (MEC) a través del programa de ayudas para la Formación del Personal Investigador (beca FPI BES-2003-1621) asociada al proyecto de investigación REN2002-03424 y co-financiada por el Fondo Social Europeo. Además, este trabajo ha sido financiado por el proyecto de investigación nacional CGL2006-04471. Finalmente, el programa *ANETUS* financiado por NASA/CNES y el programa *AMMA* financiado por la Unión Europea han hecho posible parte de la investigación contenida en la Memoria de Tesis Doctoral.

This work has been supported by the National Spanish Ministry of Education and Research (MEC) under grant (BES-2003-1621) associated with the program REN2002-03424 and co-financed by the European Social Funds. Also this work has been supported by the Spanish program CGL2006-04471. Finally, the *ANETUS* program financed by NASA/CNES and the *AMMA* program financed by European Union have made possible part of the research contained in this PhD Thesis.

INDEX

Page

MOTIVATION 1

1. STATE OF THE ART 13

1.1 *Tropical Climate Variability* 13

1.2 *Tropical Atlantic Variability* 14

1.3 *Tropical Atlantic Seasonal Cycle* 16

1.3.1 Atmosphere seasonal cycle 16

1.3.2 Ocean seasonal cycle 18

1.4 *Interannual Variability SST modes and air-sea interactions* 21

1.4.1 Equatorial Mode 22

1.4.2 Meridional Mode: Its link to the Subtropical North Atlantic 24

1.4.3 Coupled air-sea feedbacks in Tropical Atlantic Variability 27

1.5 *Aspects of Intraseasonal atmosphere and oceanic variability* 29

1.5.1 Intraseasonal wind-convection fluctuations 29

1.5.2 Oceanic adjustment through long planetary waves 32

1.5.2.1 Intraseasonal oceanic Kelvin wave: an equatorial coupled wave? 33

1.5.2.2 Intraseasonal oceanic Rossby wave: The extratropical Connection 34

1.6 *Teleconnections linked to Tropical Atlantic Variability* 34

1.6.1 External forcings 35

1.6.1.1 ENSO 35

1.6.1.2 NAO 37

1.6.2 Impacts 39

1.6.2.1 Impacts on the winter European climate 39

1.6.2.2 Impacts on the summer West African climate 40

1.7 *Predictability Issues* 41

1.8 *Aspects of Decadal to Multidecadal Variability* 42

2. HYPOTHESES AND OBJECTIVES 45

2.1 *Initial Hypotheses* 45

2.2 *Specific Objectives and Outline of Results* 47

3. METHODOLOGY AND DATA 53

3.1 *The Election of the Anomalies* 53

3.2 *Discriminant Analysis* 53

3.2.1 Empirical Orthogonal Functions Analysis 54

3.2.2 Extended Empirical Orthogonal Functions Analysis 56

3.2.3 Maximum Covariance Analysis 58

3.2.4 Extended Maximum Covariance Analysis 60

3.2.5 Significance test and Representation of Results 62

3.3 *Spectral Analysis* 64

3.3.1 Filtering the data 65

3.3.2 Spectrogram Analysis 66

3.3.3 Radon Transform 66

3.4 *Data* 68

3.4.1 Oceanic Fields 68

3.4.2 Atmospheric Fields 71

4. RESULTS 75

4.1 *Tropical-Extratropical Interannual Covariability Patterns: Air-sea interactions* 77

4.1.1 Tropical Atlantic SST and winter European precipitation 79

4.1.2 Tropical Atlantic SST and summer West African rainfall 99

4.2 *Intraseasonal Tropical Atlantic Ocean Variability: The Kelvin wave signal* 119

5. INTEGRATED DISCUSSION 167

6. CONCLUSIONS 175

REFERENCES 183

GLOSSARY 197

APPENDIXES 199

APPENDIX I: THEORETICAL FRAMEWORK

APPENDIX II: ATMOSFERIC CIRCULATION RELATED TO TROPICAL CONVECTION

MOTIVATION

Tropical oceans are a major source of heat and they contribute largely to the global oceanic and atmospheric circulation. In essence, the memory of the short-term climate of the earth resides in the tropical oceans, which affect the climate of the earth on many different time scales. The study of the Tropical Variability turns to be a very complicated task since it involves analysing different air-sea-land interactions. This, along with the fact that it affects a large rural population that depend largely on rain fed agriculture (Chang et al., 2006; Kushnir et al., 2003; Xie and Carton, 2004 for a review) makes the topic a real challenge for the scientific community.

Historically, climate studies underwent a dramatic change when Bjerknes (1969) proposed a physical relationship between the interannual oceanographic and meteorological variations and the tropical Pacific. He also explained how the Sea Surface Temperature (SST) gradients are crucial for the atmospheric pressure gradients to drive the Walker (zonal) circulation. This circulation makes de dry air to sink over the cold water of the eastern tropical Pacific, flowing westward along the equator as part of the trade winds. This air is warmed and moistened as it moves over the progressively warmer water until it reaches de western tropical Pacific, rising in towering rain clouds. The return flow in the upper atmosphere closes the Walker circulation. On the other hand, interannual SST variations in the tropical Pacific cause the Southern Oscillation (SO, Philander, 1990). Nevertheless, from the oceanographic point of view, SST changes associated with an anomalous thermocline slope are caused by surface wind fluctuations associated with the SO. These circular argumentations led to a new conceptual framework which considered the climate system as a coupled ocean-atmosphere system. From this new perspective, and especially after the big 1982 El Niño event, which affected dramatically North America, a lot of effort has been made to understand the ENSO[1] phenomenon. Important international research programs have being launched, like TOGA[2] (1985) with the aim to develop new prediction models for SO conditions.

Regarding the Tropical Atlantic (TA) Ocean, it also exhibits variability at many different time scales, with complex air-sea interactions. These are responsible for the climate variability of many surrounding areas where large populations are settled (see figure I). Unfortunately, TA has been considered up until now, less important for the scientific community compared with the Pacific Ocean. While ENSO and Tropical Pacific has been understood with considerable depth during the 80's and continues to be understood every day, the Atlantic Ocean has been relegated to play the "younger brother" role of the Pacific Ocean, which is known to have a strong influence on it. Although El Niño counterpart of the Pacific has been described for the Atlantic (Zebiak, 1993), the components of the Bjerknes mechanism and the intrinsic variability have been carelessly studied. Predictability also seems to be significantly lower for the Atlantic than for the Pacific (Keenlyside and Latif, 2007). However, in the last 30 years, exhaustive research has found a strong relationship between some extreme climatic events that have taken place in the Atlantic basin, such as droughts over NE Brazil and NW Africa, and TA SST anomaly patterns. Nowadays, Tropical Atlantic Variability (TAV), which includes the interaction between surface winds, Sea Level Pressure (SLP), the Inter-Tropical Convergence Zone (ITCZ) shifts, SST and the upper ocean, is still not well understood and is a current topic of the International CLIVAR[3] program (Hurrell et al., 2006).

Since SST is the variable that links the upper ocean and the overlying atmosphere, it plays a fundamental role in TAV. Interactions between SST and atmospheric convection associated with the ITCZ are important drivers of climate variability, especially near the convective threshold (28ºC). From seasonal to interdecadal timescales, TA SST anomalies can modulate

[1] El Niño and the Southern Oscillation; both variability modes are treated as a coupled ocean-atmosphere variability phenomenon.
[2] Tropical Ocean Global Atmosphere
[3] Climate Variability and Predictability. It provides a nurturing framework from a range of backgrounds to describe, understand and predict aspects of climate variability.

the meridional energy gradients and, consequently, the ITCZ shifts and the intensity of the West African Monsoon (WAM), among other processes. The understanding of the variability of the mixed layer is a key to correctly explain and model the SST. Nevertheless, there are still questions about how much of its dynamics could be explained by the subsurface processes in comparison with the thermodynamical response of the mixed layer to the overlying atmosphere, especially in front/upwelling areas.

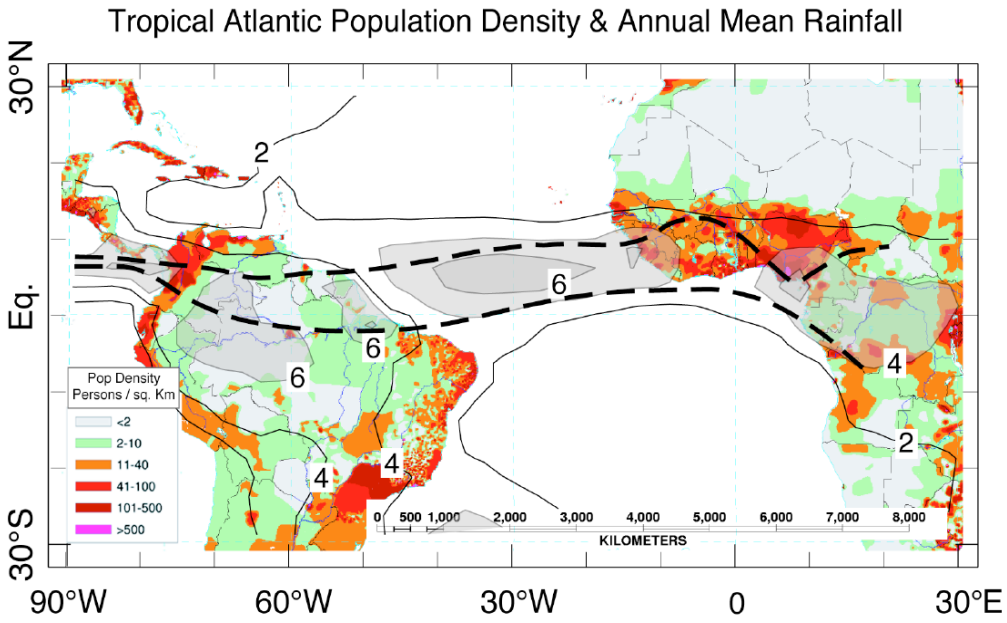

Figure I. Map of population density in persons/km^2 (colors, see inserted legend), overlaid by contour of annual rainfall (in mm/day) with values > 4 mm/day shaded in transparent gray to indicate the mean position of the ITCZ. The north (July-August) and south (March-April) limits of the ITCZ climatological annual migration are indicated by thick dashed lines. Figure from Kushnir et al. (2003).

The study of the TA SST patterns and the associated atmospheric behaviour is the most straightforward way of understanding the TAV and associated air-sea interactions. Though many studies in the last decade explore the mechanisms of SST variability, the fewer are the ones describing the mechanisms of subsurface variability (Tourre and White, 1995; Cibot et al., 2005; Yeshanew and Jury, 2007). The reason for such gap is the very sparse and inaccurate data available of the subsurface ocean, especially in the TA. Also, along the equator, the currents are ageostrophic, which makes difficult to use estimations using density gradients, being direct *in situ* measurements the only reliable data. Only since 1979 it has been possible to measure long time series equatorial currents with moored floats (Philander, 1990). Part of this data gap has been filled by international observational programs such as PIRATA[4] (Servain et al., 1998), SEQUAL/FOCAL[5], and currently the impressive ARGO-CORIOLIS[6] program. Furthermore, OGCM[7] with global ocean assimilation analysis efforts (i.e. GFDL MOM2[8], SODA[9], MERCATOR[10]), optimal interpolation of the collected available data (i.e. TAOSTA[11] dataset), as well as administrative support from CLIVAR international have also helped to fill this gap. On the other hand, and maybe in relation with the lack of oceanic data, many model-based studies have considered the ocean as an almost passive actor in the climate variability

[4] Pilot Research Moored Array in the Tropical Atlantic.
[5] Joint US/French Seasonal Response of the Equatorial Atlantic (SEQUAL) and Programme Francaise Océan-Climat en Atlantique Equatorial (FOCAL) programs of 1983–1985 were comprehensive observational efforts to date in the tropical Atlantic.
[6] ARGO is part of the integrated global observation strategy to monitor and forecast the ocean behaviour. CORIOLIS is one of the two Argo Global Data Assembly Centres.
[7] Oceanic General Circulation Models
[8] Geophysical Fuid Dynamics Laboratory (GFDL) Modular Ocean Model (MOM2)
[9] Simple Ocean Data Assimilation (SODA) is a reanalysis of the global upper ocean climate.
[10] Mercator is a French operational system that assimilates by the analysis and forecasting model input from ocean observations measured by satellites and *in situ* observations.
[11] Tropical Atlantic Ocean Subsurface Temperatura Atlas.

(Hasselmann, 1976; Barsugli and Battisti, 1998; Seager et al., 2001; Chang et al., 2006). In some studies, Atlantic Variability appears to be explained by the internal atmospheric variability (Cayan, 1992; Robertson et al., 2000), where the ocean appears as a passive agent with respect the atmosphere. Along with this, most of the oceanic models use a coarse resolution that poorly resolves dynamical processes near the equator and coastal regions (Seager et al. 2001), where theoretically, the ocean plays a more important role. In addition, the presence of coherent low-frequency signals in both, the atmospheric and the oceanic data, is a key point that supports the ocean as a forcing.

In any case, the coupled models are in development with part of the scientific community proposing relevant questions about the active role of the upper ocean. Oceans appear to be very important on very large timescales and in relation with the abrupt climate change (Johnson and Marshall, 2002), but it could also be important on timescales ranging from intraseasonal to interannual (Jayne and Marotzke, 2001; Chang et al., 2006 among others). In addition, important leads and lags between the SST, surface fluxes, and ocean heat transport can sustain oscillatory behaviour (Seager et al., 2001).
The coupling between atmosphere and ocean generates a new breed of modes whose characteristics depend on the time scale of the dynamical adjustment of the ocean relative to the time scale of SST change due to the air-sea coupling (Chang et al., 2006). In spite of the lack of upper ocean data, in the second half of the twentieth century, theoretical efforts have been made in relation with the time response of the ocean to the atmosphere variations in order to answer to questions: how does the ocean adjustment to the atmospheric variability occur? And: what “memory” do these adjustments provide to the coupled system?

Oceanic waves have an essential role in the ocean adjustment and therefore, in the climate variability. Most of the heat content in the tropical ocean is located in the upper layer and, as a result, low latitude oceans are often approximated as a two-layer system. This attribute approximation implies that variations in the depth of the thermocline, and hence of the heat content, are directly reflected in Sea Surface Height (hereafter SSH, Rebert et al., 1985; Stammer, 1997). Since Matsuno (1966) established the equations of the shallow water equatorial waves, the oceanic waves were a very intensively studied topic during the 70’s and 80’s (Moore, 1968; O’Brien et al., 1978; Clarke, 1983, among others). Theoretical works inspire the idea of the waves as a manner to communicate climate anomalies from one boundary to another in enough time to be predictable. Moreover, the oceanic adjustment by waves is an important key for the El Niño cycle (Suarez and Schopf, 1988; Philander 1990; Gill, 1982). A new stage started when TOPEX/Poseidon (T/P) was launched in 1992 and since then, ocean dynamics and oceanic wave propagations have been better described in the equatorial Pacific and Atlantic (Chelton and Schlax, 1996; Katz, 1997; Roundy and Kiladis, 2006; among others.).
The oceanic wave’s propagation interacting with SST fronts and coastal upwelling systems could be a way of producing SST anomalies which could affect the season of the fisheries (Picaut, 1983; Schouten et al., 2005, Florenchie et al., 2003; Rouault et al., 2007). In addition, the Gulf of Guinea is a main topic in the WAM study because it is a principal source of water vapor which can, in turn, constitute most of the precipitation on the continent (Fontaine et al., 1999). That region has a large SST seasonal amplitude and a well-described seasonal upwelling (Picaut, 1983), and it is very active in the described TAV modes (Carton et al., 1996; Chang et al., 1997; Sutton et al., 2000a; Frankignoul and Kesterane, 2005; Keenlyside and Latif., 2007). However, the complex interactions that concern the TAV, oceanic waves and rainfall variability are not well understood. Faced with the importance of the ocean adjustment, the TAV in relation to those waves deserves further investigation.

At the same time, TAV modes have been related with the extratropical climate anomalies. On the one hand, the controversial and singular Atlantic Meridional mode (Chang et al., 1997; Dommenget and Latif, 2000) and, in particular the northern SST branch of the mode, has been related to the North Atlantic Oscillation (NAO; Hurrell, 1995) via the Azores High (Okumura et al., 2001). The oceanic patterns could have a feedback to the atmosphere (Peng et al., 1995) and could be useful for predicting seasonal winter extratropical precipitation (Rodriguez-Fonseca and Castro, 2002). Furthermore, the fact that the Meridional mode centers coincide with the permanent West African (WA) coastal upwelling systems, makes the TAV topic more complex. On the other hand, the Atlantic Niño or equatorial mode (Zebiak, 1993; Carton et al.,

1996) has been related to the ENSO (Latif and Grötzner, 2000; Wang, 2006), and to the extratropical Southern Atlantic (Trazska et al., 2007).

Seasonal to interannual TAV has received significant attention in recent programs after TOGA decade such as; CLIVAR, which is the World Climate Research Programme (WCRP) project that addresses Climate Variability and Predictability with a particular focus on the role of ocean-atmosphere interactions in climate, the AMMA[12]-EU project which investigates the West African Monsoon, the Spanish-project CGL2006-04471 which is focused on the TAV and ANETUS[13] program which is focused on the eastern Atlantic upwelling system. A lot of work remains to be done regarding details of the involved mechanisms, and also regarding activity at smaller time-scales, in particular, and in the recent satellite observational period (1979-2003).

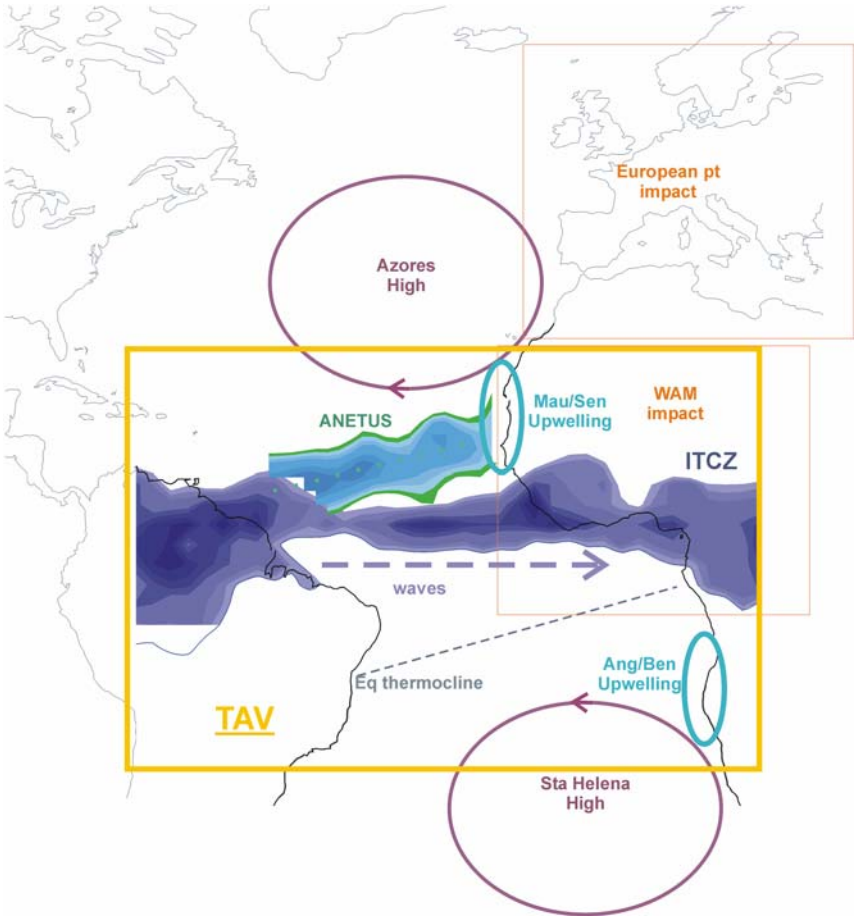

Figure II. Scheme of the TAV, its main components (ITCZ, subtropical High pressure systems, coastal upwelling systems, ANETUS, upper ocean, oceanic waves…) and the areas of impact considered in this work (Europe and West Africa).

Besides the more accurate observational data collected during this recent period (1979-2003), some singularities and tendency features have been observed; slow global warming, with large fluctuations, over the twenty century up to 1975, followed by rapid warming at a rate ~0.2ºC per decade (Hansen et al., 2006). Since the 1970's, drier than normal conditions over the Sahel region and the Amazon River basin have been observed (Janicot et al., 1996). Such a long-term downward trend in Sahelian summer rainfall is a unique feature in recent tropical fluctuations and has been associated with SST trends in the Atlantic and Indian Oceans (Folland et al., 1986; Shinoda and Kawamura, 1994; Bader and Latif, 2003; Giannini et al., 2003). A different equatorial Pacific-Atlantic relationship has also been reported (Keenlyside and Latif, 2007), as well as a clear cooling trend over the eastern equatorial Pacific due to natural variations (Cane et al., 1997) despite the strong and frequent El Niño events in the period after the 1977 climate

[12] African Monsoon Multidisciplinary Analysis
[13] Atlantic NorthEastern Tropical Upwelling System (Lazar, 2005)

transition (Miller et al., 1994; Fedorov and Philander, 2000). These unusual ENSO events have also been associated with the century-long warming trend (Trenberth and Hoar, 1996), in agreement with other authors that have explained a weakening of Pacific Walker circulation (Vecchi et al., 2006) and an expansion of the tropical belt width (Seidel et al., 2008) to be due to the global warming by anthropogenic forcing. In addition, recent Northern Hemisphere warming can be accounted for the phase-shifting events of the Pacific Decadal Oscillation (PDO) and NAO from 1970s (Palmer, 1998).

The present PhD thesis investigates the air-sea interaction in the Tropical Atlantic with observational and model data collected from 1979 to the present using statistical and mechanical diagnostics. Figure II illustrates the components of the system that is studied along the PhD Thesis. This PhD deals with different aspects of the TAV and therefore has been structured in four different blocks. In the first Chapter, the background knowledge about the TAV is presented along with the detailed main goals of the work (Chapter 2). Chapter 3 describes the methodology and data. Chapter 4 contains peer reviewed articles which describe the main results corresponding to different aspects of the TAV, in relation to the impacts on the precipitation over extra-tropical and tropical areas. Regarding extra-tropical areas, the SNA variability is investigated by considering its impacts on European rainfall and assessing the Mauritanian/Senegal upwelling variability in relation to the SST variability. Regarding tropical areas, the Equatorial mode in relation to WA rainfall variability and the air-sea interactions within the mode are shown. The last results are the product of the analysis of the oceanic Kelvin waves at intraseasonal timescales and some of their forcing. The final Chapters contain an integrated discussion together with a summary of the main conclusions. Finally, ideas for future research are proposed.

MOTIVACIÓN

Los océanos tropicales constituyen una fuente capital de calor que contribuye, en gran parte, a la circulación atmosférica y oceánica global. En esencia, la memoria a corto plazo del clima de la Tierra reside en el océano tropical. Por otro lado, las interacciones aire-océano que tienen lugar en los trópicos afectan al clima global en un amplio rango de escalas temporales. El estudio de la Variabilidad Tropical es una tarea muy compleja al involucrar a diferentes interacciones aire-mar-tierra y, además, es un importante desafío para la comunidad científica ya que afecta a una extensa población rural que depende de la agricultura pluvial (Chang et al., 2006; Kushnir et al., 2003; Xie y Carton, 2004 para una revisión).
Históricamente, los estudios climáticos experimentaron un dramático cambio cuando Bjerknes (1969) propuso una relación física entre las variaciones interanuales oceanográficas y las meteorológicas en el Pacífico tropical. En este trabajo explicó cómo el gradiente de temperatura de la superficie del mar (SST[1]) es necesario a la hora de generar gradientes de presión atmosférica que conduzcan la circulación zonal de Walker. De esta forma, el aire seco subside en las regiones de agua fría del Pacífico tropical oriental y fluye hacia el oeste a lo largo del ecuador, como parte de los vientos alisios. El aire se calienta y se humedece mientras, progresivamente, aparta el agua más caliente hasta que llega al Pacífico tropical occidental, donde se alza en altísimas nubes convectivas. El flujo de retorno en la atmósfera superior cierra esta circulación de Walker. De este modo, las variaciones interanuales de la SST en el Pacífico tropical causan la Oscilación del Sur (SO[2], Philander, 1990). Sin embargo, desde el punto de vista oceanográfico, los cambios de SST asociados con una pendiente anómala de la termoclina son causados por fluctuaciones del viento superficial, asociadas con la SO. A partir de estos argumentos circulares, un nuevo marco conceptual fomentó la idea del sistema climático como un sistema acoplado océano-atmósfera. Desde este nuevo paradigma y después del gran suceso de El Niño en 1982, que influyó dramáticamente en Norteamérica, se han realizado muchos esfuerzos para comprender el fenómeno ENSO[3], incluyendo programas internacionales de investigación (i.e. TOGA[4] se lanzó en 1985, con el objetivo de desarrollar modelos para predecir condiciones de la SO).

En particular, el clima del océano Atlántico Tropical (TA[5]) exhibe variabilidad en muchas escalas temporales. Se trata de una región en la que acontecen complejas interacciones aire-mar que, a su vez son responsables de la variabilidad climática en diferentes áreas circundantes de alta densidad demográfica (ver figura I). Desafortunadamente, el estudio de la variabilidad sobre TA ha sido hasta hoy considerado por la comunidad científica menos importante que el del Océano Pacífico. Mientras que el fenómeno ENSO y la variabilidad del Pacífico Tropical han sido comprendidos y continúan comprendiéndose desde los años 80; el Océano Atlántico ha sido relegado a jugar el papel del 'hermano pequeño' del Océano Pacífico, que lo influye poderosamente. A pesar de que un homólogo de El Niño del Pacífico ha sido descrito para el Atlántico, los componentes del mecanismo de Bjerknes y la variabilidad intrínseca asociados han sido estudiados someramente. Además, la predecibilidad también se muestra significativamente menor para el Atlántico que para el Pacífico (Keenlyside y Latif, 2007). Sin embargo, en los últimos 30 años, estudios exhaustivos han encontrado una fuerte relación entre algunos sucesos climáticos extremos que han tenido lugar en la cuenca Atlántica, como las sequías en el NE de Brasil y NO de África, y los patrones anómalos de la SST del TA. Hoy en día, la Variabilidad del Atlántico Tropical (TAV[6]), que incluye la interacción

[1] Del inglés Sea Surface Temperature
[2] Del inglés Southern Oscillation
[3] *El Niño and the Southern Oscillation*; ambos modos de variabilidad son tratados como un fenómeno de variabilidad océano-atmósfera.
[4] Estudio de la *Tropical Ocean Global Atmosphere,* que incluye datos a tiempo real de boyas marítimas amarradas para perfeccionar la detección, comprensión y predicción de El Niño y La Niña.
[5] Del inglés Tropical Atlantic
[6] Del inglés Tropical Atlantic Variability

entre los vientos superficiales, la presión al nivel del mar (SLP[7]), los cambios en la Zona de Convergencia InterTropical (ITCZ[8]), la SST y el océano superior; todavía no está bien comprendida y es un tema puntero dentro del programa Internacional CLIVAR[9] (Hurrell et al., 2006).

Dado que la SST es la variable que conecta el océano superior y la atmósfera que lo recubre, juega un papel fundamental en el entendimiento de la TAV. Las interacciones entre la SST y la convección atmosférica asociada con la ITCZ, son importantes conductores de variabilidad climática, especialmente cerca del umbral convectivo (28ºC). Desde períodos de tiempo estacionales a períodos interdecadales, las anomalías de la SST del TA pueden modular los gradientes de energía meridional y, en consecuencia, los cambios en la ITCZ y en la intensidad del Monzón del Oeste Africano (WAM[10]), entre otros procesos. La comprensión de la variabilidad de la capa de mezcla es clave para a la hora de explicar correctamente los cambios en la SST, así como para su posterior modelado. Sin embargo, quedan todavía dudas sobre en qué medida su dinámica podría ser explicada por los procesos de sub-superficie, en comparación con la respuesta termodinámica de la capa de mezcla a la atmósfera que la recubre, especialmente en áreas de frentes/afloramientos.

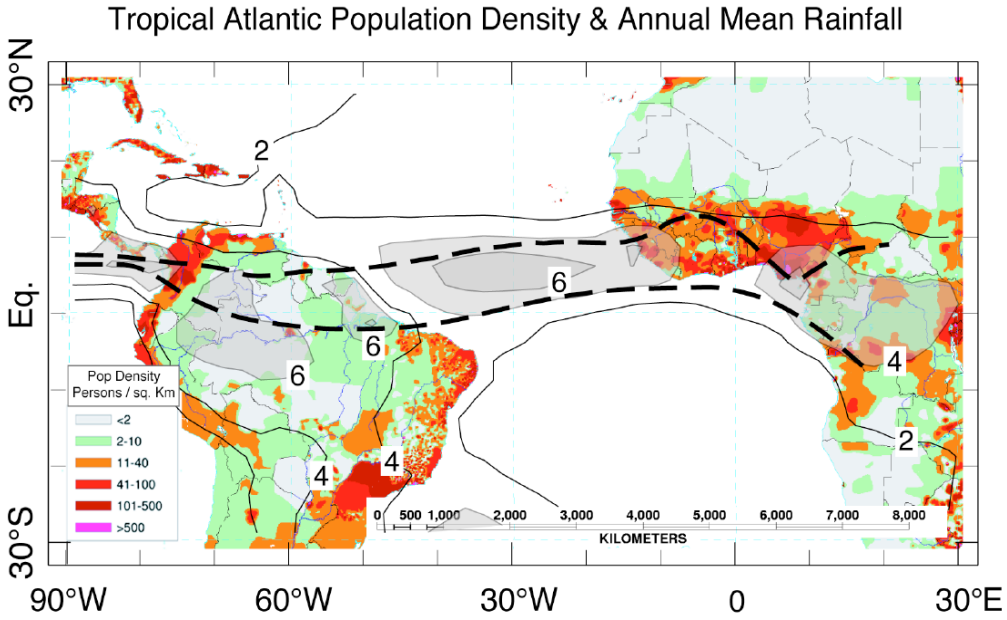

Figura I. Mapa de densidad de población en personas/km^2 (colores, ver la leyenda insertada), junto al contorno de la lluvia anual (en mm/día). Los valores > 4 mm/día aparecen sombreados en gris traslúcido para indicar la posición significativa de la ITCZ. Los límites norte (Julio-Agosto) y sur (Marzo-Abril) de la migración climatológica anual de la ITCZ se indican con líneas de puntos gruesas. Figura de Kushnir et al. (2003).

El estudio de las estructuras predominantes de variabilidad de SST en el TA y el comportamiento atmosférico asociado, es la manera más sencilla de comprender la TAV. A pesar de que, desde la pasada década, muchos estudios han explorado la variabilidad de la SST, son relativamente menos los que describen los mecanismos de la variabilidad de la sub-superficie (Tourre y White, 1995; Cibot et al., 2005; Yeshanew y Jury, 2007). La razón de esta diferencia en las investigaciones climáticas estriba, en lo escasos e inexactos que son los datos de la subsuperficie oceánica, especialmente en el TA. Además, a lo largo del ecuador las corrientes son ageostróficas, lo que hace difícil las estimaciones a partir de los gradientes de densidad; siendo los únicos datos fiables aquellos provenientes de medidas directas *in situ.* Sólo desde 1979 ha sido posible obtener series temporales de corrientes ecuatoriales

[7] Del inglés Sea Level Pressure
[8] Del inglés Inter-Tropical Convergente Zone
[9] *Climate Variability and Predictability* provee de un marco de desarrollo desde amplios antecedentes para describir, comprender y predecir aspectos de la variabilidad climática. http://www.clivar.org/
[10] Del inglés West African Monsoon

(Philander, 1990). Parte de esta falta de datos ha sido completada por programas internacionales observacionales como PIRATA[11] (Servain et al., 1998), SEQUAL/FOCAL[12] y, actualmente, por el impresionante programa ARGO-CORIOLIS[13]. Los OGCM[14], con intentos de análisis de asimilación oceánica global (i.e., GFDL MOM2[15], SODA[16], MERCATOR[17]), interpolación óptima de los datos disponibles recogidos (i.e. conjunto de datos de TAOSTA[18]), además del apoyo administrativo de CLIVAR internacional, también ayudaron a llenar este vacío.
Por otro lado, y puede que relacionado con la falta de datos oceánicos, muchos estudios basados en modelos han considerado al océano como un actor casi pasivo en la variabilidad climática (Hasselmann, 1976; Barsugli y Battisti, 1998; Seager et al., 2001; Chang et al., 2006). En algunos estudios, la Variabilidad del Atlántico aparece asociada con la variabilidad interna de la atmósfera (Cayan, 1992; Robertson et al., 2000), mientras que el océano aparece inactivo respecto a la atmósfera. No obstante, la mayoría de los modelos oceánicos utilizan una resolución baja que, a duras penas, resuelve los procesos dinámicos cerca del ecuador y las regiones costeras (Seager et al. 2001), donde teóricamente el océano juega un papel más importante. Además, la presencia de señales de baja frecuencia, coherentes en los datos atmosféricos y oceánicos, hace pensar que el océano pueda tener un papel activo forzando a la atmósfera.
En todo caso, los modelos acoplados están desarrollándose y parte de la comunidad científica está proponiendo la investigación de algunas cuestiones sobre el papel activo del océano superior. El océano parece ser muy importante en períodos de tiempo muy largos y en relación con el cambio climático abrupto (Johnson y Marshall, 2002), pero podría ser también importante en rango de períodos de tiempo de intraestacionales a interanuales (Jayne y Marotzke, 2001; Chang et al., 2006 entre otros). Además, se han encontrado importantes desfases en las relaciones entre la SST, los flujos de superficie, y el transporte de calor oceánico, que pueden apuntar a un comportamiento oscilatorio (Seager et al., 2001).
El acoplamiento entre atmósfera y océano produce una nueva generación de modos cuyas características dependen de la escala de tiempo del ajuste dinámico del océano, en relación a la escala de tiempo del cambio de la SST debido al acople aire-mar (Chang et al., 2006). A pesar de la falta de datos del océano superior, en la segunda mitad del siglo XX se han hecho esfuerzos teóricos en relación con el tiempo de respuesta del océano a las variaciones atmosféricas para responder a: ¿cómo se ajusta el océano a las variaciones atmosféricas?, y ¿Qué "memoria" proporciona este ajuste al sistema acoplado?

Las ondas oceánicas tienen un papel importante en el ajuste oceánico y, por tanto, en la variabilidad climática. La mayor parte del contenido de calor en el océano tropical está localizado en la capa superior y, como resultado, el océano de bajas latitudes es a menudo aproximado a un sistema de dos capas. Esta aproximación implica que las variaciones en la profundidad de la termoclina y, por tanto, en el contenido de calor, son directamente reflejadas en la altura de la superficie del mar (de aquí en adelante SSH[19], Rebert et al., 1985; Stammer, 1997). Desde que Matsuno (1966) estableció las ecuaciones de las ondas ecuatoriales para aguas someras, las ondas oceánicas fueron un tema estudiado muy intensamente, sobre todo en los años 70 y 80 (Moore, 1968; O'Brien et al., 1978; Clarke, 1983, entre otros). Los trabajos teóricos inspiraron la idea de las ondas como una manera de comunicar anomalías climáticas de un lado a otro, con el tiempo suficiente como para ser predecibles. Más aún, el ajuste oceánico por ondas es una clave importante para el ciclo de El Niño (Suarez y Schopf, 1988; Philander 1990; Gill, 1982). Un nuevo escenario comenzó cuando fue lanzado el TOPEX/Poseidon (T/P) en 1992 y, desde entonces, la descripción de la dinámica oceánica y la

[11] Del inglés Pilot Reseasrch Moored Array in the Tropical Atlantic
[12] El programa conjunto EEUU/Francia Seasonal Response of the Equatorial Atlantic (SEQUAL) y el programa francés Francaise Océan-Climat en Atlantique Equatorial (FOCAL) tuvieron lugar entre 1983 y 1985 para la comprensión observacional del Atlántico Tropical.
[13] ARGO es parte de una estrategia de observación global para monitorizar y predecir el comportamiento del océano. CORIOLIS es uno de los dos centros de datos globales de Argo.
[14] Del inglés *Oceanic General Circulation Models*
[15] Del inglés Geophysical Fuid Dynamics Laboratory (GFDL) y Modular Ocean Model (MOM2)
[16] Del inglés Simple Ocean Data Assimilation (SODA) es un reanálisis del océano superior global.
[17] Mercator es un sistema francés operacional que asimila con un modelo las observaciones *in situ* y de satélites.
[18] Del inglés Tropical Atlantic Ocean Subsurface Temperatura Atlas.
[19] Del inglés Sea Surface Height

propagación de ondas oceánicas ha mejorado tanto en el Pacífico como en el Atlántico (Chelton y Schlax, 1996; Katz, 1997; Roundy y Kiladis, 2006; entre otros).
La propagación de ondas oceánicas y su interacción con los sistemas de afloramiento costeros es un mecanismo candidato de producir anomalías de SST que, a su vez, podrían influir en las temporadas de pesca (Picaut, 1983; Schouten et al., 2005, Florenchie et al., 2003; Rouault et al., 2007). Además, la variabilidad del Golfo de Guinea es un tema crucial en el estudio del WAM, ya que es una región que proporciona una fuente de vapor principal que puede, a su vez, constituir la mayor parte de la precipitación del continente (Fontaine et al., 1999). La amplitud estacional de la SST en esta región es amplia, habiéndose descrito un afloramiento estacional (Picaut, 1983) y siendo una zona muy activa sobre los modos de TAV conocidos (Carton et al., 1996; Chang et al., 1997; Sutton et al., 2000a; Frankignoul y Kesterane, 2005; Keenlsyde y Latif., 2007). No obstante, las complejas interacciones que conciernen a la TAV, las ondas oceánicas y la variabilidad de la lluvia; no están todavía bien comprendidas. Ante la importancia del ajuste oceánico, la TAV en relación con esas ondas merece mayor investigación.

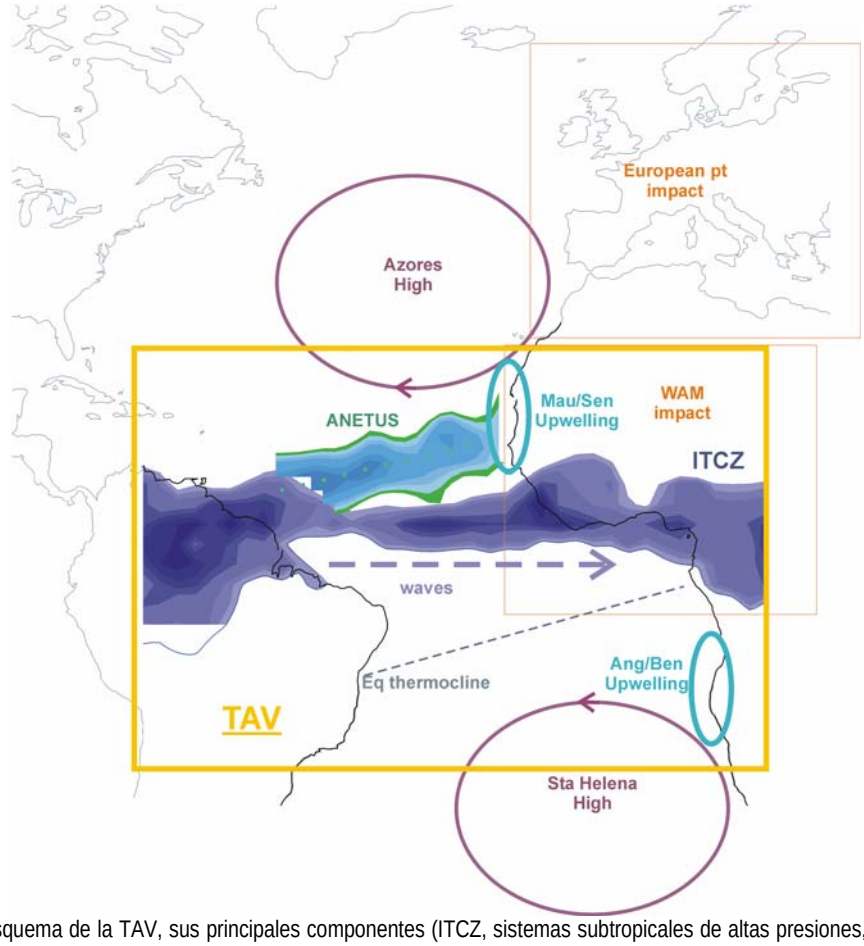

Figure II. Esquema de la TAV, sus principales componentes (ITCZ, sistemas subtropicales de altas presiones, sistemas de afloramientos costeros, ANETUS, océano superior, ondas oceánicas…) y las áreas de impacto consideradas en este trabajo (Europa y África del Oeste).

Al mismo tiempo, los modos de la TAV se han relacionado con anomalías climáticas extratropicales. Por un lado, el controvertido y singular modo Atlántico Meridional (Chang et al., 1997; Dommenget y Latif, 2000) y, en particular, la rama norte de este modo de SST, se ha relacionado con la Oscilación del Atlántico Norte (NAO[20]; Hurrell, 1995) a través del sistema de altas presiones de las Azores (Okumura et al., 2001). Los patrones oceánicos podrían tener una respuesta hacia la atmósfera (Peng et al., 1995) y podrían ser útiles para predecir precipitación estacional invernal extratropical (Rodríguez-Fonseca y Castro, 2002). Más aún, el hecho de que los centros del modo meridional coincidan con los sistemas de afloramientos

[20] Del inglés North Atlantic Oscillation

costeros permanentes de África del Oeste, convierte a la TAV en un tema más complejo. Por otro lado, el Niño Atlántico o Modo Ecuatorial (Zebiak, 1993; Carton et al., 1996) ha sido relacionado con el ENSO (Groztner y Latif, 2000; Wang, 2006), y con el Atlántico Sur extratropical (Trazska et al., 2007).

El estudio de la TAV, en el rango que abarca de escalas estacionales a interanuales, ha recibido una atención significativa en programas recientes, tras la década de TOGA. A destacar, el programa CLIVAR, como parte del Programa de Investigación Climático Mundial (WCRP[21]), focalizado en la Variabilidad y Predecibilidad Climática con atención especial en el papel de las interacciones océano-atmósfera en el clima; el proyecto AMMA[22]-EU, que investiga el Monzón de África del Oeste; el proyecto nacional del Ministerio de Educación y Ciencia CGL2006-04471 que está centrado en la TAV y el programa ANETUS[23] que estudia los sistema de afloramiento del noreste de la cuenca atlántica. Todavía queda mucho por hacer respecto al entendimiento de los mecanismos implicados, y la actividad a escalas temporales más pequeñas y, en particular, durante el reciente período de observaciones satelitales (1979-2003).
El periodo de tiempo 1979-2003, además de caracterizarse por datos observacionales más exactos, contiene algunas singularidades y rasgos de tendencias reseñables dentro del marco del calentamiento global. A lo largo del siglo XX aparecen grandes fluctuaciones hasta 1975, donde acontece un calentamiento rápido a un ritmo de ~0.2ºC por década (Hansen et al., 2006). Desde los años 70, se han observado condiciones más secas de lo normal sobre la región del Sahel y la cuenca del río Amazonas (Janicot et al., 1996). Una tendencia tan a la baja en la lluvia estival Saheliana es un rasgo único en las fluctuaciones tropicales recientes y ha sido asociada con tendencias de la SST en los océanos Atlántico e Índico (Folland et al., 1986; Shinoda y Kawamura, 1994; Bader y Latif, 2003; Giannini et al., 2003). Además, se ha mostrado una relación diferente Atlántico-Pacífico ecuatorial (Keenlyside y Latif, 2007). Por otro lado, a pesar del aumento de sucesos extremos de El Niño en el período posterior a la transición climática de 1977 (Miller et al., 1994; Fedorov y Philander, 2000), ha tenido lugar una tendencia clara al enfriamiento en el Pacífico ecuatorial oriental, debida a variaciones naturales (Cane et al., 1997). Estos inusuales sucesos del ENSO también han sido asociados con la tendencia de calentamiento del siglo (Trenberth and Hoar, 1996), de acuerdo con otros autores que han explicado un debilitamiento de la circulación de Walker del Pacífico (Vecchi et al., 2006) y una expansión de la anchura del cinturón tropical (Seidel et al., 2008). Además, el calentamiento reciente del Hemisferio Norte podría dar cuenta de los desplazamientos de fase de la PDO[24] y de la NAO, observados desde los años 70 (Palmer, 1998).

La presente Memoria de Tesis Doctoral compila los resultados relacionados con la investigación llevada a cabo en relación con las Variabilidad del Atlántico Tropical, realizadas con datos observacionales y de modelo recogidos desde 1970 hasta el presente; utilizando diagnósticos estadísticos y mecánicos. La figura II ilustra los componentes del sistema que se estudia a lo largo de la Memoria de Tesis. Esta Memoria se ocupa de diferentes aspectos de la TAV y, por tanto, ha sido estructurada en diferentes bloques. En el primer Capítulo se presentan el Estado del Arte del conocimiento del la TAV, junto con los principales objetivos del trabajo (Capítulo 2). El Capítulo 3 describe los datos y la metodología. El Capítulo 4 contiene los artículos científicos (evaluados externamente y publicados en revistas del Science Citation Index) que describen los principales resultados correspondientes a diferentes aspectos de la TAV, en relación con los impactos en la precipitación sobre áreas tropicales y extra-tropicales. Respecto a las áreas extra-tropicales, la variabilidad del Atlántico Norte Subtropical se investiga considerando sus impactos en la lluvia de Europa y Norte de Africa y evaluando la variabilidad de afloramientos de Mauritania/Senegal en relación con la variabilidad de la SST. Respecto a las áreas tropicales, se muestra el Modo Ecuatorial en relación con la variación de lluvia en el Oeste de África y las interacciones aire-mar dentro del modo. Los últimos resultados son el producto del análisis de las ondas oceánicas a escalas de tiempo intraestacionales y su papel en la TAV. Los Capítulos finales contienen las conclusiones en la que se discuten y resumen los principales resultados, proponiéndose ideas para futura investigación.

[21] Del inglés World Climate Research Programme
[22] Del inglés African Monsoon Multidisciplinary Analysis
[23] Del inglés Atlantic NorthEastern Tropical Upwelling System (Lazar et al., 2005)
[24] Del inglés Pacific Decadal Oscillation

1. STATE OF THE ART

The present Chapter summarizes the most relevant conclusions regarding Tropical Atlantic Variability (TAV) up to date. Section 1.1 is an introduction to the main features that characterizes the climate in the tropics, following by section 1.2 in which a brief description of TAV and the components at play is outlined. Section 1.3 is focused on the seasonal cycle of the Tropical Atlantic atmosphere and ocean. Section 1.4 contains a deeper description of the principal interannual TAV modes, together with the known feedback mechanisms. Some aspects of the intraseasonal variability, concerning oscillation in the convection and oceanic waves are presented in section 1.5. The teleconnections linked to TAV, the associated forcing as well as the related impacts are described in section 1.6. Section 1.7 assesses some insights into predictability issues. Finally, section 1.7 introduces some aspects regarding the lower frequencies in relation to TAV.

1.1 Tropical Climate variability

Large scale atmospheric motion in the tropics, occurring in periods of weeks and longer corresponds to direct thermal circulations. In these circulations, air converges onto the warmest regions of the earth's surface where it rises and condenses causing these regions to have widespread cloudiness and heavy precipitation. The meridional Hadley circulation (figure 1.1), in which air rises near the equator and sinks in higher latitudes, is the principal responsible of the meridional atmospheric heat transport. The zonal Walker circulation (figure 1.2), in which air rises over the warm western tropical ocean and sinks over the cold eastern tropical ocean. (Philander, 1990; Gill, 1982; Hartmann, 1994), caused by differences in heat distribution between ocean and land, is the most remarkable zonal thermal circulation. Other examples of thermal circulations include the monsoons, that bring heavy rainfall to the continents, when these regions are warmer than the surrounding oceans.

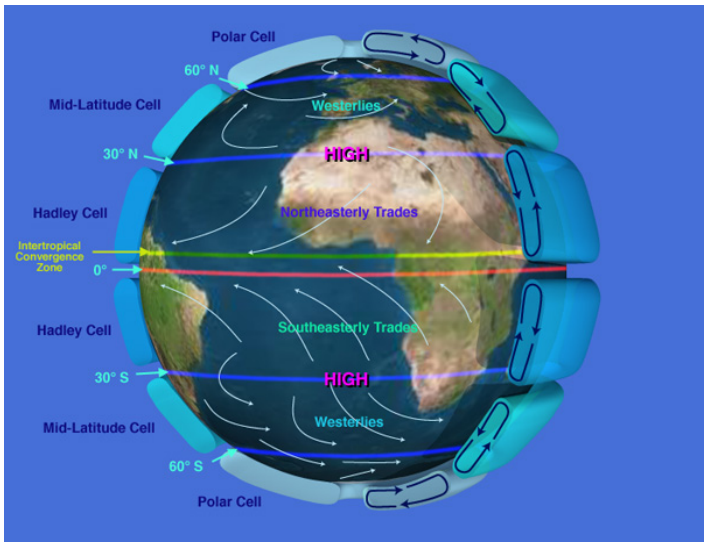

Figure 1.1. Scheme of the Meridional Circulation and winds. From NASA

Symmetrically, in the ocean there is a zonal and a meridional circulation. On the one hand, currents are westward in the surface deep tropics prevailing the upwelling at the eastern and warm water at western. This circulation is closed by an eastward undercurrent at the thermocline depth. On the

other hand, water sinks in the subdudction areas and transport cold water equatorward through the thermocline and rises at the equatorial surface which is again transported at the surface by the poleward Ekman drift.

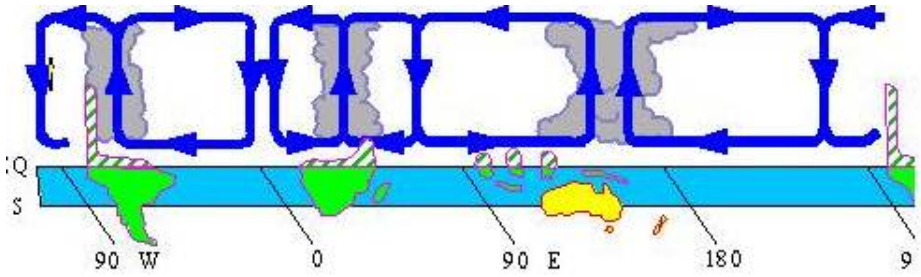

Figure 1.2. Scheme of the Walker Zonal Circulation. From Monash University webpage (Australia)

Although the Pacific is three times wider along the equator than the Atlantic, and can effortlessly influence climate around the globe, the influence of the Atlantic can be substantial, especially if its circulation changes. One part of the international research program CLIVAR (Climate Variability and Predictability) is beginning to shed light on the mechanisms and predictability of Atlantic climate variability. The most remarkable features of the Tropical Atlantic Variability are outlined next.

1.2 Tropical Atlantic Variability

The Atlantic Ocean helps to mediate the imbalance in net radiation between the tropics (where more heat is received by the Sun) and the polar regions (where more heat is radiated into space). It does so through ocean currents which transport warm water from the Tropical Atlantic (TA) to the subpolar Arctic region. The atmosphere is the largest contributor of heat, with warm air rising in the Inter-Tropical Convergence Zone (ITCZ) and moving poleward from there. On a global scale, the

Figure 1.3. Modes of climate variability in the Atlantic sector. The figure shows the path and strength of winter storms depending on the sign of the NAO; the location of tropical rainfall (determined by the ITCZ); and the transport of ocean currents (MOC). Blue arrows: cold, deep currents; red arrows: warm surface currents. From Visbeck, (2002).

North Atlantic is the largest ocean contributor, with a heat transport of 1.3 PW at 30°N; which is 25% of the total northward heat transport and is carried by the warm surface currents—North Brazil Current, Florida Current, Gulf Stream, and North Atlantic Current— from south to north (Wang and Carton, 2002; Visbeck, 2002; see figure 1.3).
The region of study is the Tropical Atlantic and is situated geographically between 30ºN and 30ºS and from 70ºW to the African coast. The Tropical Atlantic Ocean is flanked by two large tropical continents, which host major centres of atmospheric convection. As early as 320 years ago, Halley (1686) recognized the important influence of these continents on climate in the Atlantic sector and suggested that the intense surface heating over North Africa drives the southerly winds in the Gulf of Guinea (GG). It was not until 1970s, however, that the influence of the TA Ocean on continental climate variability began to come to light. The studies that followed showed that interannual variability in rainfall over the semi-arid regions of South America and Africa was associated with well-organized, repeating patterns of Sea Surface Temperature (SST) and trade wind anomalies over the tropical Atlantic. Furthermore, these patterns of ocean and atmospheric anomalies are so arranged that their interaction gives rise to positive feedback acting to amplify each other. Rapid progress has been achieved in the past decade in understanding these air-sea interaction mechanisms and modelling the resulting variability in climate over the tropical Atlantic and beyond (from Xie and Carton, 2004).

Tropical Atlantic Variability (figure 1.4) includes fluctuations in the strength of the trade and cross equatorial winds in the Tropical Atlantic, associated with changes in interhemispheric SST gradient. These have a large impact on precipitation over Northeast Brazil, Sahel, and the Guinea coastal region (Nobre and Shukla, 1996). It is important to consider that the TA is a small basin where the continental shape plays a fundamental role in its variability.

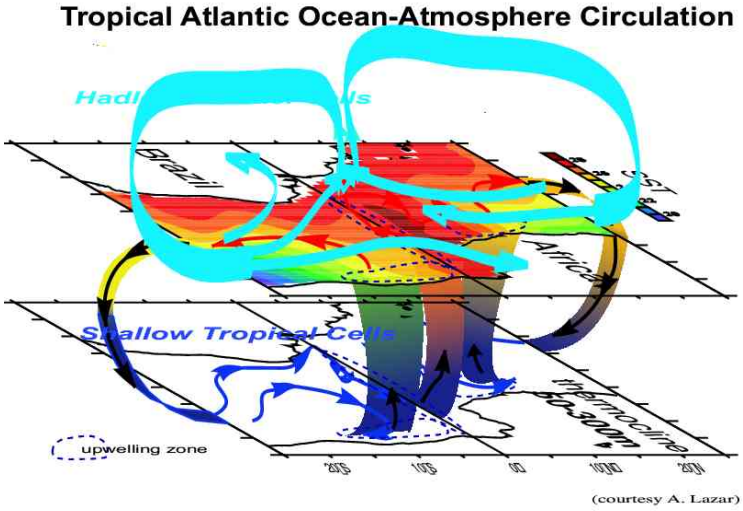

Figure 1.4. Squeme of the TA and its interactions. A schematic 3-dimensional drawing of the Atlantic shallow tropical cells, (STC's in purple arrows) and the overlying atmospheric large-scale circulation (in light blue arrows). The climatological SST field is shown in colors on the interfacing surface where the regions of upwelling are also remarked by blue dashed lines. Courtesy of A. Lazar.

The TA ocean exhibits large seasonal variability, not only in the SSTs (Merle, 1980) but also in the oceanic currents (Arnault and Périgaud, 1992; Brandt and Eden, 2005), the heat balance and upwellings (Foltz and McPhaden, 2005; Vauclair et al., 2004; Rouault et al., 2003). Also, its interannual variability leads to different modes of anomalous SST related, in turn, to the atmospheric variability. TAV has also been linked to other teleconnection patterns as the El Niño and the Southern Oscillation (ENSO, Enfield and Mayer, 1997; Saravanan and Chang, 2000) and to the North Atlantic Oscillation (NAO, Xie and Tanimoto, 1998; Pan, 2005).

In the equatorial Atlantic, changes in the north-to-south temperature distribution cause most of the observed ITCZ variability. This is quite different from the Pacific, where El Niño is associated with changes in the west-to-east surface temperature. Unlike the tropical Pacific, seasonal-to-decadal climate variability in the tropical Atlantic is not dominated by any single mode such as ENSO. Rather, this region is subject to multiple competing influences of comparable importance. Some of these influences originate in regions remote from the tropical Atlantic, while others arise from local processes; some are potentially predictable, whereas others are essentially stochastic. These influences interact in subtle ways to determine the evolution of the atmosphere–ocean system (Sutton et al., 2000a).

With all of these aspects taking in consideration, the *TAV includes the study of the variations of the Tropical Atlantic fields, such as SST, sea level pressure, surface winds, heat fluxes and currents, along with their relationships with one another.*

The study of the seasonal cycle is very important in order to understand intraseasonal to interannual variations. TA displays a very pronounced and dominant annual cycle for both the atmosphere (Philander, 1990) and the ocean (Arnault and Cheney, 1994; Peter et al., 2006). In addition, in the TA the seasons are not so symmetrical throughout the year, mainly because the solar radiation is less variant, and thus the semiannual harmonic becomes important in many fields and processes (i.e. SST and sea surface height, upwelling over the Gulf of Guinea).
The factors that influence the seasonal cycle of the movements of the convective zones, the SST gradients and variations in the heating of the continents also influence from intraseasonal to internannual variability. The seasonal cycle of the TA is described in the next section.

1.3 Tropical Atlantic Seasonal cycle

Seasonal cycle can be defined as the sum of the annual and multiple Fourier harmonics of a particular field, and describes its occurrence and evolution in a period of between one month and one year.

1.3.1 Atmosphere seasonal cycle

The atmospheric seasonal cycle of the tropical Atlantic can be explained on the basis of the location of the Intertropical Convergence Zone and the Hadley and Walker circulations.
The Atlantic Marine ITCZ is the region within the TA Ocean basin, close to the equator, where the mean rainfall associated with average effect of transient convective systems, reaches a maximum. In a broader context, the ITCZ represents a complex of phenomena, including the equatorial low-pressure trough, the trade wind convergence zone, and the regional maximum in SST values.

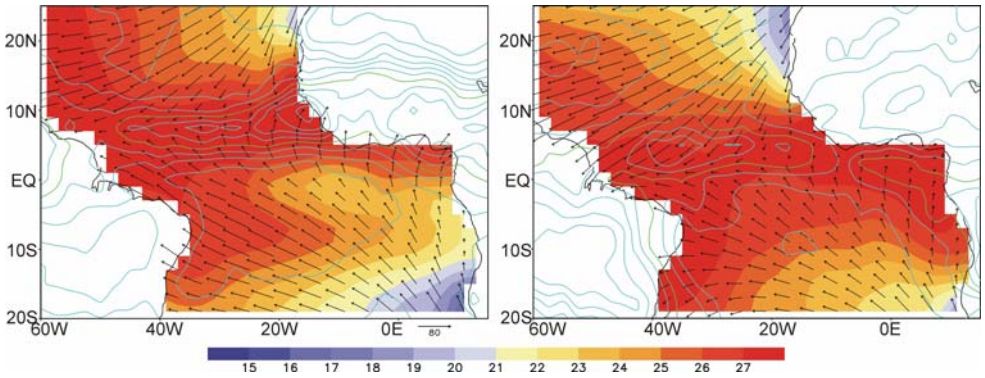

Figure 1.5. Outgoing Long-wave Radiation (contour CI=10 W/m2, the convection threshold 240 has been remarked with a green line) from NOAA and SST (shaded in ºC), wind stress (vectors in dyn/cm^2) from PIRATA in boreal summer season (left) and winter season (right).

The Marine ITCZ complex stretches across the TA basin in a east-west orientation, distorted by the effects of continental masses, and migrates north and south with the season, reaching furthest south in the boreal spring (March-April) and furthest north in the boreal summer (July-August) (Kushnir et al., 2003). Also, the Walker Atlantic circulation is weak in March and April when SST gradients and sea level pressure gradients are also small. The trade winds attain their maximum speeds around 15ºN and 15ºS. Moving from these latitudes towards the equator, the fluctuations in the intensity of the northeasterly (southeasterly) trades are relaxed (enhanced) in September (March) when the ITCZ is farthest north (equator), (see figure 1.5).
The meridional component of the circulations in the tropics, known as Hadley Circulation, has two meridional cells with moist air rising in the ITCZ then diverging poleward in the upper troposphere and descending over regions to the north and south of the ITCZ. The more intense cell has subsiding motion in the winter hemisphere where latitudinal thermal gradients are larger: the northern Hadley cell dominates from November to March and the southern Hadley cell dominates from May to September. In contrast, the centers of the subsidences, which are made up of north and south Subtropical High pressure systems (Azores and Sta Helena), are intensified in each of their own respective summer hemispheres.

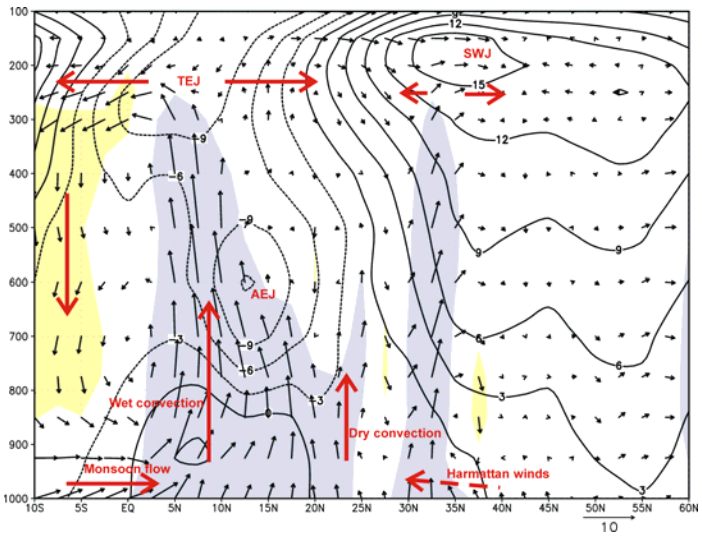

Figure 1.6a. Latitude–pressure cross section of the (10ºW–10ºE) averaged meridional circulation computed on boreal summer season (JJAS) 1979-2001. Vectors display the (*v*, *w*) circulation, colors the amplitude of the vertical velocity (negative upward), and isolines the zonal wind (m/s). From ERA reanalysis, the main WAM circulation features have been remarked in red.

The confluence of the North and South Trade winds, and thus where the ITCZ is located, takes place further north 5ºN on average, while the wind stress curl produces a seasonal upwelling band further poleward the ITCZ in boreal summer when the ITCZ is reaching its northernmost position. In summer, changes in the southern trades and the SST over the eastern equatorial Atlantic (Okumura and Xie, 2004), drive to West African Monsoon (WAM) circulation over the Gulf of Guinea. The monsoon flow crosses the continent as the ITCZ reaches its northernmost position. In addition, Harmattan winds from the Mediterranean Sea basin confluences with the monsoonal flow forming the Inter-Tropical Front (ITF). The figure 1.6 presents the mean meridional circulation, as well as the zonal wind components longitudinally averaged in boreal summer. The main features of the circulation over these regions are Hadley-type circulations from the deep convection at ~10ºN and subsiding velocities south of the equator and 25ºN-40ºN upward velocities limited to the lower troposphere associated with the dry convection in the heat low at 20ºN. The westerly wind of the monsoon layer between the equator and 20ºN and two easterly jets: African Easterly Jet (AEJ) in the midlevels and Tropical Easterly Jet (TEJ) in the upper troposphere and subtropical Westerly Jet in the upper troposphere (Sultan et al., 2003).

Despite the ITCZ annual cycle mentioned above, the ITCZ has a very irregular location along the Atlantic equator, mainly because the continental areas to the east and west of the Atlantic basin coincide with two important River basins: the Congo and the Amazon basin. In these regions, the ITCZ shows a clear semiannual variation which induces the rainfall seasons in the surrounding areas (Philander, 1990; Chiang et al., 2002). The Amazon convergence zone is also important because it interacts with both Pacific and Atlantic Walker circulation (figure 1.2).

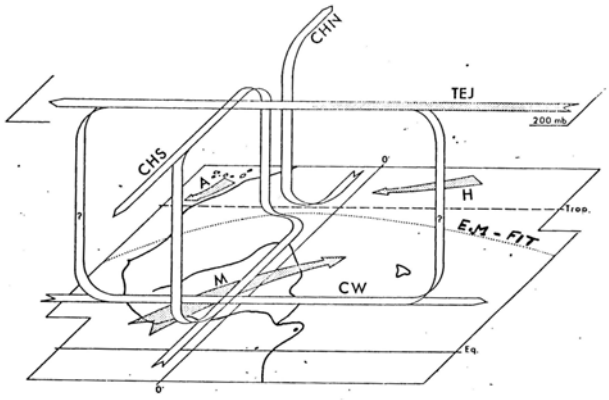

Figure 1.6b. 3-dimensional view of the West African wind circulations. CHN is the Northern Hadley Cell; CHS is the Southern Hadley Cell; TEJ is the Tropical Easterly Jet; CW is the Walker Cell Monsoonal Flow; A is Northwest Trade Wind; H is the Northeast Trade Wind (Harmattan), EM is the Surface track of the meteorological equator and FIT is the Inter-tropical Front. (Courtesy of Lambergeon-Dziatara-Janicot).

Since the equatorial pressure gradients are intimately related to the zonal SST pattern, ocean dynamics plays an important role in the seasonal cycle of the atmospheric equatorial Atlantic.

1.3.2 Ocean seasonal cycle

SST patterns reflect subsurface thermal gradients.Along the equator, the west to east decrease of SST is associated with a shoaling of the isotherms and thus of the thermocline. *The thermocline is the water column region in which very high thermal vertical gradients take place and thus it separates the warm surface waters of the mixed layer from the colder water at lower depths.* Thermocline has a depth of about 150m in the west equatorial Atlantic and is at surface level in the east, and this slope implies an eastward pressure force in the upper ocean (Philander, 1990). The 20°C isotherm occurs within the area of maximum vertical temperature gradient, and is, therefore, used to represent the tropical thermocline depth (Reverdin and McPhaden, 1986).

In general, density gradients are more due to thermal gradients than salinity gradients. For this reason, spatial variations in the depth of the thermocline are associated with large horizontal density gradients that reflect the dynamical response of the ocean to the surface winds. The pressure gradient associated with the zonal slope of the thermocline in the equatorial plane balances the wind stress (Wyrtki, 1975; Meyers et al., 1986). The thermocline is deep in the western and shallow in the eastern TA Ocean because the westward trade winds drive the warm surface waters westward and expose cold water to the surface in the east. The western TA is warmer also because the heat flux into the ocean increases. The eastward advection of warm surface waters associated with the elevation of the thermocline slope is compensated by the cooling caused by upwelling. The prevailing trade winds drive the poleward Ekman drift and hence induce equatorial upwelling that leads to a tongue of cold surface waters along the eastern-central equator in boreal spring-summer known as "*cold tongue*" (see figure 1.4, 1.7 and 1.8; Gill, 1982; Okumura and Xie, 2004). The cold tongue develops concurrently with the annual growth and eastward expansion of the Atlantic warm pool west of 50ºW (Wang and Enfield, 2001) and with the ITCZ shifts northward driven by the meridional winds. The wind stress curl produces upwelling process in a band further north of the ITCZ (figure 1.7 and figure 1.9).

The net surface heat flux is a combination of latent and sensible heat loss (turbulent fluxes), short-wave radiation absorption and net long-wave emission. In the TA, a heat budget study from observations (Foltz et al., 2003) has shown how the changes in the mixed layer heat content are balanced primarily by changes in the surface fluxes and as the equator is approached, contributions from horizontal heat advection become increasingly important. At the equator, the seasonal cycles of net surface heat flux, zonal heat advection (from currents), eddy heat advections (from tropical instability waves), entrainment (from zonal mass divergence) all contribute significantly to seasonal SST variability.
In addition, the seasonal adjustment of the ocean to the forcing of the wind stress drives a cycle of consecutive long waves. At the beginning of the year, the relaxation of the trade winds drives a first seasonal Kelvin wave eastward (February-March) and a Rossby wave westward (March-August). In boreal summer, with the strengthening of the trade winds, the Rossby wave is reflected as a Kelvin wave in phase with the second seasonal Kelvin wave (September-October) (Schouten et al, 2005).

Therefore, advection, upwelling and mixing processes, together with the heat flux across the ocean surface, influence SST in the tropical oceans.

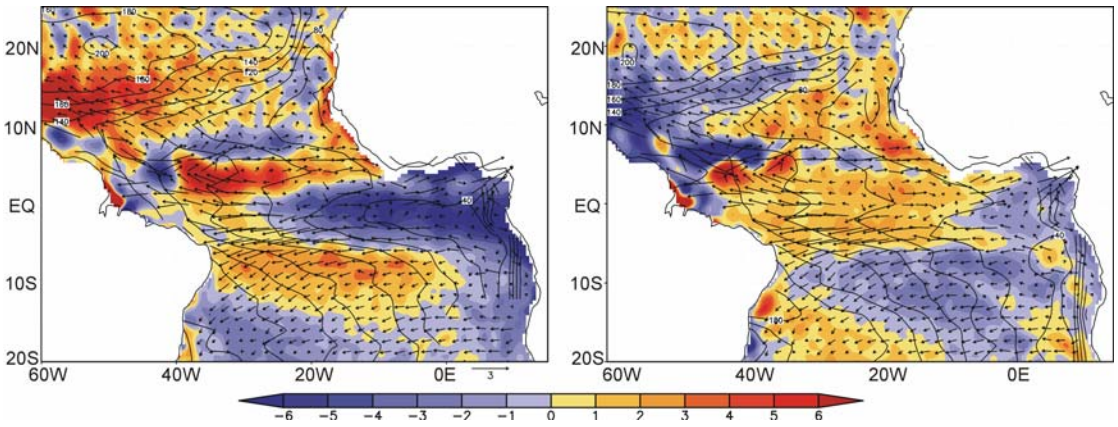

Figure 1.7. 20ºC thermocline depth (contour CI=10 m) from TAOSTA and Sea Surface Height (SSH, shaded in cm) from T/P in boreal summer season (left) and winter season (right). The mean sea surface currents (vectors in cm/s) from OSCAR analysis (Bonjean and Lagerloef, 2002).

Similarly to the equatorial upwelling processes, alongshore winds induce **coastal upwelling** along the southwest and northwest African coast by producing offshore Ekman drift. Since the vertical velocity component vanishes at the ocean surface, mixing processes determine the extent to which upwelling affects SST. The upwelling zones are narrow but currents advect the cold surface waters over considerable distances (Mittelstaedt, 1991). Two coastal upwelling systems are important over the TA: Mauritanian/Senegal and Angola/Benguela upwelling systems.
The Mauritanian/Senegal upwelling system is a complex system caused by the northeasterly trade winds and it is of special interest because it is thermodinamically very active;and in this area the seasonal and interannual variations are huge. This region of great ecological importance, has been studied from a multidisciplinary point of view by other authors (Mittelstaedt, 1991; Barton, 1998; Pelegrí et al., 2005; Santos et al., 2005; among others). The area is flanked by the cold Canarias Current (CC) and the warm water of the deep tropics, forming fronts and important mesoscales structures. Although the upwelling is confined to relatively close coastal regions, the impact of the cold SST can be felt 300-600 km offshore (Mittelstaedt, 1991) through eddies and filaments. This upwelling region has a high meridional variation and the division between the northern permanent upwelling and the southern seasonal upwelling has been identified at around 20ºN; the former is driven by the trade winds and the latter is driven by the ITCZ shifts (Mittelstaedt, 1991).
Symmetrically to the Mauritanian/Senegal upwelling area, there is another upwelling system in the south Atlantic called the Angola/Benguela upwelling system. This system is unique because it is surrounded by warm water systems, the east equatorial Atlantic and the Agulhas currents from the

Indian Ocean. The front area is a transition zone between the warm water Angola current and the waters from the Benguela upwelling system and is therefore a high productivity region and an important biomass and biodiversity reservoir (Shannon, 1985; Shannon et al., 1986). This upwelling system reaches its maximum in boreal summer, when the southeasterly winds are enhanced, and coincides with the occurrence of the seasonal eastern equatorial upwelling.
In addition, due to the fact that these two upwelling regions are part of the subtropical gyres, the processes that take place there can have an impact in more remote regions through Rossby wave propagation (Jacobs et al., 1994).

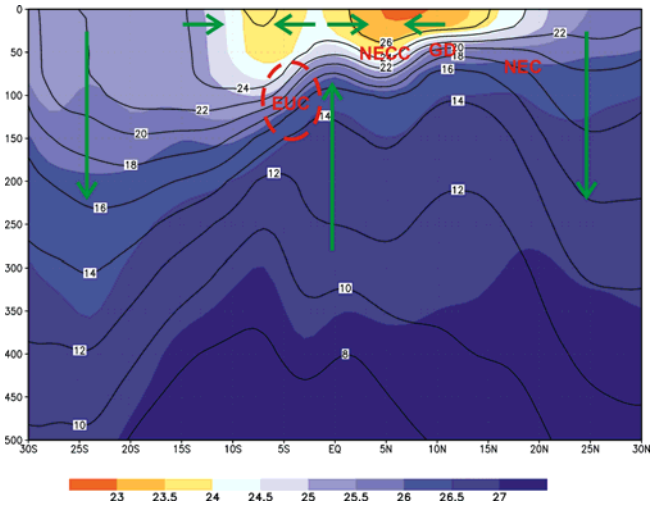

Figure 1.8. Scheme of density (shaded, potential-sigma in Kg/m^3) and temperature (contours, potential temperature in ºC) at 20ºW in the Atlantic. The figure shows some features of the tropical upper ocean circulation: NECC, NEC, EUC, GD and equatorial convergence and divergence. Data from Levitus (1998) and TAOSTA, summer season from the period 1979-1998.

Regarding the **ocean currents,** even when the prevailing winds are westward, *eastward and westward-flowing currents* characterize the oceanic circulation in the TA (see figure 1.8 and 1.9). North Equatorial Counter Current (NECC) flows eastward between 3ºN and 10ºN and has typical speeds of 50 cm/s. This narrow current is flanked by two broad westward surface currents, the North and South Equatorial Currents (NEC and SEC), to the north of 10ºN and to the south of 3ºN, respectively. Southern currents have a more intense core between 3ºN and the equator in which speeds can exceed 100 cm/s. Far from the equator, the zonal pressure force induces equatorward geostrophic motion. At the equator, the coriolis parameter vanishes and fails to balance the pressure force. The fluid that converges onto the equator will, in part, rise to the surface to sustain the divergent Ekman drift and will also, in part, accelerate eastward, down the pressure gradient, thus giving rise to an eastward current in the equatorial thermocline. Such a current is known as Equatorial Under Current (EUC), which has its core in the thermocline and extends vertically with a speed of 150 cm/s.
The SEC is intensified in the western Atlantic and continues all the way to the coast of Brazil where the fluid is absorbed by the northwestward North Brazil Current (NBC). NBC flows continuously along the coast into the Gulf of Mexico between November and April when the southeast trades are weak. The intensification of the southeast trades in May affects the NBC dramatically; It adruptly veers offshore between 5ºN and 10ºN to feed the NECC (figure 1.9) and it persists in this mode through October (Bruce and Kerling, 1984). This seasonal change is accompanied by the ITCZ movement, and in boreal summer, the NECC is strong and penetrates into the Gulf of Guinea.
The westward NEC and SEC form part of the subtropical ocean gyres in the Atlantic and are linked to the Gulf Stream in the north. The connection between the tropical and extratropical circulations is important because the oceanic circulation balances the latitudinal heat gradient between the equator and higher latitudes. In the Atlantic much of the cross-equatorial flow of warm surface

waters is in the NBC. This region is also important for the mesoscale eddy transport (Stammer, 1997).
Meridional motion in the TA Ocean is poleward Ekman drift in the surface layers and equatorward geostrophic motion at the depth of the thermocline. The intense upwelling is found at the equator, whilst downwelling occurs at the subtropical regions (figure 1.8).

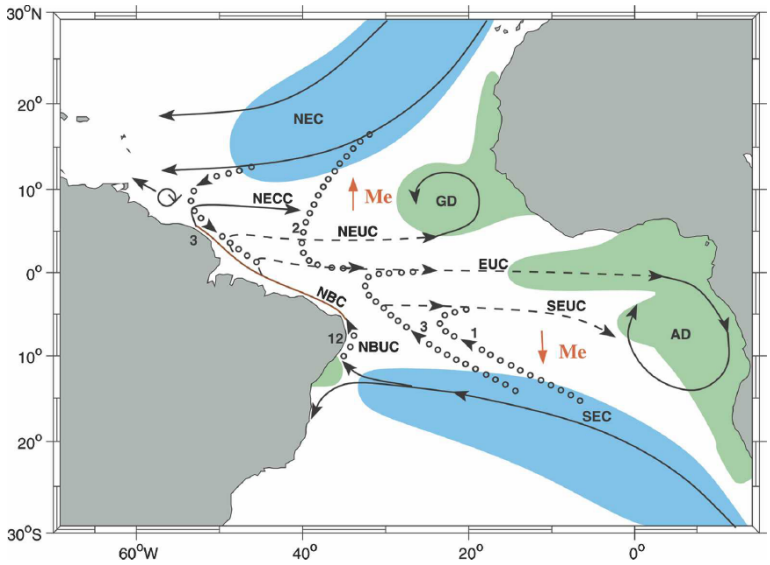

Figure 1.9. Scheme of the Equatorial surface oceanic circulation. Schematic representation of the Atlantic STC circulation with subduction (blue) and upwelling (green) zones that participate in the STC. Current branches participating in STC flows are the North and South Equatorial Current (NEC, SEC) and Countercurrent (NECC), Equatorial Undercurrent (EUC), North and South Equatorial Undercurrent (NEUC, SEUC), and the North Brazil Current and Undercurrent (NBC, NBUC); GD and AD are the Guinea and Angola domes. Interior equatorward thermocline pathways are dotted; transport estimates are marked for interior and western boundary pathways. From Schott et al. (2004).

As in the atmosphere, the ocean connects its circulations by zonal and meridional cells in the upper ocean. Zonally at the equator, the maximum upwelling occurs in the eastern Atlantic, the mean surface currents are westward, and an eastward current with the core at the thermocline (EUC) closes the zonal circulation. Meridionally, *Shallow Tropical Cells* (STCs) connect the surface water to the thermocline waters by recirculating the equatorial Ekman drift to the subduction regions (figure 1.4). Subducted water from the subtropical gyres flows toward the equator at depths of about 100-400 m, feeds into the EUC, upwells in the eastern equatorial region and returns to the subtropics in the surface layer (Luyten et al., 1983; Gu and Philander, 1997; Liu and Yang, 2003; Kushnir et al., 2003).

1.4 Interannual variability: SST Modes and air-sea interactions

TA interannual variability appears superimposed on the annual cycle and it is governed by multiple influences at different timescales, producing different anomalous SST modes. The principal Tropical Atlantic SST variability modes are the *Equatorial* mode or *Atlantic El Niño* (Zebiak, 1993), the *Meridional* mode (Ruiz-Barradas et al., 2000; Servain et al., 2003) and the Subtropical North Atlantic (Sutton et al., 2000b).

Positive feedback between the ocean and the atmosphere allows these modes of SST anomalies to persist in time. The seasonally-changing background state influences the type and strength of air-sea interaction that prevails in each season. The TAV has peculiarities related to the small ocean basin and to the shape of the boundaries continent as well as to the nearby Pacific Ocean.
Although both, the Pacific and the Atlantic share the El Niño-like equatorial mode, the Southern Oscillation and the Meridional mode are exclusive to the Pacific and the Atlantic basins,

respectively[1]. These features make the Bjerknes feedback mechanism in the TA less well understood than in the tropical Pacific in relation to the interannual variability (Keenlyside and Latif, 2007). Besides the local air-sea interaction, external forcing, most notably the Pacific ENSO, significantly influences SST variability in the TA through atmospheric teleconnections. These teleconnections will be assessed in section 5. The description of each TA mode along with the related air-sea feedbacks will be described in this section

1.4.1 Equatorial Mode

The Equatorial mode is also known as the Atlantic Niño, due to its similarity to the Pacific Niño (Zebiak, 1993; Latif et al., 1996). The first well documented Atlantic Niño event took place in 1963, and received attention not only because of its magnitude, but also because it coincided with the EQUALANT observational program (Merle, 1980). During that summer, the coincidence of warming SST, a relaxation of the trade winds and shift of convection caused to dub this phenomenon the "Atlantic Niño" (Merle, 1980).
The Atlantic Niño or *Equatorial Mode* (EM) is characterized by a relaxation in the equatorial trade winds which induces a warm water redistribution in the equatorial belt and a weakening in the equatorial thermoclime slope and also in the heat content zonal gradient (Merle, 1980; Servain et al., 1982; Carton and Huang, 1994; Carton et al., 1996), which can be the result of an oscillatory ocean-atmosphere coupled mode (Zebiak, 1993). Contrary to the Pacific Niño, for which there is an east-west movement of the convergence zone over the western tropical Pacific, this movement does not occur over the Western TA in the EM (Wang, 2002b). During the Atlantic Niño, the entire equatorial basin suffers anomalous convention conditions with ascending motions as a consequence of the zonal pressure gradient disappearance (figure 1.10).

This mode usually occurs in boreal summer season when the anomalous conditions of the eastern equatorial upwelling can modify the zonal pressure gradient. The main consequences are related to the WAM, which has its onset in summer, intimately related to the continent-ocean temperature contrast due to the "cold tongue development" (Okumura and Xie, 2004). For a positive EM event, there is an occurrence of unusually heavy rainfall over Northeastern Brazil, the coast of the GG and southwestern Africa occurs. More recently, some observational studies in the AMMA-EU framework have shown that a delay in the WAM onset with respect to the mean could be explained, in part, by air-sea interaction in the GG where the equatorial upwelling has also shown a lag with respect to the mean (Janicot et al., 2007).

During the Pacific Niño, the equatorward displacement of the ITCZ early in the year is usually followed, a few months later, by an eastward movement of the western Pacific convergence zone. In contrast, the absence of such an eastward displacement from the Atlantic is part of the reason why warm episodes in the Atlantic tend to terminate early in the second half of the year (Philander, 1990). However, Carton et al. (1996) studied the EM and identified it as having very high variability through the year possible appearing in several seasons. This ability is related to the GG upwelling seasons; an upwelling season with a very developed cold tongue occurs in boreal summer, while there is a small upwelling season from November-December (Picaut, 1983). Okumura and Xie (2006) have described the November-December mode as a particular case of the equatorial Atlantic, relating it to anomalous upwelling over the coast of the GG in its second season. This mode affects the rainfall variability in the coastal Congo-Angola during its early rainy season (Okumura and Xie, 2006).

Regarding the **oceanic component** of this mode, in the 1984 event, there was an intensification of the NECC and the appearance of an unusual eastward current south of the equator which contributed to a warming of the southeastern tropical Atlantic (Philander, 1990). Although the zonal pressure gradient along the equator disappeared (Katz et al., 1986), the intensity of the EUC was almost unaffected as was the upwelling along the northern coast of the GG. However, upwelling along the southwestern coast of Africa was significantly weakened (Shannon et al., 1986). Sterl and

[1] However, some authors have described a Meridional Mode for the Tropical Pacific (Chiang and Vimont, 2004).

Hazeleger (2003) conducted a careful budget analysis of the SST tendency and found that SST anomalies in the South Atlantic are mainly generated through heat flux and momentum exchange between the ocean and the atmosphere. The former creates thermal anomalies in the mixed layer while the latter creates vertical stirring and horizontal Ekman transport which act on the mean temperature gradient (vertical and horizontal). It is only along the Angolan coast and in the equatorial cold tongue region that they have found evidence that the ocean dynamics (i.e., transports by ocean geostrophic currents) are important. This is in agreement with heat budgets performed by other authors (Vauclair et al., 2004).

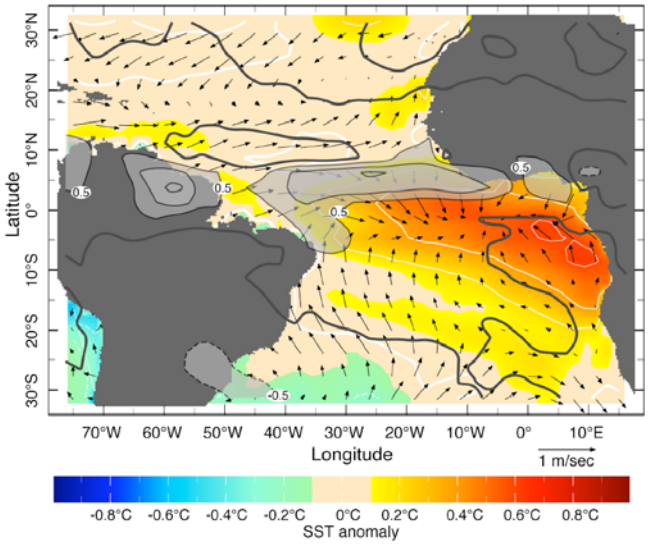

Figure 1.10a. Dominant pattern of surface ocean-atmosphere variability in the TA region during boreal summer (June-August). The black contours depict the first EOF rainfall anomaly (from GPCP data, 1979-2001) in units of mm/day. This EOF explains 23% of the seasonal variance. The colored field is the SST anomaly regressed on the PC time series of the rainfall EOF (units are ºC, see scale below, white contours every 0.2ºC are added). Arrows depict the seasonal surface wind vector anomaly in m/s, regressed on the same time series. From Kushnir et al., (2003)

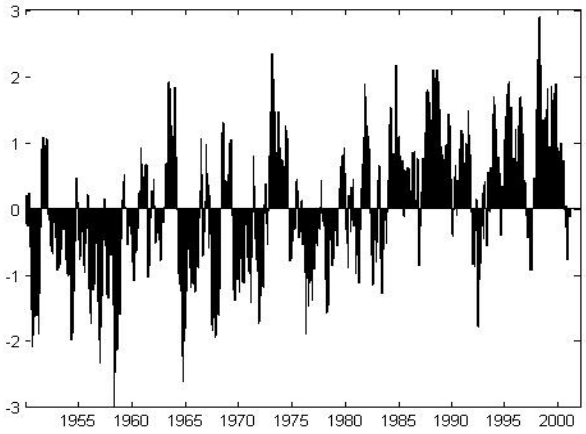

Figure 1.10b. Index of the Equatorial Atlantic mode, which peaks in summer, referred to as ATL3 index and calculated like Zebiak (1993).

Anomalous warm conditions over the coastal region of the Angola/Benguela upwelling system constitute a particular variability mode, referred to as *Benguela Niños* (Shannon et al., 1986). These events have very strong ecological and climatic consequences, such as fishing block, and anomalous rainfall over surrounding areas as Namibia and Angola (Rouault et al., 2003; Rouault et

al., 2007). However, these Benguela Niños have been associated with the EM throughout oceanic wave's mechanism; western equatorial wind anomalies induces equatorial SST anomalies (related to EM) which remotely influence Angola/Benguela coast via equatorial and coastal Kelvin waves (Vega et al., 2003; Florenchie et al., 2003; Florenchie et al., 2004; Grodsky and Carton, 2006; Rouault et al., 2007).

Although the EM appears as the leading mode in most of the discriminant analysis described in the recent literature and especially in summer (Kushnir et al., 2003), the behaviour of the *Subtropical South Atlantic* (SSA) is a controversial part of the TAV. Although Venegas et al. (1997) described the SST variations over SSA as a different mode associated more with the Sta Helena High pressure system, in many studies the EM appears together with an anomaly over the southern subtropics (Handoh et al., 2006b; Sterl and Hazeleger, 2003). On the one hand, some authors relate the subtropics to the EM, implying that the South Atlantic atmosphere could lead the equatorial part. Trzaska et al. (2007) have related the SSA mode to the south Atlantic subtropical High Sea Level Pressure (SLP) anomalies, finding that this subtropical mode is preceding the EM with the transition taking place from boreal winter-spring to summer. On the other hand, some others suggest a different origin: the equatorial part could be associated with ENSO-anomalous Walker circulation while the off-equatorial part could be due to a south extratropical wave train (Handoh et al., 2006b; Cazes-Boezio et al., 2003).
Some other authors have also investigated the question of whether the EM is related to the variability in the South Hemisphere (Venegas et al., 1997; Sterl and Hazeleger, 2003; Barreiro et al., 2005). The most prominent result is that southern summer atmospheric variability can play a preconditioning role in the onset of the anomalies in the deep tropics during the following austral fall. In spite of the fact that many works have associated the EM with the subtropical atmospheric dynamics and external forcing more than with equatorial dynamics, some authors still consider the EM as an internal self-sustaining oscillation (Zebiak, 1993; Handoh and Bigg, 2000; Latif and Grötzner, 2000; Handoh et al., 2006b; Keenlyside and Latif, 2007).

The observed **atmospheric pattern** associated with the EM resembles the baroclinic response to a deep atmospheric heat source at the equator, which has been found with AGCM by some authors (Barreiro et al., 2002; Robertson et al., 2003; Trzaska et al., 2007). This baroclinic response consists of a strong low-level westerlies flow to the heat source, a southeasterly flow from March-April near 20ºS, and the anticyclones developed at upper levels on either side of the equator as a Gill's response (Gill, 1982). A model study from Haarsma and Hazeleger (2007), have reported that the latter atmospheric response can even impact on extratropical areas.

1.4.2 Meridional Mode. Its link to the Subtropical North Atlantic

The *Meridional mode* (MM) consists of a spatial pattern of opposite SST anomalies across the equator, which is strongly linked to the anomalous rainfall in Northeast Brazil (Moura and Shukla, 1981; Nobre and Shukla 1996). By matching wet and dry years in the Nordeste with patterns of SST, it was found drought associated with an anomalous northward shift of the ITCZ in conjunction with an anomalous northward gradient of SST, an association often referred to as the *Atlantic dipole* and *cross-equatorial SST gradient* (Xie and Carton, 2004). This mode is the dominant pattern of Tropical Atlantic Variability (Nobre and Shukla 1996; Seager et al. 2001), especially in boreal spring (Kushnir et al. 2003, and has an important decadal variability. It is characterized by an anomalous meridional displacement of the Marine ITCZ (Nobre and Shukla, 1996; Ruiz-Barradas et al., 2000, Chiang et al., 2002) through the anomalous cross-equatorial winds. The observed seasonality of this SST-convection interaction is argued to be the result of the spatially uniform warm climatological SST conditions in boreal spring that make the Atlantic ITCZ highly sensitive to small perturbations in the meridional direction (Chiang et al., 2002).

The centers of this mode coincide with the subtropical high pressure systems and the eastern part of the subtropical gyres, which is important in terms of air-sea interactions. In addition, the eastern upwelling systems are located over the northern and southern braches of the MM, which makes the interactions more complex (see figure 1.11).

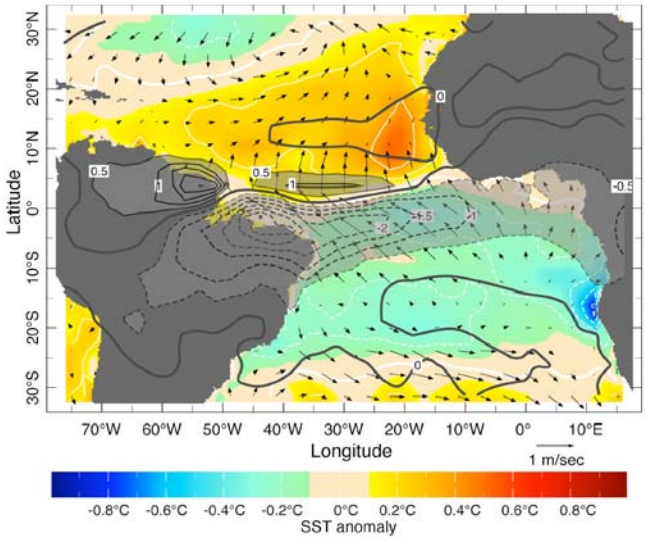

Figure 1.11a. As in Figure 1.10a but for the boreal spring season (March-April). The rainfall EOF of this season explains 33% of the variance. From Kushnir et al., (2003).

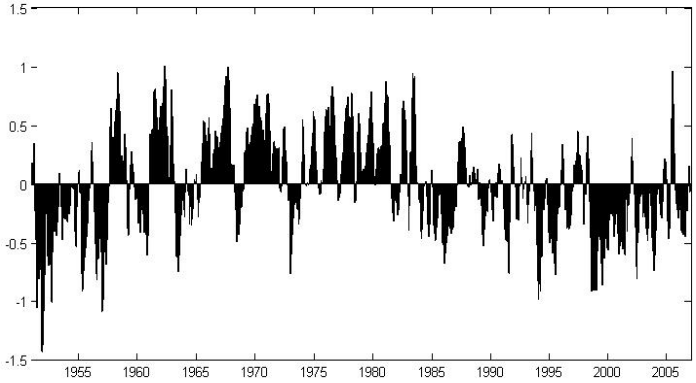

Figure 1.11b. Tropical Atlantic Dipole Index (Servain, 1991) calculated as the difference between North Tropical Atlantic (NTA) and South Tropical Atlantic (STA) index. El Niño + Trend signal has been removed from NTA and STA. The NTA and STA indices are significantly anticorrelated. Courtesy of NOAA.

Some authors have pointed out the possible close **relationship between TA modes**. Philander (1990) explains how the EM involves meridional displacements of the ITCZ, asymmetrically around the equator. However, the intensification of the Low pressure over the entire basin, which provokes anomalous high precipitation over Nordeste Brazil and the coast of GG, helps an enhanced Hadley circulation that modifies the Subtropical High pressure systems, in which the centers of action of the MM are situated. Servain et al. (1999) have suggested the following scenario: an anomalous northward ITCZ shift would be associated with a similar displacement of the entire trade winds system, weakening the northeastern trade winds and strengthening the Southeastern trade winds along the equator. These changes increase the thermocline slope at the eastern equatorial Atlantic, creating cold SST anomalies over the southern hemisphere due to increase of evaporation and upwelling, which then develops into an Atlantic La Niña event, and warm SST anomalies north of the ITCZ by decreasing evaporation. Other authors think that the EM is the first step for the development of a MM because one center by itself is enough to create cross-equatorial winds by the meridional SST gradient (Okumura and Xie, 2006; Hu and Huang, 2006). Nevertheless, an AGCM simulation forced with a dipole SST of opposite anomalies between the equator and the south subtropics has shown a southward shift of the ITCZ (Haarsma et al., 2003). These changes in

cloud cover counteract the variations in latent heat flux north of the ITCZ, thereby prohibiting the generation of a MM by a thermodynamic feedback.

The question of the **existence of the dipole pattern** is controversial (see figure 1.12). Houghton and Tourre (1992) first pointed out that the dipole may not be a realistic physical entity because the SST fluctuations in the northern and southern branches of the dipole are largely independent. Subsequent analyses with more data (i.e., Enfield and Mayer 1997; Mehta 1998; Dommenget and Latif 2000) confirmed their result, although some of the issues are still in debate. If the MM is a mathematical artefact (Dommenget and Latif 2000), then the centers of action do not necessarily appear together and, therefore, there exist two separate northern and southern modes.

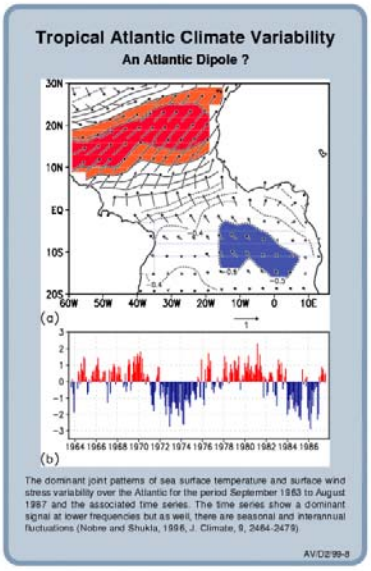

Figure 1.12. The Meridional mode or the Atlantic Dipole? From Nobre and Shukla, 1996.

Faced with these different frameworks, in this study it is assumed that the development of the EM does not necessarily create a MM. In addition, the MM could (but does not necessarily) develop from one center and usually appears with anomalous subtropical high systems in both the northern and southern hemispheres. Although the MM can be initiated from the southern center due to south Atlantic atmospheric variability (Barreiro et al., 2004), this southern center would also be related to the EM (Venegas et al., 1997; Sterl and Hazeleger, 2003). Therefore, special attention is currently made to the Subtropical North Atlantic SST variations.

The *Subtropical North Atlantic (SNA),* which can also be seen as the northern part of the MM, has been intensively studied by other authors (Czaja and Frankignoul, 2002; Czaja et al., 2002; Sutton et al., 2000b). This center is also important because it is the region that connects the tropical and the northern extratropical regions. Therefore, it is strongly influenced by both the North Atlantic Oscillation (NAO) and the ITCZ (Xie and Carton, 2004) and could have an important climatic impact on the extratropics (Okumura et al., 2001).
In the SNA region, located in the region of the Azores high pressure system, the SST variations have been attributed mainly to the turbulent heat fluxes (Cayan, 1992). Furthermore, Czaja et al. (2002) ascribe the majority of the strong North TA SST anomalies in the recent half-century to the force of ENSO and the NAO. However, Czaja (2003) has concluded that in absence of ocean dynamics in the upper ocean balance, the surface fluxes variability appears considerably weaker. Also, the SNA is flanked by the Mauritanian/Senegal upwelling system which can interact with the SNA SST anomalies.

The air-sea interactions related to the TAV are described in subsection 1.4.3.

1.4.3 Coupled air-sea feedbacks in Tropical Atlantic Variability

The simplest coupled ocean-atmosphere system is perhaps the coupled mixed layer model presented by Barsugli and Battisti (1998). The model is an extension of Hasselmann's (1976), and includes a thermodynamic air-sea coupling through surface heat exchange. Assuming that the surface heat exchange is predominately controlled by air-sea temperature differences, then the ocean and the atmosphere are subject to a negative feedback. This is because, for a given atmospheric temperature, the ocean temperature will always tend to relax toward it. The atmospheric temperature is subject to a similar constraint if an oceanic temperature is given. This leads to the so-called **"passive" coupling** between the ocean and the atmosphere. This simple coupled model has been successful in explaining some basic characteristics of climate variability in extratropical regions.

However, in the tropics, the effect of surface winds often dominates over the effect of air-sea termperature differences on surface heat flux variability, and modelling and observational studies have evidenced that large-scale surface circulation of the tropical atmosphere is responsive to SST anomalies (Bjerknes, 1969; Zebiak, 1993; Chang et al., 2000). Therefore another **"active" coupling** mechanism may be important (Chang et al., 1997).

The feedback mechanism that has received the most attention and is also the most controversial is a **thermodynamic feedback** referred to as the **Wind-Evaporation-SST (WES) feedback** (Xie and Philander, 1994; Carton et al., 1996; Chang et al., 1997). In this mechanism, the key element is the response of cross-equatorial wind to the interhemispheric SST gradient (it is characteristic of the MM). If an anomalous interhemispheric SST gradient is introduced, the atmosphere will respond with a change in meridional pressure gradient through hydrostatic adjustment of the atmospheric boundary layer (Lindzen and Nigam, 1987), as well as with midtropospheric diabatic heating. Together, these drive a cross-equatorial boundary layer flow, changing the meridional position of maximum surface wind convergence and therefore the ITCZ (Chiang et al., 2002). The anomalous cross-equatorial flow is deflected by the coriolis force in both hemispheres in such a way that it increases the wind speed over the hemisphere where a negative SST anomaly exists, cooling it further through surface evaporation. It then decreases the wind speed over the hemisphere where a positive SST anomaly exists, warming it further. The net effect is a positive feedback on the original SST anomaly (Chang et al., 1997; Chang et al., 2000; Ruiz-Barradas et al., 2000; Barreiro et al., 2004).

Almost all the GCMs show a cross-equatorial circulation pattern in response to the inter-hemispheric SST gradient in the deep tropics, as in the observations (Chang et al. 2000; Sutton et al., 2000a; Okumura et al., 2001; Terray and Cassou, 2002). However, the validity of this feedback mechanism remains controversial. While some models show a positive thermodynamics feedback (Chang et al., 1997; Chang et al., 2000), others show a negative feedback (Sutton et al., 2000a). Frankignoul et al. (2003) have compared and discussed the different WES feedback in the AGCMs and they have found that the lack of reliable surface heat flux measures is the principal source of errors in the simulations. This has prevented a rigid test of the hypothesis.

The same testing problem also occurs with the **cloud-SST feedback** (Philander et al., 1996), which has potentical relevance to TAV. Off the west coast of Africa where low level stratus clouds are formed as a result of the increased static stability of the lower atmosphere due to cold surface waters, solar radiation is blocked which causes a further cooling in surface waters. Colder SSTs produce more clouds which block more solar radiation, and so forth. The extent to which this positive feedback can really affect TAV needs further investigation. However, some authors have identified the importance of this mechanism over the eastern Atlantic, while the WES feedback is more effective at the western Atlantic (Traszka et al., 2004). In addition, massive convective activities over the Amazon basin can potentially be an active player in TAV (Chang et al., 2006; Grodsky et al., 2008).

Concerning **dynamic interactions** between the ocean and the atmosphere, the most important one involves interactions between zonal wind stress and equatorial SST anomalies, analogous to the **feedback mechanism proposed by Bjerknes** (1969) for ENSO. Modeling and observational works (Zebiak, 1993; Carton and Huang, 1994; Delecluse et al., 1994; Carton et al., 1996;

Keenlyside and Latif, 2007) have suggested that the Bjerkness feedback mechanism does operate in the equatorial Atlantic, albeit much weaker than the Pacific counterpart.
In this mechanism, the warm SST anomalies over the eastern part of the Atlantic due to the weakening of the trades is accompanied by a redistribution of heat, in which the thermocline slope raises over the western Atlantic, feeding a warmer SST and decelerating the winds due to the diminishing of the SST gradient. This positive feedback is more effective in boreal summer, when the zonal gradients are largest and the atmosphere does respond to the equatorial Atlantic SST anomalies.
The main differences of the feedback between the two basins (Chang et al., 2006; Keenlyside and Latif, 2007) can be summarized as follows;
a) The correlation between the zonal wind and equatorial SST anomaly is considerably lower in the TA than in the Pacific, while the correlation between the meridional wind in the vicinity of the ITCZ and equatorial SST anomaly remains comparable in both oceans. In addition, the spatial correlation structure between the zonal wind and SST anomaly is narrower in the tropical Atlantic than in the tropical Pacific.
b) The coherence between equatorial and eastern coastal SST is much less in the Atlantic and the zonal wind variability is displaced proportionally farther to the west in the basin than in the Pacific.
c) *While in the Pacific a zonal SST gradient occurs, being eastern SST anomalies out of phase with the western, in the Atlantic, this SST gradient is much weaker.*
d) In the Atlantic, there is no a migratory component of the zonal wind variability and the strongest variability is situated in the western portion of the basin.
e) Because of c) and d) in the Atlantic, there is no a convection migration at the eastern of the basin, the maximum convection and rainfall occurs along the entire basin.
Nevertheless, the Bjerknes mechanism works to explain part of the Atlantic EM (Zebiak, 1993; Carton et al., 1996; Keenlyside and Latif, 2007), but the components have different evolution than the Pacific counterpart and thus the predictability is lower (Keenlyside and Latif, 2007).

Another dynamic ocean-atmosphere interaction is referred to as **Ekman feedback** which involves interactions between upwelling induced by surface Ekman divergence associated with cross-equatorial wind anomaly and the cross-equatorial SST gradient (Mitchell and Wallace, 1992; Chang and Philander, 1994). If a warm SST anomaly is introduced into the northern hemisphere, a northward wind anomaly will be developed near the equator as a result of the low pressure anomaly over the warm region. The cross-equatorial wind anomaly will give rise to a surface Ekman divergence and upwelling to the south of the equator which will then cause surface cooling in the southern hemisphere and enhance north-south temperature difference, in a positive feedback way.

Outside of the tropics, air-sea interactions seem to be more like a one-way street: Changes in the atmosphere cause reactions in the ocean–sea ice system (Visbeck, 2002). Also the SST is colder and the mixing by winds deepens the thermocline. Therefore it is more difficult to identify ocean-atmosphere interactions and the response time of the system is larger (Frankignoul, 1985). However, some authors have shown evidence of air-sea interaction at the extratropical regions (Frankignoul, 1985) even in cool conditions (Xie, 2004).

Ocean circulation and **upper ocean dynamics** can contribute significantly to SST variability throughout the **Shallow Tropical Cells** or **SubTropical Cells** that transport cold mid-latitude surface water along the thermocline into the equator where this water upwells to the surface (McCreary and Lu 1994; Liu, 1994). Two main mechanisms can conceivably affect subsurface ocean temperature on the equator, which can in turn affect SST and the atmosphere at decadal and longer timescales. One is through **STC's advection of SST anomalies** from the subduction regions to the deep tropics trough a so-called **"oceanic tunnel"** (Gu and Philander 1997; Zhang et al., 1998; Schneider et al., 1999; Lazar et al., 2001; Weller, 2003). Another is through **changes in STC strength** and hence, its transport of cold water (Kleeman et al., 1999; Huang and Pedlosky, 1999) and it is found that the Southern Atlantic is by far the main source of water of the equatorial thermocline and the surface (Frantantoni et al., 2000; Malanotte-Rizzoli et al., 2000).

These **advective processes** are manifested in propagation of SST anomalies and are active in the Atlantic (Hansen and Bezdek, 1996; Sutton and Allen, 1997; Venegas et al., 1997; Mehta, 1998). Numerical modelling studies with forced ocean GCMs show that in the trade wind regions, advection by ocean currents within the ocean mixed layer acts to damp thermal anomalies that are forced by surface fluxes (Seager et al., 2001) in a negative feedback. Therefore, the ocean dynamics contribute to restore the equilibrium of the ocean-atmosphere system damping SST anomalies, e.g., by means of the meridional ocean heat transport associated with anomalous temperature gradients (Chang et al., 1997; Kushnir et al., 2002).

Another way to connect tropics-extratropics is through the **oceanic waves**. Eastward Kelvin waves can connect anomalies from one boundary to the other. Then, the poleward coastally-trapped waves and the possible Rossby wave radiation from the coast at the eastern part of the basin traveling westward, is a way of connecting the tropics-extratropics and boundaries at the subtropical regions respectively (Jacobs et al., 1994). This oceanic processes has been related to the EM (Handoh and Bigg, 2000; Vauclair and du Penhoat, 2001; Chang et al., 2006). During the development phase of the EM, the Bjerknes positive feedback dominates, which causes the anomalies to grow. However, during the decay phase, the equatorial wave adjustment process of the ocean plays a role of delayed negative feedback (Chang et al., 2006). Since the oceanic waves are the natural oceanic adjustment in the variability, and they are relevant in climate terms, the oceanic waves could be intensively described in section 4.

1.5 Aspects of Intraseasonal atmospheric and oceanic variability

As it has been described before, the SST is part of the climate variability at many different scales. At intraseasonal timescales, the SST anomalies are one of the determining elements of the convection variability in the tropical oceans, and therefore participate in the atmospheric oscillations that imply variations in the convection and the associated winds. Since the SST is the variable that links the upper ocean and the overlying atmosphere, the SST *influence*s and *is influenced* by both the atmosphere and the ocean. From this bi-directional relationship, the processes frequently appear as coupled and it is very difficult to distinguish between causes and consequences (i.e. processes described by Chelton et al., 2004; Hayes et al., 1989, Flatau et al., 1997, among others).

In addition, the ocean has a particular way of adjustment from anomalous conditions, and it is this way which is important in climate terms (Philander, 1990). Generally speaking, the oceanic response, represented as anomalous Sea Surface Height (SSH), is the sum of a strong local effect (direct heat and moisture exchange with the atmosphere) plus a dynamical response from remote disturbances, believed to be primarily wind-related (Gill and Niiler, 1973).
In this section, *the air-sea interactions based on the SST, atmospheric convection, surface winds and oceanic waves are described at intraseasonal timescales.*
Here the intraseasonnal variability is addressed since a lot of processes over the TA, and also important for the human activities, have large intraseasonal variability (i.e. WAM, the oceanic cold tongue over the eastern equatorial Atlantic, the seasonal coastal upwelling at the West African coast…). Furthermore, intraseasonal phenomena could modulate TA seasonal to interannual variability modes. Some important mechanisms for understanding the above-mentioned processes among others are remarked along the section.

1.5.1 Intraseasonal wind-convection fluctuations

The dominant intraseasonal atmospheric variability in the tropics occurs at periods from 30 to 70 days and is known as **Madden-Julian Oscillation** (MJO, Madden and Julian, 1971, 1994).
This intraseasonal fluctuation is associated with a global-scale zonally oriented circulation cell that propagates eastward. Meridionally it is confined to the tropics, the band of latitudes from 20ºN to 20ºS, with maximum amplitude along the equator (figure 1.13). Low level winds converge onto and upper level winds diverge from a region of rising air and low surface pressure. These wind

anomalies have, therefore, characteristics of the first baroclinic mode, with the low-level wind out of phase with the upper-level winds. The speed of the eastward propagation is 10 m/s approximately.

The intensity of the cell varies with longitude: it has a strong effect on cloudiness over the Indian Ocean and Western Pacific, and in recent years, a large amount of research has focused on the role of the MJO in the Indian and African monsoons from the new satellite dataset (Madden and Julian, 1994; Matthews et al., 2007; Mounier et al., 2007). Although the convection anomalies are mainly confined to the Indian Ocean and Western Pacific warm pool regions, wind perturbations tend to propagate around the equator. The eastward propagation of this phenomenon was initially explained as the manifestation of convectively driven, equatorially trapped Kelvin modes. However the MJO is not simply a free Kelvin wave because it is highly influenced by interactions between the surface wind fluctuations and the release of latent heat, and it strongly modulates tropical convection. In addition to the eastward movement of the system, individual cloud clusters propagate westward (Nakazawa, 1988)

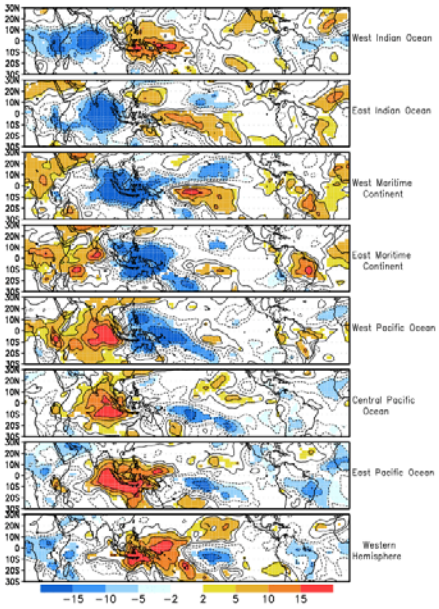

Figure 1.13. MJO composites based on a multivariate index utilizing outgoing longwave radiation for November-March season (From NOAA).

The first existing theories of MJO development and propagation (Lau and Peng, 1987; Emanuel, 1987; Neelin et al., 1987; Hu and Randall, 1994) concentrated on atmospheric processes and neglected the feedback between the SST modification by convection and the development of the cluster itself. Even the air-sea interaction theories (Emanuel, 1987; Neelin et al., 1987) consider the effect of evaporative fluxes on the atmospheric boundary layer without taking into account the effect of the fluxes on SST.

Flatau et al. (1997) formulated a conceptual model of the interaction between equatorial atmospheric processes and local SST changes: SST decreases under and west of a convective source due to the cloud shielding effect, ocean mixing and evaporative fluxes associated with strong equatorial westerly winds. East of the convective source, in the region of weak winds associated with the convergent region of an easterly propagating Kelvin wave, SST can increase. This zonal SST gradient causes zonal changes in surface moist static energy and provides surface forcing; promoting development of convection in convergent region and helping the convention propagate eastward. This theory was in agreement with Nakazawa (1995), who described episodes

observed with TOGA in the Pacific and showed that high SST preceded convective activity by 12-13 days and that the moisture increase was related to enhanced evaporation.
After the formulation of the Flatau et al.'s model (1997), which introduced the SST as an active feedback element, the convection oscillation has been drawn as coupled. The relation between the convection anomalies, SST, surface winds and heat fluxes has been shown mainly in the Indo-West Pacific basin (Hendoh et al., 1998). However, Woolnough et al., (2000) have found that the relation between variables are extended farther east consistent with the eastward extension for the warm pool and westerly winds.
Consequently, these works have also suggested coupled mechanism for the convection-oceanic wave propagation. The mechanism could be explained as follows: convection anomalies induce wind stress anomalies that can produce SSH anomalies triggering equatorial oceanic waves, which in turn contribute to the equatorial thermocline variability. In this way, observational studies have shown how the MJO is able to modify the surface ocean throughout the shortwave radiation and latent heat fluxes anomalies due to the enhancement (weakening) of the cloudiness and westerly (easterly) winds anomalies associated with the wet (dry) MJO phase over the Indian and western central Pacific and force eastward-propagating oceanic equatorial Kelvin waves (Matthews et al., 2007).
The convection oscillation-MJO within particular ENSO events has also been studied from observations (Kessler et al., 1995; Roundy and Kiladis, 2006). Roundy and Kiladis (2006) have shown how the westerlies MJO-induced anomalies contribute to the oceanic equatorial Kelvin wave triggering. They have also shown the existence of air-sea interactions as the wave is passing.

In spite of the difficulty to clearly identify a signature of the eastward convection propagation over the Atlantic basin, a type of convection fluctuations has been recognized (Park and Schubert, 1993; Foltz and McPhaden, 2005), and they have been suggested to be mainly a fingerprint of the MJO. Furthermore, 30-70 days wind variations have been documented and these patterns may play an important role in affecting the character of climate variability in the TA (Foltz and McPhaden, 2004). For instance, intraseasonal wind fluctuations and modes of convectively coupled atmospheric Kelvin waves have been detected over the Atlantic and West Africa (Mounier et al., 2007). These intraseasonal convection fluctuations could be related to WAM onset variations (Sultan and Janicot, 2001).

In the Atlantic, there are several key regions regarding the convection variability: Amazon river Basin, Nordeste Brazil and the Subtropical Atlantic Convergence Zone (SACZ) in the Western Atlantic basin, and the coast of the GG and the Congo River basin-Angola in the Eastern Atlantic basin. This convection zones can also be linked to the ITCZ movements and therefore are important in the TAV.
Although the MJO has a much weaker effect on the convective zones over the Amazon and Congo River basins (compared to the Indo-Pacific basin), the interaction of the MJO with the South America deep convection is quite well established (Kayano and Kousky, 1999). While, the the convergence over the Amazon basin and the SACZ are highly influenced by the tropical Pacific variability. For instance, Kiladis and Liebmann (2006) have suggested two ways in which the Pacific convection affects the TA: in an El Niño event the intraseasonal convection propagating eastward has more probability to reach the Amazon River basin, while in La Niña events the convection anomalies can modify the SACZ. In addition, there are extratropical described patterns that could influence tropical convection at intraseasonal scales. Liebmann et al. (1999) have shown evidence that submonthly variations in the cloudiness field that defines the SACZ are influenced by wavelike features propagating into the region from the extratropics. A signal associated with SACZ convection appears to be that of a Rossby wave originating within the midlatitude westerly belt of the Southern Hemisphere (Liebman et al., 1999; Cazes-Boezio et al., 2003).

Although there is a consensus about the forcing of oceanic waves by atmospheric signals from observational studies (Katz, 1997; Woolnough et al., 2000; Kessler et al., 1995; Hendoh et al., 1998), the oceanic anomalies impact on intraseasonal convection needs to be tested within a coupled model. As the convection oscillations are intimately related to the SST, which is in turn

strongly associated with oceanic waves within the equatorial band, in the next subsection the description and the role of the oceanic waves in the TAV are described.

1.5.2 Oceanic adjustment through long planetary waves

When the southeast trades intensify in spring, SST neat the equator start to fall. Surface waters remain warm to the north of 3ºN so that a temperature front appears near 3ºN. The latitudinal shear of the currents in that region becomes so large that instabilities result. The instabilities near 3ºN cause the thermal front to have westward-propagating undulations with a wavelength in of the order of 1000 km and a period between 3 and 4 weeks (Philander, 1990; Grodsky et al., 2005). These Tropical Instability Waves (TIW) are spatially heterogeneous and nonstationary in time and have been related to SST-wind feedback at intraseasonal scales in the equatorial Pacific (Hayes et al., 1989; Chelton et al, 2004), and they have also found over the Atlantic (Grodsky and Carton, 2006).

In addition, as shown by Matsuno (1966) and Moore (1968), the latitude band of the tropical oceans is the site of a singular set of equatorial waves that propagate eastward (equatorial Kelvin waves) or westward (Rossby waves). These waves are the result of the adjustment of the ocean to the wind stress changes (Philander, 1990; Schouten et al., 2005; Han et al., 2008). In comparison with the Pacific, where a large part of the ocean variability is explained by free waves, in the Atlantic, the narrow size of the basin induces a basin-wide response mostly in phase with the seasonal wind forcing, in an equilibrium response (Arnault and Périgaud, 1992).

Oceanic Kelvin and Rossby waves are inherent in the equatorial band and their sea level signature can be easily discerned from satellite measurements (Chelton and Schlax, 1996; Hill et al., 2000, among others, see figure 1.14). The SSH variable of the satellite measurements is more sensitive to the lowest baroclinic modes (Stammer, 1997; Brandt and Eden, 2005). These waves have been very important to explain theoretically the development of El Niño events (Suarez and Schopf, 1988).

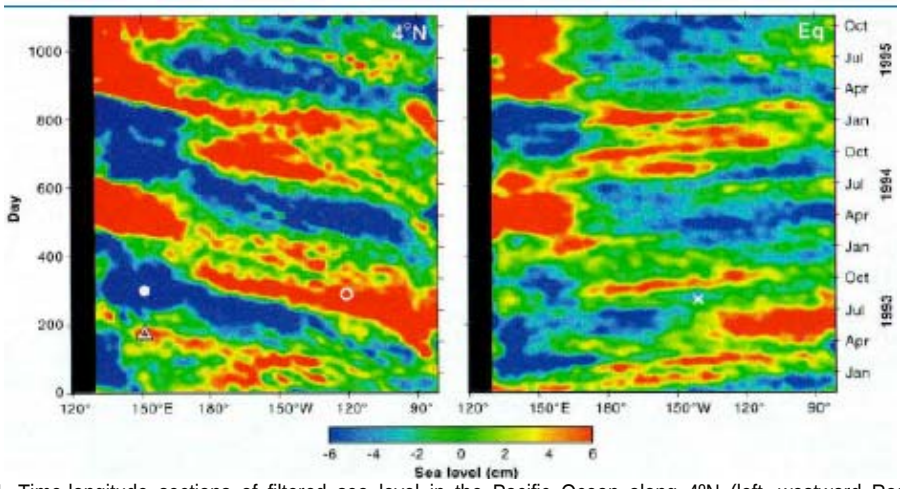

Figure 1.14. Time-longitude sections of filtered sea level in the Pacific Ocean along 4ºN (left, westward Rossby wave's propagation) and the equator (right, eastward Kelvin waves propagation). From Chelton and Schlax (1996).

While the intraseasonal variability of these waves is a current topic in relation to the convective activity at the equator (Kessler et al., 1995; Roundy and Kiladis, 2006, Matthews et al., 2007), the interannual variations of the oceanic waves are more difficult to study due to the limitation in the altimeter missions. In spite of the difficulty, some authors have suggested that the oceanic waves are active in TA interannual variability (Handoh and Bigg, 2000; Schouten et al., 2005). The oceanic Rossby wave has been already widely investigated over the Indo-Pacific and Atlantic basins and mainly over extratropical regions (Chelton and Schalax, 1996; Cipollini et al., 1996; Hill et al., 2000; Challenor et al., 2001; Brandt et al., 2002).

From the theory and the observations, the phase speed changes of these waves have been related to the stratification changes (Clarke, 1983; Johnson and McPhaden, 1993). Although it has been difficult to find a good agreement between the observations and the theory mainly off equatorial areas where the stratification changes are larger (Chelton and Schlax, 1996; Killworth et al., 1997; Greatbatch and Peterson, 1996), the two-layers model has been a good stratification simplification at the equator (Philander, 1990; Kessler et al.,1995, see appendix I), where the theoretical phase speed agrees better with the observed phase speed (Cravatte et al., 2003; Roundy and Kiladis, 2006). The amplitude of these waves is around 5 cm, the phase speed found for the first baroclinic Kelvin modes in the Atlantic has been found to be 2.6 m/s, 1.6 m/s, 0.8 m/s, and one third of this magnitude for the baroclinic Rossby modes (Chelton and Schlax, 1996; du Penhoat and Treguier, 1985; Katz, 1997; Illig et al., 2004 among others).

Off the equator, Moore (1968) established that the equatorial Kelvin waves could be reflected in the eastern boundary, and in part, could propagate poleward coastally trapped. Clarke (1983) also established analytically the equatorial wave reflection in an oceanic boundary without dissipation. Along the coast, one way of dissipation of the Kelvin wave energy is the radiation of Rossby waves from the eastern boundary (Gill, 1982). These oceanic waves features; on the one hand Kelvin waves can propagate eastward reaching the east ocean basin and poleward coastally trapped as far as the subtropics, and on the other hand Rossby waves can propagate westward radiating from the eastern boundary, make the waves a mechanism of propagating climate anomalies, meridionally from tropics to subtropics and zonally from one boundary to another, in a time able to be predictable (Kessler, 1991; Chelton and Schlax, 1996; Cipollini et al., 1996; Polito and Cornillon, 1997). Handoh and Bigg (2000) have suggested a self-sustained TA interannual mode through Kelvin-Rossby wave reflection at the coastal boundaries; however the intricacy of the Rossby reflection at the western boundary has been pointed out by many authors (Arnault et al., 1990; Handoh and Bigg, 2000; Illig et al., 2004).

Furthermore, Kelvin waves could be especially important in their interaction with the subtropical upwelling systems, in which the vertical movements partly explain the SST variations (Meyers et al., 1998; Vega et al., 2003; Hormazabal et al., 2002; Florenchie et al., 2003; Rouault et al., 2007). Rossby waves could also be important in relation to SST anomalies off equator (Hill et al., 2000; Leewenburgh and Stammer, 2001) and in impacting the western boundary currents (Jacobs et al., 1994).

1.5.2.1 Intraseasonal oceanic Kelvin wave: an equatorial coupled wave?

Kelvin waves are of particular interest because they are nondispersive, the fastest propagating wave along the equator and the only one capable to propagate eastward (see appendix I). In the Pacific, the observational analysis have found the dominant Kelvin wave period near 70 days, the dominant wavelength to be about 13000-14000 km, and the leading phase speed to be around 2.4 m/s (McPhaden and Taft, 1988; Cravatte et al., 2003), corresponding to the first vertical baroclinic-mode Kelvin wave. Other authors have found the period range of the intraseasonal Kelvin waves between 40-130 days in the Pacific (Johnson and McPhaden, 1993; Cravatte et al., 2003; Roundy and Kiladis, 2006), being the second baroclinic-mode also important (Philander, 1990; Cravatte et al., 2003). While, in the Atlantic, the Kelvin wave timescales are ranging 20-120 days, and phase speed ranging between first and second baroclinic modes (Katz, 1997; Illig et al., 2004; Han et al., 2008).

Localized surface forcing in the west can be communicated to the eastern Pacific in less than 3 months, and to the eastern Atlantic in less than one month (for the first baroclinic mode). One such mechanism by which these waves can remotely affect the SST, and hence the tropical climate, is via zonal advection of the mean SST gradients (Johnson and McPhaden, 1993; Leewenburgh and Stammer, 2001). Furthermore, a coupled mechanism feedback has been proposed between the horizontal extent of the surface westerlies/convection over the western Pacific and the strength of the intraseasonal Kelvin waves (Kessler et al., 1995), and perhaps playing a role in the onset and/or evolution of El Niño (Kessler, 1991). Vertical movements of the thermocline through the passage of

these waves also participate in affecting the SST. In addition, the wave-mean flow interactions have been documented in the EUC system (Johnson and McPhaden, 1993; Roundy and Kiladis, 2006).

In the Pacific, the main equatorial Kelvin wave forcing has been found to be the wind bursts in the western Pacific (Giese and Harrison, 1990; Philander, 1990; Johnson and McPhaden, 1993; Cravatte et al., 2003; among others). The coherence between the oceanic Kelvin wave and the wind at western equatorial Pacific has encouraged thinking that, in turn, they could be influenced by the MJO (Kessler et al., 1995) which dominates the atmospheric variability at intraseasonal scales. This hypothesis seems to be valid western date line (Hendoh et al., 1998), where the eastward phase speed propagation of the MJO-induced stress anomalies is similar to the gravest baroclinic Kelvin waves, hence, near resonant forcing results.
In the Atlantic, where the MJO forcing is not so obvious, there have been many studies suggesting and supporting the idea that part of the equatorial and coastal upwelling along the coast of the GG is remotely forced by the wind anomalies over the western equatorial Atlantic via Kelvin waves (Moore et al., 1978; Adamec and O'Brien, 1978; O'Brien et al., 1978; Servain et al., 1982; Picaut, 1983; Philander, 1990; Katz, 1997; among others). However, in comparison to the Pacific, further description of the intraseasonal Kelvin wave activity in the Atlantic, as well as its triggering mechanism is clearly needed.

1.5.2.2 Intraseasonal oceanic Rossby wave: The extratropical connection

The Rossby waves are planetary waves from the conservation of the potential vorticity on the surface of a rotating sphere (see appendix I). They are very efficient from extratropical latitudes to 5º latitude (Chelton and Schlax, 1996).
The importance attached to baroclinic planetary waves is due to two main reasons: 1) they can be regarded as the key response of the oceans to large-scale changes in atmospheric forcing by which information is transferred from the eastern ocean boundaries to the west (Gill, 1982). 2) they also interact with the strong western boundary currents such as the Kuroshio Current and the Gulf Stream, and maintain these currents (Jacobs et al., 1994). In short, as well as being one of the ways the ocean itself *responds* to climate events, Rossby waves may also delay the effects of these events and control the dynamics of climate change and weather variability (Challenor et al., 2004).

Additionally, the study of the Rossby waves is important as origin of the equatorial Kelvin wave. Indeed, analytically, one possible mechanism for the Kelvin wave triggering at western equator is the Rossby wave reflection at the American coast (Moore et al., 1978; O'Brien, 1978; Clarke, 1983, among others). Furthermore, it is interesting to note that the theoretical first baroclinic Rossby mode at ~4ºN coincide in space and phase speed with the TIW signal, therefore the Rossby waves could reinforce or hide the TIW signal at this latitude, modifying the surface winds there. Nevertheless, the Rossby-Kelvin relationship has been not clearly observed and the intraseasonal oceanic wave activity in the Atlantic has been overlooked by the scientific community.

1.6 Teleconnections linked to Tropical Atlantic Variability

Coupled feedbacks involved in TAV are much weaker than those in the Pacific, a feature that points out to an important role of the external influences that could explain its variability. At least two external sources of influence on the TAV have been proposed: Pacific ENSO and the NAO. Both of these phenomena peak during the boreal winter. The most common mechanism is by altering the northeasterly trade winds in the SNA region which can cause changes in the surface turbulent fluxes, modifying the SST with a maximum in spring (Enfield and Mayer, 1997). The external forcing is described in subsection 1.6.1.
In addition, as it has been suggested along section 1.4, TAV can impact on different climate events and basins. The impacts on rainfall variability are large in the surrounding continental areas, as the Nordeste Brazil and West Africa. TAV can also impact extratropical areas. The main impacts, on

West African (WA) summer rainfall and winter European precipitation variability are summarized in subsection 1.6.2.

1.6.1 External forcings

Atlantic surface-temperature anomalies just north of the Equator can be triggered by El Niño, as well as by changes in the strength of the trade winds associated with the NAO (Visbeck, 2002).
The well-known ENSO in the Pacific (Enfield and Mayer, 1997; Saravanan and Chang, 2000) and the NAO (Xie and Tanimoto, 1998; Okumura et al., 2001; Marshall et al., 2001) have their peaks in boreal winter and have an important influence on TAV. The Atlantic MM appears to be more affected than the EM by these remote influences. One reason for that is related to the different seasons to which these two modes are phase locked (Chang et al., 2006).
TAV is influenced not only by ENSO and the NAO, but also by atmospheric variability in the South Atlantic during boreal summer and winter (Barreiro et al., 2004), although a South Atlantic Oscillation has not been described. The variability of the South subtropical high seems to be part of a global pattern resembling the southern annular mode (Wallace, 2000).

The remote influence of ENSO, NAO and South Atlantic Atmosphere over TAV can interfere constructively or destructively regarding the acting feedback mechanisms, such as WES in the Meridional mode (Giannini et al., 2000; Barreiro et al., 2004).

1.6.1.1 ENSO

El Niño events are large climate disturbances which are rooted in the tropical Pacific Ocean, and occur every 3 to 7 years (Philander, 1990). They have a strong impact on the continents around the tropical Pacific, and climatic influence on half of the planet. The developed phase of El Niño is characterized by a temperature elevation at the ocean surface, from the coasts of Peru and Ecuador to the center of the equatorial Pacific Ocean. A consequence of such warming is the long-term perturbation of the weather systems over the lands around, notably heavy rains in usually dry areas, drought in normally wet regions. El Niño is also seen as the warm phase of the irregular climate oscillation called ENSO (El Niño/Southern Oscillation), which is caused by unstable interactions of the ocean and atmosphere.
It has been known for some time that a basin-wide warming takes place in the tropical Atlantic a few months after the El Niño in the Pacific peaks in December-January (Xie and Carton, 2004). Most of the studies suggest that, during and immediately following an El Niño event, precipitation generally decreases over the Equatorial Atlantic. The mature phase of a Pacific event occurs in November-January. ENSO warm event impacts on the northern TA SST as a basin-wide warming during its mature phase in boreal winter, and in the spring immediately following (Enfield and Mayer, 1997; Giannini et al., 2000; Saravannan and Chang, 2000; Alexander et al., 2002, see figure 1.15). This first-described remote teleconnection from statistics and modelling studies was explained as possibly mediated through a northern midlatitude "**atmospheric bridge**" (Nobre and Shukla, 1996). During warm ENSO events, diabatic heating anomalies in the tropical Pacific cause the northeasterly trades in the TA to weaken during boreal winter, which coincides with the mature phase of ENSO. This reduces the evaporational cooling, and generates a positive SST anomaly in the northern tropics. In this way, ENSO generally tends to aid the development of an SST gradient (MM) in the following boreal spring (Chiang et al., 2002; Giannini et al., 2001).
This could also be the pathway for Pacific influence on the Atlantic ITCZ. Chiang et al. (2000) have established a paradigm that suggests that the TA ITCZ has a preferred mode of variability (meridional displacement of the convection) and an increased subsidence over the TA from a warm ENSO event, forces this mode to favour a northward ITCZ displacement in April-May. Local feedbacks are likely to play an important role in setting up this response (Saravannan and Chang, 2000; Chang et al., 2008).

There have been described two main mechanisms from which the ENSO can modify TAV. On the one hand, the ENSO phenomenon can warm the northern TA Ocean **through Pacific North Atlantic (PNA) pattern** (Horel and Wallace, 1981; Handoh et al., 2006a; Kushnir et al., 2006). On

the other hand, ENSO and the subsidence associated with **Walker anomalous circulation** can interact mainly with the convection region in the Amazon basin, which can affect in turn the TA Walker circulation (Wang 2002a; Saravanana and Chang, 2000). Therefore the ENSO has a direct effect on the Atlantic Marine ITCZ through its influence on the circulation and vertical stability of the tropical atmosphere.
In addition, in boreal spring, the interplay between ENSO influence and the underlying state of the Atlantic interhemispheric SST gradient, present at the time of ENSO influence, is very important; when the gradient is preconditioned such that the North TA region is warmer than normal before the teleconnection from the equatorial Pacific affect the region, the impact of ENSO is stronger than normal and *vice versa* (Chiang et al., 2002).

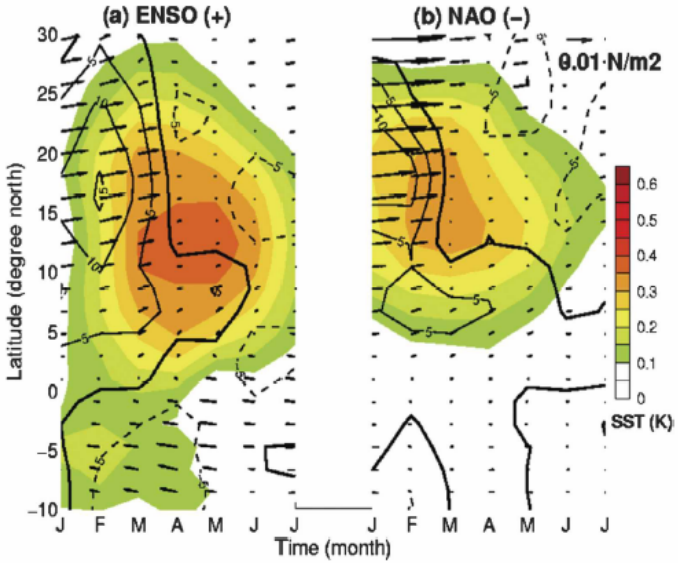

Figure 1.15. Regression of zonally averaged surface wind stresses (vector), surface heat flux (contour), and SST anomalies onto (a) Niño-3 and (b) negative NAO indexes as a function latitude and time lag (from the winter to the summer). The zonal average was taken between 40°W and 20°W. The Niño-3 index is defined as area-averaged SST anomaly over 5°S–5°N, 90°–150°W during boreal winter (December–February) and the NAO index is based on the winter (December–March) sea level pressure index of Hurrell (1995). From Czaja et al. (2002.)

The ENSO impact on the South TA is less established. Some authors (Mo and Hakinen, 2001; Handon et al., 2006b) have argued a teleconnection through the Pacific-South American pattern, but acting only on the quasi-biennial component of ENSO.

Regarding the ENSO's influence on the EM, reports from the existing literature are inconsistent. The EM has been suggested as largely independent of the ENSO (Zebiak, 1993; Latif and Grötzner, 2000). In another point of view, Wang (2002a) and Wang (2005) have shown that the Walker circulation is modified in the ENSO event, and the global equatorial band is also shifted, and it could create an EM. Carton and Huang (1994) showed that the strong 1984 warming resulted from zonal wind anomaly related to 1982/83 ENSO. Also, other authors have suggested that, at quasi-biennal timescales, a boreal winter warm ENSO event could induce an anomalous wind at the western Atlantic which can trigger an oceanic Kelvin wave reaching the eastern Atlantic in boreal summer, when it can be amplified by air-sea interactions, and thus developing an EM (Latif and Grotzner, 2000).
Nevertheless, some studies for the recent period, have observed a different Pacific-Atlantic connection that implies a **summer inter- basin SST gradient** (Wang, 2006; Keenlyside and Latif, 2007). Wang (2006) suggested the cross-Amazon winds, forced by the interhemispheric basin SLP gradient, as the major responsible of this association and influencing the tropical climate variability in a feedback way. This mechanism seems to be in agreement with other works that have shown a

sub-surface Kelvin wave propagation from the western equatorial Atlantic that could generate a Benguela Niño/EM (Florenchie et al., 2003; Rouault et al., 2007). This is also in agreement with Handoh et al. (2006b), who have shown that the link between the Amazonian rainfall and tropical Atlantic warm events is induced by ENSO.
The existence of such a simultaneous tropical Pacific-Atlantic relationship has also suggested the possibility of the more active role of the TAV over the Tropical Pacific. One possible mechanism could be through the whole convection belt shifts, and the enhancement of the convergence over the central Amazon/Panama basin or through the Western Hemispheric Warm Pool (WHWP) which is also a region of interaction between the ENSO and the TAV (Wang and Enfield, 2001).
This different Pacific-ENSO relationship could be associated with the climate shift, which took place in the late 1970s, and dramatically affected the El Niño (Miller et al., 1994) properties by changing the background tropical winds and the associated equatorial upwelling (Wang and An, 2002), the zonal pressure gradient (Cane et al., 1997) and the thermocline depth state (Federov and Philander, 2000). In addition, from decadal to multidecadal timescales, the Atlantic seems to affect ENSO (Chiang et al., 2000; Dong et al., 2006).

1.6.1.2 NAO

The NAO is the leading mode of North Atlantic climate variability, ranging from central North America to Europe and much into Northern Asia (Rogers, 1984; Hurrel, 1995; Hurrell et al., 2001). The NAO is a large scale seesaw in north Atlantic atmospheric mass, between the subtropical high and the subpolar low pressure systems. When the NAO is in its positive phase, low-pressure anomalies over Iceland and the Arctic combine with high-pressure anomalies across the subtropical Atlantic to produce stronger than-average westerly winds across the mid-latitudes. During this phase, climate is colder and drier than average over the northwest Atlantic and the Mediterranean, whereas conditions are warmer and wetter than average in northern Europe and the eastern United States (figure 1.16 and 1.17).

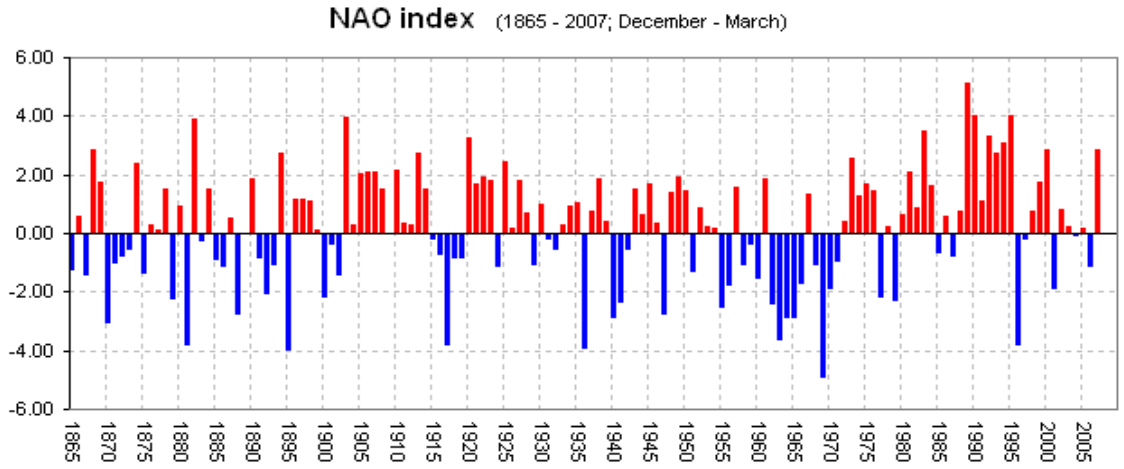

Figure 1.16. NAO index as normalized time-averaged pressure differences between Azores and Iceland stations representing its two centres of action. From NOAA.

Extensive climate impacts have been documented for the NAO (Marshall et al., 2001), and scientists speculate about its interaction with global warming (Shindell et al., 1999).
It has been defined a NAO index (figure 1.16) as normalized, time-averaged pressure differences between stations representing its two centres of action, such as the Azores and Iceland (Rogers, 1984; Hurrell, 1995; Hurrell et al., 2001). This index varies from year to year, but also exhibits a tendency to remain in one phase for intervals lasting several years, indicating the presence of an external forcing such as the ocean. A sharp increase of this index has occurred over the past 25 years. Since 1980, the NAO has remained in a strong positive phase, and displayed an upward trend that has been associated with the increase of temperature over the Northern Hemisphere (Marshall et al., 2001).

The NAO has been viewed as a regional expression of a more global pattern: the leading atmospheric mode of the winter Northern Hemisphere known as Artic Oscillation (AO) or Northern Annular mode (NAM, Thompson and Wallace, 1998; Marshall et al., 2001).

The phase of the NAO appears to be largely driven by atmospheric weather noise and, thus, internal variability. Although changes in ocean sea-surface temperatures have only a moderate effect on the NAO (Kushnir et al., 2002); the NAO has been associated with the HorseShoe (HS) SST pattern in the previous summer (Frankignoul, 1985; Cassou et al., 2004) and some predictable skill have been found from the HS subtropical lobe (Rodwell and Folland, 2002; Czaja and Frankignoul, 2002; Rodriguez-Fonseca and Castro, 2002)

The NAO causes extensive changes in the surface wind field which, in turn, strongly affects upper-ocean temperatures and circulation (Visbeck et al, 2003). The NAO is strongly coupled to the Atlantic SST Tripole pattern (Sutton and Allen, 1997). Although most of the variability of this oceanic pattern has been constrained to turbulent heat flux anomalies (Cayan 1992) and therefore considered as an atmospheric footprint, these SST anomalies could affect the atmosphere in a feedback way (Pan, 2005; Peng et al., 2005; Czaja and Frankignoul, 1999; Wen et al., 2005).

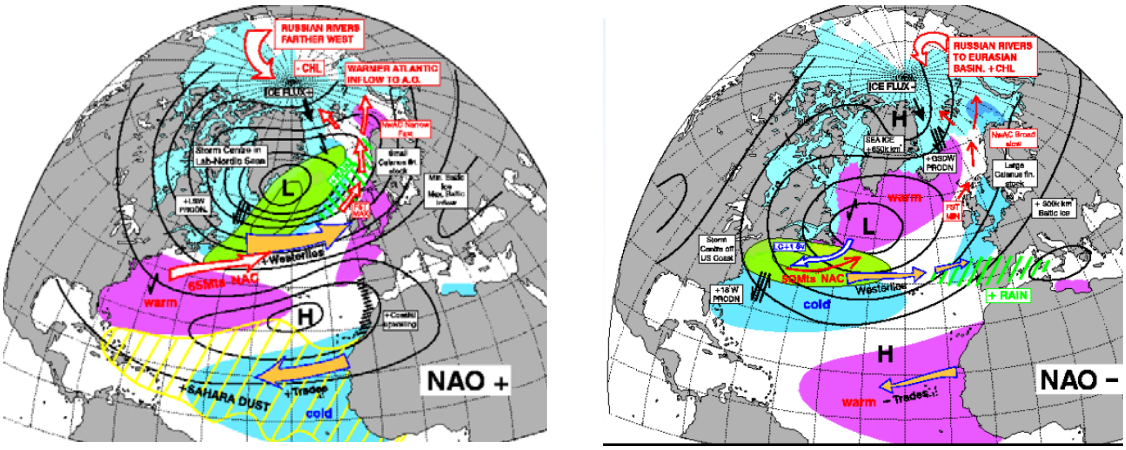

Figure 1.17. Positive (left) and negative (right) phase of the NAO and some of its impacts: the SST Atlantic Tripole, the anomalous surface winds, the modulation of the pressure systems and the anomalous precipitation in the northern Hemisphere. From NASA.

Basically, the NAO modulates the subtropical Azores High pressure system and therefore the trade winds strength, and in turn, SST variability over SNA (Okumura et al., 2001). Observational and modeling studies show that, during a strong positive (negative) NAO year northeasterly trade winds strengthen (weaken) and generate a negative (positive) SST anomaly in the tropical north Atlantic via changes in latent heat flux (Chang et al., 2000; Czaja et al., 2002; Kushnir et al., 2002). Therefore, a MM over the TA could be induced. However, there is a controversial debate about the role of the local air-sea feedback. Some authors (Kushnir et al., 2002; Chang et al., 2000) reason that local feedback is essential in maintaining the deep tropical response that consists of a cross-equatorial wind and a SST meridional gradient during boreal spring. However, Czaja et al. (2002) have argued that SST variability in 10ºN-20ºN band can be largely explained as the passive response of a slab mixed layer Ocean to changes in wind-induced latent heat flux associated with fluctuations in the subtropical high without invoking a role for local feedback.

As well as the north subtropical High variability can have an influence on the tropical north Atlantic SST, the south subtropical High largely influences the SST over the southern Atlantic hemisphere (Venegas et al., 1997; Sterl and Hazeleger, 2003).

1.6.2 Impacts

1.6.2.1 Impacts on the winter European climate

Winter climate variability over the Euro-Atlantic sector is largely linked to the *North Atlantic atmospheric variability patterns.* The main impacting atmospheric variability pattern is the NAO, which has been described above and, in less consideration, the Eastern Atlantic (EA) pattern.
Both phases of the NAO are associated with basin-wide changes in the intensity and location of the North Atlantic jet stream, storm tracks and associated synoptic eddy activity, and in large-scale modulations of the normal patterns of zonal and meridional heat and moisture transport (Hurrell, 1995). These modulations result in changes in temperature and precipitation patterns over the North Atlantic basin. In this way, one standard deviation anomaly in the NAO index is associated with more than 1ºC in the winter temperature over the northwest Atlantic and extend from northern Europe across much of Eurasia (Hurrell, 1995). During high (low) NAO index, drier (wetter) than normal conditions over much of central and southern Europe, the northern Mediterranean countries and west North Africa (from Iceland to Scandinavia) during boreal winter season (van Loon and Rogers 1978; Hurrell, 1995; Rodwell et al., 1999; Marshall et al., 2001, see figure 1.18).

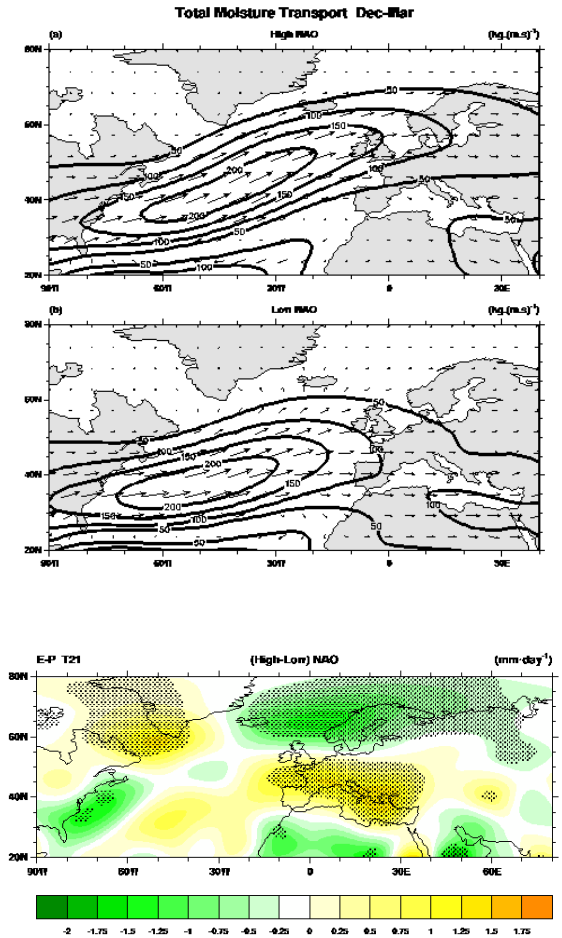

Figure 1.18. Vectors of the vertically integrated moisture transports for (A) high NAO index winters and (B) normal or low NAO index winters. Evaporation minus precipitation computed from the atmospheric moisture budget for high minus normal or low NAO index winters is shown in (C). The contour interval of the magnitudes is 50 kg/(m s) in (A) and (B). The contour interval in (C) is 0.5 mm/day, and the stippling indicates values significantly different from zero at the 5% level using a *t*-test. From Hurrell (1995).

From a regional point of view of the NAO impacts, the above described **Dipolar winter European precipitation pattern**, associated with the NAO, highly reflects part of observed winter climate variability over the Euro-Atlantic sector and, in particular, the leading mode of winter Iberian Peninsula (IP) precipitation variability, which has been largely studied by other authors (Zorita et al., 1992; Rodríguez-Fonseca, 2001; Rodriguez-Fonseca and Castro, 2002; Rodríguez-Fonseca and Serrano, 2002).

This precipitation dipolar pattern, with positive anomalous precipitation over IP and North Africa and negative anomalous precipitation over the British Isles and Scandinavian Peninsula (figure 1.18), implies a particular atmospheric signature which consists in anomalous surface southwesterly winds over the SNA, as well as positive SST anomalies and negative SLP anomalies in the region. However, the main variability mode over the European continent cannot be considered as the NAO by itself. A particular SLP dipole structure associated with SNA SST anomalies affecting specially the Iberian Peninsula and Northern Africa is an intrinsic mode (Rodriguez-Fonseca and Castro, 2002).
Regarding the TA forcing on the midlatitudes, meridional SST gradients in the tropics could act as "atmospheric brigde" through Hadley circulation changes, thus modulating NAO/mid-latitude variability (Marshall et al., 2001). The Tripole pattern of SST associated with the NAO has a strong signal in the tropics-subtropics, and the Subtropical branch has been pointed out to be the most active in affecting the atmosphere (Sutton et al., 2000b). Thus, variability of the jet stream could be exited by its southern flank (Robertson et al., 2000) through SST changes. The relatively large SST anomalies persistence (Frankignoul, 1985) from the previous summer to the next winter has been achieved as a possible predictor in winter precipitation anomalies (Rodwell et al., 1999). However, the eddies and mean flow interaction from the extratropical Atlantic has been reported to have a more important impact on winter European precipitation (Terray and Cassou, 2002; Losada et al., 2007).

1.6.2.2 Impacts on the summer West African climate

West African rainfall variability is one important topic for researches because extreme episodes, as droughts and floods in the Sahel, could be dramatic for developing countries depending on rain fed agriculture (Sultan et al., 2005).
At interdecadal timescales, the second part of the 20th century has known a very unusual evolution of Sahelian rainfall with a 20-year wet period followed by another 20-year dry period (Janicot et al., 2001). Such a devastating drought, which has consumed the entire sub-Saharan belt during boreal summer since the late 1960s, has been associated with SST trends due to multidecadal variations in the Atlantic (Folland et al, 1986; Ward, 1998) and Indian Oceans (Shinoda and Kawamura, 1994; Bader and Latif, 2003; Giannini et al., 2003; Lu and Delworth, 2005). Indeed, this observed drought tendency following the 1960s has been well reproduced with models only forced with observed SST (Giannini et al., 2003; Paeth and Hense, 2004; Lu and Delworth, 2005; Tippett, 2006; Tippett and Giannini, 2006). However, the GCMs fail to reproduce WA rainfall interannual variability (Moron et al., 2003; Tippett, 2006; Tippett and Giannini, 2006).

At interannual time scales, WA rainfall variability is modulated by both, oceanic (between 0-10ºN) and continental (between 10ºN-20ºN) convergence, by variations in the ITCZ position and land-atmosphere interactions respectively (Lamb, 1978). Historically, two main WA rainfall types have been identified: Dipole years, in which anomalies of opposite sign appear north and south of 10ºN, and non-Dipole years with anomalies of the same sign in the whole region (Motha et al., 1980; Janicot, 1992; Fontaine and Janicot, 1996; Janicot et al., 1996; Ward, 1998). In the 1979-2001 period, which is included in the drier decades, the interannual variability from enhanced precipitation dataset, has been characterized by perfect uncoupled modes between Sahelian rainfall and rainfall over the coast of the GG variability, associated with different global SST anomalies (Ward, 1998; Giannini et al., 2003).

Regarding the **rainfall variability over the coast of the GG (Guinea mode),** it is very coupled with the variability over the surrounding ocean areas. The GG has a large SST seasonal variation due to

the enhanced boreal summer eastern equatorial upwelling, which, in part, provokes the WAM onset. This minimum of SST in the GG is known as *Atlantic cold tongue*, and it is attributed to the intensification of southerly winds south of the GG during the WAM onset (Okumura and Xie, 2004).
Interannual WA rainfall anomalies occur during the normal rainy season of that region. In a regular seasonal cycle, the ITCZ starts to move northward in April and May, when the SST starts to fall and the trade winds intensify. In some cold (dry years) this northward movement can begin as early as February and in some warm, (wet years) it can begin as late as June (Philander, 1990; Janicot et al., 2007). For instance; in 1984, the ITCZ did not start to move northward until July.

The rainfall variability over the coast of the GG has been associated with the EM at very different periods of time, and at several different frequencies (Vizy and Cook, 2001; Ward, 1998; Fontaine and Janicot, 1996). The general mechanism has been shown by Vizy and Cook (2001), who have shown that such SST events enhance evaporation, and that the southerly flow across the Guinean Coast carries more moisture inland, leading to increased precipitation south from the usual latitude of the ITCZ.

Sahelian rainfall variations are influenced not only by changes in the position of the ITCZ but also by changes in the moisture flux convergence into the West African sector of the Sahel (Newell and Kidson, 1984). Warm surface waters south of the equator in the Atlantic favor the decrease of rainfall in the Sahel. If there are also high SST in the eastern tropical Pacific and cold surface waters over the northern Atlantic, then the likelihood of a drought in the Sahel is enhanced. Up to 50% of the interannual variance of Sahel rainfall is related to simultaneous interannual fluctuations in such a SST pattern (Folland et al., 1986; Philander, 1990).
Regarding this SST pattern related to Sahelian rainfall, for the wet period (1949-1969), the Sahel variations have been associated with the Atlantic MM (Janicot et al., 1996; Janicot et al., 2001). However, the role of the SNA SST on WA rainfall is still unclear. Some authors have suggested that variations in SNA SST play a passive role in WA rainfall variability (Ward, 1998; Mo et al., 2001). Vizy and Cook (2001) suggest that this region can have less influence over the Sahelian rainfall, mainly because the low-level flow between the SNA and WA is a northeasterly flow, which tends to isolate the continent from SNA, and because horizontal advection is not very effective in the tropics. However, from those GCM simulations, a response to positive SNA and GG SST anomalies together results in a westerly low-level flow perturbation that largely impacts on WA precipitation (Vizy and Cook, 2001).
The Sahelian rainfall variability has been highly associated with the Pacific oceanic basin variability (Ward, 1998; Janicot et al., 1998; Janicot et al., 2001). The ENSO seems to act by modifying the east-west divergent circulation, which modulates the vertical movements over WA, while the Pacific-Atlantic zonal atmospheric gradient, coupled to the opposite SST anomalies over both oceanic basins, can enhance the WA rainfall response (Janicot et al., 1998).
The association between the Mediterranean Sea SST anomalies and the WA rainfall has also been supported by observations (Rowell, 2001) and evidenced by model simulations (Rowell, 2003; Jung et al., 2006). Rowell (2003) has found positive Mediterranean SST anomalies related to anomalous positive Sahel rainfall through evaporation and southward moisture advection which enhances low-level convergence over the Sahel. There is still an open question about whether the Mediterranean basin plays an effective role or it is only a fingerprint of larger-scale forcing.

1.7 Predictability Issues

Since atmospheric processes have very short memory, to carry out atmospheric prediction on longer time scales, one needs to invoke some kind of memory in the boundary conditions (Marshall et al., 2001). This memory most likely resides in the ocean, and in particular in the SST anomalies. From 60's there have been a growing number of studies aimed to determine the role of the oceans in the observed short-term climate changes (Kushnir et al., 2006).
For climate forecasts, both the SST anomaly impact and its evolution have to be predicted, and work proceeded in the two directions. In the same matter, there has also been a need to obtain accurate model predictions of oceanic mixed layer depth and temperature, as well as a strong interest from the fisheries community in forecasting oceanic thermal anomalies, since their

biological implications can be important (Frankignoul, 1985). SST anomalies extend throughout the oceanic mixed layer, which has a large heat capacity. As a result, the SST anomalies are rather persistent, with a typical e-folding time of 3 months (Frankignoul, 1985).

Changes in large-scale ocean circulation may also alter tropical temperature gradients and thus modulate the location and strength of the Atlantic ITCZ. With rapid progress in the understanding of TAV, prospects are good for improved seasonal- to-interannual rainfall predictions in the tropical Atlantic (Visbeck, 2002). In the tropics, two-way interactions between ocean and atmosphere have proven to be essential, and some aspects of large-scale tropical climate anomalies, such as El Niño and the TAV, are predictable.

Regarding TA, if TAV were dominated by strong air-sea feedbacks, the variation of TAV would be largely governed by an oscillating mode and the predictability of TAV would be determined by the oscillating behavior of the coupled mode. In this case, a pronounced spectral peak near the frequency of the dominant mode would be expected, but actually pronounced spectral peaks are not found in TAV. However, there are some indications of a weak spectral structure at 11-13 years in the cross-equatorial SST gradient (Chang et al., 2006), spectral of 2-3 years in the EM has been also reported (Latif and Grotzner, 2000) as well as 2-3 years spectrum in the NAO (Marshall et al., 2001).
In addition, an important key in the TA predictability is the consideration that some processes are in a way phase-locked with the seasonal cycle. For instance, there are some evidences from observations and models that the *boreal summer*, eastern equatorial Atlantic variability involves a Bjerknes mechanism acting in EM. The *boreal spring* variability associated with the meridional SST contrast, and then the WES mechanism would be more effective.
Both statistical and dynamical models have difficulties in predicting the SST, and this partly reflects an incomplete understanding of the processes that govern SST evolution (Hurrell et al., 2006). The feedback mechanisms (explained in the previous 1.3.3 section) together with other remote impacts (explained in the section 1.5.1) all plays an important role in TAV. The existence of so many players involved in TAV, makes prediction of tropical Atlantic climate very challenging, and calls for sustained research and observations in the region.
For instance, the understanding of the adjacent oceans influence over continental rainfall is a way of improving the potential predictive skill of the different regions. This is one of the objectives of the CLIVAR panel. Substantial improvements have been done in relation to the WAM prediction in the context of the AMMA-EU project.

1.8 Aspects of Decadal to Multi-decadal Variability

World wide decadal or longer timescales variability modes can modulate interannual to intraseasonal variability. This statement has been a recent topic since there is longer observational climate record, and especially has been arisen in the last decades, when several tendencies and phase-shifts of many different climatic phenomena (tropical rainfall, NAO, ENSO…) have been observed. The background state seems to be determining to accomplish the understanding for some of these changes (Fedorov and Philander, 2000), and therefore from decadal to multidecadal footprint can be part of the explanation of the recent climate change, besides the reported global warming.

The lower frequency variability mode in the Atlantic is often called Atlantic Multi-decadal Oscillation (AMO) and constitutes a mode of natural variability of SST over the North Atlantic (Enfield et al., 2001; Zhang and Delworth, 2006). This mode usually implies an inter-hemispheric contrast of SST at both sides of the equator (i.e. Delworth and Mann, 2000). The AMO has been associated with changes in the Meridional Overturning Circulation (MOC, Vellinga and and Wood, 2002; Dong and Sutton, 2002; Latif, 2001; Latif et al., 2006), which also have variability on decadal to multidecadal timescales and it is closely tied to the poleward heat transport in the Atlantic.

Regarding the impacts, Zhang and Delworth (2006) have suggested that the AMO can cause the observed multidecadal variations of India and Sahel summer rainfall. In addition, Dong et al. (2006) have investigated the hypothesis that changes in Atlantic SST, through AMO, could play a role in the changes of the Pacific mean state and, in turn, in ENSO amplitude modulation on multidecadal scales. They have presented with coupled GCM that North Atlantic warming and South Atlantic cooling (positive phase of the AMO) leads to a reduction in ENSO variability, via atmospheric bridge, deepened thermocline and reduced vertical stratification of the equatorial Pacific Ocean, which in turn weakens ENSO variability. The link Pacific-Atlantic at multidecadal timescales have also suggested by (Chiang et al., 2000), they have reported from ITCZ proxy indices that the link Pacific-Atlantic through the walker circulation appears stronger in the 1980-90's and nonexistent in the 1950-60's. Decadal variability in the Pacific-Atlantic relationship has also been suggested by Keensilyde and Latif (2007), by analysing the different behaviour between basins in the last decades (1979-1999) in comparison with decades preceding the 1979 year.

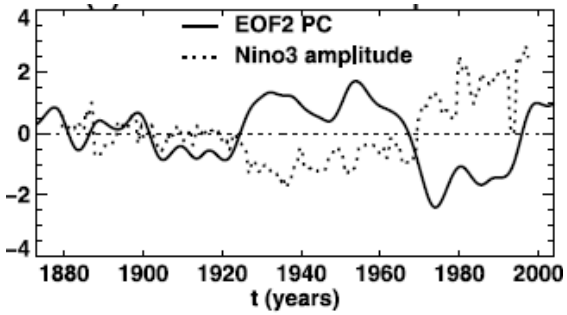

Figure 1.19. Normalized principal component PC2 of low frequency (low-pass filter with half power at period of 13.3 years) monthly SST variability (ºC) over Atlantic (full) and the normalized anomalous ENSO magnitude (defined as monthly Niño 3 index standard deviation in a running 13 year window) variation (dotted). From Dong et al., (2006).

Another mode at multidecadal timescales has been described implying the whole tropical belt divergent circulation (Chelliah and Bell, 2004). The Tropical Multidecadal Mode (TMM) captures the global climate regimes observed during the 1950s–60s and 1980s– 90s, and the 1970s transition between these climate regimes. The TMM also captures all key structural aspects of the NAO, thus, linking climate fluctuations in the global Tropics to multidecadal variations in the NAO.

As in the Atlantic, the North Pacific has a similar multidecadal variability which has also been associated with deep ocean circulation variability and it seems to affect the interannual modes. The most important is the Pacific Decadal Oscillation (PDO, Mantua and Hare, 2002). The PDO is detected as SST anomalies in the Pacific Ocean, north of 20°N. During a positive phase the west Pacific becomes cool and part of the eastern ocean warms; during a negative phase the opposite pattern occurs. The PDO can have an impact not only on the ENSO phenomena, but also on the north Atlantic variability.
The global climate seems to be more interrelated at low-frequency climate variability; the last two decades 1979-2001 (the decades preceding 1979) shows a negative (positive) phase of AMO and TMM, as well as positive (negative) phase of the PDO and NAO with stronger (weaker) Niño events.

2. HYPOTHESES AND OBJECTIVES

2.1 Initial Hypotheses:

The initial hypotheses to be considered can be summarized as follows:

- *The Tropical Atlantic Variability (TAV) is a determinant component of the global climate variability*.
  TAV has, in particular, an enormous social and economic impact on the local populations of parts of South America and Africa. Changes in the precipitation can have dramatic consequences on water resources, especially in the continental tropics, but also in the Mediterranean region.

- *Important changes in the TAV can be found for the 1979-2002 period*.
  A broad range of phenomena have been reported after the climate shift of the 70's: drier than normal conditions over the Sahel and the Amazon river basin (Janicot et al., 1996; Giannini et al., 2003), global SST tendencies, weakening of the Walker circulation (Venchi et al., 2006), expansion of the tropical belt width (Seidel et al., 2008), phase-shifts events of NAO pattern (Palmer, 1998), Atlantic influence on the ENSO-Indian monsoon relationship (Kucharski et al., 2008) and changes in the Pacific background state. Therefore, the study of the observed low-frequency variability along the 1979-2002 period could give some insights to the understanding of the climate variability in global warming conditions which can differ from the studies which focused on the decades preceding 1979.

- *The 1979-2002 period is reliable in terms of data accuracy*.
  The satellite measurements have been included in the databases, as CMAP precipitation data (Xie and Arkin 1997), ERA-40 Reanalysis (Uppala et al., 2005), etc... Also the number of observations over the TA is larger than in previous decades thanks to international programs (i.e. PIRATA, AMMA-EU...). The amount of available simulated data has also increased (Arnault and Périgaud, 1992).

- *The precipitation changes are closely related to known atmospheric variability patterns*.
  These patterns include, among others, the NAO which has been related to anomalous precipitation over the continents in the North Atlantic sector (Hurrel, 1995), and the ITCZ-Meridional mode which has been connected to the rainfall over the north of South America (Xie and Carton, 2004; Chang et al., 2006; Hurrell et al., 2006 among others).

- *Climate variability patterns linked to precipitation over Europe and West Africa covary with tropical SST anomalies*.
  The NAO, which affect rainfall over Iberian Peninsula and North Africa (Rodriguez-Fonseca, 2001), has been associated with the SST Atlantic Tripole pattern (Hurrell, 1995; Rodwell et al., 1999). The Equatorial Mode (EM) affects the rainfall over the coast of the GG (Folland et al., 1986; Janicot et al., 1996; Ward, 1998).

- *SST changes can persist and/or evolve in time and, consequently, be important for predictability issues.*
  The predictability of atmospheric patterns from the SST has been already reported by other authors (Frankignoul, 1985; see Hurrell et al., 2006 for a review).

- *Upper ocean processes can determine the TA SST variability*.
  SST variability can be due to both, atmospheric and oceanic forcing. Although the ocean's role has been neglected in many works related to climate variability (Czaja et al, 2002; Seager et al., 2001), the upper ocean processes (ocean waves, mixing

processes, upwelling…) can have a decisive role in the creation/evolution or persistence of the interannual SST patterns. Also the ocean could be important in its adjustment from wind/SST changes (Suarez and Schopf, 1988). In particular, the equator and the coast are the most exposed areas that can be driven by ocean dynamics (Carton et al., 1996; Mayer et al., 2001; Seager et al., 2001).

- *The study of the Intraseasonal processes can highlight some aspects of interannual TAV.*
  There are some ocean processes that are difficult to discern at interannual time scales. These processes can be highlighted on intraseasonal time scales and, for the particular case of the TA, they can modulate the principal annual and interannual basin signals. In particular, many processes over the TA have large intraseasonal variability (i.e. West African Monsoon, the oceanic cold tongue over the eastern equatorial Atlantic, the seasonal coastal upwelling at the western African coast …). Possible mechanisms that could be important for understanding the above-mentioned processes might imply oceanic wave propagation. Furthermore, the intraseasonal Kelvin wave activity in the Pacific Ocean has been related to convection activity, which could be important in climate terms (Kessler et al., 1995; Hendon et al., 1998; Roundy and Kiladis, 2006).

Although rapid progress has been achieved in recent years in understanding the TA air-sea interaction mechanisms, impacts and teleconnections, there are some TAV aspects that are still under debate. The study of the ocean-atmosphere feedbacks is an important key for the understanding of the SST evolution. A revision of the TAV on the basis of the new datasets is needed. In addition, only a few works have investigated the intraseasonal Kelvin waves in the TA, and there is a need to fill this gap through further investigation.

Therefore, the aim of this work is to understand the interannual and intraseasonal Tropical Atlantic Variability in the recent period (1979-2001), including the ocean role and using enhanced observations. To do this, the SST patterns, their impacts and the air-sea interactions are considered.

2.2 Specific Objectives and Outline of Results:

The specific aims to be achieved in the present PhD Thesis, considering the previous hypotheses, are divided into different separated blocks, according to the timescales of the involved processes and their impacts.

Regarding the **Interannual Tropical Atlantic Variability**, the main goal of this work is twofold:

1. To determine the TAV SST patterns with an impact on climate variability and, in particular, on the precipitation over West African during the monsoon season and over the Euro-Atlantic sector in winter, with the aim of finding possible seasonal oceanic predictors
2. To clarify the ocean's role on the origin, development and damping of these ocean-atmosphere modes.

In order to get the principal SST patterns related to the anomalous precipitation over the extratropical north Atlantic area, a discriminant analysis study of the TA SST anomalies and the winter European anomalous precipitation is performed. Also, several statistical analyses of the SST and the upper ocean processes in relation to the extratropical variability are presented. The questions posed could be:

What are the Atlantic SST patterns related to the winter European anomalous rainfall?

Is there any predictability of these patterns from the SST?

How much of the SST variability can be explained by the atmospheric forcing and oceanic processes?

In Chapter 4.1.1, the interannual SST variability related to North Atlantic anomalous climate is studied and the above-mentioned questions are attempted to be answered. The first part is the study of the European and Northern African (ENA) winter precipitation variability, determining the most influential Atlantic oceanic areas on these rainfall patterns. In this part of the chapter, the rainfall variability in ENA has been connected to changes in the Subtropical North Atlantic (SNA). Continuing this study, in the second part, the generation of the SNA SST anomalies is examined by considering the atmospheric fluxes and the subsurface thermal variability.

The Tropical Atlantic and Mediterranean SST patterns related to the summer West African rainfall variability are also studied. In this case, and in the framework of the AMMA-EU project, the interest resides in determining the time evolution of the anomalous SST patterns coupled to the WA summer rainfall variability. In this way, the WAM potential predictability will be addressed. The obtained SST patterns will be used as boundary conditions to perform sensitivity experiments with different AGCMs involved in AMMA-EU. The question to be answered will be:

What are the time-evolving SST patterns associated with the anomalous West African rainfall?

Once the covariability patterns result from the development of the EMCA methodology, these time-evolving SST patterns coupled to the WA rainfall anomalies need to be studied in order to understand:

What are the causes of the origin, development and damping of those SST modes, considering both, atmosphere and ocean dynamics in their interactions?

What is the global signature of these SST patterns?

In Chapter 4.1.2 the interannual TA SST variability related to the WA rainfall variability is studied and the above-mentioned questions are tried to be answered. The Chapter 4.1.2 consists in the analysis of the first two time-evolving SST modes which covariate with the WA rainfall. The

leading mode is investigated in depth since it shows a tight coupled behaviour and because the ocean is playing a key role in the evolution of the mode. Finally, and considering the time period of study, the global patterns of the first two covariability modes and the teleconnections with other tropical basins variability will be addressed. In this way, the recent trends in the connections found, in the context of anthropogenic and natural climate variability, will be outlined.

Concerning the **intraseasonal Tropical Atlantic Variability,** the aim of this work is to give some insights about the oceanic wave's activity over the Tropical Atlantic basin and its climate implications. The questions posed could be:

Can Kelvin waves be observed in the Atlantic and in which timescales?

What are their main characteristics?

What are the causes of triggering equatorial Kelvin waves? Is any Rossby-Kelvin relationship?

How does the wind stress affect their features along the trajectory?

What is the spatial scale of the forcing of Kelvin waves?

Can oceanic Kelvin waves have any role on the Tropical Atlantic intraseasonal variability?

Chapter 4.2 is focused on investigating the oceanic waves in the TA. The first part constitutes the morphology of the intraseasonal Kelvin wave activity. Through filtering processing, observed and modelled data and statistical tools, it is possible to characterize the main properties and to infer teleconnection mechanisms. The natural continuation is to understand the processes in its interaction with the overlying atmosphere and to give some insight on the SST impacts.
Finally, a discussion and a summary of the main conclusions will be stated in Chapter 5 and 6 respectively. In addition, the atmospheric dynamics of the extratropical teleconnections that are forced by tropical convection associated with summer SST anomalies (EM and Horseshoe/Tripole patterns) are investigated and presented in Appendix II.

2. HIPÓTESIS Y OBJETIVOS

2.1 Hipótesis iniciales:

Las hipótesis iniciales que se consideran, se enumeran a continuación:

- *La Variabilidad del Atlántico Tropical (TAV[1]) es una componente determinante en la variabilidad del clima global.*
  La TAV tiene, en particular, un enorme impacto social y económico sobre la población local de buena parte de Sudamérica y África. Los cambios en la precipitación pueden tener consecuencias dramáticas en los recursos hídricos, especialmente en los continentes tropicales, pero también en la región mediterránea.

- *Cambios importantes en la TAV podrían encontrarse en el periodo 1979-2002.*
  Se ha documentado un amplio espectro de fenómenos después de la llamada "transición climática" de los años 70: condiciones más secas de lo normal sobre el Sahel y la cuenca del río Amazonas (Janicot et al., 1996; Giannini et al., 2003), tendencias globales de la temperatura superficial del mar (SST[2]), debilitamiento de la circulación de Walker (Venchi et al., 2006), expansión de la anchura del cinturón tropical (Seidel et al., 2008), cambio de fase de los eventos de la NAO[3] (Palmer, 1998), influencia del Atlántico en la relación ENSO[4]-monzón Indio (Kucharski et al., 2008) y cambios en el estado medio del Pacífico. Por tanto, el estudio de la variabilidad de baja frecuencia observada a lo largo de este período podría aportar algunos elementos para la comprensión de la variabilidad climática en condiciones de calentamiento global. Los nuevos resultados podrían diferir de aquéllos procedentes de estudios centrados en las décadas precedentes a 1979.

- *El período 1979-2002 es fiable en términos de precisión de los datos.*
  Las mediciones desde satélite han sido incluidas en las bases de datos, como los datos de precipitación CMAP (Xie y Arkin 1997), el Reanálisis ERA-40 (Uppala et al., 2005), etc... También el número de observaciones sobre el Atlántico Tropical (TA[5]) es mayor que en décadas previas, gracias a programas internacionales (i.e. PIRATA, AMMA-EU...). El número de datos simulados disponibles también ha aumentado (Arnault y Périgaud, 1992).

- *Los cambios en la precipitación se relacionan íntimamente con patrones de variabilidad atmosférica conocidos.*
  Estos patrones incluyen, entre otros, la NAO, que se ha relacionado con precipitación anómala en los continentes del sector Nor-Atlántico (Hurrel, 1995); y el modo ITCZ[6]-Meridional, que se ha relacionado con precipitación anómala en el norte de Suramérica (Xie y Carton, 2004; Chang et al., 2006; Kushnir et al., 2006 entre otros).

- *Los patrones de variabilidad climática ligados a las precipitaciones anómalas en Europa y África del Oeste covarían con anomalías de la SST en los trópicos.*
  La NAO ha sido asociada al patrón de SST conocido como Tripolo Atlántico (Hurrell, 1995; Rodwell et al., 1999). El Modo Ecuatorial (EM[7]) tiene un patrón de SST muy

[1] Del inglés Tropical Atlantic Variability
[2] Del inglés Sea Surface Temperature
[3] Del inglés North Atlantic Oscillation
[4] Del inglés El Niño-Southern Oscillation
[5] Del inglés Tropical Atlantic
[6] Del inglés Inter-Tropical Convergence Zone
[7] Del inglés Equatorial Mode

definido y afecta a la lluvia sobre la costa del Golfo de Guinea (Folland et al., 1986; Janicot et al., 1996; Ward, 1998).

- *Los cambios de la SST pueden persistir y/o evolucionar en el tiempo y, consecuentemente, ser importantes elementos de predecibilidad.*

  La predecibilidad de los patrones atmosféricos a partir del conocimiento de las anomalías de SST ha sido ampliamente propuesto (Frankignoul, 1985; ver Hurrell et al., 2006 como resumen).

- *Los procesos del océano superior puede determinar la variabilidad de la SST en el TA*. La variabilidad de la SST puede ser debida al forzamiento tanto atmosférico como oceánico. A pesar de que el papel del océano ha sido desechado en la mayoría de los trabajos relativos a la variabilidad climática (Czaja et al, 2002; Seager et al., 2001), los procesos del océano superior (ondas oceánicas, procesos de mezcla, afloramientos...) pueden tener un papel determinante en la creación, evolución o persistencia de los patrones de la SST interanuales. También el océano puede ser importante a la hora de explicar el ajuste a los cambios en el viento/SST (Suarez y Schopf, 1988). En particular, el ecuador y la costa son las áreas más expuestas que pueden ser influidas por la dinámica del océano (Carton et al., 1996; Mayer et al., 2001; Seager et al., 2001).

- *El estudio de los procesos intraestacionales puede resaltar algunos aspectos de la TAV interanual.*
  Hay algunos procesos oceánicos que son difíciles de discernir a escalas de tiempo interanuales. Estos procesos pueden ser enaltecidos en escalas de tiempo intraestacional y, para el caso particular del TA, pueden modular las principales señales anuales e interanuales de la cuenca. En particular, muchos procesos en el TA poseen una amplia variabilidad intraestacional (i.e. el monzón de África del Oeste, la lengua fría oceánica sobre el Atlántico este-ecuatorial, el afloramiento estacional costero en la costa africana occidental etc). Posibles mecanismos que podrían ser importantes para entender los procesos mencionados anteriormente implicarían la propagación de ondas oceánicas. Más aún, la actividad de ondas de Kevin a escalas intraestacionales en el océano Pacífico ha sido relacionada con actividad convectiva, lo cual podría ser importante en términos climáticos (Kessler et al., 1995; Hendon et al., 1998; Roundy y Kiladis, 2006).

A pesar de que se ha alcanzado un rápido progreso en los últimos años en la comprensión de los impactos, las teleconexiones y los mecanismos de interacción océano-atmósfera en el TA, hay algunos aspectos de la TAV que están todavía en debate. El estudio de los mecanismos de realimentación océano-atmósfera es clave para entender la evolución de la SST. Por tanto, es necesaria una revisión de la TAV en base a los nuevos conjuntos de datos. Además, sólo unos pocos trabajos han estudiado la actividad de las ondas de Kelvin a escalas intraestacionales en el TA, y es necesario cubrir este vacío con investigación específica a este respecto.

El propósito de este trabajo es comprender la Variabilidad del Atlántico Tropical interanual e intraestacional en el período reciente (1979-2001), incluyendo el papel del océano y usando observaciones mejoradas. Para ello se han considerado los patrones de SST, sus impactos y las interacciones océano-atmósfera.

2.2 Objetivos Específicos y Perfil de Resultados:

Los objetivos específicos a alcanzar en la presente Memoria de Tesis, considerando las hipótesis previas, se dividen en dos apartados diferentes separados de acuerdo a las escalas temporales de los procesos involucrados y sus impactos.

En lo que respecta a la **Variabilidad Interanual del Atlántico Tropical**, el objetivo principal de este trabajo es doble:

1. Determinar los patrones de SST de la TAV que tienen un impacto en la variabilidad climática y, en particular, en la precipitación sobre África del Oeste durante la estación monzónica; y sobre el sector Euro-Atlántico en invierno, con el propósito de encontrar posibles predictores oceánicos estacionales.

2. Clarificar el papel del océano en el origen, desarrollo y amortiguamiento de estos modos acoplados.

Para determinar los principales patrones de SST relacionados con la precipitación anómala sobre el área extratropical Nor-Atlántica, se lleva a cabo un estudio de análisis discriminante de las anomalías de la SST del TA y la precipitación anómala del invierno europeo. Además, se presentan varios análisis estadísticos que involucran a las anomalías de SST y a los procesos del océano superior; en relación con la variabilidad extratropical. Las preguntas a plantear podrían ser:

¿Cuáles son los patrones de SST del Atlántico relacionados con la lluvia invernal anómala en el sector Euro-Atlántico?

¿Existe alguna predecibilidad de estos patrones a partir de la SST?

¿En qué medida la variabilidad de la SST puede ser explicada por el forzamiento atmosférico y los procesos oceánicos?

En el Capítulo 4.1.1 se estudia la variabilidad interanual de la SST relacionada con las anomalías climáticas del Atlántico Norte y se intenta responder a las cuestiones planteadas anteriormente. La primera parte abarca el estudio de la variabilidad de la precipitación invernal en Europa y el Norte de África (ENA), determinando las áreas oceánicas más influyentes del Atlántico en estos patrones de lluvia. En esta parte del capítulo, la variabilidad de lluvia en ENA se ha conectado con cambios en el Atlántico Norte Subtropical (SNA[8]). Como una continuación de este trabajo, en la segunda parte se estudia la generación de anomalías de SST del SNA, considerando los flujos atmosféricos y la variabilidad térmica del océano superior.

Los patrones de SST del Atlántico Tropical y el Mediterráneo relacionados con la variabilidad de la lluvia estival en el Oeste de África (WA[9]) también se analizan. En este caso, y en el marco del proyecto AMMA[10]-EU, el interés reside en determinar la evolución temporal de los patrones anómalos de la SST acoplados a la variabilidad de lluvia estival de WA. Los patrones de la SST obtenidos se utilizarán como condiciones de borde para efectuar experimentos de sensibilidad con diferentes AGCM[11] dentro de la comunidad de AMMA-UE. La pregunta a responder será:

¿Cuáles son los patrones dinámicos de SST asociados con la lluvia anómala en el Oeste de África?

[8] Del inglés Subtropical North Atlantic
[9] Del inglés West Africa
[10] Del inglés African Mosoon Multidisciplinary Analysis
[11] Del inglés Atmospheric General Circulation Model

Una vez que los patrones de covariabilidad han sido determinados, a partir del desarrollo de la metodología EMCA[12] (ver Metodología), estas estructuras de SST que evolucionan en el tiempo y que están acopladas a las anomalías de lluvia en el WA, han de ser analizadas para entender:

¿Cuáles son las causas del origen, desarrollo y amortiguamiento de estos modos de la SST, considerando tanto la dinámica atmosférica como la oceánica en sus interacciones?

¿Cuál es la estructura global que presentan estos patrones de SST?

En el Capítulo 4.1.2 se estudia la variabilidad interanual de la SST en el TA, relacionada con la variabilidad de lluvia en el WA, intentando dar respuesta a las preguntas mencionadas. El Capítulo 4.1.2 consiste en el análisis de los dos primeros modos de SST que evolucionan en el tiempo y que covarían con la lluvia en el WA. El modo principal, el Modo Ecuatorial, se investiga a fondo ya que muestra un comportamiento fuertemente acoplado con la lluvia anómala en el Golfo de Guinea; y porque el océano juega un papel clave en la evolución del mismo. Finalmente, y considerando el período de estudio, se investigan los patrones globales de los primeros dos modos de covariabilidad y las teleconexiones con la variabilidad de otras cuencas tropicales. De esta manera, se perfilarán las tendencias recientes respecto a las conexiones encontradas, en el contexto de la variabilidad antropogénica y natural del clima.

En lo que respecta a la **Variabilidad intraestacional del Atlántico Tropical,** el principal propósito de este trabajo es proporcionar algunos elementos sobre la actividad de las ondas oceánicas en la cuenca del Atlántico Tropical y sus implicaciones climáticas. Las preguntas realizadas podrían ser:

¿Se pueden observar ondas de Kelvin en el Atlántico y en qué escalas temporales?

¿Cuáles son sus principales características?

¿Cuáles son las causas que desencadenan las ondas de Kelvin ecuatoriales? ¿Hay alguna relación Rossby-Kelvin?

¿Cómo afecta el esfuerzo del viento a sus características a lo largo de la trayectoria?

¿Cuál es la escala espacial del forzamiento de las ondas de Kelvin?

¿Podrían las ondas de Kelvin oceánicas tener un papel en la variabilidad intraestacional del Atlántico Tropical?

El Capítulo 4.2 se centra en investigar las ondas oceánicas en el TA. La primera parte constituye el estudio de la morfología de la actividad de las ondas de Kelvin a escalas intra-estacionales. A través del proceso de filtración de los datos observados y modelados y las herramientas estadísticas; es posible caracterizar las propiedades más importantes e inferir mecanismos de teleconexión. La continuación natural es comprender los procesos en su interacción con la atmósfera superior, y aportar algún elemento sobre los impactos en la SST.
Finalmente, se establecerá una discusión y un resumen de las principales conclusiones en el Capítulo 5 y 6 respectivamente. Además, la dinámica atmosférica de las teleconexiones extratropicales forzada por la convección tropical asociada a las anomalías de SST estivales (patrones del EM y Herradura/Tripolo) se investiga y los resultados se presentan en el Apéndice II.

[12] Del inglés Extended Maximum Covariance Analysis

3. METHODOLOGY AND DATA

Climate variability is, to a large degree, the study of the statistics in our climate (von Storch and Zwiers, 2001). For this reason, most of the methodology used in this PhD Thesis is based on powerful tools of mathematical statistics, ranging from simple methods to determine the significance of a correlation coefficient, to sophisticated techniques that give some clues to the understanding of the dynamics of the climate system.

Classical description of the climate consisted primarily of estimates of its mean state and estimates of its variability about that state, such as its standard deviations and other simple measures of variation. The paradigm of climate research evolved from the purely descriptive approach towards an understanding of the dynamics of climate with the advent of computers and the ability to simulate the climatic state and its variability (von Storch and Zwiers, 2001).

Climate variability studies are based on the statistical analysis of large fields from different variables in the spatial-temporal domain. These fields are the basic ingredients to conform the conclusions of the hypotheses. The use of high quality data is, for this reason, an initial condition required for the correct development of the research.

In the next sections an overview of the principal statistical techniques applied along this work will be done. Sections 3.1 and 3.2 make a shallow description of the discriminant analysis techniques and spectral analysis methods used in this study, including some variants that are personal contributions to the methodology. Finally, Section 3.3 is focused in the data used along the study.

3.1 The Election of the Anomalies

The atmospheric and oceanic fields from the available datasets contain measurements from the largest and generous “laboratory”: the nature. The timeseries of the data can be considered as the sum of the mean state plus the variations from the mean known as anomalies. In this way the field Y can be decomposed as $Y=Y_m+Y'$. Therefore, the anomalies (Y') are defined as the deviation of an atmospheric or oceanic field (Y) in a given region over a specified period from the long-term average value (Y_m) for the same region. The anomalies depend on the data temporal resolution and the timescales of the processes considered: annual, monthly, or weekly anomalies.

3.2 Discriminant Analysis

The characterization of the interannual and intraseasonal variability of the different climate fields involves the use of a big amount of data, because of the large spatial and temporal extension of the study areas. For this reason, it is necessary to discriminate the available information and to resume the most susceptible areas in the system variability. Several statistical techniques are used, extracting as most information as possible that could, in turn, help to understand a particular problem. The most popular techniques are the Empirical orthogonal Functions (EOF) analysis and the Maximum Covariance Analysis (MCA). The objective of these tools is, in the case of the EOF, to look for spatial and temporal patterns that could explain the largest percentage of variance of a particular field. For MCA, the spatial and temporal patterns explaining the major percentage of covariance between two related fields is found (Wallace and Gutzler, 1981; North, 1984; Bretherton et al., 1992; von Storch and Frankignoul, 1998; von Storch and Zwiers, 2001; Rodríguez-Fonseca, 2001).

Along this work, these statistical tools and some important variants derived from them are applied. These variants are personal contributions to the methodology which have been performed to address particular problems presented in the study.

3.2.1 Empirical orthogonal Functions Analysis

The EOF analysis (also named as Principal Component Analysis, von Storch and Zwiers, 1998) searches for structures that explain the maximum temporal variance in a pool of bi-dimensional data, where one dimension (space) is used to represent the spatial structures (patterns) and the other dimension (time) represents the time samples (Von Storch and Frankignoul, 1998). The analysis produces a set of structures in the spatial dimension, the so-called Empirical Orthogonal Functions (EOFs) and complementary structures in the temporal dimension (time weights) called Principal Components (PCs), which are related one to one with EOFs (figure 3.1). Each pair of space-time structures, together with the explained percentage of variance, constitutes a mode.

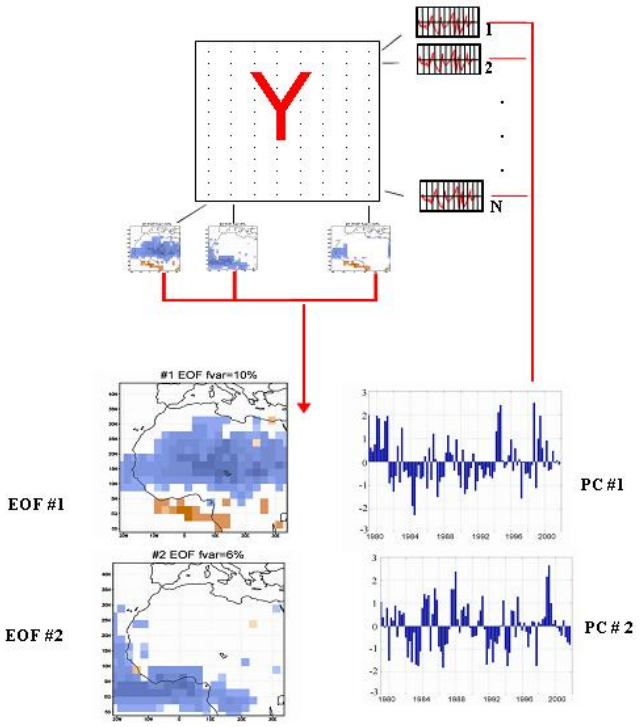

Figure 3.1. Scheme of the Empirical Orthogonal Functions methodology.

The mathematical problem and the assumptions are:
Let be a field of temporal anomalies X of a variable X_d after sustracting the mean X_m for each point of the grid, $X=X_d-X_m$, with dimension (m, n) space, time. Being R the covariance matrix of the temporal dimension t,

$$R = \frac{1}{N}\sum_t \vec{X}(t)\vec{X}(t)^T \quad , \qquad [3.1]$$

the EOF analysis consists in an eigenvalue decomposition of the covariance matrix R. The eigenvalue analysis is able to decompose any no-singular square matrix, in the way;

$$RE = LE \qquad [3.2]$$

The columns of the matrix *E* constitute the so-called eigenvectors (e_i) of *R;* and the elements of the diagonal of the matrix *L* are the eigenvalues (λ_i) of *R*. From a number of *K* modes, the field *X* could be reconstructed as a linear combination of the orthogonal spatial patterns $\vec{e}^{\,k}$ (EOFs) and the associated coefficients α_k (PCs) in the way;

$$\vec{X}(t) = \sum_{k=1}^{K} \alpha_k(t)\vec{e}^{\,k} \qquad [3.3]$$

This means that the original pool of data *X* can be reconstructed, from a determined number of modes that explain a high percentage of the variance, in such a way that the mean-squared error (mse) respect to the original data is minimum (von Storch and Frankignoul, 1998).

$$mse = \sum_{t} \left[\vec{X}(t) - \sum_{k=1}^{K} \alpha_k(t)\vec{e}^{\,k} \right]^2 \qquad [3.4]$$

From the orthogonality of the EOFs, the coefficients $\alpha_k(t)$ come from the scalar product of the vector data and the orthogonal functions in the way;

$$\alpha_k(t) = \vec{X}(t) * \vec{e}^{\,k} \qquad [3.5]$$

If the distributions are Gaussian, the coefficients $\alpha_k(t)$ are statistically independent. Therefore, if the EOFs are normalized, then the total variance of *X* can be decomposed in independent contributions of EOFs:

$$\sum_{t} \left| \vec{X}(t) \right|^2 = \sum_{t,k} \alpha_k(t)^2 \qquad [3.6]$$

The explained fraction of the variance associated with each *k* mode is resolved as;

$$f\ \mathrm{var}_k = \left[\lambda_k \Big/ \sum_{k=1}^{k} \lambda_k \right] * 100 \qquad [3.7]$$

where, λ is the corresponding eigenvalue of the *k* mode.
The main characteristic of this analysis is that the map associated with each eigenvector represents a pattern which is statistically independent with respect to the others and spatially orthogonal to them. The eigenvalue indicates the amount of variance accounted for by the pattern (North, 1984).

An important aspect of the method is the statistical significance of the analysis. The statistical problem is to what extend the estimated EOFs (eigenvectors of the sample covariance matrix) resemble the true EOFs (the eigenvectors of the true covariance matrix). The true and sample EOFs differ for two reasons (von Storch and Frankignoul, 1998). The first reason is the standard problem in statistical inference: the uncertainty due to the limited sampling. A basic empirical rule is that the low-indexed EOFs, with the largest eigenvalues, are best estimated, diminishing the certainty as *k* increases. The signals associated with low-index EOFs have large amplitudes and are in most cases sampled several times in the data set analyzed. However, the events in the sample, which are not typical of the random variable as a whole but specific to the sample, are also represented by some, usually high-indexed, sample EOFs. Unfortunately, there are not objective methods to determine the uncertainty of the sample. The second reason is the degeneracy. When an eigenvalue is multiple, or degenerate, its eigenvector directions are no longer uniquely determined, which could represent a noisy source. Degenerate eigenvalues can represent the

same dynamical processes or two no independent processes. North et al. (1982) have proposed a rule of thumb to diagnose when such indeterminacy prevails and the EOFs patterns are not uniquely determined. They resolved the question of the separation of the modes by using the slope of the estimated eigenvalue spectrum. If the sampling error of a particular mode is larger than the spacing between this mode and the precedent one, then it would mean that the mode is part of a degenerate multiplet (North et al., 1982).
In spite of these problems, the EOFs methodology responds to how the variations of a particular field are related in the spatial domain, identifying patterns of simultaneous variation. This statistical technique lets identify sub-spaces of a field from meteorology and oceanography, which contain the majority of the dynamics of an observed system (von Storch and Frankignoul, 1998; von Storch and Zwiers, 2001; Rodríguez-Fonseca, 2001).
From a **computational point of view**, Singular Values Decomposition (SVD) is an election of the solution for the traditional eingenvalue problem that is numerically more robust (von Storch and Frankinoul, 1998). The SVD of a matrix *X* (n x m) is the factorization of the matrix as;

$$X = U\Lambda V^T \qquad [3.8]$$

where *U* and *V* are orthogonal and Λ is a diagonal matrix. The columns of *U* (m x m) are the eigenvalues of XX^T and the columns of *V* (n x n) are eigenvectors of $X^T X$. The diagonal of Λ (nxm), σ_i, retains the square roots of the eigenvalues of both matrixes of covariance of *X*. If the matrix to decompose is *R* (covariance matrix of *X* from 3.1), then,

$$R = U\Lambda V^T V\Lambda^T U^T 1/n = U\Lambda\Lambda^T U^T 1/n \qquad [3.9]$$

The diagonal matrixes are related as

$$L = \Lambda\Lambda^T 1/n; \qquad \lambda_i = \sigma_i^2 1/n \qquad [3.10]$$

Along this work, the computations in matlab have been performed using SVD factorization.
Regarding the **representation of the EOFs**, throughout this PhD Thesis, three types of maps are used to represent the patterns: correlation, regression and composite maps.
The correlation maps are performed correlating the standardized PC associated with each mode and the timeseries of each spatial grid-point of the original anomalous field (Bretherton et al., 1992).
The regression maps are performed projecting the standardized PC of a determined mode onto each grid-point of the original anomalous field. Therefore, the result indicates the amplitude of the original variable associated with one standard deviation of the PC.
The spatial map is obtained for each mode, and generally, the regression pattern is represented only in those regions of the correlation map in which the scores are statistically significant (see sub-section 2.5).
The composite maps are performed averaging the anomalous maps of a particular field for those cases in which the PC associated with each mode (temporal evolution of a determined mode) is higher (lower) than an imposed threshold.

From this method, those patterns that explain the variability of one field for a particular lag are extracted. In the next section, the problem of evolving and/or propagating phenomena is solved by a variant of the EOF methodology referred to as Extended EOF analysis.

3.2.2 Extended Empirical Orthogonal Functions

A lot of processes in climate have an oscillating nature. A priori, if the nature of the propagation phenomenon is unknown, the propagation variability will not be captured by the classical EOF. The methodology known as Extended Empirical Orthogonal Functions (EEOF, first introduced by Weare

and Nasstrom, 1982) constitutes an extension of the traditional EOF technique to deal not only with spatial but also with temporal correlations observed in the data.
As it was explained above, traditional EOF analysis uses a set of time series and examines the temporal behavior of the spatial patterns. The EOF patterns describe the spatial structure, and the Principal Components (PC) characterizes its evolution in time. In contrast, the EEOF analysis recognizes that the temporal evolution of the spatial patterns is an integral part of a system's development. The EOF algorithm is applied to the concatened vector *X* of the fied *Y* at *m* consecutive times.

$$\vec{X}(t) = \left(\vec{Y}(t), \vec{Y}(t+1), ..., \vec{Y}(t+m-1)\right)^T \qquad [3.11]$$

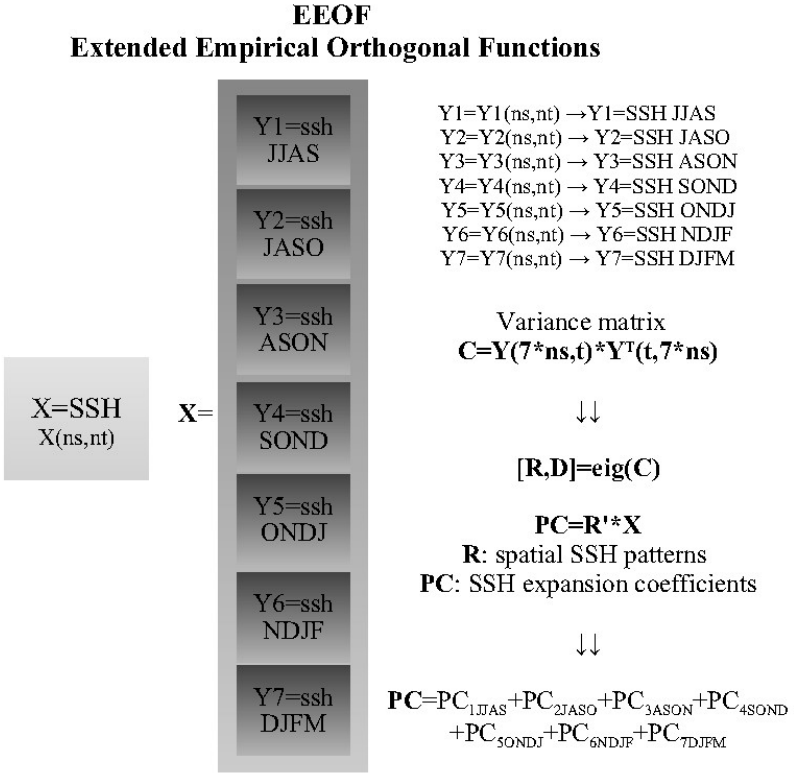

Figure 3.2. Scheme of the Extended Empirical Orthogonal Functions methodology.

This vector represents the states of the system in a *K* × *M* dimension, where *K* is the dimension of a instantaneous field *Y*, and it is spanned by time-delay coordinates *M.* An advantage of space-time EEOFs is the ability to distinguish oscillatory components with various frequencies, which makes this methodology to be suitable to study oscillatory phenomenon (Fraedrich et al., 1997). To apply EEOF, a matrix *X* is considered including positive and negative lagged time series for each of the grid points in the analysis, and EOF methodology of this pool of time series is applied.
Thus, from the EEOF analysis results PC indices which contains the information from each particular lag; and a total PC index, which is the sum of the previous indices. The latter is projected onto the original field, obtaining the EEOF pattern.
The EEOF analysis is an adaptive filtering technique (its filtering characteristics are determined by the data) in the sense that the original vector time series may be reconstructed by any of the following *j* representations (von Storch and Frankignoul, 1998):

$$Y(t) = \sum_{k+1}^{m} \alpha_k (t - j + 1) \vec{e}_{j+1}^{k} \quad , \qquad [3.12]$$

for j=1,…,m. Thus, the original vector time series are decomposed into *m* series, each of which is a space/time-filtered version of the original series. The EEOF analysis emphasizes cyclical behaviors in the evolution. If the data field *Y* features a propagating wavelike structure, then this signal will appear as a pair of EEOFs explaining a similar amount to variance, having the same frequency and de-phased by a quarter of period.
This methodology has been successfully applied to the Sea Surface Height anomalous field (see Chapter 4.2) in order to find a mode that could describe the Kelvin wave activity in the TA (see figure 6 in the first part of Chapter 4.2).

3.2.3 Maximum Covariance Analysis

Assuming two fields *Y* and *Z*, there is a method to determine the variability between these fields, extracting the patterns associated with *Y* and *Z,* and it is referred to as Maximum Covariance Analysis (MCA).

The MCA of two fields identifies pairs of spatial pattern that explain the maximum percentage of mean-square temporal covariance between the two fields (Bretherton et al., 1992; Cherry, 1996). This methodology is also usually referred to as SVD, mentioning the general technique of matrix decomposition (see Section 2.1). The MCA searches for linear combinations of the original anomalous fields in such a way that the covariance between them is maximum. These linear combinations are named as expansion coefficients and the associated weights are the spatial patterns or singular vectors (figure 3.3).
Mathematically two samples of related variables *Y* and *Z* are assumed, and the covariance matrix to factorize can be written as,

$$M = \frac{1}{N}\sum_{t}\vec{Z}(t)\vec{Y}(t)^{T} \qquad [3.13]$$

where the matrixes *Y* and *Z* are space-time distributed *Y*(ny, nt)*, Z*(nz, nt*)*. The *Y* field is considered as the predictor variable, and the *Z* field as the predicted variable. Analogously to the EOF method, after the application of the MCA, the fields can be expressed as;

$$\begin{aligned}\tilde{Y}(t) &= \sum_{k=1}^{K}\alpha_k(t)u_k \\ \tilde{Z}(t) &= \sum_{k=1}^{K}\beta_k(t)v_k\end{aligned} \quad , \qquad [3.14]$$

where *α* and *β* are so-called expansion coefficients of the fields *Y* and *Z* respectively, and they represent the temporal evolution of each variable associated with each mode. The spatial patterns (weight vectors) of the variables *Y* and *Z are u* and *v* respectively and for each mode *k*. Analogically to [3.5] the relation obtained is:

$$\begin{aligned}\alpha_k(t) &= \sum_{i=1}^{nx}u_{k,i}\vec{Y}_i(t) = u_k{}^{T}\vec{Y}(t) \\ \beta_k(t) &= \sum_{j=1}^{ny}v_{k,j}\vec{Z}_j(t) = v_k{}^{T}\vec{Z}(t)\end{aligned} \qquad [3.15]$$

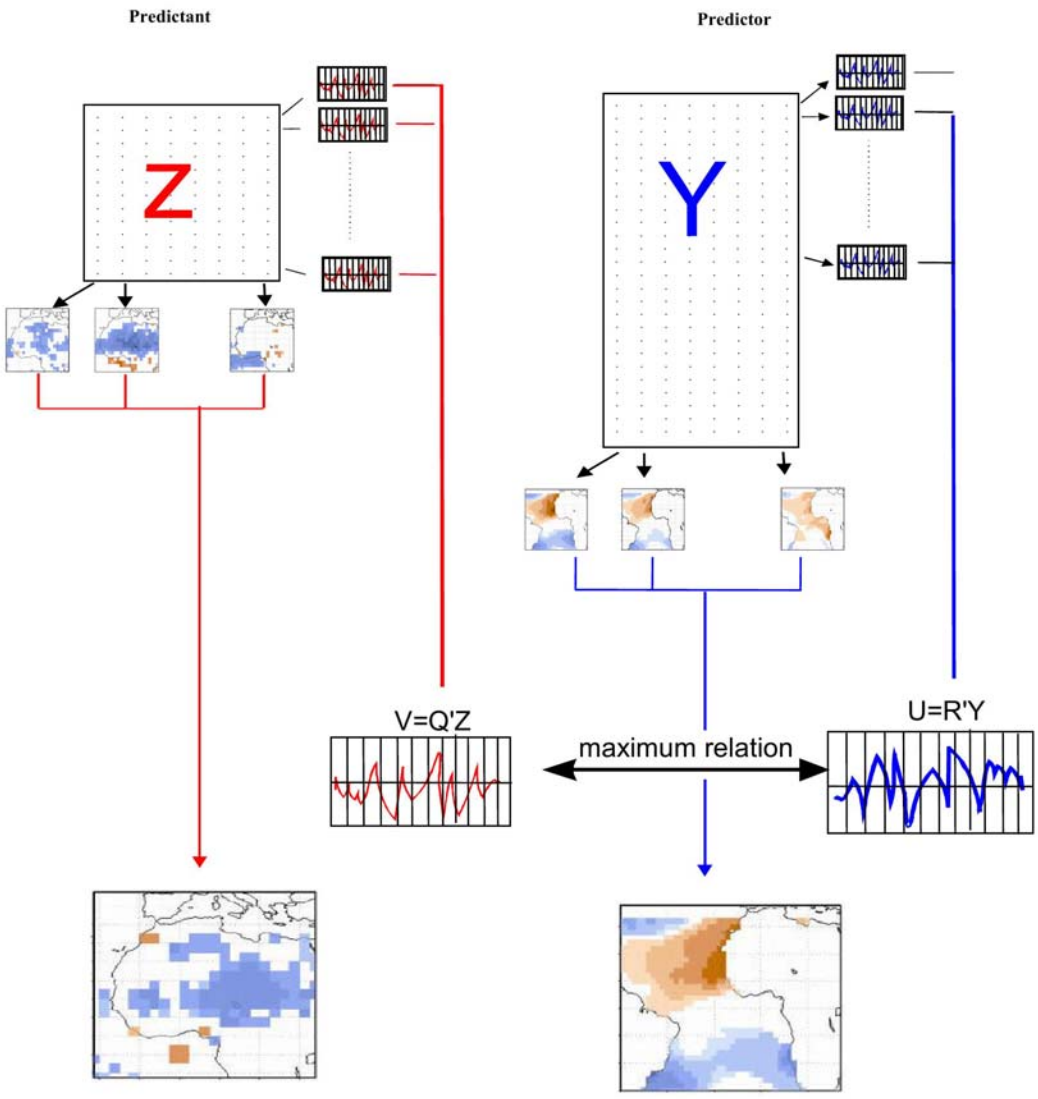

Figure 3.3. Scheme of the Maximum Covariance Analysis.

The equation [3.15], which expresses the expansion coefficients *α* and *β* for the two related variables, has the same form than the equation [3.5] for the case of just one variable. The expansion coefficients are the projections of *Y* and *Z* onto the spatial patterns. These patterns are selected in such a way that the projection of *α* onto *u* has the maximum covariance with the projection of *β* onto *v* (Bretherton et al, 1992), therefore,

$$\alpha * \beta = u^T M v = \max \qquad [3.16]$$

The parameter used to measure the explained covariance for each mode of the covariant patterns is the squared covariance fraction, which is the percentage of the explained covariance for each mode defined as,

$$scf_k = 1 - \left\| M^k - \tilde{C}_k \right\|_F^2 \Big/ \left\| M^k \right\|_F^2 = (\alpha_k * \beta_k)^2 \Big/ \left\| M \right\|_F^2 \qquad [3.17]$$

where *M* is defined in the equation [3.13], $\tilde{\tilde{C}}_k = \tilde{\tilde{Y}}_k \tilde{\tilde{Z}}_k^T$, and the norm of the vectors is the Frobenius matrix represented by the subscript F. In addition, it is given a parameter (correlation) which measures how much the expansion coefficients (representing the covariant fields *α* and *β*) are related to each other, for each *k*-mode.

$$r_k = corre(\alpha_k, \beta_k) \qquad [3.18]$$

In order to spatially represent the patterns of the MCA, three types of maps can be performed:

The correlation maps represent the correlation between the times series, for each grid point, of a particular field and the expansion coefficient associated with the *k* mode and one of the variables involved in the analysis. This spatial map will show the areas of this particular field that are highly correlated with the expansion coefficient. If the correlation is done between an expansion coefficient of a field and the same anomalous field or a different field, the maps will be homogeneous or heterogeneous, respectively. The most common procedure is to plot the homogeneous map of the predictor field and the heterogeneous map of the predicted field. The first map represents the correlations between the temporal evolution of *Y* in each of the points of the spatial domain and its expansion coefficient *α,* localizing geographically the part of the predictor field that covaries with *Z*. The second map depicts the correlation between the temporal evolution of *Z* in each of the points of the spatial domain and the expansion coefficient of the predictor field *α*. This map represents the skill of the predictor field *Y* (from *α*) to predict the field *Z*.

The regression maps represent the projection of the standardized expansion coefficients onto the temporal evolution of the variable in each point of the spatial domain. The most used are the homogeneous maps for the predictor and the heterogeneous map for the predicted field. The former represents the variation of the predictor field, for each standard deviation of the coefficient α. The latter, represent how the predicted field Z varies for one standard deviation of the coefficient α of the predictor field Y.

Finally, the composite maps (also homogeneous and heterogeneous) are performed averaging the anomalous maps of a particular field for those cases in which the expansion coefficient associated with each mode (temporal evolution of a determined mode) is higher (lower) than an imposed threshold.

3.2.4 Extended Maximum Covariance Analysis

Classical MCA resolves the question of the relation between a predictand and a predictor matrix. Some processes in the climate system imply multiple associations between variables. If a prediction of a climatic variable is done, several fields could be involved and more than one variable in the predictor array field could be considered when applying MCA and getting the patterns related to a predicted variable *Z*. For this case, an extended approach of the classical MCA (EMCA, figure 3.4) can be used.

Furthermore, as in the EEOF, sometimes the phenomena are complex time-evolving processes in the ocean and/or the atmosphere. In addition, the evolution of a system gives a substantial understanding of the processes involved and they are very important in predictability issues. Also for this case, EMCA can be applied.

Mathematically, EMCA could be described as follows. For the first case, several variables in the predictor array:

$$\vec{Y}(t) = \left(\vec{Y}a(t), \vec{Y}b(t), ..., \vec{Y}j(t)\right)^T \qquad [3.19]$$

For each predictor field *j*, the variable can be reproduced analogically as equation [3.14], as each predictor field has an associated expansion coefficient *α* and spatial pattern *u*.

$$\tilde{Y}j(t) = \sum_{k=1}^{k} \alpha_{kj}(t) u_{kj}$$
$$\tilde{Z}(t) = \sum_{k=1}^{K} \beta_k(t) v_k \qquad [3.20]$$

And the predicted field has an associated expansion coefficient *β* and spatial pattern *v*, which maximized the covariance with the *j* predictor.

For the second case, where the predictor evolves in time, the pool of timeseries can be written as

$$\vec{Y}(t) = \left(\vec{Y}(t), \vec{Y}(t+1), ..., \vec{Y}(t+m-1)\right)^T \qquad [3.21]$$

similar to the equation [3.11], and the predictor and predicted fields can be also reconstructed as

$$\tilde{Y}(t) = \sum_{k+1}^{m} \alpha_k(t-j+1) \vec{u}_{j+1}^{k}$$
$$\tilde{Z}(t) = \sum_{k=1}^{K} \beta_k(t) v_k \qquad [3.22]$$

The homogeneous/heterogeneous maps could be constructed now with the individual expansion coefficients of the predictor fields *α* or with the total timeseries of the predictor fields. The total series, which represent the expansion coefficient of all the predictor fields (variables or lagged-time variable) in relation to the predicted variable, are the sum of each individual expansion coefficients for each mode *k*,

$$\alpha_{kT} = \sum_{j=1}^{J} \alpha_{kj} \qquad [3.23]$$

Also, as in MCA, the squared covariance fraction and the correlation between the expansion coefficients give the statistical parameters associated with each mode. If the predictor evolves in time, it is the most straightforward method to isolate, in the same mode, the whole sequence of significant covariant *Y* patterns in relation to the *Z* variable, and accomplish the whole picture of the *Y* pattern evolution in relation to the *Z* with a realistic persistence feature from time 1 to time *m*. Since many processes in climate can develop rapidly from one season to another, this method, a priori, does not discriminate the season of the maximum covariability (in contrast with the classic MCA). In addition, EMCA gives the opportunity of increasing the number of time series in the analysis, having as many time series per point as time lags used in the analysis, and assessing, in this way, the statistically significance of the results.

In this work, both cases of application of the EMCA are performed. On the one hand, several variables are considered in the predictor array *Y* (SST, upper ocean temperature, windstress and latent heat flux) in order to find the relation to European precipitation (see figure 1 in the second part of Chapter 4.1.1). On the other hand, a time-varying predictor field (SST) and its relation to the WA rainfall predicted field is evaluated (see figure 3 in Chapter 4.1.2).

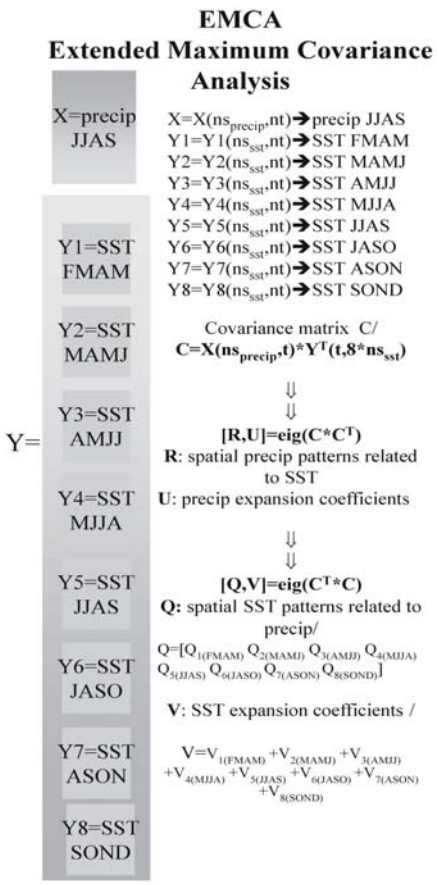

Figure 3.4. Scheme of the Extended Maximum Covariance Analysis methodology.

3.2.5 Significance tests and Representation of Results

When applying any statistical tool, it is frequently desirable to estimate the probability of obtaining a result by chance, or to estimate the "true" value of a particular parameter. Although the methods explained along this section (EOF, MCA) can give high correlations and covariances between fields, it is necessary to assess the significance of the results in order to avoid non robust patterns that could be a result of a mathematical artifact. For this reason, several statistical significance tests are going to be simply described next. The aim is to familiarize the reader with some basic tests, Monte Carlo techniques and resampling procedures that can avoid the approximations and assumptions associated with formal statistical tests.

3.2.5.1 T- test

A t-test is any statistical hypothesis test in which the test statistic has a Student's t distribution if the null hypothesis is true. It is applied when sample sizes are small and the use of the normality assumption and the associated z-test leads to incorrect inference.

In particular, this is one of the most used statistical test in meteorology and it is a very useful and simple method to test the statistical significance of the correlation between two samples, under the null hypothesis that these samples are independent and the product moment correlation coefficient is zero (Spiegel, 1993). In this way

Ho: the samples are independent; therefore the correlation *r* between them is zero.

H1: the samples are dependent

To perform this test, a low level of significance is taken (α=0.05 or α=0.01 with a 95% or 99% of significance respectively) .In this way the error of neglecting Ho being true is lessened and, therefore, there is more certainty of neglect Ho.

The statistical parameter used is

$$t = \frac{r\sqrt{N-2}}{\sqrt{1-r^2}} \qquad [3.24]$$

which is distributed following a t-Student with N-2 degrees of freedom. If $t > t_{\alpha/2}$ then the null hypothesis is neglected.

3.2.5.2 Monte Carlo test

The Random methods of computation and experimentation (generally considered forms of stochastic simulation) systematically "invert" the typical mode of simulation, treating deterministic problems by *first* finding a probabilistic analog. The previous methods of simulation and statistical sampling generally did the opposite: use simulation to test a previously understood deterministic problem. Though examples of an "inverted" approach do exist historically, they were not considered a general method until the popularity of the Monte Carlo method spread.

The name "Monte Carlo" was popularized by physics researchers Stanislaw Ulam, Enrico Fermi, John von Neumann, and Nicholas Metropolis, among others. The name is a reference to a famous casino in Monaco where Ulam's uncle would borrow money to gamble. The use of randomness and the repetitive nature of the process are analogous to the activities conducted at a casino.

Monte Carlo simulations are used to calculate the statistical distribution of a parameter under the null hypothesis that the response variable is independent of the predictors.

Ho: the response variable is independent of the predictors
H1: the response variable is dependent of the predictors

This test is very used in climate studies when using large spatial-temporal samples. In the context of this PhD Thesis, this test is used as an alternative to the t-test when the correlations found are in the limit of being considered as statistically significant. Also, this method is used, as Rodwell and Folland (2002), when the statistical significance of the scores obtained from the discriminant analysis needs to be checked. This test provides a significance level for the connection found between samples of variables, assessing if the link between the fields (i.e. relationship found from a MCA) is or not random.
The Monte Carlo test performed in this PhD Thesis consists in the combined action of shuffling the samples and applying a particular methodology (i.e computing correlations r, MCA or EMCA) *k* times (i.e. 100 times). The probability density function (PDF) of the statistical parameter (i.e. r, scf) that arises from these *k* realizations is compared to the parameter scores obtained from the non-shuffled samples. The significance level (SL) for the connection found is established from the PDF of the parameter for the permuted samples in relation to the non-shuffled parameter value.

In this work, the Monte Carlo test is used to determine the statistical significance of the EMCA applied between the time-evolving anomalous SST patterns and the WA rainfall (Chapter 4.1.2). Also, the Monte Carlo test is performed to determine the significance level of the correlation maps in the study of the subtropical north Atlantic impacts on the European precipitation (Chapter 4.1.1).

3.2.5.3 Bootstrapping

Linear regression models used in meteorology are constructed to estimate a dependent variable *y (predictands)* from a set of independent variables x_i (predictors). The crossvalidation technique offers a way of obtaining unbiased estimates of the statistical model skill and it is very used in climate prediction (Stone, 1974). Nevertheless, to give an improved estimate for very short data sets with a large low frequency contribution to the variability, the bootstrap validation technique (Efron and Tibishirani, 1993) is a more convenient procedure that can avoid possible artificial skills of the prediction.
The bootstrap is a parametric test that estimates the variance of the regression. In a first stage, bootstrap samples are obtained from the data. In a second stage, the variance about the regression for the bootstrap samples is calculated.

The method consists of permuting with replacement *B* times the residuals (e_B) obtained between the observed variable (y) and that obtained from the regression model ($\hat{y}$). Thus, for each grid point it is created a set of new estimates y_B (bootstrap replications) by adding these *B* permuted errors, e_B, to the nonpermuted estimated precipitation ($\hat{y}$) (equation 3.25). Then, the variance of each of such estimates, y_B, is calculated and compared with the variance obtained with the original model $\hat{y}$. These B estimates are arranged in a frequency distribution and count in α B/2 observations from each end to obtain (1-α)% confidence limits.

$$\hat{y} = ax + b$$
$$e = \hat{y} - y \qquad [3.25]$$
$$y_B = \hat{y} + e_B$$

As Efron and Tibishirani (1993) showed, the variance about the regression obtained from the bootstrap sample is appreciably smaller than that obtained from the original data, and the mean difference between the two variances (called *the inflation factor*) is added to the variance of the original data set to give an improved estimate.

This method is used in Chapter (4.1.1), when the winter monthly anomalous precipitation over Europe and North Africa is estimated on the basis of the previous summer subtropical Atlantic SST anomalies. This regression analysis has been applied to each of the grid points of the precipitation domain and the explained variance of the predicted rainfall has been tested using a bootstrap technique. The bootstrap improved fraction of variance over the region of interest is shown as a measure of the quantitative skill of estimating the ENA winter monthly anomalous precipitation from the previous summer subtropical Atlantic SST variability. In this validation procedure it has been used *B* = 2000.

3.3 Spectral Analysis

Spectral analysis is a basic utility used in statistics, to decompose a time series into a spectrum of cycles of different lengths. In this way a signal can be described with respect to frequency. A frequency domain graph shows how much of the signal lies within each given frequency band over a range of frequencies. The frequency domain relates to the Fourier transform or Fourier series by decomposing a function into an infinite or finite number of frequencies. This is based on the concept of Fourier series that any waveform can be expressed as a sum of sinusoids.

For climatological purposes, the spectral analysis is used, for example, to compute the seasonal cycle on. By definition, the seasonal cycle is the sum of the annual and multiple Fourier harmonics. For a variable Q periodic on time, it can be expressed as a sum of orthogonal functions (Fourier harmonics). This sum of harmonics truncated by *n*, with amplitude *q*, frequency ω and phase φ is expressed as:

$$Q = q_0 + \sum_{i=1}^{n} q_i \cos(\omega_i t - \varphi_i) \qquad [3.25]$$

Truncation of the Fourier series by semiannual harmonics is a reasonable way of performing the seasonal cycle for many climatic variables (such as SSH, OLR) with pronounced annual and semiannual cycles in the TA. Limitation of the sampling is given by the Nyquist theorem: *no information is lost if the sampling interval is smaller than 1/(2f_{max}), where f_{max} is the maximum frequency present on the series*. It is called the Nyquist frequency: for a sampling interval Δt it is given by $f_N = 1/(2\Delta t)$.

It is important that the filter design functions operate with normalized frequencies, so they do not require the system sampling rate as an extra input argument. The unit frequency is the Nyquist frequency, so, the normalized frequency, therefore, is always in the interval $0 \leq f \leq 1$.

This work uses different spectral techniques not only to compute the seasonal cycle but also to filter the data (Section 3.1), localize different frequencies on time (Section 3.2) and determine some parameters (Section 3.3).

3.3.1 Filtering the data

The variability of a time series may be caused by different processes that are characterized by their "time scales" (von Storch and Zwiers, 2001). It is therefore useful to split a time series into certain components, each one related to a different time scale.

Simple filter are very useful to avoid frequencies that could add noisy to the signal associated to a particular phenomenon. The goal of filter design is to perform a frequency dependent alteration of a data sequence. The filter only knows what is in the time record. It assumes the actual signal contains discontinuities, and they are the cause of the leakage. Leakage could be avoided if the input waveform zero crossings were synchronized with the sampling times, but this is impossible to achieve in practice. In order to reduce the effect of leakage, the data samples are multiplied by a so-called "windowing" or "weighting" function, which can have several different shapes. One of the most used windows is the Hanning window, which has the shape of one cycle of a cosine wave with 1 added to it so it is always positive.

In this work, the filter has been used to capture intraseasonal signals in the sea surface height field (Chapter 4.2). To this aim, a Hanning window is used to smooth the variable along the time of 25 and 95 days respectively, finding intraseasonal anomalies no longer than three months and smaller than three weeks. Therefore, the filtered data is the result of subtracting, the fitted signal for 95 days from the fitted signal for 25 days. This can be written as:

$$y_{t(25-95)} = y_{t(25dy)} - y_{t(95dy)} \qquad [3.26]$$

This procedure is similar to applying a running mean of the signal and it is an example of digital filter, with a set of real weights. The weights can be tailored so the filter retains variation on long, short or intermediate time scales. Each of these low-pass digital filters can be described as

$$y_t = \sum_{k=-K}^{K} a_k x_{t+k} \qquad [3.27]$$

Where, $\{a_{-K},...,a_K\}$ is a set of 2K + 1 real weights (of the Hanning function), that smooth the variable along the time of 25 (K=12) and 95 (K=47) days respectively. These transformations

replace each value on the grid to which they are applied with a weighted average of the surrounding data values along the axis specified. The spectral density function (Γ) of the output y_t is related to that of the input x_t by

$$\Gamma_{yy}(\omega) = \left|c(\omega)\right|^2 \Gamma_{xx}(\omega) \qquad [3.28]$$

where c(ω) is the *frequency response function* (von Storch and Zwiers, 2001).
For the particular case of the filtering applied to the SSH data, the frequency response function (figure 3.5) preserves about 60% of the signal amplitude within the 70-35 day band, with a maximum (80%) at 50 days, and a 10% preserving reached at about 200 and 20 day periods. Although the two low-pass filters cut off quite sharply, they do not show artificial spectral peaks and no negative side lobes are found (in contrast with the running mean filter).

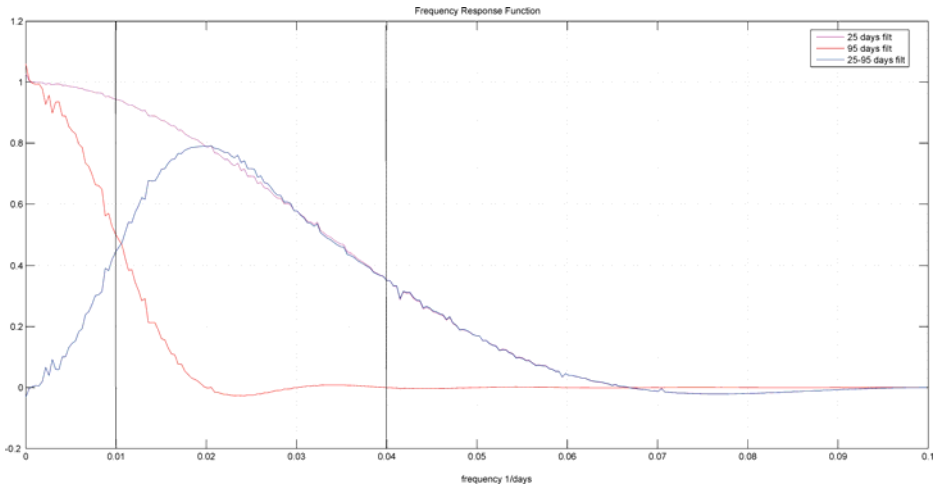

Figure 3.5. Response function of the filters performed as the ratio between the Fourier Transform of the filtered signal and the Fourier Transform of the original signal for each filter.

3.3.2 Spectrogram Analysis

To determine the frequencies that characterize a signal, different spectral techniques can be applied to the data. The spectrogram analysis is the result of calculating the frequency spectrum of windowed frames of a signal. It is a 3-dimensional plot of the energy of the frequency content of a signal as it changes over time. To calculate the spectrogram, the digitally sampled data, in the time domain, is broken up into windows, which usually overlap, and Fourier transform is performed to calculate the magnitude of the frequency spectrum for each window. Each window corresponds to a measurement of magnitude versus frequency for a specific moment in time.
In this study the analysis is performed in order to know the frequencies involved in the propagation at inter-annual and intra-annual timescales of the SSH field (Chapter 4.2). For this reason, the windows in which the spectral analysis is performed are differently chosen depending on the frequency. To find the better frequency band that describe the Kelvin wave propagation, the spectrogram along the Kelvin wave track have been performed and the energy for all the track points at different frequency bands have been plotted (figure 3 in the first part of Chapter 4.2).

3.3.3 Radon Transform

The Radon Transform (RT) function is defined for a function *f(x)* of 2-D vector *x=(x,y).* In this case *f(x)* is the wavefield in the track-time plot and *x, y* are track points and time, respectively. If L is an

arbitrary line at an angle θ with respect to the x axis, the RT (Deans, 1983) is defined as the projection of $f(x)$ on L, that is;

$$p(x',\theta) = \int_{y'} f(x,y)dy' \qquad [3.27]$$

Where y' is the orthogonal direction to L (along which the integration is performed) and x' is the coordinate on L. Note that, for a given θ, the Radon transform is a 1-D function of the line coordinate x'. The essential method is to transform two-dimensional images (i.e. hovmuller diagrams) with lines into a domain of possible line parameters (i.e., slope, which equates to speed in a track–time plot, see figure 3.6), whereby each line in the image will yield a peak at the corresponding line parameter in the transform domain (Challenor et al., 2001; Challenor et al., 2004). The Fourier Transform (FT) and RT are closely related by means of the *Projection-Slice theorem*: the RT at a given θ corresponds to the inverse FT of a slice taken at the same angle θ in the Fourier space. This is important as the lines at an angle θ, both in the track-time space and in the wavenumber-frequency space, are lines of constant speed, which can be readily computed from θ. This implies that computing the RT of the track-time plot for different values of θ, and then its energy is equivalent to computing the energy in the spectrum along lines of constant speed, and it is the most straightforward method to find the value of the speed for which that energy is maximum (Challenor et al., 2001).

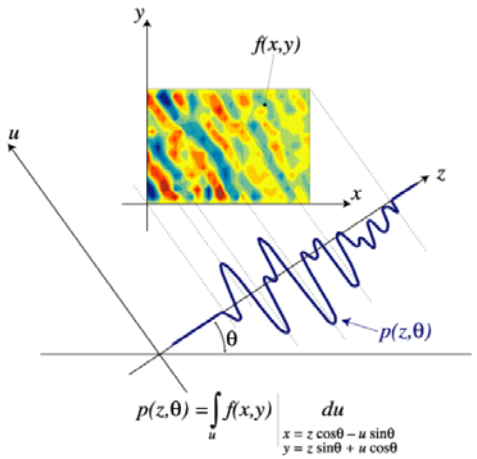

Figure 3.6. 2-D Radon transform $p(z,\theta)$ of an image $f(x,y)$ is projected sum of that image at a given angle θ. From Challenor et al. (2004).

The Radon Transform (RT) is a very useful image processing technique for the satellite images. The RT methodology has also been successfully used to characterize the phase speed of the oceanic long planetary waves (Chelton and Schlax, 1996; Cipollini et al., 1996; Polito and Cornillion, 1997; Hill et al., 2000; Challenor et al., 2001; Challenor et al., 2004; de la Rosa et al., 2007).

This methodology has been used in Chapter 4.2 to calculate the phase speed of the intraseasonal Kelvin waves in the Atlantic from hovmuller plots, as well as phase speed of Rossby waves (see figure 3 in the second part of Chapter 4.2). The data processing includes smoothing the data to avoid the signals around the frame and the RT of the images has been performed for the angle between -90 to 90 degrees every 0.25 degrees. The corresponded angle of the maximum RT standard deviation is defined as the angle of the propagation. The methodology has been applied to each track point with a radius of 10 degrees around each point (de la Rosa et al., 2007) later the phase speed for each point along the track has been calculated.

3.4 Data

The data used along this work comes from observational data and Reanalysis of oceanic and atmospheric variables. Additionally, due to the lack of data in the subsurface ocean and, especially, in the TA, some analyses have been done using model simulation outputs. The description of the data is done for the variables of interest.

3.4.1 Oceanic Fields

Sea Surface Height (SSH):
The SSH variable represents heat and pressure gradients of the upper ocean and, therefore, lot of aspects of the oceanic variability (Arnault and Périgaud, 1992; Stammer, 1997). The sea-level signature of the oceanic waves is adequate to their detection and satellite altimeters can measure their signals down to a few centimetres. The inter-comparison analyses with *in situ* measures (i.e. tide gauges records) have shown that altimetry is an important tool to study the oceanic variability (Arnault and Périgaud, 1992; Arnault et al., 1992; Musman, 1992), even in the coastal regions (Aman et al., 2007). In contrast to the sparse network of coastal tide gauges, measures of SSH from space by satellite radar altimetry, provide near global and homogeneous coverage of the world's oceans.
Along this work, SSH from the TOPEX/Poseidon (T/P) altimetry measurements are used (figure 3.7a). The data has 0.5 degrees latitude–longitude horizontal resolution and 7-days time resolution. It is produced and distributed by AVISO[1], as part of the Ssalto ground processing segment. The T/P trajectories follow polar orbits with a separation between ascendants and descents of a distance D (figure 3.7b). The cycle of the altimeter is directly related to the distances between trajectories. The parameters of the satellite missions are resumed in table 3.1.

In order to get the SSH variable, corrections applied to the data Height are performed. The SSH T/P anomalies have already been corrected by removing four-year average elevation and signals such as the ocean tide (Arnault and Le Provost, 1997), the dry tropospheric inverted barometer, tidal aliasing and vapour water. These corrections concerns to how AVISO processes the T/P signal in order to homogenize the product. Homogenisation process consists in applying the most recent corrections, models and references recommended for altimeter products. In particular, they remove the mean current circulation and the Geoid uncertainties by subtracting the 4 year (1993-1996) mean, obtaining Sea Level anomalies (See for more information AVISO handbooks, 1992; 1995).

The T/P resolution along the trajectory of the T/P altimeter is ~10km (6.91 T/P and 7km Jason), while, along the equator, the resolution diminishes to 300 km (see table 3.1 to compare with other satellite altimeters). A resolution problem exists along the coast. The altimeter has a delay for identifying the oceanic surface when it travels from land to sea to be around 50 km and, therefore, some coastal data is only reliable 50 km offshore (Arnault and Périgaud, 1992).

	Satellite mission		
Parameters	Geosat	ERS1	T/P-Jason
Cycle (days)	17	35	10
Distance in between trajectories (km)	150	30	300
Distance along the trajectory (km)			10

Table 3.1. Parameters of different satellite missions

The merged product is the best compromise between the trajectory distance and the time of cycles. All the data from the available altimeters are organized with an objective analysis, through a correlation criterion with a 15 days radius and with the information of 7.5 days before and after. The

[1] AVISO (Archivage, Validation et Interprétation des données des Satellites Océanographiques) is part of the CNES (Centre National d'Études Spatiales).

data has been ordered in grid with a 0.5x0.5 latitude-longitude spatial resolution and a time step of 5 days. The total domain for the TA Ocean is:

Latitude -44.5ºS: 0.5: 45ºN
Longitude 79.5ºW: 0.5: 20ºE
Time 1/12/1992: 5: 1/8/2002

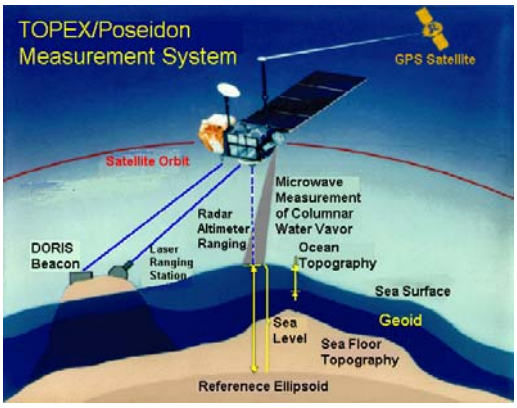

Figure 3.7a. Scheme of the T/P satellite measurements. From AVISO homepage.

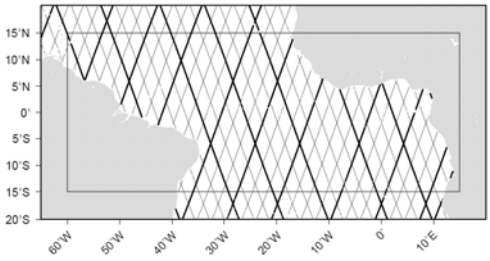

Figure 3.7b. TA region, the T/P ground-tracks are superimposed. Tracks occurring in the first third period (3.3 days) of the cycle are shown with a thicker line. From Franca et al. (2003).

Sea Surface Temperature (SST):
Since the SST is the variable that links the upper ocean to the atmosphere, it is the most important variable in the air-sea interaction studies. Therefore, several very reliable dataset are available in public access (i.e. Kaplan, ICOADS, PIRATA, ERSST, etc …).
In this PhD Thesis, Extended Reconstructed SST data (ERSST dataset, Smith and Reynolds, 2003) monthly and weekly averaged is used, in order to study interannual and intraseasonal variability respectively. This data set is based on the updated COADS SST observations, and improved new quality control statistical methods that allow stable reconstruction using sparse data. It has 2º x 2º latitude-longitude spatial resolution from 1854 to present.
For some analysis, observational monthly SST from PIRATA[2] dataset (Servain et al., 1998) has been used, in order to be consistent and give homogeneity to the analysis with other variables from PIRATA, such as wind stress.

UPPER OCEAN TEMPERATURE:
The lack of subsurface data in the TA was a constraint in the knowledge of the TAV for many years. For the last decades, TAOSTA (Tropical Atlantic Ocean Subsurface Temperature Atlas) dataset (Vauclair and du Penhoat, 2001), embedded different datasets (as PIRATA) to merge a complete description of upper ocean temperature (form 10 to 500 m in 14 depth-levels) over the TA with 2º x 2º latitude–longitude spatial resolution and monthly time resolution. The 20ºC isotherm depth, as thermocline depth proxy in the TA, is deduced from this upper ocean field.
Vauclair and du Penhoat (2001) collected all available near surface and subsurface observations of the TA between 1979-1998, in order to build a gridded data set of surface and subsurface temperatures referred to as TAOSTA. These data come from various sources: XBT (TOGA/WOCE subsurface DATA centre), CTD and Nansen casts from oceanographic cruises, moorings in 1983-1984 and PALACE floats (Profiling Autonomous Lagrangian circulation Experiment) in 1998-1999. The data from PIRATA mooring are also included for the last two years. They have compiled

[2] PIRATA (Pilot Research Moored Array in the Tropical Atlantic), is a multinational program (tripartite between Brazil, France and United States of America) established to monitor the ocean-atmosphere system in the Tropical Atlantic in order to improve our knowledge and understanding of the Ocean-Atmosphere variability in this particular world region.

approximately 120000 profiles which do not have a uniform distribution. Figure 3.8a shows the total number of profiles per month, summed over the whole basin, and the non-homogeneity of the temporal coverage of the data. Figure 3.8b illustrates the distribution of the data. The best sampled areas are along commercial lines and there is little sampling south of 10ºS in the central Atlantic.

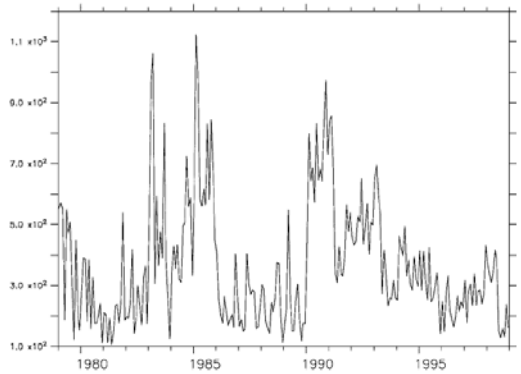

Figure 3.8a. Number of profiles per month used for the objective analysis, summed for the whole basin: 70ºW-12ºE, 30ºS-30ºN. From Vauclair and du Penhooat (2001).

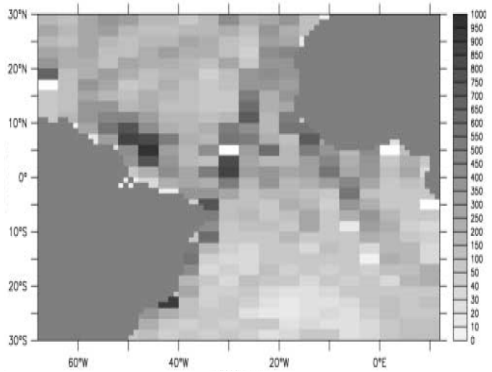

Figure 3.8b. Number of profiles by box (2ºx4º) before objective analysis summed for the 20 years. White box means number of data greater than 1000. From Vauclair and du Penhoat (2001).

The profiles on the standard Levitus levels (form surface to 500m) has been interpolated. Based on the Bretherton et al. (1976) technique, and optimal interpolation method was used, taking into account the spatial and temporal scales of the involved physics. A correlation radius of 800 km in longitude, 300 km in latitude and 31 days in time has been used. The optimal interpolation scheme solves a local problem at each grid point using the neighbouring data only, and data were weighted according to their expected accuracy estimated from the data source and the accuracy of the measurement techniques (Vauclair and du Penhoat, 2001). It is important to notice that, in regions of strong mesoscale variability, such as coastal upwelling areas, correlation radius are probably smaller than in the open basin. Therefore, this analysis tends to smooth the coastal upwelling signal too widely. Comparison with SST fields (Reynolds, 1993) showed correlation of 0.9. A reduction in the correlation coefficient (with a minimum of 0.7) has been observed in areas of strong variability (i.e. upwellings, because of the method underestimate SST in these areas). Nevertheless, this data has been used along this PhD Thesis (Chapter 4.1.1) and it has been revealed very suitable to study interannual variability in the TA, including the upwelling areas.

Model Oceanic data:

The low-frequency variability of the tropical oceans is induced primarily by fluctuations in the winds. In the tropics, phenomena can be simulated deterministically if the forcing function is known. However, OGCMs, though reasonably realistic, are far from perfect. Flaws are attributable primarily to inaccurate forcing functions (the surface winds for example), and to inadequate parameterization of mixing processes (Philander, 1990; Arnault and Périgaud, 1992).

In addition, to study the dynamics of the ocean, OGCMs have a very important use in the generation of data sets. The use of this data may address questions that cannot be answered on the basis of measurements only; for example about the heat and mass budget of the ocean. The available subsurface data (subsurface variables, currents, etc…) especially in the TA, is very insufficient for variability studies.

In this PhD Thesis, in order to study oceanic wave activity over the TA (in Chapter 4.2) observations and model data set have been used. In particular, a numerical simulation of the OPA OGCM (Madec et al., 1998) has been used. The ORCA05 configuration used was run at the LOCEAN laboratory by the NEMO (Numerical Framework for Ocean Modeling) team, for the 1992-2000 period. The configuration has, for the global ocean, 0.5 degrees latitude–longitude horizontal resolution and 30 vertical levels. The momentum flux is the weekly ERS1-2 wind stress interpolated daily, while the air-sea heat fluxes are computed in line with semi-empirical, or bulk formulas using OGCM SST, the ERS1-2 wind speed, the NCEP-NCAR reanalysis (Kalnay et al., 1996) air

temperature, and monthly climatological air humidity (Trenberth et al., 1989) and cloudiness (Berliand and Strokina, 1980). Precipitation data come from the Climate Prediction Center Merged Analysis of Precipitation (CMAP) product (Xie and Arkin, 1996). Major river runoffs are taken into account through monthly values of river discharge (UNESCO, 1996). At last, a restoring term towards Levitus (1998) Sea Surface Salinity is applied to the fresh water budget. For further details on the model configuration see de Boyer-Montégut et al. (2007).

The model has been very useful to recognize and interpret signals from the SSH and thermocline proxy (z18). However, some constrains regarding the resolution of the model must be considered when resolving some processes. For instance, the suitability of the model to show oceanic waves is limited by the spatial resolution. The distance comprised in 0.5 degrees corresponds to the Rossby radius of deformation at about ~15 degrees of latitude for a 2 m/s baroclinic phase speed (see figure 3.9). Therefore, it is certainly a limitation in the model analysis and it may affect the ability to observe coastal waves poleward of 10 to 20 degrees of latitude, which correspond to a sub-grid process (in Chapter 4.2).

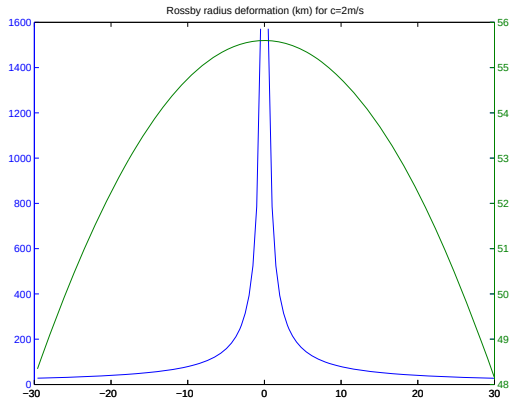

Figure 3.9a. Rossby radius of deformation for a given phase speed c=2m/s and the distance of the 0.5º longitude versus the latitude.

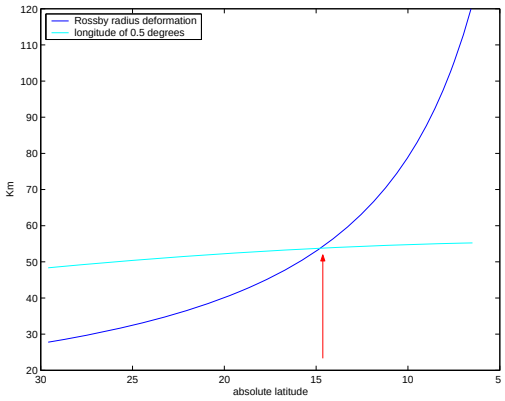

Figure 3.9b. Same as a) but focused on the latitudes between 6º -30 º of latitude to show the threshold of the model resolution to notice Kelvin wave activity.

3.4.2 Atmospheric Fields

ERA-40 and NCEP Reanalysis: Most of the atmospheric data used along this PhD Thesis comes from the ERA-40 reanalysis (Uppala and co-authors, 2005). However, in the Chapter 4.1.1, NCEP Reanalysis (Kalnay and co-authors, 1996) has also been used.
In a reanalysis, observed SST is specified as the lower boundary condition for an integration of an AGCM, which is constrained by assimilating all available meteorological observations (mainly wind, pressure and air temperatures). Every 6 hours, the atmosphere model is “pushed” towards these observations in a way not violating physical laws. A reanalysis is thus forced to follow the observed variability of the atmosphere.
The extend to which the AGCM in the reanalysis is constrained, depends on the amount of data available. In the Tropical and South Atlantic Ocean, data density is much lower than for oceans in the Northern Hemisphere or the Pacific Ocean. However, although observations were sparse during the early years of the reanalysis, there are shipping lanes from South America and South Africa to Europe and North America, and weather stations in few Islands (Vauclair and du Penhoat, 2001; Sterl and Hazeleger, 2003). With the introduction of satellites during the 1980s, observation density over the TA has increased dramatically and, thus, the reanalyses of the recent decades has improved.
Besides SST, which is imposed as the lower boundary condition, all reanalysis quantities are model output and, therefore, automatically internally consistent. This property is important when one wants

to study the interplay between different quantities, e.g., the coupled variability of ocean and atmosphere (Sterl and Hazeleger, 2003).
Along this work, **surface fields as SLP, winds, turbulent and radiative fluxes** are used and they come from the Reanalyses. Despite the limitation in reproducing realistic heat fluxes with models (Frankignoul et al., 2003), the best compromise between the consistency and the observed fluxes is the reanalysis product (Sterl and Hanzeleger, 2003). Other atmospheric variables, such as geopotential height and temperature at different atmospheric levels, also come from the Reanalysis data. ERA-40 Reanalysis data has a 2.5º x 2.5º latitude–longitude spatial resolution and monthly and daily time resolution.

WIND STRESS:

The transference of momentum from the atmosphere to the ocean is produced through the wind stress. Therefore, wind stress is the part of the surface wind that is effective with respect to the surface ocean, and it is defined as the drag force per unit area caused by wind shear (local variation of the wind vector in height). The wind stress on the sea surface applies a friction force that can drive ocean currents (Gill, 1982; Pond and Pickard, 1983). In a basic view, the wind stress module is defined as:

$$\tau = \rho c_D \left|\vec{u}\right|^2 \qquad [3.28]$$

Where ρ is the density of sea water, c_D is an empirical drag coefficient and u is the surface wind at 10m. The wind stress direction is the same as the surface wind (Gill, 1982; Pond and Pickard, 1983).

Monthly wind stress over the TA with 2º x 2º latitude–longitude spatial resolution is used from PIRATA dataset (Servain et al., 1998).
In order to study intraseasonal variability (Chapter 4.2), zonal and meridional scatterometer wind stresses have been used from the Active Microwave Instrument-Earth Resources Satellite (AMI-ERS), with a 5-day temporal resolution and 0.5º x 0.5º spatial resolution.

Outgoing Long-wave Radiation (OLR):
The OLR is the energy leaving the earth as infrared radiation at low energy. This energy radiated from the warmer earth to cooler space is derived from window channel measurements from satellites in polar orbit. Estimate of OLR from NOAA polar-orbiting satellites are often used to distinguish areas of deep tropical convection and to estimate the earth's radiation budget. Monthly and daily OLR is provided by NOAA/OAR/ERSL PSD (Liebmann and Smith, 1996). The spatial resolution is 2º x 2º latitude–longitude.

The OLR is affected by clouds and dust in the atmosphere, which tend to reduce it below clear sky values. Measurements of the outgoing long-wave radiation emitted by the tops of deep convective clouds, which are at much lower temperatures than areas of clear skies, quantify the convective activity in different regions. Quantities of OLR<240 W/m2 define the threshold of convection, and 180 W/m2 allows for better quantification of the convection in regions such as West Africa (Fontaine et al., 2007). Note that measurements of OLR, though useful, are not entirely reliable indicators of convection, especially outside the tropics, because non-convective clouds such as cirrostratus in the jet streams can also have cold tops (Philander 1990).

PRECIPITATION:

Precipitation is one of the variables to quantify the impact of the TAV and, at the same time, it is a variable very difficult to predict and simulate. In this PhD Thesis, the variability of the precipitation in tropical and extratropical areas is studied at interannual scales.
On the one hand, precipitation at tropical areas comes from, monthly CPC Merged Analysis of Precipitation (CMAP, Xie and Arkin 1997) for the period 1979-2002. This data has the benefit of the satellite measures over the ocean, which makes the dataset suitable to study rainfall variability over

the global ocean. The data over the ocean let to follow continuously the marine ITCZ, which is a very important component in the TAV (Kushnir et al., 2003).
In addition, over the tropical areas, there are not many data available from the rain gauges. The homogeneity of the CMAP contrasts with other precipitation data over the continent such as CRU-Gridded global precipitation dataset (Hulme, 1992).
On the other hand, European and Northern African monthly winter precipitation from 1960 to 1996 comes from Legates and Willmott dataset (LW, Legates, 1989; Legates and Willmott, 1990), with 1º x 1º latitude–longitude spatial resolution. This database has been constructed from 26858 precipitation stations across the world, with the highest concentration in North America and Europe, which provides a very reliable grid-data over the Northern hemisphere. The two above-mentioned datasets, CMAP (Appendix II) and LW are used for extratropical regions (Chapter 4.1.1).

4. RESULTS

4.1 Tropical-Extratropical Interannual Covariability Patterns: Air-sea interactions

4.1.1 Tropical Atlantic SST and winter European precipitation

INTERNATIONAL JOURNAL OF CLIMATOLOGY
Int. J. Climatol. **26**: 179–191 (2006)
Published online in Wiley InterScience (www.interscience.wiley.com). DOI: 10.1002/joc.1234

EVALUATION OF THE NORTH ATLANTIC SST FORCING ON THE EUROPEAN AND NORTHERN AFRICAN WINTER CLIMATE

BELÉN RODRÍGUEZ-FONSECA,[a,*] IRENE POLO,[a] ENCARNA SERRANO[a] and MANUEL CASTRO[b]
[a] *Departamento de Geofísica y Meteorología, Universidad Complutense de Madrid, 28040, Madrid, Spain*
[b] *Facultad de Ciencias del Medio Ambiente. Universidad de Castilla – La Mancha, 45071, Toledo, Spain*

Received 24 April 2005
Revised 25 May 2005
Accepted 6 June 2005

ABSTRACT

The 1960–1996 patterns of monthly anomalous winter precipitation in Europe and North Africa (ENA) and their connection with the North Atlantic SST are studied. A lag Singular Value Decomposition analysis has been applied to monthly SST and precipitation data to define the most influential Atlantic oceanic areas on the winter ENA rainfall. The results indicate a link between the subtropical North Atlantic SST and the winter precipitation anomalies in areas of the northern–southwestern Europe and northern Africa, since the preceding summer months. We also show that the SLP pattern connected with this subtropical oceanic area is not the NAO itself, and we explain this subtropical–extratropical connection through changes in the trade winds. The estimates of ENA winter precipitation anomalies, based on the previous summer SST, have been validated using a bootstrap analysis. Finally, we verify the reliability of this connection for the whole period from 1900 to 1996. Copyright © 2006 Royal Meteorological Society.

KEY WORDS: North Atlantic climate variability; winter European precipitation; North Atlantic Oscillation; tropical-extratropical teleconnections; subtropical SST; statistical seasonal forecast

1. INTRODUCTION

The North Atlantic Oscillation (NAO), defined as a large-scale atmospheric mass exchange between the Icelandic low and the Azores high semipermanent sea level pressure (SLP) systems (Rogers, 1984) is the most important atmospheric pattern controlling the precipitation variability in the region of Europe and Northern Africa (hereafter ENA, 20 °N–70 °N, 20 °W–55 °E). Hence, the prediction of this oscillation is the main goal for the European climate predictability.

It is well known that owing to the high thermal inertia of the sea, the anomalous sea surface temperature (SST) is one of the most convenient variables to be used as a climatic predictor. Although several decades ago, Bjerknes (1964) and Cayan (1992) showed a NAO-like atmospheric forcing of interannual North Atlantic SST (through the action of surface heat fluxes), observational studies suggest an oceanic forcing on the large-scale atmospheric circulation in the North Atlantic area, particularly associated with the NAO (Sutton and Allen, 1997; Rodwell and Folland, 2002). In particular, Czaja and Frankignoul (1999) found a relationship between the winter NAO-like pattern at 500-hPa level and the North Atlantic SST variations. The tropospheric signal that they found is strongest when the SST leads the atmosphere by 3 to 5 months. Drévillon *et al*. (2001) showed a relationship between the summer SST in one part of the Atlantic tripole and the storm tracks that cross Europe in winter. Rodwell *et al*. (1999) used an atmospheric general circulation model (AGCM) to show that SST anomalies force some of the variability of the wintertime NAO observed over the past 50 years. Okumura *et al*. (2001) have also carried out a set of long AGCM integrations, showing an interaction between

* Correspondence to: Belén Rodríguez-Fonseca, Departamento de Geofísica y Meteorología, Universidad Complutense de Madrid, 28040, Madrid, Spain; e-mail: brfonsec@fis.ucm.es

the tropical SSTs (Atlantic dipole pattern) and the extratropical North Atlantic atmospheric variability (mainly, the Azores high).

Observational studies of Rodríguez-Fonseca and Castro (2002, hereafter RFCA02) show that the extreme winter precipitation events (linked to the NAO) in the Iberian Peninsula and Northern Africa (IPNA, {20 °N–45 °N, 10 °W–10 °E}) are, in turn, connected with an anomalous SST pattern, which subtropical branch persists from the previous summer months. Owing to the fact that the NAO affects the north and south of the Euro–Atlantic sector in an opposite way, in this work we have extended the RFCA02 study to the whole ENA area described in the preceding text, with the aim of evaluating the SST influence on this area. Also, we have tried to look for a mechanism that can explain the air–sea interactions involved in the established connection. Finally, we have determined the reliability and significance of this link, using data for a longer time period.

In Section 2, the data and the preprocessing applied are described. The relationship between the North Atlantic SST and precipitation is discussed in Section 3. In Section 4, a closer investigation of the connection between subtropical North Atlantic SST and the ENA precipitation is made. Section 5 analyzes the consistency of the precipitation–SST connection identified, and finally, Section 6 summarizes the main conclusions.

2. DATA AND PREPROCESSING

The winter 'season' chosen in this study is the month sequence NDJF (from November to February) used in RFCA02, in order to make comparisons with some of the results of that study. European and Northern African monthly winter precipitation anomalies from 1960 to 1996 were calculated from the Legates and Willmott (LW) $1^\circ \times 1^\circ$ latitude–longitude resolution data set (Legates, 1989), the same database that was used in RFCA02. This database has been constructed from 26 858 precipitation stations across the world, with the highest concentration in North America and Europe. This helps to establish the reliability of the LW data in reproducing accurately the winter low frequency variability of the ENA precipitation. In fact, the typical and well documented precipitation dipole related to the NAO in winter (Rogers, 1984; Fraedrich *et al*., 1993; Hurrell, 1995), displayed in Figure 1(a), can be seen also in Figure 1(b), which displays the leading EOF structure of the anomalous winter precipitation in ENA calculated with the LW data. In this way, the high index polarity of the NAO is related to negative precipitation anomalies in southwestern ENA and positive precipitation anomalies in the North of Europe. The opposite occurs during cases of low NAO index. Figure 1(c) shows the second EOF structure of the ENA anomalous precipitation, a tripolar structure with a different behavior in central Europe than in the rest of ENA, which has also been documented by other authors (Zveryaev, 2004).

NDJF monthly wind velocity and SLP anomalies from the NCEP reanalysis (Kalnay *et al*., 1996) have been used to study the SST-atmospheric connection for the period 1960–1996. As can be seen in Figure 2(a), the first principal component of the winter ENA precipitation (PC1) projected onto the NCEP winter SLP anomalies exhibits a NAO-like pattern. Using the monthly timeseries of the NAO (Hurrell, 1995), the correlation coefficient between this NAO index and PC1 is 0.44, which is statistically significant at 98% (according to Monte Carlo test) but not as high as expected. In fact, the SLP pattern in Figure 2(a) does not strictly have the NAO structure, since the centers of action appear displaced to the east. In relation to the SLP pattern connected to the second precipitation EOF, it shows a dipolar structure with a main center over central Europe and a weaker one over the IPNA region (Figure 2(b)).

With regard to the SST anomalies, most of the results in this work are based on 1960–1996 SST data, derived from the Comprehensive Ocean–Atmosphere Data Set (COADS), with a spatial resolution of $2^\circ \times 2^\circ$ latitude–longitude. In order to study the lagged connection between the SST and the ENA NDJF precipitation anomalies, we have considered SST values corresponding to the sequence NDJF and the previous four-calendar month sequences: ONDJ (October to January), SOND (September to December), ASON (August to November), JASO (July to October), and JJAS (June to September).

Section 5 analyzes the reliability of the connection found in this study, using a longer time period for the SLP and the SST (1900–1996). In this section, we use the SLP Trenberth data (Trenberth and Paolino, 1980)

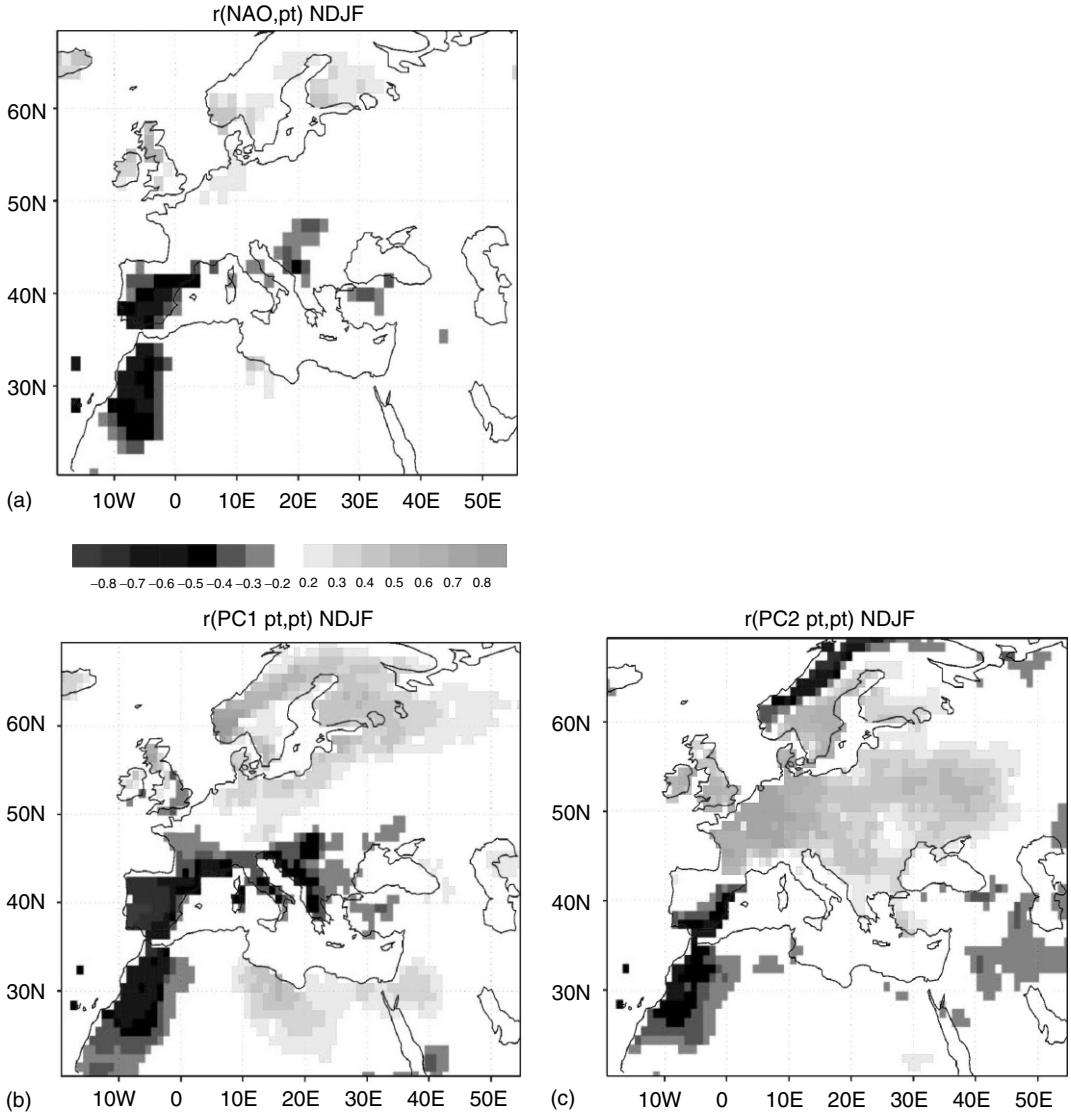

Figure 1. Correlation map between the ENA NDJF monthly precipitation anomalies and (a) the NDJF NAO index; (b) the first and (c) the second ENA winter precipitation principal components, respectively. Only the areas with 98% significant correlation (based on a Monte Carlo test) are shaded. Period: 1960–1996

and the SST derived from the Extended Reconstructed SST data (ERSST, Smith and Reynolds, **2003**). The linear trend has been first removed from the SST and precipitation, and the monthly precipitation anomalies have been standardized (not so the SST anomalies).

3. RELATIONSHIP BETWEEN ENA PRECIPITATION AND ATLANTIC SST ANOMALIES

The contemporaneous and lagged Maximum Covariance analyses (MCA, known as also as Singular Value Decomposition analyses; Bretherton *et al.*, 1992) performed in RFCA02 have been spatially enlarged to consider the winter precipitation over the entire ENA region. This has been done with the aim of verifying whether the RFCA02 conclusions can be extended to the whole European area. Figure 3 summarizes the main

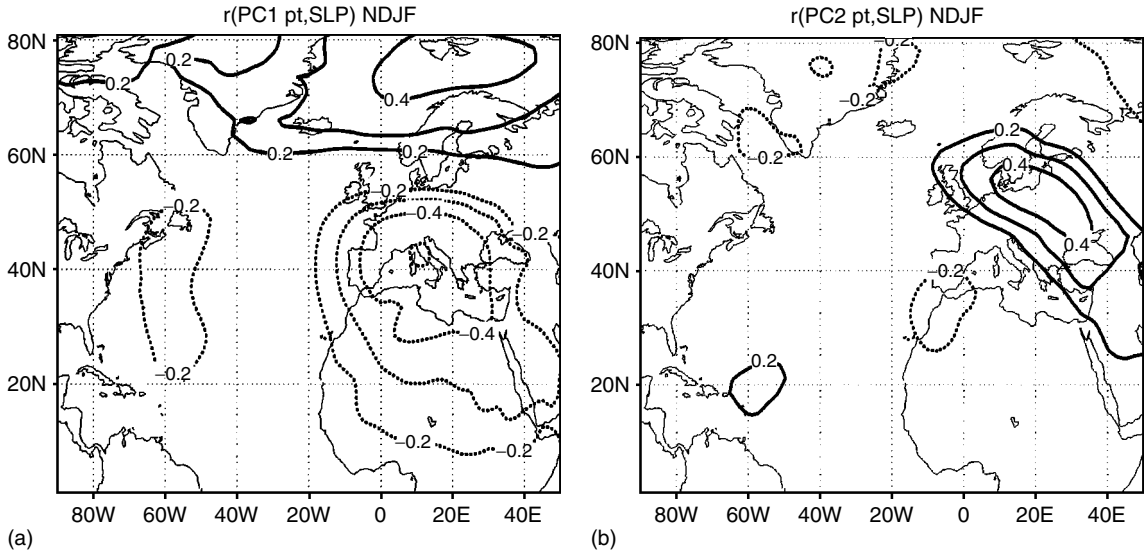

Figure 2. Correlation map between the NDJF monthly anomalous SLP over ENA and (a) the first and (b) the second ENA winter precipitation principal components, respectively. Only the areas with 98% significant correlation (from a Monte Carlo test) are shown. Contour interval of 0.1. Period: 1960–1996

results of the first mode of these MCA analyses for the simultaneous (Figure 3(a) and (b)) and 5-month lag (Figure 3(d) and (e)) winter precipitation–SST connections respectively. The statistical significance of the results has been established using a Monte Carlo test with 500 experiments, in each of which the time series of precipitation and SST are randomly permuted and the MCA analyses are repeated (Livezey, 1995). In this way, the confidence level is the percentage of experiments in which the squared covariance fraction and the values of the correlation scores, obtained when permutations are done, are smaller than the original value calculated without permutation.

As in RFCA02, the contemporaneous connection between the precipitation and the SST in NDJF shows the documented North Atlantic oceanic tripole pattern (Figure 3(b)) that reflects the winter atmospheric forcing onto the ocean through latent and sensible heat fluxes (Bjerknes, 1964; Cayan, 1992). In fact, when calculating the correlation map between the leading NDJF SST expansion coefficient and the NDJF anomalous SLP field (Figure 3(c)), we obtain a Monte Carlo significant NAO-like structure. The correlation coefficient between the NDJF SST expansion coefficient and the NDJF NAO index is 0.43, significant at the 98% level.

With respect to the precipitation structures linked to this SST pattern, the areas in the heterogeneous correlation map of Figure 3(a) coincide with those winter precipitation areas connected to the NAO (Figure 1(a)) and primarily reflect the leading EOF pattern of the winter precipitation (Figure 1(b)). The correlation coefficient between the first NDJF precipitation expansion coefficient of this simultaneous SST connection and the winter NAO is 0.46, significant at the 98% level.

Figure 3(a) and (b) reveals that during winter months, an increase (decrease) in the subtropical and subpolar North Atlantic SST, and a decrease (increase) in the Northwestern Atlantic SST are linked to positive (negative) precipitation anomalies in the IPNA and the Mediterranean areas (as shown in RFCA02) and negative (positive) anomalies in the British Isles, Scandinavian Peninsula, and Denmark. This connection is also related to a negative (positive) NAO-like structure (Figure 3(c)). The structure of this SST pattern coincides with the January–March mean SST anomalous pattern, also shown by Okumura *et al.* (2001). The wind field response shown by these authors induces highly significant anomalies in the Azorean high and also anomalies, although weaker, in the Icelandic low.

Owing to the large thermal inertia of the ocean, some of the SST-influenced regions in Figure 3(b) could have been formed in previous months, persisting until the next winter and having, for this reason, a potential predictive value. Lag-MCA analyses between NDJF monthly precipitation and 'seasonal' SST anomalies

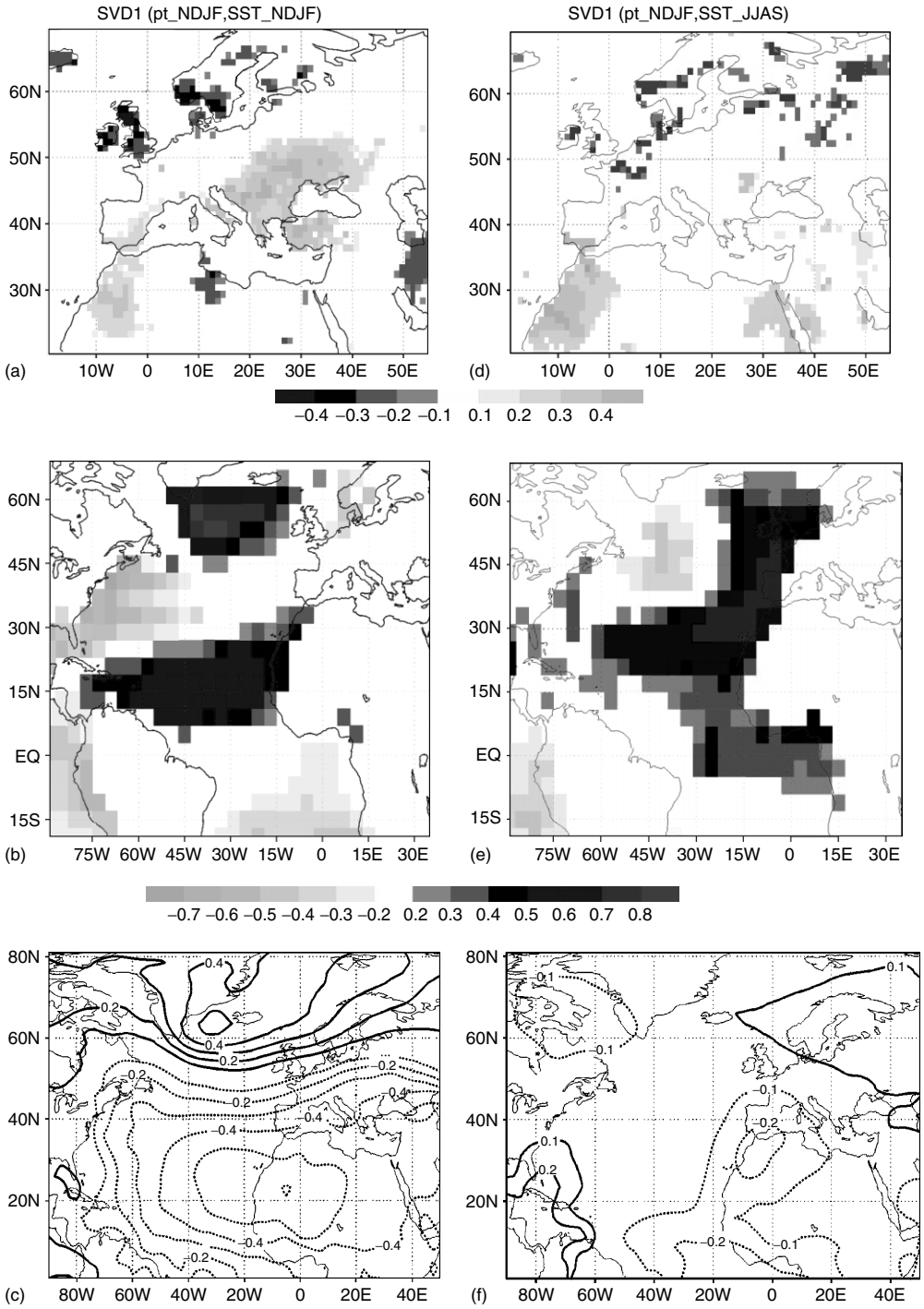

Figure 3. Left panel: results of the first mode of the MCA analysis done between NDJF ENA monthly precipitation and North Atlantic SST anomalies: (a) precipitation heterogeneous correlation map, (b) SST homogeneous correlation map. Only the areas with 98% significant correlation (from a Monte Carlo test) are shaded. (c) significant correlation map at 98% (from a Monte Carlo) between the NDJF SST first MCA expansion coefficient and the contemporaneous monthly anomalous SLP. Contour interval 0.1. Right panel: (d)–(f) similar to (a)–(c) in the left panel except the lag-MCA analysis done between the NDJF ENA monthly precipitation and the previous JJAS North Atlantic SST anomalies. Period: 1960–1996. The contour interval is 0.1, the continuous line indicates positive correlation scores and the dotted line negative correlation scores

have been performed with the aim of determining those persisting regions. From −1 to −5 months, the SST lag (not shown), the connection between the precipitation and the SST, persists in the subtropical Atlantic (as in RFCA02). Figure 3(d) and (e) shows the precipitation heterogeneous correlation map and the SST homogeneous correlation map respectively, as a result of the lag-MCA analysis carried out with the NDJF anomalous ENA precipitation and the previous JJAS SST anomalies (lag = −5 months). The summer oceanic pattern of Figure 3(e) exhibits a statistically 98% significant positive correlation (positive scores in Figure 3(d)) with the next winter precipitation in the south of the Iberian Peninsula and northwest of Africa, and a statistically 98% significant negative correlation (negative scores in Figure 3(d)) in the south of the Scandinavian Peninsula, Denmark and the British Isles, among other regions (same as Figure 3(a)).

Figure 3(f) shows the winter SLP pattern that is connected to this MCA summer SST structure. This atmospheric pattern has common features not only with the winter SLP structure associated with the first precipitation EOF (Figure 2(a)) but also with the pattern connected with the second precipitation EOF (Figure 2(b)). Indeed, 99% significant correlation coefficients (around 0.5) obtained between the leading precipitation expansion coefficient in the JJAS SST – NDJF precipitation connection (Figure 3(d)) and the first (Figure 1(b)) and second (Figure 1(c)) winter precipitation principal component, led us to conclude that the SLP pattern connected with summer SST anomalies could be a 'hybrid' of those SLP patterns linked to the leading and second winter precipitation EOF and not 'strictly' to the NAO.

In the light of these results, those significant SST areas in Figure 3(e) that coincide with those in Figure 3(b) could reduce the North Atlantic region, influencing winter ENA precipitation anomalies, to a small and easily monitored area. The coincident regions in Figure 3(b) and (e) is located, like in RFCA02, between 15 °N and 25 °N, i.e. in the subtropical North Atlantic area.

The next section focuses on the role of the summer subtropical North Atlantic SST signal (hereafter SA) in influencing the winter ENA precipitation.

4. THE SUBTROPICAL NORTH ATLANTIC AND THE WINTER EUROPEAN PRECIPITATION

Considering the above results, the SA index is defined as the standardized area-average of the monthly SST anomalies over the eastern subtropical North Atlantic region 15 °N–25 °N–30 °W–20 °W (RFCA02).

The correlation coefficient between the JJAS SA index and the leading JJAS SST expansion coefficient from 1960 to 1996 (from the MCA, between the JJAS SST and the next NDJF precipitation) is 0.74. Also, both oceanic indices exhibit statistically significant linear correlation scores with the first principal component of the winter precipitation over ENA (0.30 and 0.26 respectively). Figure 4(a) shows the connection between the ENA winter monthly precipitation and the previous summer (JJAS) SA index. The good agreement between Figure 4(a) and Figure 3(d) indicates that the influence of the North Atlantic summer SST on the ENA winter precipitation could be practically explained in terms of the connection with the subtropical North Atlantic SST variability.

With regard to the SLP, Figure 4(b) shows that a decrease (increase) of the subtropical North Atlantic SST anomalies induces an anticyclonic (cyclonic) anomaly of the circulation over the IPNA area, this result being in agreement with Okumura *et al*. (2001). These authors explained this circulation in terms of the changes in the tropical Atlantic dipolar SST mode. In this manner, Okumura *et al*. observed that the wind response to a southward SST gradient (negative SST anomalies over the SA region) is a strengthening of the trade winds in the Atlantic Northern Hemisphere, which leads to a wind evaporation–SST feedback (Chang *et al*., 1997; Chang *et al*., 2000) to the dipole interhemisphere mode. This effect on the trade winds could change the atmospheric circulation, influencing the Azores high, and ultimately the NAO pattern.

In fact, Figure 5 represents the winter mean anomalous wind for high and low SA index, showing how, when the phase of the SA index is negative (positive) in NDJF, the mean wind NDJF anomalies have an anticyclonic (cyclonic) shape over the North Atlantic region, increasing (decreasing) the precipitation in northern Europe and decreasing (increasing) in the IPNA region. These two winter anomalous wind patterns keep their opposite behavior if we consider the SA index for JJAS (in Figure 5(b) and (d)).

All these results indicate that the winter anomalous precipitation in the earlier mentioned ENA areas is susceptible to being partially described from the previous summer SST anomalies over the limited subtropical

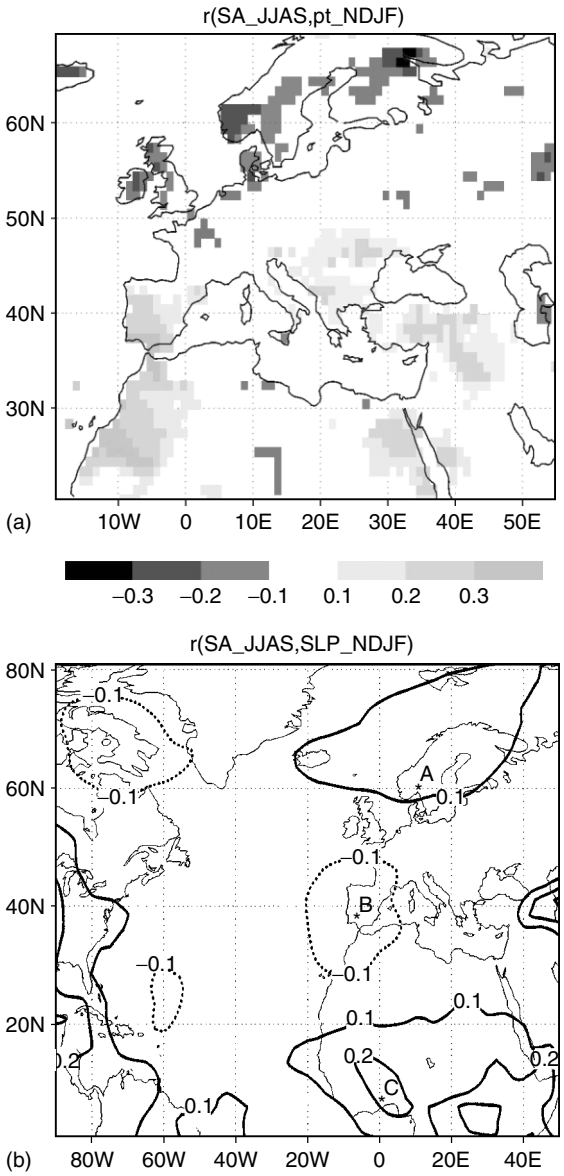

Figure 4. (a) Correlation map between the oceanic JJAS SA index and the next NDJF monthly precipitation anomalies in ENA. Only the areas with 98% significant correlation (based on a Monte Carlo test) are shaded. (b) Significant correlation map at 98% (based on a Monte Carlo test) between the summer SA index and the NDJF monthly SLP anomalies. The contour interval is 0.1, the continuous line indicates positive correlation scores and the dotted line negative correlation scores. Period: 1960–1996

North Atlantic region, a result that might represent a substantial help in the seasonal winter predictability of rainfall over ENA.

A simple linear regression model has been constructed to estimate the ENA winter monthly anomalous precipitation on the basis of the previous summer subtropical Atlantic SST anomalies. The independent variable is the JJAS oceanic SA index, and the dependent variable is the NDJF monthly precipitation anomaly in ENA. This regression analysis has been applied to each of the grid points of the precipitation domain and the explained variance of the predicted rainfall has been tested using a bootstrap technique. It should be noted that the use of a cross-validation, skipping just one year, was considered less appropriate because artificial skill could not be avoided owing to the large low frequency contribution to the variability. An alternative way

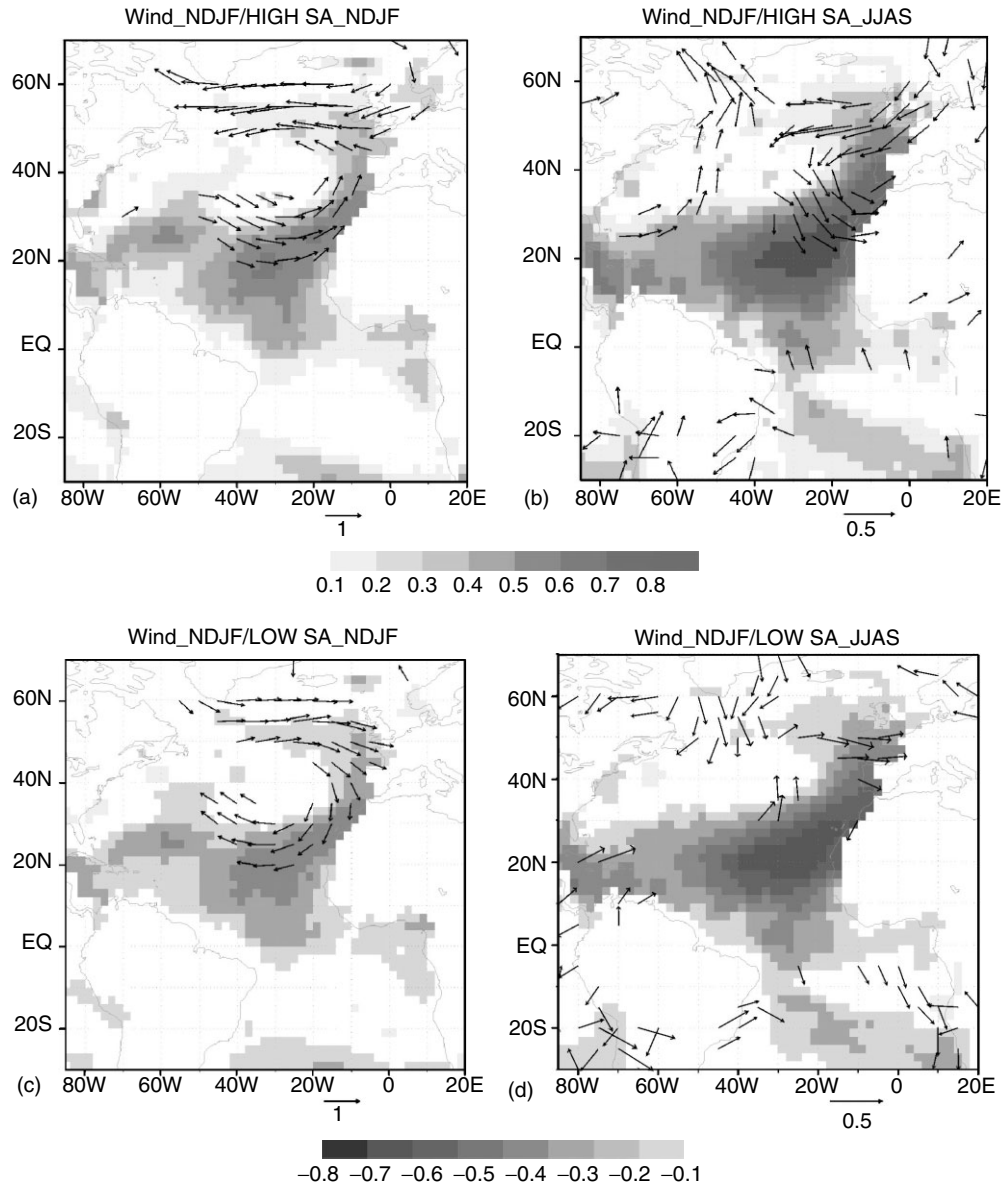

Figure 5. (a): Monthly mean wind anomalous velocity ($\geq$0.5 m·s^{-1}, arrows) during high NDJF SA index winter months. The mean SST anomaly (°C, shaded areas) for the high NDJF SA index is superimposed to the wind values. (c) Same as (a) but for low SA index. (b) and (d) Similar to (a) and (c) but considers the previous summer JJAS SA index episodes when displaying the winter anomalous wind (only mean anomalous wind $\geq$0.2 m·s^{-1} is plotted). Period: 1960–1996

of cross-validating the estimates from a model is the bootstrap technique (Efron and Tibishirani, 1993). This method consists of permuting with replacement B times the residuals (e_B) obtained between the observed (Y) and the simple regression modeled (Y_m) precipitation. Thus, for each grid point we create a set of new estimates Y_B by adding these B permuted errors, e_B, to the nonpermuted estimated precipitation (Y). Then, the variance of each of such estimates, Y_B, is calculated and compared with the variance obtained with Y_m. As Efron and Tibishirani showed, the variance about regression obtained from the bootstrap sample is appreciably smaller than that obtained from the original data, and the mean difference between the two variances (called *the inflation factor*) is added to the variance of the original data set to give an improved estimate. The

bootstrap improved fraction of variance over the region of interest is shown as a measure of the quantitative skill of estimating the ENA winter monthly anomalous precipitation from the previous summer subtropical Atlantic SST variability. In this validation procedure we have used $B = 2000$.

In Figure 6, shaded areas indicate the corresponding bootstrap improved fraction of variance of wintertime precipitation that can be explained using the winter (Figure 6(a)) or the previous summer SA SST index (Figure 6(b)) as independent variables.

This simple regression analysis explains estimated anomalies in the IPNA region (as shown by RFCA02) and also in the areas of Europe that are influenced by the subtropical North Atlantic SST variability (Figure 4(a)). These statistically significant areas in Figure 6 comprise the structure of the winter ENA precipitation pattern affected by the NAO (Figure 1(a)), which explains most of the winter ENA rainfall variability (Figure 1(b) and (c)). It is important to mention that the results of this simple regression model that only uses the summer

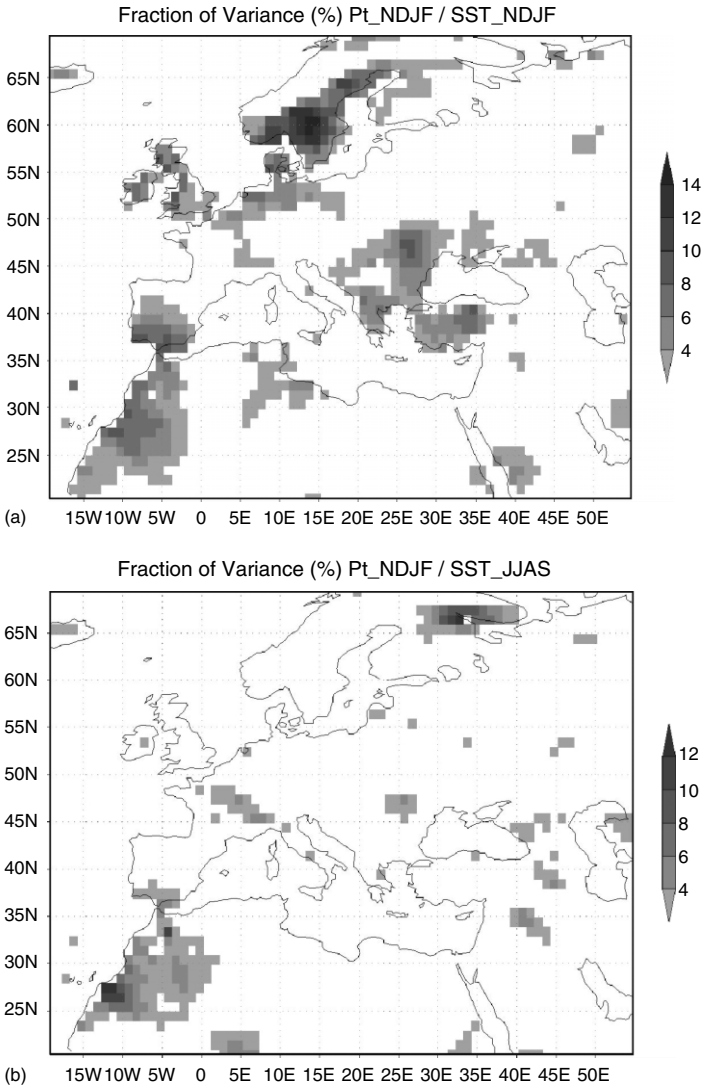

Figure 6. (a) Improved fraction of variance (%) from 2000 bootstraps of ENA NDJF anomalous precipitation calculated about linear regression with the contemporaneous oceanic SA index as independent variable. (b) Similar to (a) but using the previous summer JJAS SA index as independent variable. Period: 1960–1996

monthly SA index as an independent variable, do not differ from those regression models that use the information from the first MCA mode of the SST-precipitation connection, or the whole information from all the modes in the SST-precipitation connection (not shown). So, these results support the idea that the subtropical North Atlantic SST could be used as a tool for predicting the occurrence of significantly anomalous winter precipitation not only in the IPNA area but also in other European regions. Next, we check whether this connection is due to an artificial skill because of the short period of years used in the study (1960–1996). For this purpose, we have analyzed the connection between the precipitation and SST anomalies for the consecutive periods: 1900–1930, 1931–1960 and 1961–1996.

5. THE RELIABILITY OF THE CONNECTION BETWEEN SST AND ENA WINTER PRECIPITATION

In the previous section, it was described that the connection between summer SST anomalies and next winter ENA precipitation and SLP variability has been studied for a relatively short period (1960–1996). In order to test the reliability of such connections, and to check whether this subtropical oceanic signal is due to an artificial skill, a longer and independent data period should be used. To this end, the Trenberth and ERSST data sets mentioned in Section 2, providing SLP and SST in the areas of study respectively, were used. Although some precipitation databases for the long period 1900–1996 are also available, it must be borne in mind that, within the quite complex orographical area of interest (SW Europe and NW Africa), only a few meteorological stations were operative throughout the first half of the twentieth century. It should be also borne in mind that the interpolation for a regular grid of sparse and irregularly distributed precipitation data has higher uncertainty than for SLP data. Thus, it is reasonable to think that a statistically significant connection between SST and SLP would be reliable enough to serve as a proxy for connection with precipitation as well.

In order to test the SST–SLP connection described in the previous section, we have defined a SLP index from 1900–1996 NDJF monthly anomalies, using the information provided by the correlation pattern in Figure 3(f) and correlating this atmospheric index with the corresponding previous JJAS SST anomalies. Because of the large low frequency variations in the JJAS SST through 1900–1996, we have considered three separate sets of JJAS SST anomalies based on means for 1900–1930, 1931–1960 and 1961–1996. The SLP index has been created by adding the 1900–1996 NDJF anomalous Trenberth SLP time series of the grid points indicated in Figure 4(b) (labeled as A, B), weighted by its associated correlation score in Figure 3(f). Thus, the SLP index is defined as:

$$SLP_{\mathrm{idx}} = 0.17 \cdot SLP_{\mathrm{A}} - 0.23 \cdot SLP_{\mathrm{B}}$$

Figure 7(a)–(c) shows the 90% significant correlation maps done with the above SLP index for NDJF months and the three separate sets of JJAS ERRS SST anomalies for 1900–1930, 1931–1960 and 1961–1996. The statistical significance of the correlation scores has been established using a Monte Carlo test with 500 experiments. We can see that the areas with winter SLP index connected with JJAS SST anomalies are located over centers of action of the oceanic pattern shown in Figure 3(e) (which shows the connection between JJAS SST and winter precipitation in ENA). When correlating the winter SLP index with the contemporaneous ERRS SST anomalies for the preceding three separate periods through 1900–1996, we can appreciate a pattern similar to the *Atlantic tripole pattern*, whose centers of action are coincident for the three periods (Figure 7(d)–(f)).

On the basis of these calculations, we suggest that the subtropical North Atlantic signal is a *climatic* signal, which could improve the knowledge of the reasons of winter climate variability (in terms of precipitation) over ENA. Nevertheless, there are other regions of the Atlantic tripole with statistically significant correlation with the ENA precipitation (the subpolar region) that could be the topic of future studies.

6. SUMMARY AND CONCLUSIONS

The main findings of this study can be summarized as follows:

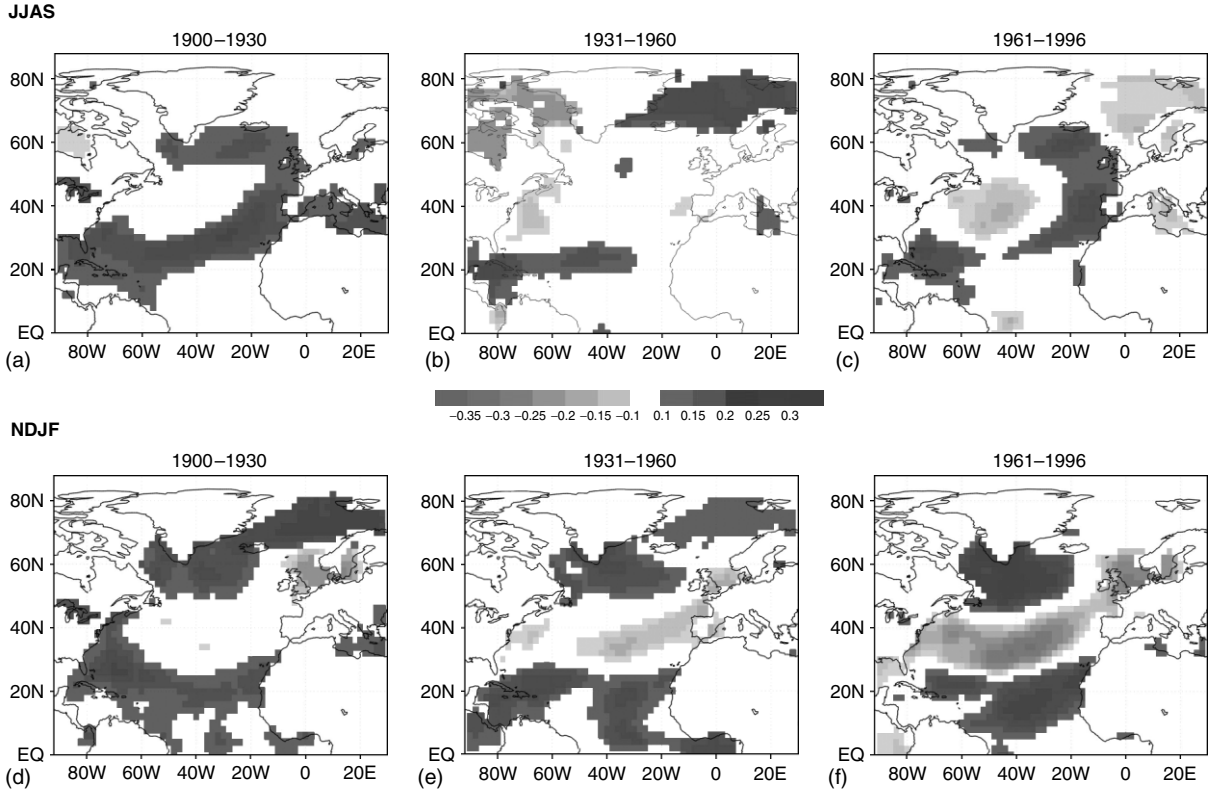

Figure 7. (a)–(c) Significant correlation maps at 90% (from a Monte Carlo test) between the SLP index, derived from Figure 3(f), in NDJF and the separate sets of previous JJAS ERSST SST anomalies for 1900–1930, 1931–1960, and 1961–1996, respectively. (d)–(f) Similar to (d)–(f) but considers the contemporaneous NDJF ERSST SST anomalies

1. The leading North Atlantic SST pattern connected to the ENA winter anomalous monthly precipitation exhibits a tripole structure with centers of action located at the south of Greenland, the central North Atlantic and the subtropical Atlantic. The persistence of the signal over the subtropical North Atlantic from the previous summer months could be helpful in seasonal winter predictability of rainfall over ENA, although this connection is higher in the southwestern ENA area.
2. The areas with anomalous precipitation connected with this SST structure form a dipolar pattern with opposite behavior in the rainfall variability between the north and the south of ENA. This dipolar precipitation pattern has common areas with those linked to the NAO and with the two main ENA precipitation EOFs.
3. This oceanic summer pattern appears to be connected with a winter SLP structure that differs from the NAO and which seems to be a 'hybrid' of the SLP pattern linked to the first and second ENA precipitation EOFs.
4. The wind velocity composite maps for high and low subtropical North Atlantic SST index (SA, established by the authors in RFCA02) show that this SST signal propagates to the extratropics and influences on the ENA precipitation. In this way, a decrease (increase) in the SA SST intensifies (weakens) the trade winds, producing variations in the North Atlantic circulation (as shown also by Okumura *et al*., 2001), and mainly in the subtropical high-pressure system.
5. A simple regression model with the summer subtropical oceanic index as an independent variable and the ENA winter monthly precipitation anomalies as a dependent variable shows statistically significant results over the same areas that define the leading patterns of the winter ENA precipitation variability, this connection being stronger in the southwestern ENA area.

6. The possibility of artificial skill in this oceanic subtropical influence on the ENA precipitation, due to the short period of the study (1960–1996), has been checked from SLP 1900–1996 independent data. The oceanic signal obtained for 1960–1996 exhibits a pattern with common centers of action to the structures found for 1900–1930 and 1931–1960 respectively.

We have still no answer to the question of how the oceanic subtropical signal persists from summer to the next winter. Nowadays we are performing studies of the underlying northern subtropical Atlantic water column temperature profiles during the extreme SA SST cases. We have found (Polo *et al*., 2005) that during summer there is an opposite connection between the coastal upwelling and the increase of the SST due to the surface wind forcing. This suggests the existence of a feedback mechanism to explain the connection found in this paper between summer subtropical Atlantic SST and the winter ENA climate variability.

This will be the focus of future studies that will try to explain the mechanisms involved in this connection. Also, we are working with other SST indices in the Atlantic, and we are considering the stratospheric influence as well (Baldwin and Dunkerton, 2001). The inclusion of these factors could help improve the winter European seasonal forecasting, and could also be useful as tools for GCM simulations that are designed to look for the causes of the teleconnection between SST and the European and North Africa precipitation variability.

ACKNOWLEDGEMENTS

We would like to thank Professor J. Michael Wallace very much for his helpful suggestions during his visit to the Department of Geophysics and Meteorology in 2002. We sincerely would like to thank the referees for providing us with careful reviews that have considerably improved the manuscript. This study was supported by the Spanish MCYT projects REN2000-0770 and REN2002-03424.

REFERENCES

Baldwin MP, Dunkerton TJ. 2001. Stratospheric harbingers of anomalous weather regimes. *Science* **294**: 581–584.

Bjerknes J. 1964. Atlantic air-sea interaction. *Advances in Geophysics* **10**: 1–82.

Bretherton CS, Smith C, Wallace JM. 1992. An intercomparison of methods for finding coupled patterns in climate data. *Journal of Climate* **5**: 541–560.

Chang P, Ji L, Li H. 1997. A decadal climate variation in the tropical Atlantic ocean from thermodynamic air-sea interactions. *Nature* **385**: 516–518.

Chang P, Saravanan R, Ji L, Hegerl GC. 2000. The effect of local sea surface temperatures of atmospheric circulations over the tropical Atlantic sector. *Journal of Climate* **13**: 2195–2216.

Cayan DR. 1992. Latent and sensible heat flux anomalies over the northern oceans: driving the sea surface temperature. *Journal of Physical Oceanography* **22**: 859–881.

Czaja A, Frankignoul C. 1999. Influence of the North Atlantic SST on the atmospheric circulation. *Geophysical Research Letters* **26**: 2969–2972.

Drévillon M, Terray L, Rogel P, Cassou C. 2001. Midlatitude Atlantic SST influence on European winter climate variability in the NCEP reanalysis. *Climate Dynamics* **18**: 331–344.

Efron B, Tibishirani R. 1993. *An Introduction to the Bootstrap*. Chapman & Hall: London.

Fraedrich K, Bantzer C, Burkhardt U. 1993. Winter climate anomalies in Europe and their associated circulation at 500 hPa. *Climate Dynamics* **8**: 161–175.

Hurrell JW. 1995. Decadal trends in the North Atlantic Oscillation: regional temperatures and precipitation. *Science* **269**: 676–679.

Kalnay E, Kanamitsu M, Kistler R, Collins W, Deaven D, Gandin L, Iredell M, Saha S, White G, Woollen J, Zhu Y, Chelliah M, Ebisuzaki W, Higgins W, Janowiak J, Mo KC, Ropelewski C, Wang J, Leetmaa A, Reynolds R, Jenne R, Joseph D. 1996. The NCEP/NCAR 40-Year Reanalysis Project. *Bulletin of the American Meteorological Society* **77**: 437–471.

Legates DR. 1989. A high-resolution climatology of gauge-corrected global precipitation. In *Precipitation Measurement. Proceedings of the WMO/IAHS/ETH International Workshop on Precipitation Measurement, St. Moritz, Switzerland, Dec. 3–7, 1989*, Sevruk B (ed) Swiss Federal Institute of Technology: Zurich, 519–526.

Livezey RE. 1995. The evaluation of forecasts. In *Analysis of Climate Variability: Applications of Statistical Techniques*, von Storch H, Navarra A (eds) Springer-Verlag: Berlin 177–196.

Okumura Y, Xie S-P, Numaguti A, Tanimoto Y. 2001. Tropical Atlantic air-sea interaction and its influence on the NAO. *Geophysical Research Letters* **28**: 1507–1510.

Polo I, Rodríguez-Fonseca B, Sheinbaum J. 2005. Northwest Africa upwelling and the Atlantic climate variability. *Geophysical Research Letters* **32**: DOI:10.1029/2005GL023883.

Rodríguez-Fonseca B, Castro M. 2002. On the connection between winter anomalous precipitation in the Iberian Peninsula and North West Africa and the summer subtropical. *Geophysical Research Letters* **29**: No. 18, 1863. DOI 10.1029/2001GL014421.

Rodwell MJ, Folland CK. 2002. Atlantic air-sea interaction and seasonal predictability. *Quarterly Journal of the Royal Meteorological Society* **128**: 1413–1443.

Rodwell MJ, Rowell DP, Folland CK. 1999. Oceanic forcing of the wintertime North Atlantic Oscillation and European climate. *Nature* **398**: 320–323.
Rogers JC. 1984. The association between the North Atlantic Oscillation and the Southern Oscillation in the Northern Hemisphere. *Monthly Weather Review* **112**: 1999–2015.
Smith TM, Reynolds RW. 2003. Extended reconstruction of global sea surface temperatures based on COADS data (1854–1997). *Journal of Climate* **16**: 1495–1510.
Sutton RT, Allen MR. 1997. Decadal predictability of North Atlantic sea surface temperature and climate. *Nature* **388**: 563–567.
Trenberth KE, Paolino DA. 1980. The Northern Hemisphere sea-level pressure data set: trends, errors and discontinuities. *Monthly Weather Review* **108**: 855–872.
Zveryaev I. 2004. Seasonality in precipitation variability over Europe. *Journal of Geophysical Research* **109**: D05103. vol doi:10.1029/2003JD003668.

Northwest Africa upwelling and the Atlantic climate variability

Irene Polo,[1] Belén Rodríguez de Fonseca,[1] and Julio Sheinbaum[2]

Received 22 June 2005; revised 26 October 2005; accepted 28 October 2005; published 2 December 2005.

[1] Summer Subtropical North Atlantic (SNA) Sea Surface Temperature (SST) anomalies have recently been connected to winter atmospheric variability in the Atlantic European sector. Wind-induced surface heat flux changes are believed to be the major cause of SNA SST anomalies. However, the impact of coastal upwelling off northwest Africa, on SNA SST variability has been overlooked. Since the area is known to have a richer dynamical behavior than other regions of the central SNA, subsurface thermal anomalies are included in our analysis. Results show that this upwelling region affects significantly the patterns of covariability between climatically relevant variables, suggesting that more intricate processes may be involved in generating surface anomalies that, in turn, may influence the European sector climate variability. **Citation:** Polo, I., B. R. de Fonseca, and J. Sheinbaum (2005), Northwest Africa upwelling and the Atlantic climate variability, *Geophys. Res. Lett.*, *32*, L23702, doi:10.1029/2005GL023883.

1. Introduction

[2] Extreme winter precipitation events in the Euro Atlantic and Northern Africa sector, which are clearly linked to the North Atlantic Oscillation (NAO), have been related to the previous summer SST variations in the Subtropical North Atlantic (SNA) area [*Rodríguez-Fonseca and Castro*, 2002; *Rodríguez-Fonseca et al.*, 2005, hereinafter referred to as RF05]. These results highlight the important role of SNA-SST anomalies as a possible predictor of winter extra-tropical precipitation events.

[3] SNA region shares its variability with two SST patterns, as it is the southernmost lobe of the SST tripole [*Sutton and Allen*, 1997] and also the northern part of the tropical Atlantic SST dipole. *Carton et al.* [1996] and *Chang et al.* [1997] suggest that SST anomalies in the tropical Atlantic are caused by anomalies in the wind-induced surface heat fluxes. However, in the coastal region off northwest Africa, north of the Guinea Dome, coastal upwelling by alongshore winds significantly affects the SST [*Carton et al.*, 1996]. *Seager et al.* [2001] point out that, changes in coastal upwelling and offshore advection are probably responsible for some of the observed SST changes in the region west of Morocco. All these numerical studies do not find evidence that off equatorial SSTs are influenced by subsurface thermal anomalies except near the African coast.

[4] In contrast, other studies suggest that the role of the ocean should be taken into account in order to study the SST variability. *Leeuwenburgh and Stammer*'s [2001] observational study finds remarkable correlation between SST and Sea Surface Height (SSH) anomalies in all ocean basins. Since, SSH anomalies are mainly associated with barotropic and first mode baroclinic signals [*Stammer*, 1997], the internal ocean dynamics cannot be neglected in air-sea interaction processes. In relation to this, the work of *Mayer et al.* [2001] described the subtropical region as a transition area where both, the thermocline dynamics and the surface fluxes contribute to the SSH anomalies, noting the particular behavior of the subtropical area between 10°N and 20°N. Furthermore, *Weller*'s [2003] analysis of the Northeast Atlantic subduction mooring array, concludes that several processes are at work in controlling the mixed layer dynamics around the SNA area including advection, Ekman pumping and eddies.

[5] The lack of climate studies looking at the role of subsurface variability in SST anomalies is due, to a large extent, to the absence (until recently) of adequate observational databases to carry out this task, but also to model studies, which suggest that surface fluxes are the key factor, which determine subtropical SST variability.

[6] Our report attempts to fill this gap by using the recently created *Tropical Atlantic Ocean Subsurface Temperature Atlas* data set (TAOSTA) of monthly 0 to 500 m depth subsurface temperatures [*Vauclair and du Penhoat*, 2001] together with other standard surface data sets, analyzing and quantifying the covariability patterns.

[7] The oceanic region along the northwest African coast is a complex system forced by the northeast Trade winds. *Santos et al.* [2005] have related decadal changes in the Canary coastal upwelling system to alongshore wind changes, having an important impact in the ecosystem productivity. Although the NW Africa upwelling is confined to the waters relatively close to the coast, the impact of the cold SST is felt 300 to 600 km offshore [*Mittelstaedt*, 1991], though eddies and filaments. Besides, being the eastern boundary of the subtropical gyre, processes occurring there could impact regions elsewhere through propagation of Rossby waves.

[8] The TAOSTA data set used in this study may not resolve all details of the processes occurring along the boundary but does capture the impact of cold SST and deeper temperature anomalies close to the coast, the ocean interior and their low frequency variability.

[9] In the next section the data and methodology used in the study are described, followed by the results of the different multiple MCA analysis and the summary of main conclusions.

2. Data and Methodology

[10] To study the anomalous thermal structure of SNA water column, the 0-to-500 meters depth (14 levels) sub-

[1]Departamento de Geofísica y Meteorología, Universidad Complutense de Madrid, Madrid, Spain.
[2]Departamento de Oceanografía Física, CICESE, Ensenada BC, México.

0094-8276/05/2005GL023883$05.00

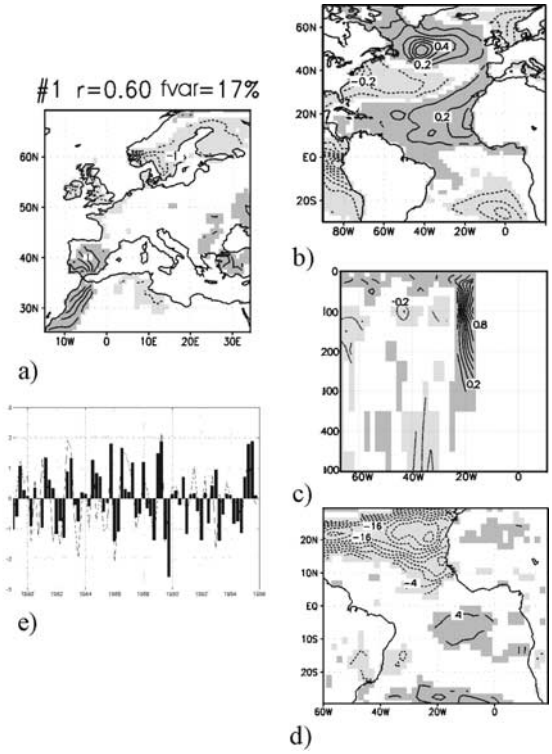

Figure 1. Leading mode of the multiple MCA analysis between a) European precipitation (htm map CI = 0.5 cm month^{-1}), b) Atlantic SST (hmm map CI = 0.1°C), c) 15°N water column temperature profile (hmm map CI = 0.1°C) and d) surface latent heat flux (hmm map CI = 2 W m^2). Only those areas 98% statistically significant, evaluated with a t-test, are shaded (dark and light shaded areas correspond to positive and negative values respectively). The zero contour line has been removed. The standardized expansion coefficients from the predictand (bars) and the predictor (continuous line) fields are plotted in (e). See color version of this figure in the HTML.

surface temperature (Tp) data, from the TAOSTA database, has been used. The available data period is 1979 to 1998, and the spatial grid resolution is 2° × 2° lat-long, having adequate statistics for using in climate variability studies [*Vauclair and du Penhoat*, 2001].

[11] Preliminary analysis showed that the maximum SST and Tp covariability takes place between 15°N to 20°N. This feature, together with the fact that the 15°N has good temporal-spatial resolution in the TAOSTA database, has made us choose the 15°N water column thermal profile (Tp15) to characterize the subtropical subsurface.

[12] The Atlantic observational SST data comes from the Extended Reconstructed Sea Surface Temperatures (ERSST [*Smith and Reynolds*, 2003]). The observational wind stress over the Tropical Atlantic has been obtained from the Pilot Research Moored Array in the Tropical Atlantic (PIRATA-CLIVAR) dataset [*Servain et al.*, 2003].

[13] As the former databases do not include observed surface wind and latent heat flux, we obtained these data from the NCEP/NCAR re-analysis dataset [*Kalnay et al.*, 1996]; considering positive latent heat flux when it is a gain for the atmosphere.

[14] The whole study will analyze the winter variability with a spatial resolution of 2° × 2° lat-lon and from 1979–1998, as this is the available time period of the TAOSTA data set.

[15] With regard to the European precipitation, we have used Legates and Willmott [*Legates*, 1989], 1° × 1° lat-lon resolution dataset from 1979 to 1996.

[16] Taking into account the fact that the NW Africa upwelling reaches its southernmost extent in winter (15°N is therefore a good profile), and with the aim of making comparisons with previous studies (RF05), the analysis will be done during the winter anomalous seasonal monthly sequence November–December–January–February (NDJF). The linear trend has been removed from the anomalous data before performing the analysis (average values for the removed trend are: −0.003°C y^{-1} for the subsurface temperature, −0.02°C y^{-1} for the SST, 0.03 cm month^{-1} y^{-1} for the precipitation, and −0.55 W m^{-2} y^{-1} for the latent heat flux).

[17] Multiple Maximum co-variance analysis (MCA, or SVD [*Bretherton et al.*, 1992]) is used to identify the modes that explain the maximum co-variance between a dependent and several independent fields. Each mode comprises different spatial structures and time series (expansion coefficients) for all the fields involved in the analysis. The results are shown in terms of heterogeneous and homogeneous regression maps for the dependent and independent fields respectively. For each mode, the dependent heterogeneous map (htm) shows the amplitude of the projection (for each grid point) of the expansion coefficient of the independent fields on the grid point anomaly time series of the dependent one. The independent homogeneous maps (hmm) show the amplitude of the projection of the independent mode on the grid point anomaly time series of each independent field. Only those areas that are 98% statistically significant (evaluated with a t-test) are mapped. The covariance fraction (fvar), a measure of the fraction of explained covariability by each mode; and the correlation coefficient (ruv) between the independent and dependent expansion coefficients, completes the information.

3. Results

[18] The multiple MCA analysis linking the anomalous winter European precipitation with the Atlantic SST, the sea sub-surface temperature at 15°N and the surface latent heat flux, has been performed (Figure 1). The leading mode, which explains a 17% of fvar, shows the dipolar precipitation pattern and north Atlantic SST tripole structure, both known to be related to the NAO pattern (RF05), with a correlation coefficient of 0.46 between the NAO and the precipitation expansion coefficient.

[19] In the subtropical region the SST pattern (Figure 1b) has the same structure as the meridional mode [*Chang et al.*, 1997], and the signal can also be seen in the surface latent heat flux structure, where the action centers are located over the SNA and the central-eastern equatorial areas (Figure 1d), although the southern hemisphere contribution is weaker. The leading 15°N temperature profile pattern shows an anomalous water column located eastern 20°W and extended down to 350 m depth (Figure 1c). This is a

region close to the NW African coast characterized by the well-known seasonal coastal upwelling. Western to this column, there is an anomalous Tp15 shallower structure covering the mixed layer (Figure 1c). The temporal evolution of the expansion coefficients shows high frequency interannual variability of the precipitation, that correlates with a 0.6 score with the oceanic variables. This suggests that the oceanic fields explain part of the European winter precipitation low frequency variability.

[20] All these results are consistent with other author findings. In this way, the NAO, which is the cause of the European dipole pattern (Figure 1a) [*Hurrell*, 1995; RF05], is strongly coupled to the Atlantic SST Tripole suggesting a positive feedback between them [*Rodwell et al.*, 1999; *Pan*, 2005]. *Chang et al.* [1997] also shows that the SST anomalies in the SNA region are mainly driven by wind-induced latent heat fluxes (Figure 1d) but they do not say anything about the subsurface thermal contribution (Figure 1c).

[21] Our study considers the influence of all the components that could be involved in this coupled system, quantifying not only the thermodynamics associated with heat flux exchanges but also the dynamics associated with the NW Africa upwelling, a system that has been pointed out to significantly affect the SST variability in the Guinea Dome region [*Carton et al.*, 1996]. Figure 2 shows the leading mode of the multiple MCA analysis between the Atlantic SST, the Tp15 and the surface heat flux. The Equatorial Pacific has been masked out for the analysis in order to remove the ENSO effect. The Atlantic tripole, together with the Atlantic dipole, appear as the leading mode of the Atlantic SST related to the Tp15 anomalies and the surface latent heat flux (Figure 2a). The latent heat flux pattern in the tropical Atlantic (Figure 2c) shows the interhemispheric gradient related to the cross-equatorial wind [*Chang et al.*, 1997]. The subsurface temperature pattern (Figure 2b) is highly correlated with the one found in Figure 1c (0.8 correlation score between them) and also with the leading Tp15 EOF (not shown). Again, this feature reminds us that we cannot forget the subsurface when describing the SST variability in the SNA region.

[22] We now consider two different analyses to quantify the surface latent heat flux, and the subsurface thermal contributions, separately; the MCA analysis done with the SST and the Tp anomalies, and the MCA analysis done with the SST and the latent heat flux anomalies. Both analyses (not shown) represent the same structures as those in the previous figures but they explain a significantly different percentage of the covariance fraction (27% when considering the Tp15 as the predictor, versus 19% when considering the latent heat fluxes). The expansion coefficient related to the Tp15 leading MCA mode shows lower frequency variability than the heat flux leading MCA mode, when explaining the same SST pattern. This feature indicates that the subsurface variability is related to the slow-varying decadal SST variability, explaining a higher percentage of the SST variance.

[23] But, is the subsurface thermal variability east of 20°W due to coastal upwelling? Wind stress is accepted as the most important driving force for coastal upwelling. For this reason, we have performed an analysis of the wind stress and its curl in relation to anomalous subtropical SST.

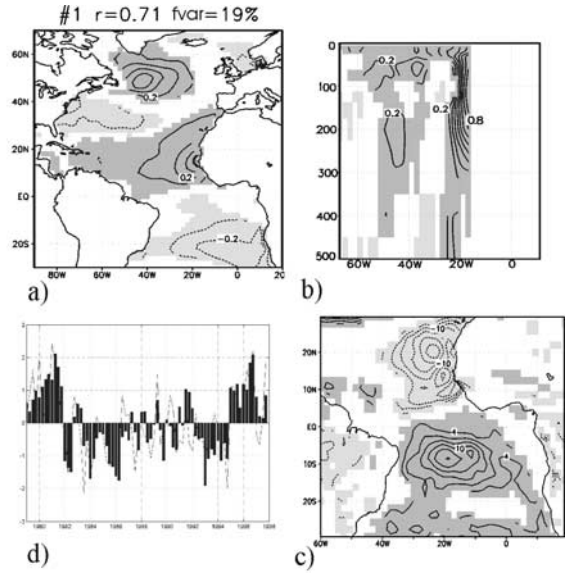

Figure 2. As Figure 1 but for the leading mode of the multiple MCA analysis between a) Atlantic SST (htm map CI = 0.1°C), b) 15°N water column temperature profile (hmm map CI = 0.1°C) and c) surface latent heat flux (hmm map CI = 2 W m^2). See color version of this figure in the HTML.

Also the latent heat flux for a positive and a negative month lag will be analyzed. In this way, the role of the dynamics and the thermodynamics in the anomalous SST is shown.

[24] To reach this aim, the leading mode of the winter SNA SST principal component (fvar = 68%), is projected, for the tropical Atlantic, on the anomalous SST (Figure 3a), the anomalous latent heat flux and surface wind (Figure 3b); and also onto the anomalous wind stress and its curl (Figure 3c). For positive SNA anomalous SST event, the results are interpreted as follows: one month before NDJF season, the wind-induced latent heat flux anomalies are negative, whilst the wind stress curl anomalies are inducing negative upwelling anomalies along the coast. The regression map done with the Tp15 anomalies shows the same structure as the previous figures (not shown). In NDJF, the wind stress curl is more intense, and the latent heat flux is still negative except for the upwelling area (Figure 3b, central panel). One month later, the latent heat flux is positive over the SNA region, the upwelling is reduced but still negative and the SST anomalies persist. From these findings, a thermodynamic budget study of the SNA region is necessary.

4. Conclusions

[25] This study have evidenced that the connection between the European precipitation and the SST is, not only through latent heat flux exchanges but also through the water column temperature variability in the SNA region.

[26] The results show how SST anomalies over the SNA region, related to the meridional mode of the TAV and to the southern branch of the Atlantic tripole, which in turn are connected to the European precipitation, cannot be explained just by the wind-induced latent heat flux changes.

[27] The wind-induced latent heat flux positive (negative) anomalies lead to negative (positive) anomalous SSTs in the

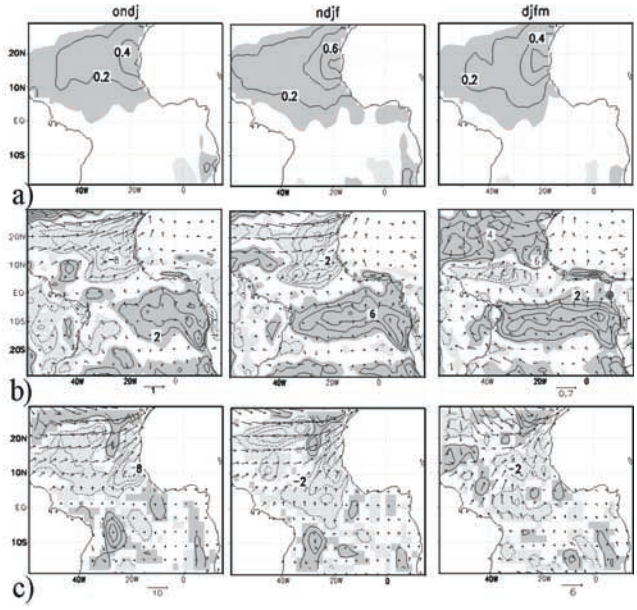

Figure 3. Regression maps of the first winter SNA SST Principal Component onto the: a) SST anomalies (shaded areas and contour lines CI = 0.2°C), b) surface latent heat flux (shaded areas and contour lines CI = 2 W m^2) and wind (vectors in m s^1) anomalies, c) wind stress curl (shaded areas and contour lines CI = 2 $\times$ 10^{-6} N m^{-3}) and wind stress (vectors in 10^{-1} N m^{-2}) anomalies. Dark and light grey shaded areas correspond to positive and negative values respectively. The zero contour line has been removed. The maps are shown from one month before (sond) to one month after (djfm) the winter sequence (ndjf). See color version of this figure in the HTML.

SNA region, increasing the cross-equatorial gradient. Furthermore, a strengthening (weakening) of the northerly wind stress induces positive (negative) anomalous coastal upwelling, contributing to a decrease (increase) in the SST from the previous months. The heat flux seems to be responsible for damping these SST anomalies one month later.

[28] The ocean dynamics associated with the NW Africa upwelling system are playing a role that needs further investigation. A thermodynamic budget of the SNA region is in progress by the authors. Also, the relation between wind-induced upwelling off NW Africa, SST anomalies and ENSO, that have been pointed out by other authors [*Roy and Reason*, 2001], should be analyzed in this context with more detail.

[29] **Acknowledgments.** We would very much like to thank the anonymous referees for their helpful suggestions. This study has been supported through the Spanish MCYT project REN2002-03424, which also funds Irene Polo.

References

Bretherton, S. B., C. Smith, and J. H. Wallace (1992), An intercomparison of methods for finding coupled patterns in climate data, *J. Clim.*, *5*, 541–560.

Carton, J. A., X. Cao, B. S. Giese, and A. M. Da Silva (1996), Decadal and interannual SST variability in the tropical Atlantic Ocean, *J. Phys. Oceanogr.*, *26*, 1165–1175.

Chang, P., L. Ji, and H. Li (1997), A decadal climate variation in the tropical Atlantic Ocean from thermodynamic air-sea interaction, *Nature*, *385*, 516–518.

Hurrell, J. W. (1995), Decadal trends in the North Atlantic Oscillation: Regional temperatures and precipitation, *Science*, *269*, 676–679.

Kalnay, E., et al. (1996), The NCEP/NCAR 40-year reanalysis project, *Bull. Am. Meteorol. Soc.*, *77*, 437–470.

Leeuwenburgh, O., and D. Stammer (2001), The effect of ocean currents on sea surface temperature anomalies, *J. Phys. Oceanogr.*, *31*, 2340–2358.

Legates, D. R. (1989), A high-resolution climatology of gauge-corrected global precipitation, in *Precipitation Measurement: Proceedings of the WMO/IAHS/ETH International Workshop on Precipitation Measurement, St. Moritz, Switzerland, Dec. 3–7, 1989*, edited by B. Sevruk, pp. 519–526, Swiss Fed. Inst. of Technol., Zurich, Switzerland.

Mayer, D. A., R. L. Molinari, M. Baringer, and G. J. Goñi (2001), Transition regions and their role in the relationship between sea surface height and subsurface temperature structure in the Atlantic Ocean, *Geophys. Res. Lett.*, *28*(20), 3943–3946.

Mittelstaedt, E. (1991), The ocean boundary along the northwest African coast: Circulation and oceanographic properties at the sea surface, *Prog.Oceanogr.*, *26*, 307–355.

Pan, L.-L. (2005), Observed positive feedback between the NAO and the North Atlantic SSTA tripole, *Geophys. Res. Lett.*, *32*, L06707, doi:10.1029/2005GL022427.

Rodríguez-Fonseca, B., and M. Castro (2002), On the connection between winter anomalous precipitation in the Iberian Peninsula and North West Africa and the summer subtropical Atlantic Sea Surface Temperature, *Geophys. Res. Lett.*, *29*(18), 1863, doi:10.1029/2001GL014421.

Rodríguez-Fonseca, B., I. Polo, E. Serrano, and M. Castro (2005), Evaluation of the North Atlantic SST forcing on the European and Northern African winter climate, *Int. J. Climatol.*, in press.

Rodwell, M. J., D. P. Rowell, and C. K. Folland (1999), Oceanic forcing of the wintertime North Atlantic Oscillation and European climate, *Nature*, *398*, 320–323.

Roy, C., and C. Reason (2001), ENSO related modulation of coastal upwelling in the eastern Atlantic, *Prog. Oceanogr.*, *49*, 245–255.

Santos, A. M. P., A. S. Kazmin, and A. Peliz (2005), Decadal changes in the Canary upwelling system as revealed by satellite observations: Their impact on productivity, *J. Mar. Res.*, *63*, 359–379.

Seager, R., Y. Kushnir, P. Chang, N. Naik, J. Miller, and W. Hazeleger (2001), Looking for the role of the ocean in tropical Atlantic decadal climate variability, *J. Clim.*, *14*, 638–655.

Servain, J., G. Clauzet, and I. C. Wainer (2003), Modes of tropical Atlantic climate variability observed by PIRATA, *Geophys. Res. Lett.*, *30*(5), 80031, doi:10.1029/2002GL015124.

Smith, T. M., and R. W. Reynolds (2003), Extended reconstruction of global sea surface temperatures based on COADS data (1854–1997), *J. Clim.*, *16*, 1495–1510.

Stammer, D. (1997), Global characteristics of ocean variability from regional TOPEX/POSEIDON altimeter measurements, *J. Phys. Oceanogr.*, *27*, 1743–1769.

Sutton, R. T., and M. R. Allen (1997), Decadal predictability of the North Atlantic sea surface temperature and climate, *Nature*, *388*, 563–567.

Vauclair, F., and Y. du Penhoat (2001), Interannual variability of the upper layer of the tropical Atlantic Ocean from in situ data between 1979 and 1999, *Clim. Dyn.*, *17*(7), 527–546.

Weller, R. A. (2003), Subduction, paper presented at the 'Aha Huliko'a Winter Workshop, U.S. Off. of Nav. Res., Honolulu, Hawaii.

B. R. de Fonseca and I. Polo, Departamento de Geofísica y Meteorología, Universidad Complutense de Madrid, E-28040 Madrid, Spain. (ipolo@fis.ucm.es)

J. Sheinbaum, Departamento de Oceanografía Física, CICESE, Ensenada, BC 22860, México.

4.1.2 Tropical Atlantic SST and summer West African rainfall

Tropical Atlantic Variability modes (1979-2002). Part I: time-evolving SST modes related to West African rainfall.

IRENE POLO
Departamento de Geofísica y Meteorología, UCM, Madrid, Spain.

BELÉN RODRÍGUEZ-FONSECA
Departamento de Geofísica y Meteorología, UCM, Madrid, Spain.

TERESA LOSADA
Departamento de Geofísica y Meteorología, UCM, Madrid, Spain.

JAVIER GARCÍA-SERRANO
Departamento de Geofísica y Meteorología, UCM, Madrid, Spain.

(*JCLI 9716, Journal of. Climate, accepted May 2008*)

ABSTRACT

This work presents a description of the 1979-2002 Tropical Atlantic (TA) SST variability modes coupled to the anomalous West African (WA) rainfall during the monsoon season. The time-evolving SST patterns, with an impact on WA rainfall variability, are analysed using a new methodology based on Maximum Covariance Analysis. Enhanced CMAP dataset, which includes measures over the ocean, gives a complete picture of the interannual WA rainfall patterns for the Sahel dry period. The leading TA SST pattern, related to the Atlantic-Niño, is coupled to anomalous precipitation over the coast of the Gulf of Guinea, which corresponds to the second WA rainfall principal component. The thermodynamics and dynamics involved in the generation, development and damping of this mode are studied and compared with previous works. The SST mode starts at the Angola/Benguela region and is caused by alongshore wind anomalies. It then propagates westward via Rossby waves and damps due to latent heat flux anomalies and to Kelvin wave eastward propagation from an off-equatorial forcing. The second SST mode includes the Mediterranean and the Atlantic ocean, showing how the Mediterranean SST anomalies are those that are directly associated with the Sahelian rainfall. The global signature of the TA SST patterns is analysed, adding new insights about the Pacific-Atlantic link in relation to WA rainfall during this period. Also, this global picture suggests that the Mediterranean SST anomalies are a finger-print of large scale forcing.

This work updates the results given by other authors, whose studies are based on different datasets back to the 50´s, including both, the wet and the dry Sahel periods. The obtained SST patterns are being used as boundary conditions for future sensitivity experiments done in the framework of the AMMA-EU project.

1. Introduction

The study of the Tropical Atlantic Variability (TAV) is an important challenge for the scientific community because its impacts affect to a large rural population, which depends on rain fed agriculture. TAV implies SST patterns, which are linked to extreme climate conditions over the Atlantic Basin and in particular over West Africa (WA).

At interdecadal timescales, the second part of the 20th century has known a very unusual evolution of Sahelian rainfall with a 20-year wet period followed by another 20-year dry period. Such a long-term downward trend in Sahelian summer rainfall is a unique feature in recent tropical fluctuations, and it has been associated with SST trends in the Atlantic and Indian Oceans (Folland et al., 1986; Shinoda and Kawamura, 1994; Bader and Latif, 2003; Giannini et al., 2003; Lu and Delworth, 2005). Indeed, this observed drought tendency following the 1960s has been well reproduced with models only forced by observed SST (Giannini et al., 2003; Paeth and Hense, 2004; Lu and Delworth, 2005; Tippett, 2006; Tippett and Giannini, 2006). In addition, Zhang and Delworth (2006) have pointed out that the Atlantic Multidecadal Oscillation, which was in its negative phase in the 1980's-1990's, can cause the observed multidecadal variations of Sahel summer rainfall, suggesting that the important role of the multidecadal variability in the interpretation of the recent climate change cannot be ignored.

In spite of this recent understanding about WA rainfall at decadal timescales as well as improvements in seasonal prediction, the General Circulation Models (GCMs) fail to reproduce WA rainfall interannual variability (Moron et al., 2003; Tippett, 2006; Tippett and Giannini, 2006). Some authors have suggested that the model error observed in the Sahel rainfall could be related to the error in the representation of ocean-atmosphere

interaction (Tippett, 2006). Faced with this, the SST modulation of the interannual variability of WA rainfall during the Sahel dry period, deserves more investigation.

At interannual scales, WA rainfall variability is modulated by both, oceanic (between 0-10N) and continental (between 10N-20N) convergence, by variations in the ITCZ position and land-atmosphere interactions respectively. Historically, two main WA rainfall types have been identified; Dipole years, in which anomalies of opposite sign appear north and south of 10N, and non-Dipole years with anomalies of the same sign in the whole region (Motha et al., 1980; Janicot, 1992; Fontaine and Janicot, 1996; Ward, 1998). This classification, based on the available *in situ* precipitation data from land stations over WA, has been useful in order to discriminate some associated processes and SST influences (Fontaine and Janicot, 1996; Janicot et al., 1998; Ward, 1998). However, it accounts for a large variability occurrence in the different wet and dry decadal periods over Sahel (Janicot et al., 1996; Ward, 1998; Janicot et al., 2001). Some of these studies have suggested that the occurrence of Dipole years, which are most closely associated with TA SST, is dominant during the wetter epoch, whereas non-Dipole years are particularly numerous in the dry Sahel period (Ward, 1998; Janicot et al., 2001), when the ENSO is more active in relation to WA rainfall (Janicot et al., 1998; Janicot et al., 2001). Paeth and Stuck (2004) have suggested that warm TA SSTs could enhance the rainfall Dipole, which is the prevailing precipitation pattern in the CRU observational dataset as well as in the global and regional climate models outputs. However, some discriminant analyses have shown perfect uncoupled rainfall variability modes between Sahel and the coast of the Gulf of Guinea (GG), associated with different global SST anomalies (Ward, 1998; Giannini et al., 2003). This work will present rainfall patterns calculated from the enhanced satellite-based CMAP dataset, which includes measures over the ocean, a feature that needs to be discussed with respect to other WA rainfall observational studies.

Regarding rainfall variability of the coast of the GG, it seems to have a very tight ocean-atmosphere coupling at interannual and decadal time scales (Wagner and da Silva, 1994; Fontaine and Janicot, 1996; Ward, 1998; Vizy and Cook, 2001; Giannini et al., 2003), linked with the well-known Atlantic–Niño mode (Zebiak, 1993; Carton et al., 1996). Vizy and Cook (2001) have shown that such SST events enhance evaporation, and that the southerly flow across the coast of the GG carries more moisture inland, leading to increased precipitation south from the usual latitude of the ITCZ. The Atlantic-Niño mode is characterized by a relaxation in the equatorial trade winds which induces a redistribution of warm water in the equatorial belt and a weakening in the equatorial thermoclime slope and also in the heat content zonal gradient (Carton et al., 1996; Vauclair et al., 2004). In cold years (dry years in the GG region), the northward ITCZ movements can begin as early as February. Conversely, the warm years (wet years over the GG) are characterized by a reduction of the southerly flow between April and June, followed by a rapid increase later in July (Fontaine et al., 2003). Although the Atlantic-Niño has been investigated from 80's, the related air-sea interactions mechanisms are still a current topic (Keenlyside and Latif, 2007), mainly because of the lack of reliable ocean data in the TA. This work makes special attention to address the main question about the development and damping of this SST mode coupled to GG rainfall.

The relation between the Sahelian rainfall and the so-called Atlantic SST Meridional mode (Chang et al., 1997) was pointed out to be more important before 1970, during the wet Sahel period (Janicot et al., 1996; Janicot et al., 2001) and at interdecadal timescales (Lamb, 1978; Hastenrath, 1984). However, the role of the Subtropical North Atlantic (SNA) SST on WA rainfall is still unclear. Some authors have suggested that SNA SST plays a passive role with regard to WA rainfall (Ward, 1998; Mo et al., 2001). Vizy and Cook (2001) suggest that this region can have less influence over the Sahelian rainfall, mainly because the low-level flow between the SNA and WA is a northeasterly flow, which tends to isolate the continent from SNA, and because horizontal advection is not very effective in the tropics. However, from their GCM simulations, a response to positive SNA and GG SST anomalies results in a westerly low-level flow perturbation that largely impacts on WA precipitation (Vizy and Cook, 2001).

The possible Sahelian impact from other regions, such as the Mediterranean Sea, has also been supported (Rowell, 2001). From AGCM simulations, Rowell (2003) has found positive Mediterranean Sea SST anomalies related to anomalous positive Sahel rainfall through evaporation and southward moisture advection that enhances low-level convergence over the Sahel. Jung et al. (2006) have simulated significant increased Sahelian rainfall for the warm Mediterranean event of 2003, derived from enhanced evaporation in the Mediterranean Sea. Nevertheless, there is still an open question about whether the Mediterranean basin plays an effective role or it is only a fingerprint of larger-scale forcing.

Regarding the global signature of the TAV, some studies have evidenced an association between ENSO events and the Atlantic-Niño mode (Latif and Grötzner, 2000; Wang, 2006), and both phenomena are related to WA rainfall patterns (Rowell, 2001; Janicot et al., 1998; Janicot et al.,

2001). The ENSO seems to act by modifying the east-west divergent circulation, which modulates the vertical movements over WA, while the Pacific-Atlantic zonal atmospheric gradient, coupled to the opposite SST anomalies over both oceanic basins, can enhance the WA rainfall response (Janicot et al., 1998). However, the setup of a Pacific-Atlantic zonal atmospheric oscillation in the dry Sahel period could be the responsible of recent changes in the anomalous SST and WA rainfall trends after 1970. The Pacific- Atlantic relationship has dramatically changed in this recent period (Keenlyside and Latif, 2007); and therefore the study of such relationship is important for understanding the interannual influences over WA.

The aim of this work is to clearly identify and describe the SST modes of variability over the WA adjacent oceans that are coupled to summer WA rainfall during 1979-2002 period and their seasonal-time evolution (origin, development and damping). To accomplish this objective, we have developed an extended methodology of the classical Maximum Covariance Analysis and we have applied it to the WA monthly anomalous summer (JJAS) precipitation and the monthly TA and Mediterranean SST anomalies from FMAM to SOND. Since the methodology highlights the seasonal dependence of the time-evolving SST, it will give a new and valuable insight on the understanding of these interannual variability modes.

The SST patterns found in this paper are being used as boundary conditions in some of the sensitivity experiments that the EU-AMMA project has planned to perform with different AGCMs, with the aim of understanding the response of the WA rainfall to the SST in the adjacent oceans and its potential predictability. The same EMCA methodology has been applied in Part II (García-Serrano et al., 2008), focusing on the relation between the summer TA SST patterns and summer to winter Atlantic precipitation variability, addressing TAV-extratropical connection through tropical convection.

In the next section 2, the data and the methodology used in this work are described. Section 3 describes the principal components of the WA rainfall and the main SST-WA rainfall covariability modes. The air-sea interactions related to the leading SST pattern, as well as the global SST signature of every mode is analysed. Finally the main conclusions are discussed in section 4.

2. Data and Methodology

1979-2002 monthly CPC Merged Analysis of Precipitation (CMAP, Xie and Arkin 1997) and ERSST dataset (Smith and Reynolds, 2003) for the SST variable have been used to study the main coupled modes between summer WA precipitation and TA SST. 1979-2002 is very reliable period regarding data accuracy because satellite data is included in the precipitation datasets. Also, the use of this data provides information on the precipitation over the ocean, something important if we want to follow the patterns over the basin. As a first step of the analysis, June-July-August-September (JJAS) monthly standardized precipitation Empirical Orthogonal Functions (EOF) are computed to quantify the principal modes of WA precipitation during the whole monsoon season. Then, the anomalous SST patterns coupled to the summer WA rainfall variability is described and analyzed. Eight different four-month sequences, centered in JJAS, and lagging one month forward and backward, are computed to know the state of the ocean in relation to the WA rainfall variability. Time series are linearly detrended and anomalies are calculated with respect to the considered period.

In order to follow and give and interpretation of the air-sea processes related to the leading SST coupled mode, several oceanographic and atmospheric key variables have been analyzed. The oceanic variables are the wind stress (from PIRATA dataset, Servain et al., 1998), the 20ºC isotherm depth as tropical thermocline depth proxy (from TAOSTA dataset, Vauclair and du Penhoat, 2001), and the Sea Level Anomalies (SLA, from the altimetry measures TOPEX/Poseidon in the period 1993-2001, which is provided by CNES-AVISO). The atmospheric variables are the interpolated Outgoing Long-wave Radiation (OLR, provided by NOAA/OAR/ERSL PSD, Liebmann and Smith, 1996), the surface heat fluxes, the surface winds and the Sea Level Pressure (SLP). The latter surface variables come from the ERA-40 dataset (Uppala et al., 2005), which includes satellite data from 1973.

The methodology of *Extended Maximum Covariance Analysis* (hereafter EMCA, Figure 1) is developed and implemented in this study. This methodology is an extension of the Maximum Covariance Analysis (Bretherton et al., 1992, Frankignoul and Kestenare, 2005; Polo et al., 2005) but considering all the lagged SST time series in the same array (see Figure 1, matrix Y). Using EMCA we can isolate, in the same mode, the whole sequence of significant covariant SST patterns in relation to the JJAS precipitation, and accomplish the whole picture of the SST pattern evolution in relation to the precipitation with a realistic persistence feature from boreal late winter to summer. Since the TA SST signals can develop rapidly from early spring to late summer, in our method, a priori, we do not discriminate the season of the maximum SST covariability with the summer rainfall (in contrast with the classic MCA).

In addition, EMCA gives the opportunity of increasing the number of time series in the analysis,

having as many time series per point as time lags used in the analysis, and assessing, in this way, the

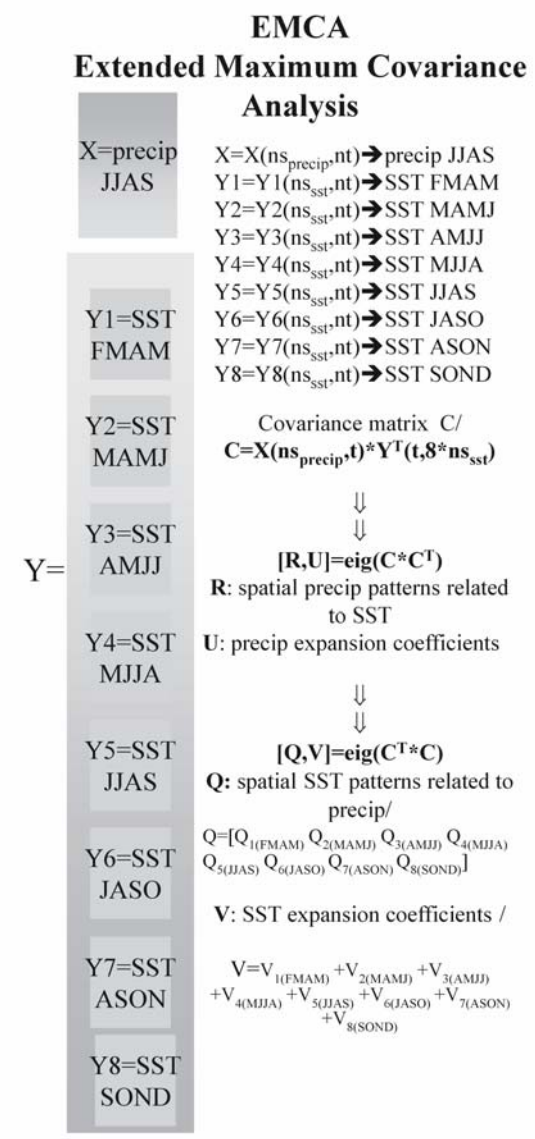

Figure 1: Scheme of the Extended Maximum Covariance Analysis (EMCA) used in this study.

statistically significance of the results. As in the classical MCA, each mode comprises different spatial structures (singular vectors) and time series (expansion coefficients) for every involved field in the analysis. The results are shown in terms of homogeneous and heterogeneous regression maps, for the SST sequence and the summer precipitation field respectively. For each mode, the SST homogeneous map (hm) shows the amplitude of the projection (for each grid point and each lag) of the total SST expansion coefficient onto the TA SST anomalies, giving a measure of the SST anomaly per standard deviation. The precipitation heterogeneous maps (ht) show the amplitude of the projection of the total SST expansion coefficient onto summer WA rainfall anomalies, giving a measure of the precipitation anomalies associated with one standard deviation of the anomalous SST. Only those areas that are 98% statistically significant (evaluated with a t-test) are mapped. A measure of the fraction of explained covariability (square covariance fraction, scf), and the correlation coefficient (ruv) between the independent and dependent expansion coefficients complete the information for each mode. To quantify the statistical significance of the EMCA, additional statistical information is given. In order to test if the SST-precipitation link found is not random, we have checked the results using a Monte Carlo test. In this way, the combined action of shuffling and applying the EMCA is performed 100 times. The probability density function of the scf parameter that arises from these 100 realizations, is compared to the non-shuffled EMCA scf scores, giving a significance level (SL) for the connection found.

3. Results

a) Principal Component Analysis:

In this section, interannual WA rainfall modes (over the region 5ºS-32ºN; 21.25ºW-33.75ºE) are computed for the dry Sahel period using CMAP precipitation dataset, with the aim of updating the results given by previous authors. The first two EOFs of WA monthly-standardized anomalous precipitation during the rainy season (JJAS), which account for around 20% of the total variance, are shown in Figure 2. The following third mode has not been considered since its sampling error is larger than the spacing between second and third eigenvectors, which means that the third PC is part of a degenerate multiplet (North et al., 1982). The significant precipitation pattern of the leading Principal Component (PC) shows the anomalous Sahelian rainfall (*Sahelian Mode*, Figure 2a) as the first mode, with more no-rain than wet periods during the whole sequence. This pattern accounts for the 10% of the total variance and its study is of great importance because it explains part of the WA monsoon variability, which is a hot topic for the agriculture and health in developing countries (Sultan et al., 2005). The regression map of the second PC represents the rainfall pattern of the coast of the GG (*Guinean Mode*, Figure 2b). The pattern exhibits interannual and interdecadal variability, with more dry events over the coast of the GG in the 1990's than in the 1980's.

While other works present the Guinean mode as the leading WA rainfall mode (Giannini et al., 2003), from our results, during the 1979-2002, most of the rainfall interannual variability is concentrated over the Sahel region, being the Guinean mode the second EOF. A prior normalization of the rainfall anomalies has confirmed the reversion of the order of the first two modes (not shown). Without the standardization of the rainfall anomalies (as done in Giannini et al., 2003), the rainfall anomalies of the

coast of the GG have higher amplitudes and appear as the leading mode.

In addition, although several authors have pointed out that a significant part of the interannual variability of WA anomalous rainfall is due to the opposite evolution between central Sahelian and Guinean rainfall indexes as a Dipole pattern (Janicot, 1992; Fontaine et al., 1995; Fontaine and

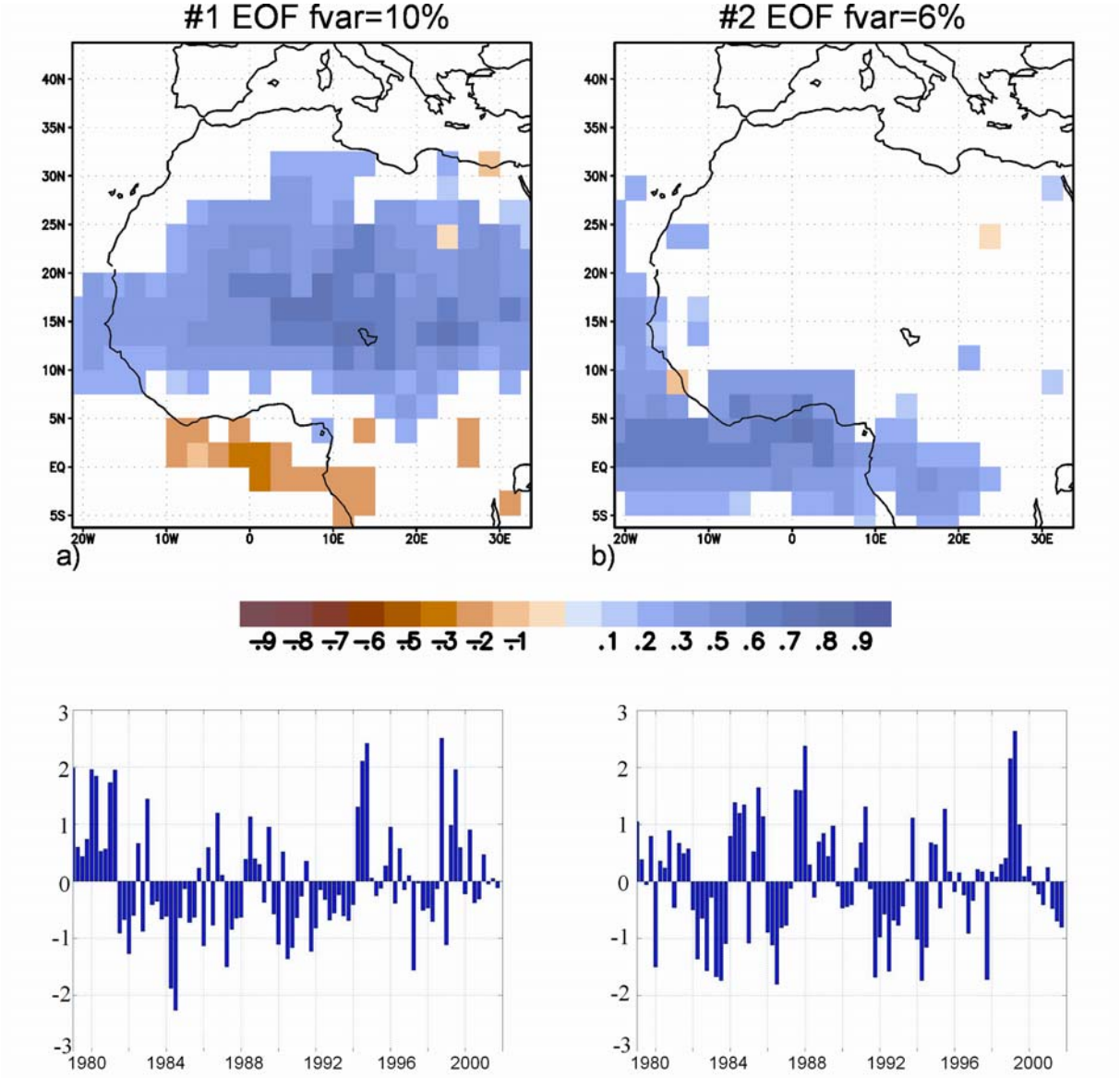

Figure 2: First two CMAP JJAS precipitation Empirical Orthogonal Functions over WA. Only 98% statistically significant areas, evaluated with a t-test, have been shaded. Times series of the associated Principal Components are in bars.

Janicot, 1996; Ward, 1998; Douville et al., 2007), our results separate the Sahelian and the Guinean rainfall in two different modes. Furthermore, the Dipole classification is under the assumption that both, the Sahel and the coast of the GG have the same variability patterns, while it is clear that they have different variability especially in the last dry period (Ward, 1998). Since the processes associated with both are operating and competing (Ward, 1998), for some analysis, the Dipole and non-Dipole subdivisions appear useless. The absence of the Dipole pattern in our analysis could be caused by the used dataset; CMAP rainfall comes from satellite data with land-sea continuity and a smaller time span (1979-2002), which is contained in the dry Sahel period. In order to check this hypothesis, we have analysed the same patterns considering CRU dataset for a longer period (1949-1996) and for part of the dry period (1975-1996). For the same data treatment and for both periods, we have obtained the same uncoupled Sahelian and Guinean modes (not shown). Likewise, standardization produces a reversal of the modes in the sense of percentage of variability. A kind of dipole pattern is found for the second period without standardizing the WA rainfall anomalies, although it has the maximum loadings over the coast of GG region. Therefore, this data-treatment dependence reveals

that the Dipole is not robust enough to be considered as a canonical pattern.

b) SST-precipitation coupled modes:

In order to determine the TA SST patterns related to summer WA precipitation anomalies, we apply EMCA between the TA SST from FMAM to SOND and JJAS WA rainfall. For the **leading EMCA mode**, which accounts for the 31% of the scf, the SST significant homogeneous regression maps shows positive SST anomalies over the Atlantic equatorial tongue region from the previous spring (AMJJ), related to an increase of summer precipitation along the coast of the GG (Figure 3, upper panel). The precipitation expansion coefficient of this mode has a strong relation to the Guinean mode in Figure 2b (0.89 correlation coefficient), and the SST expansion coefficient is very well correlated (0.84 correlation coefficient) with the equatorial Atlantic SST index (ATL3, Zebiak, 1993), which describes the Atlantic-Niño mode. It is important to mention that the Guinean rainfall pattern appears now as the leading mode of covariability with TA SST, implying that an important part of the rainfall variability of the coast of the GG can be explained by TA SST anomalies. Conversely, Sahelian rainfall has been related to more global SST patterns as Pacific (Giannini et al., 2003; Janicot et al., 1998) and Indian or northern basin ocean (Giannini et al., 2003; Ward, 1998) and to land-surface processes (Douville, 2002; Philippon and Fontaine, 2002).

The **second EMCA mode** (Figure 3, lower panel) represents the 14% of the total scf and describes a spatial pattern with positive summer rainfall anomalies over the Sahel and positive SST anomalies over the SNA and Mediterranean Sea, persisting from some months in advance. The precipitation expansion coefficient has a strong relation to the Sahelian mode in Figure 2a (0.87 correlation coefficient). Nevertheless, this is not a robust mode as the SL obtained from the Montecarlo test indicates that the results can be reproduced in half of the shuffled cases. For this reason, this mode will be discussed and re-calculated in the next sections.

In the following section, these two covariability modes are intensely analysed. On the one hand the leading mode, which corresponds to the Guinean rainfall and the Atlantic- Niño, is discussed in terms of air-sea interactions. On the other hand, the second covariability mode will be analysed and discussed in order to better understand the role of the SNA and Mediterranean Sea SST on the Sahelian rainfall. The global picture of these SST patterns will also be discussed.

b.1) EQUATORIAL ATLANTIC SST-GUINEAN RAINFALL MODE: AIR-SEA INTERACTIONS

Figure 3 (upper panel, from FMAM to SOND) shows the sequence of SST homogeneous regression maps, related to the Atlantic-Niño or Equatorial Mode (EM), linked to the Guinean anomalous precipitation. Here, it can be seen how the EM develops from FMAM to JJAS, starting with a maximum of anomalous SST over the Angola/Benguela upwelling region and a second relative maximum around 20S. Afterwards, the mode shows a strengthening and/or northward (westward) propagation of the coastal (equatorial) anomalies and a weakening of the anomalies in 20S. Then, the whole mode starts to weaken, disappearing in SOND. The Bjerknes mechanism components in the EM have been analysed by other authors (Keenlyside and Latif, 2007), but there are still some gaps about the development and damping of the mode. Therefore, we will analyze the thermodynamics and dynamics involved in the mode's evolution by regressing the SST expansion coefficient onto different thermodynamic and oceanographic variables.

The role of the TA heat fluxes in relation to the EM is investigated in Figure 4, which shows the balance between the radiative fluxes (shortwave radiation minus longwave) and the turbulent fluxes (latent heat fluxes). Regarding the EM evolution from FMAM to JJAS, heat fluxes are not responsible for the SST anomalies located in the Angola/Benguela upwelling region (10S-20S; 0-10E), as the SST warming is concomitant with more evaporation over this region. On the contrary, the west-equatorial North-Atlantic warming (0-10N; 50-30W) can be attributed to an increase of solar radiation (associated with less clouds) and a decrease of evaporation. The damping of the SST anomalies at the southern lobe (0-10S; 40-20W) starts in MAMJ due to an increase of the latent heat flux to the atmosphere and a decrease of the solar radiation. From JJAS to SOND, negative latent heat fluxes anomalies could be responsible for the damping at the south of the tongue, while radiative fluxes reduce the SST anomalies at the east, in agreement with Trzaska et al. (2006). From the thermodynamics analysis of the EM, we conclude that, although both, negative radiative and latent heat fluxes anomalies, could be important in damping the SST in the EM, heat fluxes cannot explain the generation and persistence of the SST anomalies at the southeastern region.

In order to find an explanation for the SST anomalies generation at the southeastern part of the tongue from the previous winter, regression of the SST expansion coefficient onto the surface winds and the SLP is displayed in Figure 5. Noticeable is an enhancement of the clockwise circulation together with a weakening of the subtropical Santa Helena high-pressure system from the previous NDJF winter sequence. Such a feature could be responsible for the anomalous southeastward surface winds, and hence the SST warming. However, both wind anomalies over the eastern

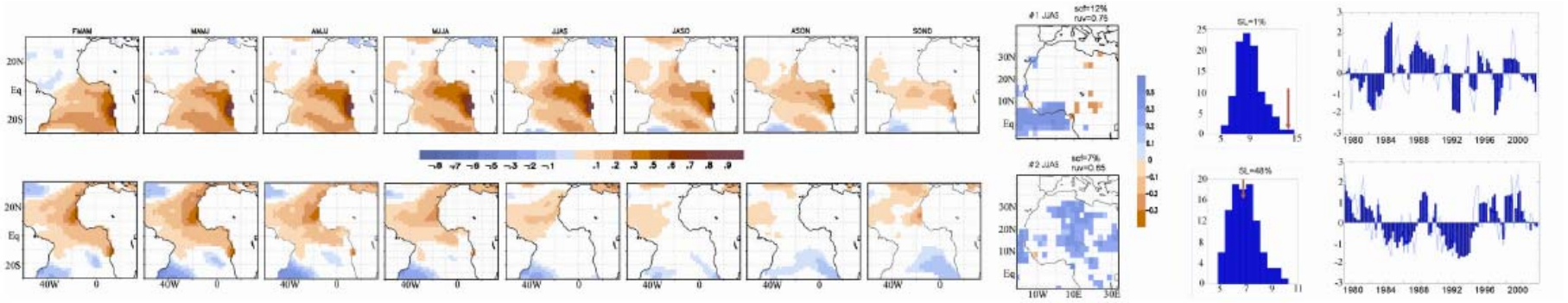

Figure 3: First two covariability modes obtained from the EMCA between summer WA precipitation and the anomalous SST (ºC) 4-months sequences from FMAM to SOND. Only 98% statistically significant areas, evaluated with a t-test, have been shaded. The probability density function of the scf from 100 times montecarlo tests (histogram) is compared with the original EMCA scf score (arrow) to show its significance level. The expansion coefficients (SST in bars, precipitation in continuous line) are shown for each mode.

South Atlantic and positive SST anomalies over the Angola/Benguela region (not shown) are significant two months before SLP negative ones, from SOND indeed. At that moment, positive SLP anomalies cover the Amazon basin and the equatorial band (Figure 5a-b) suggest that subsequent weakening of the Santa Helena High could be forced by inversion of the local Hadley cell via atmospheric bridge.

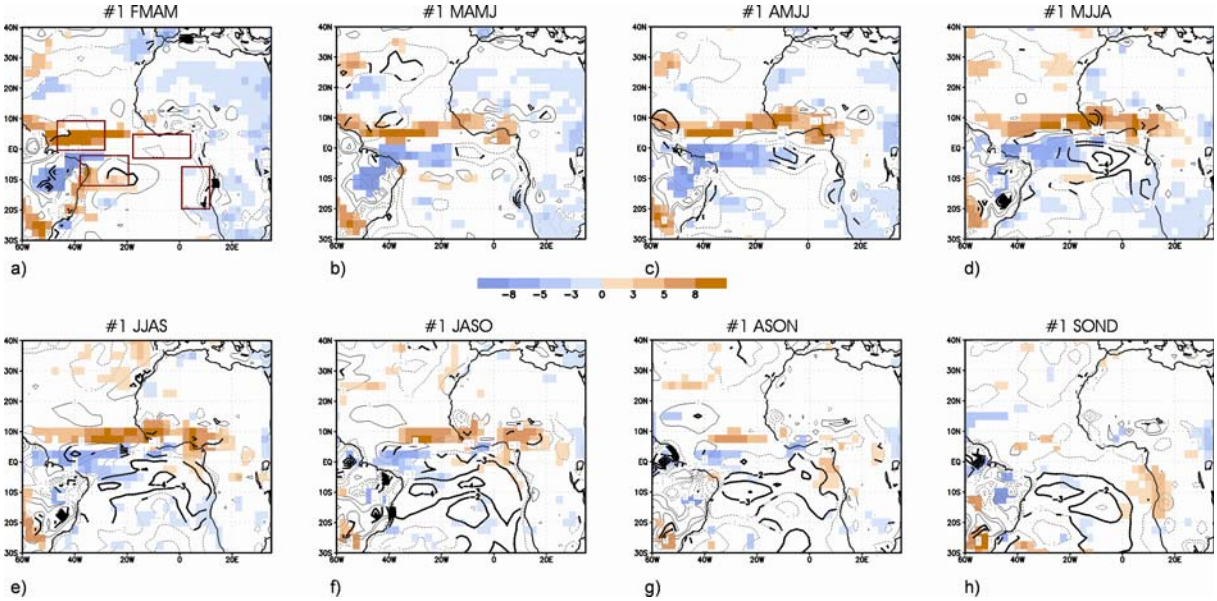

Figure 4: Regression of the total SST expansion coefficient associated with the leading EMCA mode onto the radiative flux anomalies (shortwave minus longwave radiation, W m^{-2}, positive downward, 98% statistically significant areas, evaluated with a t-test, have been shaded), and the latent heat flux anomalies (contour lines, CI=1 W m^{-2} positive downward, 98% statistically significant areas, evaluated with a t-test, have been remarked) for the 4-months sequences from FMAM (a) to SOND (h). The boxes in (a) are regions considered in the heat balance.

Such type of mechanism has been proposed in the Northern Hemisphere for explaining the anomalous-indirect Atlantic Hadley circulation during the mature and decay phases of El Niño (Wang, 2002a; 200b). However, this result is not totally in agreement with other authors' findings. Trzaska et al. (2006) have shown the EM as a consequence of the Subtropical South Atlantic SST mode (SSA, consistent with Venegas et al., 1997) which is associated with the south Atlantic subtropical High SLP anomalies, and no mention is done to the equatorial contribution.

Despite most of the works have associated the origin and development of the EM with subtropical atmospheric dynamics, some authors have suggested that Ekman pumping and the wind stirring may also play a role in the SST evolution over the TA (Sterl and Hazeleger, 2003; Barreiro et al., 2004). In view of this, the oceanic component is analysed in Figure 6, which shows the regression of the leading EMCA mode SST expansion coefficient onto the wind stress and the Ekman pumping. Figure 6a (and Figure 5a-b) shows how, from the previous winter months, anomalous southward wind stress, locally changes the upwelling over the Angola/Benguela front, and thus the SST and the thermocline depth over the region (not shown). In particular, in DJFM, this positive SST anomaly over the southern Atlantic produces a meridional and zonal-basin gradient, which increases the northwesterly wind stress over the south Atlantic (Figure 6b). From DJFM to AMJJ (Figure 6b-e), southeastward anomalous wind stress changes the thermocline slope, rising at the west and sinking at the east in the Equator (not shown). In MAMJ (Figure 6d) in the Southwest Atlantic, the wind stress curl starts to be anomalously cyclonic creating upward Ekman pumping and cooling the mixed layer at the west-central basin, as the latent heat flux decreases (Figure 4c). From JASO, the positive Ekman pumping anomalies are located over the eastern part of the basin, as the southerly alongshore wind starts to be significant over 10S, helping to damp the mode.

The SLA pattern associated with the EM consists of anomalous eastern equatorial Atlantic tongue (as the SST) and western equatorial Atlantic opposite sign SLA, in a see-saw-like thermocline configuration (not shown), in agreement with other authors (Wang, 2006; Keenlyside and Latif 2007). Since the EM strongly involves subsurface equatorial dynamics through equatorial waves adjustment (Vauclair and Penhoat, 2001; Vauclair et al., 2004; Handoh and Bigg, 2000), and looking for a mechanism that, on the one hand could explain the development of the EM (from winter to summer) and, on the other hand, the fading of the EM (from summer to autumn), time-longitude plots

of SLA have been done for extreme positive and negative events of the expansion coefficient. We have chosen the years 1995 and 1997, positive and negative EM years respectively (see expansion coefficients in Figure 3, upper panel), following the SLA from 40W to 10E and from February to October.

The time-longitude SLA plots (Figure 7) at 5S shows for 1995 (1997) how the positive (negative) SLA signal at Southeast Atlantic is propagating clearly westward as a Rossby wave (Chelton and Schlax, 1996; Polito and Cornillion, 1997). This eastern perturbation travels as far as 30W-20W and does not propagate further west (Figure 7-left, A-B), as an anomaly of the opposite sign appears. This SLA anomaly could be originated and/or reinforced by the Ekman pumping at this longitude, from AMJJ season, and it is also propagating westward with the same phase speed, cancelling the positive (negative) SLA propagation further west.

Simultaneously to the westward upwelling (downwelling) Rossby wave travelling along 5S (Figure 7-left, A-B), there is an upwelling (downwelling) Rossby wave travelling westward along the 5N latitude (not shown), and the wind stress over 30W-20W is also favouring (inhibiting) the Ekman pumping at both sides of the equator for the year 1995 (1997). At the beginning of July, this negative (positive) SLA signal appears in the western equatorial Atlantic and reflects as an eastward Kelvin wave travelling up to September reaching the eastern equator (Figure 7-right, C-D), and helping to damp the EM. The wind stress anomalies over 30W-20W, the associated Ekman pumping at both sides of the equator (Figure 6g) and the possible relation to anomalous SLA signal triggering a Kelvin wave, support the hypotheses proposed by Polo et al. (2008) that Ekman pumping ITCZ shift-induced anomalies are, in part, source for equatorial Atlantic Kelvin waves.

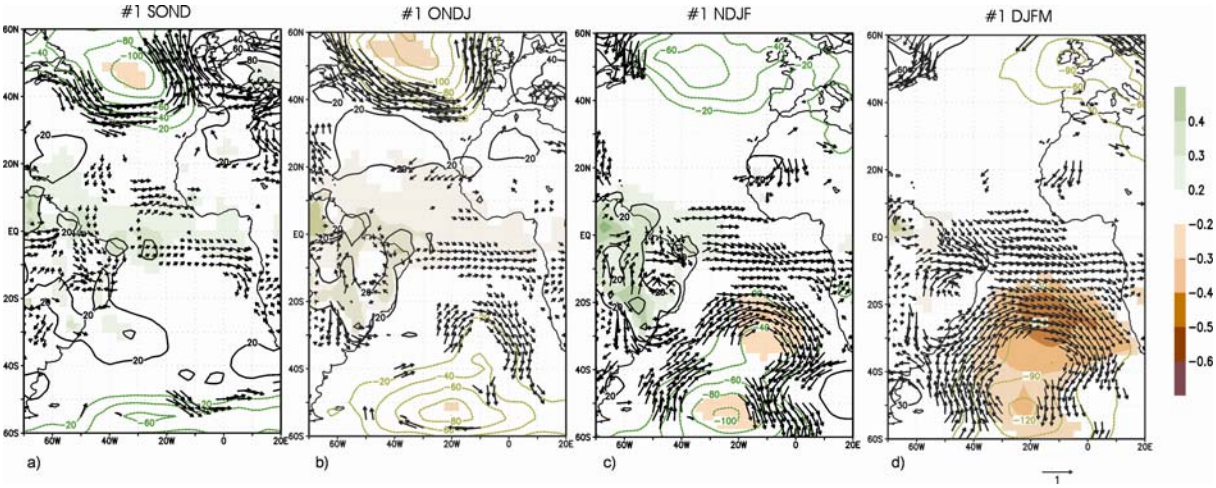

Figure 5: Regression of the total SST expansion coefficient associated with the leading EMCA mode onto the surface wind anomalies (vectors, m s^{-1}, 98% statistically significant areas, evaluated with a t-test, have been plotted), and the Sea Level Pressure (contours, CI=20 mbar, 98% statistically significant areas, evaluated with a t-test, have been shaded), for the 4-months sequences from previous SOND (a) to DJFM (d).

Although the hypothesis needs to be checked using a model, we have found that the EM starts at the Angola/Benguela upwelling region. The SLA anomalies radiate and propagate westward as Rossby waves, and damp due to the latent heat flux anomalies at the south Atlantic and Kelvin wave eastward propagation from an off-equatorial forcing. The phase speed for the westward and eastward propagation has been computed with the Radon Transform technique (Hill et al., 2000). The mean phase speed calculated for the westward propagation at 10S, 5S and 2.5S is -0.5 m/s, and for the equatorial eastward propagation is around 3 m/s, corresponding approximately to the first baroclinic mode (Philander, 1990; França et al., 2003). Longitudinally, the area around 30W-25W seems to be a threshold for the first baroclinic Rossby wave. Nevertheless, for both westward Rossby wave and eastward Kelvin wave propagations there is more homogeneity in the middle of the basin (from 20W to 5W). In addition, other non-linear processes could interfere in the propagation continuity onshore, however these tasks are out of scope of this study and future research lines.

Our results presented above disagree with Latif and Grotzner (2000), Florenchie et al. (2003) and Wang (2006) with regard to the oceanic wave propagation's role in the origin of the equatorial and South Atlantic SST variability. In particular, Florenchie et al., (2003) have suggested that the generation of the Benguela Niños could be remotely generated by wind anomalies at the west-central equatorial Atlantic via oceanic Kelvin wave propagation, and Wang (2006) has supported this result. Also, Latif and Grötzner (2000) have showed an eastward SLA propagation from western equatorial Atlantic in winter that reaches the eastern

equatorial Atlantic the next summer when it can be amplified by air-sea interactions and the SST can be modified. Our results show that neither west equatorial SLA Atlantic in winter nor anomalous winds in the west-central equatorial Atlantic have been found to force Benguela Niños/EM via Kelvin waves.

Regarding the Pacific-Atlantic connection, Latif and Grotzner (2000) showed how, at quasi-biennal time scales, a winter El Niño event leads an Atlantic-Niño the following summer with no significant simultaneous relationship. Recently, Wang (2006) has discussed the importance of the Pacific-Atlantic SST gradient driving the atmospheric circulation across equatorial South America via SLP gradient and influencing the tropical climate variability in a feedback way. In order to assess these relationships between basins, the EM has been regressed onto the global SST and precipitation anomalies (Figure 8), showing a global rainfall pattern that involves the whole tropical belt. The equatorial Atlantic positive precipitation anomalies from FMAM to AMJJ are related to negative precipitation anomalies over the central Pacific. From JJAS to SOND, the Atlantic-Niño is being damped, with a westward displacement of the global tropical convection

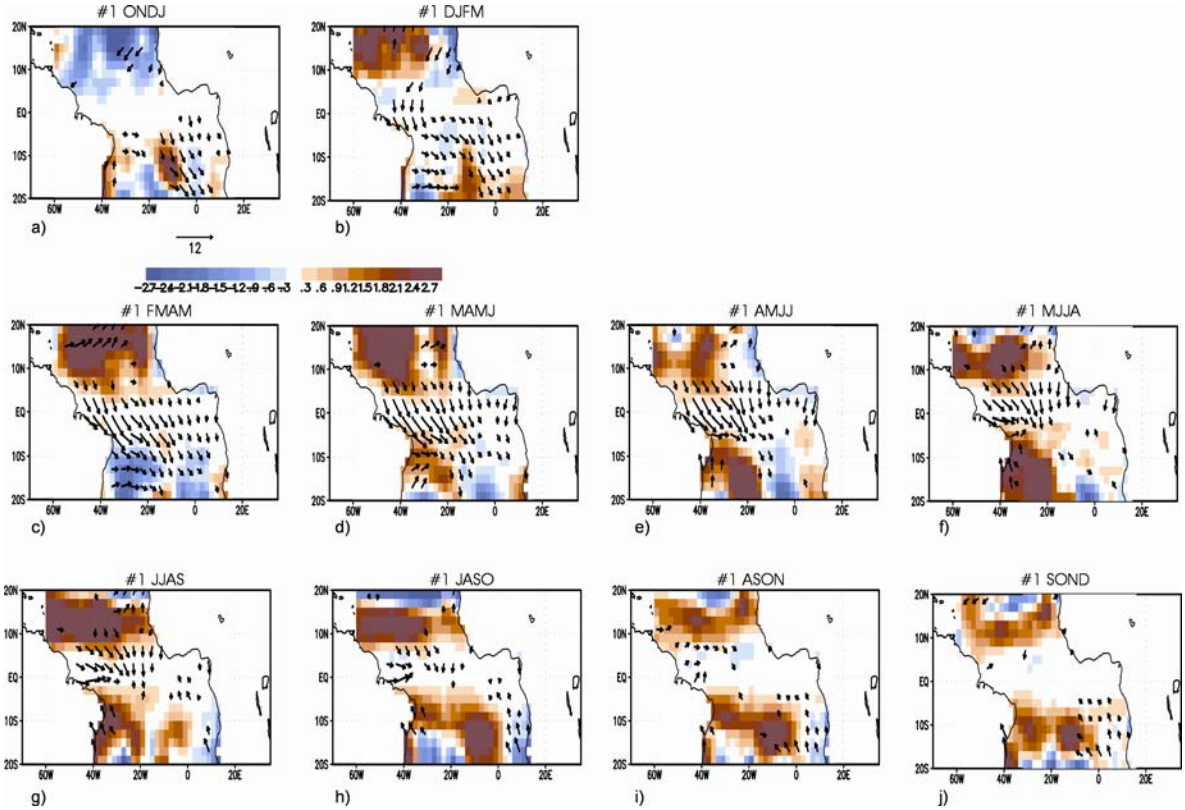

Figure 6: Regression of the total SST expansion coefficient associated with the leading EMCA mode onto the wind stress anomalies (vectors, 10^{-1} N m^{-2}, 98% statistically significant areas, evaluated with a t-test, have been plotted), and Ekman pumping anomalies (positive upward, shaded areas CI=6 10^{-3} m month^{-1}) for the 4-months sequences from the previous ONDJ (a) to the following SOND (j).

anomalies; increasing the West Asian precipitation and decreasing from central to eastern Pacific precipitation (Niña-like pattern). This is more evident considering the global SST anomalies associated with the EM; SST anomalies decreasing from the central to the east Pacific Ocean, and increasing at the western Pacific (Figure 8a-d contour lines). In order to address a possible EM modulation, we have correlated the lagged Niño3-index with the EMCA-SST expansion coefficient (Figure 8e). The maximum correlation occurs when warm EM phase in summer leads the Pacific Niña by 6-8 months, during the following winter. This is a very relevant result that points out a different equatorial Pacific-Atlantic connection in the 1979-2002 period: the Atlantic-Niño can lead the Pacific Niña and this situation seems to be related to the Guinean rainfall mode instead of Sahelian rainfall. Jury et al. (2002) have found that upper zonal winds in the central Atlantic lead the Niño-3 SST index, particularly in the 1980s and 1990s. They suggest that both the Niño-3 and the Atlantic winds are responding to atmospheric convective forcing in the western Pacific, but that the upper wind reacts more quickly to eastward-shifted convection in the Pacific than does the Niño-3 SST, which depends on the comparatively slow eastward propagation of ocean anomalies. These upper winds could force, through the Walker circulation, the SST in the tropical Atlantic to react more quickly that the

Niño-3 SST, explaining in this way the relation found between the Atlantic and the Pacific. Melice and Servain (2003) have also showed the south tropical Atlantic leading the SOI from 1984 to 1998 by ~4 months, although they do not know how South Tropical Atlantic could be dynamically linked with the Southern Ocean or even if such a link exists. Nevertheless, the importance of the later result in Figure 8, about the recent trends in the Pacific-Atlantic connection needs further investigation and will be the focus of future studies.

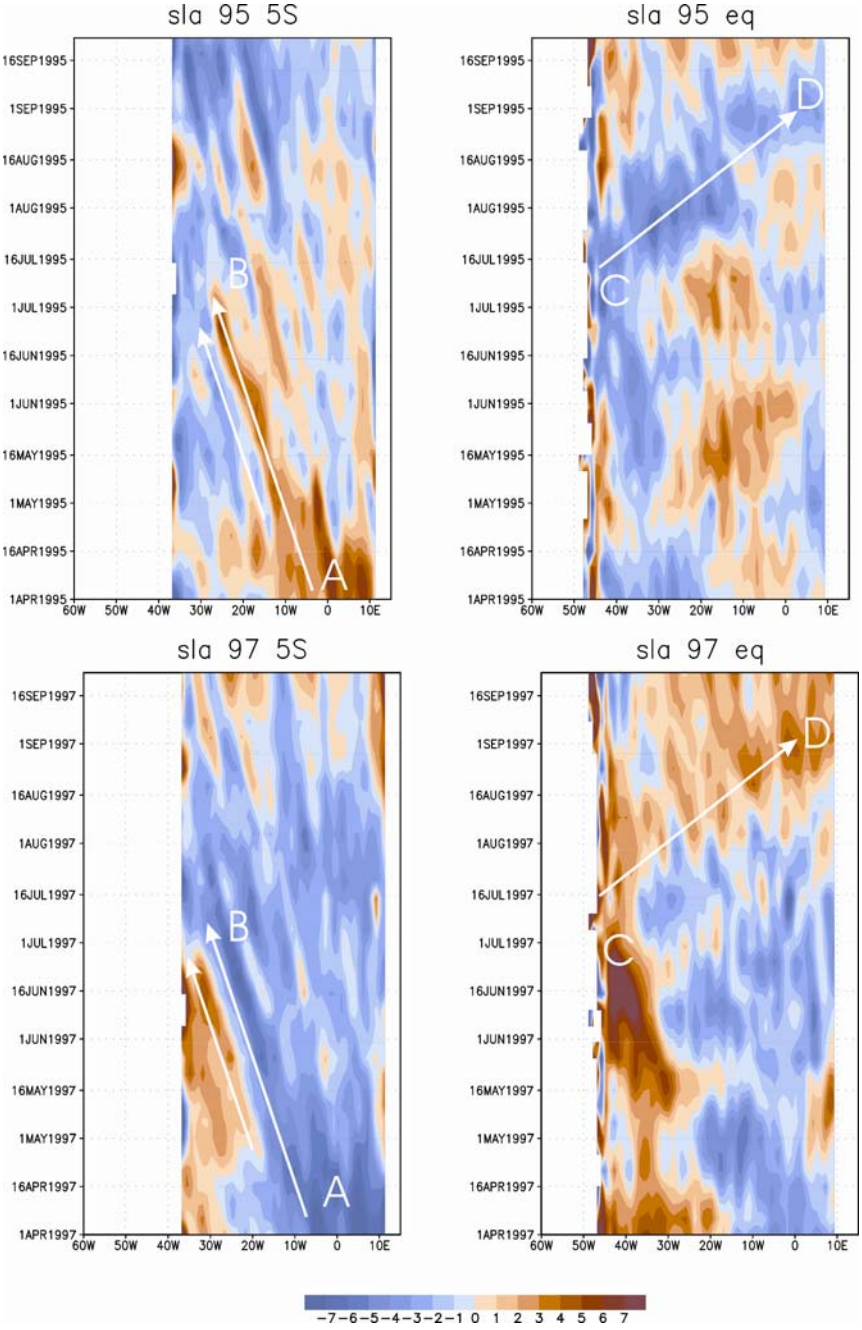

Figure 7: Sea Level Anomalies (shaded areas in cm) from April to September along 5S (left panel) and along the equator (right panel) for the 1995-year (top panel) and 1997-year (bottom panel).

b.2) SUBTROPICAL NORTH ATLANTIC AND MEDITERRANEAN SEA SST-SAHELIAN RAINFALL MODE: A DISCUSSION

The second mode in Figure 3 (lower panel) associates, in JJAS, the Sahelian anomalous rainfall with Mediterranean Sea SST anomalies, persisting from FMAM, and SNA SST anomalies, damping from AMJJ. The Mediterranean Sea influence on the WA monsoon regime has already been evidenced (Rowell, 2001) and studied with AGCM simulations (Rowell, 2003). Regarding SNA, there are some studies suggesting its influence (Paeth and Friedrichs, 2004; Rodríguez- Fonseca et al., 2006),

although there are some authors proposing that SNA SST has a passive role or very limited effects on WA rainfall (Ward, 1998; Mo et al., 2001; Vizy and Cook, 2001). For this reason, a discussion about the covariability between SNA and Mediterranean Sea SST anomalies and WA rainfall is considered in this section.

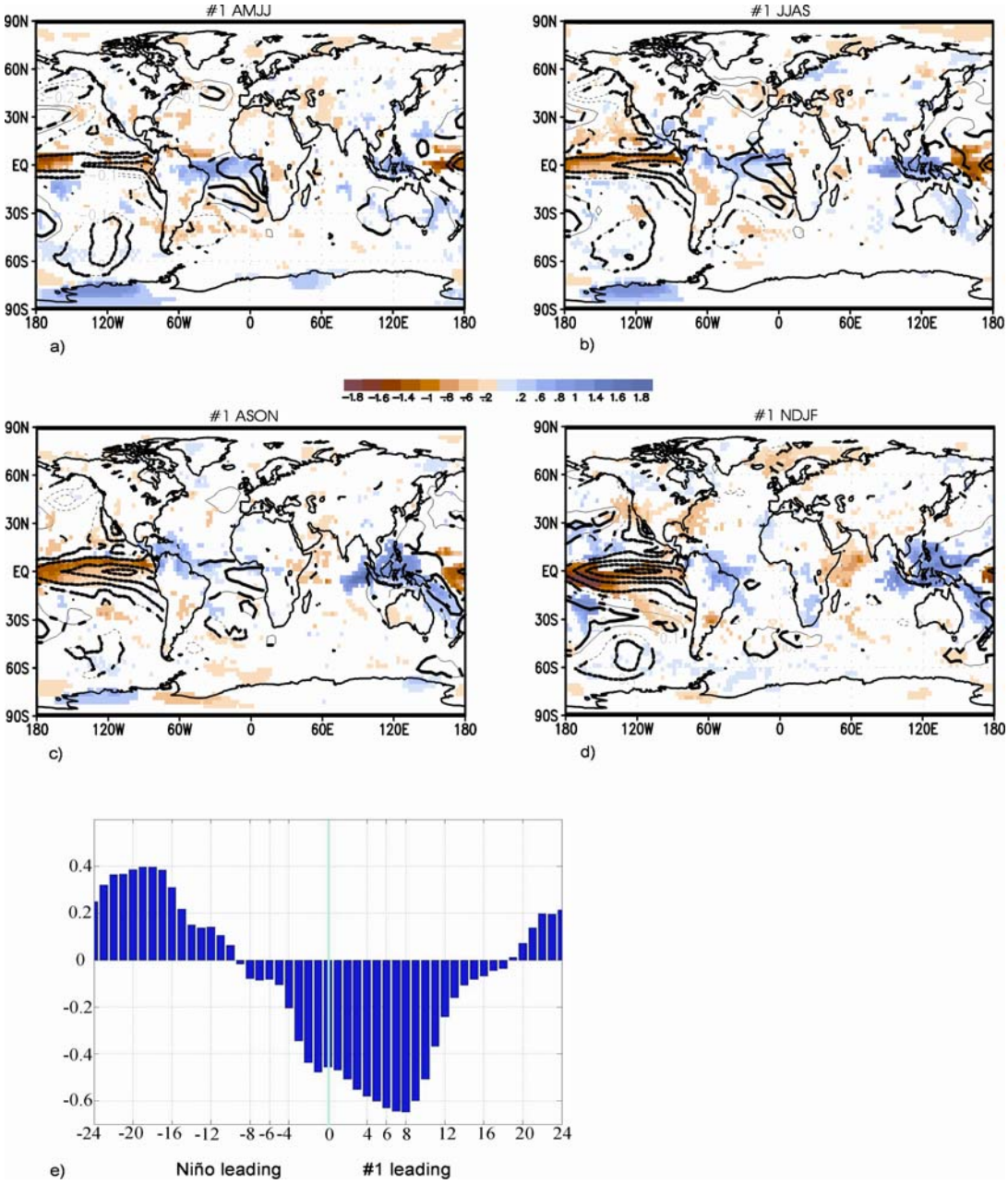

Figure 8: Regression of the total SST expansion coefficient associated with the leading EMCA mode onto the global SST anomalies (contour lines, CI=0.1ºC, 98% statistically significant areas, evaluated with a t-test, have been bolded) and the precipitation (shaded areas, mm day^{-1}, 98% statistically significant areas, evaluated with a t-test, have been shaded), for AMJJ (a), JJAS (b), ASON (c) and NDJF (d) seasonal sequences. Correlation coefficient between the leading mode SST expansion coefficient (lag 0) and the Niño3 index, leading and lagging 24 months (e).

In order to separate the possible contribution of the Mediterranean Sea SST anomalies from those of the SNA on the summer WA anomalous rainfall, we have performed two different EMCA analyses; one between the Mediterranean Sea and the WA rainfall, and another between the TA and the WA rainfall. The leading EMCA mode obtained when considering just the Mediterranean SST anomalies (Figure 9a), explains more than 33% of the covariance and it is a very robust mode. The mode relates positive SST over the Mediterranean, maximum at the east, with increasing rainfall over the Sahel, in particular over the region 10N-25N; 5E-25E. The correlation of the precipitation

expansion coefficient is statistically significant with both, the first WA rainfall PC in Figure 2a, and the second EMCA rainfall expansion coefficient in Figure 3 (0.96 and 0.90, respectively: see Table 1).

The same analysis done just for the TA SST presents a second mode (Figure 9b) with maximum loadings over Congo River basin and northern Sahel region. This pattern is itself more related to the third mode of variability when including the Mediterranean (not shown, the correlation coefficient between the both SST expansion coefficients is 0.83).

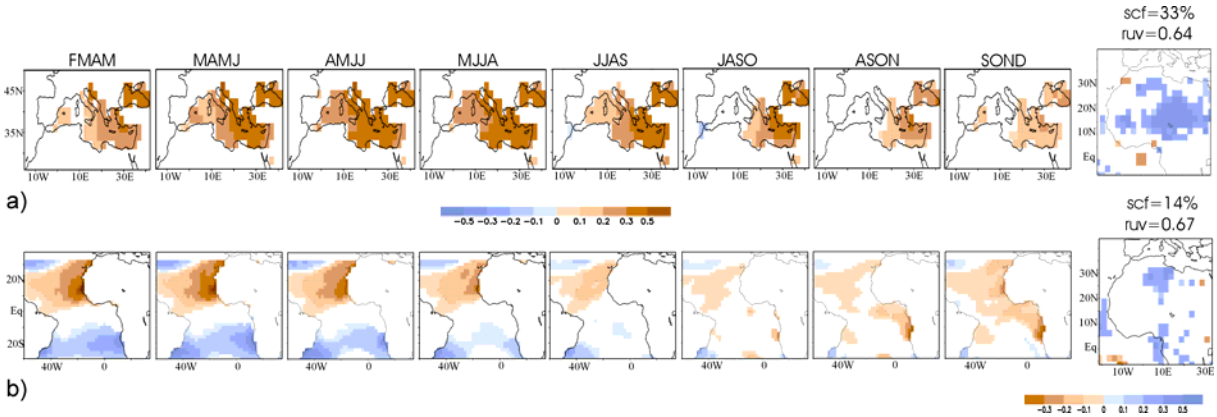

Figure 9:
a) Leading covariability mode obtained from the EMCA between summer WA precipitation and the anomalous Mediterranean Sea SST, 4-months sequences from FMAM to SOND. Only 98% statistically significant areas, evaluated with a t-test, have been shaded.
b) Second covariability mode obtained from the EMCA between summer WA precipitation and the anomalous TA SST (avoiding the Mediterranean Sea) corresponding to the 4-months sequences from FMAM to SOND. Only 98% statistically significant areas, evaluated with a t-test, have been shaded.

The correlation coefficients between the expansion coefficients of the three analyses are presented in Table 1. The three precipitation EMCA expansion coefficients obtained for the three EMCA analyses (trop+med, med, trop) are significantly correlated with the leading WA rainfall PC. However, regarding the SST expansion coefficients, the result from the total analysis (trop+med) is very similar to the TA analysis (r=0.71), but is less significant for the Mediterranean Sea analysis (r=0.49), and there is a very poor correlation between TA and the Mediterranean Sea analyses (r=0.09).

These results imply that both, TA and Mediterranean Sea SST anomalies, covary with the anomalous WA precipitation, but not necessary in the same way. Indeed, the sum of the SST expansion coefficients of both analyses; considering the SNA and Mediterranean Sea separately (Figure 9), is very similar to the SST expansion coefficient of the trop+med mode (Figure 3, lower panel), with a correlation coefficient of 0.82 versus the low correlations in Table 1. This linear relationship evidences that the Mediterranean Sea and the SNA SST are independent components of the WA rainfall variability: the Mediterranean Sea SST influences Sahelian rainfall, while SNA SST influences Congo River Basin rainfall.

To characterize the large-scale ocean pattern associated with these two modes, the regression of the SST expansion coefficients onto the global SST anomalies is performed (Figure 10a-b). The analysis reveals that both large-scale patterns are different. On the one hand, tropical SST anomalies related to the Mediterranean mode, are confined to the Pacific. On the other hand, for the SNA mode the whole tropical ocean basin is also significant. The SST signal over the Pacific is also different for both modes: the Mediterranean mode is related to central equatorial Pacific SST, while the SNA mode is related to the central-eastern equatorial Pacific.

The central equatorial Pacific SST signal related to the Mediterranean mode corresponds to the evolution of an extratropical Pacific mode from the previous summer (not shown), but not to a canonical El Niño event. However, the lead-lag correlation analysis between the Mediterranean expansion coefficient and the Niño3-index shows, with weak but significant scores, a 2-year correlation cycle that could give some insight into predictability issues (Figure 10c). Hence, the previously suggested connection between tropical Pacific SST and Sahelian rainfall (Janicot et al., 1996; Janicot et al., 2001) seems to be pointing at the Mediterranean Sea as relevant mediator. Thus, the relationship could be interpreted as a Tropical Pacific-Mediterranean - Mediterranean- Sahel interaction. The physical mechanisms involved in the remote relation between Mediterranean and Pacific SST anomalies (Figure 10a) could include

atmospheric teleconnections through Rossby waves. In addition, significant simultaneous correlations are found between Pacific Decadal Oscillation index and the Mediterranean mode. This is an important area of research in progress by the authors through observational and model analyses. However, it is worthy to notice that the regression of the leading WA rainfall PC (from Figure 2a) onto the global SST anomalies is significant only over the Mediterranean Sea region (not shown), giving robust weight to the Mediterranean influence during the dry Sahel period.

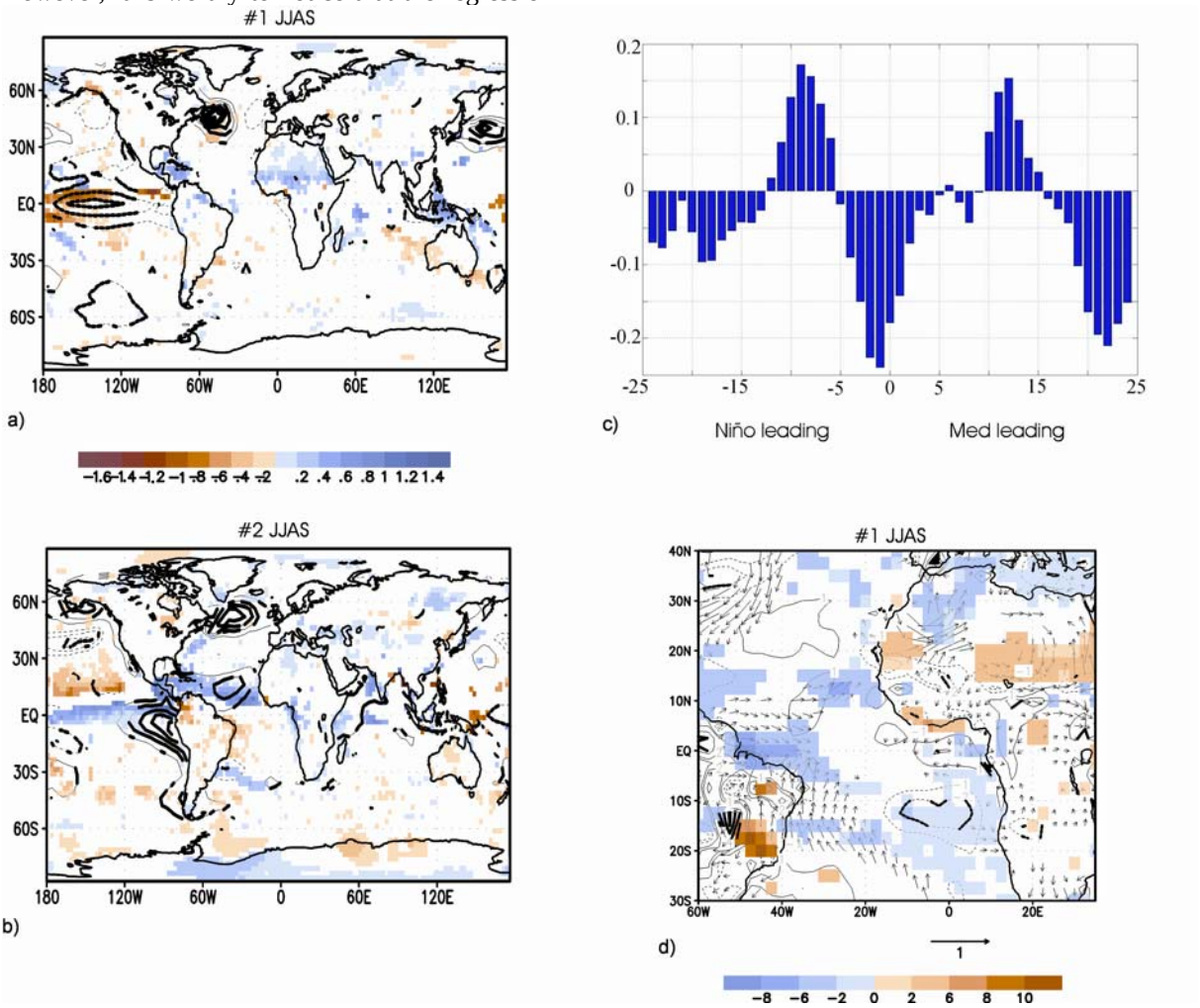

Figure 10:
a) Regression of the total SST expansion coefficient associated with the Mediterranean Sea EMCA leading mode onto the global SST anomalies (contour lines, CI=0.1ºC, 98% statistically significant areas, evaluated with a t-test, has been bolded) and the precipitation (shaded areas, mm day^{-1}, 98% statistically significant areas, evaluated with a t-test, have been shaded), for JJAS. Note that SST anomalies over the Mediterranean Sea are significant (same as Figure 9a) but the contour lines in the global map are not enough visible.
b) Same as a) but for the total SST expansion coefficient associated with the TA EMCA second mode.
c) Correlation coefficient between the total SST expansion coefficient associated with the Mediterranean Sea EMCA leading mode (lag 0) and the Niño3 index, leading and lagging 24 months.
d) Regression of the total SST expansion coefficient associated with the Mediterranean Sea EMCA leading mode onto the radiative flux anomalies (shortwave minus longwave radiation, W m^{-2}, positive downward, only 98% statistically significant areas, evaluated with a t-test, have been shaded), the surface wind anomalies (vectors, m s^{-1}, only 98% statistically significant areas, evaluated with a t-test, have been plotted) and the latent heat flux anomalies (contour lines, CI=1 W m^{-2}, positive downward, only 98% statistically significant areas, evaluated with a t-test, has been remarked), for the JJAS season.

Regarding the large-scale SST signal related to the SNA mode, Figure 10b yields both a North Atlantic pattern which is reminiscent of the previous winter Tripole SST pattern (not shown) and a tropical Pacific pattern which resembles the decay phase of El Niño (eastern remaining anomaly accompanied by western opposite-surrounding one). Some authors have pointed out how ENSO phenomenon can warm the SNA through PNA pattern and via Atlantic Walker-related anomalies (Wang, 2002b; Kushnir et al., 2006), while the NAO modulates trade winds strength and, in turn, SNA SST (Okumura et al., 2001). The regressed precipitation for this SNA mode shows positive anomalous

rainfall over Eastern equatorial Pacific, the Western Hemisphere Warm Pool (Wang, 2002b), and the Congo River basin region; and negative loadings over Northeastern Brazil.

Our results conclude that interannual Sahelian rainfall variability for the period 1979-2002 is mainly related to Mediterranean SST anomalies, instead of Pacific basin or SNA region. Figure 10d shows the Mediterranean SST expansion coefficient regressed onto the surface wind, the latent heat flux and the radiation flux anomalies for JJAS season. There is a positive radiative flux anomaly over Sahel region, which means that the Mediterranean influence is mainly non convective. The monsoon flow is weak, and the Harmattan winds over the Sahel are strengthened. This result coincides with those of Rowell (2003), who has shown that in years in which Mediterranean SSTs are warmer than average, increased evaporation leads to an enhanced moisture content of the air that is advected southwards by the low-level mean flow across the eastern Sahara into the Sahel, feeding the increased moisture convergence and leading to increased rainfall. Jung et al. (2006), simulates the 2003 Mediterranean warm event showing how the anomalously high moisture is advected from the Mediterranean by the climatological Harmattan and Etesian winds, where enhanced moisture flux convergence leads to more precipitation. Rowell (2003) also shows how the additional heating over the Sahel could induce a stronger low-level in-flow from the TA, which can be an explanation for the appearance of the Mediterranean and SNA SST anomalies together associated with anomalous Sahel rainfall.

	Tropical Atlantic (2# mode)	Mediterranean Sea (1# mode)	1# **PC** WAM	Tropical Atlantic+ Med (#3 mode)	
Tropical Atlantic + Mediterranean (2# mode)	0.75	0.90	0.89		**U**
	0.71	0.49	0.41		**V**
Tropical Atlantic (2# mode)		0.49	0.49	0.36	**U**
		0.09	0.12	0.83	**V**
Mediterranean Sea (1# mode)			0.96		**U**
			0.48		**V**

Table 1: Correlation coefficients between precipitation expansion coefficients (**U**) and SST expansion coefficients (**V**) from the different EMCA modes (Figure 3, lower panel and Figure 9), and WA rainfall PC modes (Figure 2).

4. Conclusions

This work characterize the most relevant observational TA (and Mediterranean Sea) SST modes coupled to the summer WA rainfall, in order to understand the possible predictability of the interannual WA rainfall variability for the Sahel dry period. We have evidenced the reliability of the precipitation dataset as well as the use of EMCA technique as a tool for resolving time-evolving SST patterns in relation to the anomalous WA rainfall. Using CMAP rainfall dataset for the period 1979-2002, the first two summer WA rainfall EOF variability modes have been determined as Sahelian and Guinean rainfall patterns, which appear as uncoupled ones. In contrast to other works that use CRU dataset, different time period and/or different methodologies, no evidences for a Dipole pattern are found for this period.

The leading SST-precipitation EMCA mode shows the evolution of the equatorial Atlantic mode associated with anomalous precipitation over the coast of the GG. The SST pattern is persisting for almost the complete sequence. Results suggest that the origin of the SST pattern occurs at the Angola/Benguela upwelling area due to an anomalous alongshore wind stress over this region. The wind anomalies over the Southeast Atlantic could be associated with a previous anomalous subsidence over the Amazon basin. The eastern anomalous SST creates a zonal gradient over the equatorial band, changing the thermocline slope. The SLA associated with the SST propagates westward as a Rossby oceanic wave from Southeastern Atlantic as far as West-central equatorial Atlantic. A different sign SLA anomaly, induced by anomalous Ekman pumping at the West Atlantic, propagates eastward as Kelvin oceanic wave, helping to damp the EM. The latent heat fluxes anomalies and the reversion of the wind anomalies also contributes to restore the normal conditions over the TA. Nevertheless, in order to asses these hypotheses about the EM air-sea interactions, coupled model would be need.

We have also evidenced that the leading TA EMCA mode could be important in driving Pacific anomalies. This different equatorial Pacific-Atlantic connection during the dry Sahel period implies a less active role of the ENSO events on the Sahelian rainfall anomalies, while the Pacific-Atlantic relationship has more influence on the rainfall over the coast of the GG, as the Walker circulation is anomalous along the entire equatorial band.

Although the Atlantic-Niño mode by itself does not seem to have a large influence on Sahelian rainfall, a seasonal correlation between autumn Guinean rainfall and the following summer Sahel rainfall has been found and evaluated by other authors, mainly as the result of the soil moisture conditions persistence and the developed vegetation interactions (Philippon and Fontaine, 2002; Fontaine et al., 2002; Douville et al., 2007).

The second SST-WA rainfall covariability mode, relates the anomalous Sahelian rainfall to an anomalous SST pattern over the SNA and Mediterranean Sea. This mode shows how, from AMJJ to JJAS, the warm Mediterranean SST anomalies enhance the Sahel precipitation by more evaporation and southward low level flow to the Sahel. The westerly winds from the Atlantic are also favored, strengthening the deep and dry convection over the Sahara low. Different EMCA-analyses have shown that the Mediterranean SST pattern has the major contribution on Sahel rainfall, while the direct influence of the SNA is not clear. The global SST pattern associated with the Mediterranean Sea mode shows SST anomalies over central Pacific and North Atlantic. It suggests that the Pacific-Sahel connection could be via the Mediterranean Sea. However, during this period, the Sahelian rainfall variability seems to be influenced only by the Mediterranean Sea (the leading WA rainfall PC regressed onto global SST has shown significant SST anomalies just over Mediterranean Sea).

This work outlines the TA role over the WA rainfall, indicating that, for the 80's and 90's the EM is the most relevant mode affecting the GG region and no significant link with the Sahelian Rainfall. The Mediterranean is shown to affect just over the Sahel precipitation. Nevertheless, there are some constrains that should be outlined. On the one hand, the ocean is not the only factor explaining the WA rainfall variability; and the interaction with land surface processes and the role-played by soil moisture and vegetation are also crucial factors (Douville, 2002; and Philippon and Fontaine, 2002). On the other hand, the Atlantic Ocean is not the only basin that influences WA rainfall variability. The role of other ocean basins has been also analyzed in an intercomparison exercise that is being developed in the framework of the AMMA-EU project. In this work, the same analysis for different ocean basins has been done, finding that, for this period, the Mediterranean Sea SST anomalies are the most important in driving Sahel anomalies, while the Central Pacific SST and Eastern Indian ocean SST explains less than 10% and 14%, respectively, of the SST-WA rainfall covariability, and the SST evolution of those patterns is not very clear.

Acknowledgments. We would like to thank to the editor Dr. Clara Deser, Dr. Carlos Roberto Mechoso, Dr. Elsa Mohino and anonymous reviewers for their helpful comments. The study was supported by the Global change and Ecosystems programme (EU Integrated project: African Monsoon Multidisciplinary Analysis (AMMA). AMMA has been the beneficiary of a major financial contribution from the European Community's Sixth Framework Research Programme. Detailed information on scientific coordination and funding is available on the AMMA International web site http://www.amma-international.org. Also, the study has been supported through Spanish MEC project CGL2006-04471.

REFERENCES

Bader, J., and M. Latif, 2003: The impact of decadal-scale Indian ocean ST anomalies on Sahelian rainfall and the North Atlantic Oscillation. *Geophys. Res. Lett.*, **30**, 2169, doi: 10.1029/2003GL018426.

Barreiro, M, A. Giannini, P. Chang, and R. Saravanan, 2004: On the role of the South Atlantic atmospheric circulation in Tropical Atlantic Variability. *In Earth's Climate: The Ocean-atmosphere interaction. Geophysical Monograph Series*, **147**, AGU, Washingto n DC, pp 143156.

Bretherton, S. B., C. Smith, and J. H. Wallace, 1992: An Intercomparation of methods for finding coupled patterns in climate data, *J. Climate*, **5**, 541-560.

Carton, J. A., X. Cao, B. S. Giese, and A. M. Da Silva, 1996: Decadal and Interannual SST Variability in the Tropical Atlantic Ocean. *J. Phys. Oceanogr.*, **26**, 1165–1175.

Chang, P., L. Ji, and H. Li, 1997: A decadal climate variation in the tropical Atlantic Ocean from thermodynamic air–sea interactions. *Nature*, **385**, 516–518.

Chelton, D. B., and M. G. Schlax, 1996: Global observations of oceanic Rossby waves, *Science*, **272**, 234-238.

Douville, H., 2002: Influence of soil moisture on the Asian and African monsoons. Part II. Interannual variability. *J. Climate*, **15**, 701-720.

Douville, H., S. Conil, S. Tyteca and A. Voldoire, 2007: Soil moisture memory and West African monsoon predictability: artefact or reality?, *Clim. Dyn.*, **28**, 723-742.

Florenchie, P., J. R. E. Lutjeharms, C. J. C. Reason, S. Masson, and M. Rouault, 2003: The source of Benguela Niños in the South Atlantic Ocean. *Geophys. Res. Lett.*, **30**, DOI 10.1029/2003GL017172.

Folland, C. K., T. N. Palmer and D. E. Parker, 1986: Sahel rainfall and worldwide sea temperatures, *Nature*, **320**, 602-607.

Fontaine, B., S. Janicot, and V. Moron, 1995: Rainfall Anomaly Patterns and Wind Field Signals over West Africa in August (1958–1989). *J. Climate*, **8**, 1503-1510.

Fontaine, B. and S. Janicot, 1996: Sea surface temperature fields associated with West African rainfall anomaly types. *J. Climate*, **9**, 2935-2940.

Fontaine, B., 2002: Spring to summer changes in the West African monsoon through NCEP/NCAR reanalyses (1968-1998). *J. Geophys. Res.* 107(d14): 4186.

Fontaine, B., P. Roucou, and S. Trzaska, 2003: Atmospheric water cycle and moisture fluxes in the West African monsoon: mean annual cycles and relationship using NCEP/NCAR reanalyses, *Geophys. Res. Lett.*, **30**, 10.1029-10.1032.

França, C., I. Wainer, A. R. De Mesquita, and G. J. Goni, 2003: Planetary equatorial trapped waves in the Atlantic Ocean from TOPEX/Poseidon altimetry, *in*: Goni, G.J.; Malanotte-Rizzoli, P. *Ed. Interhemispheric water exchange in the Atlantic Ocean. Elsevier Oceanography Series*, **68**, 213-232.

Frankignoul, C., E. Kestenare, 2005: Air-sea interactions in the tropical Atlantic: A view based on lagged rotated maximum covariance analysis. *J. Climate*, **18**, 3874-3890.

García-Serrano, J., T. Losada, B. Rodríguez-Fonseca and I. Polo, 2008: On the Origin, Impacts and Teleconnections of Tropical Atlantic Variability Modes. Part II: time-evolving atmospheric circulation related to SST-forced tropical convection. *J. Climate*, accepted.

Giannini, A., R. Saravannan and P. Chang, 2003: Oceanic Forcing of Sahel Rainfall on Interannual to Interdecadal Time Scales. *Science*, **302**, 1027-1030.

Handoh, I. C. and G. R. Bigg, 2000: A self-sustaining climate mode in the Tropical Atlantic, 1995-97: Observations and modelling. *Quart. J. Roy. Meteor. Soc.*, **126**, 807-821.

Hastenrath, S., 1984: Interannual Variability and Annual Cycle: Mechanisms of Circulation and Climate in the Tropical Atlantic Sector. *Mon. Wea. Rev.*, **112**, 1097-1107.

Hill, K. L., I. S. Robinson, and P. Cipollini, 2000: Propagation characteristics of extratropical planetary waves observed in the ATSR global sea surface temperature record. *J. Geophys. Res.*, **105**, 21927-21945.

Janicot, S., 1992: Spatio-temporal variability of West African rainfall. Part I: Regionalization and typings. *J. Climate*, **5**, 489-497.

Janicot, S., V. Moron, and B. Fontaine, 1996: Sahel droughts and ENSO dynamics. *Geophys. Res. Lett.*, **23**, 515-518.

Janicot, S., A, Harzallah, B. Fontaine, and V. Moron, 1998: West African Monsoon dynamics and Eastern Equatorial Atlantic and Pacific SST anomalies (1970-1988). *J. Climate*, **11**, 1874-1882.

Janicot, S., S. Trzaska, and I. Poccard, 2001: Summer Sahel-ENSO teleconnection and decadal time scale SST variations. *Climate Dyn.*, **18**, 303-320.

Jury, M. R, D. B. Enfield, and J. L. Mélice, 2002: Tropical monsoons around Africa: stability of El Niño-Southern Oscillation associations and links with continental climate. *J Geophys Res* **107** (C10): 15–1, 15–17.

Jung, T., L. Ferranti, and A. M. Tompkins, 2006: Response to the Summer of 2003 Mediterranean SST Anomalies over Europe and Africa. *J. Climate*, **19**, 5439–5454.

Kushnir Y., W.A. Robinson, P. Chang, and A. W. Robertson, 2006: The Physical Basis for Predicting Atlantic Sector Seasonal-to-Interannual Climate Variability. *J. Climate*, **19**, 5949-5970.

Keenlyside, N. S., and M. Latif, 2007: Understanding Equatorial Atlantic Interannual Variability. *J. Climate*, **30**, 131-142.

Lamb, P. J., 1978: Large-Scale tropical Atlantic surface circulation patterns associated with sub-Saharan weather anomalies. *Tellus*, **30**, 240-251.

Latif, M., and A. Grötzner, 2000: On the equatorial Atlantic oscillation and its response to ENSO. *Climate Dyn.*, **16**, 213-218.

Liebmann, B., and C. A. Smith, 1996: Description of a Complete (Interpolated) Outgoing Longwave Radiation Dataset. *Bull. Amer. Meteor. Soc.*, **77**, 1275-1277.

Lu, J., and T. L. Delworth, 2005: Oceanic forcing of the late 20th century Sahel drought. *Geophys. Res. Lett.*, **32**, L22706, doi:10.1029/2005GL023316.

Melice, J.L., and J. Servain, 2003: The tropical Atlantic meridional SST gradient index and its relationships with the SOI, NAO and Southern Ocean. *Clim. Dyn.* **20**, 447–464. DOI 10.1007/s00382-002-0289-x.

Mo, K., G. D. Bell, and W. M. Thiaw, 2001: Impact of Sea Surface Temperature Anomalies on the Atlantic Tropical Storm Activity and West African Rainfall. *J. Atmos. Sci.*, **58**, 3477-3496.

Moron, V., N. Philippon, and B. Fontaine, 2003: Skill of Sahel rainfall variability in four atmospheric GCMs forced by prescribed SST. *Geophys. Res. Lett.*, **30**, 2221, doi:10.1029/2003GL018006.

Motha, R. P., S. K. Leduc, L. T. Steyaert, C. M. Sakamoto, and N. D. Strommen, 1980: Precipitation patterns in West Africa. *Mon. Wea. Rev.*, **108**, 1567–1578.

North, G. R., T. L. Bell, F. Cahalan, and F. J. Moeng, 1982: Sampling Errors in the Estimation of Empirical Orthogonal Functions. *Mon. Wea. Rev.*, **110**, 699-706.

Okumura, Y., S. P. Xie, A. Numaguti, and Y. Tanimoto, 2001: Tropical Atlantic air-sea interactions and its influence on the NAO. *Geophys. Res. Lett.*, **28**, 1507-1510.

Paeth, H., and J. Stuck, 2004: The West African dipole in rainfall and its forcing mechanisms in global and regional climate models. *Mausam* **55**, 561–582.

Paeth, H., and P. Friederichs, 2004: Seasonality and time scales in the relationship between global SST and African rainfall. *Climate Dyn.*, **23**, 815-837, doi: 10.1007/s00382-004-0466-1.

Paeth, H., and A. Hense, 2004: SST versus climate change signals in West African rainfall: 20th century variations and future projections. *Climatic Change* **65**,179–208.

Philander, S. G. H., 1990: *El Niño, La Niña, and the Southern Oscillation.* International Geophysics Series, Vol. 46, Academic Press, 293 pp.

Philippon, N., and B. Fontaine, 2002: The relationship between the Sahelian and previous second Guinean rainy seasons: a monsoon regulation by soil wetness?. *Ann. Geophys.*, **20**, 575-582.

Polito, P. S., and P. Cornillon, 1997: Long baroclinic Rossby waves detected by TOPEX/POSEIDON. *J. Geophys. Res.*, **102**, 3215-3235.

Polo, I., B. Rodríguez-Fonseca, and J. Sheinbaum, 2005: Northwest Africa upwelling and the Atlantic climate variability. *Geophys. Res. Lett*., **32**, L23702, doi:10.1029/2005GL023883**.**

Polo I, A. Lazar, and B. Rodríguez-Fonseca, 2008: Oceanic Kelvin Waves and Tropical Atlantic intraseasonal Variability. Part II: Mechanisms and Impacts. Submitted

Rodríguez-Fonseca, B., I. Polo, E. Serrano, and M. Castro, 2006: Evaluation of the north Atlantic SST forcing on the European and northern African winter climate, *Int. J. Climatol*., **25**, doi: 10.1002/7joc.1234

Rowell, D. P., 2001: Teleconnections between the tropical Pacific and the Sahel, *Quart. J. Roy. Meteor. Soc*., **127**, 1683-1706

Rowell, D. P., 2003: The impact of the Mediterranean SSTs on the Sahelian rainfall season. *J. Climate*, **16**, 849-862.

Servain, J., A. J. Busalacchi, M. J. McPhaden, A. D. Moura, G. Reverdin, M. Vianna, and S. E. Zebiak, 1998: A Pilot Research Moored Array in the Tropical Atlantic (PIRATA). *Bull. Ame. Meterorol. Soc.*, **79**, 2019-2032.

Shinoda, M., and R. Kawamura, 1994: Tropical rainbelt, circultation, and sea surface temperatures associated with the Sahelian rainfall trend, *J. Meteorol. Soc. Jpn.*, **72**, 341-357.

Smith, T. M., and R.W. Reynolds, 2003: Extended Reconstruction of Global Sea Surface Temperatures Based on COADS Data (1854-1997). *J. Climate*, **16**, 1495-1510.

Sterl, A. and W. Hazeleger, 2003: Coupled variability and air-sea interaction in the South Atlantic Ocean. *Clim.Dyn.*, **21**, 559-571. DOI: 10.1007/s00382-003-0348-y.

Sultan, B., K. Labadi, J. F. Guegan, and S. Janicot, 2005. Climate drives the meningitis epidemics onset in West Africa. *Plos Medicine*, **2**, 43-49.

Tippett, M. K., 2006: Filtering of GCM simulated Sahel precipitation. *Geophys. Res. Lett.*, **33**, L01804, doi: 10.1029/2005GL024923.

Tippett, M. K., and A. Giannini, 2006: Potentially predictable components of African summer rainfall in a SST-forced GCM simulation. Submitted to *J. Climate*.

Trzaska, S., A. W. Robertson, J. Farrara, and C. R. Mechoso, 2006: South Atlantic variability arising from air-sea coupling: local mechanisms and tropical-subtropical interactions. *J. Climate*, in press.

Uppala, S. M., and co-authors, 2005: The ERA-40 Reanalysis. *Quart. J. Roy. Meteor. Soc.*, **131**, 2961-3012. doi: 10.1256/gj04176.

Vauclair, F., and Y. du Penhoat, 2001: Interannual variability of the upper layer of the Tropical Atlantic Ocean from in situ data between 1979 and 1999. *Climate Dyn.*, **17**, 527-546.

Vauclair, F., Y. du Penhoat, and G. Reverdin, 2004: Heat and Mass Budgets of the Warm Upper Layer of the Tropical Atlantic Ocean in 1979-99. *J. Phys. Oceanogr*., **34**, 903-919.

Venegas, S. A., L. A. Mysak, and D. N. Straub, 1997: Atmosphere–Ocean Coupled Variability in the South Atlantic. *J. Climate*, **10**, 2904–2920.

Vizy, E. K, and K. H. Cook, 2001: Mechanisms by Which Gulf of Guinea and Eastern North Atlantic Sea Surface Temperature Anomalies Can Influence African Rainfall. *J. Climate*, **14**, 795-821.

Wagner, R. G., and A. M. da Silva, 1994: Surface conditions associated with anomalous rainfall in the Guinea coastal region. *Int. J. Climatol.*, **14,** 179–199.

Wang, C., 2002a: Atmospheric circulation cells associated with the El Niño-Southern Oscillation. *J. Climate*, **15**, 399-419.

Wang, C., 2002b: Atlantic climate variability and its associated atmospheric circulation cells. *J. Climate*, **15**, 1516–1536.

Wang, C., 2005: ENSO, Atlantic climate variability, and the Walker and Hadley circulations. In: *The Hadley Circulation: Present, Past, and Future*. H. F. Diaz and R. S. Bradley, Eds., Kluwer Academic Publishers, 173-202.

Wang, C., 2006: An overlooked feature of tropical climate: Inter-Pacific-Atlantic variability. *Geophys. Res. Lett.*, **33**, L12702, doi: 10.1029/2006GL026324.

Ward, M. N., 1998: Diagnosis and short-lead time prediction of summer rainfall in tropical North Africa at interannual and multidecadal timescales. *J. Climate*, **11**, 3167-3191.

Xie, P., and P.A. Arkin, 1997: Global precipitation: A 17-year monthly analysis based on gauge observations, satellite estimates, and numerical model outputs. *Bull. Amer. Meteor. Soc.*, **78**, 2539 – 2558.

Zebiak, S. E., 1993: Air–sea interaction in the equatorial Atlantic region. *J. Climate*, **6,** 1567–1586.

Zhang, R., and T. L. Delworth, 2006: The impact of Multidecadal Atlantic Oscillation on Indian/ Sahel rainfall and Atlantic Hurricanes. Geophys. Ress, Lett, vol 33, L17712, doi:10.1029/2006GL026267, 2006

4.2 Intraseasonal Tropical Atlantic Ocean Variability: the Kelvin wave signal

Oceanic Kelvin Waves and Tropical Atlantic intraseasonal Variability.

Part I: Kelvin wave characterization.

IRENE POLO
Departamento de Geofísica y Meteorología, UCM, Madrid, Spain.

ALBAN LAZAR
LOCEAN - IPSL / Univ. Paris VI. 4 pl. jussieu, 75252 Paris cedex 05, France

BELEN RODRIGUEZ-FONSECA
Departamento de Geofísica y Meteorología, UCM, Madrid, Spain.

SABINE ARNAULT
LOCEAN - IPSL / Univ. Paris VI. 4 pl. jussieu, 75252 Paris cedex 05, France

(*Journal of Geophysical Research, accepted March 2008*)

ABSTRACT

Oceanic Kelvin waves from the equator to the West African coast are investigated in the framework of Tropical Atlantic (TA) intraseasonal variability. In order to better highlight the wave propagations, a 25-95 day band-pass filter was applied to the Sea Surface Height (SSH) product derived from the TOPEX/Poseidon altimeter and an OGCM simulation for the 1993-2000 period. In addition to equatorial eastward propagations, our analysis reveals recurrent and continuous propagations distinguishable over thousands of kilometers poleward along the coasts as far as about 10-15 degrees of latitude, a novel result with altimeter data. The variance of the filtered SSH signal goes from 1 cm at the equator to 2 cm at the African coast. Estimates of the phase speed range from 1.5 m/s to 2.1 m/s along the equator and the West African coastline. Such values are very close to those of equatorial Kelvin wave propagations, likely dominated by the first two baroclinic modes, supporting the fact that the coastal propagations are coastally trapped Kelvin waves. In order to simplify the description of these Kelvin waves, we present an intraseasonal climatology which reveals regular boreal autumn-winter equator to coast propagations. An improved description is achieved thanks to the computation of an extended empirical orthogonal function for the boreal autumn-winter propagations. Lag correlation of SSH signals allows for a twofold quantification; the phase speed and the importance of remote forcing along the coast. The remote forcing effect of intraseasonal Kelvin waves is clearly evidenced over coastal upwelling regions as far as 10-15 degrees latitude. The physical mechanism associated with the forcing of the Kelvin waves and its impacts are investigated in Part II of this work.

1 Introduction

Most of the heat content variability in the tropical ocean is located in the upper layer and, as a result, low latitude oceans are often approximated as a two-layer system. This attribute approximation implies that variations in the depth of the thermocline, and hence of the heat content, are directly reflected in Sea Surface Height (hereafter SSH, Rebert et al., 1985) with the first baroclinic mode being dominant.

As shown by Matsuno (1966) and Moore (1968), the latitude band of the tropical oceans is the site of a singular set of equatorial waves that propagate eastward (equatorial Kelvin waves) or westward (Rossby waves). Their sea-level signature is adequate to their detection and satellite altimeters can measure the signals down to a few centimetres. Although altimeter measurements primarily reflect the movement of the thermocline, because of the near-surface intensification of baroclinic modes (Stammer, 1997), second and third baroclinic modes could also be important in the actual Tropical Atlantic (du Penhoat and Trequier, 1985; Illig et al., 2004; Shouten et al, 2005). The phase speed estimated of the equatorial Atlantic is 2.6 m/s for the first vertical mode Kelvin wave, and 1.4 m/s and 0.8 m/s for the second and third vertical modes (Schouten et al., 2005; Illig et al., 2004).

The Tropical Atlantic (TA) dynamic sea level variability is dominated by the seasonal cycle (Arnault and Cheney, 1994). The seasonal adjustment of the ocean to the forcing of the wind stress causes a cycle of consecutive Rossby and Kelvin waves. Figure 1a shows the seasonal cycle of the sea level and the wind stress along the equator and the West African coast. This standard figure (similar to the one shown by Shouten et al., 2005 and Rouault et al., 2007) computed here as the sum of the annual and semiannual harmonics, is characterized at the eastern equator by an upwelling season (May to October) and a downwelling season (November to April), coinciding with the strengthening and weakening of the trade winds at the equator. Along the coast of the Gulf of Guinea (GG), coinciding with the two upwelling seasons (February-March and August-September; Picaut, 1983), there are some apparent coastal propagations of the sea level (February-March and August-September in figure 1a-left) which, are slower than the one expected from theoretical first mode Kelvin wave propagations (Schouten et al., 2005) and whose wave nature is not clear. One might wonder from this figure whether there are only high-order slow modes along the coast, or if the lowest-order baroclinic modes are masked by wind changes associated with the ITCZ migration or other large-scale processes. In order to answer this question an additional processing of the signal is thus necessary to verify the latter-mentioned coastal propagations.

Since Matsuno (1966) established the equations of the shallow water equatorial waves, several studies early advocated the idea that part of the equatorial and coastal upwelling in the GG is remotely forced by the wind in the western equatorial Atlantic via Kelvin waves (Moore et al., 1978; Adamec and O'Brien, 1978; O'Brien et al., 1978; Clarke, 1978; Servain et al., 1982). Further elements were presented in support of coastal wave propagation in the TA with Sea Surface Temperature (SST, Picaut, 1983) and tide gauges records (Aman et al., 2007). A new stage started when TOPEX/Poseidon (T/P) was launched in 1992 and, since then, Kelvin wave propagations have been better described in the equatorial Atlantic (Katz, 1997; França et al., 2003; Illig et al., 2004; Schouten et al., 2005; Han et al., 2008) and equatorial Pacific (Kessler et al., 1995; Meyers et al., 1998; Cravatte et al., 2003; Roundy and Kiladis, 2006). These studies used band-pass filters in order to avoid the masking effect of large-scales signals and this is also the strategy we adopted in this paper.

Regarding theoretical studies about the continuity of the equatorial Kelvin waves along the eastern boundary, Moore (1968) established that the equatorial Kelvin waves could be reflected in the eastern boundary, and in part, could propagate poleward coastally trapped. Although Clarke (1983) also established analytically the equatorial wave reflection in an oceanic boundary, he found that the reflection occurred without dissipation. Greatbatch and Peterson (1996) described how the stratification changes could slow down the coastally trapped wave propagation in high latitudes. Using observational data, convincing elements have been presented of Kelvin wave propagations from the equator to the coast in the eastern Pacific at intraseasonal (Hormazabal et al., 2002), and interannual timescales, especially during ENSO events (Jacobs et al., 1994; Meyers et al., 1998; Vega et al., 2003). Grodsky and Carton (2006) have found coherent interannual variations of SSH in the equatorial Atlantic and the southern subtropical Atlantic. They hypothesized that a link between the two is provided by coastal waves propagating southward along the African coast.

Along the coast, one way of dissipation of the Kelvin wave energy is the radiation of Rossby waves from the eastern boundary (Gill, 1982). The Rossby wave when reaching the western boundary can then potentially trigger a new Kelvin wave at the western equator. However several works have argued that the small Atlantic basin and the presence of the North Brazil Current (NBC) could inhibit the Rossby reflection (Arnault et al., 1990, Handoh and Bigg, 2000, Illig et al., 2004). These authors have experienced difficulties at tracking back equatorial waves up to the American coast.

In this paper, we have focused our analysis on intraseasonal timescales. At these scales, the Kelvin wave activity has been pointed out, mainly in the Pacific basin, to be associated with the convection activity, which can be important in climate terms (Kessler et al., 1995; Hendon et al., 1998; Roundy and Kiladis, 2006). In the TA, intraseasonal variability modulates the main annual to interannual basin signals of important processes (i.e. West African Monsoon, oceanic cold tongue over the eastern equatorial Atlantic, seasonal coastal upwelling at the African West coast, etc…). Therefore it is important to investigate the nature of the intraseasonal SSH signal, and in particular its contribution to the teleconnection processes within the tropics. Furthermore, an unambiguous detection of continuous propagating signals from the equator to the subtropical along the eastern Atlantic ocean coastlines at intraseasonal scales is still missing, and we understand there is a need of filling this gap through further investigation. It is the goal of this first paper to provide a sound description of this phenomenon over the TOPEX/Poseidon 1993-2000 time period, using the satellite measurements combined with an Ocean General Circulation Model (OGCM) simulation. In the second part of this paper, we analyse the various forcing of these waves as well as some of its impacts in relation to the TA intraseasonal variability. The

current manuscript presents a detailed description of the data used (section 2). After a discussion of the choice of the band-pass filter (section 4), we study the intraseasonal propagating SSH anomalies in the observations and the OGCM (section 5), through a climatology and, focusing on boreal autumn-winter season, the main propagating mode. Then apparent propagation phase speeds are quantified and the remote impacts characterized (section 6). Finally the main conclusions are summarized.

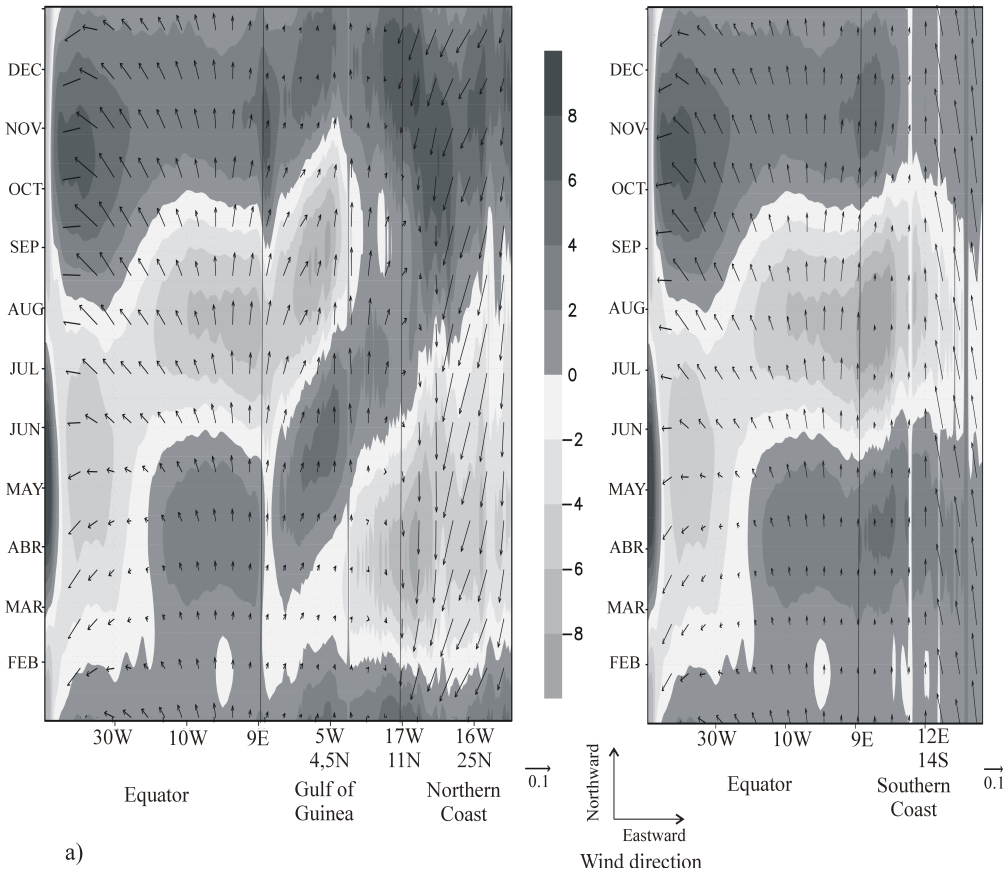

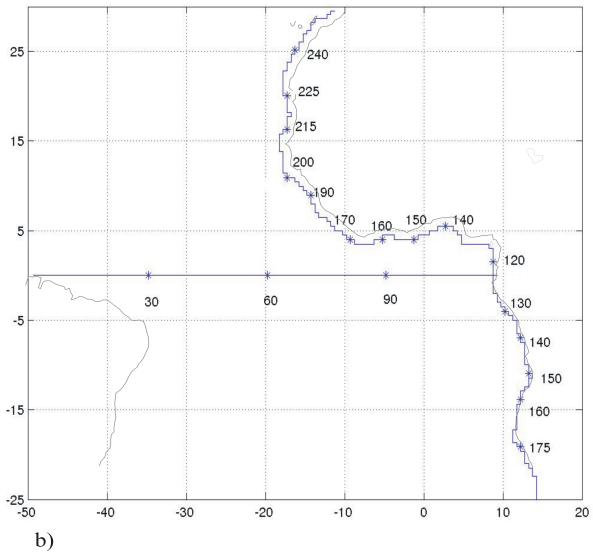

Figure 1: a) Seasonal cycle of the observed T/P SSH (shaded areas in cm) and the wind stress (vectors in 10^{-1} N/m^2), for the equatorial Atlantic and the northern (left) and southern (right) African coast. The wind stress is projected over virtual xy-axes, positive eastward and northward respectively. **b)** Map of the Grid points along the Equator and the African coast used in the study as Kelvin wave-tracks.

2 Description of the data

We use SSH TOPEX/Poseidon altimetry measurements, with 0.5 degrees horizontal resolution and 7-days time resolution produced and distributed by Aviso, as part of the Ssalto ground processing segment. The T/P SSH anomalies have already been corrected by removing four-year average elevation and signals such as the ocean tide, the dry tropospheric, inverted barometer, tidal aliasing and vapour water. The inter-comparison analyses with *in situ* measurements (i.e. tide gauges records) have demonstrated that the altimetry is an important tool to observe oceanic variability (Arnault et al., 1992), even in the coastal regions (Aman et al., 2007). In contrast to the sparse network of coastal tide gauges, measurements of SSH from space by satellite radar altimetry provide near global and homogeneous coverage of the world's oceans. The weekly temporal resolution of the T/P SSH is expected to be high enough for the description of the baroclinic Kelvin waves, since the theoretical first baroclinic mode takes about 30-45 days to cross the Atlantic along the equator and more than 20 days to leave the tropical latitudes studied here. However, the 0.5 degree spatial resolution corresponds to the Rossby radius of deformation at about 15 degrees of latitude for a 2 m/s baroclinic phase speed. Therefore it is certainly a limitation to our analysis, and it may in particular affect our ability to observe coastal waves poleward of 10 to 20 degrees of latitude.

In order to complete the study with synchronous subsurface oceanic quantities that are not available in the observations, in particular the thermocline depth, we use a numerical simulation of the OPA OGCM (Madec et al., 1998). The ORCA05 configuration used here was run at the LOCEAN laboratory by the NEMO (Numerical Framework for Ocean Modeling) team, for the 1992-2000 period. The configuration is for the global ocean with a 0.5 degrees horizontal resolution and 30 vertical levels. The momentum flux is the weekly ERS1-2 wind stress interpolated daily, while the air-sea heat fluxes are computed in line with semi-empirical, or bulk formulas using OGCM SST, the ERS1-2 wind speed, the NCEP-NCAR reanalysis (Kalnay et al., 1996) air temperature, and monthly climatological air humidity (Trenberth et al., 1989) and cloudiness (Berliand and Strokina, 1980). Precipitation data come from the Climate Prediction Center Merged Analysis of Precipitation (CMAP) product (Xie and Arkin, 1996). Major river runoffs are taken into account through monthly values of river discharge (UNESCO, 1996). At last, a restoring term towards Levitus (1998) Sea Surface Salinity is applied to the fresh water budget. For further details on the model configuration see de Boyer-Montégut et al. (2007).

In this work we have used 5-day average output of SSH and 18°C isotherm depth (hereafter z18). We have chosen the 18°C isotherm depth as the thermocline depth proxy after having analysed the isotherms ranging from 15°C to 25°C. The 18°C isotherm depth appears to be the most representative thermocline proxy over the African coastlines, in particular within upwelling areas where the isotherms outcrop. Note that the pycnocline (represented as sigma-26 isopycnal depth $z\sigma 26$) is theoretically more closely related to waves and it has more physical meaning than z18. However the z18 it is much better geographically defined than $z\sigma 26$, especially in the coastal areas, therefore z18 will be used along the study. In the next section, some basic statistics are performed to show the ability of the model to reproduce the SSH observations for the 1993-2000 period.

To follow the Kelvin wave propagation, wave-tracks have been defined along the equator and the African coast following the model grid, thus the distance between two grid points is 0.5° (~55 km). For the sake of minimizing data gaps, the northern coastal track-points have been shifted 0.5° offshore. The corresponding wave-tracks are shown in figure 1b, along the equator and poleward along the African coast. For the north, the track moves along the GG westward and continues northward up to 30°N, having twice more track-points than the south. For the south, the track runs up to 25°S along the coast (named hereafter southern African coast). Note that both, north and south wave-tracks, share the first ~120 points corresponding to the equatorial Atlantic. It bears mentioning that following the coastline along different isobaths (0, 200, 400, 1000 meters) does not make substantial differences and no remarkable properties changes are found (not shown). In this paper generally, for the sake of simplicity, the term "Kelvin wave" refers to the equatorial and coastally trapped propagations, even though the coastal wave nature may be a mixed of Kelvin and topographic wave.

3 Interannual SSH anomalies

The annual and semiannual components dominate the sea level variability over the equator and the African coast (Wilson and Adamec, 2002; Schouten et al., 2005; Aman et al., 2007). Figure 2 shows Hovmuller diagrams of the observed SSH interannual anomalies along the wave-tracks, which are the result of removing the seasonal cycle relative to the above-mentioned harmonics to the total signal. The result of this truncation (figure 1a) is similar to the one obtained when performing the seasonal cycle with

higher truncation or with a simple climatologycal average (not shown). Although propagations are difficult to identify unequivocally due to basin-scale interannual SSH anomalies (Handoh and Bigg, 2000; França et al., 2003), many propagating-like signals appear strikingly going from the equator to the African coast; along the GG (figure 2-left) and along the southern African coast (figure 2-right). It is also noticeable that some points are particularly noisy: in the western equator (0-20 equatorial track-points), at 5°S (140 south track-point), and at 10°N (200 north track-point). The first two locations correspond to the Amazon and the Congo River run off. Whereas the last location corresponds to the large offshore extension of the continental plateau, likely associated with strong tidal signals.

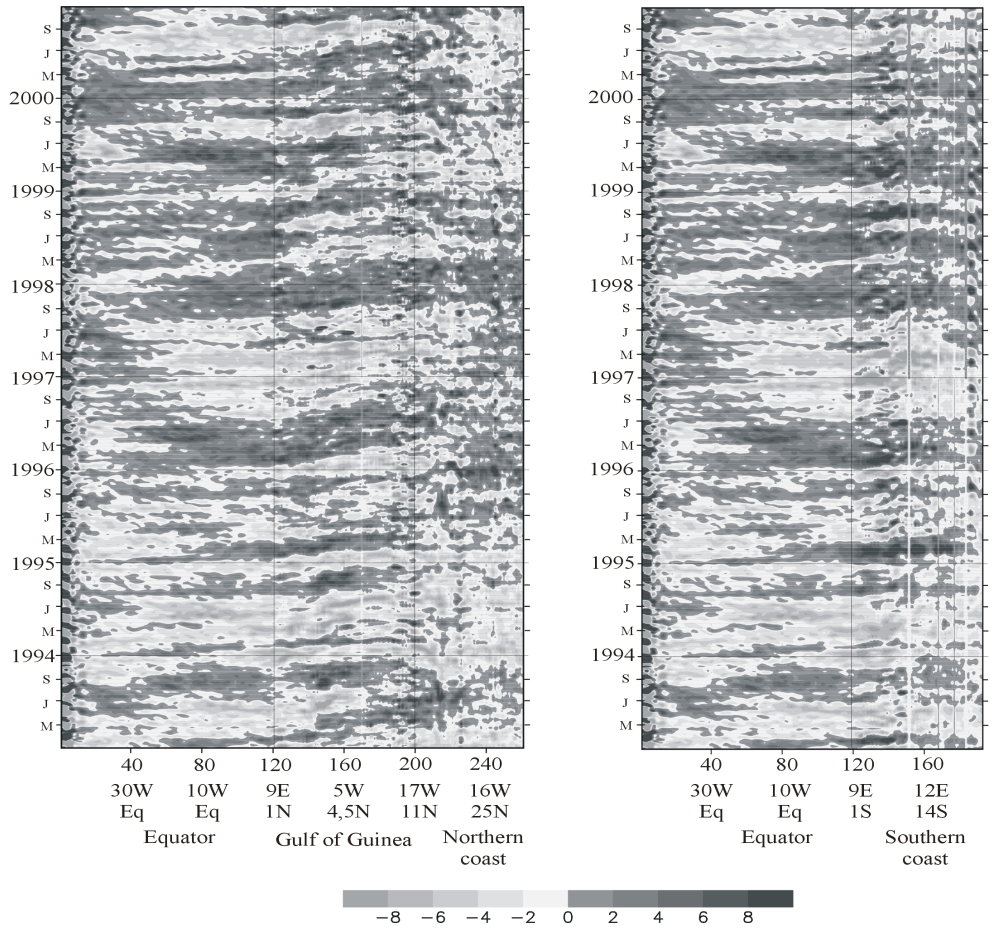

Figure 2: Hovmuller diagrams for the observed SSH interannual anomalies (cm), following the track of the figure 1b, for the equator and the northern African coast (left) and the southern African coast (right), for the 1993-2000 period.

The diagrams show extreme positive and negative events, associated with the 1995-1996, 1998, 1999 warm events and the 1994, 1997 and 2000 cold events. Some of those years have been described by other authors in relation to a self-sustaining Atlantic climate mode (Handoh and Bigg, 2000), to interannual variability modes (Sutton et al., 2000; Illig et al, 2006), to ENSO (Saravanan and Chang, 2000) and to the extratropical north Atlantic climate variability (Rodriguez-Fonseca et al., 2006). Interestingly, this figure suggests a quasi-permanent intraseasonal modulation of the interannual signals. The aim of the rest of this article is to characterize the intraseasonal SSH component.

4 Selection of the intraseasonal frequency band

Figure 3a presents the energy spectra of the observed SSH along the wave-tracks computed up to a period of 500 days. The annual and semiannual cycles appear the most energetic and are present along the equator and the coast; they are followed by a 120 days signal (top panel). For periods smaller than 100 days, energy is less concentrated in a specific periodicity (bottom panel). However, there are some relative maximum at the 100 to 95 day and 60 to 50 day periods. Below 30 days approximately, there is

no energy as expected when reaching close to the T/P time resolution. Periodicity peaks at intraseasonal scales in the Atlantic have been studied in details by Katz (1997) who found enhanced variance at about 25 and 50 days, as well as Han et al. (2008) have found dominant spectral peaks within the intraseasonal windows at 10-40 and 40-60 days. In the Pacific, Kessler et al. (1995) or Cravatte et al. (2003) have also evidenced a peak at 120 days, but the next smaller period is 75 days, with neither 60 days nor 95 days peaks. It appears in the Atlantic with no clear single peak but rather with a wide range of active periods. As Roundy and Kiladis (2006) proposed for the Pacific equatorial Kelvin waves, this spreading of the wave frequencies may occur in part because phase accelerations and amplitude variations are forcing the waves to become not sinusoidal in time.

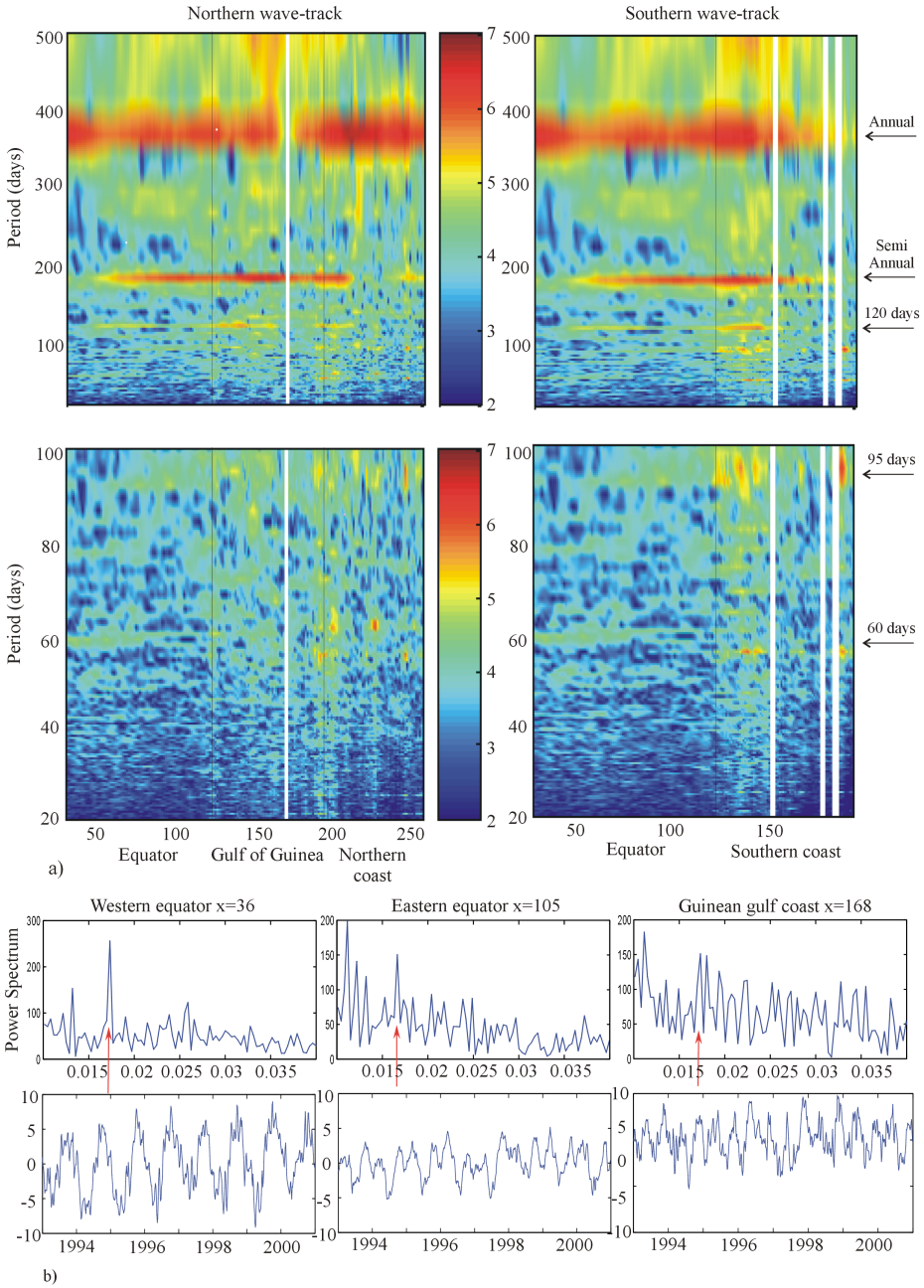

Figure 3: a) Variance-preserving spectra of observed SSH data (in cm^2). Periodicity versus track-points for the north (left panel) and south (right panel) Kelvin wave-track. Top panel corresponds to 20-500 days periodicity range, and bottom panel corresponds to 0-100 day periodicity range. **b)** Power spectrum ranging from 20 to 100 days (top panel) of three points along the north wave-track corresponding to the western equator, eastern equator and Gulf of Guinea (from left to right) and the associated timeseries (bottom panel). The frequency around 50-66 days period has been remarked.

Figure 3b shows an example of three points along the northern wave-track (x=36, 105 and 168, which correspond to western equator, eastern equator and GG respectively). Although depending on the location the SSH signals differ (figure 3b-bottom panel), the power spectrums from 100 to 25 days, show a relative peak in between 67-50 days (figure 3b-top panel).

Finally we chose to retain the 25-95 day periodicity. The filter has been performed by subtracting two low-pass filters, which have been constructed by smoothing the signal with a Hanning weighting function of 21 days and 91 days time-window, respectively (25-95 days for the modelled data). The smoothing replaces each value on the grid to which they are applied with a weighted average of the surrounding data values along the time axis. The subtraction of the two low-pass filters results in a 25-95 day band-pass filter, whose frequency response function (not shown) preserves about 60% of the signal amplitude within the 70-35 day band, with a maximum (80%) at 50 days, and a 10% preserving reached at about 200 and 20 day periods. Note that the filter preserves the frequencies, and it neither creates artificial spectral peaks nor phase shifts associated with negative lobes.

5 Description of the intraseasonal Kelvin wave propagations

Figure 4a shows the result of filtering the T/P SSH data in the entire period along the north (left panel) and south (right panel) wave-tracks. It can be noticed the almost-permanent eastward/poleward propagating signals along the year and for all the years. A first gross visual estimation of the slopes for continuous signals suggests a regular propagation phase speed of ~1.8 m/s. The diagram shows downwelling and upwelling Kelvin wave propagation with a ~2 month period. It is important to notice that, although the filter is preserving the 50 day period, the 2 month period signal is not just a filter product since figure 3 support the importance of the 2 month period, and similar SSH signals are found when filtering the SSH within different windows (i.e. 25-150 day band, not shown).

The absolute mean value of the SSH signal amplitude is 1-2 cm at the equator and the signal is amplified to 2-4 cm at the beginning of the coast, at the coast of the GG (from 120 to 180 north track-points) and at the southern African coast (from 120 to 150 south track-points). This intraseasonal SSH signal represents approximately 50% of the seasonal cycle amplitude (comparing with figure 1a). The SSH variance (figure 4b) shows 1 cm at the equator that increases at the African coast to 2 cm, with higher variance at some coastal track-points.

Although there are horizontal SSH bands (i.e. October-November 1993; October-November 1997 in figure 4a), corresponding to a whole basin equatorial events, most of the SSH signals are associated with an eastward propagation. After the equatorial Kelvin wave splits at the African coast, poleward propagation can be noticed as far as 12 degrees (200 north track-point and 160 south track-point). Beyond these points, no propagation can be detected. Some exceptions, as for the southern track, that shows clearer propagation at higher latitudes for some events (see November-December 1993 events in figure 4a), could be due to some “in phase” SSH variations forced locally by wind burst. This latitudinal propagation threshold is explained by the limitation of the data resolution (~0.5°) versus the radius of deformation. Poleward 15 degrees latitude, the distance comprised in 0.5° longitude exceeds the radius of deformation computed for 2 m/s baroclinic phase speed (not shown), which makes the wave to be hardly detectable.

Strikingly, the Hovmuller diagrams repeatedly display equatorial and coastal downwelling Kelvin wave in September, December and March; and whereas equatorial and coastal upwelling Kelvin wave appears frequently in November, January and July. The September-November and December-January pairs are representative for most years. However, an interannual modulation of the intraseasonal variability is also clear (for example comparing autumn-winter 1994 and 1999 years in figure 4a).

The Hovmuller diagram for the modelled SSH (not shown), exhibits even clearer anomaly propagation at those frequencies than the observed SSH. In order to test the ability of the ORCA05 configuration to simulate the intraseasonal SSH, we have correlated the model and the T/P data at intraseasonal scales (figure 4c). Along the equator the correlation is statistically significant except for the western equatorial Atlantic, because of the noisy SSH signal in this area, as it has been discussed before (likely due to the low time-resolution of the river runoff data in the model, T/P error near the Amazon mouth, or incorrect NBC rings in the model). Along the coast, the correlation is good for most of the points, decreasing poleward for the north and south wave-tracks.

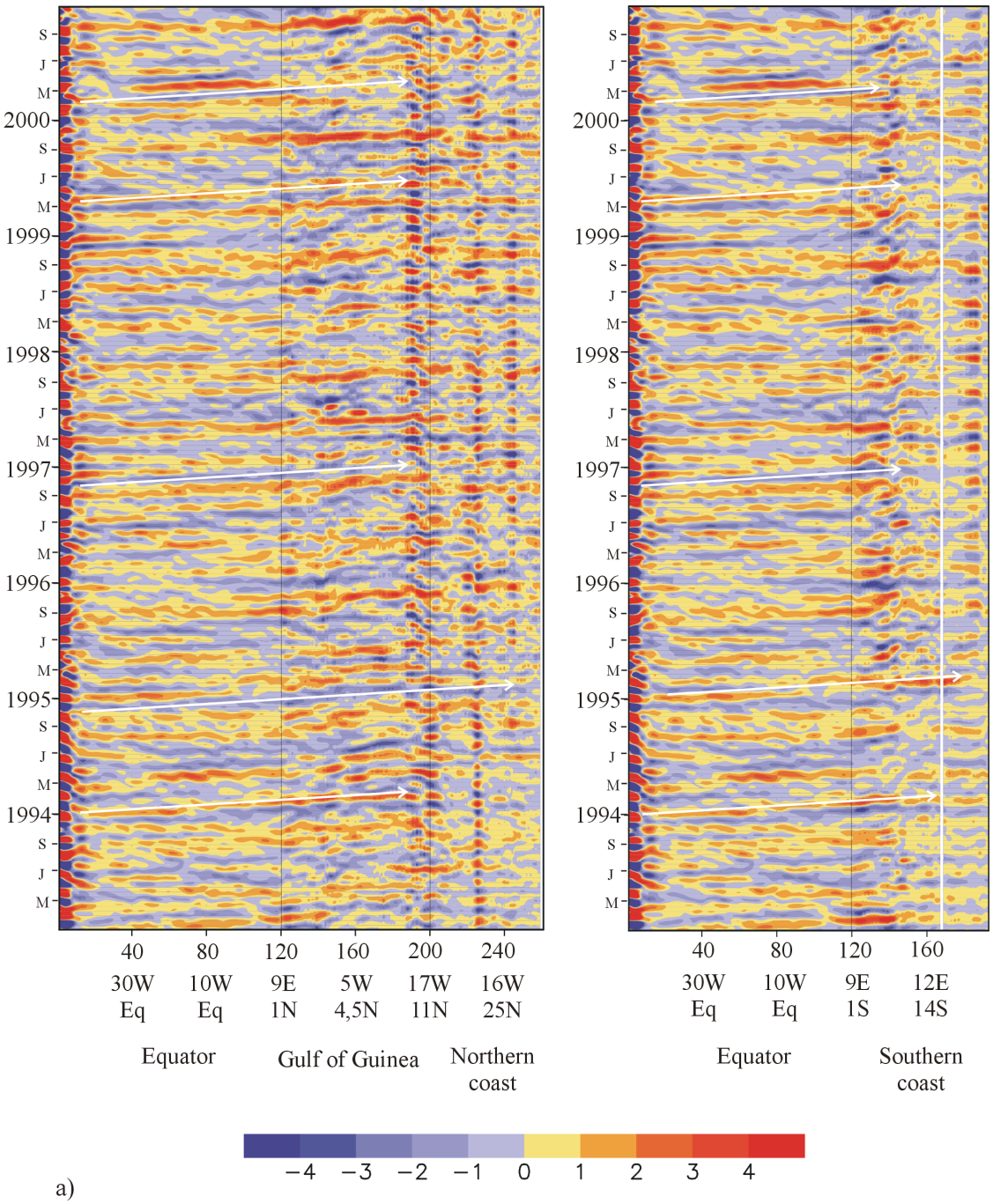

Figure 4: a) Hovmuller diagrams of the observed intraseasonal SSH (in cm), following the wave-track of figure 2, for the equator and the northern African coast (left) and the southern African coast (right), for the 1993-200 period. The filtered SSH signals are the result of applying a 21-91 day band-pass filter. The white arrows correspond to 1.8 m/s propagation phase speed.

The differences of the variances for the model and for the observations can be seen in figure 4b, being the amplitude of the observations larger than the model one. In particular, the variance differs very much for the point 190 of the north wave-track, a point that is probably very affected by the tide of two month period (Arnault and Le Provost, 1997). The differences at 0-20 equatorial track-points and 140 south track-point are related to the Amazon (not shown because it has a very large value) and the Congo River runoff respectively. The main differences also appear at 220-240 north track-points and 185 south track-point, which correspond to the permanent coastal upwelling regions, likely not very well represented by the altimetry and/or due to the model resolution. Note that the correlation between the modelled and observed non-filtered SSH data is statistically significant for all the points (not shown),

although the lower correlation occurs at the GG for the north wave-track and at 15°S for the south wave-track (r=0.5). Although a thorough inter-comparison study between the model and the T/P data is out scope of our work, the statistical basic test suggests that the model configuration is suitable to study the SSH intraseasonal variability at the equator and the tropical African coast. Hereafter, the model and the observations will be used along the paper to understand the SSH variability, as well as its dynamics in the companion paper.

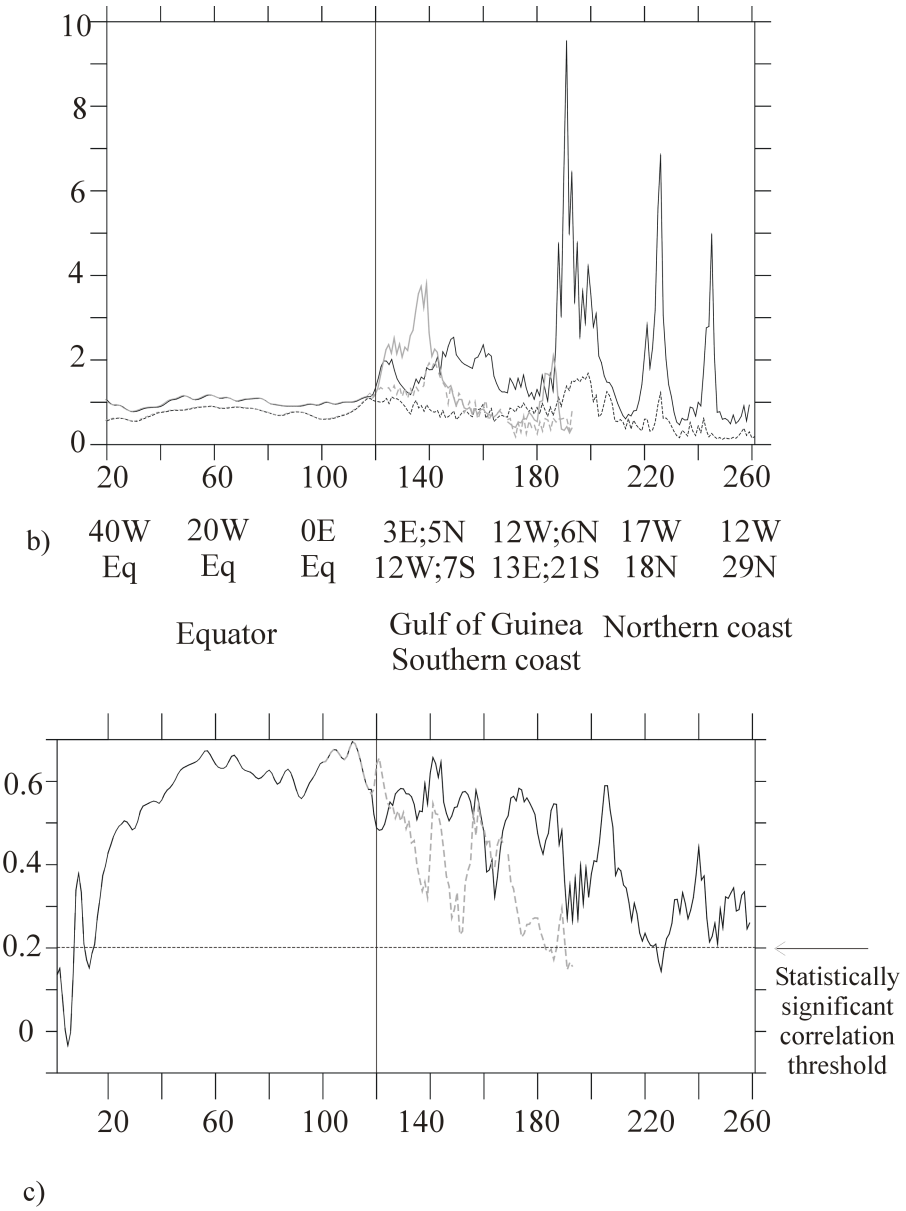

Figure 4: b) Variance of the intraseasonal SSH anomalies for the observations (solid line) and the model (dotted line) for the north track (black lines) and the south track (grey lines). **c)** Correlation between the observed and modelled intraseasonal SSH anomalies, for the north wave-track (black-solid line) and south wave-track (grey-dotted line).

At last, it is worth noting that the same Hovmuller diagram as figure 4a for the modelled z18 variable (not shown) displays similar characteristics in term of propagation, suggesting that the observed SSH is a very good proxy for the study of propagations in the real thermocline. This is in agreement with studies of the relationship between sea level and stratification in the tropics, which have suggested that a 1-2 cm rise in the sea level reflects a 2-4 m deepening of the thermocline (Carton et al., 1996).

5.1 Intraseasonal climatology: Main recurring propagation

To clarify the main propagation properties described before, and particularly bring to light the most regular intraseasonal signals, the 5-day climatological average of the band-pass filtered SSH for the period 1993-2000 has been computed for the observations and the simulation. This intraseasonal climatology (figure 5a) displays some events clearly related to wave propagations, along parts of the tracks. The equator shows more positive propagation during the downwelling season (September to February, figure 1a), and more negative and quite less propagating signals during the climatological upwelling season of the western basin (March to August). The most pronounced features in figure 5a appear in the boreal autumn-winter season, in particular September and December downwelling propagations. They are associated with November and January upwelling propagations, they seem to reach quite far poleward in both hemispheres, and are comparable in the model and the observations. The phase speed of these events range from 1.6 m/s (grey arrow) to 1.8 m/s (white and black arrows), the latter corresponds to the one estimated from the figure 4a. The SSH slope suggests that the phase speed slows slightly down from the equator to the African coast.

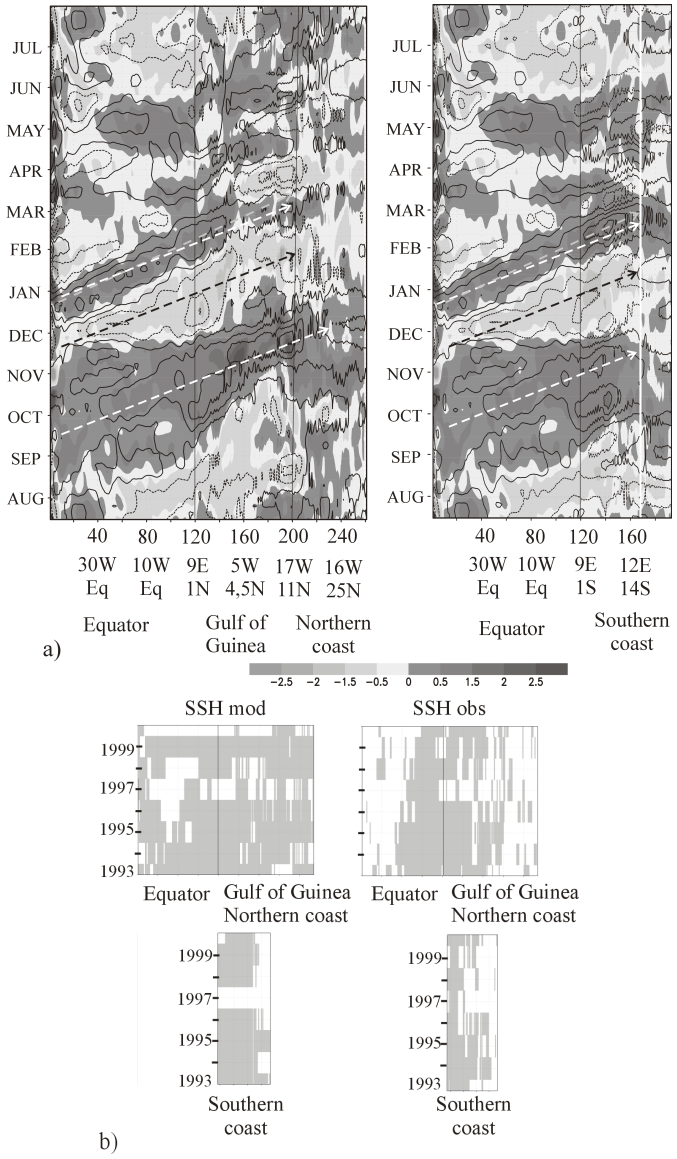

Figure 5. a) Climatology of the intraseasonal SSH anomalies (in cm) for the observations (shaded areas) and the model (contour lines, CI=0.5, the zero line has been removed), for the north wave-track (left panel) and the south wave-track (right panel). The arrows correspond to 1.8 m/s (white and black lines) and 1.6 m/s (grey line) propagation phase speeds. **b)** Significant areas are shaded from a significance t-test, at 99% confidence level, for the correlation between the sampled average of SSH (intraseasonal climatology from figure 4a) and the temporal series for each year and for each point along the north (top panel) and the south (bottom panel) wave-tracks, for the model (left panel) and the observations (right panel).

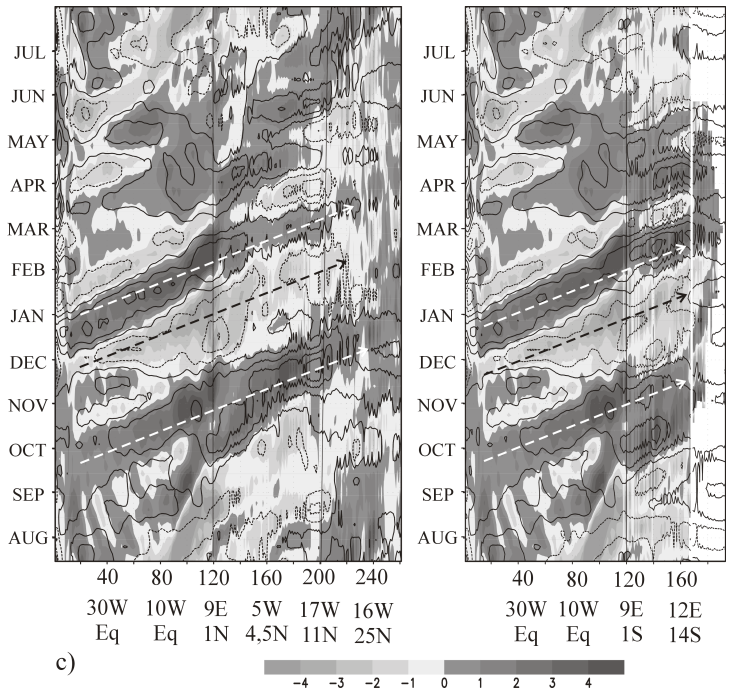

Figure 5: c) Climatology of the intraseasonal 18°C isotherm depth anomalies (shaded areas, in m), and modelled intraseasonal SSH anomalies (contour lines, CI=0.5 cm, the zero line has been removed), for the north wave-track (left panel) and the south wave-track (right panel). The arrows correspond to 1.8 m/s propagation phase speed.

Despite weaker amplitude compared to the non-averaged signals (figure 4a), the amplitude of this climatology still represents more than 20% of the seasonal cycle amplitude (from figure 1a). In order to represent the significance of this intraseasonal climatology for all the years considered here in observations and model, we have performed a significance parametric test under; on the one hand, the null hypothesis of "equal means" and on the other hand the null hypothesis of "independent fields". Each year has been compared to the sampled mean constructed without that particular year under 95% and 99% confidence levels. The mean is statistically significant, at 95% and 99% confidence level, for all the years for observations and model and for north and south wave-tracks (not shown). The correlation is statistically significant at 99% confidence level from a t-test, for most of the years along the track (figure 5b). The observed SSH intraseasonal climatology is significant over the central-eastern equatorial Atlantic for all the years, but it is not significant at the western equatorial Atlantic and subtropical regions (figure 5b right-panel). Regarding the model, the intraseasonal climatology is not significant for some particular years (1997, 1998 and 2000) over central equatorial Atlantic (figure 5b left-panel). The year 1997 does not seem to be significant mostly along both, north and south wave-tracks, and for observations and model. The most significant regions for both, observations and model are the central-eastern equatorial Atlantic, the GG and the southern coast from the equator up to 12°S.

In order to assess the thermocline vertical displacements associated with the SSH anomalies, the intraseasonal climatology of the 18°C isotherm depth is presented in figure 5c (the intraseasonal climatology of the modelled SSH is also superimposed). Whereas the consistency between the SSH and the z18 is high, the latter is often more continuous from the equator to the coast, and further north and south than the former (see the December downwelling wave that reaches the most northern point at approximately constant speed). Note that the SSH and z18 are more in agreement over the equatorial band than poleward of 10° latitude where the SSH-z18 relation is more complex, likely due to larger compensation effects by additional thermodynamical processes such as surface heat fluxes (Mayer et al., 2001).

From z18 intraseasonal climatology (figure 5c), the August-September downwelling Kelvin event can be seen as a particular wave starting at the African coast, rather than propagation from the western equator. At this event there is a different behaviour of the SSH and z18; the z18 splits between the equator and the GG and it is interpreted as split of modes, which is coherent with Illig et al's results (2004). Once trapped at the coast, SSH and z18 September and December donwelling signals appear to be amplified in the coast of the GG (140-200 north track-points) and in the southern coast (120-160 south

track-points). This amplification was also noticeable over the whole 93-00 period for the T/P SSH and its variance (figure 4a left panel, and figure 4b). The propagation pattern disappears further 215 north and 170 south track-points, and beyond these points (near subtropics) the signal seems to be stationary (figure 4a, figure 5a and figure 5c).

To isolate and quantify the spatial-temporal structure of the robust September to February Kelvin waves, we present in the next section an Extended Principal Component Analysis.

5.2 A mode for boreal autumn-winter intraseasonal Kelvin waves

A canonical mode of the boreal autumn-winter Kelvin waves can be established thanks to a discriminant analysis technique known as Extended Empirical Orthogonal Functions (EEOF), which constitutes an extension of the traditional EOF technique. It deals not only with spatial but also with temporal correlations observed in weather/climate data (Weare and Nasstrom, 1982), and it is suitable to study oscillatory phenomenon (Fraedrich et al., 1997). We consider positive and negative lagged timeseries for each track-point, and we apply an EOF analysis of this pool of time series. The EEOF analysis recognizes that the temporal evolution of the spatial patterns is an integral part of a system's development. Consider a track–time section (Hovmuller), which can be described by a vector of K components ordered according to the track and evolving with time. Sliding a time window of length W over this vector time series leads to a new vector, this vector represents the states of the system in a $K \times W$ dimensional phase space spanned by time-delay coordinates.

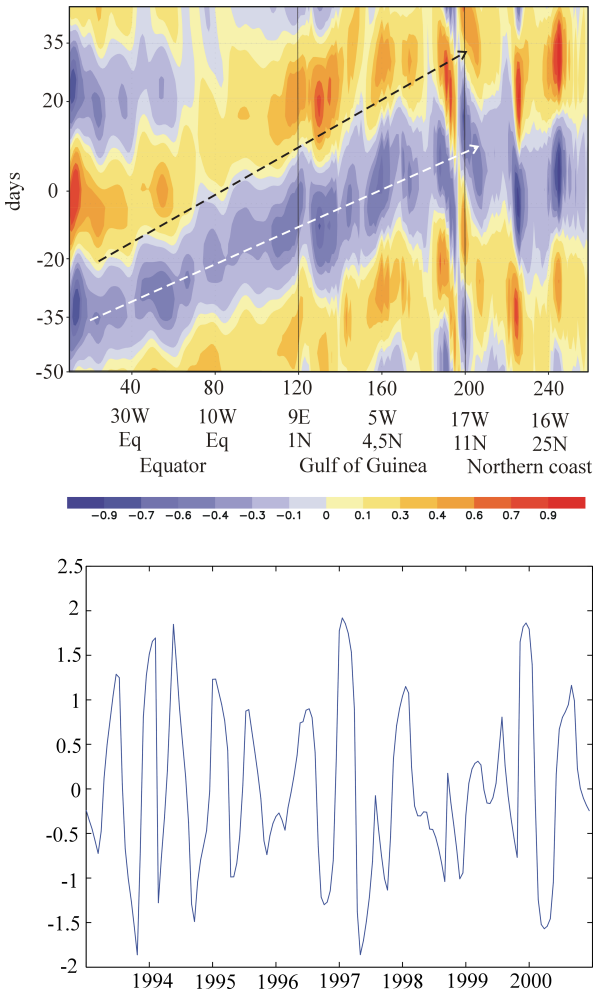

Figure 6: Leading Extended Empirical Orthogonal Function mode of the observed intraseasonal SSH along the north wave-track (top panel, in cm), and the associated Extended Principal Component for the period 1993-2001 (bottom panel) in boreal autumn-winter (September to February). The EEOF has been performed after interpolate the T/P SSH to 5-day temporal outputs and obtaining 21 lags. The white (black) arrow corresponds to 2.5 m/s (2 m/s) propagation phase speed.

As it has been seen previously, the autumn-winter is a particularly active season for the Kelvin waves, therefore the EEOF analysis is performed for the boreal autumn-winter season (from September to February) for all the years from 1993 to 2000. The EEOF analyses are performed on time wave-track series of observed filtered SSH, and applying a window of 5 days to the data obtaining 21 lags, and thus calculating the EOFs of the time development of the Kelvin wave-track structure. From the analysis, a resultant total Extended Principal Component (EPC) index is computed, which is projected onto the original field to represent the EEOF spatial pattern. For simplicity only the north wave-track is analyzed, since both, north and south wave-tracks share the equatorial Atlantic and the leading mode of the south wave-track (not shown) is highly correlated with the leading mode of the north wave-track.

The leading EEOF variability mode of boreal autumn-winter filtered T/P SSH, which explains 10% of the variance of the filtered signal, is shown in figure 6. It shows the upwelling-downwelling Kelvin waves along the equator and the coast of the GG (figure 6-top panel). The SSH anomalies propagate from the western equator to 15°N approximately (220 track-point) at a rather stable speed ranging from 2 m/s to 2.5 m/s, a higher phase speed than the one estimated from the previous Hovmuller plots. Further north, in the subtropical coastal region other processes seem to explain the SSH variability, as previously discussed. The leading EPC (figure 6-bottom panel) shows one cycle per autumn-winter of positive and negative SSH over the wave-track. The remarkable interannual modulation of the EPC index is in agreement with those noticed previously in figure 4a. Although special years of variability are found for the 1996-1998 period, the main periodicity of the wave from the EEOF analysis is around 50 days. The second mode (not shown) corresponds to Kelvin wave propagation along the western-central equatorial Atlantic (in quadrature-like with the leading mode) but without continuity along the coastal wave-track.

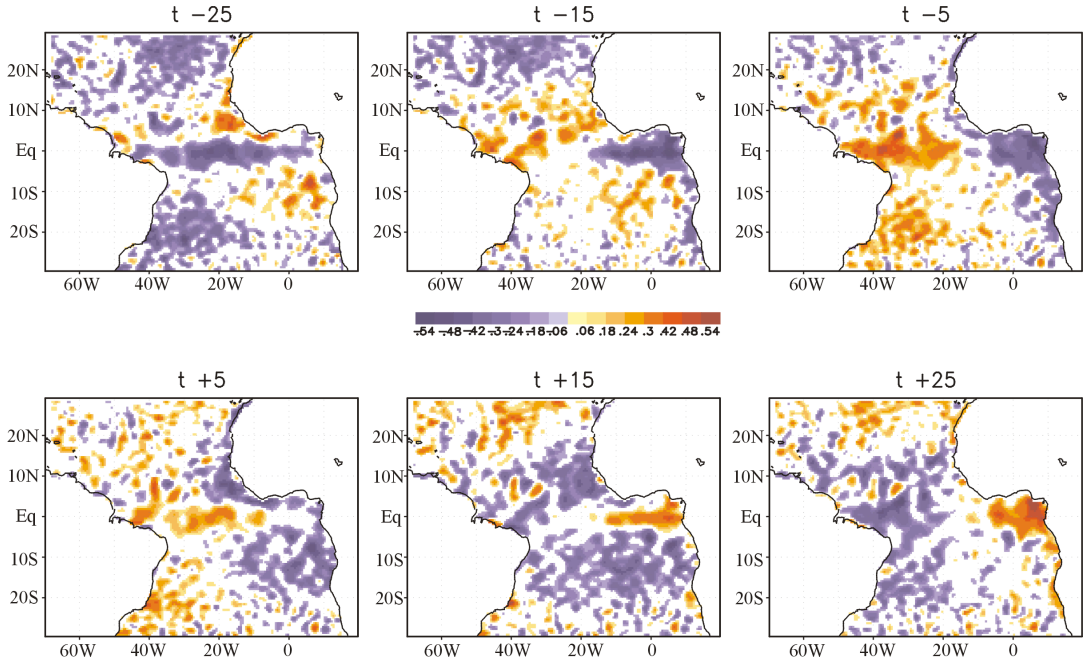

Figure 7: Regression of the observed intraseasonal SSH anomalies over the whole Tropical Atlantic on the leading EEOF mode from figure 6 at different lags (shaded areas, CI=0.1 cm), only statistically significant areas at 95% confidence limit are plotted.

In order to visualize the spatial structure of the leading EEOF mode, the observed SSH over the whole TA basin has been regressed onto the EPC and it is shown in figure 7. The projection has been done for different lags (lagging the SSH field from –25 days to +25 days) to show the time evolution over the whole TA as the wave is propagating. The projection shows very clear spatial structure for the beginning of the downwelling (upwelling) equatorial Kelvin wave at the western equator at lag -15 (lag +15). The Kelvin wave propagates equatorially trapped at lag +5 (lag -25) reaching the African coast at lag +25 (lag -5). At the Guinean Dome and 5°S, it is visible a Rossby wave-like radiation propagating westward al lag -15 (lag +15). Finally, the coastally trapped Kelvin wave propagates as far as ~15 degrees of latitude at lag -25 (lag +5).

The EEOF analysis has discriminated a very robust propagating pattern associated with equatorial and coastally trapped Kelvin wave. We have evidenced the importance of the intraseasonal propagating signals, and particularly in boreal autumn-winter, with different methodologies. The fact that Kelvin wave appears as a mode achieves the importance of the waves in the context of the TA variability. The EEOF information will be used in the second part of the paper to study the associated air-sea interactions.

6 Finer estimates of propagation phase speed and teleconnections

Once the intraseasonal climatology and the leading boreal autumn-winter mode are underlined, it is worth coming back to the intraseasonal timeseries through a lead-lag correlation analysis. It allows for both, a finer quantification of the phase speed and the teleconnections sustained by the waves.

6.1 Propagation phase speed

The speed of oceanic wave propagation is important in determining the oceanic response time to disturbances from the equilibrium state. A thorough estimate offers also a sound way to evidence the wave nature of the apparent propagations in the band-pass filtered data. The equatorial Kelvin wave has a phase speed defined by the linear theory as:

$$c_n = \left(g h_n \right)^{1/2}$$

where h_n is the equivalent depth for each n mode. The Atlantic equatorial Kelvin wave propagations have been shown in observational data and linear theory to have a phase speed range 2.4-2.9 m/s phase speed for the first baroclinic mode, 1.2-1.5 m/s for the second mode and 0.8-1 m/s for the third mode (du Penhoat and Treguier, 1985; Philander, 1990; Katz, 1997; França et al, 2003; Illig et al., 2004; Guiavarc'h et al., 2008).

Figure 8 shows the one point lag correlation for the intraseasonal climatology shown in figure 5, at 99% confidence level, for the modelled (top panel) and the observed (bottom panel) SSH and z18 variables. We have chosen four different points along the north (figure 8a) and south (figure 8b) wave-track corresponding to different regions; eastern equator, GG, southern African coast, and subtropical regions. The lag correlation for the z18 is also shown in contours, giving a similar phase speed than the one from the SSH. At the subtropics (i.e. the 220-260 north track-points and the 160-190 south track-points), the slope tends towards zero as the SSH signal shows nearly horizontal structure poleward of ~12 degrees latitude for both model and observations (as shown in figures 4a, 5a and 6).

The phase speed can be easily computed by linear regression of the maximum correlations at each point and lag in figure 8. The different linear fittings corresponding to 2.5, 1.8 and 1.5 m/s are included in figure 8. The visual comparison with the arrows indicate that the observed climatological Kelvin wave phase speed is ranging from 1.5 to 2 m/s. Due to the large dispersion of the data in the lag correlation plots, we have also computed the phase speed with Radon Transform (RT) methodology, which is a more accurate technique. The RT is very useful image processing technique for the satellite images, and it has been used before to characterize the phase speed of the oceanic Rossby waves (Chelton and Schlax, 1996; Polito and Cornillion, 1997; Hill et al., 2000; Challenor et al., 2001). To compute the RT of the track-time plot (hovmuller) for different values of direction is equivalent to compute the energy in the spectrum along lines of constant speed, and it is the most straightforward method to find the value of the speed for which that energy is maximum (Challenor et al., 2001). The corresponding angle of the maximum RT standard deviation is defined as the angle of the propagation. The methodology has been applied following the Hill et al.'s work (2000), for the observed and modelled SSH hovmuller, for the north and the south wave-track in the entire 1993-2000 period (table 1). The phase speed calculated by RT, in average, does not change significantly the phase speed calculated by linear regression of the maximum lag correlation. The propagation phase speed ranges from 1.5 to 2.1 m/s, which is also found by other authors (Katz, 1997; França et al., 2003), and it could corresponds to a mix between the first and the second theoretical Kelvin baroclinic modes, or a modulation of the first baroclinic Kelvin wave mode speed by the first baroclinic Rossby wave mode. In addition, topography effects, stratification changes and the beers of modes can intricately be disturbing the measurements. It is important to notice that performing the RT for each point results in important variations along the tracks (not shown), especially from the equator to the coast, which can be also observed from figures 4a, 5a and 8. The differences

between the observed and the theoretical phase speed, as well as the speed variations along the wave-track will need further investigations.

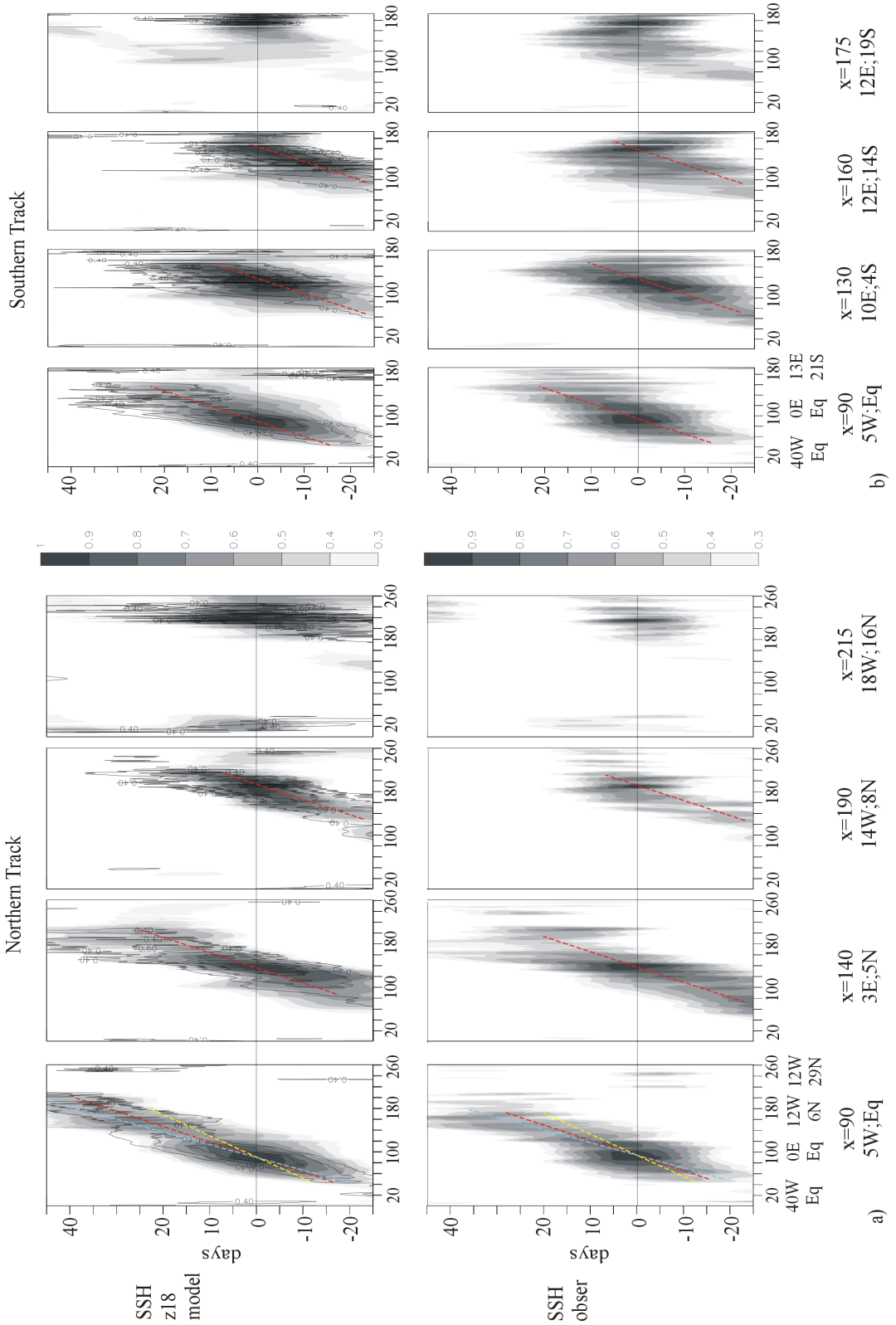

Figure 8. a) One point observed SSH (shaded) and modelled z18 (contour lines) intraseasonal climatology lag correlation map for several track-points for the north, and for the model (upper panel) and the observations (bottom panel). Correlation significant at the 99% confidence limit is plotted. The yellow, red and blue lines correspond to 2.5 m/s, 1.8 m/s and 1.5 m/s propagation phase speeds respectively. **b)** As figure a) but for the south African coast wave-track.

between the observed and the theoretical phase speed, as well as the speed variations along the wave-track will need further investigations.

Nevertheless, the velocities found for both, north and south wave-tracks, for the modelled and the observed SSH and with different methods show a satisfactory agreement of the model with the satellite estimates (table 1). This means that, even with a low resolution, the model is suitable to study oceanic Kelvin wave propagations, at least equatorward of about 12 degrees of latitude. Overall, the amplitude (figure 4b, and 5a) and the phase speed (figure 8), are both important wave factors and are well reproduced by the OGCM simulation. This result will be important in order to diagnose the forcing mechanisms in the second part of this study.

From the calculated phase speed, we can conclude that the Kelvin wave propagation seen in figures 4, 5 and 6, is expressing mainly the first two baroclinic Kelvin wave modes along the equator and the African coast.

Hovmuller SSH Field	Phase speed (m/s) from linear fitting	Phase speed (m/s) from RT
Model North	1.6	1.60
Observ North	1.5	1.86
Model South	1.8	1.86
Observ South	1.9	2.10

Table 1: Phase speed calculated by linear best-fitting and Radon Transform of the observed and modelled SSH of the north and south wave-tracks. The linear best-fitting has been computed and averaged from figure 8. The RT has been computed for each hovmuller for the observed (from figure 4) and modelled SSH, smoothing with at hanning window avoiding the signals around the frame. The RT of the images has been performed for the angle between -90 to 90 degrees every 0.05 degrees.

6.2 How far Kelvin wave travels? Evidence for teleconnections

Figure 8 can also be used to quantify how SSH intraseasonal variability along the coast and as far as about 12 degrees (around 200 north track-point and 150 south track-point) is remotely controlled by the wave propagating signal.

In these plots, we consider that the teleconnection breaks down where the apparent slope changes drastically, in particular where it becomes more horizontal. Although, as further away from each point smaller is the lag correlation with the point, and the propagation direction is difficult to discern due to the large physical processes implied, it can be seen equatorial connection driving SSH anomalies along the coastal track. Hence, starting with the northern coastline, the correlation centered at 5°W-0°N (90 track-point) shows continuity from the equator to the coast, although there is a change in the slope at the coast of the GG as noted previously (~120 track-point, transition between the equatorial and coastal wave-guide), and the slope break latitude is reached at about 10N (195 track-point) with a correlation of about 0.4. It suggests that this equatorial point still remotely controls 16% of the intraseasonal variance at ~10°N. The correlations centred at 3°E over the GG (140 north track-point) indicate, as expected, a clear control from the eastern equator, as well as a significant impact in the propagation direction up to ~16°W; 10°N (195 north track-point) in the observations, and further poleward in the model. At these latitudes, the explained variance drops down to about 10-20%. In the third panel, centered at 14°W-8°N (190 track-point) the correlations for the observations show that the point is partly controlled by locations behind, but no signal seems to propagate further north. Beyond 12°N (figure 8a, 215 track-point), the SSH is more related to neighbouring points at lag zero, suggesting other type of coherent local forcing.

For the south (figure 8b), the correlation shows even more continuity between the equator and the coast than for the north, probably due to the more straight coastline. The correlation slope appears to break in the vicinity of 12°S (150 track-point). Beyond this point the correlation is significant but the slope is not coherent with a teleconnection via Kelvin wave propagations and suggests a control by other processes. The lack of propagation beyond 12°S is seen clearer for z18 (figure 8b-top 175 track-point), while the observed SSH (figure 8b-bottom 175 track-point) shows more correlation with the equatorial points.

In conclusion, the T/P SSH support the importance of teleconnection through Kelvin waves along the tropical African coast, from the equator up to 12°S and 10°N (12°N in the model). These latitudinal teleconnection thresholds could be due, in part, to the limits of the data resolution relative to the Rossby radius of deformation (close to 15 degrees of latitude). They are likely as well associated with

the location of the intense coastal Mauritanian/Senegal and Angola/Benguela upwelling systems. Roughly, it is in the vicinity of 10 degrees of latitude, depending on the season, where the isopycnal surfaces start to outcrop in these upwelling regions. Hence, the signals carried out by the waves are partly transferred into the mixed layer, and correspondingly limit the ability of the waves to propagate information.

In practice, because the dissipative effects, there should be a limit to the distance to which the information is carried poleward by waves (Gill, 1982; Clarke and Shi, 1991). The lack of correlation at higher latitudes could be because of a great deal of energy is also found in smaller-scale motions; these may be eddies, wave motions due to small-scale features by bottom topography or loss of energy by Rossby waves radiation from the African coast (Mittelstaedt, 1991). At last, the orientation relative to the coast, the regularity and intensity of the trade winds exhibit major changes between the deep tropics, equatorward of 10°N, and the tropical-subtropical regions. We will show in the second part of this study that, the SSH variability poleward of 12 degrees of latitude is essentially controlled by local wind to the expense of teleconnection processes.

7 Conclusions

This paper is an attempt to provide new and sound insights into TA intraseasonal Kelvin wave activity. This topic has been little considered in comparison with the Pacific basin (Kessler et al., 1995; Cravatte et al., 2003; Roundy and Kiladis, 2006). It is essential to investigate it thoroughly, in light of the recent Aviso T/P dataset and state of the art OGCM, considering how often is remote forcing by Kelvin waves invoked to interpret TA variability, particularly in the vicinity of the Angola/Benguela upwelling system (Florenchie et al., 2003; Rouault et al., 2007), as well as in the coast of the GG (Servain et al., 1982; Picaut, 1983; Aman et al., 2007).

In order to study the SSH intraseasonal variability, we have band-pass filtered the data in the 25-95 day period, emphasizing the relative active 50 day period. This processing, frequently used along the equator, enlightens here the propagation of Kelvin wave signals polewards along the African coast. In the present part of this study, we demonstrate the possibility of visualizing equator to coast propagations of observed and modelled SSH and thermocline intraseasonal anomalies over several years in the TA. The TOPEX/Poseidon and 0.5° resolution OGCM simulation datasets have proved to be suitable for the identification and characterization of equatorial Kelvin waves and their continuity within the tropical band as coastally trapped Kelvin waves at intraseasonal frequencies. Such signals can clearly be followed over distance of thousands of kilometres along the coasts, especially equatorward of 10 to 15 degrees of latitude. However, the filter reduces the variance of the total signal by about a factor of two, down to one centimetre at the equator and two along the coast.

The estimated propagation phase speeds are found to be in the range between the first and second theoretical Kelvin baroclinic modes (from 1.4 m/s to 2.6 m/s). The results are homogenous for the observed and modelled SSH, for the northern and the southern wave-tracks, and from the different methodologies (RT and linear regression). Nevertheless, a finer understanding of the phase speeds and the thermocline response would require a modal analysis along the coast.

In addition, lag correlation plots allowed for the quantification of the remote effects of the waves along the coast. It is possible to state that the eastern equator SSH can explain about 25% of the intraseasonal variability of the GG so-called coastal upwelling and 16% of the intraseasonal variability of the Benguela upwelling. Although the SSH variability over the Mauritanian/Senegal upwelling region is less influenced by the wave propagations, the results support the existence of a remote forcing via eastward and poleward intraseasonal Kelvin waves of the lowest latitudes of the north and south eastern tropical upwellings.

The major result of our study is the demonstration that it is possible and useful to simplify the complex intraseasonal activity down to two synthetic signals; an intraseasonal climatology and an Extended EOF mode. From the intraseasonal climatology, a particularly striking result is that major Kelvin wave activity occurs with a high degree of recurrence in boreal autumn-winter season (September-December downwelling and November-January upwelling Kelvin waves). The model simulation helped to quantify the associated stratification changes, which are very well correlated and reach a few meters for a few centimers surface signals. The most robust continuity develops in early boreal winter from the west equator eastward and poleward towards the Benguela upwelling system and the coast of the GG in late boreal winter, in observed and modelled SSH (figure 5a) as well as within the thermocline (figure 5c).The connecting signals propagation velocity, ~1.8 m/s, supports the existence of some remote forcing via Kelvin waves.

The extended EOF mode for this boreal autumn-winter Kelvin wave propagation is the second synthetic view of this phenomenon. The mode, albeit of weak amplitude, provides an associated spatial structure that proves well the Kelvin wave nature of these teleconnections. The fact that Kelvin wave appears as a mode achieves the importance of the waves in the context of the TA SSH variability. Its principal component timeseries can be used to identify interannual modulations, as well as construct through regression associated signals in pertinent variables, such as the wind stress and SST, which will be presented in the second part of the study.

In order to develop a detailed description of SSH propagations and coastal teleconnections in this paper, we have left aside the analysis of the complementary process controlling the SSH: the local atmospheric forcing. In the second part of this study, we will focus on the causes for the equatorial Kelvin wave triggering at the western equatorial Atlantic, its relationship with the atmosphere, the possible impacts on the SST and the particular behaviour in the subtropics.

Acknowledgements: We would like to thank to the editor Raghu Murtugudde and anonymous reviewers for their helpful comments on the manuscript. We are grateful to Christian Ethe and Gurvan Madec for kindly providing the model run outputs, and Gildas Mainsant for his help in the analysis. We also thank Serge Janicot, Vincent Echevin and Frédéric Vivier for stimulating discussions. This study has been supported by ANETUS (CNES/NASA) and the Spanish MCYT CGL2006-04471 and REN2002-03424 programs, which has also funded Irene Polo and her research stage at LOCEAN laboratory as part as her phD thesis.

References

Adamec, D., and J. J. O'Brien (1978), The Seasonal Upwelling in the Gulf of Guinea Due to Remote Forcing, *J. Physical Oceanog.*, **8**, 1050-1060.

Aman, A., L. Testut, P. Woodworth, T. Aarup, and D. Dixon (2007), Sesonal Sea Level Variability in the Gulf of Guinea from altimetry and tide gauge. Submitted.

Arnault, S., Y. Menard, and J. Merle (1990), Observing the tropical Atlantic Ocean in 1986--1987 from altimetry, *J. Geophys. Res.,* **95** (C10), doi: 10.1029/90JC00347.

Arnault, S., L. Gourdeau, and Y. Menard (1992), Comparison of the altimetric signal with in-situ measurements in the tropical Atlantic ocean, *Deep Sea Res*., **39** (3/4), 481-499, 1992.

Arnault, S., and R. E. Cheney (1994), Tropical Atlantic sea-level variability from Geosat (1985-1989), *J. Geophys. Res.,* **99**, 18207-18223.

Arnault, S., and C. Le Provost (1997), Regional identification in the tropical Atlantic Ocean of residual tide errors from an empirical orthogonal function analysis of TOPEX/POSEIDON altimetric data, *J. Geophys. Res.*, **102**, 21022-21036.

Berliand, M. E., and T. G. Strokina (1980), Global distribution of the total amount of clouds, *Hydrometeorological Publishing House*, Leningrad,Russia, 71 pp.

Carton, J. A., X. H. Cao, B. S. Giese, and A. M. daSilva (1996), Decadal and interannual SST variability in the tropical Atlantic Ocean, *J. Phys. Oceanogr.,* **26**, 1165-1175.

Challenor, P.G., P. Cipollini, and D. Cromwell (2001), Use of the 3D radon transform to examine the properties of oceanic Rossby waves, *J. Atmos. Oceanic Technol.,* **18**, 9*,* 1558-1566.

Chelton, D. B., and M. G. Schlax (1996), Global observations of oceanic Rossby waves, *Science*, *272*, 234-238.

Clarke, A. J. (1978) , On the generation of the seasonal coastal upwelling in the Gulf of Guinea, *J. Geophys. Res.,* **84**, 3743-3751.

Clarke, A. J. (1983), The Reflection of Equatorial Waves from Oceanic Boundaries, *J. Phys. Oceanogr.,* **13**, 1193-1207.

Clarke, A. J., and C. Shi (1991), Critical frequencies at ocean boundaries, *J. Geophys. Res., 96*, 10 731–10 738.

Cravatte S., J. Picaut and G. Eldin (2003), Second and first Kelvin modes in the equatorial Pacific at intraseasonal timescales, *J. Geophys. Res*., **108**, doi:10.1029/2002JC001511.2003.

de Boyer-Montégut, C., J. Vialard, S. S. C. Shenoi, D. Shankar, F. Durand, C. Ethé, and G. Madec (2007), Simulated seasonal and interannual variability of mixed layer heat budget in the northern Indian Ocean, *J. Climate*, **20**, 3249-3268

du Penhoat, Y., and A.-M. Treguier (1985), The seasonal linear response of the Atlantic Ocean, *J. Phys. Oceanogr*., **15**, 316-329.

Florenchie, P., J. R. E. Lutjeharms, C. J. C. Reason, S. Masson, and M. Rouault (2003), The source of Benguela Niños in the South Atlantic Ocean, *Geophys. Res. Lett*., **30**, 10, 1505.

França, C., I. Wainer, A. R. De Mesquita, and G. J. Goni (2003), Planetary equatorial trapped waves in the Atlantic Ocean from TOPEX/Poseidon altimetry, *in*: Goni, G.J.; Malanotte-Rizzoli, P. (Ed.) (2003). *Interhemispheric water exchange in the Atlantic Ocean. Elsevier Oceanography Series,* **68***,* 213-232.

Fraedrich, K., J. L. McBride, W. M. Frank, and R. Wang (1997), Extended EOF Analysis of Tropical Disturbances: TOGA COARE, *J. Atmos. Sci*, **54**, 19, 2363–2372.

Gill, A. E. (1982), *Atmosphere-Ocean Dynamics*, Academic Press. 662 pp. ISBN 0122835220.

Greatbatch, R. J. and K. A. Peterson (1996), Interdecadal variability and oceanic thermohaline adjustment, *J. Geophys. Res.,* **101**, 20467–20482.

Grodsky, S.A., and J.A. Carton (2006), Influence of the tropics on the climate of the South Atlantic, *Geophys. Res. Letts.*, Art. No. L06719.

Guiavarc'h, C., A. M. Treguier, A. Vangriesheim (2008), Remotely forced biweekly deep oscillations on the continental slope of the Gulf of Guinea, *J. Geosphys. Res*., in press.

Han, W., P.J. Webster, J. Lin, W.T. Liu, R. Fu, D. Yuan, and A. Hu (2008), Dynamics of intraseasonal sea level and thermocline variability in the equatorial Atlantic during 2002-2003*, J. Phys. Oceanogr.*, in press

Handoh, I. C. and G. R. Bigg (2000), A self-sustaining climate mode in the Tropical Atlantic, 1995-97: Observations and modelling, *Q JR. Meteo. Soc.,* **126**, 807-821.

Hendon, H. H., B. Liebmann, and J. D. Glick (1998), Oceanic Kelvin Waves and the Madden-Julian Oscillation, *J. Atmos. Sci.,* **55**, 88-101.

Hill, K. L., I. S. Robinson, and P. Cipollini (2000), Propagation characteristics of extratropical planetary waves observed in the ATSR global sea surface temperature record, *J. Geophys. Res.,* **105**(C9), 21927-21945.

Hormazabal, S., G. Shaffer and O. Pizarro (2002), Tropical Pacific control of intraseasonal oscillations off Chile by way of oceanic and atmospheric pathways, *Geophys. Res. Lett*., **29**, doi: 10.1029/2001GL013481.

Illig S., D. Gushchina, B. Dewitte, N. Ayoub, and Y. du Penhoat (2006), The 1996 equatorial Atlantic warm event: Origin and mechanisms, *Geophys. Res. Lett*., **33**, doi: 10.1029/2005GL025632.

Illig S., B. Dewitte, N. Ayoub, Y. du Penhoat, G. Reverdin, P. De Mey, F. Bonjean, and G. S. Lagerloef (2004), Interannual long equatorial waves in the tropical Atlantic form a high resolution ocean general circulation model experiment in 1981-2000, *J. Geophys. Res*., **109**, C02022, doi. 101029/2003JC001771.

Jacobs, G.A., H. E. Hurlburt, J. C. Kindle, E. J. Metzger, J. L. Mitchell, W. J. Teague, and A. J. Wallcraft (1994), Decade-scale trans-Pacific propagation and warming effects of an El Niño anomaly, *Nature,* **370**, 360-363.

Kalnay, E. and co-authors (1996): The NCEP/NCAR 40-year Reanalysis Project. *Bull Amer. Meteor. Soc*., **77**, 437-471.

Katz, E.J. (1997), Waves along the equator in the Atlantic, *J. Phys. Oceanogr.*, *27*, 2536–2544.

Kessler, WS, MJ McPhaden, and KM Weickmann (1995), Forcing of intraseasonal Kelvin waves in the equatorial Pacific, *J. Geophys. Res.,* **100**, 10613-10631.

Levitus, S. (1998), Climatological Atlas of the world ocean. *Tech. Rep.* **13**, NOAA, Rockville, Md.

Madec, G., P. Delecluse, M. Imbard, and C. Lévy (1998), OPA 8.1 Ocean General Circulation Model reference manual. *Note du Pôle de modélisation*, Institut Pierre-Simon Laplace, N°11, 91 pp.

Matsuno, T. (1966), Quasi-geostrophic motions in the equatorial area, *J. Met. Soc. Japan*, **44**, 25–43.

Mayer, D. A., R. L. Molinari, M. O. Baringer, and G. J. Goni (2001), Transition regions and their role in the relationship between sea surface height and subsurface temperature structure in the Atlantic Ocean, *Geophys. Res. Lett.,* **28**, 3943–3946.

Meyers, S. D., A. Melsom, G. T. Mitchum and J. O'Brien (1998), Detection of the fast Kelvin Wave teleconnection due to El Nino-Southern Oscillation, *J. Geophys. Res.,* **103**, 27655-27663.

Mittelstaedt, E. (1991), The ocean boundary along the northwest African coast: Circulation and oceanographic properties at the sea surface, *Progress in Oceanography*, **26**, 307-355.

Moore, D. W. 1968: Planetary-gravity waves in an equatorial ocean. Ph. D. thesis, Harvard University, Cambridge, Mass.

Moore, D. W., P. Hisard, J.P. McCreary, J. Merle, J. J. O'Brien, J. Picaut, J. Verstraete, and C. Wunsch (1978), Equatorial adjustment in the eastern Atlantic, *Geophys. Res. Lett*., **5**, 637-640.

O'Brien, J. J., D. Adamec, and D. W. Moore (1978), A simple model of upwelling in the Gulf of Guinea, *Geophys. Res. Lett.,* **5**, 8, 641-644.

Philander, S. G. H. (1990), El Niño, La Niña, and the Southern Oscillation*.* International Geophysics Series, Vol. **46**, Academic Press, 293 pp.

Picaut, J. (1983), Propagation of the seasonal upwelling in the eastern equatorial Atlantic, *J. Phys. Oceanogr.,* **13**, 18-37.

Polito, P. S., and P. Cornillon (1997), Long baroclinic Rossby waves detected by TOPEX/POSEIDON, *J. Geophys. Res.*, **102**, 3215-3235.

Rebert, J., J. Donguy, G. Eldin, and K. Wyrtki (1985), Relations between sea level, thermocline depth, heat content, and dynamic height in the tropical Pacific Ocean, *J. Geophys. Res.*, **90**, 11719–11725.

Rodriguez-Fonseca, B., I. Polo, E. Serrano, and M. Castro (2006), Evaluation of the north Atlantic SST forcing on the European and northern African winter climate, *Int. J. Climatology*., **25**, doi: 10.1002/7joc.1234.

Rouault, M., S. Illig, C. Bartholomae, C. J. C. Reason, and A. Bentamy (2007), Propagation and origin of warm anomalies in the Angola Benguela upwelling system in 2001, *J. Mar. Sys.,* doi: 10.1016/j.jmarsys.2006.11.010.

Roundy, P. E., and G. N. Kiladis (2006), Observed Relationships between Oceanic Kelvin Waves and Atmospheric Forcing, *J. Climate,* **19**, 5253-5271.

Saravanan, R., and P. Chang (2000), Interaction between tropical Atlantic variability and El Niño–Southern Oscillation, *J. Climate,* **13**, 2177–2194.

Servain, J., J. Picaut, and J. Merle (1982), Evidence of Remote Forcing in the Equatorial Atlantic Ocean, *J. Phys. Oceanogr.,***12**, 457-463.

Schouten, M. W., R. P. Matano, and T. P. Strub (2005), A description of the seasonal cycle of the equatorial Atlantic from altimeter data, *Deep Sea Res*., **52**, 477-493.

Stammer, D. (1997), Global Characteristics of Ocean Variability Estimated from Regional TOPEX/POSEIDON Altimeter Measurements, *J. Phys. Oceanogr.,* **27***,* 1743-1769.

Sutton, R. T., S. P. Jewson, and D. P. Rowell (2000), The elements of climate variability in the tropical Atlantic region, *J. Climate,* **13***,* 3261–3284.

Trenberth, K. E., J. G. Olson, and W. G. Large (1989), A global ocean wind stress climatology based on the ECMWF analyses. National Center for Atmospheric Research, NCAR/TN-338+STR, Boulder, Colorado, 93 pp.

UNESCO (Ed.) (1996), Discharge of selected rivers of the world. Volume II (Part II), UNESCO Publishing.

Vega, A., Y. Du-Penhoat, B. Dewitte, and O. Pizarro (2003), Equatorial forcing of interannual Rossby waves in the eastern South Pacific, *Geophys. Res. Lett*., **30**, 5, 1197.

Weare, B. C., and J. S. Nasstrom (1982), Examples of extended empirical orthogonal function analysis, *Mon. Weath. Rev.,* **110**, 481-485.

Wilson, C., and D. Adamec (2002), A global view of bio-physical coupling from SeaWiFS and TOPEX satellite data, 1997–2001, *Geophys. Res. Lett*., **29**, 8. 10.1029/2001GL014063.

Xie, P., and P. A. Arkin (1996), Analysis of global monthly precipitation using gauge observations, satellite estimates and numerical model predictions, *Climate,* **9**, 840-858.

Oceanic Kelvin Waves and Tropical Atlantic intraseasonal Variability.

Part II: Mechanisms and Impacts

IRENE POLO
Departamento de Geofísica y Meteorología, UCM, Madrid, Spain.

ALBAN LAZAR
LOCEAN - IPSL / Univ. Paris VI. 4 pl. jussieu, 75252 Paris cedex 05, France

BELEN RODRIGUEZ-FONSECA
Departamento de Geofísica y Meteorología, UCM, Madrid, Spain.

(*Journal of Geophysical Research*)

ABSTRACT

Oceanic intraseasonal Kelvin waves over the Tropical Atlantic (TA) were defined and characterized in part I of this work. The present paper addresses the Kelvin wave interaction within the TA intraseasonal variability. This includes the causes which trigger the equatorial Kelvin wave, the different behaviour of the SSH signals along the wave-track, and the wave propagation impacts on the SST along the West African coast. In order to understand the Kelvin wave sources, SSH and wind stress covariability over the TA is investigated, as well as the possible Rossby-Kelvin reflection mechanism. On the one hand, though the wind stress variability reveals an SSH/z18 forcing at the central-east equator and subtropical areas, it does not seem to trigger the Kelvin wave locally at the western equatorial Atlantic. On the other hand, although the Rossby-Kelvin wave interaction analysis shows oceanic Rossby waves radiation from Guinea Dome and 4ºS in boreal spring-summer and propagation westward, the wave reflection at the Western boundary is very difficult to identify in boreal autumn-winter. In this season, in a two month period, it shows TA basin-scale atmospheric oscillation that suggests Ekman pumping ITCZ shift-induced anomalies over the western off-equatorial Atlantic can be responsible for SSH/z18 anomalies over the 2-6ºN band, which can trigger the equatorial Kelvin waves. The Kelvin wave impacts on SST, via mean SST gradient advection by anomalous geostrophic current, have been evidenced at some parts of the coast of the Gulf of Guinea and at the northern African coast from 10ºN to 25ºN.

1 Introduction

Intraseasonal Kelvin wave activity in the Tropical Atlantic (TA) from observational and model data has been described in part I (Polo et al., 2008). It has been found that the boreal autumn-winter is the most active season for the oceanic intraseasonal Kelvin wave. Kelvin waves start at the western equatorial Atlantic and propagate along the equator. At the eastern equator, they split and propagate coastally trapped along the West African coast as far as 12 degrees latitude, beyond this latitude the Sea Surface Height (SSH) signal is a result of other processes. The purpose of this second part is to address the mechanism for the Kelvin wave source and to analyse the behaviour of the SSH along the West African coast in relation to the oceanic wave activity and its impacts.

Regarding the mechanism for triggering equatorial Kelvin waves, the principal source has been related to western equatorial zonal wind changes (Adamec and O'Brien, 1978 Philander, 1990; Katz, 1997; Han et al., 2008). Wider studies for the equatorial Pacific have found convectively coupled equatorial waves related to the Madden-Julian Oscillation (MJO), an intraseasonal oscillation of the atmospheric convection, which affects the entire troposphere and is stronger at the boreal winter with a period of between 30 to 60 days (Madden and Julian, 1994). These works have analyzed the Pacific equatorial intraseasonal Kelvin waves and its relation to the Outgoing Long-wave Radiation (OLR) anomalies associated with the MJO (Hendon et al., 1998; Matthews et al., 2007), and in particular, during El Niño phases (Kessler et al., 1995; Roundy and Kiladis, 2006). Roundy and Kiladis (2006) have found that, for some events, the surface westerly wind convection-induced anomalies associated with the MJO

are triggering the oceanic Kelvin waves at the western-central equatorial Pacific. They have also found proof for air-sea interactions in the convection anomalies propagation as the wave is passing. Observational coherent relationship between atmospheric convection, surface fluxes and Sea Surface Temperature (SST) has been suggested over the Tropical Indian and Pacific Ocean basins on intraseasonal timescales (Woolnough et al, 2000). They have found a sequence that relates positive SST anomalies with enhanced convection, anomalous westerly wind and enhanced evaporation, in an intraseasonal oscillation, in agreement with the coupled mechanism proposed by Flatau et al. (1997).

In the Atlantic, Foltz and McPhaden (2004) have shown significant correlation between MJO and western equatorial Atlantic zonal winds. Foltz and McPhaden (2005) have shown the consistency between convergence, precipitation and wind velocity at 50-60 days period in the western TA. Park and Schubert (1993) have found TA OLR 20-70 days period and the maximum northeastern South America convergence fluctuations have been connected to the MJO. The MJO influence at the Amazon region and the interaction with the South America deep convection is well established (Kayano and Kousky, 1999), however, MJO impacts over TA and the equatorial Kelvin Atlantic wave's generation at intraseasonal time scales has not been completely explained.

Analytically, another possible mechanism for the Kelvin wave appearance at West equator is the Rossby wave reflection. However several works have argued that the small Atlantic basin and the presence of the North Brazil Current (NBC) could inhibit the Rossby reflection (Arnault et al., 1990; Handoh and Bigg, 2000; Illig et al., 2004). These authors have experienced difficulties at tracking back equatorial waves up to the American coast. The oceanic Rossby waves have already been widely investigated, although most of these works are concerned with extratropical Rossby waves (Chelton and Schlax, 1996; Cipollini et al., 1996; Hill et al., 2000; Challenor et al., 2001).

Although there have been many studies suggesting and supporting the idea that part of the equatorial and coastal upwelling in the Gulf of Guinea (GG) is remotely forced by the wind in the western equatorial Atlantic via Kelvin waves (Moore et al., 1978; Adamec and O'Brien, 1978; Servain et al., 1982; Picaut, 1983, among others), and some observational works have shown evidence of oceanic waves activity in the TA interannual variability (Handoh and Bigg, 2000; Schouten et al., 2005; Polo et al., 2007b), there is a lack of investigation about the origin of the Kelvin wave, and the Rossby-Kelvin relationship in the deep tropics, especially at intraseasonal timescales.

Concerning the oceanic waves impacts, oceanic waves have demonstrated its climate forcing by modifying SST via anomalous current advection (Leewenburgh and Stammer 2001; Hill et al., 2000). An important challenge of this work is to discern some of the Kelvin wave impacts on the SST along the African coast, which includes the coast of the GG, the coast of the Guinea dome, the coast of the Angola dome and northern and southern subtropical areas. These regions, which are the environment for the oceanic wave activity, are also region of important processes and the Kelvin wave could be a way of producing SST variations: i.e. GG is a principal source of water vapor, constituting the most of the precipitation on the continent (Fontaine et al., 1999); the subtropical coastal areas are permanent upwelling system and the SST variations could affect the season of the fisheries (Picaut, 1983; Schouten et al., 2005; Florenchie et al., 2003). Furthermore, the Kelvin wave interactions with some regions could be important in climate terms; the Northern African coast SST variability over the Subtropical North Atlantic (SNA) has been connected to the anomalous winter European precipitation events (Rodríguez-Fonseca et al, 2006). The SNA region is flanked and influenced by the Mauritanian/Senegal upwelling system (Polo et al., 2005) therefore, the interaction with the Kelvin waves could be important for the upwelling and extratropical climate variability. Kelvin waves could interact with the Angola/Benguela upwelling system, which can be also relevant in climate terms, since this area has been already discussed in relation to the Equatorial interannual mode (Latif and Grötzner, 2000; Wang, 2006; Polo et al., 2008b) and the Benguela Niño events (Florenchie et al., 2003; Rouault et al., 2007). In addition, tropics could be connected to extratropics through equatorial-coastal Kelvin waves that radiate as a Rossby wave, propagating climate anomalies (Kessler, 1991; Chelton and Schlax, 1996; Cipollini et al., 1996; Polito and Cornillon, 1997; Jacobs et al., 1994).

Faced with the importance of the oceanic waves and due to the fact that only a few works have studied the processes in relation to Tropical Atlantic Variability (TAV), in this study we attempt to clarify the mechanism for triggering the Kelvin wave and its impacts, by focusing attention on the interaction with TA intraseasonal variability, and considering the boreal autumn-winter equatorial and coastal Kelvin wave mode found in part I. The paper follows this order; section 2 discusses the variables and data. The results are shown in sections 3 and 4. In order to find the Kelvin wave source, the SSH variability along the wave-track is investigated in section 3.1. The Kelvin-Rossby relation and a mechanism for triggering the equatorial Kelvin wave are explained in subsection 3.2 y 3.3 respectively. A discussion about oceanic and atmospheric oscillations is in subsection 3.4. Section 4 gives some insights about particular SSH

variability over the subtropics, as well as the Kelvin wave impacts on SST along the coast. Finally, the main results are summarized.

2 Data and Analysis tools

We use SSH TOPEX/Poseidon altimetry measurements, with 0.5 degrees horizontal resolution and 7-days time resolution produced and distributed by Aviso, as part of the Ssalto ground processing segment. The T/P SSH anomalies have already been corrected by removing four-year average elevation and signals such as the ocean tide, the dry tropospheric, inverted barometer, tidal aliasing and vapour water. The inter-comparison analyses with *in situ* measurements (i.e. tide gauges records) have demonstrated that the altimetry is an important tool to observe oceanic variability (Arnault et al., 1992), even in the coastal regions (Aman et al., 2007). In contrast to the sparse network of coastal tide gauges, measurements of SSH from space by satellite radar altimetry provide near global and homogeneous coverage of the world's oceans. The weekly temporal resolution of the T/P SSH is expected to be high enough for the description of the baroclinic Kelvin waves, since the theoretical first baroclinic mode takes about 30-45 days to cross the Atlantic along the equator and more than 20 days to leave the tropical latitudes studied here. However, the 0.5 degree spatial resolution corresponds to the Rossby radius of deformation at about 15 degrees of latitude for a 2 m/s baroclinic phase speed. Therefore it is certainly a limitation to our analysis, and it may in particular affect our ability to observe coastal waves poleward of 10 to 20 degrees of latitude. However, the T/P orbit configuration and the repeat period is the best compromise between the spatial and temporal resolution. Katz (1997) was able to measure TIW and Kelvin waves over the TA from T/P SSH. More details about the uncertainty of the SSH estimated from T/P can be found in part I of this work and in França et al., (2003).

In order to complete the study with synchronous subsurface oceanic quantities that are not available in the observations, in particular the thermocline depth, we use a numerical simulation of the OPA OGCM (Madec et al., 1998). The ORCA05 configuration used here was run at the LOCEAN laboratory by the NEMO (Numerical Framework for Ocean Modeling) team, for the 1992-2000 period. The configuration is for the global ocean with a 0.5 degrees horizontal resolution and 30 vertical levels. The momentum flux is the weekly ERS1-2 wind stress interpolated daily, while the air-sea heat fluxes are computed in line with semi-empirical, or bulk formulas using OGCM SST, the ERS1-2 wind speed, the NCEP-NCAR reanalysis (Kalnay et al., 1996) air temperature, and monthly climatological air humidity (Trenberth et al., 1989) and cloudiness (Berliand and Strokina, 1980). Precipitation data come from the Climate Prediction Center Merged Analysis of Precipitation (CMAP) product (Xie and Arkin, 1996). Major river runoffs are taken into account through monthly values of river discharge (UNESCO, 1996). At last, a restoring term towards Levitus (1998) Sea Surface Salinity is applied to the fresh water budget. For further details on the model configuration see de Boyer-Montégut et al. (2007).

In this work we have used 5-day average output of SSH and 18°C isotherm depth (hereafter z18, see part I for details). The ability of the model to reproduce the observed SSH and to recognize propagating signals has been demonstrated in part I.

In order to investigate TAV associated with the winter EEOF Kelvin waves, some observational variables have been used: the weekly mean SST comes from the Reynolds data set, and daily OLR, as tropical convection proxy, comes from NOAA/OAR/ERSL PSD data resources (Liebmann and Smith, 1996). From the Active Microwave Instrument-Earth Resources Satellite (AMI-ERS), zonal and meridional scatterometer wind stresses have been used, with a 5-day temporal resolution. Some additional fields have been also used such as Sea Level Pressure (SLP), geopotential height and surface winds from ERA-40 reanalysis (Uppala et al., 2005). To follow the Kelvin wave propagation, the same wave-track defined in part I has been used (figure 1b in part I). The track moves along the equator and poleward along the West African coast. , starting at the western equatorial Atlantic, and following the equator and continuing poleward along the African coast. For the north, the track moves along the GG westward and continues northward up to 30°N, having twice more track-points than the south. For the south, the track runs up to 25°S along the coast (named hereafter southern African coast).

Throughout the study, and in order to understand the variability associated with the wave as it is passing, we use the Extended Principal Component (EPC) timeseries from the leading mode of the Extended Empirical Orthogonal Function (EEOF) performed in part I (figure 6 in part I). This mode has determined the signal of the intraseasonal equatorial Kelvin wave propagating along the equator and splitting at the west Africa and propagating poleward along the coast as far as ~12ºN in boreal autumn-winter season, and it will be referred as Winter EEOF Kelvin Wave (hereafter WEK). As in part I, the data is filtered with a 25-95 days band-pass filter (see part I for further discussion) in order to isolate the intraseasonal variability of each field. Different variables are projected onto this WEK timeseries with the

aim of understanding the horizontal structure of the Kelvin wave in the TA, the relation to the atmosphere through the wind stress and the convection, and its impacts.

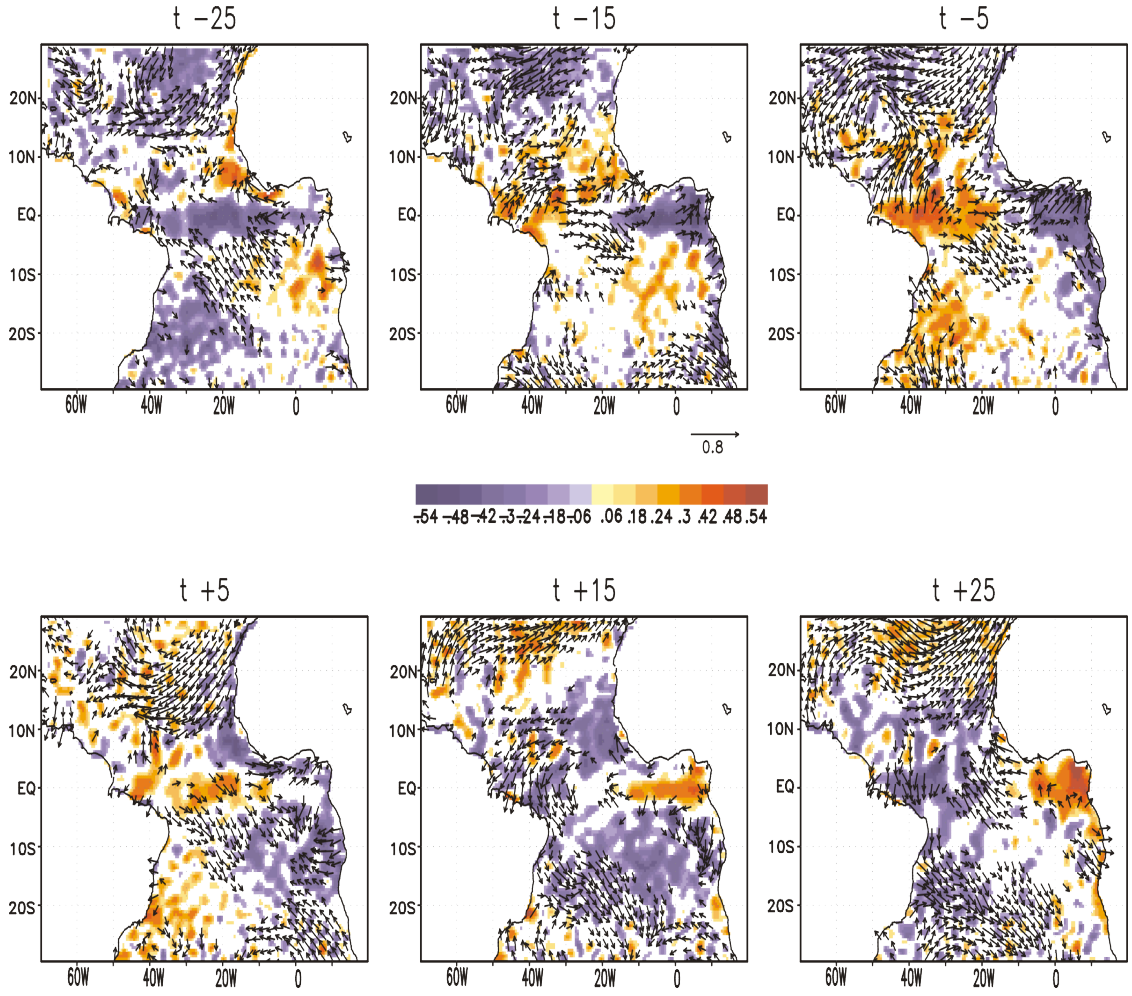

Figure 1: Regression of the EEOF from boreal autumn-winter SSH along the northern wave-track on to the SSH (shaded areas, CI=0.1 cm) and the wind stress (vectors, in 10^{-2} N/m^2) from lag -25 to lag +25.

3 Which processes are co-varying with the Kelvin waves?

As has been summarized in the introduction, some authors have already investigated Kelvin waves at intraseasonal scales. However, there is a lack of investigation about the origin of the Kelvin wave and the Rossby-Kelvin relationship in the deep tropics and especially in the TA at intraseasonal scales. Faced with this, some issues are raised about the Kelvin wave nature, and the main aim of this section is to answer the following question:
What is the source of the TA intraseasonal Kelvin wave? In order to investigate that, we reformulate two more questions;
How does the wind force the SSH along the wave-track?
Is there Rossby-Kelvin interaction?

The present section investigates all those questions in the context of TA intraseasonal variability. In section 3.1 the wind stress influence is analysed. Rossby-Kelvin relationship is explained in section 3.2, while the section 3.3 expounds a possible mechanism for Kelvin wave source. A discussion is posed in section 3.4.

3.1 SSH-Wind stress covariability

Since the wind stress is the most important SSH variability factor, we first check whether the wind stress field is coherent with the SSH variations, on the one hand with the WEK propagation and on the other hand with the local SSH changes.

3.1.1 SSH-wind stress covariability broadening the WEK picture

To understand the TA SSH spatial pattern associated with the boreal autumn-winter Kelvin waves, the observational SSH and wind stress anomalies are regressed onto the WEK timeseries (from part I). The projection has been done for different lags (lagging the SSH and wind stress fields from –25 days to +25 days) to show the time evolution over the whole TA as the wave is propagating (figure 1). Two striking results must be considered from the whole picture: the wind stress signal appears associated with large-scale structures, and both fields, SSH and wind stress also oscillates coherently at large-scales, especially in the northern hemisphere.

Starting with the equatorial signals, at lag –15 (lag +15), at 50-40ºW within equatorial band, the wind stress shows a northward (southward) component and a downwelling (upwelling) SSH signal in the region. This appears controversial because at the equator, this wind stress signal would be associated with wind divergence (convergence), and in turn with upwelling (downwelling) SSH signal. The zonal wind stress is weak and positive for both cases. However, if we consider the signal offshore (~5N), the wind stress divergence, the wind stress curl and the meridional wind stress are working to produce downwelling (upwelling). The Ekman pumping's contribution associated with the wind stress signal will be quantify later in the text.

At lat –5 (lag +25), the downwelling (upwelling) SSH signal is completely developed. At central equator the decrease (increase) of the southern trade winds could correspond to an anomalous convergence (divergence) of the meridional Ekman current. This could reinforce the positive (negative) SSH anomaly. Simultaneously, the subtropical trade winds between 10-30ºN are clockwise (anticlockwise) and thus strengthened (weakened), which is favourable to Ekman currents divergence (convergence). This is coherent with the observed upwelling (downwelling) SSH signal at the northern African coast.

At lag +5 (lag –25), the equatorial downwelling (upwelling) SSH signal travels all along the equator with weak equatorial winds above it, which would favour the SSH signal at the central equator. The positive (negative) equatorial SSH signal arrives at the GG and the African coast at lag +15 (lag -15), and then it seems to propagate poleward up to 20ºS and 20ºN at lag +25 (lag -5). However, simply coastal propagations are not at work at this latitudes (see part I); simultaneous and favourable coastal wind stress anomalies are capable to generate the actual coastal SSH over the northern subtropics. Poleward 10 degrees latitude along the coast, the synchronous arrival of SSH and development of coherent wind stress anomalies is an interesting phenomenon. It suggests a striking coherence between Kelvin wave propagations timescales and northern basin- scale wind oscillations. This particular issue will be discussed in section 4.1.

At lag –25 (lag +5) the coastal signal is developed into an open ocean downwelling (upwelling) signal at 5-10ºN;10-20ºW and 5-15ºS;0-10ºW. This pattern could correspond with Rossby radiation from the African coast. This feature will be analysed in the section 3.2.

The wind stress anomalies seem to be consistent with the anomalous SSH associated with the WEK, at central equator and Northern African coast. Whereas, west of the equator, where the Kelvin wave starts, the wind stress signal is not coherent with SSH. In the next section we quantify the local relationship between the wind stress and the SSH along the Kelvin wave-track.

3.1.2 SSH-wind stress covariability following the wave-track

In order to quantify the simultaneous relationship between the SSH and the local wind stress along the equator, we have performed the correlation between the filtered SSH changes (time centered derivative of the variable) and the along-track filtered wind stress anomalies in the boreal autumn-winter season (figure 2a). We can discriminate several regions by the covariability behaviour; the western equator, the central-eastern equator, the equatorial coastal region and the Subtropics.

Close to the American coast, over the Amazon mouth, the SSH exhibits a very high variability (as has been seen before at the beginning of the wave-track in figure 4 in part I), due to the multiple and

complex processes in the region and the lack of reliability of the SSH data there. Therefore, we have discarded this region and we do interpret the effective influence of the wind stress (from ~50ºW to 45ºW, not shown in figure 2a).

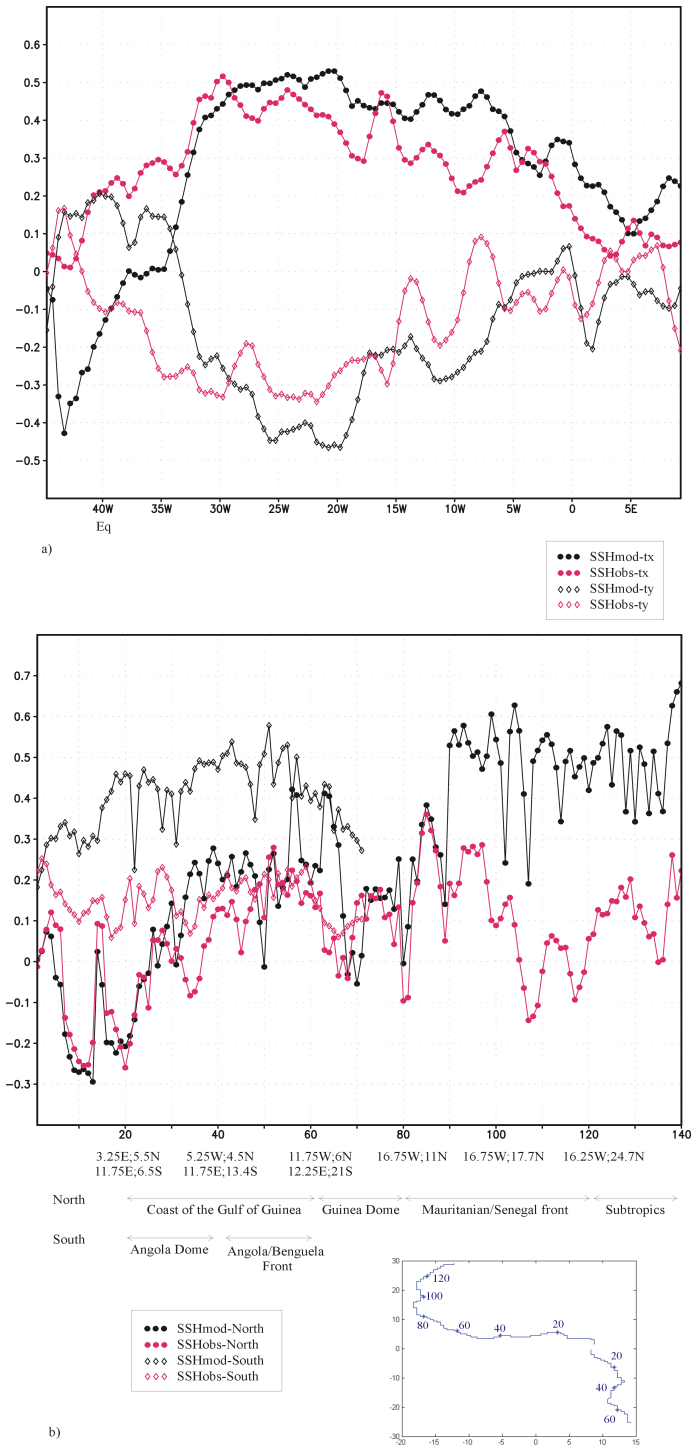

Figure 2: a) Correlation between the SSH and Z18 changes and the wind stress along the equator **b)** correlation between the SSH and Z18 changes and alongshore wind, for the northern and southern African coast.

At the western equatorial Atlantic (45ºW-35ºW), a key region as shown in figure 1, the correlations are low but it is interesting to see that the observed and the modelled SSH respond to the wind stress in an opposite way; a positive (negative) zonal wind stress and a negative (positive) meridional wind stress are related to a positive (negative) SSH in the observations (model). While, over this area, a northwestward wind stress is expected to force an upwelling SSH signal (Philander, 1990;

Katz, 1997). Therefore, the low correlation for the observations suggests that the forcing is not the classical equatorial zonal wind burst. This is an important result because the wind stress over the western equatorial Atlantic by itself seems not to explain satisfactorily the SSH changes and thus the source for Kelvin waves (from figure 1 and figure 2a), although the modelled and the observed SSH are well correlated (figure 4c in part I). Therefore, other processes that could force the Kelvin wave at the western equatorial Atlantic need to be investigated in the successive sections.

From 35ºW Kelvin track-point, the correlations for observations and model suggest that the wind stress amplitudes are driven a large part of the SSH changes (r=0.4 for the observations and 0.5 for the model). Along central and eastern equatorial Atlantic, as trade winds strengthen (weaken), SSH decreases (increases). Over the GG (10ºW-10ºE), there is a significant decrease of correlation value for both, zonal and meridional wind stress with SSH; this is likely to be due to other forcing mechanism, such as remote control Kelvin wave from the western equator, are at work in the eastern equatorial Atlantic (see also part I). This behaviour can also be seen in figure 2b, which shows the correlation between the SSH changes and the alongshore wind stress, and the lower values over the coast of the GG (<~0.25), indicate the possible dominance of the remote forcing in this region.

Along the northern African coast (Figure 2b), the correlation between the SSH and the alongshore wind stress increases poleward up to 15N with a very good agreement between observations and model. North of 15ºN, the observed SSH stays poorly correlated to the wind, whereas the model SSH reaches ~0.5 correlation score. The correlation value difference could be due to the model over-estimating local wind control or higher signal to noise ration for the coastal observed SSH data (see the decrease of correlation poleward between model and observations in figure 4c in part I). However, the shape of the correlation along the northern wave-track is quite similar for both, the observed and modelled SSH. This suggests that the model is reproducing well the spatial alongshore variations of the SSH-wind relationship.

Along the southern African coast, the correlation between the observed SSH with the alongshore winds is very low. For the modelled SSH, the correlation increases poleward reaching a 0.5 correlation score at the Angola/Benguela upwelling region. The particular behaviour in the subtropical areas will be analysed in section 4.1.

We are now looking for the source of the Kelvin wave and, as we have seen before, the wind stress does not explain completely the modelled/observed SSH variations at the western equatorial Atlantic, where the WEK starts. For this reason, we are going to explore other possible triggering mechanism as the Rossby wave reflection. This will be examined in the following section.

3.2 Is there a Rossby Kelvin exchange in the deep tropics?

The Rossby wave radiation from the African coast and the Rossby-Kelvin reflection at the American coast could be possible in an oscillatory loop-like mode (Handoh and Bigg, 2000). The next section tries to identify Rossby wave radiation from the African coast followed by reflection at the American coast at intraseasonal scales. Rossby wave description at the equatorial band is done in the context of the Kelvin wave activity, therefore this is not an extensive study of the Rossby waves itself; which have been studied more precisely by other authors (Chelton and Schlax, 1996; Cipollini et al., 1997, among others).

3.2.1 Rossby wave identification and characterization

We want to identify and characterize, on the one hand, the Rossby wave radiation from the African coast, which is a feature that makes the Kelvin wave dissipate poleward (Gill, 1982), and on the other hand the Rossby reflection at the American coast, which could be responsible of some intraseasonal Kelvin waves events. This scenario would describe an oscillatory loop-like system of which trajectory is illustrated in figure 3a.

The track is defined in order to differentiate the first meridional Rossby mode (maximum amplitude at 4ºN and 4ºS; Illig et al., 2004) from the rest of the meridional modes. For simplicity and to better identify the possible continuity, figure 3b shows the Hovmuller for Rossby-Kelvin-Rossby trajectory for the Northern Hemisphere during 1998-1999, which are representative of wave activity (see figure 4 and figure 5b in part I) and WEK activity (see figure 6 in part I). The Rossby wave-track corresponds to the coast of the GG at the beginning, shared with the Kelvin wave-track (figure 1b in part I), and 4ºN offshore. Figure 3b (central panel) shows the SSH and z18 along the equator as Kelvin waves, and figure 3b (right panel) shows the SSH and z18 anomalies along the GG again (same as the beginning of figure 3b-left panel). The modelled SSH (not shown) is in good agreement with the z18 signal. In

general, propagating features at 4N and the equator can be seen for both observed and modelled SSH signals.

From figure 3b, observed SSH does not support the idea of Rossby radiation from the GG (~13ºW; 4ºN) and continuity offshore, whereas the model z18 shows more continuity that could correspond to Rossby wave. This feature can be seen for the event November 1998, in which negative z18 anomaly at the GG propagates and continues offshore reaching 43ºW; 4ºN in July 1999 (figure 3b-left panel). Later, there is an intensification of the signal at the western part of the track (23ºW-43ºW), probably due to local effects (figure 3b-left panel). There are some particular events, which could be considered as propagation from the coast to the western Atlantic (figure 3b-left panel, i.e. from January 1998 at eastern track to June 1998 at 38ºW negative modelled z18 and observed SSH signals; from February 1998 at eastern track to September 1998 at 40ºW positive observed SSH signal). However, to identify Rossby propagations phase speed calculation is needed.

In the same manner, continuity from the western Atlantic (figure 3b right panel) and the equatorial Kelvin waves (figure 3b central panel) is visible for some events (i.e. September 1998, November 1998, December 1998, January 1999, September 1999), although further analysis in needed in the next subsection to demonstrate this continuity. Figure 3b (right panel) shows the SSH and z18 anomalies along the GG again, with clear continuity from the equator and which could represent a mix between the Rossby and coastally trapped Kelvin wave (phase speed ranges the first and second baroclinic Kelvin modes, see part I).

In order to quantify if the propagation along ~4ºN corresponds to Rossby wave, we have calculated the propagation phase speed along the northern Rossby wave-tracks of modelled and observed filtered SSH signal for the entire period by Radon Transform technique (figure 3c). The phase speed at the coast of the GG is in the range 1-2.4 m/s (see part I). There is a threshold for the Rossby wave phase speed after the coast of the GG; the open ocean phase speed decreases from 1 to 0.2 m/s at the western-most position. The main phase speed is 0.5 m/s, which roughly corresponds to the phase speed found from the T/P as the first baroclinic Rossby wave at that latitude (Chelton and Schlax, 1996; Fu and Chelton, 2001; Killworth at al., 1997). We conclude that, the propagation found for most events in figure 3b-left panel are Rossby wave radiation since the phase speed by RT is coherent with the theoretical one. In the next section we will go further checking the possible Kelvin-Rossby radiation at the eastern Atlantic in boreal spring-summer season, as well as the Rossby wave forcing western equatorial Atlantic in boreal autumn-winter season on equatorial Kelvin waves.

3.2.2 Kelvin wave forcing eastern equatorial Atlantic and Rossby wave forcing western equatorial Atlantic

As can be seen in figure 3b-left panel, the boreal spring-summer signal at 4ºN generally strengthens westward (i.e. spring summer 1998 and spring-summer 1999, between 23ºW-43ºW in figure 3b-left panel). This could correspond with seasonal development of Tropical Instability Waves (TIW). These waves are indeed detected in boreal summer in the TA from altimetry measurements at 4ºN, and they have been described as periodic 20-30 days fluctuations (Grodsky et al., 2005), propagating westward at 0.45 m/s with a period around 25 days (Musman, 1992), and at 0.23 m/s with a 28 days period (Katz, 1997). The region of maximum SSH/z18 activity in figure 3b-left is at 4N in between 34ºW-38ºW, and the beginning of the Kelvin waves occurs at the equator ~38ºW in figure 3b-central. In order to investigate how the Rossby waves/TIW at 4N, from the GG, could reach and impact at western Atlantic in boreal late spring-summer season, the lagged correlation between the signal at 34-38ºW; 4ºN and the signal along Rossby wave-track has been computed for the SSH and z18 variables (figure 4a).

Although for the observations (figure 4a-top panel), the signal is noisier than for the modelled SSH/z18 (figure 4a-central and top panels), for the three variables the shape of the lag correlation appears similar to Rossby wave propagation from ~13ºW; 4ºN to the western region 34-38ºW; 4N. For the modelled SSH (figure 4a-central panel), the signal is complex, with positive correlation at –60 days between the point 34-38ºW; 4ºN and the points at the coast of the GG, which implies that the African coast could be a source for the SSH signal at western Atlantic, although the signal does not necessarily come propagating from the coast of the GG, because the correlation is not significant at eastern 13ºW. However, the slope of the correlation west of 13ºW is close to the z18 one. The figure 4a (bottom panel) shows nearly continuous z18 positive correlation beam linking the point 34-38ºW; 4ºN at lag 0 to the point 13ºW-4ºN at lag –70 days. It suggests that Rossby wave could originate from eastern 13ºW-4ºN, and propagates to western Atlantic, in agreement with the RT phase speed estimated in figure 3c (the 70 days corresponds to the propagation time for a Rossby wave to travel from 13ºW-4ºN to ~38ºW-4Nº at 0.5 m/s). Hence, the model signal in the western Atlantic could be partially explained by the arrival of the

Rossby wave/TIW from the African coast; however, the observations do not support this teleconnection clearly. Note that it does not hold for boreal winter (not shown).

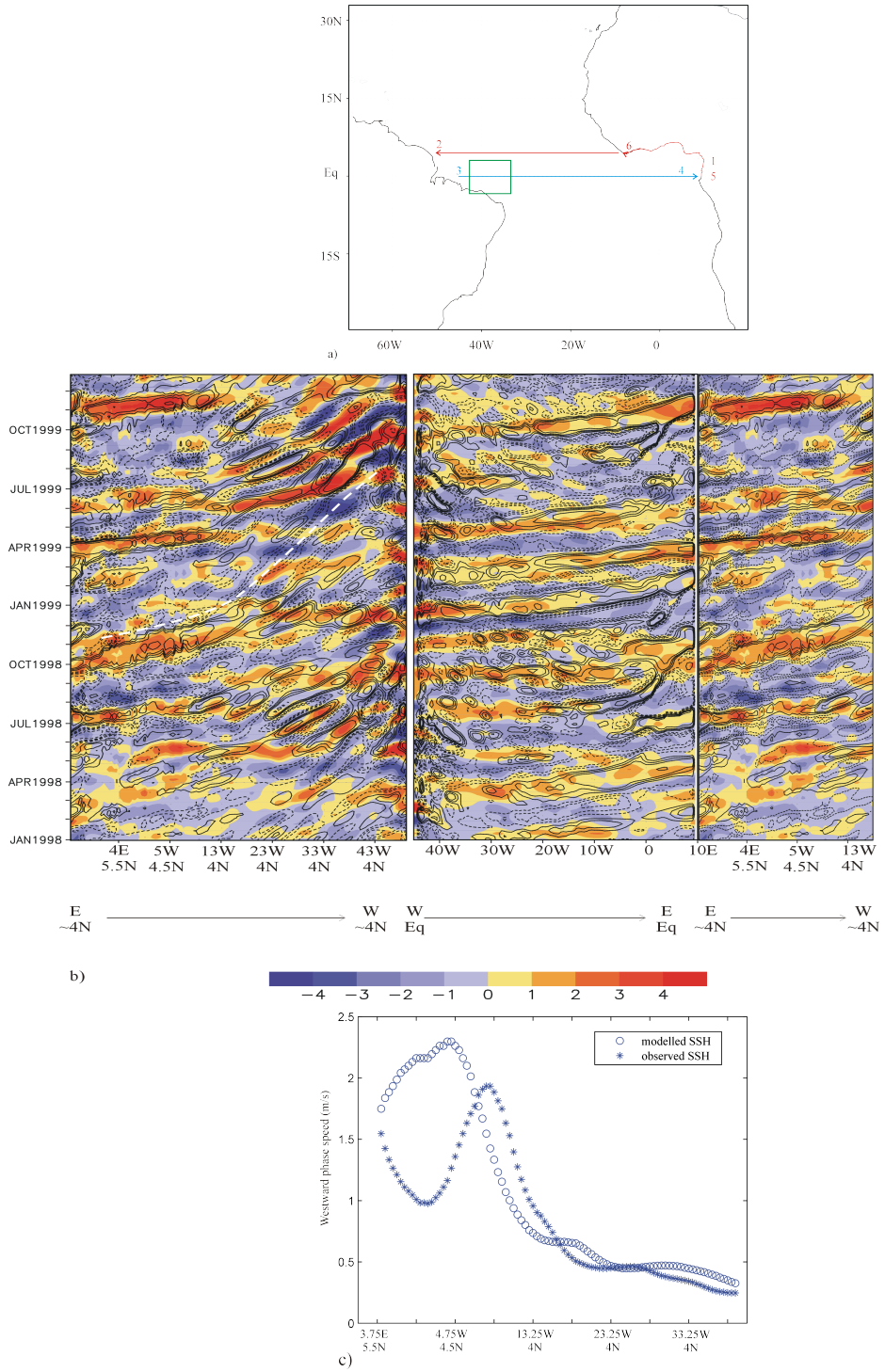

Figure 3. a) Grid map for the Rossby-Kelvin wave-tracks; following the coast of Gulf of Guinea and 4ºN offshore for the northern Rossby wave-track westward (red line from 1 to 2), equatorial Kelvin wave-track eastward (blue line from 3 to 4) and turn back again along the coast of the Gulf of Guinea (red line from 5 to 6). **b)** Hovmuller plots of the SSH (shaded areas, in cm) and z18 (contour lines, labels ±.1, 2, 3, 5 m) from 1998 to 2000, following 4ºN from east to west (left panel), following the equator from west to east (central panel) and following again the Gulf of Guinea at ~4ºN from east to west (right panel), as the map in (a) shows. **c)** Phase speed (-1*m/s) of the Rossby wave along the northern and southern wave-tracks for the model SSH, computed by Radon Transform technique with a 10 degrees radius window around each point and shifting the angle from –90 to 90 degrees each 0.25 degree. The positive phase speed is considered westward since the Rossby wave-track is defined from east to west

Despite the boreal spring-summer increase of SSH/z18 activity at 4ºN in the west, there is not a clearly apparent corresponding increase of west equatorial Kelvin wave activity (in figure 3b and along the entire period, not shown). It suggests that Kelvin waves are not particularly excited by the arrival of Rossby wave/TIW. To illustrate this, we can see an example in the event of the 1998 boreal summer (figure 3b-left panel). At west-4ºN there is a high activity, but this high amount of activity is not especially reflected in the west equatorial Kelvin wave propagation that occurs later, which one would expect to be higher (figure 3b-central panel). In boreal autumn-winter the Rossby wave/TIW activity at the western part of the basin seems to be weaker (figure 3b-left panel). However, there are standing coherent signals over 30W-40W (i.e. from figure 3b-left panel: December 1998) that could be related to the triggering of Kelvin waves, and its nature would be studied in section 3.3.

To provide evidence of the possible Rossby-Kelvin reflection close to the American coast in boreal autumn-winter, figure 4b shows the lagged correlation between SSH and z18 signal at western Atlantic (34-38ºW; 4ºN) and the signal along the Equator. The observations and the model simulation suggest a clear relation between the occurrences of SSH/z18 anomalies at 34-38ºW; 4ºN and the later equatorial Kelvin wave propagation (figure 4b). Nevertheless, the mechanism does not seem to be a Rossby reflection itself, because the time required to propagate the SSH/z18 anomaly from 38ºW-4ºN to the west-equatorial Atlantic with the phase speed above-resolved for the Rossby waves, would be more than 20 days. However, 5-10 days is the time for reaching the maximum correlation between SSH/z18 signal at 34-38ºW; 4ºN and equator-40ºW (figure 4b). Although this result is noisier for the observed SSH (figure 4b-bottom panel) significant correlation also occurs with the point 34-38ºW; 4ºN. The result does not hold for boreal summer (not shown).

Although the Rossby to Kelvin reflection mechanism over the American coast is not a complete explanation for the equatorial Kelvin generation, the relation between SSH anomalies at western Rossby wave-track (western Atlantic) and the equatorial Kelvin wave propagation is confirmed in the boreal autumn-winter season. The SSH at western equator is partly explained by the SSH at 4ºN (r=0.5 more 25% of explained variance). The relation between SSH variability ~34- 38ºW; 4ºN and SSH at equator-40ºW 10 days later, could be explained by processes around that longitude at 4ºN which imply large-scale SSH anomalies that are capable of influencing the equator some days later, mechanism that will be discussed in the next section.

3.3 Ekman pumping ITCZ shift- induced anomalies

Our previous results indicate that the wind stress at the western equatorial is not triggering the wave by itself, furthermore, a complete Rossby-Kelvin reflection is not found. However it is believed that the anomalous zonal wind stress is a major source for the SSH variability at the western equatorial Atlantic, as many authors have suggested (Adamec and O'Brien, 1978; Philander, 1990; Kessler et al., 1995; Katz, 1997; Roundy and Kiladis, 2006), this poses the question; Where is the system's energy coming from? In the next section, we investigate the processes involved in the SSH/z18 intraseasonal variability over the Western Atlantic, given that SSH/z18 anomalies over 34-38ºW; 4ºN are related to the equatorial Kelvin waves around ~5-10 days later (figure 3b and figure 4b). The wind stress and the Ekman pumping are the natural candidates to force that high SSH/z18 variability at ~4ºN (Vivier et al., 1999). The Ekman pumping is computed as follows;

$$ek = \frac{1}{\rho}\left(\nabla \times \frac{\tau'}{f}\right)$$

where ρ is a mean density, τ ' is the anomalous wind stress vector and f the Coriolis parameter. The Ekman pumping in this way is defined as positive upward (i.e. upwelling process). In this section, firstly we analyze the 1998/1999 winter event in order to describe a complete picture of the particular upwelling/downwelling Kelvin wave from the western equator. Finally we propose a mechanism for the Kelvin source considering the WKE phenomenon and implying TAV at intraseasonal scales.

3.3.1 Boreal winter 1998/1999 event and WEK triggering

We first focus on the period running from early spring to late winter 1998 (see figure 3b). This period is characterized by Rossby/TIW activity at the western part of the Rossby-track (figure 3b-left panel) in boreal spring-summer. In boreal autumn-winter, there was an amplification of the SSH signal

between 23ºW to 43ºW at 4ºN (figure 3b-left panel), and Kelvin wave activity along the equator (figure 3b-central panel).

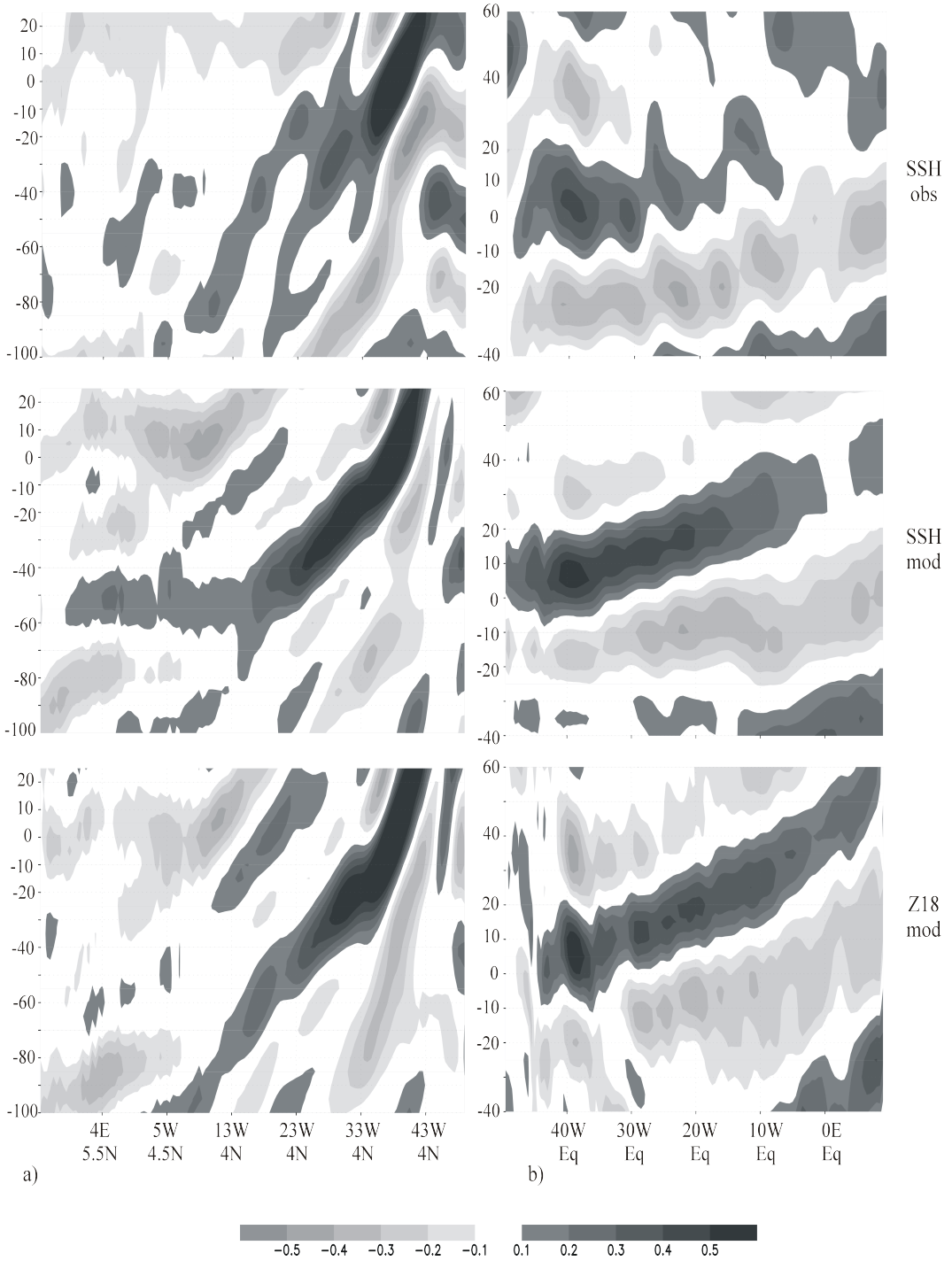

Figure 4: a) Lagged correlation between the z18 (top panel), modelled SSH (central panel) and observed SSH (bottom panel) along the Rossby wave-track and the variable at 34-38ºW; 4ºN track-point in boreal spring-summer (May to September). **b)** Lagged correlation between the z18 (top panel), modelled SSH (central panel) and observed SSH (bottom panel) along the equatorial Kelvin wave-track and the variable at 34-38ºW; 4ºN track-point in boreal autumn-winter season (September to February). Figure 5. November 1998- February 1999 event.

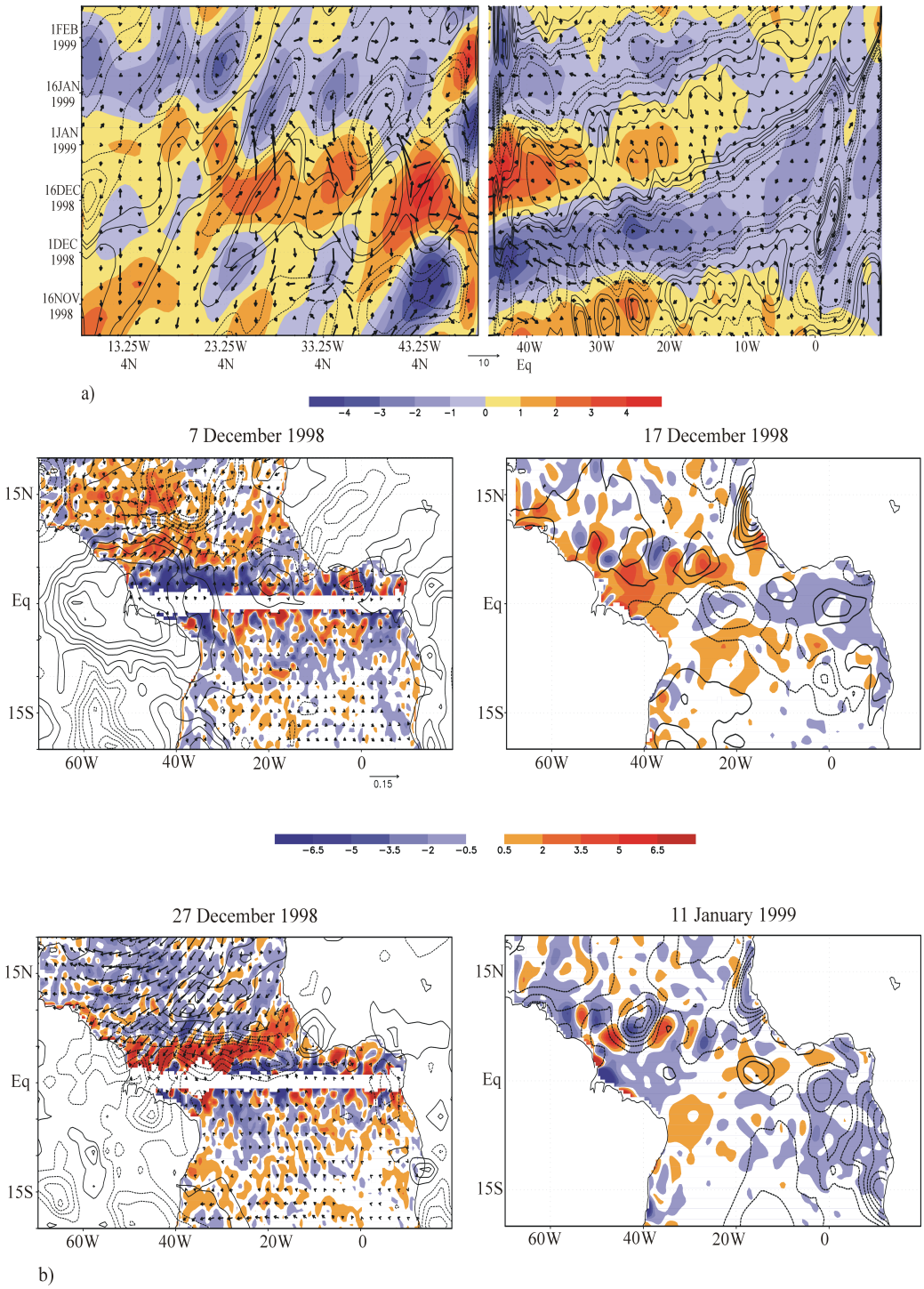

Figure 5: a) Left panel: observed SSH (shaded areas, in cm), z18 (contour lines, levels ±1, 2, 3, 5 m) and the vector consisiting in the zonal wind stress (0.5 10^{-2} N/m^2 positive rightward) and the Ekman pumping (m/5days positive upward) for the northern Rossby wave-track. Right panel: SSH (shaded areas, in cm), z18 (contour lines, levels ±1, 2, 3, 5 m) and the wind stress (vectors, 0.5 10^{-2} N/m^2) along the equator. **b)** Left panel: Wind stress anomalies (vectors, 10^{-2} N/m^2), Ekman pumping anomalies (shaded areas, 10^{-6} N/m^3 positive upward), OLR anomalies (contour lines, CI=5 W/m^2, the zero line has been removed) at 7 December (27 December), the beginning of the downwelling (upwelling) Kelvin wave event. Right panel: observed SSH (shaded areas, in cm) and SST anomalies (contour lines, in ºC) at 17 December (11 January).

Looking closely in the boreal winter 1998/1999 event, which is a representative year in relation to the WEK phenomenom (part I), we concentrate in the two phase's phenomenon that took place from beginning December 1998 to February 1999. Figure 5a shows the observed SSH and the modeled z18 anomalies along 4N (left) and along the equator (right) from November 1998 to February 1999. During December 1998 (January 1999), there are positive (negative) SSH/z18 anomalies over the western TA, from ~30ºW to 40ºW. These anomalies seem to be led by downward (upward) Ekman pumping anomalies over this region from ~15-10 days before (meridional vectors in figure 5a-left panel). These SSH/z18 anomalies over the western equatorial Atlantic at 4N from 40ºW to 30ºW, which are coherent with the Ekman pumping anomalies, suggest a continuity of the signal that propagates along the equator (figure 5a-right panel).

From previous analysis (figure 1, 2a), northwesterly (southeasterly) wind stress anomalies at the equatorial western Atlantic do not seem to lead up to positive (negative) SSH/z18 signal at the western equator. The large-scale wind stress structure and the associated Ekman pumping anomalies are illustrated in Figure 5b (left panel), which shows the anomalous wind stress, Ekman pumping and OLR anomalies over the whole TA at 7 December (27 December), ~5 days before the maximum Ekman pumping anomalies over 2-6ºN band, and 10 days before the maximun of the equatorial SSH at 17 December (11 January) (figure 5b-right). At the begginning (end) of December, the large-scale anomalous northward (southward) wind stress anomalies over the northwestern TA are associated with an anomalous positive (negative) OLR over west equator and with downward (upward) Ekman pumping anomalies over the 2ºN-6ºN band in the western-central Atlatnic, while at ~12ºN, the behaviour appears to be the opposite for OLR and Ekman pumping anomalies.

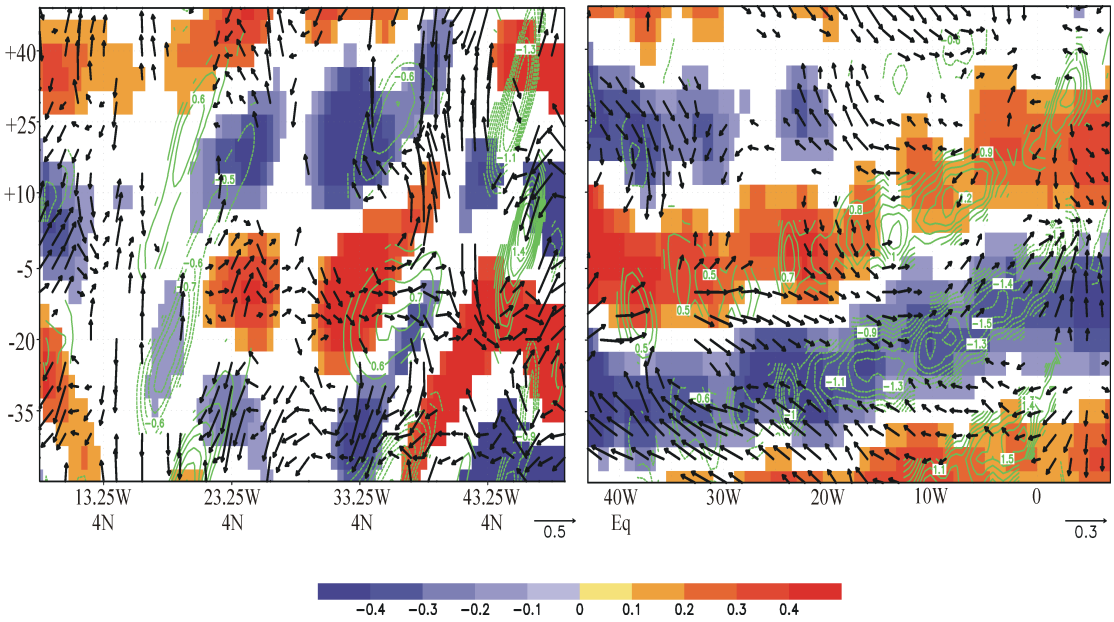

Figure 6: Left panel: observed SSH (shaded areas), modelled z18 (green contour lines) and zonal wind stress (zonal vector, in 0.5 10^{-2} N/m^2) and Ekman pumping (meridional vector, in m/5days) at 4N regressed onto the WEK timeseries. Only the areas statistically significant have been plotted.

This situations implies a basin-scale wind stress intraseasonal anomalies, coherent with maximun convergence shifts at the western Atlantic, as well as with Ekman pumping anomalies over the band centered at ~4N west-central Atlantic, and over the coastal Mauritanian/Senegal region (figure 5b).

In order to generalize the hypothesis of the particular behaviour of the 1998/99 boreal winter event, several variables; z18, Ekman pumping and wind stress at Western Atlantic has been regressed onto WEK timeseries (figure 6, comparable to the figure 5a for the 1998/99 event). Although the signals are noiser at the western Atlantic (left panel), over ~40ºW and 30ºW, the local downward (upward) Ekman pumping from ~lag -25 (~lag +5) is coherent to lead to a positive (negative) SSH/z18 signal around 10 days later. Simultaneously, the wind stress shows a northward (southward) component at western Atlantic, coinciding with the beginning of the downwelling (upwelling) signal as it has been shown before in figure 1. The continuity from off-equatorial forcing to equatorial propagation, figure 6a

(right panel) shows the well-known WEK propagation (from part I) in both, observed SSH and modeled z18.

3.3.2 Behavior at the western equator and related mechanism

Both, the particular 1998/1999 event and the WEK have suggested that wind stress, OLR, Ekman pumping signals over western off-equatorial Atlantic are consistent with SSH/Z18 signals that could trigger Kelvin waves. Now, we want to understand the processes that take place at the western equatorial Atlantic considering the seasonal cycle at the western Atlantic.

The seasonal cycle of the Ekman pumping, OLR and observed SSH variables is performed latitudinally averaging over 40ºW-30ºW (figure 7a). In boreal spring-summer season (from May to August), with the strengthening of the south trade winds, as the ITCZ shifts to its northernmost position (OLR < 240W/m2, Liebmann and Smith, 1996), the upwelling system, which is located poleward of the ITCZ, shifts and covers the entire basin around 10ºN and coherently the SSH shallows. In the boreal autumn-winter season, the ITCZ is moving towards the equator from its northernmost position, having a southern location in the late winter by the northern trade winds intensification. In the same manner, the Ekman pumping shows the diminishing of both, the downwelling over 2-6ºN and the upwelling at 10ºN, as the upwelling band shifts southward.

These two different configurations that imply Southward and Northward ITCZ shifts, and the associated winds, the Ekman pumping and the oceanic response will be named as SIC-like configuration for boreal autumn-winter and NIC-like configuration for boreal spring-summer. Since the deviations from these configurations could explain the intraseasonal variability of the variables, we can describe the situation found in the 1998/1999 winter event and in WEK (in figure 5 and 6a) as follows; if a southerly (northerly) wind stress anomalies occur at the Northwest Atlantic, the ITCZ position shows an anomalous NIC-like (SIC-like) configuration, that is, the ITCZ shifts anomalous northward (southward) as the upwelling band, leaving an anomalous downwelling (upwelling) over 2-6ºN ~5 days later. The Ekman pumping anomalies are then creating a positive (negative) SSH/z18 anomaly that affects the western equator 5-10 days after.

In order to check the hypothesis of the ITCZ-shift induced Ekman pumping anomalies anomalies at western off-equatorial Atlantic could trigger Kelvin waves, and to understand the different phases between variables, we have constructed the lagged correlation between the observed SSH averaged over the box-region (3ºN-3ºS; 40ºW-30ºW) and the variables; wind stress anomalies at 5N and Ekman pumping and OLR anomalies at 3N at lag 0, for the boreal autumn-winter season (figure 7). In this way, the SSH-box is "moving" from the reference of the others variables, and we will check if the processes that take place at lag 0 along 3-5N are oscillating as the wave, or if they are *being influenced by* (negative lags) and *have an influence onto* (positive lags) observed SSH-box. The SSH averaged over the box in the boreal autum-winter season is well correlated with the WEK (figure 7b-right), and shows significant eastward equatorial propagation (figure 7b, overlaid contours in red shows the SSH correlation along x-axis which represents the equator).

The southerwesterly wind stress at 5ºN together with positive anomalous OLR over 3N are correlated to positive SSH-box signal from 5 to 20 days after. The downward Ekman pumping anomalies shows correlation with SSH-box 5-10 days after, the significant correlation is confined between 45ºW-35ºW. The opposite phase is consistent with the oscillation of the SSH in a period around 50 days.

Figure 7b (and figures 1 and 5) have suggested that these west equatorial SSH anomalies are associated with large-scale movements in the whole Atlantic basin; the wind stress, the OLR and the Ekman pumping are oscillating at intraseasonal timescales and they are related to the SSH at the beginning of the equatorial Kelvin waves. The oscillatory patterns could be explained by intraseasonal ITCZ shifts; although these oscillations are part of a really coupled process it is very difficult to distinguish the cause and the consequence in the system (see the oscillation of every variable in figure 7b). Therefore we conclude that wind stress variations at the western Atlantic and the Ekman pumping over the western off-equatorial Atlantic, which could be induced by ITCZ-shifts, could act on SSH/z18 anomalies in that region over enough spatial scale for triggering the equatorial Kelvin wave 10-15 days after. However, model simulation is needed with a particular forcing in order to test the hypothesis of the mechanism. A discussion about the origin of these basin-scale oscillation is sought in the next section.

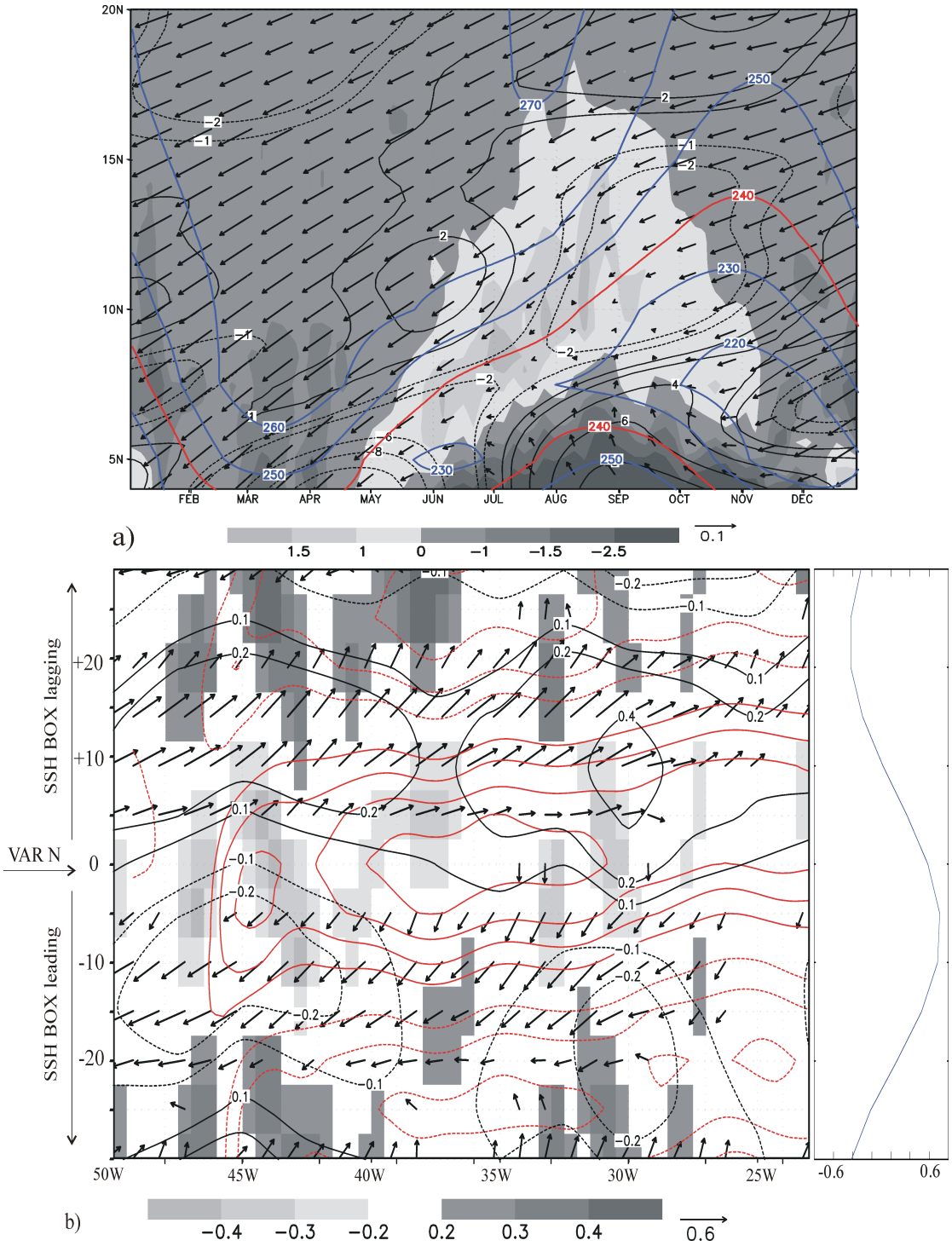

Figure 7: a) Seasonal cycle, 40ºW-30ºW longitude averaged of Ekman pumping (shaded areas, in m/5days), OLR (blue contour lines, in W/m^2 , OLR<240W/m^2 in red line as convection threshold), observed SSH (black contour lines, in cm) and wind stress (vectors, in N/m^2). **b)** Boreal autumn-winter correlation between the lagged observed SSH anomalies averaged over 40W-30W; 3N-3S and the variables at lag 0: wind stress anomalies at 5N (only statistically significant vectors has been plotted), OLR anomalies at 2N (black contour lines) and the Ekman pumping anomalies at 3ºN (only statistically significant areas has been shaded). The horizontal axis shows the west-east direction for each variable. The overlaid red contours (CI=0.1, the zero line has been removed) represent the correlation between the averaged SSH and the lagged SSH along the equator. The correlation between the averaged SSH and the WEK timeseries are plotted in the right panel.
Figure 8. Leading (left panel) and sec

3.4 Discussion

As has been shown in section 3, we believe that intraseasonal ITCZ shifts are able to explain the origin of some equatorial Atlantic Kelvin wave events. Nevertheless, this result must be discussed because the OLR intraseasonal variability at the western Atlantic has been largely associated with the MJO (Park and Schubert 1993; Kayano and Kousky, 1999; Foltz and McPhaden, 2004). In the Pacific basin, westerlies-MJO seems to influence the equatorial Kelvin waves (Kessler et al., 1995; Hendoh et al., 1998; Roundy and Kiladis, 2006; Matthews et al., 2007). With the aim of clarifying and discussing the possible MJO role in triggering equatorial Kelvin waves, we have made some additional computation using a MJO index (provided by NOAA Climate Prediction Center). This index shows different MJO phases, one of these phases regressed onto the OLR and the SSH is characterized by anomalous convection over NW Africa and NE South America and SSH anomalies over the GG (not shown).

To discern the regional OLR pattern related to the SSH along the wave-track and to quantify the link between the anomalous convection and the SSH, we have performed a Maximum Covariance Analysis (MCA) between the anomalous TA OLR and the observed SSH along the northern wave-track in boreal autumn-winter (figure 8).

The leading mode explains 24% of the covariance and associates positive SSH anomalies over the western equatorial Atlantic with positive convection over the southern Atlantic. Also a remarkable two tilted bands of OLR anomalies of different sign occurs along ~10N with a NE-SW direction.

The second mode, explaining 16% of the covariance, associates positive SSH anomalies over the coast of the GG and poleward 14ºN, with positive anomalous convection over NW Africa and NE South America (figure 8-upper panel). This OLR homogeneous pattern associated with this mode is very similar to the one found by Park and Schubert (1993), which is a convection mode in the Atlantic associated with the MJO.

The patterns associated with the leading mode shows positive OLR anomalies over the western Atlantic and weak northeasterly winds (10 days before) and, as a stage of the mechanism similar to the one shown in figure 1 (lag -15) before the Kelvin wave starts. Indeed, the SSH expansion coefficient is much related to the SSH-box from figure 7b (r=0.68), and to the WEK timeseries (r=0.46). While, the second mode corresponds to an MJO impact and has a simultaneous impact over the coast of the GG and the northern African coast and it also has a significant correlation with the WEK timeseries (r=0.4). We believe that both covariability modes are explaining part of the Kelvin wave propagation along the equator and the African coast as it is stated from figure 8 bottom panel. Indeed the sum, of the leading and the second SSH expansion coefficients, shows a correlation coefficient of 0.67 with the WEK timeseries. Furthermore, the OLR global pattern projected onto the OLR expansion coefficients show, for the leading mode significant anomalies over the Atlantic, while for the second mode, significant anomalies are found over the Indian-West-central Pacific (not shown), showing complementary patterns of the WEK projected onto the global OLR (not shown).

Therefore, part of the energy for the intraseasonal wind-OLR-Ekman anomalies that could force Kelvin waves, comes from global OLR patterns (MJO) and part comes from local OLR patterns (TA). The MJO is able to impact the Azores High pressure system and the associated winds (Foltz and McPhaden, 2004) and the North subtropical anomalies can, in turn, modify the tropical convection via Hadley circulation. In addition, south hemisphere extratropical circulation could force tropical convection and some authors have shown evidence that sub-monthly variations in the cloudiness field that defines the South Atlantic Converge Zone (SACZ) are influenced by wavelike features propagating into the region from the extratropics (Liebmann et al., 1999; Cazes-Boezio et al., 2003).

To show these possible extratropical interactions we have plotted extratropical geopotential height at 500 hPa (z500) and tropical Sea Level Pressure (SLP) and surface wind anomalies for December 1998 event (figure 9). During December 7th (December 27th) 1998, the dipole-like SLP over the western TA (linked to Ekman pumping ITCZ-shift-induced anomalies mechanism in figure 5b) appears with positive (negative) SLP anomalies over the Equator and negative (positive) further north, associated with anomalous surface wind pattern. This anomalous Subtropical pattern can influence and be influenced by anomalous tropical convection over the Amazon region. In addition, the extratropics show an anomalous Rossby wave-like circulation pattern at intraseasonal scales in both hemispheres. Nevertheless, the global pattern associated with the atmospheric-oceanic oscillations in the western Atlantic needs an extended study.

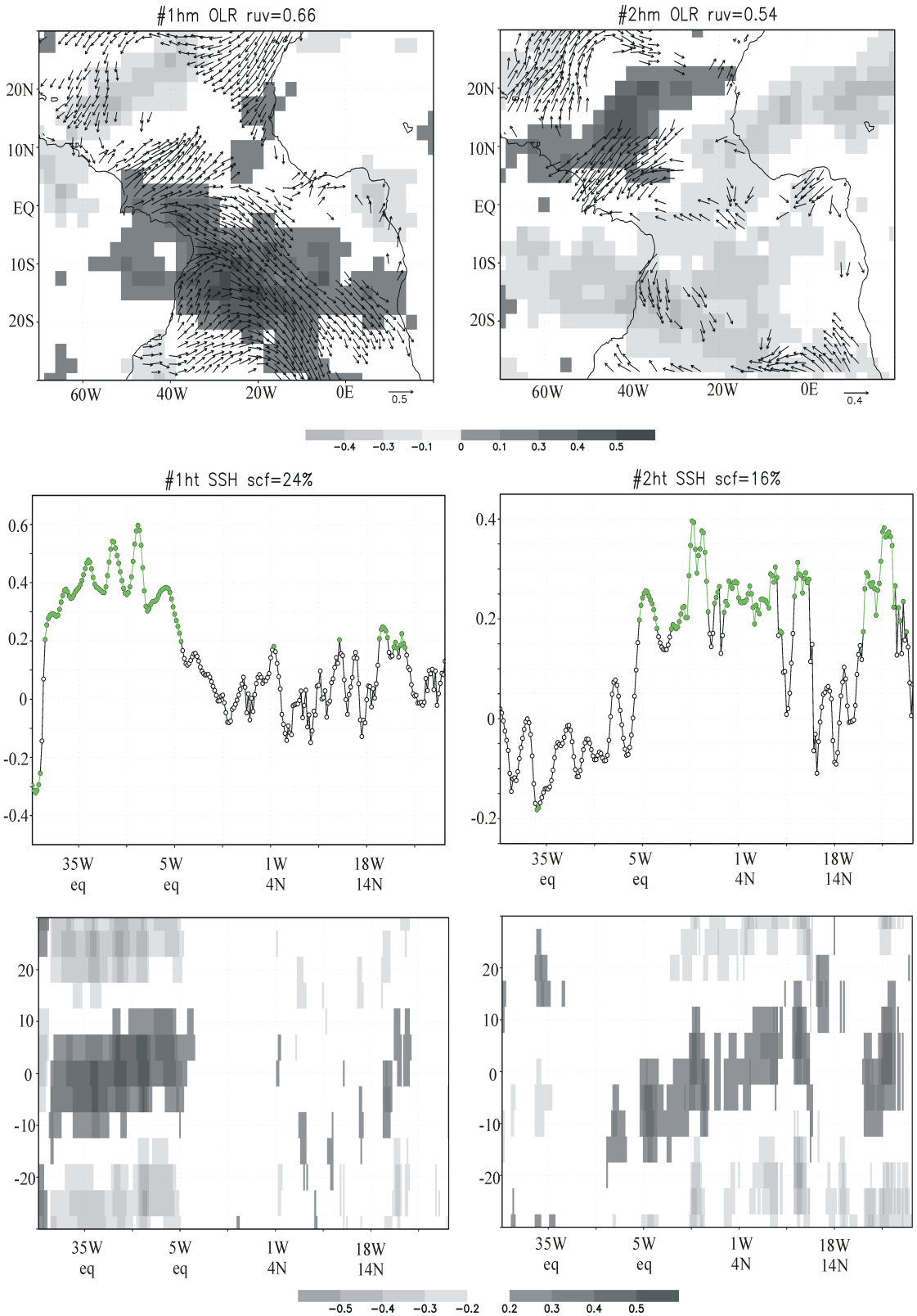

Figure 8: Leading (left panel) and second (right panel) covariability modes from Maximum Covariance Analysis between the observed SSH anomalies along the Kelvin wave-track and the OLR anomalies over the Tropical Atlantic. Top panel: OLR homogeneous regression map (shaded areas, in W/m^2) and OLR expansion coefficient regressed onto the wind stress anomalies 10 days before (vectors, in N/m^2). Central panel: observed SSH heterogeneous regression map (in cm). Bottom panel: correlation between the OLR expansion coefficient and the lagged SSH anomalies along the track (in cm). Only statistically significant areas has been plotted.

4 Kevin wave reaching the subtropical latitudes

In this section the impacts along the African coast are investigated. We want to answer two main questions. First, why does intraseasonal SSH coastal propagations when reaching the subtropics, frequently end as apparent coherent anomalies over large portions of the coast? Is this a wind forced behaviour and then why is it often in phase with the arrival of coastal waves, or is this an acceleration of the phase speed in the highly stratified upwelling areas?. Second, how the anomalous movements generated by the arrival of a wave affect the SST along the coast?. Therefore, the analysis is focused on the coastal-track, first by studying the SSH-wind covariability and later by considering the anomalous geostrophic advection of heat associated with the intraseasonal SSH signal.

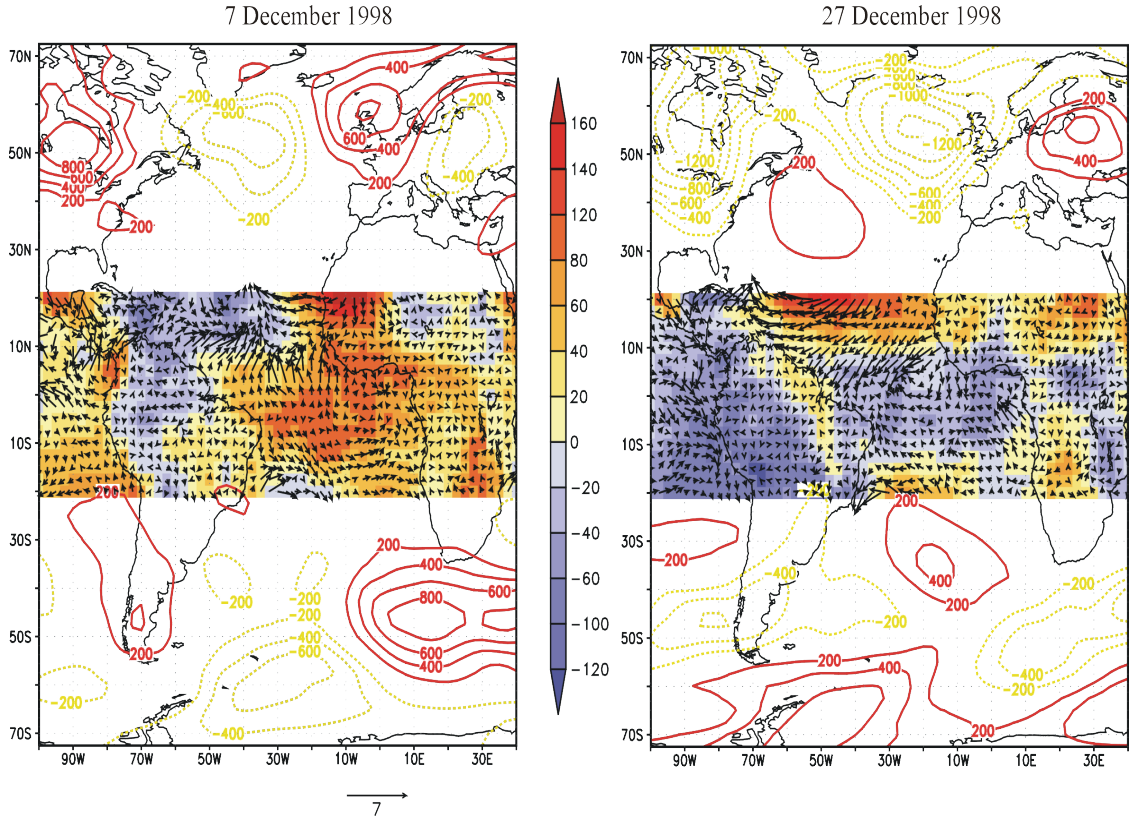

Figure 9: Geopotential height intraseasonal anomalies at 500 hPa over extratropics (contours, in m), Sea Level Pressure anomalies (shadead areas, in mbar) and surface winds (vectors in m/s) over the Tropical band for the 1998 event, 7th December 1998 (left panel) and 27th December 1998 (right panel).

4.1 SSH-wind variability at the subtropics

As has been described in part I and at the beginning of this paper, poleward of 10-15 degrees latitude the coastal Kelvin waves seem not to propagate due to the data resolution (see part I), and the correlation between the SSH and the alongshore wind-stress changes is significant (figure 2b). However, from figure 1, the coastal SSH signal shows coherence with the arrival of the WEK and also with the wind stress over several hundreds of km along the coast. In order to explain this feature, we now search for coherent patterns through the EOF analysis of the boreal autumn-winter meridional wind stress for both the north and the south wave-tracks (figure 10).

The leading modes, associated with north and south coastal areas, display anomalies that occupy the whole coast segment poleward of about 15 degrees of latitude and account for 60% and 40% of the variance respectively (figure 10a). The timeseries associated with these patterns (figure 10b) exhibit intraseasonal variability with approximately a 2 month period.

The 15-30ºN band wind forcing is dominated by large-scale signals involving the entire hemispheric basin (figure 10c) which bear the same structure as the subtropical Azores and Sta Helena High pressure systems ~2 month oscillations, for the north and the south respectively. This would explain the large coherent scale of the meridional wind stress EOF and suggest that they also dominate the large-

scale signals observed in figure 1 and figure 5. Moreover, the leading modes of winter meridional wind stress variability shows significant correlation with SSH poleward ~12 degrees of latitude (one standard deviation of the wind anomalies correspond to nearly 1cm in the SSH), being more effective in the north (figure 10c). Note that we have not found systematic interferences between the two High pulsations at any lag.

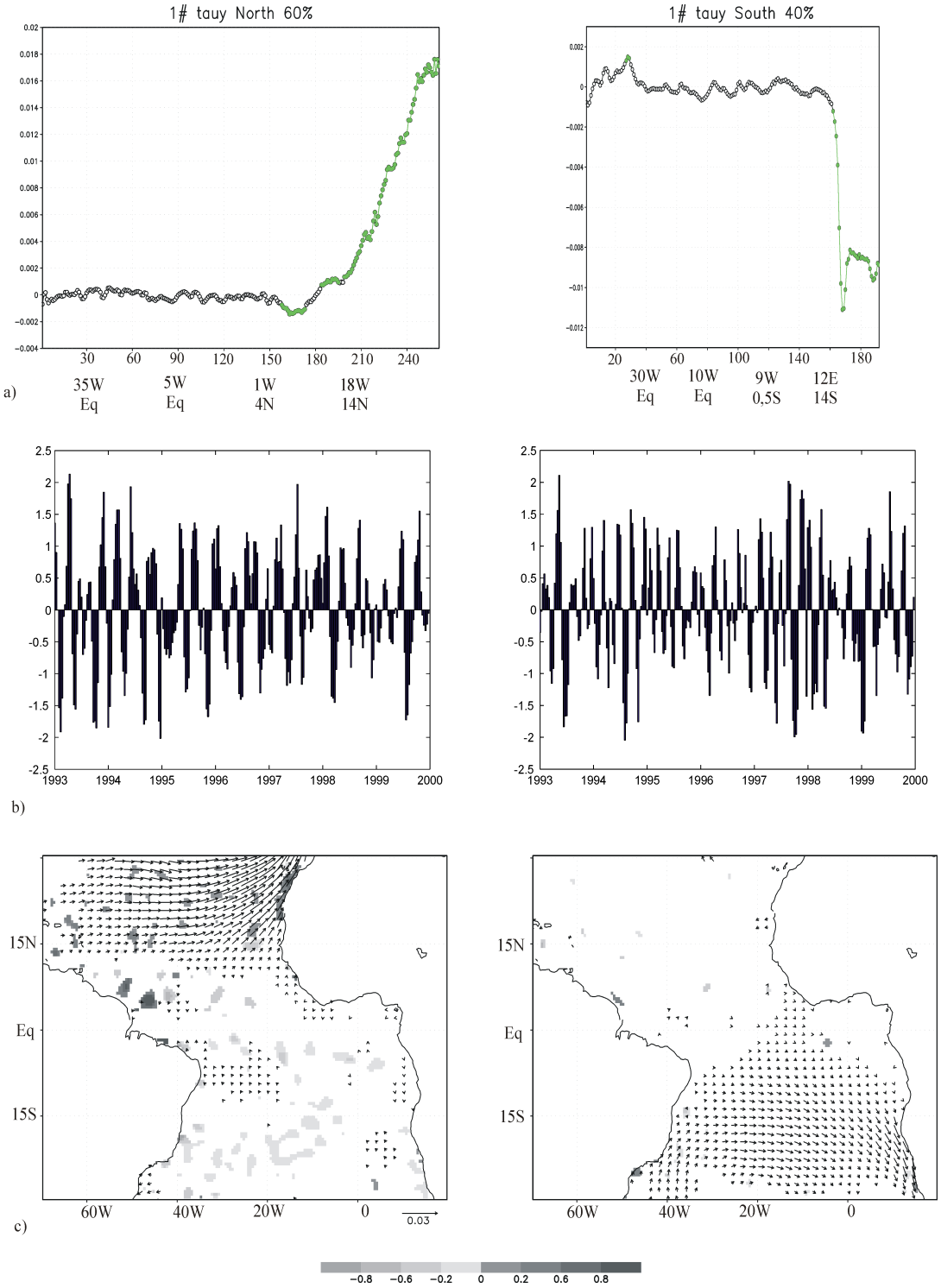

Figure 10: a) EOF leading mode for the filtered meridional wind stress (N/m^2) along the equator and the northern wave-track (left panel) and southern wave-track (right panel). **b)** PCs associated to the previous leading EOF mode (standard deviation) for the period 1993-2000. **c)** Regression of the meridional wind stress PC for the northern wave-track (left panel) and for the southern wave-track (right panel) onto the Tropical Atlantic wind stress (N/m^2) and the observational SSH (cm).

This 2 month period is very important especially in the north, because the Kelvin wave takes around 2 months to arrive close to the subtropical areas from the western equatorial Atlantic (following the wave-track, from the western Atlantic to 12N the distance is ~100 degrees, and from the linear theory $c=\sigma\lambda$ so, if λ is 100 degrees, and c is 2.2 m/s, T ~ 60 days). This fact makes both, the SSH from the wave and the SSH resulting from an anomalous meridional wind stress alongshore, be in phase. In the south, the Kelvin wave takes around one month and a half to arrive at the subtropical areas from the western equatorial Atlantic (If λ is 80 degrees, and c is 2.2 m/s, T ~ 45 days), which contributes to out phasing the SSH from the wave and the SSH from the anomalous meridional wind stress. All of this also explains the coherent signal in figure 1. Figure 1 shows a basin-scale wind stress pattern associated with the WEK; the north subtropical high oscillates with a period that doubles the time of the wave propagation from the west equator to the close northern subtropical upwelling system (in figure 1 cyclonic at lag -25 and anticyclonic at lag +5). This generates simultaneously local SSH anomalies over the subtropics, with opposite sign than those at the west equator. When the equatorial signal reaches the subtropical upwelling about a half oscillation period later, it is in phase with the new locally wind-forced signal. Then, the local and remote signals tend to reinforce each other. As can be seen in figure 1; for lag –25 (lag +5), the wind stress is imposing an anomalous downwelling (upwelling) signal at the Mauritanian/Senegal upwelling system, coinciding with the arrival of the equatorial downwelling (upwelling) Kelvin wave. For a different basin scale pattern (as happens with the southern wave-track) or a different oscillation period far away from the propagation time, the configuration for remote and local signals is more favorable to be out-phase.

From figure 10, we conclude that the meridional wind stress oscillations at the subtropics, which correspond to large-scale trade winds anomalies at both hemispheres, have similar scales than WEK phenomenom. The leading modes of meridional wind variability are important in driving SSH changes at the subtropical coastal areas. Poleward 20 degrees latitude, EKman pumping anomalies are significantly correlated to the SSH variability (not shown). Indeed, the origin and efficiency of the SSH changes at the subtropical coastal areas belongs to coastally trapped waves, Ekman pumping and wind driven latent heat flux changes and the efficiency of every process needs further investigation. The next subsection gives some insights about the SST intraseasonal variability connected to the coastally trapped Kelvin wave propagation.

4.2 Coastal waves influence on SST

Some authors have pointed out that the oceanic waves can have an impact on the SST mainly through advection (Leewenburgh and Stammer 2001; Hill et al., 2000). In this section we try to identify the intraseasonal SST variability in relation to the WEK. The projection of the WEK timeseries onto the observed SSH and the wind stress (figure 1), and the leading meridional wind mode (figure 10) have revealed that the SSH variability at the subtropical coast has a twofold cause; the trade wind oscillations and the coastally trapped Kelvin wave arrival (although the data resolution limits its visualization, the WEK is in phase with the wind stress in the northern wave-track). Now, we analyze the efficiency of the mean SST advection by anomalous current in modifiyng the SST along the West African coast.

First, in order to identify the regions where the WEK is linked to anomalous SST, the WEK timeseries has been projected onto the observed SSH, SST and wind stress anomalies along the African coast and it is shown in figure 11a. From the former figure, there is coherence between the negative (positive) SSH with a strengthening (weakening) of the alongshore winds, however, the associated negative (positive) SST signal is so clear.

Over the coast of GG, westerly wind anomalies from lag -10 to lag +10 are related to anomalous negative SST and SSH by upwelling process between 35-50 track-points (figure 11a-left). Over the Mauritanian/Senegal from (10-25ºN), both the SST and the SSH are coherent with the wind stress anomalies; northerly wind stress from lag -10 to lag +5 correspond to negative SST and SSH anomalies between 80-120 track-points (figure 11a-left). Hence both SST and SSH are coherent with the mechanism of wind stress forcing over 10-25N. At the southern wave-track the northerly wind is coherent with the negative SST and upwelling SSH signal around 40 track-point from lag -10 to lag +5 (figure 11a-right).

To show how the SST changes respond to the advection by geostrophic anomalous currrents associated with the WEK along the African coast, we have calculated the advection term. Based on the scaling results from Leewenburgh and Stammer (2001) for the SST budget associated with Rossby wave propagation, we balance the local SST changes with the advection of the mean SST by anomalous geostrophic currents. We neglect the advection by the mean currents, and the forcing terms such as wind-

driven entrainment, and we simply have a wave field acting on the winter background temperature gradient, without dissipation. This is done by substituting the zonal and meridional quasi-geostrophic velocity by the meridional and zonal altimetric sea surface slope, respectively and it is expressed as follows;

$$u' \approx -\frac{g}{f}\frac{\partial \eta'}{\partial y}$$
$$v' \approx \frac{g}{f}\frac{\partial \eta'}{\partial x}$$

Where f is the coriolis parameter and η represent the SSH. The advection of the mean SST by anomalous geostrophic currents from the wave results;

$$\frac{\partial SST'}{\partial t} \approx \nabla SST \cdot \vec{u}' = \frac{g}{f}\left(\frac{\partial \overline{SST}}{\partial x}\frac{\partial \eta'}{\partial y} - \frac{\partial \overline{SST}}{\partial y}\frac{\partial \eta'}{\partial x} \right) \qquad [1]$$

The figure 11b shows the anomalous advection along the coast versus the SST changes (°C/5days) regressed onto the WEK timeseries. It is important to notice that the advection calculated in this way, is smaller than the SST anomaly rate itself associated with the WEK. The simplification executed in the equation [1], masks other processes that are involved in resting the warming and cooling as the wave is passing. However, in spite of the geostrophic approximation in equation [1], we show next that the advection term is able to explain part of the SST behavior along the coast associated with the WEK.

Regarding the Northern coast (figure 11b-left panel), the SST changes are coherent with the anomalous advection over 10-25ºN African coast (from 80-120 track-points), and some parts of the coast of the GG (from 35-50 track-points). Over the coast of the GG, the anomalous zonal currents are effective over a negative background SST zonal gradient (figure 11c), implying a positive advection (figure 11b-left panel) for an upwelling Kelvin wave (figura 11a-left panel). While, northward 10ºN the anomalous meridional current affects over a negative background SST meridional, resulting in a negative SST advection for an upwelling Kelvin wave. This means that a negative SSH from the WEK from lag -5 to lag +5 (from lag -10 to lag +15) tend to warm (cool) the coast of the GG (subtropical coast) region (figure 11b-left panel). Concerning the Southern coast (figure 11b-right panel), the anomalous advection does not hold the SST changes along the wave-track, and the fields are too noisy to distinguish impacts on the SST.

The WEK seems to be efficient at some parts of the coast to affect the SST by anomalous current. The climate consequence of that could be important, especially over the GG, which is intensively studied for being intimately related to the West African monsoon onset, from intraseasonal to interannual timescales. Furthermore, the coastal and subtropical region has special importance; the Mauritanian upwelling system variability, has been previously related to the European climate variability (Polo et al., 2005) and the Angola/Benguela upwelling system has been related to the Benguela Niños (Rouault et al., 2007). For that reason, further investigation about the wave forcing on the SST, considering all the processes involved are already being analysed by the authors.

5 Summary

In part I of this work, we have found Kelvin wave activity from the western equatorial Atlantic propagating eastward along the equator and poleward coastally trapped along the African coast as far as 12 degrees latitude. The major activity for the intraseasonal Kelvin waves appears in boreal autumn-winter with a predominant two month period.

Looking for the causes of the phenomenon, one hypothesis largely assumed is that the source of the equatorial Kelvin wave is the zonal wind stress at the equatorial western Atlantic (Philander, 1990; Katz, 1997). Later, other authors have suggested that the atmospheric Oscillation (MJO) can be coupled to the wind and SSH changes (Hendon et al., 1998; Kessler et al., 1995; Foltz and McPhaden, 2004; Roundy and Kiladis, 2006). We have found no significant correlation between the SSH changes and the wind stress at the western equatorial Atlantic; therefore the source of the winter intraseasonal Kelvin wave is more complex and it has needed further exploration. Other established mechanism for equatorial

Kelvin waves is the Rossby wave reflection at the west of the basin. From the analysis of the Rossby-Kelvin wave relationship, we have evidenced Rossby wave radiation from the GG mostly in boreal late spring-summer season at some events. However, there is not a well established and completed loop between Kelvin-Rossby-Kelvin waves.

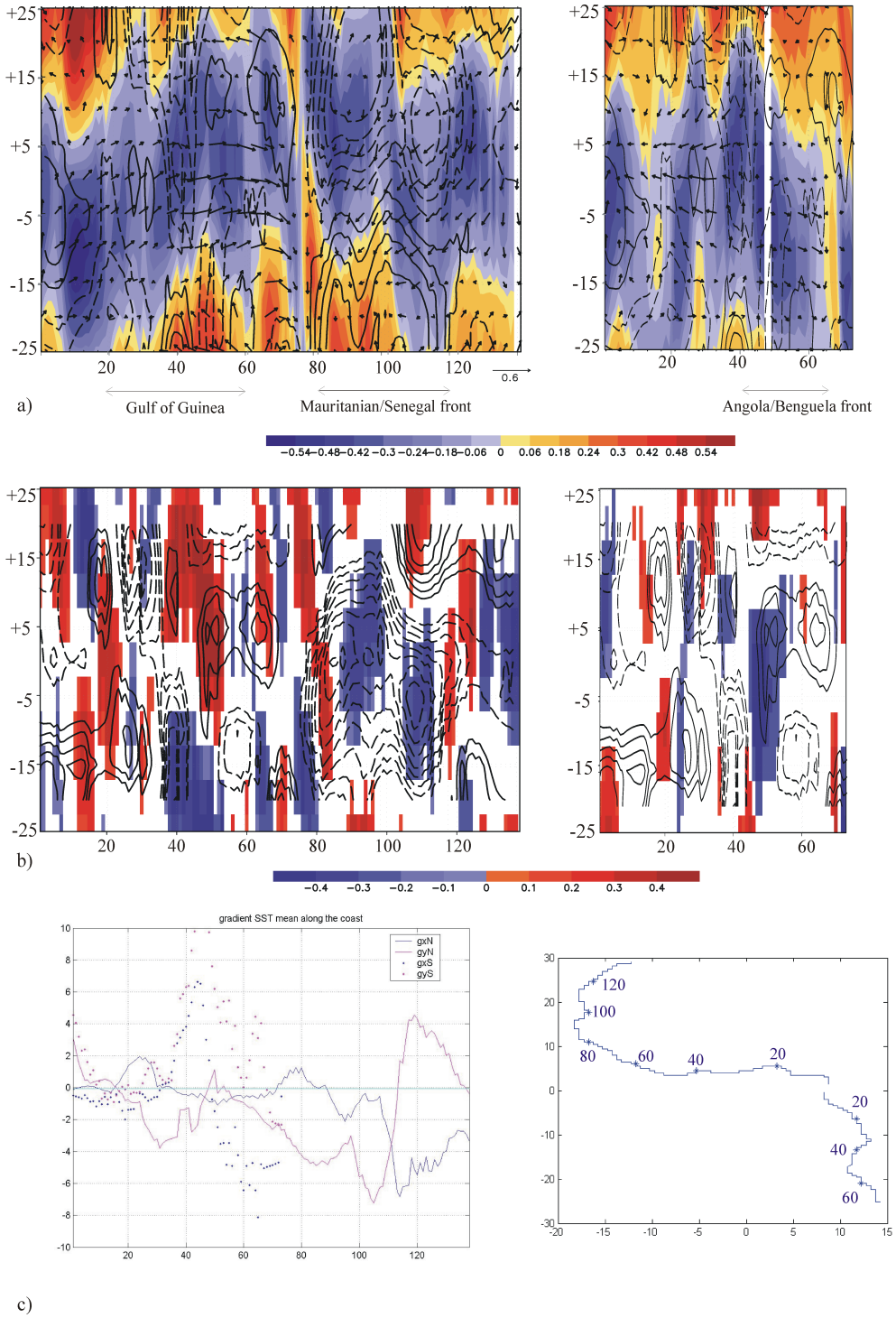

Figure 11: a) Regression of the EEOF from boreal autumn-winter SSH along the northern wave-track onto the observed SSH (shaded areas, in cm), and onto the SST (contour along $\pm 10^{-2}$ 4, 8, 12, 16, 20 ºC), along the northern African coast (left panel) and the southern African coast (right panel). **b).** Regression of the EEOF from boreal autumn-winter SSH along the northern wave-track onto the observed advection by anomalous current (only statistically significant areas are shaded, 10^{-1} ºC/5day), and onto the SST changes (contour lines, $\pm 10^{-2}$ 4, 6, 8, 10, 12, 14, 16, 18 ºC/5days), along the northern African coast (left panel) and the southern African coast (right panel). **c)** Mean winter SST gradient along the northern and southern African coast (in 10^{-6} ºC/m).

We propose a mechanism that explains the triggering of Kelvin waves namely *Ekman pumping ITCZ shift-induced anomalies*. A basin-scale wind stress anomalies over the Northwest TA, coherent with anomalous convection at both sides of 10N and anomalous Ekman pumping at west-central off-equatorial band, are inducing anomalous SSH/z18 anomalies over a wide band, which shows continuity to equatorial Kelvin waves. The wind stress oscillation and the associated OLR anomalies are a signature of the ITCZ shifting and its position at intraseasonal scales. When southwesterly (northeasterly) wind stress anomalies occurs at the Northwestern Atlantic, the ITCZ and the upwelling band shift northward (southward) position. This situation allows the western equatorial band to be in an anomalous divergence (convergence), represented by the OLR anomalies ~5 days after the winds start to be anomalous, and ~2-6ºN latitudinal band in an anomalous downwelling (upwelling) region. The downward (upward) Ekman pumping anomalies over ~4ºN impose a positive (negative) SSH anomalies with a maximum 5-10 days after, triggering the equatorial Kelvin wave.

The triggered equatorial Kelvin wave propagates eastward along the equator, with a phase speed corresponding with a mix between the first and second baroclinic modes, splits poleward along the African coast where it propagates coastally trapped as far as 12 degrees latitude (see part I). As the Kelvin wave is moving poleward, the wave has less impact on the SSH changes, while the alongshore winds become important at these regions. The oscillating winds at the subtropical Atlantic regions could act as a feedback for the wave SSH perturbation. The period of that oscillation seems to be around 60 days; therefore the SSH signal associated with these wind stress anomalies would be in phase with the arrival of the wave at the northern African coast.

The SST anomalies associated with the winter equatorial and coastal EEOF Kelvin wave show an influence from the anomalous advection by quasi-geostrophic currents over background SST gradient at the northern 10ºN over the African coast and some parts of the coast of the GG.

There are still many open questions that the authors would like to answer, such as the understanding of the global pattern associated with the atmospheric-oceanic oscillations in the Western Atlantic, the SSH impact on the SST along the African coast including all the terms of the heat budget, the interaction with the upwelling areas and the interannual study of the Kelvin waves in relation to the proposed mechanism. The study of those topics is already in progress by the authors.

Acknowledgements: We are grateful to Christian Ethe and Gurvan Madec for kindly providing the model run outputs. We also thank Sabine Arnault, Serge Janicot, Vincent Echevin and Frédéric Vivier for stimulating discussions. This study has been supported by ANETUS (CNES/NASA) and the Spanish MCYT CGL2006-04471 and REN2002-03424 programs, which has also funded Irene Polo and her research stage at LOCEAN laboratory as part as her phD thesis.

References

Adamec D., and J. J. O'Brien (1978), The Seasonal Upwelling in the Gulf of Guinea Due to Remote Forcing, *J. Physical Oceanog., 8,* 1050-1060.

Aman A., L. Testut, P. Woodworth, T. Aarup and D. Dixon (2007), Seasonal Sea Level Variability in the gulf of Guinea from altimetry and tide gauge. Submitted.

Arnault, S., Y. Menard, and J. Merle (1990), Observing the tropical Atlantic Ocean in 1986--1987 from altimetry, *J. Geophys. Res., 95* (C10), doi: 10.1029/90JC00347.

Arnault S., L. Gourdeau and Y. Menard (1992), Comparison of the altimetric signal with in-situ measurements in the tropical Atlantic ocean, *Deep Sea Res., 39*(3/4), 481-499, 1992.

Berliand, M. E., and T. G. Strokina, (1980), Global distribution of the total amount of clouds, *Hydrometeorological Publishing House*, Leningrad, Russia, 71 pp.

Cazes-Boezio G., A. W. Robertson and C. R. Mechoso (2003), Seasonal Dependence of ENSO Teleconnections over South America and Relationships with Precipitation in Uruguay, *J. of Climate, 16*, 1159-1176.

Challenor, P.G., P. Cipollini, and D. Cromwell (2001), Use of the 3D radon transform to examine the properties of oceanic Rossby waves, *J. Atmos. Oceanic Technol., 18*,(9),1558-1566.

Chelton, D. B. and M. G. Schlax (1996), Global observations of oceanic Rossby waves, *Science*, *272*, 234-238.

Cipollini, P., D. Cromwell and G.D. Quartly (1996), Variability of Rossby wave propagation in the North Atlantic from TOPEX/POSEIDON altimetry. *Proc. IGARSS '96*, Lincoln, Nebraska, vol.1, 91-93.

Flatau M., P. J. Flatau, P. Phoebus and P. P. Niiler (1997), The Feedback between Equatorial Convection and Local Radiative and Evaporative Processes: The Implications for Intraseasonal Oscillations, *J. Atmos. Sci.*, 54, 2373-2386.

Florenchie P., J. R. E. Lutjeharms, C. J. C. Reason, S. Masson and M. Rouault (2003), The source of Benguela Niños in the South Atlantic Ocean, *Geophys. Res. Lett., 30*, 10, 1505.

Foltz, G. and M. McPhaden (2004), The 30-70 day oscillations in the tropical Atlantic. *Geophys. Res. Lett*., *31*(15): doi: 10.1029/2004GL020023.

Foltz, G.R. and M.J. McPhaden (2005), Mixed layer heat balance on intraseasonal time scales in the northwestern tropical Atlantic Ocean, *J. Climate, 18,* 4168-4184.

Fontaine, B., S. Janicot, and P. Roucou (1999), Coupled ocean–atmosphere surface variability and its climate impacts in the tropical Atlantic region, *Clim. Dyn., 15*, 451–473.

França, C., I. Wainer, A. R. De Mesquita, and G. J. Goni (2003), Planetary equatorial trapped waves in the Atlantic Ocean from TOPEX/Poseidon altimetry, *in*: Goni, G.J.; Malanotte-Rizzoli, P. (Ed.) (2003). *Interhemispheric water exchange in the Atlantic Ocean. Elsevier Oceanography Series, 68,* 213-232.

Fu, L. L., and D. B. Chelton (2001), *Satellite Alitmetry and Earth Sciences*, chapter Large scale ocean circulation, pp. 133–169, Academic Press.

Garcia-Serrano J., T. Losada, B. Rodriguez-Fonseca and I Polo (2007), Tropical Atlantic Variability modes (1979-2002). Part II: Atmospheric response to SST-forced tropical convection. J. Climate (under revision).

Gill A. E. (1982), Atmosphere-Ocean Dynamics. Academic Press. 662 pp. ISBN 0122835220

Grodsky S. A., J. A. Carton, C. Provost, J. Servain, J. A. Lorenzzetti and M. J. McPhaden (2005), Tropical instability waves at 0ºN, 23ºW in the Atlantic: A case study using Pilot Research Moored Array in the Tropical Atlantic (PIRATA) mooring data, *J. Geophys. Res*., *110*,C08010, doi: 10.1029/2005JC002941.

Han, W., P.J. Webster, J. Lin, W.T. Liu, R. Fu, D. Yuan, and A. Hu (2008), Dynamics of intraseasonal sea level and thermocline variability in the equatorial Atlantic during 2002-2003*, J. Phys. Oceanogr*., in press

Handoh I. C. and G. R. Bigg (2000), A self-sustaining climate mode in the Tropical Atlantic, 1995-97: Observations and modelling, *Q J R. Meteo. Soc., 126*, 807-821.

Hendon, H. H., B. Liebmann, and J. D. Glick (1998), Oceanic Kelvin waves and the Madden-Julian Oscillation, J. Atmosph. Sci., 55, 99-101.

Hill, K. L., I. S. Robinson, and P. Cipollini (2000), Propagation characteristics of extratropical planetary waves observed in the ATSR global sea surface temperature record, *J. Geophys. Res., 105*(C9), 21927-21945.

Illig S., B. Dewitte, N. Ayoub, Y. du Penhoat, G. Reverdin, P. De Mey, F. Bonjean and G. S. Lagerloef (2004), Interannual long equatorial waves in the tropical Atlantic form a high resolution ocean general circulation model experiment in 1981-2000, *J. Geophys. Res*., *109,* C02022, doi. 101029/2003JC001771.

Jacobs G.A., H. E. Hurlburt, J. C. Kindle, E. J. Metzger, J. L. Mitchell, W. J. Teague, and A. J. Wallcraft (1994), Decade-scale trans-Pacific propagation and warming effects of an El Niño anomaly, *Nature*, 370, 360-363.

Katz, E.J. (1997), Waves along the equator in the Atlantic, *J. Phys. Oceanogr., 27*, 2536–2544.

Kayano, M. and V. Kousky (1999), Intraseasonal (30-60 day) variability in the global tropics: principal modes and their evolution, *Tellus , 51*, 373-386.

Kessler W. S. (1991), Can Reflected Extra-equatorial Rossby Waves Drive ENSO?, *J. Phys. Oceanogr., 21*, 444-452.

Kessler, WS, MJ McPhaden, and KM Weickmann (1995), Forcing of intraseasonal Kelvin waves in the equatorial Pacific, *J. Geophys. Res., 100*, 10613-10631.

Killworth, P. D., D. B. Chelton and R. de Szoeke (1997), The speed of observed and theoretical long extratropical planetary waves, *J. Phys. Oceanogr., 27,* 1946-1966.

Latif, M., and A. Grötzner (2000), On the equatorial Atlantic oscillation and its response to ENSO, *Clim. Dyn.*, *16*, 213-218.

Leewenburgh O., and D. Stammer (2001), The Effect of Ocean Currents on Sea Surface Temperature Anomalies. *J. Phys. Oceanogr., 31*, 2340-2358.

Levitus, S., (1998), Climatological Atlas of the world ocean. Tech. Rep. 13, NOAA, Rockville, Md.

Liebmann B. and C. A. Smith (1996), Description of a Complete (Interpolated) Outgoing Longwave Radiation Dataset, *Bull. Amer. Meteor. Soc., 77*, 1275-1277.

Liebmann B., G. N. Kiladis, J. A. Marengo, T. Ambrizzi and J. D. Glick (1999), Submonthly Convective Variabiltiy over South America and the South Atlantic Convergence Zone, *J. Climate, 12*, 1877-1891.

Madden R. and P. Julian (1994), Observations of the 40-50 day tropical oscillation: A review. *Mon. Wea. Rev* ., *112*, 814-837.

Madec, G., P. Delecluse, M. Imbard, and C. Lévy (1998), OPA 8.1 Ocean General Circulation Model reference manual. *Note du Pôle de modélisation*, Institut Pierre-Simon Laplace, N°11, 91pp.

Matthews, A., P. Singhruck and K. J. Heywood (2007), Deep Ocean Impact of a Madden-Julian Oscillation Observed by Argo Floats, *Scienc*e, vol. 318, 1765-1769.

Moore, D. W., P. Hisard, J.P. McCreary, J. Merle, J. J. O'Brien, J. Picaut, J.;. Verstraete and C. Wunsch (1978), Equatorial adjustment in the eastern Atlantic, *Geophys. Res. Lett*., 5, 637-640.

Musman, S. (1992), Geosat altimeter observations of long waves in the equatorial Atlantic, *J. Geophys. Res. 97*, 3573–3579.

Park, C. K, S. D. Schubert (1993), Remotely Forced Intraseasonal Oscillations over the Tropical Atlantic, *J. Atmos. Sci., 50*, 1, 89-103.

Philander, S. G. H. (1990), *El Niño, La Niña, and the Southern Oscillation.*International Geophysics Series, Vol. 46, Academic Press, 293 pp.

Picaut J. (1983), Propagation of the seasonal upwelling in the eastern equatorial Atlantic, *J. Phys. Oceanogr*., vol 13, 18-37.

Polito, P. S., and P. Cornillon (1997), Long baroclinic Rossby waves detected by TOPEX/POSEIDON, *J. Geophys. Res.*, *102*, 3215-3235.

Polo I., B. Rodríguez-Fonseca and J. Sheinbaum (2005), Northwest Africa upwelling and the Atlantic climate variability, *Geophys. Res. Lett., 32*, L23702, doi:10.1029/2005GL023883.

Polo I., A. Lazar, B. Rodriguez-Fonseca, S. Arnault and G. Mainsant (2008a), Oceanic Kelvin Waves and Tropical Atlantic intraseasonal Variability. Part I: Kelvin wave characterization, J. Geophys. Res (under revision).

Polo I., B. Rodriguez-Fonseca, T. Losada and J. Garcia-Serrano (2008b), Tropical Atlantic Variability modes (1979-2002). Part I: time- evolving SST modes related to West African rainfall, J. Climate (under revision).

Rodríguez-Fonseca B., I. Polo, E. Serrano and M. Castro (2006), Evaluation of the north Atlantic SST forcing on the European and northern African winter climate, *Int. J. Climatology*., *25* doi: 10.1002/7joc.1234

Rouault, M. S. Illig, C. Bartholomae, C. J. C. Reason and A. Bentamy (2007), Propagation and origin of warm anomalies in the Angola Benguela upwelling system in 2001, *J. Mar. Syst*. doi: 10.1016/j.jma jmarsys.2006.1 rsys. 2006.11.010 1.010

Roundy P. E., and G. N. Kiladis (2006), Observed Relationships between Oceanic Kelvin Waves and Atmospheric Forcing, *J. Climate, 19*, 5253-5271.

Servain, J., J. Picaut, and J. Merle (1982), Evidence of Remote Forcing in the Equatorial Atlantic Ocean, *J. Phys. Oceanogr.,* 12, 457-463.

Schouten M. W., R. P. Matano and T. P. Strub (2005), A description of the seasonal cycle of the equatorial Atlantic from altimeter data, *Deep Sea Res*., *52*, 477-493.

Stammer, D. (1997), Global Characteristics of Ocean Variabiltiy Estimated from Regional TOPEX/POSEIDON altimeter Measurements, *J. Phys. Oceanogr., 27*, 1743-1769.

Trenberth, K. E., J. G. Olson, and W. G. Large (1989), A global ocean wind stress climatology based on the ECMWF analyses. National Center for Atmospheric Research, NCAR/TN-338+STR, Boulder, Colorado, 93 pp.

UNESCO (Ed.), (1996), Discharge of selected rivers of the world. Volume II (Part II), UNESCO Publishing.

Uppala, S. M., and co-authors (2005), The ERA-40 Reanalysis, *Quart. J. Roy. Meteor. Soc.*, 131, 2961-3012. doi: 10.1256/gj04176.

Vivier, F., K. A. Kelly and L. Thompson (1999), Contributions of wind forcing, waves, and surface heating to sea surface height observations in the Pacific Ocean, *J. Geophys. Res. (Oceans)*, *104*(C9), 20767-20788.

Wang, C. (2006), An overlooked feature of tropical climate: Inter-Pacific-Atlantic variability, *Geophys. Res. Lett.*, *33*, L12702, doi: 10.1029/2006GL026324.

Woolnough S. J., J. M. Slingo and B. J. Hoskins (2000), The Relationship between Convection and Sea Surface Temperature on Intraseasonal Timescales, *J. Climate*, 13, 2086-2104.

Xie, P., and P. A. Arkin, (1996), Analysis of global monthly precipitation using gauge observations, satellite estimates and numerical model predictions, *J. Climate,* 9, 840-858.

5. INTEGRATED DISCUSSION

A discussion that integrates the aspects of Tropical Atlantic Variability (TAV) at interannual and intraseasonal scales examined in this PhD Thesis is presented in this section. Thus, the initial hypotheses (Chapter 2) and the results will be evaluated and compared with the recent literature (Chapter 1).

Regarding the **interannual TAV** (Chapter 4.1), it was first hypothesized that the TAV could have an important impact over the European winter precipitation and West African (WA) summer rainfall.

Concerning the precipitation modes, the leading winter European and Northern Africa (ENA) precipitation mode appears as a dipole-like structure with opposite sign anomalies over the North (British Isles and Scandinavia peninsula) and the South (Iberian Peninsula, North Africa and some Mediterranean regions). This dipolar pattern is mainly related to the North Atlantic Oscillation (NAO), in agreement with other authors (Hurrrell, 1995). The first two summer WA rainfall Empirical Orthogonal Functions (EOF) variability modes have been determined as Sahelian and Guinean rainfall patterns, which appear as uncoupled modes. In contrast to other works that use CRU dataset, different time period and/or different methodologies (Bader and Latif, 2007; Douville et al., 2007), no evidences for a Dipole pattern are found with CMAP dataset.

The Sea Surface Temperature (SST) modes with an impact on the precipitation over these areas have been filtered out. On the one hand, Subtropical North Atlantic (SNA) SST mode is found to have an impact on the winter ENA precipitation anomalies resulting in the NAO-like precipitation pattern (Chapter 4.1.1). Despite other authors have explained the European precipitation dipole by the NAO influence (Hurrell, 1995), a particular Sea Level Pressure (SLP) pattern is found associated with the SNA SST anomalies impacting winter European precipitation. This SLP pattern seems to be a hybrid of the SLP modes linked to the first two European precipitation modes.
Other authors have recognized the persistence, from summer to winter, of the SST Tripole pattern from lag to lag Maximun Covariance Analysis (Czaja and Frankignoul, 1999; Wen et al., 2005). In this PhD Thesis, it is found that the Atlantic Tripole SST pattern seems to develop from summer Horseshoe SST pattern in interaction with the atmosphere (see Appendix II).
On the other hand, the Equatorial Mode (EM) is found to have an impact on the West African summer rainfall constituting a tight coupled mode (Chapter 4.1.2) in agreement with other authors (Fontaine and Janicot, 1996; Ward, 1998). In this work, the EM affects the anomalous rainfall along the coast of the Gulf of Guinea (GG) in summer, and over the Amazon region in autumn-winter. The SST anomalies over the Mediterranean Sea are closely associated with the Sahelian rainfall variability, a relationship also suggested by other authors (Rowell et al., 2001), although underestimated in comparison with the Pacific influence. From an Extended Maximum Covariance Analysis (EMCA), some seasonal predictability features of these modes have been evidenced, such as SST persistence and time evolution from previous seasons.

The second main hypothesis proposed in the objectives was that the mechanisms at work in the TAV are not only related to thermodynamics, but also to the ocean dynamics. The latter could be important for explaining the SST variability, through the oceanic waves, mixing and upwelling processes.

In contrast with other authors that have related the SST variability over the Subtropical areas mainly to turbulent and radiative heat fluxes (Frankignoul and Kestenare, 2005; Barreiro et al., 2004; Sterl and Hazeleger, 2003), in this study, the SNA appears to be also affected by the ocean dynamics. The results suggest a positive feedback between the SST and the surface winds over the SNA region (Chapter 4.1.1) as shown also by Okumura et al., (2001). In addition, it is found that the Mauritanian/Senegal upwelling system can, in part, be responsible

of the appearance and/or persistence of the SNA SST anomalies, while the latent heat fluxes tend to damp the SST anomalies one month later (Chapter 4.1.1).

Regarding the EM, some studies from different time periods have shown that this mode is driven by anomalous winds over the western equatorial Atlantic (Zebiak, 1993; Ruiz-Barradas et al., 2000), which can be forced by the Pacific basin (Latif and Grötzner, 2000). Some authors have also linked the Benguela Niños with equatorial Kelvin waves from the SST anomalies over the central equator (Florenchie et al., 2003). However, the results from this PhD Thesis have highlighted the different behaviour of this mode in recent decades. The analysis (Chapter 4.1.2) has pointed out that, in the period studied, this mode starts from the Angola/Benguela region from the previous late-winter, and the development of the mode occurs from ocean-atmosphere feedbacks. The evolution could be related to westward oceanic Rossby waves propagation from the southwest African coast, while the damping is, in part, based on the oceanic adjustment by equatorial waves from an offshore forcing. The impact on the WA rainfall comes from heat flux anomalies over the warm SSTs that, besides the decay of the mode, help to transfer anomalous moisture inland in summer (Chapter 4.1.2).

Therefore, the Tropical Atlantic (TA) coastal upwelling systems (Mauritanian/Senegal and Angola/Benguela upwelling systems) have a decisive role on the TAV, as was hinted at by other authors (Carton et al., 1996; Mayer et al., 2001; Seager et al., 2001). Moreover, these upwelling systems are important in SST variability modes that have an impact on precipitation.

Regarding the methodology, it has been revealed that the application of the EMCA, which includes the lagged-time series on the predictor field matrix, is very reliable for predictability issues, especially in those modes that evolve phase-locked with the seasonal cycle. This cannot be achieved with the traditional MCA applied lag-to-lag individually (Peng et al., 1995; Frankignoul and Kestenare, 2005, Wen et al., 2005, among others).

The new observational data network over the TA (TAOSTA, PIRATA, T/P) have allowed to determine the thermal upper ocean role on the SST variability, in comparison with previous works that are based on model data (Carton et al., 1996; Seager et al., 2001) or on very sparse observed data (Hastenrath and Merle, 1987). The period of study has shown several tendencies that could be related, in part, to the “climate shift” and/or to decadal variability (Zhang and Delworth, 2006; Dong et al., 2006). One of these peculiarities is the linkage between the EM and the equatorial Pacific. Although the Atlantic Niño and Pacific Niño relationship was also suggested by Wang (2006) and Keenlyside and Latif, (2007), here EM-WA rainfall coupled mode is found to be possibly leading the Pacific Niña by 6 months in advance (Chapter 4.1.2). An Atlantic-Pacific SST gradient oscillation coupled to the anomalous equatorial convection belt had never been reported before.

Due to the above-explained evidences about the ocean role on TAV, this work has also studied in depth the air-sea interaction mechanisms implied in the **intraseasonal TAV** (Chapter 4.2). In particular, this work has provided new and sound insights into TA intraseasonal Kelvin wave activity. It was essential to investigate it thoroughly, in the light of the recent Aviso T/P dataset and state of the art OGCM[1], considering how often the remote forcing by Kelvin waves has been invoked to interpret TA variability, particularly in the vicinity of the Angola/Benguela upwelling system (Florenchie et al., 2003; Rouault et al., 2007), as well as in the coast of the GG (Servain et al., 1982; Picaut, 1983; Aman et al., 2007).

One hypothesis largely assumed has been that the source of the equatorial Kelvin wave can be attributed to zonal wind burst over the western equatorial Atlantic (Philander, 1990; Katz, 1997; Han et al., 2008) and/or Rossby reflection from the eastern South American coast. Also it has been hypothesized that these equatorial and coastal areas could highly be affected by the oceanic waves mainly by impacting the SST (Leewenburgh and Stammer 2001), which in turn, could have a feedback to the atmosphere.
The available data of the satellite period and the spatial-time scales of the oceanic waves, make the intraseasonal timescales the most useful to study waves. The 30-60 days period is found to be important for the Kelvin wave activity in the TA (Chapter 4.2), which is also an important

[1] Ocean General Circulation Model

range-scale for convection and wind variability. For instance, the Madden Julian Oscillation (MJO) occurs at these timescales (Madden and Julian, 1994) and an intraseasonal oscillation over the Azores High has been evidenced in the TA (Chapter 4.2).

The analysis of the atmospheric forcing in boreal autumn-winter has underlined the importance of an off-equatorial anomalous Ekman pumping, maximum around 4ºN in the western basin, associated with basin-scale wind stress anomalies over the North Atlantic. The western pumping is responsible for triggering equatorial Kelvin waves. Regarding Rossby waves, they are found to radiate from the West African coast and to reach the American coast. However, the reflection at the coast and the transformation to Kelvin waves is very difficult to identify (Chapter 4.2) as other authors had reported (Illig et al, 2004). The same interaction at interannual scales is suggested for the EM development and damping: Rossby waves radiating from the African coast, and propagating anomalies up to 30ºW, and equatorial Kelvin waves generated off-equator (Chapter 4.2).

In the same manner, the scenario of coastally trapped Kelvin waves propagating along the African coast and reaching the Mauritanian/Senegal Upwelling system in not clearly supported by the available data, although they could be acting as a feedback in phase with the wind stress perturbation (Chapter 4.2). In the south, however, lag correlation suggests, to the contrary, a significant control (about 15% of the variance) by Kelvin waves over the front of the Angola-Benguela upwelling (~12ºS). In fact, it is believed that the lack of clear propagation within the upwelling region is due to the wind forcing, which dominates the Sea Surface Height (SSH) variability and hence masks the wave effect. Nevertheless, Kelvin waves should have an impact on the SST variability through anomalous advection by quasi-geostrophic currents and vertical mixing changes due to thermocline depth anomalies. These effects are expected to be the largest near the strong SST gradients observed within the eastern basin upwellings.

5. DISCUSIÓN INTEGRADORA

Una discusión integradora sobre los aspectos de la Variabilidad del Atlántico Tropical (TAV[1]) a escalas interanuales e intraestacionales, tratados en esta Memoria de Tesis doctoral, es presentada en este Capítulo. De este modo, las hipótesis iniciales (Capítulo 2) y los resultados serán evaluados y comparados con la literatura reciente (Capítulo 1).

En lo que respecta a la **Variabilidad interanual el Atlántico Tropical** (Capítulo 4.1), primero se hipotetizó que la TAV podría tener un impacto importante sobre los regímenes anómalos de la precipitación invernal en Europa y de la lluvia estival en el Oeste de África (WA[2]).

Respecto a los modos de precipitación, el principal modo de precipitación invernal en Europa y el Norte de África (ENA) aparece como una estructura dipolar con anomalías de signo opuesto en el norte (Islas Británicas y Península Escandinava) y el sur (Península Ibérica, África del Norte y algunas regiones mediterráneas). Este patrón dipolar está principalmente relacionado con la NAO[3], de acuerdo con otros autores (Hurrrell, 1995). Los dos primeros modos EOF[4] de variabilidad de lluvia estival en WA han sido determinados como patrones de lluvia del Sahel y de Guinea y aparecen como modos desacoplados. En contraste con otros trabajos que usan datos procedentes de CRU, diferentes períodos de tiempo y/o diferentes metodologías (Bader y Latif, 2007; Douville et al., 2007), no se han encontrado evidencias de un patrón Dipolar mediante el empleo de datos CMAP.

Se han filtrado los modos de la Temperatura Superficial del Mar (SST) con un impacto en la precipitación sobre estas áreas. Por un lado, se ha encontrado que las anomalías de la SST sobre el Atlántico Norte Subtropical (SNA[5]) tienen un impacto en las anomalías de la precipitación invernal en ENA, con un patrón de precipitación similar a la NAO (Capítulo 4.1.1). A pesar de que otros autores han explicado el dipolo de precipitación europeo por la influencia de la NAO (Hurrell, 1995), se ha encontrado un patrón de presión al nivel de mar (SLP[6]) particular asociado con las anomalías en la SST sobre SNA que impacta en la precipitación invernal europea. Este patrón de SLP parece ser un híbrido de los patrones de SLP ligados a los dos primeros modos de precipitación en Europa.
Otros autores han descrito la persistencia desde el verano hasta el invierno de las anomalías subtropicales ligadas al Tripolo Atlántico de SST con la metodología MCA[7] desfase a desfase (Czaja y Frankignoul, 1999; Wen et al., 2005). En esta Memoria, el patrón del Tripolo Atlántico de SST parece desarrollarse desde el patrón estival de Herradura de SST, en interacción con la atmósfera (ver apédice II).
Por otro lado, se ha encontrado que el Modo Ecuatorial (EM[8]) tiene un impacto en la lluvia estival del Oeste de África constituyendo un modo fuertemente acoplado (Capítulo 4.1.2), de acuerdo con otros autores (Fontaine and Janicot, 1996; Ward, 1998). El EM afecta a la lluvia anómala a lo largo de la costa del Golfo de Guinea (GG) en verano y sobre la región amazónica en otoño-invierno. Las anomalías de SST sobre el mar Mediterráneo están estrechamente asociadas con la variabilidad de la lluvia en el Sahel, una relación sugerida también por otros autores (Rowell et al., 2001), aunque subestimada en comparación con la influencia del Pacífico. A partir de una metodología Extendida del Analisis de Máxima Covarianza (EMCA[9]), se han detectado algunas características de la predecibilidad estacional

[1] Del inglés Tropical Atlantic Variability
[2] Del inglés West Africa
[3] Del inglés North Atlantic Oscillation
[4] Del inglés Empirical Orthogonal Functions
[5] Del inglés Subtropical North Atlantic
[6] Del inglés Sea Level Pressure
[7] Del inglés Maximum Covariance Analysis
[8] Del inglés Equatorial Mode
[9] Del inglés Extended Maximum Covariance Analysis

de estos modos de SST que impactan en la precipitación, tales como la persistencia y la evolución temporal de las anomalías de SST desde estaciones previas.

La segunda hipótesis propuesta en los objetivos fue que los mecanismos que operan en la TAV no sólo están relacionados con la termodinámica, sino también con la dinámica oceánica. Ésta última podría ser importante para explicar la variabilidad de la SST, a través de las ondas oceánicas, procesos de mezcla y de afloramiento.

En contraste con otros autores que han relacionado la variabilidad de la subtropical de la SST principalmente con flujos de calor radiactivos y turbulentos (Frankignoul y Kestenare, 2005; Barreiro et al., 2004; Sterl y Hazeleger, 2003), en este estudio, la SST sobre el SNA parece estar afectada también por la dinámica oceánica. Los resultados sugieren una realimentación positiva entre la SST y los vientos superficiales sobre la región del SNA (Capítulo 4.1.1) como ya mostró Okumura et al., (2001). Además, se ha encontrado que el sistema de afloramiento de Mauritania/Senegal puede, en parte, ser responsable de la aparición y/o persistencia de las anomalías de SST en el SNA, mientras que los flujos de calor latente tenderían a amortiguar las anomalías de la SST un mes después (Capítulo 4.1.1).

Respecto al EM, algunos estudios a partir de diferentes períodos de tiempo han mostrado que este modo es originado por vientos anómalos sobre el Atlántico ecuatorial occidental (Zebiak, 1993; Ruiz-Barradas et al., 2000), que podrian ser forzados desde la cuenca del Pacífico (Latif y Grötzner, 2000). Algunos autores han relacionado también los Niños de Benguela con las ondas ecuatoriales de Kelvin provenientes de las anomalías de la SST sobre el ecuador central (Florenchie et al., 2003). Sin embargo, los resultados de esta Memoria han resaltado el distinto comportamiento de este EM en décadas recientes. El análisis (Capítulo 4.1.2) ha apuntado que, en el período de estudio, este modo comienza en la región de Angola/Benguela desde el finales del invierno anterior; y el desarrollo del modo ocurre a partir de interacciones océano-atmósfera. La evolución podría estar relacionada con la propagación hacia el oeste de ondas de Rossby desde la costa del suroeste de África. El amortiguamiento del modo, en parte, se basaría en el ajuste oceánico a través de una onda ecuatorial de Kelvin forzada fuera del ecuador. El impacto sobre la lluvia en el WA vendría por las anomalías de flujo de calor latente sobre las SSTs cálidas, que además de amortiguar el modo, ayudan a transferir humedad anómala sobre continente en verano (Capítulo 4.1.2).

Por tanto, los sistemas de afloramiento costero del TA (sistemas de afloramiento de Mauritania/Senegal y de Angola/Benguela) tienen un papel decisivo en la TAV, como aludieron otros autores (Carton et al., 1996; Mayer et al., 2001; Seager et al., 2001). Aún más, estos sistemas de afloramientos son importantes en los modos de SST que tienen un impacto en la precipitación.

Respecto a la metodología, se ha revelado que la aplicación del EMCA, que incluye series desfasadas en la matriz del campo predictor, ha sido muy fiable para el estudio de predecibilidad estacional, especialmente en los modos que evolucionan en fase con el ciclo estacional. Esto no puede lograrse aplicando el método tradicional MCA individualmente desfase a desfase como muchos autores lo han usado (Peng et al., 1995; Frankignoul y Kestenare, 2005, Wen et al., 2005; entre otros).

La nueva red de datos observacionales sobre el TA (TAOSTA, PIRATA, T/P) ha permitido determinar el papel térmico del océano superior en la variabilidad de la SST, en comparación con trabajos previos que estaban basados en datos de modelos (Carton et al., 1996; Seager et al., 2001) o muy escasos datos observados (Hastenrath y Merle, 1987). El período de estudio ha mostrado varias tendencias que podrían estar, en parte, relacionadas con la llamada “transicion climática” y/o con variabilidad interdecadal (Zhang y Delworth, 2006; Dong et al., 2006). Una de estas peculiaridades es el vínculo entre el EM y el Pacífico ecuatorial. Aunque la relación entre el Niño Atlántico y Pacífico fue también sugerida por Wang (2006) y Keenlyside y Latif, (2007), aquí se ha encontrado que posiblemente el modo acoplado de SST y lluvia podría liderar a una Niña del Pacífico seis meses antes (Capítulo 4.1.2). Una oscilación del gradiente de la SST entre el Atlántico y el Pacífico, acoplado con la convección anómala en el cinturón ecuatorial, no había sido descrita anteriormente.

Debido a las evidencias arriba explicadas sobre el papel del océano en la TAV, este trabajo también ha estudiado en profundidad los mecanismos de interacción aire-mar implicados en la **Variabilidad intraestacional del Atlántico Tropical** (Capítulo 4.2). En particular, este trabajo ha aportado nuevos y sólidos elementos sobre la actividad de ondas de Kelvin a escalas intraestacionales en el TA. Era esencial investigar a fondo esta actividad, a la luz del reciente conjunto de datos Aviso T/P[10] y el estado del arte de OGCM[11], considerando con qué frecuencia el forzamiento remoto de las ondas de Kelvin ha sido invocado para interpretar la variabilidad del sistema de afloramiento de Angola/Benguela (Florenchie et al., 2003; Rouault et al., 2007), así como del afloramiento en la costa del GG (Servain et al., 1982; Picaut, 1983; Aman et al., 2007).

Una hipótesis ampliamente asumida ha sido que la fuente de la onda de Kelvin ecuatorial puede ser atribuida a ráfagas de viento zonal sobre el Atlántico ecuatorial occidental (Philander, 1990; Katz, 1997; Han et al., 2008) y/o la reflexión de ondas de Rossby en la costa oriental de Sudamérica. También se ha hipotetizado que las áreas ecuatoriales y costeras podrían ser altamente afectadas por las ondas oceánicas, impactando principalmente sobre la SST (Leewenburgh y Stammer 2001), la cual a su vez, podría tener una respuesta hacia la atmósfera.

Los datos disponibles del período de satelite y las escalas de espacio-temporales de las ondas oceánicas hacen que las escalas de tiempo intraestacionales sean las más útiles para el estudio de las ondas. Se ha visto que la periodicidad de 30-60 días es importante en la actividad de las ondas de Kelvin en el TA (Capítulo 4.2). Esta periodicidad es también importante en la variabilidad del viento y la convección a gran escala. Por ejemplo, la MJO[12] (Madden and Julian, 1994) ocurre a esas escalas de tiempo, y se ha evidenciado sobre el TA una oscilación intraestacional sobre la Alta de Azores (Capitulo 4.2).

El análisis del forzamiento atmosférico en el otoño-invierno ha indicado la importancia de un bombeo de Ekman anómalo fuera del ecuador, máximo sobre 4ºN, en el oeste de la cuenca, asociado con anomalías del esfuerzo del viento a gran escala sobre el Atlántico Norte. El bombeo en el oeste es responsable del disparo de las ondas de Kelvin ecuatoriales. Respecto a las ondas de Rossby, se han encontrado evidencias de radiación de estas ondas desde la costa de África occidental, alcanzando la costa tropical Americana. Sin embargo, la reflexión en la costa y la transformación en ondas de Kelvin es muy difícil de identificar (Capítulo 4.2), como otros autores ya habian apuntado (Illig et al., 2004). El papel de las ondas oceánicas en la TAV a escalas interanuales ha sido evidenciado como importante en el desarrollo y amortiguamiento del EM: ondas de Rossby radiando desde la costa africana, propagando anomalías hacia el oeste hasta 30ºW y ondas ecuatoriales de Kelvin hacia el este que son generadas fuera del ecuador (Capítulo 4.2).

De la misma forma, el escenario de las ondas de Kelvin atrapadas en la costa propagándose a lo largo de la costa africana y alcanzando el sistema de afloramiento de Mauritania/Senegal está claramente apoyado con los datos disponibles, a pesar de que podrían estar actuando en fase con la respuesta a la perturbación del esfuerzo del viento (Capítulo 4.2). En el sur, sin embargo, correlaciones desfasadas sugieren, por el contrario, un control significativo (sobre 15% de la varianza) por ondas de Kelvin sobre el frente de Angola/Benguela (~12ºS). De hecho, se cree que la falta de claridad en la propagacion en estas zonas de afloramiento es por el forzamiento del viento, el cual domina la variabilidad de la altura de la superficie del mar (SSH[13]) y por tanto enmascaran el efecto de la onda. No obstante, las ondas de Kelvin deberían tener un impacto en la variabilidad de la SST a través de la advección anómala por corrientes cuasi-geostróficas y cambios en la mezcla vertical por anomalías de la profundidad de la termoclina. Estos efectos se esperan que sean más grandes cerca de los fuertes gradientes de SST que se observan en los afloramientos del este de la cuenca.

[10] Del inglés: Topex/Poseidon Satellite
[11] Del inglés Ocean General Circulation Model
[12] Del inglés Madden Julian Oscillation
[13] Del inglés Sea Surface Height

6. CONCLUSIONS

The main contributions of this PhD Thesis to the state of the art of TAV at interannual and intraseasonal timescales are summarized as follows:

- The leading Atlantic SST mode, connected to winter European and North of Africa anomalous precipitation, coincides with the Atlantic Tripole which is known to be coupled to the NAO. The subtropical branch of this SST pattern persists from the previous summer months giving a predicting value to this region. The better skill scores have been found over the Iberian Peninsula and North of Africa when predicting the anomalous winter precipitation from summer SNA SST anomalies.

- The anomalous SST signal obtained for 1960–1996 is a robust pattern, also present in 1900–1930 and 1931–1960 periods. However, the Horseshoe-Atlantic Tripole transition is enhanced in the last period.

- The mode that captures the time-evolution of the summer Horseshoe SST pattern into the winter Tripole SST pattern for 1979-2001 suggests that the transition is forced to a large extent by changes in the TA atmosphere.

- The winter SNA SST anomalies are explained by wind-induced latent heat flux changes and by the water column temperature variability over Mauritanian/Senegal coast. A strengthening (weakening) of the northerly wind stress induces more (less) latent heat flux release to the atmosphere and an enhancement (weakening) of the coastal upwelling. Both factors are contributing to the decrease (increase) in the SSTs from the previous months. The heat flux seems to be responsible for damping these SST anomalies one month later.

- An Extended MCA has been designed in order to extract covariability modes, using a time-evolving predictor in relation to a predictand field. This methodology is reliable to find varying patterns that are phase-locked to the seasonal cycle.

- The leading TA SST- WA rainfall EMCA mode shows the evolution of the EM associated with the Guinean rainfall pattern. The origin of the SST pattern occurs at the Angola/Benguela upwelling area due to an anomalous alongshore wind stress over this region. The wind anomalies over the Southeast Atlantic could be associated with a previous anomalous subsidence over the Amazon basin, which could have had an influence on weakening the South Subtropical High pressure system.

- The SSH anomalies associated with this SST mode suggest a westward propagation, as a Rossby oceanic wave, from Southeastern Atlantic as far as 30ºW. An opposite sign SSH anomaly induced at west off-equator propagates eastward as an equatorial oceanic Kelvin wave, helping to damp the SST anomalies. The latent heat flux anomalies and the reversion of the wind anomalies also contribute to restore the normal conditions over the TA.

- The EM appears associated with opposite SST and rainfall anomalies over the central-eastern equatorial Pacific. The results suggest that the summer EM could be leading the development of a Pacific La Niña the following winter.

- The EM is associated with anomalous rainfall over the whole equatorial Atlantic band from summer to autumn. The precipitation evolves westward, restoring the deep convection and finally it is confined over the northeastern Brazil in winter. No significant rainfall has been evidenced over the North Atlantic-Europe during these seasons.

- The second TA SST- WA rainfall EMCA mode relates the anomalous Sahelian rainfall with an anomalous SST pattern over the SNA and Mediterranean Sea. The analyses done for the independent basis have shown the Mediterranean SST pattern as the major contributor to WA rainfall, while the direct influence of the SNA on the WA rainfall is not clear.

- Oceanic Kelvin wave activity has been found over the TA at intraseasonal timescales for the period 1993-2000, with a predominant 50 day period and ~2 cm of amplitude. The estimated propagation phase speeds are found to be in the range between the first and second theoretical Kelvin baroclinic modes (from 1.4 m/s to 2.6 m/s). The results are consistent with the observed and modelled SSH.

- The Kelvin waves propagate eastward from west equatorial Atlantic to the west African coast where they split and travel poleward, coastally trapped as far as ~12 degrees latitude. This Kelvin wave activity is associated with thermocline depth changes.

- The western equator SSH can explain about 25% of the intraseasonal variability of the GG coastal upwelling and 15% of the intraseasonal variability of the Angola/Benguela upwelling via Kelvin waves. However, the SSH variability over the Mauritanian/Senegal upwelling region is less influenced by the wave propagations.

- The complex intraseasonal Kelvin wave activity has been simplified down to two synthetic signals: an intraseasonal climatology and an Extended EOF mode. Intraseasonal climatology has shown that the main Kelvin wave activity occurs in boreal autumn-winter season. The fact that winter Kelvin wave activity appears as a SSH variability mode highlights the importance of the waves in the context of the TAV.

- The local wind anomalies over the western equatorial Atlantic cannot explain the beginning of the Kelvin waves in the western equator. However, over the Central-eastern equatorial Atlantic, the wind stress is controlling part of the SSH variability. There is evidence of some Rossby wave radiation events from the GG, mostly in boreal late spring-summer season. However, the Rossby waves' reflection at the American coast mechanism does not explain the triggering of the identified equatorial Kelvin waves.

- A mechanism, *Ekman pumping ITCZ shift-induced anomalies,* is proposed to explain the triggering of Kelvin waves. Basin-scale wind stress anomalies over the Northwest TA are coherent with anomalous convection at both sides of 10N and anomalous Ekman pumping at west-central off-equator, which induces SSH anomalies over a wide band ~2ºN-6ºN. These SSH anomalies show continuity with the beginning of the equatorial Kelvin waves. The wind stress and the convection oscillations are signatures of Inter-Tropical Covergence Zone (ITCZ)-shifts at intraseasonal scales.

- When southerly (northerly) wind stress anomalies occur at the western Atlantic, the ITCZ and the upwelling band shift northward (southward). This situation leaves the west-central band at ~4N in an anomalous downwelling (upwelling) stage. The downward (upward) Ekman pumping anomalies impose positive (negative) SSH anomalies in a sufficient spatial scale for triggering equatorial Kelvin waves ~10 days after.

- Two TA convection patterns are found to be associated with the EEOF SSH mode: one associated with the proposed mechanism and the other associated with the MJO. The MJO seems to affect the SSH over the GG coast.

- The oscillating winds at the subtropical north Atlantic region are in phase with the arrival of the wave at the northern African coast. The EEOF SSH mode describes this in-phase relationship.

- Anomalous advection of mean SST by quasi-geostrophic currents associated with the winter EEOF SSH mode seems to affect the SST north of 10ºN over the African coast and some regions over the coast of the GG.

Future Research

The ocean dynamics associated with the upwelling areas over the TA need further investigation. An oceanic model is needed to discern and accurately quantify the ocean contribution to the SST variability, in order to include all the terms implying in the mixed layer variability.

In the same manner, the ocean-atmosphere interaction proposed mechanisms that explain the evolution of the SST modes which have an impact on precipitation, need to be tested using a coupled model.

From the EM-equatorial Pacific relationship, the study of the possible influence of the Atlantic atmospheric variations in summer onto the equatorial Pacific ocean dynamics from summer to winter need to be tested with a coupled model.

Despite oceanic Kelvin waves have been characterized over the TA, a finer understanding of the phase speeds and the thermocline response would require a modal analysis. The impacts on SST and the proposed mechanism for the triggering would require deeper analysis with a coupled model.

6. CONCLUSIONES

Las principales contribuciones de la Tesis al estado del arte de la Variabilidad del Atlántico Tropical (TAV[1]), a escalas interanuales e intraestacionales, podrían resumirse como sigue:

- El modo principal de covariabilidad entre la temperatura de la superficie del mar (SST[2]) anómala en el Atlántico y la precipitación invernal anómala en Europa y el norte de África coincide con el Tripolo Atlántico de SST; el cual es conocido por estar acoplado a la Oscilación del Atlántico Norte (NAO[3]). La rama subtropical de este patrón de SST (SNA[4]), persiste desde los meses de verano anteriores, lo que da un valor predictivo a esta región. La bondad de la predicción de la precipitación anómala inviernal es alta en algunas regiones de la Península Ibérica y el norte de África.

- La estructura de SST anómala obtenida para el periodo 1960-1996 es un patrón robusto, que también se encuentra presente en los periodos 1900-1930 y 1931-1960. Sin embargo, la transición del patrón de SST de Herradura a Tripolo Atlántico, se encuentra intensificada en el último periodo.

- El modo que captura la evolución temporal del patrón de SST de Herradura en el verano, a el patrón del Tripolo Atlántico en invierno, para el periodo 1979-2001; sugiere que la transición es forzada en gran medida por cambios en la atmósfera del Atlántico Tropical (TA[5]).

- Las anomalías de SST invernales sobre el SNA, son explicadas por cambios en el flujo de calor latente inducidos por el viento y por la variabilidad térmica de la columna de agua sobre la costa de Mauritania/Senegal. Un fortalecimiento (debilitamiento) del esfuerzo del viento del norte, induce más (menos) liberación de calor latente hacia la atmósfera y una intensificación (debilitamiento) del afloramiento costero. Ambos factores están contribuyendo a la disminución (aumento) de la SST desde meses anteriores. El flujo de calor latente parece ser el responsable del amortiguamiento de estas anomalías de SST un mes después.

- Una forma extendida del método de Análisis de Covarianza Máxima (MCA[6]) ha sido diseñada para extraer modos de covariabilidad con un campo predictor que evoluciona en el tiempo, en relación con un campo a predecir. Esta metodología EMCA es muy fiable para encontrar patrones que varían en fase con el ciclo estacional.

- El modo principal EMCA entre la SST en el TA y la lluvia sobre el Oeste Africano (WA[7]), muestra la evolución del Modo Ecuatorial (EM[8]) asociado con el patrón de lluvia de Guinea. El origen del patrón de SST transcurre en el área de afloramiento de Angola/Benguela, debido a un esfuerzo de viento anómalo a lo largo de la costa sobre esta región. Las correspondientes anomalías del viento sobre el Sureste Atlántico podrían estar, a su vez, relacionadas con una subsidencia anómala previa sobre la cuenca amazónica. Esta subsidencia anómala podría estar influyendo en el debilitamiento del sistema de Altas presiónes subtropicales de Santa Helena y, por tanto, en el viento.

[1] Del inglés Tropical Atlantic Variability
[2] Del inglés Sea Surface Temperature
[3] Del inglés North Atlantic Oscillation
[4] Del inglés Subtropical North Atlantic
[5] Del inglés Tropical Atlantic
[6] Del inglés Maximum Covariance Analysis
[7] Del inglés West Africa
[8] Del inglés Equatorial Mode

- Las anomalías de altura del nivel del mar (SSH[9]) asociadas con este modo de SST sugieren una propagación hacia el oeste, con caracterísitcas de onda oceánica de Rossby desde el Sureste Atlántico hasta 30ºW. Una anomalía de SSH de signo opuesto, inducida fuera del ecuador, se propaga hacia el este como onda ecuatorial de Kelvin oceánica, ayudando a amortiguar el EM. Las anomalías de flujo de calor latente y el restablecimiento de las anomalías del viento también contribuyen a restaurar las condiciones normales sobre el TA.

- El EM aparece asociado a anomalías de SST y de lluvia, de signo opuesto, sobre el Este y Centro del Pacífico ecuatorial. Los resultados sugieren que el EM en verano podría estar liderando el desarrollo de una Niña Pacífica en el siguiente invierno.

- El EM se encuentra asociado a lluvia anómala sobre toda la banda equatorial Atlántica desde el verano hasta el otoño. La precipitación evoluciona hacia el oeste, restaurando la convección profunda, y finalmente es confinada sobre el noreste de Brasil en invierno. No se ha encontrado lluvia significativa sobre el sector Euro-Atlántico durante estas estaciones.

- El segundo modo EMCA entre la SST en el TA y la lluvia sobre el WA, relaciona la precipitación anómala sobre el Sahel con un patrón de SST anómalo sobre el Mar Mediterráneo y el SNA. Los análisis realizados tomando las cuencas por separado, han mostrado que el patrón de anomalías de SST sobre el Mar Mediterráneo es el que tiene una mayor contribución en la lluvia sobre el WA; mientras que la influencia directa de la región SNA sobre la lluvia en el WA no parece significativa.

- Se ha encontrado actividad de ondas de Kelvin oceánicas sobre el TA a escalas de tiempo intraseacionales para el periodo 1993-2000, con un periodo predominante de 50 dias y ~2 cm de amplitud. Las velocidades de fase estimadas se encuentran dentro del rango teórico establecido para los dos primeros modos baroclínicos de Kelvin (desde 1.4 m/s a 2.6 m/s). Los resultados son consistentes tanto para las SSH observadas como simuladas.

- Las ondas de Kelvin se propagan hacia el este desde el oeste equatorial Atlántico hasta la costa oeste de África, donde se divide y viaja hacia los polos atrapada en la costa hasta ~12 grados de latitud. Esta actividad de ondas de Kelvin está asociada con cambios en la profundidad de la termoclina.

- La SSH sobre el oeste ecuatorial puede explicar el 25% de la variabilidad intraestacional del afloramiento de la costa del Golfo de Guinea (GG) y el 15% de la variabilidad intraestacional del afloramiento de Benguela via ondas de Kelvin. Sin embargo, la variabilidad de SSH sobre el afloramiento de Mauritania/Senegal está menos influida por las propagaciones de las ondas.

- La compleja actividad de las ondas de Kelvin intraescionales ha sido simplificada a dos señales sintéticas: una climatología intraestacional y un modo extendido de EOF[10]. La climatología intraestacional ha mostrado que la actividad de ondas de Kelvin ocurre principalmente en el otoño-invierno boreal. El hecho de que la actividad invernal de ondas de Kelvin aparezca como un modo de variabilidad de la SSH, resalta la importancia de las ondas en el contexto de la TAV.

- Las anomalías de viento local sobre el Atlántico oeste ecuatorial no pueden explicar el comienzo de las ondas en el oeste ecuatorial. No obstante, sobre el centro-este ecuatorial Atlántico, el esfuerzo del viento controla parte de la variabilidad de la SSH. Se han encontrado evidencias, en algunos eventos, de radiación de ondas de Rossby desde el GG sobre todo en la estación de primavera-verano. Sin embargo, la reflexión de las ondas de Rossby en la costa de America no explica el disparo de las ondas de Kelvin indentificadas.

[9] Del inglés Sea Surface Height
[10] Del inglés Empirical Orthogonal Functions

- Se ha propuesto un mecanismo para explicar el disparo de las ondas de Kelvin denominado *anomalías del bombeo de Ekman inducidas por movimientos de la Zona de Convergencia Inter-Tropica (ITCZ[11])*. El mecanismo se describe mediante anomalías del esfuerzo del viento a gran escala sobre el noreste del TA, que son coherentes con la convección anómala a ambos lados de 10ºN y el bombeo de Ekman anómalo fuera del ecuador en el oeste-centro Atlántico. Estas anomalías inducen anomalías de SSH sobre la banda 2ºN-6ºN y muestran continuidad con el comienzo de las ondas de Kelvin ecuatoriales. Las oscilaciones del esfuerzo del viento y de la radiación de onda larga son una señal de los movimientos de la ITCZ a escalas intraestacionales.

- Un esfuerzo del viento anómalo del sur (norte) sobre el oeste Atlántico induce un movimiento anómalo de la ITCZ y de la banda de afloramiento hacia el norte (sur). Esta situación deja la banda centrada en 4ºN sobre el Atlántico oeste-central en un estado de hundimiento (afloramiento) anómalo. Las anomalías del bombeo de Ekman hacia abajo (arriba) crean anomalías positivas (negativas) de SSH en una escala espacial sufientemente grande como para disparar ondas de Kelvin ecuatoriales ~10 dias después.

- Se han encontrado dos patrones de convección asociados con el modo EEOF de SSH: uno asociado al mecanismo propuesto y otro asociado a la MJO[12]. La MJO parece afectar a la SSH sobre la costa del GG.

- Los vientos oscilando en la región del Atlántico norte Subtropical están en fase con la llegada de la onda a la costa norte de Africa. El modo EEOF de SSH describe esta relación en fase.

- La advección anómala del estado medio de la SST por corrientes cuasi-geostróficas asociadas con el modo invernal EEOF de SSH, parece afectar a la SST en la costa africana al norte de 10ºN y en algunas zonas de la costa de GG.

[11] Del inglés InterTropical Convergence Zone
[12] Del inglés Madden-Julian Oscillation

Investigación futura

La dinámica oceánica asociada con las regiones de afloramiento del TA necesita ser investigada con profundidad. Un modelo oceánico sería necesario para discernir y cuantificar con precisión la contribución oceánica a las variaciones de la SST, para incluir todos los términos que están implicados en la variabilidad de la capa de mezcla.

De la misma forma, los mecanismos de interación océano-atmósfera propuestos para explicar la evolución de los modos de SST que tienen un impacto en la precipitación, necesitan ser comprobados usando un modelo acoplado.

A partir de la relación del EM con el Pacífico ecuatorial, el estudio de la posible influencia de las variaciones de la atmósfera Atlántica en verano en la dinámica del océano Pacífico ecuatorial desde el verano hasta el invierno, necesita ser testado con un model acoplado.

A pesar de que las ondas oceánicas han sido caracterizadas sobre el TA, un entendimiento más profundo tanto de las velocidades de fase como de la respuesta de la termoclina, requiere un análisis modal. Los impactos en la SST y el mecanismo propuesto para el disparo de las ondas requerirían ser analizados con un modelo acoplado.

REFERENCES

Adamec, D. and J. J. O'Brien (1978), The Seasonal Upwelling in the Gulf of Guinea Due to Remote Forcing, *J. Phys. Oceanogr*., **8**, 1050-1060.

Alexander, M. A., I. Bladé, M. Newman, J. R. Lanzante, N. C. Lau and J. D. Scott (2002), The Atmospheric Bridge: The influence of ENSO teleconnections on air-sea interaction over the global oceans, *J. Climate*, **15**, 2205-2231.

Aman, A., L. Testut, P. Woodworth, T. Aarup and D. Dixon (2007), Seasonal Sea Level Variability in the Gulf of Guinea from altimetry and tide gauge, *Rev. Ivoir. Sci. Technol.,* **09** 105-118. ISSN 1813-3290.

Arnault, S., and R. E. Cheney (1994), Tropical Atlantic sea-level variability from Geosat (1985-1989), *J. Geophys. Res.,* **99**, 18207-18223.

Arnault, S., and Périgaud, (1992), Altimetry and models in the tropical oceans: A review, *Oceanologia acta*, **15**, 411-430.

Arnault, S., L. Gourdeau and Y. Menard (1992), Comparison of the altimetric signal with in-situ measurements in the tropical Atlantic ocean, *Deep-Sea Res*. I, **39**, 481-499.

Arnault, S., Y. Menard, and J. Merle (1990), Observing the tropical Atlantic Ocean in 1986--1987 from altimetry, *J. Geophys. Res.,* **95** (C10), doi: 10.1029/90JC00347.

Arnault, S., and C. Le Provost (1997), Regional identification in the tropical Atlantic Ocean of residual tide errors from an empirical orthogonal function analysis of TOPEX/POSEIDON altimetric data, *J. Geophys. Res.*, **102**, 21022-21036.

AVISO (1992), "*AVISO Handbook: Merged TOPEX/POSEIDON Products*", AVI-NT-02-101-CN, Edition 2.1

AVISO (1995), "*AVISO User Handbook: Sea Level Anomaly files*", AVI-NT-011-312-CN, Edition 1.

Bader, J. and M. Latif (2007), Combined Tropical Oceans Drive Anomalous Sub- Saharan West African Rainfall, *J. Climate*, in press

Bader, J., and M. Latif (2003), The impact of decadal-scale Indian ocean ST anomalies on Sahelian rainfall and the North Atlantic Oscillation, *Geophys. Res. Lett*., **30**, 2169, doi: 10.1029/2003GL018426.

Barreiro, M., P. Chang and R. Saravanan (2002), Variability of the South Atlantic Convergence Zone simulated by an Atmospheric General Circulation Model, *J. Climate*, **15**, 745–763.

Barreiro, M, A. Giannini, P. Chang, and R. Saravanan (2004), On the role of the South Atlantic atmospheric circulation in Tropical Atlantic Variability. *In Earth's Climate: The Ocean-atmosphere interaction. Geophysical Monograph Series,* **147**, AGU, Washington DC, pp 143-156.

Barreiro, M., P. Chang, L. Ji, R. Saravanan and A. Giannini (2005), Dynamical Elements of Predicting Boreal Spring Tropical Atlantic Sea-Surface Temperatures, *Dyn. Atmos. Oceans*, **31**, 61-85.

Barsugli, J. J., and D. S. Battisti (1998), The basic effects of atmosphere-ocean thermal coupling on midlatitude variability, *J. Atmos. Sci.,* **55,** 477-493.

Barton, E. D. (1998), Eastern boundary of the North Atlantic - northwest Africa and Iberia. A.R.Robinson and K.Brink eds, in *The Sea*, **11**, 633-657.

Berliand, M. E. and T. G. Strokina (1980), Global distribution of the total amount of clouds, *Hydrometeorological Publishing House*, Leningrad, Russia, 71 pp.

Bjerknes, J. (1969), Atmospheric teleconnections from the Equatorial Pacific, *Mon. Wea. Rev.*, **97**(3), 163-172.

Blanke, B., M. Arhan, G. Madec, and S. Roche (1999), Warm water paths in the equatorial Atlantic as diagnosed with a general circulation model. *J. Phys. Oceanogr*., **29**, 2753-2768.

Bonjean, F., and G. S. E. Lagerloef (2002), Diagnostic model and analysis of the surface currents in the tropical Pacific Ocean. *J. Phys. Oceanogr.,* **32,** 2938–2954.

Brandt, P., L. Strammaa, F. Schott, J. Fishera, M. Dengler, and D. Quadfasel, (2002), Annual Rossby waves in the Arabian Sea from TOPEX/POSEIDON altimeter and in situ data, *Deep-Sea Research II,* **49** 1197–1210.

Brandt, P., and C. Eden (2005), Annual cycle and interannual variability of the mid-depth tropical Atlantic Ocean, *Deep-Sea Res. I,* **52**, 199-219.
Bretherton, F. P., R. E. Davis and C. B, Fandry (1979), A technique for objective analysis and design oceanographic experimentes applied to mode-73, *Deep-Sea Res.*, **23**, 559-582.
Bretherton, S. B., C. Smith, and J. H. Wallace (1992), An intercomparation of methods for finding coupled patterns in climate data, *J. Climate,* **5***,* 541-560.
Bruce, J. G. and J. L. Kerling, (1984), Near Equatorial eddies in the North Atlantic, *Geophys. Res. Lett.*, **11**, 779-782.
Cane, M. A., A. C. Clement, A. Kaplan, Y. Kushnir, D. Pozdnyakov, R. Seager, S. E. Zebiak, R. Murtugudde (1997), Twentieth-Century Sea Surface Temperature trends, *Science,* **275**, 957–960. DOI: 10.1126/science.275.5302.957
Carton, J. A. and Y B. Huang (1994), Warm Events in the Tropical Atlantic, *J. Phys. Oceanogr.,* **24**, 888-903.
Carton, J. A., X. H. Cao, B. S. Giese, and A. M. daSilva (1996), Decadal and interannual SST variability in the tropical Atlantic Ocean, *J. Phys. Oceanogr.,* **26**, 1165-1175.
Cassou, C., C. Desert, L. Terray, J. W. Hurrell and M. Drévillon (2004), Summer Sea Surface Temperature conditions in the North Atlantic and their impact upon the atmospheric circulation in early winter, *J. Climate*, **17**, 3349-3363.
Cayan D. R. (1992), Latent and sensible heat flux anomalies over the northern oceans: driving the Sea Surface Temperature, *J. Phys. Oceanogr.,* **22**, 859–881.
Cazes-Boezio G., A. W. Robertson and C. R. Mechoso (2003), Seasonal dependence of ENSO teleconnections over South America and relationships with precipitation in Uruguay, *J. Climate,* **16**, 1159-1176.
Challenor, P.G., P. Cipollini and D. Cromwell (2001), Use of the 3D radon transform to examine the properties of oceanic Rossby waves, *J. Atmos. Oceanic Technol.,* **18**(9)*,* 1558-1566.
Challenor, P.G., P. Cipollini, D. Cromwell, K. L. Hill, G. D. Quartly and I. S. Robinson (2004), Global characteristics of Rossby wave propagation from multiple satellite datasets, International, *J. Remote Sens.*, **25**(7-8) 1297-1302.
Chang P. and S. G. Philander (1994), A Coupled Ocean-Atmosphere Instability of Revelance to the Seasonal Cycle, *J. Atmos. Sci.*, **51**, 3621-3648
Chang, P., L. Ji and H. Li (1997), A decadal climate variation in the tropical Atlantic Ocean from thermodynamic air–sea interactions, *Nature*, **385**, 516–518.
Chang P., R. Saravanan, L. Ji and G. C. Hegerl (2000), The effect of local Sea Surface Temperatures of atmospheric circulations over the tropical Atlantic sector, *J. Climate,* **13**, 2195–2216.
Chang P., T. Yamagata, P. Shopf, S. K. Behera, J. Carton, W. S. Kessler, G. Meyers, T. Qu, F. Schott and S. P. Xie (2006), Climate Fluctuations of Tropical Coupled Systems-The Role of Ocean Dynamics, *J. Climate*, **19**, 5122-5174.
Chang P., Y. Fang, R. Saravannan, L. Ji and H. Seidel (2008), The cause of the fragile relationship between the Pacific El Niño and the Atlantic Niño, *Nature*, **443**, 324-328.
Chelliah M. and G. D. Bell (2004), Tropical Multidecadal and Interannual Climate Variability in the NCEP–NCAR Reanalysis, *J. Climate*, **17**, 1777-1802.
Chelton, D. B. and M. G. Schlax (1996), Global observations of oceanic Rossby waves, *Science*, **272**, 234-238.
Chelton, D.B., M.G. Schlax, M.H. Freilich and R.F. Milliff (2004), Satellite measurements reveal persistent small-scale features in ocean winds, *Science,* **303**, 978–983.
Cherry, S. (1996), Singular Value Decomposition and Canonical Correlation Analysis. *J. Climate*, **9**, 2003-2009.
Chiang J. C. H., Y. Kushnir and S. E. Zebiak (2000), Interdecadal changes in eastern Pacific ITCZ variability and its influence on the Atlantic ITCZ, *Geophys. Res. Lett*., **27**, 3687-3690.
Chiang, J. C. H., Y. Kushnir and A. Giannini (2002), Deconstructing Atlantic ITCZ variability: influence of the local cross-equatorial SST gradient, and remote forcing from the eastern equatorial Pacific, *J. Geophys. Res., (Atmos.)*, **107**(D1), 4004, doi:10.1029/ 2000JD000307.
Chiang J. C. H. and D. J. Vimont (2004), Analogous Pacific and Atlantic Meridional Modes of Tropical Atmosphere-Ocean Variability. *J. Climate*, **17**, 4143-4158.
Cibot C., E. Maisonnave and L. Terray (2005), Mechanisms of tropical Pacific Interannual to decadal variability in the ARPEGE/ORCA global coupled model, *Climate Dyn*., **24**, 823-842.
Cipollini, P., D. Cromwell and G.D. Quartly (1996), Variability of Rossby wave propagation in the North Atlantic from TOPEX/POSEIDON altimetry. *Proc. IGARSS '96*, Lincoln, Nebraska, **1**, 91-93.

Clarke, A. J. (1983), The reflection of equatorial waves from oceanic boundaries, *J. Phys. Oceanogr.,* **13**, 1193-1207.

Cravatte, S., J. Picaut and G. Eldin (2003), Second and first Kelvin modes in the equatorial Pacific at intraseasonal timescales, *J. Geophys.Res*., **108**, doi:10.1029/2002JC001511.

Cushman-Roisin, B. (1994), *Introduction to Geophysical Fluid Dynamics*. Prentice Hall, 320 pp.

Czaja A. (2003), On the time variability of the net ocean to atmosphere heat flux in midlatitudes, with application to the North Atlantic basin. *Quart. J. Roy. Meteor. Soc.,* **129**, no. 594, 2867-2878 (12).

Czaja, A. and C. Frankignoul (1999), Influence of the North Atlantic SST on the atmospheric circulation, *Geophys. Res. Lett.*, **26**, 2969-2972.

Czaja, A. and C. Frankignoul (2002), Observed impact of Atlantic SST anomalies on the North Atlantic Oscillation, *J. Climate*, **15**, 606-623.

Czaja A., P. Van Der Vaart, and J. Marshall (2002), A diagnostic Study of the Role of remote forcing on the Tropical Atlantic Variability, *J. Climate,* **15**, 3280-3290.

de Boyer-Montégut, C., J. Vialard, S. S. C. Shenoi, D. Shankar, F. Durand, C. Ethé, and G. Madec (2007), Simulated seasonal and interannual variability of mixed layer heat budget in the northern Indian Ocean, *J. Climate*, **20**, 3249-3268.

de la Rosa, S., P. Cipollini and H. M. Snaith (2007), An Application of the Radon Transform to study Planetary waves in the Indian Ocean. (personal communication from Cipollini).

Deans, S. R. (1983), *The Radon Transform and Some of Its Applications.* John Wiley and Sons, 289 pp.

Delecluse, P., J. Servain, C. Levy, K. Arpe and L. Bengtsson (1994), On the connection between the 1984 Atlantic warm event and the 1982-1983 ENSO, *Tellus*, **46**A, 448-464.

Delworth, T. L. and M. E. Mann (2000), Observed and simulated multidecadal variability in the Northern Hemisphere, *Climate Dyn.*, **16**, 661– 676.

Dommenget, D. and M. Latif (2000), Interannual to decadal variability in the tropical Atlantic*, J. Climate*, **13**, 777–792.

Dong B. W. and Sutton (2002), Adjustment of the coupled ocean–atmosphere system to a sudden change in the Thermohaline Circulation, *Geophys. Res. Lett.,* **29**, doi: 10.1029/2002GL015229

Dong, B., R. T. Sutton and A. A. Scaife (2006), Multidecadal modulation of El Niño-Southern Oscillation (ENSO) variance by Atlantic Ocean sea surface temperatures, *Geophys. Res. Lett.*, **33**, L08705, doi:10.1029/2006GL025766.

Douville, H. (2002), Influence of soil moisture on the Asian and African monsoons. Part II. Interannual variability, *J. Climate,* **15**, 701-720.

Douville, H., S. Conil, S. Tyteca and A. Voldoire (2007), Soil moisture memory and West African monsoon predictability: artefact or reality?, *Climate Dyn.*, **28**, 723-742.

du Penhoat, Y. and A.-M. Treguier (1985), The seasonal linear response of the Atlantic Ocean, *J. Phys. Oceanogr*., **15**, 316-329.

Efron, B. and R. Tibishirani (1993), *An Introduction to the Bootstrap*. Chapman & Hall, London.

Enfield, D. B. and D. A. Mayer (1997), Tropical Atlantic Sea Surface Temperature variability and its relation to El Niño–Southern Oscillation, *J. Geophys. Res.*, **102**, 929-945.

Enfield, D. B., A. M. Mestas-Nunez and P. J. Trimble (2001), The Atlantic multidecadal oscillation and its relation to rainfall and river flows in the continental U.S. *Geophys. Res. Lett.,* **28**, 2077-2080.

Emanuel, K. A. (1987), An air-sea interaction model of intraseasonal oscillations in the tropics, *J Atmos Sci,* **44**, 2324-2340.

Fedorov, A. and S. G. Philander (2000), Is El Niño changing?, *Science,* **288**,1997-2002.

Flatau, M., P. J. Flatau, P. Phoebus and P. P. Niiler (1997), The feedback between equatorial convection and local radiative and evaporative processes: the implication for Intraseasonal oscillations, *J. Atmos. Sci.*, **54**, 2373-2386

Florenchie, P., J. R. E. Lutjeharms, C. J. C. Reason, S. Masson and M. Rouault (2003), The source of Benguela Niños in the South Atlantic Ocean, *Geophys. Res. Lett*., **30**(10), 1505, doi:10.1029/2003GL017172.

Florenchie P., C. J. C. Reason, J. R. E. Lutjeharms, M. Rouault, C. Roy and S. Masson (2004), Evolution of interannual warm and cold events in the South-East Atlantic Ocean, *J. Climate* **17**, 2318-2334.

Folland, C. K., T. N. Palmer and D. E. Parker (1986), Sahel rainfall and worldwide sea temperatures, *Nature*, **320**, 602-607.

Foltz, G. R., S. A. Grodsky, J. A. Carton and M.J. McPhaden (2003), Seasonal mixed layer heat budget of the tropical Atlantic Ocean, *J. Geophys. Re*s., **108**, 3146, doi:10.1029/2002JC001584.

Foltz, G. R. and M. J. McPhaden (2004), The 30-70 day oscillations in the Tropical Atlantic, *Geophys. Res. Lett.*, **31**(15), L15205, doi: 10.1029/2004GL020023.

Foltz, G. R. and M. J. McPhaden (2005), Mixed layer heat balance on intraseasonal time scales in the northwestern tropical Atlantic Ocean, *J. Climate,* **18***,* 4168-4184.

Fontaine, B. and S. Janicot (1996), Sea Surface Temperature fields associated with West African rainfall anomaly types, *J. Climate*, **9**, 2935-2940.

Fontaine, B., S. Janicot and P. Roucou (1999), Coupled ocean–atmosphere surface variability and its climate impacts in the tropical Atlantic region, *Climate Dyn.,* **15**, 451–473.

Fontaine, B., S. Louvet and P. Roucou (2007), Definition and predictability of an OLR-based West African monsoon onset, *Int. J. Climatol.*, DOI:10.1002/joc.1674.

Fraedrich, K., J. L. McBride, W. M. Frank and R. Wang (1997), Extended EOF Analysis of Tropical Disturbances: TOGA COARE, *J. Atmos. Sci*, ***54*****,** 19, 2363–2372.

França, C., I. Wainer, A. R. De Mesquita and G. J. Goñi (2003), Planetary equatorial trapped waves in the Atlantic Ocean from TOPEX/Poseidon altimetry, *in*: Goñi, G. J.; Malanotte-Rizzoli, P. (Ed.). *Interhemispheric water exchange in the Atlantic Ocean. Elsevier Oceanography Series,* **68***,* 213-232.

Frankignoul, C. (1985), Sea surface temperatures, planetary waves, and air-sea feedback in the middle latitudes, *Rev. Geophys*., **23**, 357-390

Frankignoul, C., E. Kestenare, M. Botzet, A.F. Carril, H. Drange, A. Pardens, L. Terray and R. Sutton (2003), An intercomparison between the surface heat flux feedback in five coupled models, COADS, and the NCEP reanalysis, *Climate Dyn.,* **22**, 373-388.

Frankignoul, C. and E. Kestenare (2005), Air-sea interactions in the tropical Atlantic: A view based on lagged rotated maximum covariance analysis, *J. Climate*, **18**, 3874-3890.

Frantantoni, D. M., W. E. Johns, T. L. Townsend, and H. E. Hurlburt, (2000), Lowlatitude circulation and mass transport pathways in a model of the tropical Atlantic Ocean. *J. Phys. Oceanogr.,* **30,** 1944–1966.

Giannini, A., J. C. H. Chiang, M. A. Cane, Y. Kushnir and R. Seager (2001), The ENSO teleconnection to the Tropical Atlantic Ocean: Contribution of the remote and local SSTs to rainfall variability in the Tropical Americas, *J. Climate*, **14**, 4530-4544.

Giannini, A., Y. Kushnir and M. A. Cane (2000), Interannual variability of Caribbean rainfall, ENSO, and the Atlantic Ocean, *J. Climate*, **13**, 297-311.

Giannini, A., R. Saravannan and P. Chang (2003), Oceanic forcing of Sahel rainfall on interannual to interdecadal time scales, *Science*, **302**, 1027-1030.

Gill, A. E. (1982), *Atmosphere-Ocean Dynamics*, Academic Press. 662 pp. ISBN 0122835220.

Gill, A. E. and P. P. Niiler (1973), The theory of the seasonal variability in the ocean, *Deep-Sea Res.*, **20**, 141-177.

Giese, B. S. and D. E. Harrison (1990), Aspects of the Kelvin wave response to episodic wind forcing, *J. Geophys. Res.,* **95** (C5), 7289–7312..

Greatbatch, R. J. and K. A. Peterson (1996), Interdecadal variability and oceanic thermohaline adjustment, *J. Geophys. Res.,* **101**, 20467–20482.

Grodsky, S. A., J. A. Carton, C. Provost, J. Servain, J. A. Lorenzzetti and M. J. McPhaden (2005), Tropical instability waves at 0ºN, 23ºW in the Atlantic: A case study using Pilot Research Moored Array in the Tropical Atlantic (PIRATA) mooring data, *J. Geophys. Res*., **110**, C08010, doi: 10.1029/2005JC002941.

Grodsky, S. A. and J. A. Carton (2006), Influence of the tropics on the climate of the South Atlantic, *Geophys. Res. Lett.,* **33***,* L06719, doi:10.1029/2005GL0.

Grodsky, S. A., J. A. Carton and C. R. McClain (2008), Variability of upwelling and chlorophyll in the equatorial Atlantic, *Geophys. Res. Lett.,* **35**, L03610, doi:10.1029/2007GL032466

Gu, D. and S. G. H. Philander (1997), Interdecadal climate fluctuations that depend on exchange between the tropics and extratropics, *Science*, **275**, 805-807.

Guiavarc'h, C., A. M. Treguier and A. Vangriesheim (2008), Remotely forced biweekly deep oscillations on the continental slope of the Gulf of Guinea, *J. Geophys. Res*., in press.

Haarsma, R. J., E. J. D. Campos and F. Molteni (2003), Atmospheric response to South Atlantic SST dipole, *Geophys. Res. Lett.*, **30**, doi: doi:10.1029/2003GL017829

Haarsma, R. J. and W. Hazeleger (2007), Extra-tropical atmospheric response to equatorial Atlantic cold tongue anomalies, *J. Climate,* **20**(10), 2076–2091.

Halley, E. (1686), An Historical Account of the Trade Winds, and Monsoons, Observable in the Seas Between and Near the Tropicks; With an Attempt to Assign the Phisical Cause of Said Winds, *Philosophical Transactions*, **183**, 153-168.

Han, W., P.J. Webster, J. Lin, W.T. Liu, R. Fu, D. Yuan and A. Hu (2008), Dynamics of intraseasonal sea level and thermocline variability in the equatorial Atlantic during 2002-2003*, J. Phys. Oceanogr*., **38**, 945–967.

Handoh, I. C. and G. R. Bigg (2000), A self-sustaining climate mode in the Tropical Atlantic, 1995-97: Observations and modelling, *Quart. J. R. Meteor. Soc.,* **126**, 807-821.

Handoh, I. C., A. J. Matthews, G. R. Bigg and D. P. Stevens (2006a), Interannual variability of the Tropical Atlantic independent of and associated with ENSO: Part I. The North Tropical Atlantic, *Int. J. Climatol*., **26**, 1937-1956, DOI: 10.1002/joc.1343.

Handoh, I.C., G. R. Bigg, A. J. Matthews and D. P. Stevens (2006b), Interannual Variability of the tropical Atlantic independent of and associated with ENSO: Part II. The south tropical Atlantic, *Int. J. Climatol.*, **26**, 1957-1976, DOI: 10.1002/joc.1342.

Hansen, D.V. and H. F. Bezdek (1996), On the nature of decadal anomalies in the North Atlantic sea surface", *J. Geophys. Res.*, **101**, 8749-8758.

Hansen, J., M. Sato, R. Ruedy, K. Lo, D. W. Lea and M. Medina-Elizade (2006), Global temperature change, *Proc. Natl. Acad. Sci.*, **103**, 14288-14293, doi: 10.1073/pnas.0606291103.

Hartmann, D. L. (1994), *Global Physical Climatology*. Ed Academic Press, International Geophysics Series, vol 56.

Hasselmann, K. (1976), Stochastic climate models. I- Theory, *Tellus*, **28**, 473-485.

Hastenrath, S. and J. Merle (1987), Annual cycle of subsurface thermal structure in the tropical Atlantic Ocean, *J. Phys. Oceanogr.,* **17,** 1518–1538.

Hayes, S. P., M. J. McPhaden and J. M. Wallace (1989), The influence of sea surface temperature upon surface wind in the eastern equatorial Pacific: Weekly to monthly variability, *J. Climate.,* **2**, 1500-1506.

Hendon, H. H., B. Liebmann, and J. D. Glick (1998), Oceanic Kelvin Waves and the Madden-Julian Oscillation, *J. Atmos. Sci.,* **55**, 88-101.

Hill, K. L., I. S. Robinson and P. Cipollini (2000), Propagation characteristics of extratropical planetary waves observed in the ATSR global Sea Surface Temperature record, *J. Geophys. Res.,* **105**(C9), 21927-21945.

Horel, J. D. and J.M. Wallace (1981), Planetary-Scale Atmospheric Phenomena Associated with the Southern Oscillation, *Mon. Wea. Rev.*, **109**, 813–829.

Hormazabal, S., G. Shaffer and O. Pizarro (2002), Tropical Pacific control of intraseasonal oscillations off Chile by way of oceanic and atmospheric pathways, *Geophys. Res. Lett*., **29**, doi: 10.1029/2001GL013481.

Hough, S. S. (1897), On the application of harmonic analysis to the dynamical theory of the tide. Part I: On Laplace's 'oscillations of the first species' and on the dynamics of ocean currents, *Philos. Trans. R. Soc. London*, Ser. A, **189**, 201-257.

Houghton, R.W. and Y.M. Tourre (1992), Characteristics of low-frequency sea surface temperature fluctuations in the tropical Atlantic, *J. Climate,* **5**, 765-771.

Hu, Z.-Z. and B. Huang (2006), Physical processes associated with tropical Atlantic SST Meridional gradient, *J. Climate*, **19**, 5500-5518.

Hu, Q. and D. A. Randall (1994), Low-frequency oscillations in radiative–convective systems, *J. Atmos. Sci.* **51**, 1089–1099.

Huang, R. X. and J. Pedlosky (1999), Climate variability inferred from a layered model of the ventilated thermocline, *J. Phys. Oceanogr.*, **29**, 779–790.

Hulme, M. (1992), A 1951-80 global land precipitation climatology for the evaluation of General Circulation Models, *Climate Dyn.*, **7**, 57-72.

Hurrell, J.W. (1995), Decadal Trends in the North Atlantic Oscillation: Regional Temperatures and Precipitation, *Science,* **269**, 676-679.

Hurrell, J. W., Y. Kushnir and M. Visbeck (2001), Climate - The North Atlantic oscillation, *Science*, **291** (5504), 603-605.

Hurrell, J.W., M. Visbeck, A. Busalacchi, R. A. Clarke, T. L. Delworth, R. R. Dickson, W. E. Johns, K.P. Koltermann, Y. Kushnir, D. Marshall, C. Mauritzen, M. S. McCartney, A. Piola, C. Reason, G. Reverdin, F. Schott, R. Sutton, I. Wainer and D. Wright (2006), Atlantic Climate Variability and Predictability: A CLIVAR Perspective, *J. Climate*, **19**, 5100-5121.

Illig, S., B. Dewitte, N. Ayoub, Y. du Penhoat, G. Reverdin, P. De Mey, F. Bonjean and G. S. Lagerloef (2004), Interannual long equatorial waves in the tropical Atlantic form a high

resolution ocean general circulation model experiment in 1981-2000, *J. Geophys. Res*., **109**, C02022, doi. 101029/2003JC001771.
Jacobs, G. A., H. E. Hurlburt, J. C. Kindle, E. J. Metzger, J. L. Mitchell, W. J. Teague and A. J. Wallcraft (1994), Decade-scale trans-Pacific propagation and warming effects of an El Niño anomaly, *Nature,* **370**, 360-363.
Janicot, S. (1992), Spatio-temporal variability of West African rainfall. Part I: Regionalization and typings, *J. Climate*, **5**, 489-497.
Janicot, S., V. Moron and B. Fontaine (1996), Sahel droughts and ENSO dynamics, *Geophys. Res. Lett.*, **23**, 515-518.
Janicot, S., A, Harzallah, B. Fontaine and V. Moron (1998), West African Monsoon dynamics and Eastern Equatorial Atlantic and Pacific SST anomalies (1970-1988), *J. Climate*, **11**, 1874-1882.
Janicot, S., S. Trzaska and I. Poccard (2001), Summer Sahel-ENSO teleconnection and decadal time scale SST variations, *Climate Dyn.,* **18**, 303-320.
Janicot, S., A. Ali, N. Asencio, G. Berry, O. O. Bock, B. Bourles, G. Caniaux, F. Chauvin, A. Deme, L. Kergoat, J.-P. Lafore, C. Lavaysse, T. Lebel, B. Marticorena, F. Mounier, J.-L. Redelsperger, F. Ravegnani, C. Reeves, R. Roca, P. de Rosnay, B. Sultan1, C. Thorncroft, M. Tomasini, A. Ulanovsky and ACMAD forecasters team (2007), Large-scale overview of the summer monsoon over West and Central Africa during the AMMA field experiment in 2006. Submitted to *Annales Geophysicae*.
Jayne, S. R. and J. Marotzke (2001), The dynamics of ocean heat transport variability, *Rev. Geophys.*, **39**, 385-411.
Johnson, E. S. and M.J. McPhaden (1993), Structure of Intraseasonal Kelvin Waves in the Equatorial Pacific Ocean, *J. Phys. Oceanogr.*, **23**, 608–625.
Johnson, H. L. and D. P. Marshall (2002): A theory for the surface Atlantic response to thermohaline variability, *J. Phys. Oceanogr.*, **32**, 1121-1132.
Jung, T., L. Ferranti, and A. M. Tompkins (2006), Response to the summer of 2003 Mediterranean SST anomalies over Europe and Africa, *J. Climate,* **19***,* 5439–5454.
Kalnay, E. M., M. Kanamitsu, R. Kistler, W. Collins, D. Deaven, L. Gandia, M. Iredell, S. Saha, G. White, J. Woollen, Y. Zhu, M. Chelliah, W. Ebisuzaki, W. Higgins, J. Janowiak, K. C. Mo, C. Ropelewski, J. Wang, A. Leetmaa, R. Reynolds, R. Jenne and D. Joseph (1996), The NMC/NCAR 40-Year Reanalysis Project, *Bull. Amer. Meteor. Soc*., **77***,* 437-471.
Katz, E. J., P. Hisard, J.. Verstraete and S. L. Garzoli (1986), Annual change of sea surface slope along the equator of the Atlantic Ocean in 1983 and 1984, *Nature*, **322**, 245-247.
Katz, E. J. (1997), Waves along the equator in the Atlantic, *J. Phys. Oceanogr.*, **27**, 2536–2544.
Kayano, M. and V. Kousky (1999), Intraseasonal (30-60 day) variability in the global tropics: principal modes and their evolution, *Tellus,* **51**, 373-386.
Keenlyside, N. S. and M. Latif (2007), Understanding Equatorial Atlantic interannual variability, *J. Climate*, **30**, 131-142.
Kessler, W. S. (1991), Can reflected extra-equatorial Rossby waves drive ENSO?, *J. Phys. Oceanogr.,* **21**, 444-452.
Kessler, W. S., M. J. McPhaden and K. M. Weickmann (1995), Forcing of intraseasonal Kelvin waves in the equatorial Pacific, *J. Geophys. Res.,* **100**, 10613-10631.
Kiladis, G. N. and B. Liebmann (2006), Interannual Variability of Atmospheric Kelvin Wave Activity over South America, *Proceedings of AGU Fall meeting. San Francisco, USA*.
Killworth, P. D., D. B. Chelton and R. de Szoeke (1997), The speed of observed and theoretical long extratropical planetary waves, *J. Phys. Oceanogr.,* **27***,* 1946-1966.
Kleeman, R. J.P. McCreary and B.A. Klinger (1999) A mechanism for generating ENSO decadal variability, *Geophys. Res. Lett.*, **26**, 1743-1746.
Kucharski, F., A. Bracco, J. H. Yoo and F. Molteni (2008), Atlantic forced component of the Indian monsoon interannual variability, *Geophys. Res. Lett*., **35**, L04706, doi:10.1029/2007GL033037.
Kundu, P. and I. M. Cohen (2002), *Fluid Mechanics*. Academic Press, 730 pp.
Kushnir, Y., W. A. Robinson, I. Bladé, N. M. J. Hall, S. Peng and R. Sutton (2002), Atmospheric GCM response to Extratropical SST anomalies: Synthesis and Evaluation, *J. Climate*, **15**, 2233-2256.
Kushnir, Y., M. Barreiro, P. Chang, J. Chiang, A. Lazar and P. Malanotte-Rizzoli (2003), The role of the south Atlantic in the Variability of the ITCZ, White paper for CLIVAR/IAI/OOPC.

Kushnir, Y., W. A. Robinson, P. Chang and A. W. Robertson (2006), The Physical Basis for Predicting Atlantic Sector Seasonal-to-Interannual Climate Variability, *J. Climate*, **19**, 5949-5970.

Lamb, P. J. (1978), Large-Scale tropical Atlantic surface circulation patterns associated with sub-Saharan weather anomalies, *Tellus,* **30**, 240-251.

Latif, M., A. Groetzner and H. Frey (1996), El Hermanito: El Nino's overlooked little brother in the Atlantic. Max-Planck-Institut für Meteorologie, Report No.196.

Latif, M. and A. Grötzner (2000), On the equatorial Atlantic oscillation and its response to ENSO, *Climate Dyn.*, **16**, 213-218.

Latif, M. (2001), Tropical Pacific/Atlantic Ocean Interactions at Multi-Decadal Time Scales, *Geophys. Res. Lett.*, **28**, 539-542.

Latif, M., C. Böning, J. Willebrand, A. Biastoch, J. Dengg, N. Keenlyside, U. Schweckendiek and G. Madec (2006), Is the Thermohaline Circulation Changing?, *J. Climate*, **19**, 4631–4637.

Lau, K. M. and L. Peng (1987), Origin of low-frequency (intraseasonal) oscillations in the tropical atmosphere. I. Basic theory, *J. Atmos. Sci.,* **44**, 950–972.

Lazar, A., R. Murtugudde and A. Busalacchi (2001), A model study of temperature anomaly propagation from the subtropics to tropics within the South Atlantic thermocline, *Geophys. Res. Lett.*, **28,** 1271-1274.

Lazar, A. (2005), Seasonal to interannual variability of the Atlantic North-eastern upwelling system (ANETUS): Looking for causes and basin-scale consequences, NASA/CNES Research Announcement SALP-BC-MA-EA-14810-CN.

Leewenburgh, O. and D. Stammer (2001), The effect of ocean currents on Sea surface Temperature anomalies, *J. Phys. Oceanogr.,* **31**, 2340-2358.

Legates, D. R. (1989), A high-resolution climatology of gauge-corrected global precipitation, *Proceedings of the WMO/IAHS/ETH International Workshop on Precipitation Measurement, St. Moritz, Switzerland, Dec. 3–7,* Sevruk B (ed) Swiss Federal Institute of Technology: Zurich, 519–526.

Legates, D. R. and C. J. Willmott (1990), Mean Seasonal and Spatial Variability in Gauge-Corrected, Global Precipitation, *Int. J. Climatol*., **10**, 111-127.

Levitus, S. (1998), Climatological Atlas of the world ocean, *Tech. Rep.* **13**,NOAA, Rockville, Md.

Liebmann, B. and C. A. Smith (1996), Description of a complete (interpolated) outgoing longwave radiation dataset, *Bull. Amer. Meteor. Soc.,* **77**, 1275-1277.

Liebmann B., G. N. Kiladis, J. A. Marengo, T. Ambrizzi and J. D. Glick (1999), Submonthly convective variabiltiy over South America and the South Atlantic convergence zone, *J. Climate,* **12**, 1877-1891.

Lindzen, R. S. and S. Nigam (1987), On the role of sea-surface temperature gradients in forcing low-level winds and convergence in the tropics, *J. Atmos. Sci.,* **44**, 2440-2458.

Liu, Z. (1994), A simple model of the mass exchange between the subtropical and tropical ocean, *J. Phys. Oceanogr.,* **24,** 1153–1165.

Liu, Z. and H. Yang (2003), Extratropical Control of Tropical Climate: Atmosphere Bridge and Ocean Tunnel, *Geophys. Res. Lett.*, **30**(5),DOI:10.1029/2002GL016492.

Losada, T., B. Rodríguez-Fonseca, C. R. Mechoso and H.-Y. Ma (2007), Impacts of SST anomalies on the North Atlantic atmospheric circulation: a case study for the northern winter 1995/1996, *Climate Dyn.*, doi 10.1007/s00382-007-0261-x.

Lu, J. and T. L. Delworth (2005), Oceanic forcing of the late 20th century Sahel drought, *Geophys. Res. Lett.*, **32**, L22706, doi:10.1029/2005GL023316.

Luyten, J. R., J. Pedlosky and H. Stommel (1983), The ventilated thermocline, *J. Phys. Oceanogr*., **13**, 292-309.

Madden, R. A. and P. R. Julian (1971), Detection of a 40-50 day oscillation in the zonal wind in the tropical Pacific, *J. Atmos. Sci.,* **28**, 702-708.

Madden, R. and P. Julian (1994), Observations of the 40-50 day tropical oscillation: A review, *Mon. Wea. Rev*., **112**, 814-837.

Madec, G., P. Delecluse, M. Imbard and C. Lévy (1998), OPA 8.1 Ocean General Circulation Model reference manual. *Note du Pôle de modélisation*, Institut Pierre-Simon Laplace, N°11, 91 pp.

Malanotte-Rizzoli, P., K. Hedstrom, H. Arango and D. B. Haidvogel (2000), Water mass pathways between the subtropical and tropical ocean in a climatological simulation of the North Atlantic ocean circulation, *Dyn. Atmos. Oceans*, **32,** 331-371.

Mantua, N. J. and S. R. Hare (2002), *The Pacific Decadal Oscillation*, *J. Oceanogr.*, **58**, p. 35–44. doi:10.1023/A:1015820616384

Marshall, J., Y. Kushnir , D. Battisti, P. Chang, A. Czaja, R. Dickson, J. Hurrell, M. McCartney, R. Saravanan and M. Visbeck, (2001), North Atlantic climate variability: phenomena, impacts and mechanisms, *Int. J. Climatol*., **21**, 1863-1898. DOI: 10.1002/joc.680

Matsuno, T. (1966), Quasi-geostrophic motions in the equatorial area, *J. Meteor. Soc. Japan*, **44,** 25–43.

Matthews, A. J., P. Singhruck and K. Heywood (2007), Deep Ocean Impact of a Madden-Julian Oscillation Observed by Argo Floats, *Science*, **318**, 1765-1769.

Mayer, D. A., R. L. Molinari, M. O. Baringer and G. J. Goñi (2001), Transition regions and their role in the relationship between sea surface height and subsurface temperature structure in the Atlantic Ocean, *Geophys. Res. Lett.,* **28**, 3943–3946.

McCreary, J. P., Jr. and P. Lu (1994), On the interaction between the subtropical and the equatorial oceans: The subtropical cell, *J. Phys. Oceanogr.,* **24**, 466–497.

McPhaden, M. J and B. A. Taft (1988), Dynamics of seasonal and interannual variability in the eastern equatorial Pacific, *J. Phys. Oceanogr.,* **18,** 1713–1732..

Mehta, V. M. (1998), Variability of the tropical ocean surface temperatures at decadal multidecadal time scales. Part I: The Atlantic Ocean, *J. Climate,* **11,** 2351–2375.

Merle, J. (1980), Variabilité thermique annuelle et interannuelle de l'Océan Atlantique équatorial Est: L'hypothèse d'un "El Nino" Atlantique, *Oceanol. Acta* **3**, 209-220.

Meyers, G., J. R. Donguy and R. K. Reed (1986), Evaporative cooling of the western equatorial Pacific Ocean by anomalous winds, *Nature,* **323**, 523–526.

Meyers, S. D., A. Melsom, G. T. Mitchum and J. O'Brien (1998), Detection of the fast Kelvin Wave teleconnection due to El Nino-Southern Oscillation, *J. Geophys. Res.,* **103**, 27655-27663.

Miller, J. R., G. L. Russell and G. Caliri (1994), Continental-scale river flow in climate models, *J. Climate*, **7**, 914-928, doi:10.1175/1520-0442.

Mitchell, T. O. and J. M. Wallace (1992), The annual cycle in equatorial convection and sea surface temperature, *J. Climate*, **5**, 1140-1156.

Mittelstaedt, E. (1991), The ocean boundary along the northwest African coast: Circulation and oceanographic properties at the sea surface, *Prog. Oceanogr.*, **26**, 307-355.

Mo, K. C. and S. Häkkinen (2001), Interannual Variability in the Tropical Atlantic and Linkages to the Pacific, *J. Climate*, **14**, 2740–2762.

Mo, K., G. D. Bell and W. M. Thiaw (2001), Impact of Sea Surface Temperature Anomalies on the Atlantic Tropical Storm Activity and West African Rainfall, *J. Atmos. Sci.,* **58**, 3477-3496.

Moore, D. W. (1968), Planetary-gravity waves in an equatorial ocean. PhD. thesis, Harvard University, Cambridge, Mass.

Moore, D. W., P. Hisard, J.P. McCreary, J. Merle, J. J. O'Brien, J. Picaut, J. Verstraete and C. Wunsch (1978), Equatorial adjustment in the eastern Atlantic, *Geophys. Res. Lett*., **5**, 637-640.

Moron, V., N. Philippon and B. Fontaine (2003), Skill of Sahel rainfall variability in four atmospheric GCMs forced by prescribed SST, *Geophys. Res. Lett*., **30**, 2221, doi:10.1029/2003GL018006.

Motha, R. P., S. K. Leduc, L. T. Steyaert, C. M. Sakamoto and N. D. Strommen (1980), Precipitation patterns in West Africa, *Mon. Wea. Rev.,* **108**, 1567–1578.

Mounier, F., G. Kiladis and S. Janicot (2007), Analysis of the Dominant Mode of Convectively Coupled Kelvin Waves in the West African Monsoon, *J. Climate*, **20**, 1487-1503

Moura, A. D. and J. Shukla (1981), On the dynamics of droughts in northeast Brazil: Observation, theory, and numerical experiments with a general circulation model, *J. Atmos. Sci.,* **38,** 2653–2675.

Musman, S. (1992), Geosat altimeter observations of long waves in the equatorial Atlantic, *J. Geophys. Res.,* **97**, 3573–3579.

Nakazawa, T. (1988), Tropical cloud clusters within the intraseasonal variations over the western Pacific, *J. Meteor. Soc. Japan,* **66**, 823-839.

Nakazawa, T. (1995), Intraseasonal oscillations during the TOGA-COARE IOP, *J. Meteor. Soc. Japan*, **73**, 305-319.

Neelin, J. D., I. M. Held and K. H. Cook (1987), Evaporation-wind feedback and low frequency variability in the tropical atmosphere, *J. Atmos. Sci.,* **44,** 2241-2248.

Newell, R. E. and J. E. Kidson (1984), African mean wind changes between Sahelian wet and dry periods, *J. Climatol.,* **4,** 27–33.

Nobre, P. and J. Shukla (1996), Variations in sea surface temperatura, wind stress, and rainfall over the tropical Atlantic and South America, *J. Climate,* **9**, 2464-2479.

North, G. R., T. L. Bell, F. Cahalan and F. J. Moeng (1982), Sampling errors in the estimation of empirical orthogonal function, *Mon. Wea. Rev.*, **110**, 699–706.

North, G. R. (1984), Empirical Orthogonal Functions and Normal Modes, *J Atmos. Sci.*, **41**, 879-887.

Okumura, Y., S. P. Xie, A. Numaguti and Y. Tanimoto (2001), Tropical Atlantic air-sea interactions and its influence on the NAO, *Geophys. Res. Lett.*, **28**(8), 1507-1510.

Okumura, Y. and S. P. Xie (2004), Interaction of the Atlantic Equatorial Cold Tongue and the African Monsoon, *J. Climate,* **17**, 3589–3602.

Okumura, Y. and S. P. Xie (2006), Some overlooked features of tropical Atlantic climate leading to a new Nino-like phenomenon, *J. Climate*, **19**, 5859-5874.

O'Brien, J. J., D. Adamec and D. W. Moore (1978), A simple model of upwelling in the Gulf of Guinea, *Geophys. Res. Lett.,* **5**, 8, 641-644.

Paeth, H. and A. Hense (2004), SST versus climate change signals in West African rainfall: 20th century variations and future projections, *Climatic Change,* **65**,179–208.

Palmer, T.N. (1998), Nonlinear Dynamics and Climate Change: Rossby's Legacy, *Bull. Amer. Meteor. Soc.*, **79**, 1411–1424.

Pan, L. L. (2005), Observed positive feedback between the NAO and the North Atlantic SSTA tripole, *Geophys. Res. Lett.*, **32**, L06707, doi:10.1029/2005GL022427.

Park, C. K. and S. D. Schubert (1993), Remotely Forced Intraseasonal Oscillations over the Tropical Atlantic, *J. Atmos. Sci.,* **50**, 1, 89-103.

Pelegrí, J. L., J. Arístegui, L. Cana, M. González-Dávila, A. Hernández-Guerra, S. Hernández-León, A. Marrero-Díaz, M.F. Montero, P. Sangrà and M. Santana-Casiano (2005), Coupling between the open ocean and the coastal upwelling region off northwest Africa: water recirculation and offshore pumping of organic matter, *J. Mar. Syst.*, **54,** 3–37.

Peng, S., L. A. Mysak, H. Ritchie, J. Derome and B. Dugas (1995), The differences between early and midwinter atmospheric response to Sea Surface Temperature anomalies in the northwest Atlantic, *J. Climate*, **8**, 137–157.

Peng, S., W. A. Robinson, S. Li and M. P. Hoerling (2005), Tropical Atlantic SST forcing of coupled North Atlantic seasonal responses, *J. Climate*, **18**, 480-496.

Peter, A.C., M. L. Hénaff, Y. du Penhoat, C. E. Menkes, F. Marin, J. Vialard, G. Caniaux and A. Lazar.(2006), A model study of the seasonal mixed layer heat budget in the equatorial Atlantic, *J. Geophys. Res.*, **111**, C06014, doi:10.1029/2005JC003157, 2006

Philander, S. G. H. (1990), *El Niño, La Niña, and the Southern Oscillation.* International Geophysics Series, 46, Academic Press, 293 pp.

Philander, S. G. H., D. Gu, D. Halpern, G. Lambert, N. C. Lau, T. Li and R. C. Pacanowski (1996), The role of low-level stratus clouds in keeping the ITCZ mostly north of the equator, *J. Climate,* **9,** 2958–2972.

Picaut, J. (1983), Propagation of the seasonal upwelling in the eastern equatorial Atlantic, *J. Phys. Oceanogr.,* **13**, 18-37.

Polito, P. S. and P. Cornillon (1997), Long baroclinic Rossby waves detected by TOPEX/POSEIDON, *J. Geophys. Res.*, **102**, 3215-3235.

Pond, S. and G. Pickard (1983), *Introductory Dynamical Oceanography*. Pergamon Press, New York, 329 pp.

Rebert, J., J. Donguy, G. Eldin and K. Wyrtki (1985), Relations between sea level, thermocline depth, heat content, and dynamic height in the tropical Pacific Ocean, *J. Geophys. Res.*, **90**, 11719–11725.

Reverdin, G. and M. J. McPhaden (1986), Near surface current and temperature variability observed in the equatorial Atlantic from drifting buoys, *J. Geophys. Res*., **91**, 6569-6581.

Reynolds, R. W. (1993), Improved global surface temperature analyses using optimum interpolation, *J. Climate*, **2**, 114-119.

Robertson, A. W., C. R. Mechoso and Y.J. Kim (2000), The influence of Atlantic Sea Surface Temperature Anomalies on the North Atlantic Oscillation, *J. Climate,* **13**, 122-138.

Robertson, A. W., J. D. Farrara and C. R. Mechoso (2003), Simulations of the Atmospheric Response to South Atlantic Sea Surface Temperature Anomalies, *J. Climate*, **16**, 2540-2551.

Rodríguez-Fonseca, B. (2001), Relación entre el Régimen de precipitación anómalo en la península Ibérica y la variabilidad de baja frecuencia del sistema climático en el Atlántico Norte. PhD Thesis, UCM.

Rodríguez-Fonseca, B. and M. Castro (2002), On the connection between winter anomalous precipitation in the Iberian Peninsula and North West Africa and the summer subtropical

Atlantic Sea Surface Temperature, *Geophys. Res. Lett.*, **29**(18), 1863, doi:10.1029/2001GL014421

Rodríguez-Fonseca, B. and E. Serrano (2002), Winter 10-Day Coupled Patterns between Geopotential Height and Iberian Peninsula Rainfall Using the ECMWF Precipitation Reanalysis, *J. Climate*, **15**, 1309–1321.

Rodwell, M. J. and C. K. Folland (2002), Atlantic air-sea interaction and seasonal predictability, *Quart. J. Roy. Meteor. Soc.*, **128,** 1413-1443.

Rodwell, M. J., D. P. Rowell and C. K. Folland (1999), Oceanic forcing of the wintertime North Atlantic Oscillation and European climate, *Nature*, **398**, 320–323.

Rogers, J. C. (1984), The association between the North Atlantic Oscillation and the Southern Oscillation in the Northern Hemisphere, *Mon. Wea. Rev.,* **112**, 1999–2015.

Rossby, C. G. (1940), Planetary flow patterns in the atmosphere. *Quart. J. Roy. Meteor. Soc*., **66**, suppl. 68-69.

Rouault, M., P. Florenchie, N. Fauchereau and C. J. C. Reason (2003), South east tropical Atlantic warm events and southern African rainfall, *Geophys. Res. Lett.,* **30,** 8009, doi:10.1029/2002GL014840.

Rouault, M., S. Illig, C. Bartholomae, C. J. C. Reason and A. Bentamy (2007), Propagation and origin of warm anomalies in the Angola Benguela upwelling system in 2001, *J. Mar. Syst.,* doi: 10.1016/j.jmarsys.2006.11.010.

Roundy, P. E. and G. N. Kiladis (2006), Observed Relationships between Oceanic Kelvin Waves and Atmospheric Forcing, *J. Climate,* **19**, 5253-5271.

Rowell, D. P. (2001), Teleconnections between the tropical Pacific and the Sahel, *Quart. J. Roy. Meteor. Soc*., **127**, 1683-1706.

Rowell, D. P. (2003), The impact of the Mediterranean SSTs on the Sahelian rainfall season, *J. Climate*, **16**, 849-862.

Ruiz-Barradas, A., J. A. Carton and S. Nigam (2000), Structure of Interannual-to-Decadal Climate Variability in the Tropical Atlantic Sector, *J. Climate,* **13**, 3286-3297.

Santos, A. M. P., A. S. Kazmin and A. Peliz (2005), Decadal changes in the Canary upwelling system as revealed by satellite observations: Their impact on productivity, *J. Mar. Res.*, **63**, 359–379.

Saravannan, R. and P. Chang (2000), Interaction between tropical Atlantic variability and El Niño–Southern Oscillation, *J. Climate,* **13**, 2177–2194.

Schneider, E. K., B. Huang, Z. Zhu, D. G. DeWitt, J. L. Kinter III, B. Kirtman and J. Shukla (1999), Ocean data assimilation, initialization, and predictions of ENSO with a coupled GCM. *Mon. Wea. Rev*., **127**, 1187-1207.

Schouten, M. W., R. P. Matano and T. P. Strub (2005), A description of the seasonal cycle of the equatorial Atlantic from altimeter data, *Deep-Sea Res*. I, **52**, 477-493.

Schott, F., J. P. McCreary Jr. and G. C. Johnson (2004), Shallow overturning circulations of the tropical-subtropical oceans. *Earth's Climate: The Ocean–Atmosphere Interaction, Geophys. Monogr.,* **147**, Amer. Geophys. Union, 261–304.

Seager, R., Y. Kushnir, P. Chang, N. Naik, J. Miller and W. Hazeleger (2001), Looking for the role of the ocean in tropical Atlantic decadal climate variability, *J. Climate*, **14**, 638– 655.

Seidel, D. J., Q. Fu, W. J. Randel and T. J. Reichler (2008), Widening of the tropical belt in a changing climate, *Nature geoscience*, **1**, 21-24, doi:10.1038/ngeo.2007.38

Servain, J., J. Picaut, and J. Merle (1982), Evidence of Remote Forcing in the Equatorial Atlantic Ocean, *J. Phys. Oceanogr., **12***, 457-463.

Servain, J., A. J. Busalacchi, M. J. McPhaden, A. D. Moura, G. Reverdin, M. Vianna and S. E. Zebiak (1998), A Pilot Research Moored Array in the Tropical Atlantic (PIRATA), *Bull. Amer. Meteor. Soc.*, **79**, 2019-2032.

Servain, J., I. Wainer, J. P. McCreary and A. Dessier (1999), Relationship between the equatorial and meridional modes of climatic variability in the tropical Atlantic, *Geophys. Res. Lett*., **26**, 485-488.

Servain, J., G. Clauzet and I. C. Wainer (2003), Modes of tropical Atlantic climate variability observed by PIRATA, *Geophys. Res. Lett.*, **30**(5), 80031, doi:10.1029/2002GL015124.

Shannon, L. V. (1985). The Benguela ecosystem. 1. Evolution of the Benguela, physical features and processes, *Oceanogr. Mar. Biol. A. Rev*, **23**, 105-182.

Shannon, L. V., A. J. Boyd, G. B. Brundrit and T. Taunton-Clark (1986), On the existence of an El Niño-type phenomenon in the Benguela System, *J. Mar. Res*., **44**, 495-520

Shindell, D.T., R.L. Miller, G.A. Schmidt and L. Pandolfo (1999), Simulation of recent northern winter climate trends by greenhouse-gas forcing, *Nature,* **399**, 452-455, doi:10.1038/20905.

Shinoda, M. and R. Kawamura (1994), Tropical rainbelt, circulation, and Sea Surface Temperatures associated with the Sahelian rainfall trend, *J. Meteor. Soc. Japan,* **72**, 341-357.

Smith, T. M., and R.W. Reynolds (2003), Extended Reconstruction of Global Sea Surface Temperatures Based on COADS Data (1854-1997), *J. Climate*, **16**, 1495-1510.

Spiegel, M.R. (1993), *Estadística*. MacGrawHill, 2 Ed.

Stammer, D. (1997), Global Characteristics of Ocean Variability Estimated from Regional TOPEX/POSEIDON Altimeter Measurements, *J. Phys. Oceanogr.,* **27***,* 1743-1769.

Sterl, A. and W. Hazeleger (2003), Coupled variability and air-sea interaction in the South Atlantic Ocean, *Climate Dyn.,* **21**, 559-571. DOI: 10.1007/s00382-003-0348-y.

Stone, M. (1974), Cross-validatory choice and assessment of statistical predictors. *J. Res. Statist. Soc*., **36**, 111-14.

Suarez, M. J. and P. S. Schopf (1988), A delayed action oscillator for ENSO, *J. Atmos. Sci.*, **45**, 3283-3287.

Sultan, B. and S. Janicot (2001), Intraseasonal modulation of convection in the West African monsoon, *Geophys. Res. Lett.*, **28**, 523-526.

Sultan, B., S. Janicot and A. Diedhiou (2003), The West African monsoon dynamics. Part I: Documentation of intra-seasonal variability, *J. Climate,* **21,** 3389–3405.

Sultan, B., K. Labadi, J. F. Guegan and S. Janicot (2005), Climate drives the meningitis epidemics onset in West Africa, *Plos Medicine,* **2**, 43-49.

Sutton, R. T. and M. R. Allen (1997), Decadal predictability in North Atlantic Sea Surface Temperature and climate, *Nature*, **388**, 563-567.

Sutton, R. T., S. P. Jewson, and D. P. Rowell (2000a), Elements of climate variability in the tropical Atlantic region, *J. Climate,* **13***,* 3261–3284.

Sutton, R. T., W. Norton and S. Jewson (2000b), The North Atlantic Oscillation —What role for the ocean?, *Atmos. Sci. Lett.,* **1,** 89–100.

Terray, L. and C. Cassou (2002), Tropical Atlantic Sea Surface Temperature forcing of quasi-decadal climate variability over the North Atlantic-Europe region, *J. Climate,* **15,** 3170–3187.

Thomson, W. (Lord Kelvin) (1891), *"Popular Lectures"*, **3**. Macmillan, London.

Thompson, D. W. J. and J. M. Wallace (1998), The Arctic Oscillation signature in the wintertime geopotential height and temperature fields, *Geophys. Res. Lett.*, **25**, 1297-1300.

Tippett, M. K. (2006), Filtering of GCM simulated Sahel precipitation, *Geophys. Res. Lett.*, **33**, L01804, doi: 10.1029/2005GL024923.

Tippett, M. K. and A. Giannini (2006), Potentially predictable components of African summer rainfall in a SST-forced GCM simulation, *J. Climate*, **19**, 3133-3144.

Tourre, Y. M. and W. B. White (1995), ENSO signals in global upper ocean temperature, *J. Phys. Oceanogr.,* **25,** 1317–1332.

Trenberth, K. E. and T. J. Hoar (1996), The 1990-1995 El Niño-Southern Oscillation Event: Longest on record, *Geophys. Res. Lett.*, **23**, 57-60.

Trenberth, K. E., J. G. Olson and W. G. Large (1989), A global ocean wind stress climatology based on the ECMWF analyses. National Center for Atmospheric Research, NCAR/TN-338+STR, Boulder, Colorado, 93 pp.

Trzaska, S., A. Robertson and J. Farrara (2004), "Quasi-biennial Variability in the Tropical South Atlantic Simulated by an Atmospheric GCM Coupled to an Ocean Mixed Layer", *Proceedings of the 26th Conference on Hurricanes and Tropical Meteorology*, Miami (USA), 552-553.

Trzaska, S., A.W. Robertson, J.D. Farrara and C.R. Mechoso (2007), South Atlantic Variability Arising from Air–Sea Coupling: Local Mechanisms and Tropical–Subtropical Interactions, *J. Climate*, **20**, 3345–3365.

UNESCO (Ed.) (1996), *Discharge of selected rivers of the world*, II (Part II), UNESCO Publishing.

Uppala, S., Kallberg, P., Simmons, A. J., Andrae, U., Bechtold, V. D. C., Fiorino, M., Gibson, J. K., Haseler, J., Hernandez, A., Kelly, G. A., Li, X., Onogi, K., Saarinen, S., Sokka, N., Allan, R. P., Andersson, E., Arpe, K., Balmaseda, M. A., Beljaars, A. C. M., van de Berg, L., Bidlot, J., Bormann, N., Caires, S., Chevallier, F., Dethof, A., Dragosavac, M., Fisher, M., Fuentes, M., Hagemann, S., Holm, E., Hoskins, B. J., Isaksen, L., Janssen, P. A. E. M., Jenne, R., 25 McNally, A. P., Mahfouf, J. F., Morcrette, J. J., Rayner, N. A., Saunders, R. W., Simon, P., Sterl, A., Trenberth, K. E., Untch, A., Vasiljevic, D., Viterbo, P., and Woollen, J (2005), The ERA-40 Reanalysis, *Quart. J. Roy. Meteor. Soc.*, **131**, 2961-3012. doi: 10.1256/gj04176.

Van Loon, H. and J. C. Rogers, (1978), The seesaw in winter temperatures between Greenland and Northern Europe. Part I: General description, *Mon. Wea. Rev.*, **106**, 296-311.
Vauclair, F. and Y. du Penhoat (2001), Interannual variability of the upper layer of the Tropical Atlantic Ocean from in situ data between 1979 and 1999, *Climate Dyn.*, **17**, 527-546.
Vauclair, F., Y. du Penhoat and G. Reverdin (2004), Heat and mass budgets of the warm upper layer of the Tropical Atlantic ocean in 1979-99, *J. Phys. Oceanogr*., **34**, 903-919.
Vecchi, G. A., B. J. Soden, A. T. Wittenberg, I. M. Held, A. Leetmaa and M. J. Harrison (2006): Weakening of Tropical Pacific Atmospheric Circulation due to Anthropogenic Forcing, *Nature*, **441**, 73-76. doi:10.1038/nature04744.
Vega, A., Y. Du-Penhoat, B. Dewitte and O. Pizarro (2003), Equatorial forcing of interannual Rossby waves in the eastern South Pacific, *Geophys. Res. Lett*., **30**, 1197, doi:10.1029/2002GL015886.
Vellinga, M. and R. A. Wood (2002), Global Climatic Impacts of a Collapse of the Atlantic Thermohaline Circulation, *Climatic Change,* **54**, 251–267.
Venegas, S. A., L. A. Mysak and D. N. Straub (1997), Atmosphere–Ocean Coupled Variability in the South Atlantic, *J. Climate,* **10**, 2904–2920.
Visbeck, M. (2002), The Ocean's Role in Atlantic Climate Variability, *Science*, **297**, 2223-2224.
Visbeck, M., E. P. Chassignet, R. G. Currry, T. L. Delworth, R. R. Dickson, and G. Krahmann (2003), The Ocean's response to North Atlantic Oscillation variability. *The North Atlantic Oscillation: Climatic significance and environmental impact*, J. W. Hurrell, Y. Kushnir, G Ottersen y M. Visbeck, Eds., AGU Geophysical Monograph Series, 113-145.
Vizy, E. K and K. H. Cook (2001), Mechanisms by Which Gulf of Guinea and Eastern North Atlantic Sea Surface Temperature Anomalies Can Influence African Rainfall, *J. Climate*, **14**, 795-821.
Von Storch, H. and C. Frankignoul (1998), Empirical Modal Decomposition in costal oceanography, *The Sea,* **10**, 419-455.
Von Storch, H. and F. W. Zwiers (2001), *Statistical Analysis in Climate Research.* Cambridge University Press. 484 pp.
Wagner, R. G. and A. M. da Silva (1994), Surface conditions associated with anomalous rainfall in the Guinea coastal region, *Int. J. Climatol.,* **14,** 179–199.
Wallace, M. (2000), North Atlantic Oscillation/Annular Mode: Two Paradigms - One Phenomenon, *Quart. J. Roy. Meteor. Soc*., **126**, 791-805
Wallace, J. M. and D. S. Gutzler (1981), Teleconnections in the geopotential height field during the Northern Hemisphere winter, *Mon. Wea. Rev.,* **109**, 784–812.
Wang, C. (2002a), Atmospheric circulation cells associated with the El Niño-Southern Oscillation, *J. Climate*, **15**, 399-419.
Wang, C. (2002b), Atlantic climate variability and its associated atmospheric circulation cells, *J. Climate,* **15**, 1516–1536.
Wang, B. and S. I. An (2002), A mechanism for decadal changes of ENSO behavior: roles of background wind changes, *Climate Dyn.*, **18**, 475-486.
Wang, J. and J. A. Carton (2002), Seasonal heat budgets of the North Pacific and North Atlantic Oceans, *J. Phys. Oceanogr*., **32**, 3474-3489.
Wang, C. and D. B. Enfield (2001), The tropical Western Hemisphere warm pool, *Geophys. Res. Lett.*, **28**, 1635-1638.
Wang, C. (2005), ENSO, Atlantic climate variability, and the Walker and Hadley circulations. In *The Hadley Circulation: Present, Past, and Future.* H. F. Diaz and R. S. Bradley, Eds., Kluwer Academic Publishers, 173-202.
Wang, C. (2006), An overlooked feature of tropical climate: Inter-Pacific-Atlantic variability, *Geophys. Res. Lett.*, **33**, L12702, doi: 10.1029/2006GL026324.
Ward, M. N. (1998), Diagnosis and short-lead time prediction of summer rainfall in tropical North Africa at interannual and multidecadal timescales, *J. Climate,* **11**, 3167-3191.
Weare, B. C. and J. S. Nasstrom (1982), Examples of extended empirical orthogonal function analysis, *Mon. Weath. Rev.,* **110**, 481-485.
Weller, R. A. (2003), Subduction, paper presented at the 'Aha Huliko'a Winter Workshop, *U.S. Off. of Nav. Res.*, Honolulu, Hawaii.
Wen, N., Z. Liu, Q. Liu and C. Frankignoul (2005), Observations of SST, heat flux and North Atlantic Ocean-atmosphere interaction, *Geophys. Res. Lett.*, **32**, L24619, doi:10.1029/2005GL024871.
Woolnough S. J., J. M. Slingo and B. J. Hoskins (2000), The relationship between convection and Sea Surface Temperature on intraseasonal timescales, *J. Climate*, **13**, 2086-2104.

Wyrtki, K. (1975), El Niño—The Dynamic Response of the Equatorial Pacific Ocean to Atmospheric Forcing, *J. Phys. Oceanogr.*, **5**, 572–584.

Xie, S. P. and S. C. H. Philander (1994), A coupled ocean-atmosphere model of relevance to the ITCZ in the eastern Pacific, *Tellus*, **46-A**, no4, 340-350.

Xie, S. P. and P. A. Arkin (1996), Analysis of global monthly precipitation using gauge observations, satellite estimates and numerical model predictions, *J. Climate,* **9**, 840-858.

Xie, S. P. and P. A. Arkin (1997), Global precipitation: A 17-year monthly analysis based on gauge observations, satellite estimates, and numerical model outputs, *Bull. Amer. Meteor. Soc.*, **78**, 2539–2558.

Xie, S. P. (2004), Satellite observations of cool ocean-atmosphere interaction, *Bull. Amer. Meteor. Soc.,* **85**, 195-208.

Xie, S. P. and J. A. Carton (2004), Tropical Atlantic variability: patterns, mechanisms, and impacts, in "*Ocean-Atmosphere Interaction and Climate Variability*", edited by C. Wang, S. P. Xie, and J. A. Carton, AGU Press.

Xie, S. P. and Y. Tanimoto (1998), A pan-Atlantic decadal climate oscillation, *Geophys. Res. Lett.,* **25**, 2185-2188.

Yeshanew, A. and M. R. Jury (2007), North African climate variability Part 2: Tropical circulation systems, *Theor. Appl. Climatol.*, **89**, 37-49

Zebiak, S. E. and M. A. Cane (1987), A model El NinoSouthern Oscillation, *Mon. Wea. Rev.,* **115**, 2262-2278.

Zebiak, S. E. (1993), Air–sea interaction in the equatorial Atlantic region, *J. Climate,* **6,** 1567–1586.

Zhang, Y., J.R. Norris and J.M. Wallace (1998), Seasonality of Large-Scale Atmosphere–Ocean Interaction over the North Pacific, *J. Climate*, **11**, 2473–2481.

Zhang, R. and T. L. Delworth (2006), The impact of Multidecadal Atlantic Oscillation on Indian/ Sahel rainfall and Atlantic Hurricanes, *Geophys. Res. Lett.*, **33**, L17712, doi:10.1029/2006GL026267.

Zorita, E., V. Kharim and H. von Storch (1992), The atmospheric circulation and sea surface temperature in the North Atlantic area in winter: their interaction and relevance for Iberian precipitation, *J. Climate,* **5**, 1097-1108.

GLOSSARY

AD: Angola Dome
AEJ: African Easterly Jet
AGCM: Atmospheric General Circulation Model
AMMA: African Monsoon Mutidisciplinary Analysis
AMO: Atlantic Multidecadal Oscillation
ANETUS: Atlantic NorthEastern Tropical Upwelling System
AO: Artic Oscillation
CC: Canarias Current
CLIVAR: Climate Variability and Predictability
COADS: Comprehensive Ocean-Atmosphere Data Set
EA: Eastern Atlantic mode
EEOF: Extended EOF
EM: Equatorial Mode
EMCA: Extended MCA
ENSO: El Nino and the Southern Oscillation
EOF: Empirical Orthogonal Function
ERA: ECMWF Re-Analysis
EUC: Equatorial UnderCurrent
EWFPC: European Weather Forecast Prediction Center
FT: Fourier Transform
GCM: General Circulation Model
GD: Guinea Dome
GG: Gulf of Guinea
GOOS: Global Ocean Observing Systems
GPCP: Global Precipitation Climatology Project
HS: Horseshoe
IP: Iberian Peninsula
ITCZ: InterTropical Convergence Zone
ITF: Inter-Tropical Front
MCA: Maximum Covariance Analysis
MJO: Madden Julian Oscillation
ML: Mixed Layer
MM: Meridional Mode
MOC: Meridional Overturning Circulation
NAM: Northern Annular Mode
NAO: North Atlantic Oscillation
NBC: North Brazil Current
NBUC: North Brazil UnderCurrent
ND: November-December mode
NEC: North Equatorial Current
NECC: North Equatorial ConterCurrent
NEUC: North Equatorial UnderCurrent
NOAA: National Oceanic and Atmospheric Administration
NTA: North Tropical Atlantic
OCGM: Ocean Circulation Model
OLR: Outgoing Longwave Radiation
OSCAR: Ocean Surface Current Analyses-Real Time
PC: Principal Component
PDO: Pacific Decadal Oscillation

PIRATA: PIlot Research Atmosphere Tropical Atlantic
PNA: Pacific North Atlantic
RT: Radon Transform
SACZ: South Atlantic Convergence Zone
SEC: South Equatorial Current
SECC: South Equatorial Conter Current
SEUC: South Equatorial UnderCurrent
SLP: Sea Level Pressure
SNA: Subtropical North Atlantic
SO: Southern Oscillation
SSA: Subtropical South Atlantic
SSH: Sea Surface Height
SST: Sea Surface Temperature
STA: South Tropical Atlantic
STC: Subtropical/Shallow Tropical Cell
SVD: Singular Value Decomposition
TA: Tropical Atlantic
TAOSTA: Tropical Atlantic Ocean Subsurface Temperature Atlas
TAV: Tropical Atlantic Variability
TEJ: Tropical Easterly Jet
TIW: Tropical Instability Waves
TMM: Tropical Multidecadal Mode
TOGA: Tropical Ocean Global Atmosphere
TP: Topex/Poseidon
WA: West African
WAM: West African Monsoon
WEK: Winter EEOF Kelvin wave
WES: Wind-Evaporation SST
WHWP: Western Hemisphere Warm Pool
WOCE: World Ocean Circulation Experiment

APPENDIXES

APPENDIX I: THEORETICAL FRAMEWORK

BASIC EQUATIONS ON OCEANIC WAVES AND HEAT BUDGET

Along this PhD Thesis, the causes of the SST changes (Chapter 4.1) and the oceanic waves (Chapter 4.2) has been studied in the TAV context. In this Appendix, some basic equations in relation to a simple model that can describe the tropical oceans and solve oceanic waves in the equatorial band are presented. In addition, some aspects of the terms that are at work in the SST variations are also described.

The shallow-water model

A simple model of the tropical oceans can provide singular answers to the oceanic adjustment and the air-sea interaction[1]. In the model, the interface between two inmiscible layers of fluids, each of constant density, simulates the sharp and shallow tropical thermocline that separates the warm surface waters from the cold waters of the deep ocean. The upper layer has density ρ_1, has a mean depth H, and it is bounded above by a rigid lid. The lower layer has density ρ_2 and is infinitely deep so that is must be motionless for the kinetic energy to be finite (Philander, 1990).
The ocean equations are simplified from:
-Boussinesq approximation: ignoring variations in density in the horizontal momentum equations, and taking full account of them when they have a buoyancy implication i.e. in the vertical momentum equation. This is valid when the scale of motion is small compared to the scale height.
-Fluid of constant density, from the continuity equation the flow is incompressible $\nabla \vec{v} = 0$.
-Hydrostatic balance; vertical scales are much smaller than horizontal scales; therefore the pressure does not depend on depth.
Linear hydrostatic motion in the upper layer is driven by the windstress τ that acts as a body force. This motion is associated with a displacement η of the interface and is described by the shallow-water equations

$$\frac{\partial u}{\partial t} - fv + g' \frac{\partial \eta}{\partial x} = \frac{\tau_x}{H} \qquad \text{[I.1a]}$$

$$\frac{\partial v}{\partial t} + fu + g' \frac{\partial \eta}{\partial y} = \frac{\tau_y}{H} \qquad \text{[I.1b]}$$

$$g' \frac{\partial \eta}{\partial t} + c^2 \left(\frac{\partial u}{\partial x} + \frac{\partial v}{\partial y} \right) = 0 \qquad \text{[I.1c]}$$

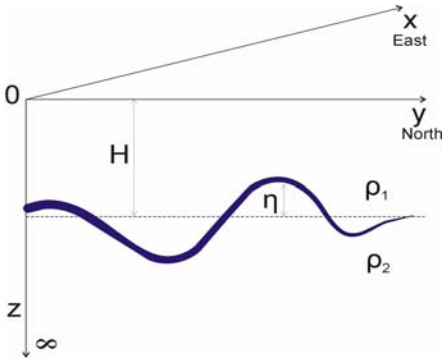

Figure I.1. Scheme of shallow water model described in this section

The Cartesian coordinate system, which is fixed in the rotating earth, is show in figure I.1. The velocity components in the eastward (x) and northward (y) directions are *u* and *v*, respectively, while *t* measures time. The equator is at y=0. Effects caused by the rotation and curvature of the earth enter through the Coriolis parameter *f*, $f = 2\Omega \sin\theta$, where Ω is the rotation of the Earth and θ is the

[1] The theory of the shallow water model and of the oceanic waves has been summarized from Gill (1982), Philander (1990), Cushman-Roisin (1994) and Kundu and Cohen (2002).

latitude. *g* is the gravitational acceleration and, because of the stratification, it is reduced to $g' = \frac{\rho_2 - \rho_1}{\rho_1} g = hg$. The gravity wave phase speed is $c = \sqrt{gh}$, where *h* is the equivalent depth.

Regarding the discussion about the suitability of the shallow water model to describe the observed processes, Kessler et al., (1995) argued that the shallow water model was able to accurately depict the observed thermocline perturbations produced, for instance, by the intraseasonal Kelvin waves despite apparent contribution from at least two baroclinic modes of the continuosly stratified system. As long as the forcing is not too far removed from the response, proper choice of the reduced gravity parameters allows close simulation of the variability resulting from multiple vertical modes (Kessler et al., 1995; Hendon et al., 1998). However, the tuning of the model can be very important. For instance, the observed change in stratification may lead to a shift in frequency and increase in amplitude of individual vertical modes (Gill, 1982). For further discussion see Arnault and Périgaud (1992), who have made a complete review of the altimetry and models in the TA.

Oceanic waves

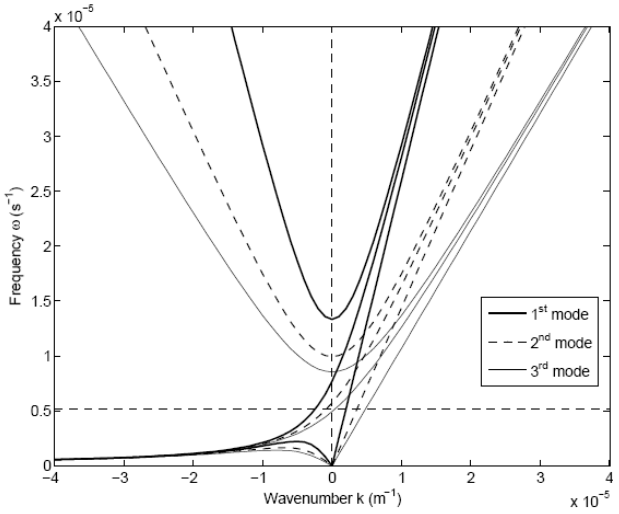

Figure I.2a. Dispersion relations for the first meridional mode equatorial trapped waves in the Atlantic ocean. Curves are drawn for the first three baroclinic modes. Baroclinic mode velocities have been computed using the mean stratification in the Atlantic ocean between 5◦N and 5◦S. The velocities are equal to 2.35 m/s, 1.35 m/s and 0.92 m/s for the 1st, 2nd and 3rd baroclinic mode, respectively. The horizontal dashed line indicates the 14-day period. From Guiavarc'h et al., (2008).

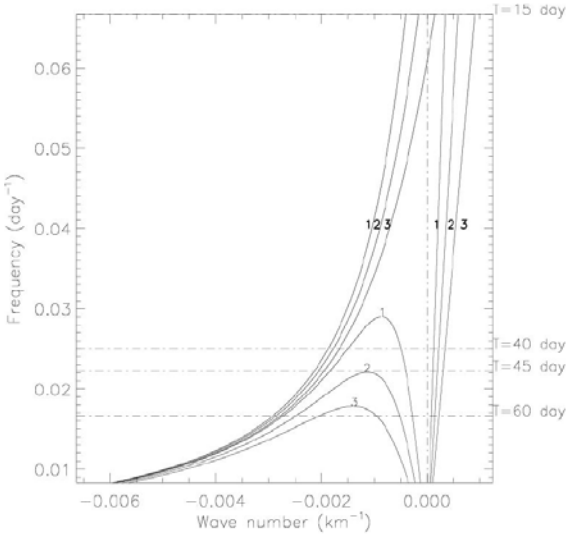

Figure I.2b. Zoom of the dispersion relation of a) from 0 to 15 day period. Dispersion relation for equatorial Kelvin, Rossby and Yanai oceanic waves for the first 3 baroclinic modes of a linear model from Han et al., (2008).

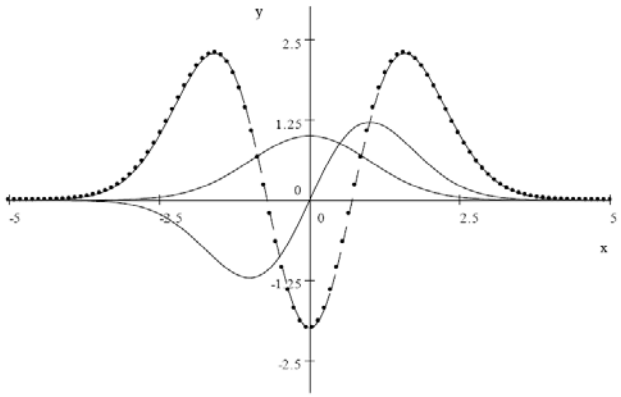

Figure I.2c. The first three Hermite functions that can be used for approximating the amplitude of the first baroclinic meridional Kelvin mode and the first two baroclinic meridional Rossby wave mode at the Equator.

The solutions of simple models (as shallow water model) help to drive the solutions of long waves acting in the ocean in the adjustment to an equilibrium state.
The introduction of two particular waves that are able to observe from satellite measurements are in this section. Figure I.2 shows the dispersion relation of the first three baroclinic modes of the more prominent waves in the equatorial band: gravity-Poincaré waves, long waves and planetary waves.

Kelvin wave

A Kelvin wave is the wave discovered by Kelvin (Thomson, 1879) as a particular solution of long-gravity waves and named the "Kelvin wave" in his honor. From the shallow water model for a homogeneous ocean (a single layer) and a flat bottom, the equations [I.1] can be simplified as:

$$\frac{\partial u}{\partial t} - fv + g\frac{\partial \eta}{\partial x} = 0 \qquad \text{[I.2a]}$$

$$\frac{\partial v}{\partial t} + fu + g\frac{\partial \eta}{\partial y} = 0 \qquad \text{[I.2b]}$$

$$g\frac{\partial \eta}{\partial t} + c^2\left(\frac{\partial u}{\partial x} + \frac{\partial v}{\partial y}\right) = 0 \qquad \text{[I.2c]}$$

Assuming the meridional velocity is null, *v=0* the equation [I.2] can be written as:

$$\frac{\partial u}{\partial t} + g\frac{\partial \eta}{\partial x} = 0 \qquad \text{[I.3a]}$$

$$fu + g\frac{\partial \eta}{\partial y} = 0 \qquad \text{[I.3b]}$$

$$g\frac{\partial \eta}{\partial t} + c^2\left(\frac{\partial u}{\partial x}\right) = 0 \qquad \text{[I.3c]}$$

The equation [I.3b] implies geostrophic movement in the x-axis. Manipulating the [I.3a] and [I.3c], the equation results:

$$\frac{\partial^2 \eta}{\partial t^2} - c^2\frac{\partial^2 \eta}{\partial x^2} = 0 \qquad \text{[I.4a]}$$

$$\frac{\partial^2 u}{\partial t^2} - c^2\frac{\partial^2 u}{\partial x^2} = 0 \qquad \text{[I.4b]}$$

The general solution for [I.4] is

$$\begin{aligned} \eta(x,y,t) &= \tilde{F}(x-ct,y) + \tilde{G}(x+ct,y) \\ u(x,y,t) &= \frac{g}{c}\left[\tilde{F}(x-ct,y) - \tilde{G}(x+ct,y)\right] \end{aligned} \qquad \text{[I.5]}$$

substituting in [I.3], the functions *F* and *G* are exponential functions by:

$$-\frac{f}{c}\tilde{\tilde{F}} = \frac{\partial \tilde{\tilde{F}}}{\partial y}$$
$$\frac{f}{c}\tilde{\tilde{G}} = \frac{\partial \tilde{\tilde{G}}}{\partial y} \qquad \text{[I.6]}$$

If f>0, then G increase exponentially indefinitely, G=0 and $\tilde{\tilde{F}} = e^{-\frac{y}{a}}\tilde{\tilde{F}}(x-ct)$ where $a = \frac{c}{f}$ is the radius of deformation. Therefore, the complete solution is:

$$\eta = e^{-y/a}\tilde{\tilde{F}}(x-ct)$$
$$u = \frac{g}{c}e^{-y/a}\tilde{\tilde{F}}(x-ct) \qquad \text{[I.7]}$$

If F is sinusoidal, then

$$\eta = \eta_0 e^{-y/a}\cos(kx-wt)$$
$$u = \frac{g}{c}e^{-y/a}\cos(kx-wt) \qquad \text{[I.8]}$$

Equation [4] is a wave equation, mathematically can be expressed as $(u,\eta) = (u_0,\eta_0)e^{-y/a}e^{i(kx-\omega t)}$. The determination of the dispersion relationship from the complete solution in [4] leads to:

$$\begin{vmatrix} -iw & gik \\ ik & -\frac{g}{c^2}wi \end{vmatrix} = 0\,;\ w = ck \qquad \text{[I.9]}$$

Where c is the phase speed for long waves without rotation effects. From [I.9] this Kelvin wave results no dispersive (phase speed and group velocity coincide), and its form does not change along the trajectory. The relation is shown in figure I.2. The Kelvin waves are long-gravity waves coastally trapped or equatorially trapped because of earth rotation. If consider vertical planes parallel to the waveguide (the equator or the coast), along the plane, the geostrophic balance occurs. In the perpendicular direction, the amplitude exponentially decays by the factor of -y/a. If the consideration of the ocean is a reduced gravity model (or continuously stratified model), then the phase speed is renamed as $c = \sqrt{hg}$, where h is the equivalent depth.

As the tropics can be considered as two-layer system, this approximation acts to prevail the first baroclinic mode as dominant. The first baroclinic mode in the Atlantic is around 2 m/s (França et al., 2003; du Penhoat and Treguier 1985, among others)

Therefore, Kelvin wave is a free wave, no dispersive, it can have subinertial and inertial frequencies, it is the only one capable to propagate eastward between boundaries and they can be forced by wind burst (Philander, 1990). They can also be coastally trapped and the variation of the amplitude perpendicular to the trajectory is exponential. These waves are studied over the TA in Chapter 4.2.

Rossby Waves

The conservation of potential vorticity is the principle from which planetary waves arise. When a parcel of fluid is displaced in the N-S direction on the surface of a rotating sphere, then the fluid is subject to a variation of the Coriolis parameter. For instance, when a small region of the ocean responds to a change in conditions (e.g. a change in current direction or additional wind stress) the system is disturbed locally. If the response has involved a latitudinal displacement of water, then potential vorticity provides a restoring force. Since the restoring force is proportional to the displacement the result is a sinusoidal signal, an intriguing property of which is that the propagation is westward although the displacements are meridional.

Hough (1897) was the first to formulate the equations for planetary wave motion on the rotating sphere and discussed the solutions in spherical coordinates. Rossby (1940) approximated the problem into Cartesian coordinates on a '*β-plane'* by linearizing the latitudinal variation of the Coriolis parameter $f = 2\Omega sin\theta$ as $f=f_0+\beta y$, where y is the meridional (north-south) coordinate and $\beta = \frac{\partial f}{\partial y}$, and identified the planetary waves patterns in the atmosphere.

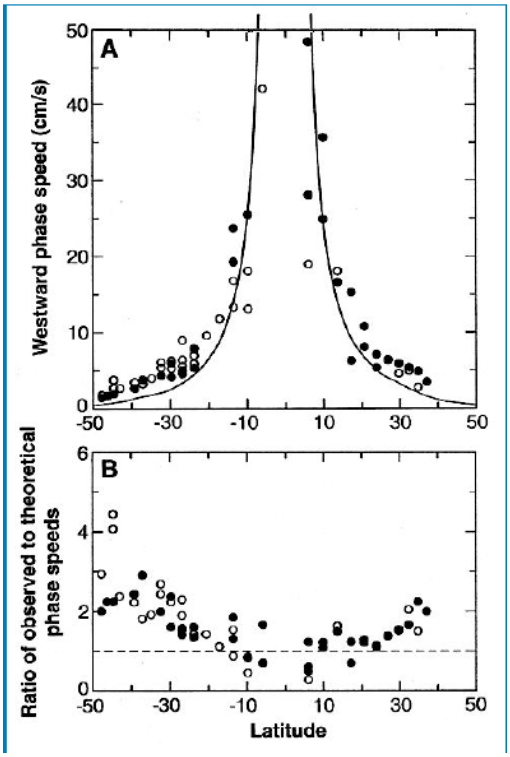

Figure I.3. (A) Globally distributed estimates of the phase speeds of westward-propagating sea level signals estimated from 3 years of TOPEX/POSEIDON altimeter observations. The solid circles correspond to Pacific estimates, and the open circles correspond to Atlantic and Indian Ocean estimates. The global average latitudinal variation of the phase speed predicted by the standard theory for extratropical freely propagating, nondispersive, linear, first-mode baroclinic Rossby waves is superimposed as the continuous line. (B) Ratio of the observed phase speeds to the phase speeds predicted by the standard theory at the same geographical locations as the observations. From Chelton and Schlax, (1996).

The *β*-plane approximation for the ocean implies $\beta y << fo$. In virtue of Carl-Gustav Rossby's essential contribution to the subject, planetary waves are also widely known as Rossby waves. The discussion of the Rossby waves is extra-equatorial (outside the 5°S-5°N latitude band). Although the Rossby waves are superimposed to the mean flow, the low-frequency propagating solutions of the planetary wave equations outside the equatorial band are classically obtained with a further

linearization about a state of zero background flow. From the potential vorticity conservation for shallow water model (single layer and flat bottom):

$$\frac{D}{Dt}\left(\frac{\xi + f}{h}\right) = 0\,, \qquad \text{[I.10]}$$

where ζ is the relative vorticity, *f* the planetary vorticity and *h*=*H*-*η*. Linearizing and in a *β*-plane approximation for a quasi-geostrophic motion:

$\frac{\partial}{\partial t}\left(\frac{\partial^2 \eta}{\partial x^2} + \frac{\partial^2 \eta}{\partial y^2} - \frac{f_0^2}{c^2}\eta\right) + \beta\frac{\partial \eta}{\partial x} = 0$, this equation has a solution of the way $\eta = \hat{\eta} e^{i(kx+ly-wt)}$ and the dispersion relationship results:

$$\omega = \frac{-\beta k}{k^2 + l^2 + f_0^2 / c^2}\,. \qquad \text{[I.11]}$$

For a continuously stratified models $c = \frac{NH}{n\pi}$. Therefore, the solutions can be cast on a number of orthogonal vertical *modes* with different depth structures. All the modes have a westward zonal (east-west) phase speed c_{nx} of the form:

$$c_{nx} = -\frac{\beta}{k^2 + l^2 + \lambda_n^{-2}} \qquad \text{[I.12]}$$

where *n* is the mode number, *k, l* are the zonal (east-west) and meridional (north-south) wavenumbers and λ_n is a characteristic length scale known as *Rossby radius of deformation* for mode *n*. The Rossby radius depends on density stratification and on 1/ |*f* |. The depth-invariant or *barotropic* mode (*n*=0) travels at many metres per second, traversing ocean basins in a matter of weeks, often too fast to be observed by satellites. However there is a great deal of interest in the much slower *baroclinic* (depth-varying) modes, especially the first baroclinic mode (*n*=1), which is the one depicted in figure I.3. The baroclinic modes travel at speeds of the order of 1-10 cm/s, and can affect the western boundary currents and thus have major repercussions on climate.
The minus sign on the right hand side of equation [I.12] indicates that the zonal speed of planetary waves is always westward. Their meridional speed is usually negligible, i.e. they tend to propagate westward or quasi-westward. Their wavelength is typically of hundreds or thousands of kilometres so they can be considered 'long' with respect to the Rossby radius, that is $k, l << 1/\lambda_n^2$ as a consequence $c_{nx} = -\beta\lambda_n^2$, and the waves can also be regarded as non-dispersive. The speed in that case varies with latitude approximately as $\cos\theta / \sin^2\theta$ *(*see the solid line in the figure I.3). It can be demonstrated that, in the long-wave approximation both the phase and group velocities are exactly westward, and that there exists a poleward latitude limit (called *turning latitude*) beyond which, planetary wave solutions become evanescent, i.e. no propagation exists (Gill, 1982).
Rossby waves has been analysed in the PhD Thesis (Chapter 4.2) in relation to the Kelvin waves in the TA.

Heat Balance of the ocean

Since the TA SST interannual variability has been studied in this PhD Thesis (Chapter 4.1) and the question of how much SST variability can be explained by each term is still a topic by itself, in the next section of this appendix, some basic equations about the components of the mixed layer changes are presented.

SST tendencies

The variations of the SST are specified by considering the atmospheric and oceanic components in just one layer (the mixed layer) and the time evolution of the temperature of it. From the conservation equation:

$$\frac{\partial T}{\partial t} + \vec{v}\nabla T = \nabla(k\nabla T) \qquad \text{[I.13]}$$

Where *k* is the thermal diffusion, v fluid velocity and *T* temperature. Considering that each field is the sum of the mean field plus the anomaly, lets say $\zeta = \zeta_m + \zeta'$, the evolution of the surface temperature *T'* in the mixed layer with an *h* depth can be expressed by:

$$\frac{\partial T'}{\partial t} = -\overline{u}\nabla T' - \frac{1}{\overline{h}}\left[(hu)'\nabla\overline{T} + h'\frac{\partial\overline{T}}{\partial t} + \omega_e\left(T - T_h\right)\right] + \frac{Q'}{\rho C_p} + \kappa\nabla^2 T' \qquad \text{[I.14]}$$

This equation has been used by other authors (Frankignoul, 1985; Leewenburgh and Stammer, 2001; Vauclair et al., 2004; Sterl and Hazeleger, 2003), and *u* is the fluid velocity, ω_e is the entrainment considered always positive to the mixed layer, T_h is the temperature in the bottom of the mixed layer or thermocline layer, ρ is the density, *Q* is the heat fluxes with the atmosphere, C_p is the specific heat and κ the diffusion coefficient. The fluid velocity can be considered as the sum of the Ekman plus geostrophic velocities, simplifying for a shallow water model,

$$u_g = -\frac{g}{f}\frac{\partial\eta'}{\partial y}$$
$$v_g = \frac{g}{f}\frac{\partial\eta'}{\partial x} \qquad \text{[I.15]}$$

$$w_e = \frac{1}{\rho f}\left(\frac{\partial\tau_y'}{\partial x} - \frac{\partial\tau_x'}{\partial y}\right) \qquad \text{[I.16]}$$

Where g is the gravity, *f* is the Coriolis parameter and τ is the wind stress. Some simplifications can be done scaling each term. The horizontal Ekman velocity has been neglected as well as the diffusion term (the last right-hand term in equation [I.14]). The equation [I.14] can be written as:

$$\frac{\partial T'}{\partial t} = \underbrace{-\left(\overline{u}\frac{\partial T'}{\partial x} + \overline{v}\frac{\partial T'}{\partial y}\right)}_{1} \underbrace{-\frac{h'}{\overline{h}}\left(\overline{u}\frac{\partial\overline{T}}{\partial x} + \overline{v}\frac{\partial\overline{T}}{\partial y}\right)}_{2} \underbrace{+\frac{g}{f}\left(\frac{\partial\eta'}{\partial x}\frac{\partial\overline{T}}{\partial y} - \frac{\partial\eta'}{\partial y}\frac{\partial\overline{T}}{\partial x}\right)}_{3} \underbrace{-\frac{h'}{\overline{h}}\frac{\partial\overline{T}}{\partial t}}_{4} \underbrace{-\frac{1}{\rho f\overline{h}}\left(\nabla\times\tau'\right)\Delta T'}_{5} + \underbrace{\frac{Q'}{\rho C_p\overline{h}}}_{6}$$

[I.17]

In the right-hand of the equation [I.17], the term 1 corresponds to the advection of the anomalous temperature by the mean flow, the second term consider the mean advection, the term 3 represents

the advection by the anomalous geostrophic currents of the mean temperature, the term 4 considers the temperature mean time variation in anomalous mixed layer depth, the term 5 corresponds to the entrainment by Ekman pumping anomalies, and finally, the term 6 is the atmospheric fluxes result.

The equation can be simplified depending of the considered problem. In Chapter 4.2, the consideration of the SST evolution is observed and then calculated with respect to the anomalous currents by oceanic waves. In this way the equation [I.17] is simplified by the advection terms, neglecting the term $u'\nabla T'$ and the term 4.

$$\frac{\partial T'}{\partial t} \approx -\overline{u}\nabla\overline{T} - \overline{u}\nabla T' - u'\nabla\overline{T} \qquad \text{[I.18]}$$

To study the SNA SST variability and EM variability from Chapter 4.1 (not shown), the importance of the advection terms 1, 2 and 3 as well as the term 4 can neglected. It can be only considered the vertical mixing by the wind stress as Ekman pumping (term 5) anomalies and the turbulent heat fluxes with the atmosphere in the term 5 by scaling to the SST evolution the following terms;

$$\frac{\partial T'}{\partial t} \approx w_e\left(T_s - T_h\right) + u\left(q_s - q_a\right) + u\left(T_s - T_a\right) \qquad \text{[I.19]}$$

The atmospheric turbulent fluxes are considered in the next subsection.

Atmospheric Fluxes

The heat budget is based on the considerations of the atmospheric fluxes, which are;

$$Q_T = Q_l + Q_s + Q_e + Q_w \qquad \text{[I.19]}$$

Qs and *Ql* are the sensible and latent heat fluxes respectively (turbulent fluxes), and correspond to the conduction and evaporation processes. *Qe* and *Qw* are the short and longwave radiation respectively (solar **radiative fluxes)**. The small effects of condensation on the ocean surface and heat transferred by precipitation can be omitted (Gill, 1982). The fluxes are considered as positive upward (to the atmosphere).

Regarding the **turbulent fluxes**, which correspond to the variation in the interface by the conduction and the evaporation, they can be extended expressed as:

$$\begin{aligned} Q_l &= L_v E \\ E &= c_E \rho_a u\left(q_s - q_a\right) \end{aligned} \qquad \text{[I.20]}$$

Where E is the evaporation rate and L_v is the latent heat of vaporization of water (given by L_v=2.5 10^6 J Kg^{-1}), c_E is dimensionless coefficient, u is the wind speed, ρ_a is the air density, q_a is the specific humidity at the standard level (mass of water vapor per mass of air), and q_s is the saturation specific humidity of the air at temperature T_a. The humidity difference is suggesting an air-sea humidity gradient, as the gradient increases, the atmosphere gains heat from the ocean via latent heat flux wind-induced.

The transference of sensible heat can be expressed as proportional to the air-sea temperature difference;

$$Q_s = c_p c_H \rho_a u\left(T_s - T_a\right) \qquad \text{[I.21]}$$

T_s is the sea surface temperature, T_a is air temperature, c_p is the heat capacity, c_H is dimensionless coefficient, ρ_a is the air density, u is the wind speed.

To compute the equation [I.27] of latent heat flux, the saturated specific humidity at air temperature T_a can be calculated from the mixing ratio (r) following the equations;

$$q_{sat} = \frac{r}{1-r} \quad \text{and} \quad r = \frac{0.622 e_w}{1000 - e_w} \qquad \text{[I.22]}$$

Where e_w, the vapour pressure (in hPa) can also easily calculated from the T_a (Gill, 1982).

$$e_w = 6.1078 \bullet 10^{\left(7.5 \frac{T_a}{(273.3+T_a)}\right)} \qquad \text{[I.23]}$$

The ocean is gaining energy mainly because the atmosphere (turbulent fluxes) and the solar radiation (radiative fluxes). But the heat content is also the result of consider other processes as the advection through currents and diffusion. The SST variation, in fact, is the sum of all these processes and the equation of that could be represented by the so called SST tendencies equation (equation I.13 above-mentioned). From the equation [I.19], the SST variations can be simplified. If the terms are linealized and scaled in units of SST rate of change (ºC/month), then the turbulent heat surface anomalies can be determined by:

Latent heat flux: $$Qlat' \approx (u\Delta q)' \approx \underbrace{u'\overline{\Delta q}}_{forcing} + \underbrace{\overline{u}\Delta q'}_{damping} \qquad \text{[I.24]}$$

$$damping\ term = \overline{u}\Delta q' \frac{L_v}{C_p \overline{\overline{H}}_{ML}} \qquad \text{[I.25]}$$

$$forcing\ term = u'\overline{\Delta q} \frac{L_v}{C_p \overline{\overline{H}}_{ML}} \qquad \text{[I.26]}$$

Sensible heat flux: $$Qsen' \approx [u(T_{SST} - T_a)]' \approx u'\overline{\Delta T} + \overline{u}\Delta T' \qquad \text{[I.27]}$$

$$damping\ term = \frac{\overline{u}\Delta T'}{\overline{\overline{H}}_{ML}} \qquad \text{[I.28]}$$

$$forcing\ term = \frac{u'\overline{\Delta T}}{\overline{\overline{H}}_{ML}} \qquad \text{[I.29]}$$

Some considerations on upwelling processes

The maximum changes in the wind stress occur at the equatorial Atlantic, where the upwelling is forced by the currents divergence, inducing an anomalous Ekman drift. Since there is a lack of reliable observational oceanic currents data and therefore it is not possible to calculate the currents divergence at interannual scales.
From Zebiak and Cane, (1987) and Okumura and Xie (2004), the upwelling at the equator can be estimated by the zonal wind stress and the wind stress divergence, proportionally to:

$$we \approx -r_s \tau_x + \nabla \tau \qquad \text{[I.30]}$$

where r_s is a friction coefficient for the shear current. If the τ_x is negative and the divergence is positive, the velocity of the Ekman is positive (upward).
This simplification was done in Chapter (4.1.2) when studying the mechanism related to the EM. The maximum of the wind stress occurs at the west equator, with anomalous convergence over this area, in consistence with more clouds and more precipitation. However, this is not related to maximum anomalous SST (that occurs at the eastern equator). It will work to sustain the SST anomalies at the western Atlantic and along the coast of the GG, but it is not the responsible of the EM evolution.
Slightly off the equator, the term involving the meridional wind stress and the wind stress curl becomes more important. Thus, the Ekman pumping is simplified as:

$$ek = \frac{1}{\rho}\left(\nabla \times \frac{\tau}{f} \right) \qquad \text{[I.31]}$$

This Ekman pumping is important in off-equatorial areas. At 5 degrees of latitude, the anomalous upwelling can create thermocline anomalies and trigger oceanic Kelvin wave (Chapter 4.1.2 and Chapter 4.2).

The entrainment by Ekman pumping in the equation [I.19] can be performed just for one term, the anomalous Ekman pumping via anomalous wind stress.

$$entr = \frac{1}{\rho}\left(\nabla \times \frac{\tau'}{f} \right)\overline{\left(\frac{(T_{SST} - T_{therm}}{H_{ML}} \right)} \qquad \text{[I.32]}$$

The term of anomalous stratification is much more difficult to quantify, although this term can be extracted as:

$$entr = \frac{1}{\rho}\overline{\left(\nabla \times \frac{\tau'}{f} \right)}\left(\frac{(T_{SST} - T_{therm}}{H_{ML}} \right)' \qquad \text{[I.33]}$$

However this term is very simplified and hides two more factors in relation to the stratification changes: one related to the anomalous vertical temperature gradient and another related to anomalous mixed layer depth.

APPENDIX II: ATMOSPHERIC CIRCULATION RELATED TO TROPICAL CONVECTION

Tropical Atlantic Variability modes (1979-2002). Part II: time-evolving atmospheric circulation related to SST-forced tropical convection

JAVIER GARCÍA-SERRANO
Departamento de Geofísica y Meteorología, UCM, Madrid, Spain

TERESA LOSADA
Departamento de Geofísica y Meteorología, UCM, Madrid, Spain

BELÉN RODRÍGUEZ-FONSECA
Departamento de Geofísica y Meteorología, UCM, Madrid, Spain

IRENE POLO
Departamento de Geofísica y Meteorología, UCM, Madrid, Spain

(*JCLI 2191, J. Climate, accepted April 2008*)

ABSTRACT

The ways in which deep convection over tropical Atlantic affects the mid-latitude climate variability through meridional circulation, planetary wave teleconnection and wave-mean flow interaction is examined for the 1979-2002 period, by following the North Atlantic summer to late winter anomalous rainfall evolution. In this way, the first two co-variability modes between anomalous summer tropical Atlantic sea surface temperature (SST) and anomalous summer to late winter precipitation over the North Atlantic basin are analysed using the same methodology of Extended Maximum Covariance Analysis developed for Part I. This work updates the results given by other authors, whose studies are based on different datasets back to the 50´s. To this aim, CMAP precipitation dataset, which includes measures over the ocean, is used to give a complete picture of the interannual rainfall patterns for the last decades.

The first mode, which accounts for more than 40% of the squared covariance fraction (scf), involves SST anomalies related to the Equatorial mode or Atlantic Niño. Its atmospheric response shows variations of the Atlantic Hadley and Ferrel circulations, reinforcing the direct and indirect circulation cells respectively; displacements of the Atlantic Walker circulation, and the excitation of Rossby waves which are trapped into the North African-Asian jet.

The second one, which accounts for 15% of the scf, is associated with the summer Horseshoe pattern and the winter NAO-Tripole. The related atmospheric circulation anomalies include direct thermal forcing (altering the local Hadley cell), perturbations in the ITCZ and a wave-like responses from the Caribbean region.

The method used in this work highlights the seasonal dependence of the modes, in contrast to previous works that lack in taking into account the month-to-month evolution of these modes. The results add new and valuable information to the understanding of these modes from the important period back to the 80's.

1. Introduction

The study of the dynamics of the teleconnections between tropics and extratropics continue to
be a priority in climate research. Several studies have focused on the atmospheric link
between Tropical Atlantic variability (TAV) and mid-latitudes climate on seasonal to decadal
timescales (e.g., Kushnir 1994; Mehta and Delworth 1995; Sutton and Allen 1997; Czaja and Frankignoul 1999).

The study of atmospheric teleconnections involves different processes and mechanisms. First, the excitation of Rossby waves by tropical convection and its associated divergent outflow in regions of strong vorticity gradient, characterized by the rotational component of the flow (Hoskins and Karoly 1981; Sardeshmukh and Hoskins 1988). Second, the deep vertical motion through the divergent part of the flow; these induced anomalies are thermally driven and associated with alterations in the zonal (Walker) and meridional (Hadley) circulations Krishnamurti 1971; Krishnamurti et al. 1973). The perturbations that propagate to the extratropics are further influenced by interactions with asymmetries in the zonal mean flow and with the midlatitude storm tracks

(Hoskins et al. 1983; Simmons et al. 1983; Trenberth 1986).

The dominant modes of SST variability in the tropical Atlantic ocean are the Equatorial Atlantic mode or Atlantic Niño and the Atlantic Meridional pattern. Previous studies show that the Equatorial Mode owes its interannual variations to the Bjerknes positive feedback mechanism (Zebiak 1993; Keenlyside and Latif 2007), while the Atlantic Dipole is not a coupled ocean-atmosphere variability mode (Sutton et al. 2000). The Equatorial Mode is characterized by anomalous SST and heat content at the eastern equatorial basin, and the displacement of the convective region southward and eastward (Zebiak 1993; Ruiz-Barradas et al. 2000; Vauclair et al. 2004). The Atlantic Meridional pattern shows SST anomalies of opposite sign at both sides of the equator. Some studies maintain that it constitutes an intrinsic mode of variability (e.g., Chang et al. 1997; Servain et al. 1999), whilst others support that the two lobes are independent modes (e.g., Dommenget and Latif 2000; Wang 2002). In any case, the centres of action represent an interhemispheric SST gradient and its subtropical northern branch shares SST anomalies with the North Atlantic Horseshoe (NAH, Czaja and Frankignoul 2002) during summer and with the North Atlantic Tripole (NAT, Sutton and Allen 1997) during winter.

Several modelling and observational studies suggest an influence of the summer tropical Atlantic SST on the fall-winter NAO, though the nature of this connection is still unclear. Proposed mechanisms involve the excitation of Rossby waves toward Europe from the Amazon-Caribbean (Drévillon et al. 2003) or the central tropical Atlantic (Peng et al. 2005); and a direct response to the extratropical SST anomalies added to changes in storm activity (Cassou et al. 2004).

The transition between the summer-NAH and the winter-NAT is an important issue still under debate as well as the oceanic forcing in winter atmospheric circulation. Some studies suggest the NAH as the SST forcing (Czaja and Frankignoul 1999; 2002; Drévillon et al. 2001; Cassou et al. 2004; Frankignoul and Kestenare 2005), while others fundamentally point to Subtropical North Atlantic SST anomalies (Rodríguez-Fonseca and Castro 2002; Polo et al. 2005; Rodríguez-Fonseca et al. 2006), in agreement with the dominant tropical forcing (Sutton et al. 2001; Terray and Cassou 2002). In contrary, different works point to the equatorial SST anomalies as the responsible oceanic forcing for the NAO (Drévillon et al. 2003; Peng et al. 2005) or the East Atlantic pattern (Frankignoul and Kestenare 2005; Haarsma and Hazelerger 2006).

The coupled low-frequency variability involved in the connection between the North Atlantic-European atmospheric circulation and the tropical SST anomalies is, thus, controversial and requires further investigation. Therefore, we consider that a clear and robust observational evidence of the tropical-extratropical teleconnections is necessary.

In Part I of this work (Polo et al. 2008), the authors addressed the study of these TAV modes associated with West African rainfall from boreal early spring to late summer, this paper studies the principal mechanisms of the tropical-extratropical atmospheric connection for both the Atlantic Niño damping and the Horseshoe-Tripole transition from summer to late winter.

To investigate the TAV SST-impact on the tropical convection and the summer to winter tropical-extratropical teleconnections described above, we perform an Extended Maximum Covariance Analysis (hereafter EMCA) between summer tropical Atlantic SST and summer to winter North Atlantic precipitation fields.

The paper is organized as follows: Data and methods used are described in the next section. Summer-late winter precipitation sequences related to TAV modes are described in section 3.1, the tropospheric circulation anomalies associated with these sequences are discussed in section 3.2, and section 4 summarizes the concluding remarks.

2. Data and Methodology

1979-2002 monthly Climate Prediction Center (CPC) Merged Analysis of Precipitation (CMAP) (Xie and Arkin 1997) and Extended Reynolds SST (Smith and Reynolds 2003) have been used to study the main coupled modes between summer (JJAS) tropical Atlantic SST anomalies (from 30S to 38N, and from 60W to 34E) and Atlantic anomalous precipitation (pcp) (from 30S to 70N, and from 90W to 35E) . To quantify the anomalous rainfall and compare with Part I results precipitation anomalies have been standarized. Monthly SST and pcp anomalies are calculated subtracting the monthly SST climatology for the period of study, and removing the linear trend.

1979-2002 period is very reliable in the sense of data accuracy because satellite data is included in the precipitation data set and provides information of the precipitation over the ocean, which allows us to follow the deep convection over the basin. In addition to this, several recent papers have addressed the changes in the

observed climate trends from the 70's (Vecchi et al.2006, Hansen et al. 2006, Seidel et al. 2008). This makes the revision of previous studies an interesting task, in order to determine the possible change in the issues already described for longer periods of time.

In order to study the dynamical mechanisms involved in the teleconnections found, different atmospherics fields are extracted from the ERA-40 re-analysis project (Uppala et al. 2005) for 1979-2002. The monthly anomalies have been calculated sustracting the monthly mean climatology for that period. The variables used are: horizontal wind at 925hPa and 200hPa; vertical velocity at 500hPa; geopotential height from 1000hPa to 100hPa; streamfunction and velocity potential at 200hPa. Rotational and divergent components of the upper tropospheric flow are computed applying a finite difference scheme to the streamfunction and velocity potential respectively.

The EMCA methodology implemented in the first part of the study is also applied in this study. It is an extension of the Maximum Covariance Analysis (MCA, Bretherton et al. 1992; Frankignoul and Kestenare 2005) but considering more than one time-lag in one of the arrays.

In this way, we can isolate in the same mode the whole sequence of significant covariant precipitation patterns in relation to the JJAS anomalous SST, obtaining the whole picture of the evolution of the rainfall from summer to winter (JJAS-DJFM). Also, this new methodology increases the number of time series in the analysis, having as many time series per point as time lags used in the analysis.

We have used this kind of statistical methodology with the aim of take into account the intrannual evolution of the interannual variability modes. In this way, EMCA method highlights the seasonal dependence of these modes. In contrast, previous works lack in taking into account the month-to-month evolution of these modes, maximizing lagged covariability independently of the other adjacent seasons and presuming the persistence of the anomalies as a function of time. Thus, we think that the EMCA results could be more robust, particularly regarding to the time-dependence of a mode's evolution.

The results are shown in terms of homogeneous and heterogeneous regression maps for the summer SST and the pcp sequence respectively. The SST homogeneous maps show the amplitude of the projection (for each grid point) of the JJAS SST expansion coefficient (EC) on the grid point anomaly time series of the SST. The pcp heterogeneous maps show the amplitude of the projection of the JJAS SST EC on the grid point anomaly time series (for each of the lags) of the precipitation. Only those areas that are 98% statistically significant with a t-test, are mapped. The squared covariance fraction (scf), a measure of the fraction of covariability explained by each mode, and the correlation coefficient between the independent and dependent Ecs (ruv), completes the information for each mode. To test if the results are statistically significant and the SST-pcp link found is not random, we check the results using a Monte Carlo test, shuffling and applying the EMCA 100 times. The probability density function (PDF) of the scf that arises from these 100 realizations is compared to the non-shuffled - EMCA scf score, giving a significance level (SL) for the connection found.

3. Results

3.1. SST-precipitation patterns

In this section, the first two EMCA modes between the summer to winter precipitation sequence and the summer SST are described, with the aim of finding those tropical Atlantic SST patterns that could be responsible of the rainfall anomalies over the Atlantic region. This description gives us some insights about possible extratropical teleconnections through tropical convection.

a. First Mode: the Equatorial Mode

The leading ECMA mode (Fig. 1h) is characterized by a JJAS SST pattern that resembles the well-known Equatorial Mode (Zebiak 1993); indeed, the correlation coefficient between its EC and ATL3 SST index (Zebiak 1993), during JJAS is 0.93. This mode coincides with the leading mode described in Part I, with a correlation of 0.91. Their first mode has its origin at the southeastern tropical Atlantic basin during the previous late boreal winter season; it evolves into an anomalous SST tongue in summer (related to the Equatorial Mode), and damps at early winter due to a dynamically active ocean, together with the contribution of the anomalous heat fluxes; finally, this mode leads in an opposite way the winter anomalous SSTs at the equatorial Pacific. For positive SST anomalies this pattern is associated with a wide band of positive anomalous precipitation that, in JJAS, covers the entire equatorial Atlantic, accompanied by drier conditions at both sides of the band (Fig. 1a).

Fig. 1b-g show the rest of precipitation sequence of this mode, from JASO to DJFM. In JASO (Fig. 1b), the anomalous rainfall pattern

is similar to the JJAS one, but the rainfall equatorial band seems to split into two regions, western and eastern of the 20W. The negative precipitation anomalies at both sides of the equatorial band decay. In ASON (Fig. 1c), the split of the rainfall equatorial band is clearer, tropical convection over the Gulf of Guinea weaken, whilst anomalous rainfall increases over northern South America. In contrast, during the following lagged season (SOND), last rainfall anomalies suffer a decrease in magnitude; while the anomalous rainfall along the Guinean coast has nearly disappeared. In ONDJ (Fig. 1e), the precipitation anomaly over northern Brazil continues its southern confinement. Negative rainfall anomalies arise over the Gulf of Florida, which could be indicating the upper in-flow convergence along the northern subtropical latitudes. Fig. 1f shows a strengthening of the negative precipitation anomalies over the Gulf of Florida during NDJF. The South America positive rainfall anomaly is reduced spatially to northeastern Brazil. Finally, during DJFM, the Amazonian positive rainfall anomalies show the major spatial confinement to northeastern Brazil (eq-10S / 55W-30W) despite that the tropical-subtropical precipitation dipole is maintained.

The JJAS SST anomalies associated with the rainfall anomalous sequence described above are confined to the tropical Atlantic. The same analysis considering the whole Atlantic basin (not shown), results in a SST anomaly pattern significant just for the tropical region. The correlation between the SST ECs of the leading modes of this two analysis is 0.99; meaning that this is a very robust mode in the sense of spatial domain. Moreover, the PDF of scf shows 1% significance level for this leading mode (Fig. 1j), which reveals the pattern robustness.

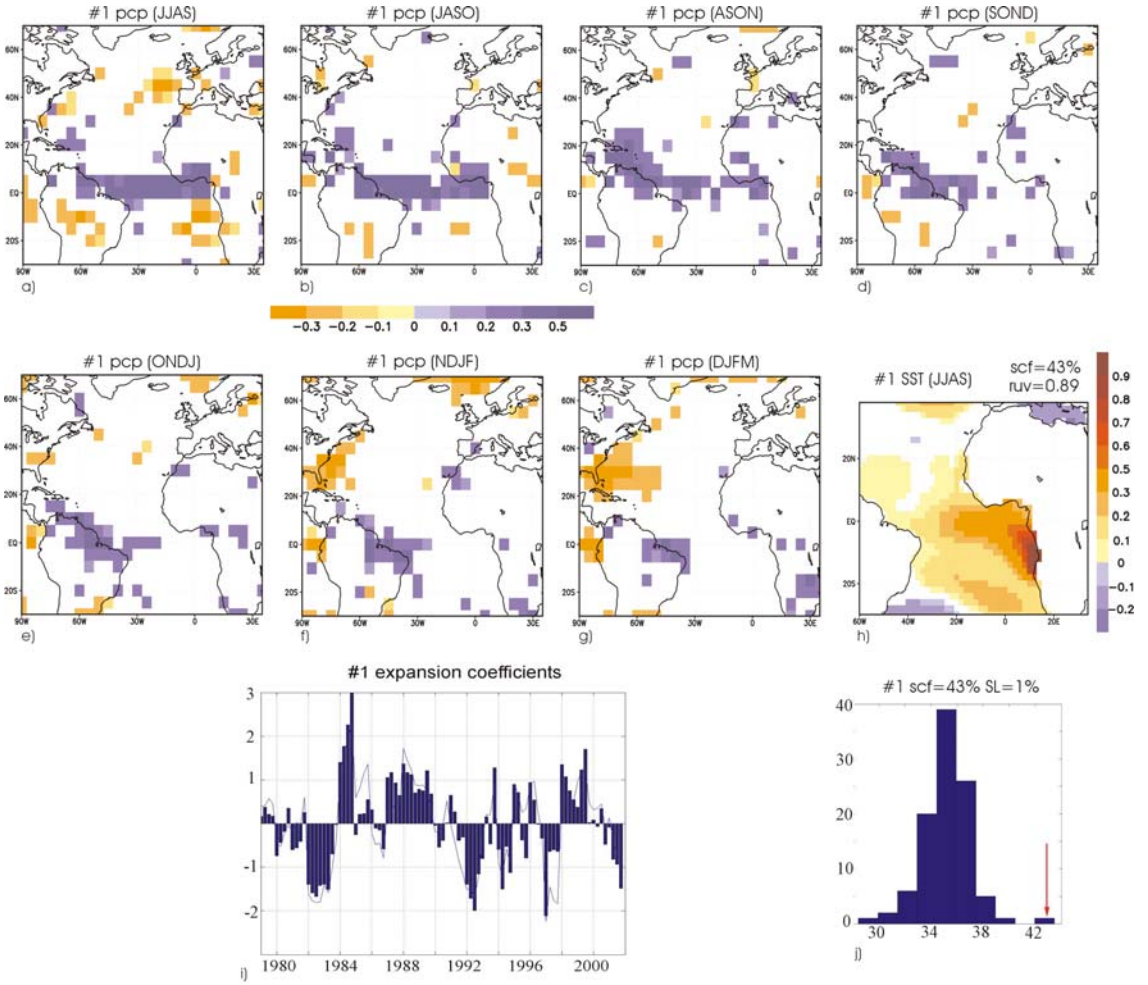

Figure 1. a-h) Regression maps of the summer to winter precipitation and the summer SST onto the leading SST expansion coefficient obtained from the EMCA done between the anomalous summer Tropical Atlantic SST (ºC, JJAS) and summer to winter monthly Atlantic standardized anomalous precipitation (mm/day, JJAS to DJFM). Only 98% statistically significant areas (evaluated with a t-test) are shaded. Square covariance fraction explained by this mode (scf) and linear correlation between expansion coefficients (ruv) is indicated. i) Standardized SST (bars) and precipitation (continuous line) expansion coefficients corresponding to the first EMCA mode. j) Probability Density

Function of the scf from 100 times montecarlo test (histogram) is compared with the original EMCA scf score arrow) to show its significance level (SL).

b. Second Mode: Subtropical North Atlantic

The second ECMA mode (Fig. 2), which explains the 15% of the squared covariance, with 17% significance level for scf (Fig. 2j), relates the SST over the Subtropical North Atlantic (SNA) to a sequence of rainfall patterns that, from summer to autumn, are significant over SNA and, from autumn to winter are significant over Europe. The pcp and SST expansion coefficients are very well correlated (ruv=0.93).

The SST-EMCA second mode projected onto the whole Atlantic Ocean (see Fig. 8) points out a more global-Atlantic structure, identified as the well-known NAH pattern. Moreover, when computing the ECMA considering the whole Atlantic basin (not shown) the obtained pattern reveals the same NAH SST mode (0.93 correlation).

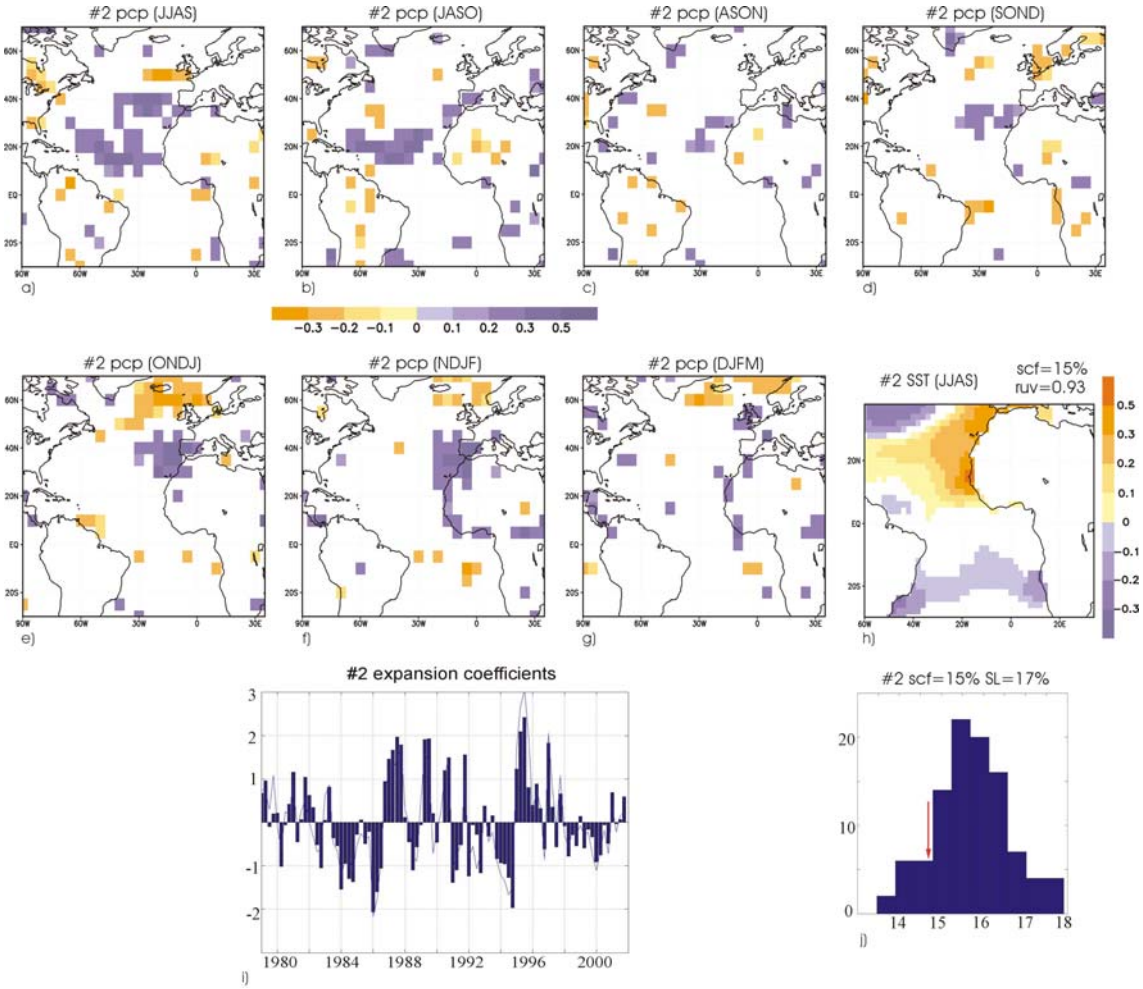

Figure 2. As Fig. 1 but for the second SST-precipitation EMCA co-variability mode.

Fig. 2a shows the spatial distribution of the summer (JJAS) precipitation anomalies over the North Atlantic connected with the contemporaneous SST NAH. It displays positive anomalies over a broad tropical-subtropical region from Mauritanian coast to Caribbean Sea (10N-25N / 60W-15W). In JASO (Fig. 2b), the North Atlantic rainfall dipole at midlatitudes disappears, and the spatial extension of the subtropical positive precipitation band is reduced. In ASON (Fig. 2c) the tropical-subtropical positive anomaly of the North Atlantic basin vanishes. From SOND to DJFM an anomalous rainfall dipole pattern between southwestern and northwestern Europe appears (Fig. 2d-g). Even so, strictly speaking, only the fourth and fifth lags (ONDJ, NDJF; Fig. 2e-f) display a precipitation NAO-signature over North Atlantic-European region: positive (negative) rainfall anomaly covering the Iberian

Peninsula and north-western Africa (northern latitudes). Indeed, the correlation coefficient between the second SST-EMCA EC and NAO index (Hurrell 1995) is statistically significant only during these two seasons (–0.40 and –0.25 respectively).

During late winter (DJFM), the positive precipitation anomaly has moved to the north, and it is located over Western Central Europe, although with a general decreasing in magnitude; and the negative anomalies suffer a slightly northeastward displacement.

The dynamical mechanisms between the tropics and extratropics associated with the EMCA modes will be discussed in section 3.2.b.

3.2. Atmospheric response to SST anomalies

We have used the SST-EMCA ECs as a time index which collects the complete information of the summer to winter time-evolving precipitation mode. Now, we compute regression maps of atmospheric variables to illustrate the dynamical mechanisms associated with the evidence of precipitation-related teleconnections.

a. The decay of the Atlantic Niño

To illustrate how the Atlantic Niño is able to significantly force rainfall anomalies through tropical deep convection, the regression maps of the leading SST-EMCA EC onto the 500hPa anomalous vertical velocity (w500) and the 200hPa upper troposphere divergent wind are shown in Fig. 3. The dynamical information associated with thermally driven vertical movements is completed in Fig. 4, with the projection onto 925hPa wind field and SST. The horizontal upper tropospheric response is characterized by regressing this SST-EMCA EC onto the streamfunction and its derived rotational wind at 200hPa (Fig. 5). The tropical component of the Rossby wave sources (trws; Sardeshmukh and Hoskins 1988; Qin and Robinson 1993), which comprises the advection of the climatological absolute vorticity by the anomalous divergent wind, is also shown in Fig. 3.

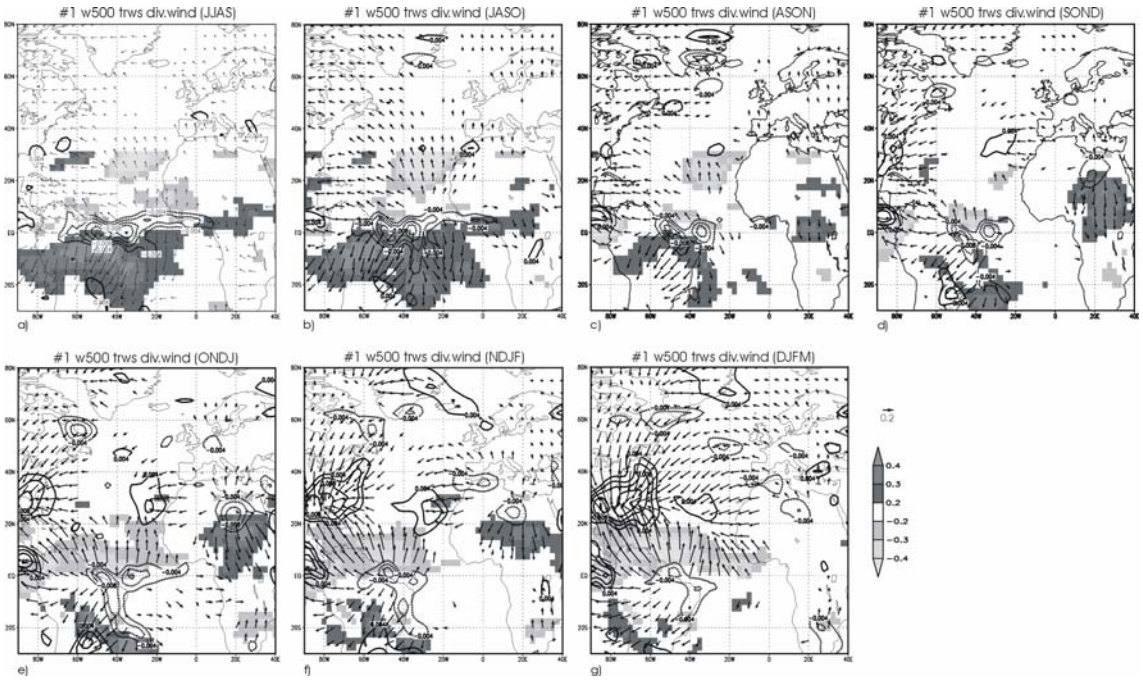

Figure 3. Regression maps of 500hPa vertical velocity (w500; contours, ci=0.002 hPa/s) and 200hPa divergent wind (arrows, m/s), together with the correlation maps of 200hPa tropical Rossby wave sources (trws; shaded) onto the leading SST-EMCA standardized expansion coefficient from JJAS to DJFM . Only 98% statistically significant areas (evaluated with a t-test) are plotted (for divergent wind, vectors in which at least one of the components is statistically significant are shown).

As found by Wang (2002, 2005), Fig. 3a shows how the Atlantic Walker circulation is extended eastward during the peak phase of the Atlantic Niño (JJAS). The anomalous ascending motion is located in the equatorial Atlantic between 60W-0E, while its summer climatological behaviour is associated with upward motions around 60W-50W and downward motions over 20W-0E. Also, observational and model results have shown that the effect of the anomalously warm (cool) cold tongue on the West African summer precipitation consists of a southward (northward) migration of the monsoon ITCZ-rainband and above (below) normal rainfall

along the coast of the Gulf of Guinea (Fontaine et al. 1999; Okumura and Xie 2004). These results are reproduced in Figs. 1a, 3a and 4a: the equatorial eastern Atlantic shows anomalous northwesterly trades winds and upper-tropospheric anomalous divergent outflow, involving positive precipitation anomalies over the region.

Consequently, this mode is associated with variations in the descent Hadley branches of both hemispheres, being responsible of the negative precipitation anomalies in the northern subtropical-midlatitudes (30N-45N) and tropical latitudes in the South Atlantic (5S-20S) respectively (Figs. 1a, 3a). Also, Fig. 5a shows how the upper tropospheric response is dominated by anomalous anticyclonic circulations, according to the subsidence over those regions.

During JASO and ASON, the anomalous rainfall moves away from the Gulf of Guinea (Fig. 1b-c), ascending motions weakens over this region and upper tropospheric divergent outflow migrates westward (Fig. 3b-c). SST anomalies also show a relaxation in the eastern tropical Atlantic (Fig. 4b-c). In fact, the correlation between SST-EMCA and ATL3 declines rapidly: 0.93 (JJAS), 0.72 (JASO), 0.53 (ASON), 0.37 (SOND). SOND is the last season in which SST anomalies cover the entire equatorial Atlantic (Fig. 4d).

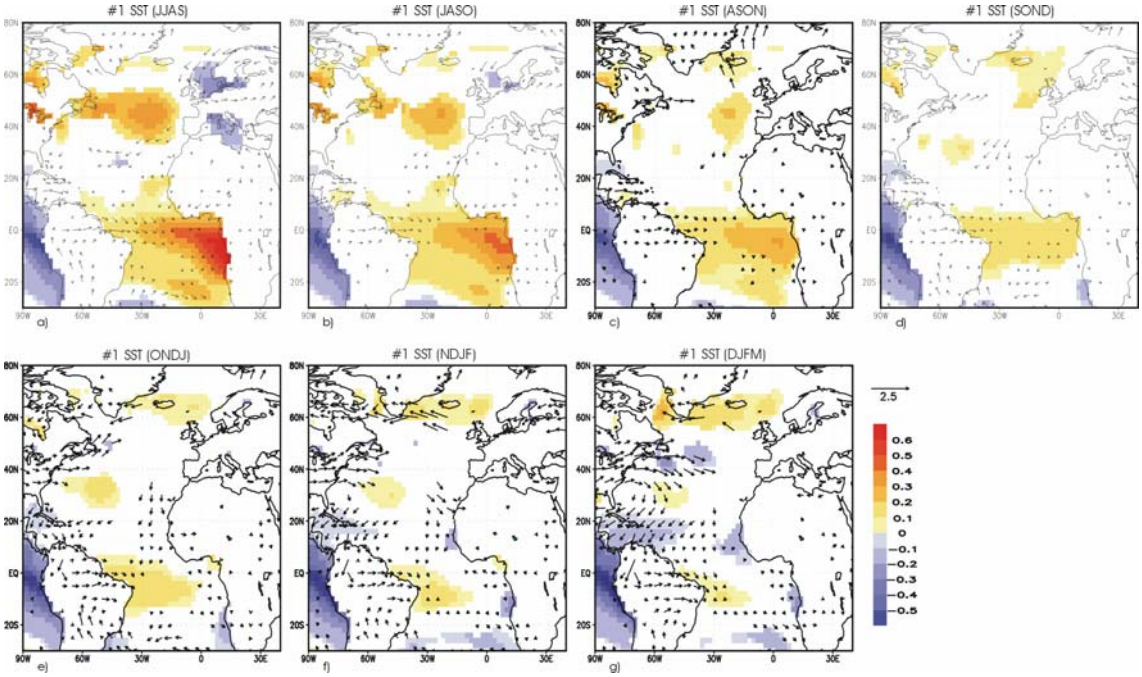

Figure 4. Regression maps of SST (shaded, ºC) and 925hPa horizontal wind (arrows, m/s) onto the first SST-EMCA standardized expansioncoefficient from JJAS to DJFM. Only 98% statistically significant areas (evaluated with a t-test) are plotted (for surface wind, vectors in which atleast one of the components is statistically significant are shown).

The growth of the equatorial SST interannual variations owes its existence to the Bjerknes positive ocean-atmosphere feedback mechanism that involves ocean dynamics, atmospheric convection, and equatorial winds over the ocean basin (Zebiak 1993; Keenlyside and Latif 2007; Polo et al. 2008). The surface convergence and upper divergence, associated with deep convection, tend to move in the direction of positive thermal forcing (Figs. 3a, 4a). Hence, if the Bjerknes positive feedback weakens, the mode decays. As expected, Fig. 4 shows how surface winds tend to displace tropical convection towards South America, so the Atlantic Walker circulation comes back to its climatological position (Figs. 3b-g, 4b-g).

An evidence of this damping-mode is illustrated in Fig. 6, which shows the correlation coefficient scores between the SST-EMCA EC and the Atlantic Walker and Hadley circulation indices created by Wang (2002) for 6 different positive lags (from JASO to DJFM) and 4 different negative lags (from FMAM to MJJA), being JJAS the period corresponding to lag 0. The correlation curves indicate that the anomalous upward motions and divergent outflow gradually increase over the equatorial Atlantic basin. Thus, during the spring-summer transition (negative lags), the SST-EMCA Equatorial mode is associated with an extension of the Atlantic Walker circulation and with a strengthening of the Atlantic Hadley circulation. The maximum correlation appears for the lag 0

(JJAS): -0.67 with the Atlantic Walker index, and 0.50 with the Atlantic Hadley index. Later, correlation curves decrease towards the statistical significance threshold. Such a feature is interpreted as the decrease of the anomalous ascending movements over the equatorial Atlantic, associated with the progressive westward displacement of the divergent circulations from the summer-maximum location (Fig. 3a-g).

Regarding the atmospheric extratropical impacts of the Atlantic Niño, vertical velocity anomalies depict a strengthening of the direct subsidence over the Florida Gulf Coast starting in ASON (Fig. 3c), and more clearly defined from SOND to DJFM (Fig. 3d-g). The associated sequence of negative precipitation anomalies confirms these results during ONDJ-DJFM (Fig. 1e-g), reflecting the local Atlantic Hadley enhancement (divergent wind; Fig. 3e-g). A continuous energy source is required to maintain the divergent meridional circulation in an anomalous state. This source could be linked to the Atlantic SST warming but, although the SST regression maps show the presence of SST anomalies off the northeastern Brazilian coast during all the lags, they clearly decay from ONDJ to DJFM (Fig. 4e-g), accompanied by a damping of the precipitation over the Amazon region (Fig. 1e-g), associated with a weakening of vertical movements (Fig. 3e-g). For this reason, such a feature is not enough to explain the increase of negative rainfall anomalies over the Florida Gulf Coast during the three last EMCA seasons.

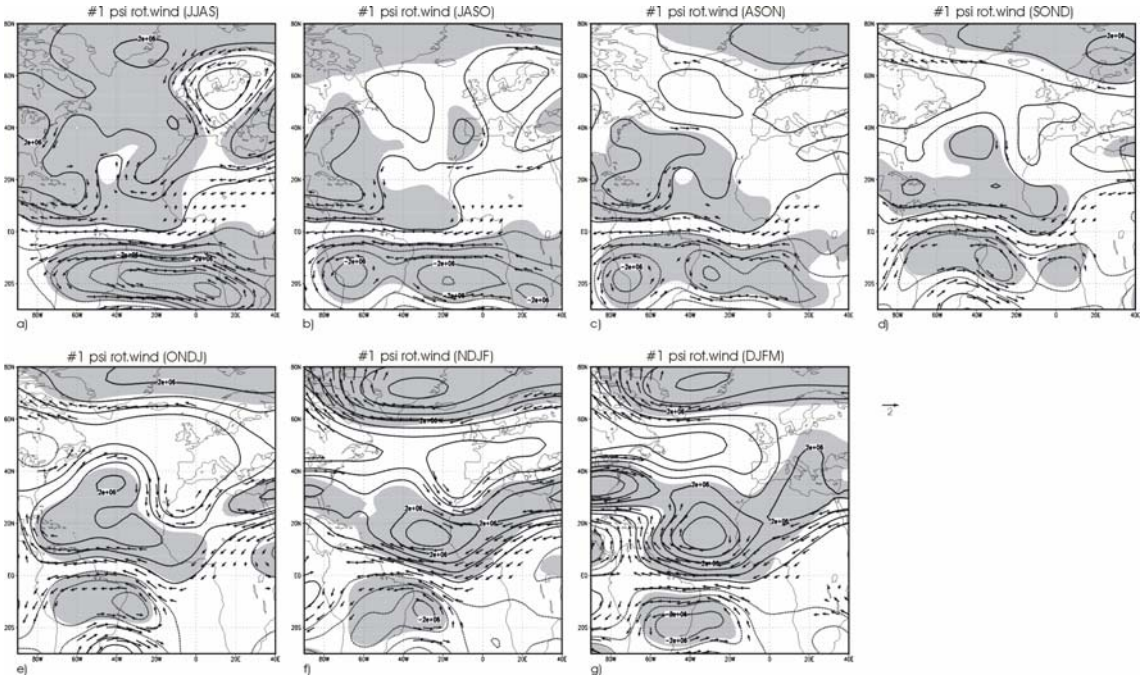

Figure 5. Regression maps of the streamfunction (contours, ci=0.5 106 m/s2) and rotational wind (arrows, m/s) at 200hPa onto the first SST-EMCA standardized expansion coefficient from JJAS to DJFM. Statistically significant areas greater than 98% (evaluated with a t-test) forstreamfunction are shaded. For rotational wind, vectors in which at least one of the components is 98% statistically significant are shown.

As the weakening of the ascending motion over eastern Brasil does not support the progressive subtropical reinforcement, we expect another contributing mechanism to maintain the increasing amplitude of the upper convergent inflow over the subtropical western Atlantic in ONDJ-DJFM (Fig. 3e-g). The analysis of the Rossby waves dynamics (Fig. 5) could give us some insights. But, given that theory predicts that there is not possible poleward rotational propagation following a latitudinal circle (Hoskins and Karoly 1981), the horizontal projection (at 200hPa) of the Rossby response is unable to support the time-evolving subtropical precipitation pattern (Fig. 1e-g).

To diagnose the physical mechanisms involved in the midlatitudes response, a study of the internal atmospheric variability (transient dynamics) is performed. The horizontal components of the Eliassen-Palm vector (E-vector) gives a description of the interaction between synoptic transients eddies and the mean flow due to barotropic processes (Hoskins et al. 1983; Trenberth 1986):

$$\vec{E} = \left(\frac{1}{2} \overline{v'v' - u'u'}, -\overline{u'v'} \right)$$

The convergence (divergence) of E depicts the eddy-induced tendency to decrease (increase) the mean zonal wind. Here we compute the E-

vector components for the horizontal wind filtered daily data using the 24h difference filter described in Wallace et al. (1988).

Fig. 7 shows its regression over the North Atlantic region from SOND to DJFM. In midlatitudes, the E-vector field shows both a clear north-south orientation and a convergence (divergence) in the region about 30N (50N) (Fig. 7b-d). Hence, regressed eddy momentum transports tend to decelerate (accelerate) the westerly mean flow along subtropical (subpolar) latitudes. These findings are in good agreement with the upper wind anomaly depicted in the regression maps of the SST-EMCA expansion coeffcient onto the zonal wind at 200hPa for early-to-late winter (ONDJ-DJFM, Fig. 7). In spite of the weak amplitude of the transient activity (specially during NDJF), the eddy-mean flow interaction is acting like in its climatological direction (Edmon et al. 1980; Hoskins et al. 1983) and, hence, reinforcing the indirect-midlatitudes Ferrel circulation (poleward westerly-injection, equatorward easterly-injection; Held and Hoskins 1985). Such a feature, although weak, could also be contributing to the excited subsidence in the subtropical Atlantic region.

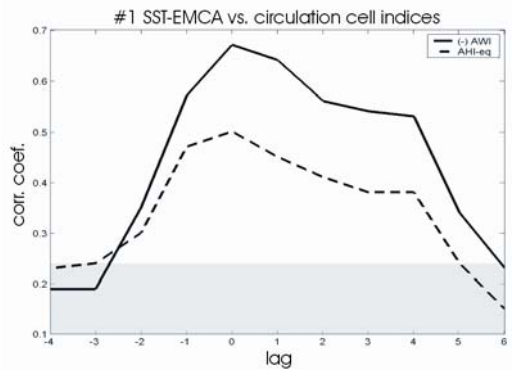

Figure 6. Time evolution of the linear correlation between the first SST-EMCA expansion coefficient (JJAS, lag-0) and the Atlantic Walker circulation index (solid line) and Hadley circulation index (dashed line) (AWI and AHI respectively, as defined by Wang 2002). The time axis is centred in the JJAS monthly sequence (lag-0), lagging one month backward (negative lags) and forward (positive lags), to cover the spring-winter transition (FMAM-DJFM). Shading represents 98% statistical significance threshold.

As none of the possible sources detailed above can totally explain the reinforcement of the subsidence over Florida, an external forcing must be also acting. Fig. 4 depicts the presence of a La Niña SST condition (with steady amplitude) related to the positive phase of the equatorial mode.The lead-lagged connection between Atlantic and Pacific Niños has been discussed in the Part I of this paper. El Niño-Southern Oscillation (ENSO) anomalies could be transferred to the Atlantic sector via the atmospheric bridge (Wang 2002, 2005) or through the PNA (Enfield and Mayer 1997; Giannini et al. 2001); mechanisms that involve reinforced subsidence over subtropical latitudes. Nevertheless, the atmospheric bridge needs a more prominent upper divergence over northern South America, and the only significant temporal-correlation between the SST-EMCA EC and the PNA index (Wallace and Gutzler 1981) occurs during DJFM (r=-0.30). Moreover, the rainfall anomalies associated with the first EMCA mode do not reproduce the observed ENSO impacts in the Tropical Atlantic, associated with more pronounced and northern equator-flank Amazon precipitation and much more weak rainfall over Florida (Giannini et al. 2000, 2001; Alexander et al. 2002). The correlation coefficient between Niño3.4 (Philip and van Oldenborg 2006) and SST-EMCA EC is statistically significant during all lags (~ -0.4); although latter values are lower compared to the correlation with ATL3 index. These results point to an important role of ENSO in the atmospheric response found on the EMCA analysis. It seems like both equatorial coupled phenomena have an impact on the autumn-winter anomalous precipitation dipole in the western subtropical Atlantic. Prescribed SST simulations with an AGCM are needed to quantify this impact.

Finally, over northern African subtropical latitudes, another region of barotropic conversion of energy from the transient eddies to mean flow is present during whole SOND to DJFM transition (Fig. 7a-d). There, the transient dynamics is primarily active in the region of North Africa-Asian jet (Hoskins and Ambrizzi 1993). The E-vector exhibits a divergence (convergence) above (below) 20N inland; thus, the North Africa-Asian jetstream suffers an increase of the zonal wind velocity (Fig. 7). Contrary to North Atlantic midlatitudes transient forcing, here the E-vectors show an east-west orientation indicating a clear zonally elongated axis of Rossby perturbations (Kiladis 1998).

The trws are represented in Fig. 3 (shading areas), indicating the upper tropospheric divergent wind efficiency to disturb downstream the mean flow. Fig. 3 shows upper tropospheric divergent outflow in the equatorial western Atlantic (over South American coast), being the effective trws extended along the subtropical central-eastern Atlantic from SOND to DJFM (Fig. 3d-g). Then, a Rossby wavetrain is excited by the vorticity source at the entrance of the North African-Asian jet, propagating eastward from the tropical eastern Atlantic. The results indicate that anomalies remain trapped in a

narrow meridional band and propagate zonally along the waveguide jet (Figs. 5d-g, 7).

Previous studies (Sardeshmukh and Hoskins 1988; Branstator 2002; Shaman and Tziperman 2005) seems to corroborate the teleconnection presented here, also supporting the suggested response of the sensitivity experiments by Haarsma and Hazeleger (2006).

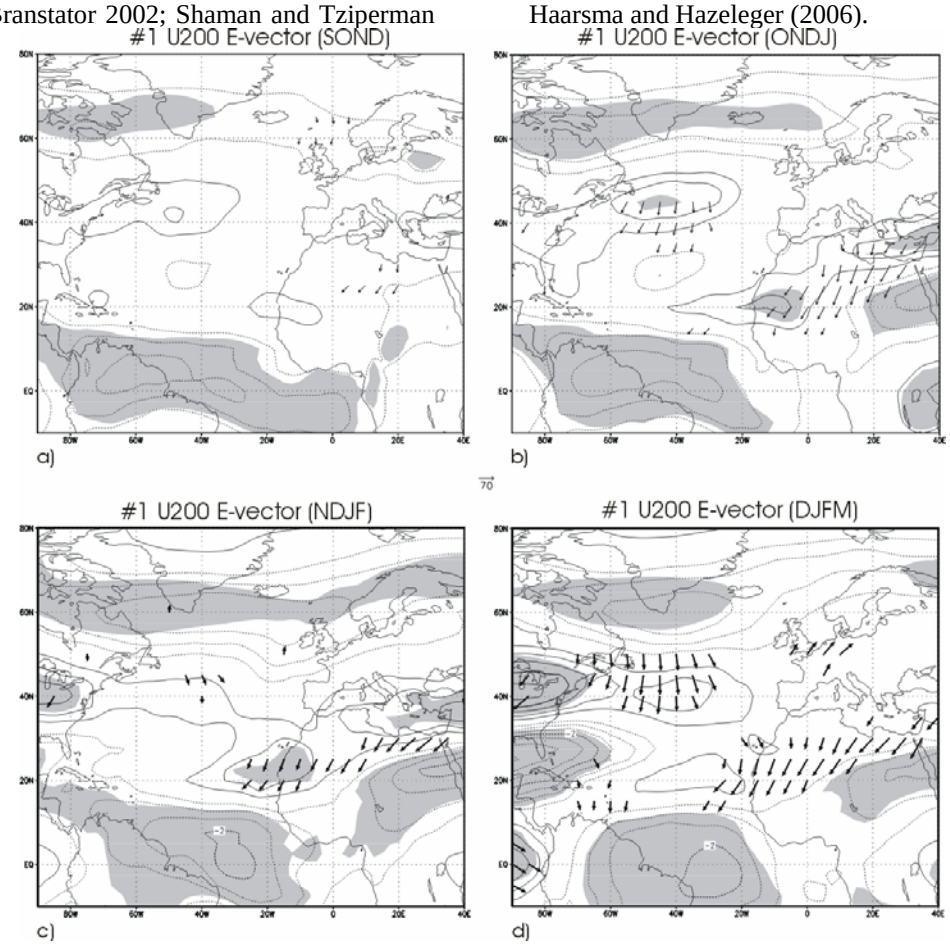

Figure 7. Regression maps of the 200hPa zonal wind (U200; contours, ci=0.5 m/s) and horizontal components of the Eliassen-Palm flux (E-vector; arrows, m2/s2) onto the leading SST-EMCA standardized expansion coefficient from SOND to DJFM. Statistically significant areas greater than 98% (evaluated with a t-test) for U200 are shaded. For E-vector, vectors in which at least one of the components is 98% statistically significant are shown.

b. Horseshoe to Atlantic Tripole transition

Figs. 8 to 10 show the regression, from summer (JJAS) to late winter (DJFM), of the second SST-EMCA EC onto different variables: Fig. 8 shows the regression onto the Atlantic SST and surface winds anomalies, while the regression onto the divergent and rotational components of the circulation are shown in Figs. 9 and 10 respectively.

In section 3.1b it was shown that the oceanic pattern associated with this mode resembles the well defined NAH during JJAS (Fig. 8a).

From JASO the pattern weakens progressively, being the positive subtropical lobe the only one practically persisting in ASON. In SOND, cold SST anomalies over central North Atlantic are reinforced and slightly displaced towards east, and warm anomalies emerge off Newfoundland; also, there is a weakening of the trade winds in the eastern warmer subtropical basin (Fig. 8d). At this stage, the anomalous SST pattern resembles more the obtained in the winter SST-EMCA regressions than the JJAS-associated one; results of Czaja and Frankignoul (2002) also point to this feature.

In ONDJ, the subtropical positive anomalies strengthen again as well as the negative anomalies in the central Atlantic, and positive anomalies at high latitude cover the whole basin width. The anomalous SST pattern resembles now the North Atlantic Tripole (NAT) pattern, just as the atmospheric projection resembles the NAO (Fig. 2e, 9e, 10e). This NAT pattern, which persists until DJFM, peaks in NDJF supporting the Czaja and Frankignoul (2002) and Rodwell and Folland (2002) results of the main atmospheric forcing of the NAT during winter. Thus, we also find that the maximum covariance is reached with the atmosphere (ONDJ-NAO) leading the ocean by one month (NDJF-SST).

During JJAS there is a weakening of the Azores high-related winds (Fig. 8a) and, in turn, of the

trades (Cassou et al. 2004). During JASO and ASON (Fig.8b-c), the midlatitude circulation becomes anticyclonic, the weakening of the trades persists over the subtropical warm SSTs, though it is confined to a narrower subtropical band. In SOND the first stage of an anomalous cyclonic circulation arises in midlatitudes, and it is totally formed in ONDJ, centered on 40N-20W, corresponding with the equivalent barotropic structure of the NAO-seesaw (Fig. 8d-e). During ASON and SOND, a reduction of the trade winds over the warm SST remains, and could act extracting less heat from the tropical western Atlantic, thus reinforcing the SST anomalies, in agreement with results of Chang et al. (1997) and Okumura et al. (2001). The regression of the latent heat flux onto the second mode expansion coefficient (not shown) shows positive values (atmosphere gains heat) over the tropical Atlantic except in the Caribbean Sea during ASON, thus the latent heat flux at this stage acts mostly damping the SST anomalies everywhere but in the western tropical basin. During SOND, the negative latent heat flux anomalies extend to the central tropical Atlantic; the SST anomalies in the western tropical Atlantic could be now reinforced by the heat flux. Nevertheless, the reinforcement of the SST anomalies in the subtropical North Atlantic would be just partially explained by this mechanism and further investigation is required, maybe using a couple model, in order to totally understand it.

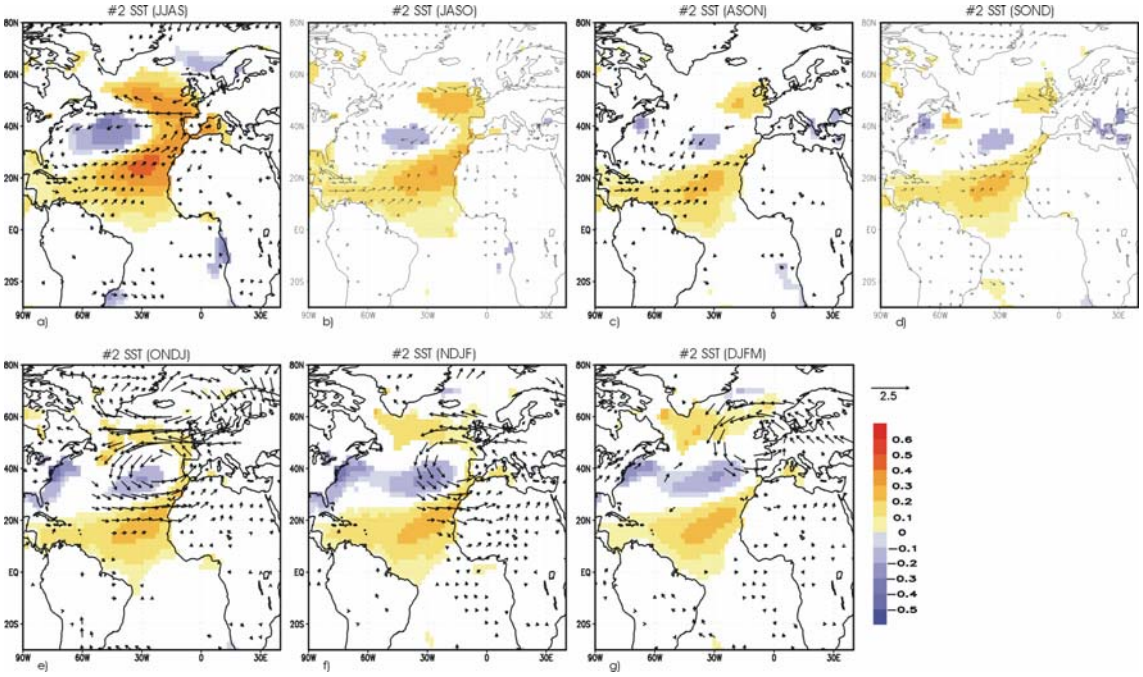

Figure 8. As Fig. 4 but for the second SST-EMCA mode.

Our results show the non persistence of the whole NA anomaly structure throughout the late summer to early winter in relation to the north Atlantic precipitation variability, contrary to Drévillon et al. (2001), Czaja and Frankignoul (2002), Cassou et al. (2004) and Frankignoul and Kestenare (2005) who pointed out that the summer NAH and its persistence could be considered as an isolated forcing of the winter NAO. In the same way, the transition of the NAH to NAT does not correspond to the dominating evolution of the equatorial Atlantic SST anomaly suggested by Peng et al. (2005).

However, the summer NAH exhibits a strong covariability with the next winter NAO-like pattern, as it has been described in the above studies. Our results point out this relationship (Figs. 2e, 8e, 9e, 10e), although including a prior transition towards the winter NAT. Indeed, from the summer NAH it seems that the more effective oceanic forcing of the extratropical winter precipitation is confined to the Subtropical North Atlantic (SNA), in accordance with Rodríguez-Fonseca and Castro (2002) and Rodríguez-Fonseca et al. (2006). Such a feature also is partially in accordance with Peng et al. (2005) whose affirmed the NAH SST is not effective in forcing the following NAO. In our opinion, both the NAH-NAO connection and the NAH-NAT transition are not casual, but causal. Thus, we suggest that the EMCA statistical tool is filtering the summer NAH SST anomaly information which is really connected to the winter NAO (or NAT SST).

We want to understand the NAH damping from JJAS to ASON and how the Atlantic Tripole appears in ONDJ. In JJAS, the warm SST

anomaly over the SNA produces anomalous convection over this region, which generates anomalous divergent wind aloft and anomalous convergence over the Amazon basin, associated with negative rainfall anomalies (Figs. 2a, 8a, 9a). This anomalous upper troposphere convergence over the Amazon persists in JASO and slightly remains in ASON, in agreement with the negative precipitation anomalies over this region (Figs. 2a-c, 9a-c). Similar results are found by Wang (2002, 2005), that relates positive SNA SST anomalies to an inversion of the direct Hadley circulation.

In JASO, the anomalous convergence over the Amazon (Fig. 9b) efficiently modulates the mean flow and triggers a Rossby wave (Fig. 10b-c). The anomalous midlatitudes-anticyclonic circulation is well defined and could be responsible of the anomalous low rainfall located in 35N-55W (Fig. 2b-c). This anomalous high could act damping the anomalous surface westerlies and producing the weakening of the Horseshoe pattern until ASON (Figs. 8b-c, 10b-c).

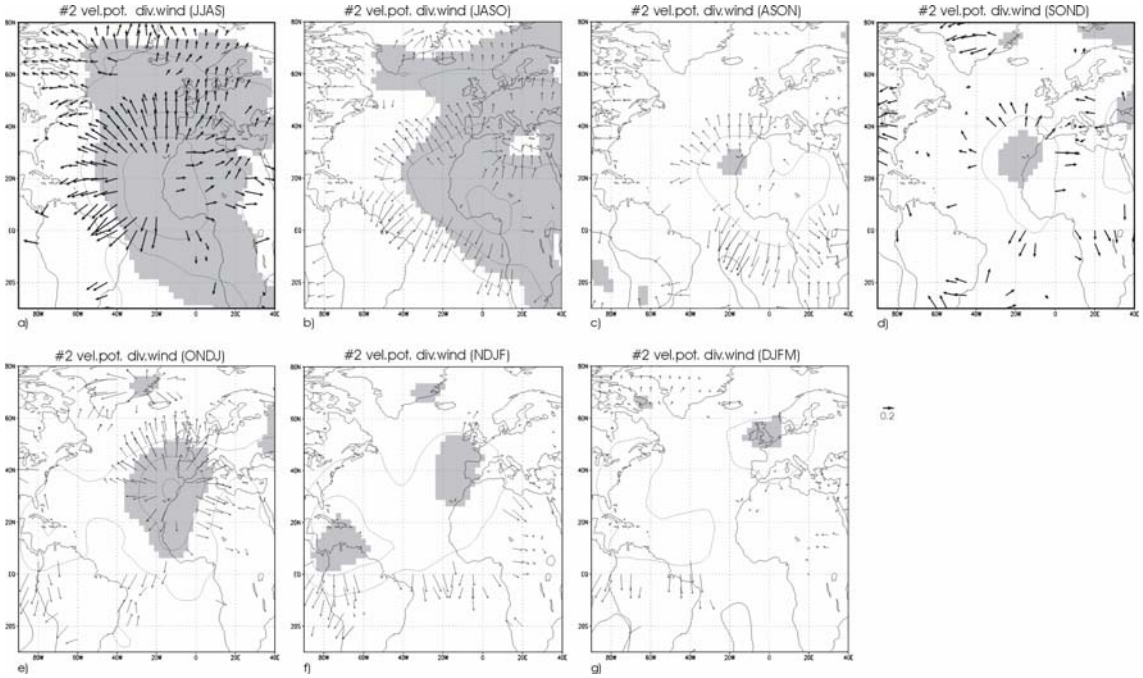

Figure 9. Regression maps of the 200hPa velocity potential (contours, ci=0.2 106 m/s2) and divergent wind (arrows, m/s) onto the second SST-EMCA standardized expansion coefficient from JJAS to DJFM. Statistically significant areas greater than 98% (evaluated with a t-test) for velocity potential are shaded. For divergent wind, vectors in which at least one of the components is 98% statistically significant are shown.

Anomalous trws, associated with large upper convergence, are present in northern South America during JASO and ASON (Fig. 10b-c), supporting the above statement. From SOND this trws weakens and is localized over north-western South America, persisting like this during ONDJ-NDJF.. As the upper convergence over the Amazon basin is weaker in ASON than in JASO (Fig. 9b-c), the associated Rossby response is also weaker in this season, although the anomalous anticyclonic circulation remains in midlatitudes (Figs. 8c, 10c).

During JASO and ASON, significant positive anomalous precipitation are present in the eastern Atlantic (20N-30N; Fig. 2b-c). This could be related to a Gill-type response to the anomalous warm SST centered in 15N, with a local baroclinic structure over the warm SST and barotropic to the north (not shown for these seasons).

During SOND, and more clear in ONDJ-NDJF, the subtropical warm SST anomalies lead to a direct response of the atmosphere that resembles the Gill's solution for oceanic forcing in the tropics: baroclinic in the tropics and equivalent barotropic in the extratropics (Fig. 11a-c, e-g). The geopotential anomalies for atmospheric column show anomalous low pressure in midlatitudes and anomalous high pressure further north, strongly resembling a negative phase of the NAO (Figs. 8e, 9e, 10e). The precipitation anomalies confirm this negative-NAO structure, being positive in the Iberian Peninsula and Northern Africa and negative over northern Europe (Fig. 2d-f).

The divergent wind pattern shows anomalous divergence over the Caribbean sea, very weak in SOND but more clear in ONDJ-NDJF (Fig. 9d-f). This can be indicative of a migration of the Hadley-ITCZ further north than its

climatological position for this season (around 10N instead of 0N), that triggers another Rossby wave associated with high pressure in the upper troposphere (divergence) over the Caribbean sea and low pressure (cyclonic circulation) in midlatitudes (Fig. 8d-f). This mechanism is in accordance with the simulations of Terray and Cassou (2002). Our suggestion is that the effects of the Rossby wave triggered from the Caribbean sea and the response to the warm SST in the eastern part of the Atlantic basin add each other, producing a clear enhancement of the precipitation anomalies in the Iberian Peninsula and Northern Africa during winter (Fig. 2d-f).

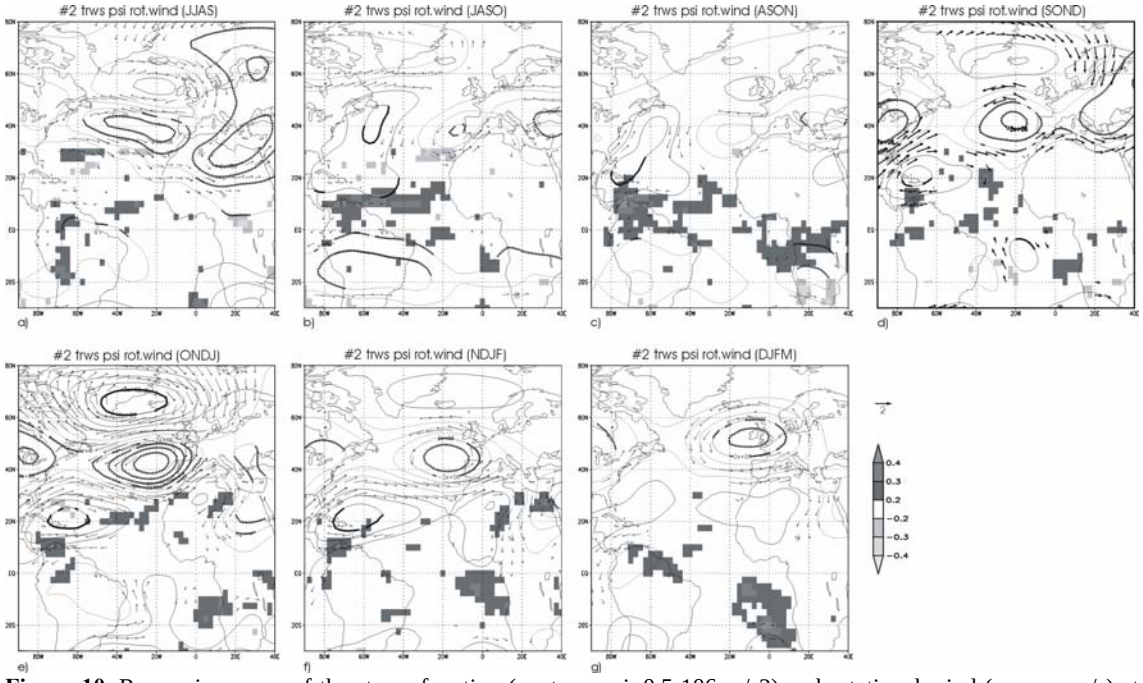

Figure 10. Regression maps of the streamfunction (contours, ci=0.5 106 m/s2) and rotational wind (arrows, m/s) at 200hPa, and correlation maps of 200hPa tropical Rossby wave sources (trws; shaded) onto the second SST-EMCA standardized expansion coefficient from JJAS to DJFM. Statistically significant areas greater than 98% (evaluated with a t-test) for streamfunction are bolded. For rotational wind, vectors in which at least one of the components is 98% statistically significant are shown.

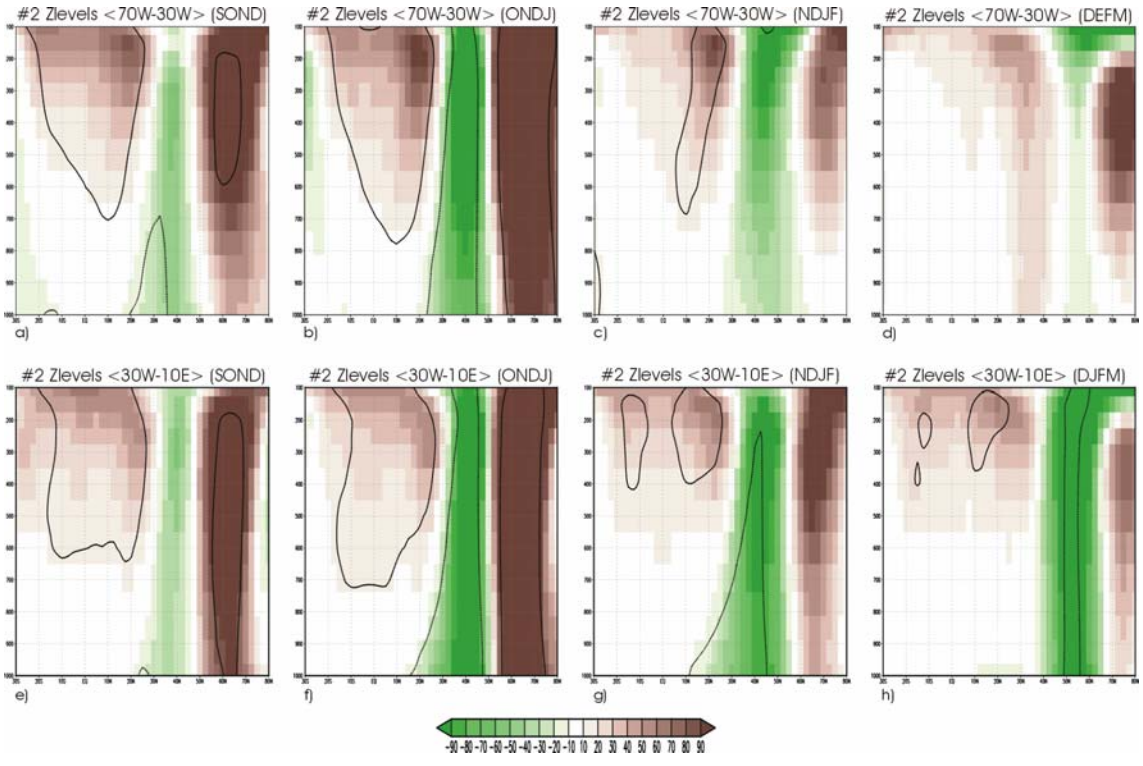

Figure 11. Regression latitude by height profiles (30S-80N, 1000-100hPa) of anomalous geopotential heights (shaded, m) onto the second SST-EMCA standardized expansion coefficient from SOND to DJFM. top) averaged over 70W-30W; bottom) averaged over 30W-10E Contours represent statistical significance greater than 98% (evaluated with a t-test).

Although these processes seem to be at work during SOND-to-NDJF evolution (Figs. 9d-f, 10d-f, 11), some effect is clearly dominating the midlatitudes atmospheric response from ONDJ to determine the NAO-phase structure (the #2 SST-EMCA EC is correlated with the NAO index only during ONDJ and NDJF). From early winter, there is a reinforcement of the anomalous meridional SST gradient at midlatitudes off Newfoundland (Fig. 8e-f), which could have an influence on the precipitation pattern. Losada et al. (2007) have suggested that the anomalous extratropical SST gradient lead to increase the kinetic energy of the transient eddies that is transferred to the mean flow in the upper troposphere.

In order to quantify the activity of transients and associated eddy-mean flow interactions, the regression of the second mode over the anomalous horizontal Eliassem-Palm flux (E-vector) is computed. Fig. 12 shows these results from SOND to DJFM, together with the regression of the anomalous 200hPa zonal wind. The behaviour of the anomalous E-vector varies from autumn to late winter, possibly, as stated by other works (Peng et al. 1995; Cassou et al., 2004) because of the influence of the background state on the efficiency of the eddy-mean flow interaction.

In SOND (Fig. 12a), the anomalous E shows divergence around 50N and convergence around 20N-30N. Thus, transient activity can be interpreted as a deceleration of the subtropical jet and acceleration of the flow further north. From ONDJ to DJFM (Fig. 12b-d), E is divergent around 40N, with E-vector pointing to the pole and giving an acceleration of the jet over midlatitudes with a more zonal extension.

We argue that, during SOND the synoptic eddy activity counteracts the effects of the SST direct forcing-Rossby mechanism explained above, so the anomalous atmospheric cyclonic circulation is weak at this stage. During ONDJ, the transients accelerate the jet around 30N-40N due to barotropic conversion (Fig. 12b), adding its action to the other two and leading to a strong anomalous cyclonic circulation in midlatitudes. Consequently, the exchange of air-mass between the Azores and Iceland is disturbed and a negative phase of the NAO is completely established.

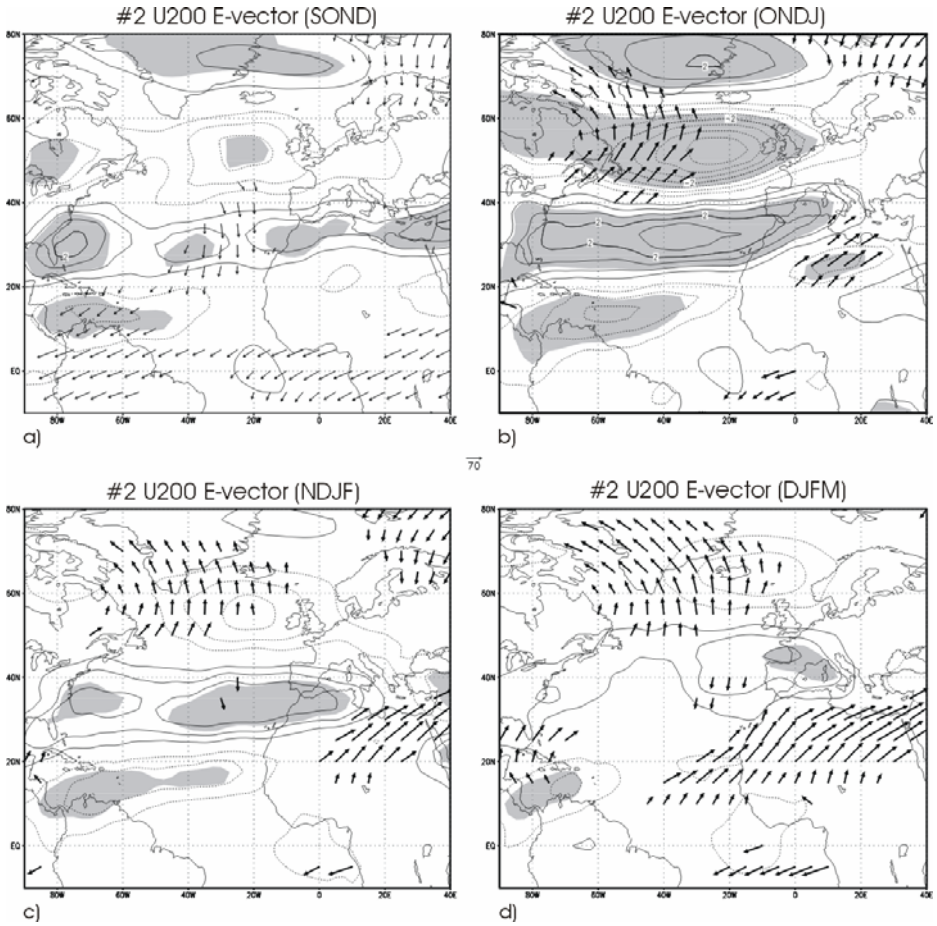

Figure 12. As Fig. 7 but for the second SST-EMCA mode.

During NDJF, the anomalous 200hPa zonal wind around 30N is weaker (Fig. 12c) and the negative lobe of the precipitation anomalous dipole diminishes (Fig. 2f). As the Rossby wave activity does not significantly change compared with ONDJ (Figs. 9e-f, 10e-f), the effective transient flux (Fig. 12c) seems to play again the dominant factor in the NAO-like seesaw (Figs. 2f, 11c-g): the westerly eddy-forcing of mean horizontal circulation (E divergence) is located northward (50N), being less effective in forcing a negative NAO phase. However, the midlatitudes rainfall anomalies persist in magnitude and location (Fig. 2e-f), supporting that the tropical influence in the NAO pattern is not negligible (Figs. 10f, 11g).

During DJFM, neither rotational wind anomalies, nor trws appear over the Caribbean (Fig. 10g). Positive precipitation anomalies are located over British Isles (Fig. 2g), in the region of anomalous cyclonic circulation (Fig. 8g). They might be caused, in part, by the remote effect of the positive SST anomalies in the eastern subtropical Atlantic as there is a Gill-response in this part of the column (Fig.11d-h). The streamfunction and easter-trws distribution in this area (Fig. 10g) could be an indicative of a direct Rossby wave that would be responsible of the cyclonic circulation located over western Europe. The divergence of E-vector around 45N-50N (Fig. 12d) indicates transference of energy to the Atlantic jet, that would strengthen the anomalous circulation generated by the Rossby wave.

4. Conclusions

The different ways in which SST forced tropical convection can trigger teleconnections are analysed in this study by describing the atmospheric response associated with the first two coupled modes between the summer Tropical Atlantic SST and North Atlantic summer to late winter time-evolving anomalous precipitation.

This impact of the summer tropical SST anomalies is analysed applying the Extended MCA (EMCA) developed and described in Part I (Polo et al. 2008), which is an extension of the Maximum Covariance Analysis (MCA). Polo et al. (2008) have investigated the modes of boreal early spring to late summer anomalous Tropical Atlantic SST related to the summer West African rainfall anomalies. Analogously, in the present study, the EMCA has allowed us to determine modes characterized by a time sequence of anomalous precipitation structures related to the summer Tropical Atlantic SST variability, improving our understanding of the role of tropical convection and its subsequent extratropical connection.

The analysis has been done for the 1979-2002 period, for which important changes in the observed climate trends have been documented, using an enhance data set with information over the ocean.

The above mentioned features have made this work an interesting task that revises previous studies in order to determine the possible change in the issues already described for longer periods of time and different methodologies.

The leading SST-precipitation EMCA mode is associated with the Equatorial mode or Atlantic Niño, which origin and associated air-sea interaction processes have been already analysed in Part I. In the present paper, this SST mode has been related to a precipitation anomalous band that, during the peak phase (JJAS), covers the whole tropical Atlantic basin from the Brazilian coast to the Gulf of Guinea, affecting the position of the ascendant branch of the Atlantic Walker circulation, the Atlantic Hadley cell and the displacement of the ITCZ. As the eastern equatorial SST anomalies decay, the precipitation and vertical motions associated with the Atlantic Walker cell come back to its climatological location generating large upper tropospheric divergence over northern South America. This upper-divergent outflow, located over the remaining SST anomalies (SOND-DJFM), leads the extratropical climate by, both, zonal and meridional circulation. Zonally, generating Rossby waves that appear to be trapped in the North Africa-Asian jet, supporting the hypothesis of a circumglobal response to the Equatorial mode suggested by Haarsma and Hazeleger (2006); these waves and the transient-eddy feedback can reinforce the wind velocity within the jet. Meridionally, the subtropical subsidence is coherent with the transient activity of midlatitudes synoptic eddies, as the eddy-momentum convergence reinforces the indirect circulation in the western North Atlantic. However, all this features are not enough to explain the more pronounced Subtropical Atlantic rainfall anomalies during the ONDJ-DJFM lags; and a forcing from other basins must be at work. The EMCA results point at the possibility of a remote Pacific-ENSO influence (Fig. 4). Albeit the constant Pacific SST amplitude, thetemporal correlations between the EMCA EC and the Niño3.4 and PNA time-series are weak, and the autumn-winter time-evolving precipitation anomalies are not exactly like the ones described as the Tropical Atlantic response to ENSO. Thus,

although it seems that both Pacific and Atlantic Niños have an influence on the Florida-Amazon anomalous rainfall regions, model simulations are required to clarify the impact of the interaction between both basins. Results of simulations done in the framework of the AMMA-EU project will be the scope of future studies in order to clarify these hypothesis.

One of the novelties of this work resides in the fact of considering as a entire mode the summer to late winter precipitation sequence in relation to the Atlantic Niño, which complements other authors findings (Fontaine et al. 1999; Wang 2002; Okumura and Xie 2004; Wang 2005). Our results reveal that the summer Atlantic Niño pattern and its autumn-winter damping are ineffective in forcing a correlated response over Europe.

Regarding the second SST-pcp EMCA mode, the authors associate it with a thermal forcing located over the Subtropical North Atlantic during all lagged seasons. This SST anomaly is part of a complete North Atlantic pattern present in summer (Horseshoe, NAH) and winter (Tripole, NAT).

The associated EMCA precipitation anomalies cover the tropical north Atlantic during the summer to fall transition (JJAS-ASON) and the North Atlantic-European sector during the fall to late winter transition (SOND-DJFM). During the first stage, with the damping of the Horseshoe, the rainfall pattern decays in the tropical-subtropical Atlantic. The responsible mechanism involves changes in tropical convection, the weakening of the Atlantic Hadley cell, and the emergence of a Rossby wavetrain from Caribbean-Central America that affects the midlatitude circulation, damping the NAH SST anomaly via anticyclonic barotropic circulation (JJAS-ASON). In SOND, the SST anomaly weakly resembles the NAT, and the subtropical forcing leads to a displacement of the ITCZ and changes in the upper divergence over northwestern South America. Such anomalous outflow forces another Rossby wavetrain of opposite polarity from the Caribbean, affecting the trade winds (cyclonic barotropic circulation), which also acts during ONDJ-NDJF. That SOND-SST pattern, associated with a dipole-like precipitation anomaly in Europe, is previous to the NAO pattern. Later, during ONDJ-NDJF, the transient eddy activity adds its effects by affecting the air-mass exchange between Azores-high and Iceland-low through changes in the zonal extension of the subtropical Atlantic jet. Finally, in DJFM, the dipolar precipitation anomaly is displaced northward. The anomalous circulation seems to be the response of the atmosphere to the Subtropical SST anomaly, adding the direct-Gill and forced-Rossby responses, not via perturbations in the ITCZ. The transient activity acts as a positive feedback inducing a large cyclonic anomaly over western Europe.

The above EMCA results, concerning the second EMCA, provide outstanding future research lines. Cassou et al. (2004) evidenced that the NAH's origin could be interpreted as the remote footprint of tropical atmospheric changes, and here we suggest that the damping showed by the NAH through JASO-ASON transition could be understood as a decaying forced by alterations in the Atlantic Hadley cell, and associated with the subtropical warming, via Rossby wave extension from the Amazon convergence zone.

The second EMCA mode shows that the damp in the SST could be due to the negative feedback produced as response to tropical atmosphere alterations. This feature could also explain the gap in the covariance between autumn NAH and winter NAO found in previous studies (Czaja and Frankignoul 1999, 2002; Rodwell and Folland 2002; Frankignoul and Kestenare 2005).

We have also addressed the possibility of a positive feedback between the NAT pattern and the NAO. Note that this feedback begins before the established NAO phase: the SOND tropical-emerging Rossby wavetrain associated with oncoming SST-NAT occurs just in the previous season to winter NAO (ONDJ). Thus, this work also point at tropical atmospheric perturbations as contributors in exciting the midlatitudes transient activity (final responsible of the NAO event).

This study has explored the potential predictability of European fall-winter climate on the basis of the knowledge of summer Tropical Atlantic Variability modes. Although the above relationships are robust and physically coherent regarding temporal and spatial structures, we cannot forget that we are following a linear approach through all the study, thereby missing all the asymmetric remote effects of the tropical convection. Further modelling studies are required to elucidate the potential connections described above, as well as investigate the non-linear atmospheric response to the tropical forcing.

Acknowledgments. This research was supported by the European Project AMMA-EU and the national CGL2005-06600-C03-02 and CGL2006-04471 projects of the Spanish MEC. We wish to thank Dr. C. Roberto Mechoso (UCLA) and Dr. Pablo Zurita (UCM) for useful discussions and comments regarding this study. The ERA-40 not available online datasets were

kindly provided by Dr. Paul Berrisford (University of Reading).

REFERENCES

Alexander, M. A., I. Bladé, M. Newman, J. R. Lanzante, N.-C. Lau and J. D. Scott, 2002: The Atmospheric Bridge: The influence of ENSO teleconnections on air-sea interaction over the global oceans. J. Climate, 15, 2205-2231.

Branstator, G., 2002: Circumglobal Teleconnections, the Jetstream Waveguide, and the North Atlantic Oscillation. J. Climate, 15, 1983-1910.

Cassou, C., C. Desert, L. Terray, J. W. Hurrell and M. Drévillon, 2004: Summer Sea Surface Temperature conditions in the North Atlantic and their impact upon the Atmospheric Circulation in early winter. J. Climate, 17, 3349-3363.

Chang P., L. Ji, and H. Li, 1997: A decadal climate variation in the tropical Atlantic Ocean from thermodynamic air–sea interactions. Nature, 385, 516–518.

Czaja, A. and C. Frankignoul, 1999: Influence of the North Atlantic SST on the atmospheric circulation. Geophys. Res. Lett., 26, 2969-2972.

Czaja, A. y C. Frankignoul, 2002: Observed impact of Atlantic SST anomalies on the North Atlantic Oscillation. J. Climate, 15, 606-623.

Dommenget, D., and M. Latif. 2000: Interannual to decadal variability in the tropical Atlantic. J. Climate, 13, 777–792.

Drévillon, M., L. Terray, P. Rogel and C. Cassou, 2001: Mid latitude Atlantic SST influence on Europe winter climate variability in the NCEP Reanalysis. Climate Dyn., 18, 331-344.

Drévillon, M., C. Cassou and L. Terray, 2003: Model study of the North Atlantic region atmospheric response to autumn tropical Atlantic sea-surface-temperature anomalies. Q. J. R. Meteorol. Soc., 129, 2591-2611.

Edmon, H. J., B. J. Hoskins and M E. McIntyre, 1980: Eliassen-Palm cross sections for the troposphere. J. Atmos. Sci., 37, 2600-2616.

Enfield, D. B. and D. A. Mayer, 1997: Tropical Atlantic sea surface temperature variability and its relation to El Niño–Southern Oscillation. J. Geophys. Res., 102, 929-945.

Fontaine B., N. Philippon and P. Camberlin, 1999: An improvement of June-September rainfall forecasting in the Sahel based upon region April-May moist static energy content (1968-1997). Geophy. Res. Lett., 26, 2041-2044.

Frankignoul, C. and E. Kestenare, 2005: Air-sea interactions in the tropical Atlantic: A view based on lagged rotated maximum covariance analysis. J. Climate, 18, 3874-3890.

Giannini, A., Y. Kushnir and M. A. Cane, 2000: Inteannual variability of Caribbean rainfall, ENSO, and the Atlantic Ocean. J. Climate, 13, 297-311.

Giannini, A., J. C. H. Chiang, M. A. Cane, Y. Kushnir and R. Seager, 2001: The ENSO teleconnection to the Tropical Atlantic Ocean: Contribution of the remote and local SSTs to rainfall variability in the Tropical Americas. J. Climate, 14, 4530-4544.

Haarsma, R. J. and W. Hazeleger, 2006: Extra-tropical atmospheric response to equatorial Atlantic cold tongue anomalies. J. Climate (in press).

Handoh, I. C., A. J. Matthews, G. R. Bigg and D. P. Stevens, 2006: Interannual variability of the Tropical Atlantic independent of and associated with ENSO: Part I. The North Tropical Atlantic. Int. J. Climatol., 26, 1937-1956, DOI: 10.1002/joc.1343.

Hansen J., M. Sato, R. Ruedy, K. Lo, D. W. Lea, and M. Medina-Elizade, 2006: Global temperature Change. Pnas, 103, 14288-14293.

Held, and B. J. Hoskins, 1985: Large-scale eddies and the general circulation of the troposphere. Advances in Geophysics, Vol. 28A, Academic Press, 3-31.

Hoskins, B. J. and D. J. Karoly, 1981: The steady linear response of a spherical atmosphere to thermal and orographic forcing. J. Atmos. Sci., 38, 1179-1196.

Hoskins, B. J. and T. Ambrizzi, 1993: Rossby wave propagation on a realistic longitudinally varying flow. J. Atmos. Sci., 50, 1661-1671.

Hoskins, B. J., I. N. James and G. H. White, 1983: The shape, prop agation, and mean-flow interaction of large-scale weather sys tems. J. Atrnos. Sci., 40, 1595-1612.

Hurrell, J.W., 1995: Decadal Trends in the North Atlantic Oscillation: Regional Temperatures and Precipitation. Science, 269, 676-679.

Janicot, S., V. Moron and B. Fontane, 1996: Sahel droughts and ENSO dynamics. Geophys. Res. Lett., 23, 515-518.

Janicot S., S. Trzaska and I. Poccard, 2001: Summer Sahel-ENSO teleconnection and decadal time scale SST variations, Clim. Dyn, 18, 303-320.

Keenlyside N. S. and M. Latif, 2007: Understanding Equatorial Atlantic Interannual Variability. J. Climate, 30, 131-142.

Kiladis, G.N., 1998: Observations of Rossby waves linked to convection of the eastern tropical Pacific. J. Atmos. Sci., 55, 321-339.

Krishnamurti, T.N., 1971: Tropical east-west circulations during the northern summer. J. Atmos. Sci., 28, 1342–1347.

Krishnamurti, T.N., M. Kanamitsu, W.J. Koss and J.D. Lee, 1973: Tropical east-west circulations during the northern winter. J. Atmos. Sci., 30, 780–787.

Kushnir, Y., 1994: Interdecadal variations in North Atlantic sea surface temperature and associated atmospheric conditions. J. Climate, 7, 141-157.

Kushnir, Y., W. A. Robinson, I. Bladé, N. M. J. Hall, S. Peng and R. Sutton, 2002: Atmospheric GCM response to Extratropical SST anomalies: Synthesis and Evaluation. J. Climate, 15, 2233-2256.

Losada, T., B. Rodríguez-Fonseca, C.R. Mechoso and H.-Y. Ma, 2007: Impacts of SST anomalies on the North Atlantic atmospheric circulation: a case study for the northern winter 1995/1996. Clim. Dyn., doi 10.1007/s00382-007-0261-x.

Mehta, V.M. and T. Delworth, 1995: Decadal variability of the tropical Atlantic ocean surface temperature in shipboard measurements and in a global ocean-atmosphere model. J. Climate, 9, 172-190.

Okumura, Y., S.-P. Xie, A. Numaguti and Y. Tanimoto, 2001: Tropical Atlantic air-sea

interaction and its influence on the NAO. Geophys. Res. Lett., 28 (8), 1507-1510.

Okumura, Y. and S.-P. Xie, 2004: Interaction of the Atlantic Equatorial Cold Tongue and the African Monsoon. J. Climate, 17, 3589–3602.

Peng, S., L. A. Mysak, H. Ritchie, J. Derome, and B. Dugas, 1995: The differences between early and midwinter atmospheric response to sea surface temperature anomalies in the northwest Atlantic. J. Climate, 8, 137–157.

Peng, S., W. A. Robinson, S. Li and M. P. Hoerling, 2005: Tropical Atlantic SST forcing of coupled North Atlantic seasonal responses. J. Climate, 18, 480-496.

Philip, S. and G. J. van Oldenborgh, 2006: Shifts in ENSO coupling processes under global warming. Geophys. Res. Lett., 33, L11704, doi:10.1029/2006GL026196.

Polo, I., B. Rodríguez-Fonseca, and J. Sheinbaum, 2005: Northwest Africa upwelling and the Atlantic climate variability. Geophys. Res. Lett., 32, L23702, doi:10.1029/2005GL023883.

Polo, I., B. Rodríguez-Fonseca, T. Losada and J. García-Serrano, 2007: On the Origin, Impacts and Teleconnections of Tropical Atlantic Variability Modes. Part I: Air-Sea Interactions related to West African Monsoon. J. Climate (submitted).

Qin, J. and W. A. Robinson, 1993: On the Rossby wave source and the steady linear response to tropical forcing. J. Atmos. Sci., 50, 1819-1823.

Rodríguez-Fonseca, B., and M. Castro, 2002: On the connection between winter anomalous precipitation in the Iberian Peninsula and North West Africa and the summer subtropical Atlantic Sea Surface Temperature. Geophys. Res. Lett., 29(18), 1863, doi:10.1029/2001GL014421.

Rodríguez-Fonseca B., I. Polo, E. Serrano and M. Castro, 2006: Evaluation of the North Atlantic SST forcing on the European and northern African winter climate. Int. J. Climatol., 25, doi: 10.1002/7joc.1234.

Rodwell, M. J. and C. K. Folland 2002: Atlantic air-sea interaction and seasonalpredictability. Q. J. R. Meteorol. Soc., 128, 1413-1443.

Rodwell, M. J., M. Drévillon, C. Frankignoul, J. W. Hurrell, H. Pohlmann, M. Stendel and R. T. Sutton, 2004: North Atlantic forcing of climate and its uncertainty from a multi-model experiment. Quart. J. Roy. Meteor. Soc., 130, 2013-2032.

Ruiz-Barradas, A., J. A. Carton, y S. Nigam, 2000: Structure of Interannual-to-Decadal Climate Variability in the Tropical Atlantic Sector. J. Climate, 13, 3286-3297.

Sardeshmukh, P. D. and B. J. Hoskins, 1988: The generation of global rotational flow by steady idealized tropical divergence. J. Atmos. Sci., 45,1228-1251.

Seidel D.J., Q. Fu, W. J. Randel and T. J. Reichler, 2008: Widening of the tropical belt in a changing climate. Nature Geoscience, 1, 21 – 24.

Servain J., I. Wainer, J. P. McCreary and A. Dessier, 1999: Relationship between the equatorial and meridional modes of climatic variability in the tropical Atlantic. Geophys. Res. Lett., 26, 485-488.

Shaman, J. and E. Tziperman, 2005: The effect of ENSO on Tibetan Plateau snow depth: a stationary wave teleconnection mechanism and implications for the South Asian monsoons. J. Climate, 18, 2067–2079.

Simmons, A. J., J. M. Wallace and G. W. Branstator, 1983: Barotropic wave propagation and instability, and atmospheric teleconnections patterns. J. Atmos. Sci., 40, 1363-1392.

Smith, T.M. and R.W. Reynolds, 2003: Extended Reconstruction of Global Sea Surface Temperatures Based on COADS Data (1854-1997). J. Climate, 16, 1495-1510.

Sutton, R. T. and M. R. Allen, 1997: Decadal predictability in North Atlantic sea surface temperature and climate. Nature, 388, 563-567.

Sutton R.T., S. P. Jewson, and D. P. Rowell, 2000: Elements of climate variability in the tropical Atlantic region. J. Climate, 13, 3261-3284.

Sutton R. T., W. Norton and S. Jewson, 2001: The North Atlantic Oscillation —What role for the ocean? Atmos. Sci. Lett., 1, 89–100.

Terray, L. and C. Cassou, 2002: Tropical Atlantic Sea surface temperature forcing of quasi-decadal climate variability over the North Atlantic-Europe region. J. Climate, 15, 3170–3187.

Trenberth, K. E., 1986: An assessment of the impact of transient eddies on the zonal flow during a blocking episode using localized Eliassen–Palm flux diagnostics. J. Atmos. Sci., 43, 2070–2087.

Vauclair F., Y. du Penhoat, and G. Reverdin, 2004: Heat and Mass Budgets of the Warm Upper Layer of the Tropical Atlantic Ocean in 1979-99. J. Physical Oceanogr., 34, 903-919.

Vecchi G. A., B. J. Soden, A. T. Wittenberg, I. M. Held, A. Leetmaa and M. J. Harrison, 2004: Weakening of tropical Pacific atmospheric circulation due to anthropogenic forcing. Nature, 441, 73-76.

Wallace, J. M. and D. S. Gutzler, 1981: Teleconnections in the geopotential height field during the Northern Hemisphere winter. Mon. Wea. Rev. 109, 784–812.

Wallace, J. M., G.H. Lim and M. L. Blackmon, 1988: Relationship between cyclone tracks, anticyclone tracks, and baroclinic waveguides. J. Atmos. Sci., 45, 439-462.

Wang, C., 2002: Atlantic Climate Variability and Its Associated Atmospheric Circulation Cells. J. Climate, 15, 1516–1536.

Wang C., 2005: ENSO, Atlantic Climate Variability and the Walker and Hadley Circulations. Revised to the book of the Hadley Circulation: Present, Past and Future, H. F. Diaz and R. S. Bradley, Eds., Cambridge University Press.

Xie, P. and P.A. Arkin, 1997: Global precipitation: A 17-year monthly analysis based on gauge observations, satellite estimates, and numerical model outputs. Bull. Amer. Meteor. Soc., 78, 2539 - 2558.

Zebiak, S. E. (1993): Air–sea interaction in the equatorial Atlantic region. J. Climate, 6, 1567–1586.